Project No. 11-3097

Feasibility and Safety Assessment for Advanced Reactor Concepts Using Vented Fuel

Reactor Concepts

Dr. Andrew Klein
Oregon State University

In collaboration with:
General Atomics

Thomas Sowinski, Federal POC
John Valente, Technical POC

NEUP Nuclear Energy University Programs
U.S. Department of Energy

NUCLEAR ENGINEERING
&
RADIATION HEALTH PHYSICS

FEASIBILITY AND SAFETY ASSESSMENT FOR ADVANCED REACTOR CONCEPTS USING VENTED FUEL

Final Report

OSU-NE-VF-1204

Topher Matthews
Renae Lenhof
Wesley Deason
Jackson Harter
Dr. Andrew Klein

January 2015

Contents

1. Executive Summary **6**

2. Introduction **13**
2.1. Summary . . . 13
2.2. Fission Products . . . 15
2.3. Extending Fuel Lifetime . . . 16
2.4. Previous Vented Fuel Designs . . . 18
2.4.1. Peach Bottom Unit 1 . . . 18
2.4.2. Gas-Cooled Fast Reactor . . . 19
2.4.3. Gen-IV Gas-Cooled Fast Reactor . . . 19
2.4.4. Energy Multiplier Module . . . 20
2.4.5. Other gas-cooled reactors . . . 21
2.4.6. Sodium Fast Reactors . . . 21
2.5. Previous Helium Purification System Designs . . . 23
2.5.1. Peach Bottom Unit 1 . . . 23
2.5.2. Gas-Cooled Fast Reactor . . . 23
2.5.3. EM^2 . . . 26
2.6. Previous Vented Fuel Subsystems Safety Analyses . . . 26
2.6.1. Peach Bottom Unit 1 . . . 26
2.6.2. Other gas-cooled reactors . . . 28

3. Fuel Modeling **29**
3.1. Introduction . . . 29
3.2. Fission Gas Behavior . . . 29
3.2.1. Bubble types . . . 31
3.2.2. Diffusivity dependence . . . 34
3.3. R/B curves . . . 37
3.3.1. Peach Bottom . . . 37
3.3.2. MHTGR model . . . 38
3.3.3. R/B model discussion . . . 42
3.4. UC Material Property Database . . . 43
3.4.1. Density . . . 44
3.4.2. Melting point . . . 45
3.4.3. Specific Heat Capacity . . . 45
3.4.4. Thermal Conductivity . . . 46
3.4.5. Thermal Expansion . . . 50

3.4.6. Young's Modulus . . . 51
3.4.7. Poisson's Ratio . . . 51
3.4.8. Thermal Creep . . . 52
3.4.9. Irradiation Creep . . . 52
3.4.10. Fission products . . . 53
3.4.11. Irradiation induced swelling and densification . . . 53
3.4.12. Fission gas release . . . 56
3.5. The BUCK Fuel Performance Code . . . 57
3.5.1. BUCK software classes . . . 57
3.5.2. Representative pin model . . . 58
3.5.3. Representative sphere model . . . 58
3.6. Re-solution Rate Calculation . . . 62

4. Systems Modeling **70**
4.1. Theory . . . 70
4.1.1. Fission Product Transport Phenomena . . . 70
4.1.2. Helium purification system design . . . 75
4.2. System Model . . . 78
4.2.1. Selection of radionuclides . . . 80
4.2.2. Evaluation of the chemical state of fission products . . . 83
4.2.3. Discussion of an appropriate model . . . 84
4.2.4. Analytical treatment of vented fuel and HPS components . . . 87
4.2.5. System model verification and validation . . . 91
4.3. Results and Discussion . . . 91
4.3.1. Helium purification system significance . . . 91
4.3.2. Benefits of a complex helium purification system . . . 99
4.3.3. Evaluation of system uncertainties . . . 105
4.4. System Modeling Conclusions . . . 112
4.5. Updated Values using MHTGR model . . . 113
4.5.1. R/B model comparison . . . 113
4.5.2. Tracked fission product list update . . . 113
4.5.3. Updated case study results . . . 118

5. Safety Analysis **120**
5.1. Background . . . 120
5.1.1. History of safety analysis in commercial nuclear power . . . 120
5.1.2. Probabilistic Risk Assessment . . . 122
5.1.3. Atmospheric transport modeling . . . 128
5.1.4. Past PRAs of gas-cooled reactors . . . 132
5.1.5. Recent PRAs of gas-cooled reactors . . . 134
5.2. Vented Fuel System Design . . . 136
5.2.1. Choice of fission product vent system components . . . 136
5.2.2. Fission product vent system component layout . . . 137
5.3. Probabilistic Risk Assessment Modeling Assumptions . . . 140

5.4. Probabilistic Risk Assessment Inputs . . . 140
5.4.1. Initiating event frequency . . . 141
5.4.2. Component reliability . . . 141
5.4.3. Common Cause Failure (CCF) . . . 142
5.4.4. Human reliability . . . 143
5.4.5. Fault tree analysis . . . 144
5.4.6. Event tree analysis . . . 144
5.4.7. Accident progression event tree analysis . . . 144
5.4.8. Source term analysis . . . 145
5.4.9. Consequence analysis . . . 146
5.5. Vented Fuel System PRA Integration . . . 148
5.6. Level 1 PRA Model . . . 148
5.6.1. Selection of initiating event frequencies . . . 148
5.6.2. Selection of component reliability data . . . 150
5.6.3. Selection of a Common Cause Failure (CCF) model . . . 155
5.6.4. Selection of a Human Reliability Assessment (HRA) model . . . 155
5.6.5. Level 1 fault tree development . . . 156
5.6.6. Level 1 event tree development . . . 158
5.6.7. Level 1 system damage state determination . . . 159
5.7. Level 2 PRA Model . . . 160
5.7.1. Level 2 Accident Progression Event Tree (APET) development . . . 160
5.7.2. Selection of APET top event probabilities . . . 163
5.7.3. Selection of Source Term Groups (STGs) . . . 164
5.7.4. Estimating source terms using STELLA model of FPVS . . . 165
5.8. Level 3 PRA Model . . . 171
5.8.1. Building an atmospheric transport model in GENII . . . 171
5.9. Level 1 PRA Results . . . 175
5.9.1. System Evaluation: Normal Operations . . . 175
5.9.2. System Evaluation: Accident Conditions . . . 180
5.9.3. System damage states . . . 188
5.10. Level 2 PRA Results . . . 189
5.10.1. Accident progression event tree results . . . 189
5.10.2. Source term estimation results . . . 191
5.11. Level 3 PRA Results . . . 194
5.11.1. Overall risk profile . . . 194
5.12. Conclusions . . . 199

6. Conclusions **202**
6.1. Summary . . . 202
6.2. Gap Analysis . . . 205
6.2.1. Fuel modeling . . . 206
6.2.2. Fission Product Vent System . . . 209
6.2.3. PRA . . . 210
6.3. Recommended Experiments . . . 211

References 215

Appendices 227

A. Fuel modeling appendicies 228

B. System Design Appendicies 229

C. PRA Appendices 280

1. Executive Summary

Recent interest in fast reactor technology has lead to renewed analysis of past reactor concepts such as Gas Fast Reactors and Sodium Fast Reactors. In an effort to make these reactors more economic, the fuel is required to stay in the reactor for extended periods of time; the longer the fuel stays within the core, the more fertile material is converted into useable fissile material. However, as burnup of the fuel-rod increases, so does the internal pressure buildup due to gaseous fission products. In order to reach the 30 year lifetime requirements of some reactor designs, the fuel pins must have a vented-type design to allow the buildup of fission products to escape.

The present work aims to progress the understanding of the feasibility and safety issues related to gas reactors that incorporate vented fuel. The work was separated into three different workscopes:

1. Quantitatively determine fission gas release from uranium carbide in a representative helium cooled fast reactor.

2. Model the fission gas behavior, transport, and collection in a Fission Product Vent System.

3. Perform a safety analysis of the Fission Product Vent System.

Each task relied on results from the previous task, culminating in a limited scope Probabilistic Risk Assessment (PRA) of the Fission Product Vent System. Within each task, many key parameters lack the fidelity needed for comprehensive or accurate analysis. In the process of completing each task, the data or methods that were lacking were identified and compiled in a Gap Analysis included at the end of the report.

The most fundamental question regarding the Safety and Feasibility of Vented Fuel Systems is "How much fission gas gets out of the fuel?" This is an essential input into the Fission Product Vent System loading, and ultimately determines the resulting consequences from the safety analysis. Unfortunately, this is also the most difficult problem to tackle. The hostile environment of a reactor core reduces nearly all experimental data to post irradiation measurements. This is further compounded by the lack of available uranium carbide data, the representative fuel form used for the current work.

There are two approaches to modeling the fission gas release from fuel pellets. The first is through experimentally determining a R/B, or Release Rate over Birth Rate line. This method condenses all of the complexity involved with fission gas release into a single relationship that produces a release rate as a function of isotope half-life. While this method is simple to implement, it quickly loses validity as the reactor design and irradiation parameters diverge from the original conditions the R/B line was formulated from.

The second approach is through mechanistic modeling of the behavior of the gas atoms themselves. This requires a even larger set of experimental data in order to validate the vast applicable

time and space scales. While a model of such depth seems to work well for uranium oxide fuels for which an immense library of irradiation data is available, carbide fuel release models have yet to capture the true phenomena.

We initially started with a simple R/B model based on the previously operating commercial Peach Bottom gas reactor. A temperature dependent R/B model based on Modular High Temperature Gas Reactor (MHTGR) information was eventually implemented to provide better data for the PRA modeling.The calculation includes an exponential temperature correction factor, necessitating application of the MHTGR model to a temperature distribution rather than an average. Estimated Beginning of Life (BOL) and End of Life (EOL) fuel temperature distributions provided by GA allowed calculation of R/B at two contrasting operating conditions. Initially, it was believed that the complexities present in the new model would result in lower fission gas release than the single Peach Bottom curve. While the narrow EOL temperature distribution does result in less release of gaseous fission products, the release actually increases for the BOL temperature distribution: a small percentage of hot fuel rods at BOL cause an increase in fission gas release, especially of isotopes with short half-lives. In general, the Peach Bottom curve lies between the BOL and EOL. The uncertainties involved affect both models equally (i.e. similar but different fuel types, thermal vs. fast reactor design, close packed vs. graphite dispersed particles), thus neither model is fully adequate. Regardless, the temperature dependence of the MHTGR allows for potentially more interesting calculations.

Along with the release rates from the fuel, the list of volatile elements that escape from the fuel has a high impact on the fission gas loading. A cut-off boiling temperature of 1500° C was initially implemented that based the volatility of fission products on the peak fuel temperatures. However, a cut-off temperature based on coolant temperatures has been deemed more appropriate. Even still, it is unclear what elements actually reach the Fission Product Vent System.

Simultaneously, a more robust mechanistic model was developed to try and model the fission gas release phenomena. This involved the creation of BUCK (Basic Uranium Carbide Kernels), a fuel performance code that builds on Idaho National Lab's BISON code. While this code handled the macro-scale fuel behavior such as swelling, creep, and thermal conduction, it lacked the microscopic data necessary to track fission gas bubble behavior.

Regardless, macro-scale simulations were conducted that modeled representative uranium carbide fuel pins. The simulations incorporated the important phenomena in a fully coupled non-linear solve. Behavior such as porosity, thermomechanical properties, and creep were captured. Simple models to account for volume swelling and fission gas release were also incorporated, but failed to accurately capture the complex behavior resulting from the accumulation of fission gas bubbles.

In order to capture some of the microscopic behavior of fission gas release, a rate equation type model that tracks the bubble size distribution is necessary to determine the behavior of the small and large bubbles present in uranium carbide. As a first step, the Binary Collision Approximation code 3DOT was created to model the re-solution event in uranium carbide, an important loss term necessary for bubble size distribution simulations. The re-solution rate as a function of bubble radius was determined for uranium carbide fuels to a fidelity not previously modeled. Due to the relatively high energy transfer material properties in uranium carbide, fission gas re-solution can be modeled using the homogeneous, atom-by-atom loss model. We found a re-solution parameter that was an order of magnitude lower than previous studies due to the

inclusion of electronic ion energy losses. A decrease in the re-solution parameter as a function of radius occurred for small bubble radii, with a nearly constant re-solution parameter for radii above 50 nm. The BCA approximation allowed the computationally inexpensive analysis of many different types of bubbles, and it was shown that the fundamental BCA assumption is appropriate for use in the simulations presented here. Through comparative studies on the re-solution parameter for various values of implantation energy and atomic density in the bubble, we found that while the re-solution parameter did change, the overall shape did not. The re-solution parameter calculated here can be used in rate-equation type simulations to model fission gas bubble behavior, and ultimately fission gas release.

Despite the success with the calculation of the re-solution rate and the ability of BUCK to model the macroscale phenomena, the final linkage between the two codes was not achieved within the scope of this project. Ultimately the R/B relationships were utilized in the systems modeling and the PRA analysis.

Although a vented fuel design directly changes the fuel pin design, the biggest safety concerns focus on the ability of the Fission Product Vent System to capture and contain the radioactive fission products. As such, the bulk of the safety analysis for this project focused on the helium purification system design and performance. The vented fission gases must be collected in a system that not only cools the vented purge stream to temperatures that will allow condensation of the gases, but also must provide enough space for the shear volume of vented gases.

In order to model the Fission Product Vent System, a model was created in the system analysis software STELLA that was able to track gas concentrations throughout a representative Fission Product Vent System (FPVS). This required a massive network of individual isobaric decay chain models to capture the expansive list of volatile isotopes. The original model was then extended to a more complex fission release model based on the MHTGR release model, with a reduced number of tracked isotopes based on more recent temperature data.

The system model was used to test seven case scenarios, ranging from a completely open system with no FPVS, to an attempt at a system with a slightly optimized FPVS. These results revealed that the following design constraints and considerations are necessary for implementation of vented fuel within a helium-cooled GFR:

1. The quantity of fission products accumulated in the FPVS is likely very large. The system must be designed to accommodate the fission product load or be regenerated at regular intervals to prevent breakthrough into the primary coolant from occurring in the last fission product trap.

2. The activity and power generation rate of fission products collected in the FPVS is also very large. Cooling the purge stream to temperatures necessary for the adsorption of noble gas fission products may present a large power requirement for the helium-cooled GFR plant. Additionally, extensive shielding systems will be required to allow operations and maintenance to occur in the vicinity of the FPVS.

3. Safety systems will be necessary to prevent overheat and release of the contents of a FPVS in an accident scenario. Use of defense-in-depth strategies to reduce the impact of a possible release of gaseous fission products is recommended.

4. Determination of the purge stream leakage rate is of crucial importance for predicting the level of radioactivity in the primary coolant.

5. Determination of the fuel release rate is of crucial importance for predicting the level of radioactivity in all areas of the plant and for the design of a safe and economical FPVS.

The original STELLA model was then extended to a more complex fission release model based on MHTGR data. In general, the the BOL MHTGR model calculates powers 30-50% higher than the Peach Bottom model, while the EOL model predicts about 1/4 of the Peach Bottom values. The accumulated masses are roughly the same for each model. The tracked element list was updated to reflect a more accurate purge stream temperature, resulting in a roughly 50% reduction in mass, power, and activity loading in the hot fission product trap.

Finally, the last task resulted in the completion of a limited scope Level 1, 2, and 3 PRA model. Taking the mass accumulations calculated in the STELLA model, the failure mechanisms and their consequences were analyzed using modern PRA tools to determine the ultimate risk involved with the current design of the representative reactor model used for this study, General Atomic's (GA) Energy Multiplier Module (EM^2). A Level 2 PRA analysis was applied to the vented fuel system using the PRA software SAPHIRE to understand how the accident progresses for each system damage state. To characterize the quantity of release for each damage state, the STELLA model was used to describe the time-dependent fission product transport in the vented fuel system. Attenuation factors were applied to the STELLA model results to account for the various fission product barriers and retention mechanisms in place to prevent or mitigate a release. Lastly, a Level 3 PRA analysis was applied to the vented fuel system using the atmospheric transport tool GENII. The acute transport model is used to determine the resulting dose and risk consequences associated with each source term group with a frequency that merits further analysis.

The present work found several vulnerabilities that require further assessment to ensure the safety of the vented fuel system. This is typical for new systems undergoing PRA for the first time. First, the motor operated isolation control valve, identified as V-15, is a single point failure having the sole ability to maintain the pressure differential required to ensure the purge stream does not counter diffuse into the primary coolant. In addition, each of the three 100% FPVS trains may be made unavailable by an inadvertent closure of V-15. Although the consequences of such an event were not further analyzed in the present work, a failure of the valve to function is shown in the Level 1 PRA to be an important component, contributing largely to the failure of the vented fuel system to function under normal conditions. The current system model is unable to analyze the effects of a failure of V-15 to maintain the required pressure differential resulting in counter diffusion of fission products into the primary system however this modeling deficiency needs to be addressed in future safety analyses.

System failures initiated by transient events dominate the overall system failure frequency as a direct consequence of the larger initiating event frequency. The most probable system damage states are a release from the vented fuel system within the containment building and within the auxiliary building. It is assumed for the present analysis that the containment building has a leak rate of 0.1% per day and is equipped with a filter allowing filtered venting of the containment whereas no retention capabilities of the auxiliary building are credited. As a result

of the reduced fission product boundaries present in the event of a release within the auxiliary building, consequences of these events prove to be more severe.

Based on the results of the present analysis, additional design and analysis of the vented fuel system is required. It should be noted that the present work operates under several highly conservative assumptions. Consequently, the vented fuel system, as modeled, may be safely operated without design changes pending the refinement of the models used to determine source term estimates and atmospheric transport. Specifically, the conservative modeling assumptions that have the potential to greatly reduce the estimated consequences if refined include the fraction of the activity within the adsorber beds that is released under accident conditions, the specific attenuation factors applied to the various fission product boundaries, and the atmospheric conditions selected for the atmospheric transport model. In addition, design changes such as an increase in the Exclusion Area Boundary or placement of the entire vented fuel system within the containment building may further reduce the consequences of a release.

As with many advanced reactor concepts, there is a large gap between the analysis required for licensing, and the data, techniques, and methods to allow accurate analysis to be completed. While completing the work for the current project, holes in the current state of the art were compiled to provide to provide a list of workscopes to further the knowledge-base on the array of subjects touched on during this project.

No topic within this project is hampered as much as the ability to accurately estimate fission gas behavior. The phenomena that drives the movement and growth of gas atoms and bubbles determines not only the fission gas release, but the swelling of the fuel as bubbles begin to populate the fuel grains.

Despite the issues with the currently implemented R/B curve, fission gas release estimations based on R/B curves in general would be the easiest to obtain and utilize, requiring only irradiation data to obtain release rates. While expensive, fueled irradiation capsules would provide the most accurate data. The major drawback of such models is that each test is integral, meaning the models may lose validity for designs or conditions deviate from the reactor type, fuel design, and irradiation conditions used to initially create the model. A broad experimental matrix may allow for interpolation between variables, improving the robustness of the model. Regardless, R/B curves could provide release rates with high confidence if licensability is necessary for only a small range of fuel types or irradiation conditions.

In order to move away from fission gas release estimates hindered by the available data, a mechanistic model that captures the relevant physics of fission gas behavior is necessary. Such a model requires several layers of complexity.Within this project, a Macroscopic model was created to model the bulk phenomena in uranium carbide fuels, however an appropriate microstructural code that can model the bubble population distribution is really necessary to capture the swelling and fission gas release.

The steps necessary to accurately model fission gas release in carbide fuel can be summarized as follows:

1. In order to estimate fission gas release only from a standardized fuel form, a R/B model should be adequate. Many irradiations are necessary across a carefully chosen number of parameters to ensure that the variations in design can be captured by an R/B model. Although potentially costly, the R/B model presents a brute-force method that will provide

adequate results within an operating envelope. Empirical models for fuel swelling due to gas bubbles are also necessary in order to correctly predict the behavior of the fuel-cladding contact.

2. In order to estimate fission gas beyond normal designs or normal operation, a mechanistic model of the fission gas release phenomena is necessary. This method requires a much more thorough understanding of the physics at hand, but will allow modeling of the fuel during off-normal events. Such a model could predict both gas release and swelling due to gas bubbles. While many macro-scale models exist, microstructural models that adequately capture bubble behavior need to be created. A broad supporting experimental database is also necessary.

3. An intermediate solution combining an R/B-type model with a fuel performance model may capture the advantages of both. Although somewhat limited by the experimental data used to produce the R/B model, gas release calculations may benefit from higher fidelity results from fuel performance models such as temperature and stress distributions.

Another limiting factor found during the current study is in the accurate determination of fission product behavior in the reactor and Fission Product Vent System. This requires comprehensive knowledge of the operating parameters of the reactor itself, such as temperature distributions, pressures, and core materials, as well as knowledge of how fission products behave at those conditions.

One of the biggest gaps is the accurate estimation of the fission product trap's ability to trap and hold onto the fission gases. This is important not only at their standard operating temperature, but as a function of temperature and time for determination of gas release during accident conditions.

In addition to the delay beds, plateout of certain elements will occur on all of the Fission Product Vent System piping. The concentration of the plateout and its behavior to temperature is important to estimate the activity levels of these pipes so as to adequately shield them during repairs.

An important design parameter that is necessary to calculate in order to determine the primary coolant activity is the purge stream leakage fraction. Though the purge stream leakage fraction is very specific to the plant design that it refers to, research into techniques which would decrease the probability of release of fission products into the primary coolant would be valuable.

Another issue of concern that could be addressed is the development of a more complex and more precise system model of a helium-cooled GFRs plant utilizing vented fuel. With a more complex and precise model, many more delay bed arrangements in the Fission Product Vent System could be tested and the plateout distribution in the primary coolant and behavior of short-lived fission products in the system could be better understood.

Although not attempted in the current work, a better understanding of transient behavior is necessary.The presence of pressure transients in the vented fuel system could have a significant impact on the transport of volatile fission products from the core and throughout the plant. If possible, these pressure transients should be evaluated in an in-pile fuel test that is also capable a measuring fission product plateout and adsorption to properly verify the analytical models of the system behavior.

The breadth of PRA analysis conducted in the present project revealed several avenues by which the safety implications of using vented fuel might be better understood. The first is in establishing a more detailed software tool capable of analyzing the transient effects of an accident scenario which challenge the vented fuel system. STELLA has inherent limitations requiring conservative assumptions regarding source term attenuation factors and the retention capabilities of the adsorber modules under various accident conditions. While some conservatism is good practice, failure to address such deficiencies in the analysis may lead to a misguided understanding of the risks associated with the application of a vented fuel system for advanced gas reactor concepts. A more refined and precise model including pressure and temperature feedback from accident progression could assist in a more accurate, and likely less conservative, assessment of the safety significance of a release from the vented fuel system. This includes an improved method for determining fuel release fractions.

Another issue of concern that could be addressed is the general lack of gas reactor component reliability data, which increases the uncertainty associated with the reliability of several important components whose failure directly impacts the potential source term and associated consequences. The Level 1 results indicate that the failure of the motor operated valves in the system hold the highest importance. As the design matures, an effort to refine the component reliability database, specifically for components with high importance factors such as valves, should be pursued to ensure adequate reliability of the system. The relevance and value of the PRA analysis conducted in the present project ultimately depends on the quality of component reliability data and initiating event frequency data input into the analysis.

Finally, to better understand the cost-benefit ratio of utilizing a vented fuel system, a full plant wide PRA should be performed to assess the risks related to a release of fission products for a base design utilizing vented fuel and a design which elects to increase the plenum volume to allow for storage of fission gas accumulation over the extended operating life. Although there is risk introduced by removing the fission products from the core, there is also a benefit of isolating these fission products from the effects of a challenging event in the reactor core. The risks identified in the present project may be of less concern than the risks associated with choosing to preserve the fission products in the core for the full projected thirty year core life.

2. Introduction

2.1. Summary

Recent interest in fast reactor technology has lead to renewed analysis of past reactor concepts such as Gas Fast Reactors and Sodium Fast Reactors. In an effort to make these reactors more economic, the fuel is required to stay in the reactor for extended periods of time; the longer the fuel stays within the core, the more fertile material is converted into useable fissile material. However, as burnup of the fuel-rod increases, so does the internal pressure buildup due to gaseous fission products. In order to reach the 30 year lifetime requirements of some reactor designs, the fuel pins must have a vented-type design to allow the buildup of fission products to escape.

The present work aims to progress the understanding of the feasibility and safety issues related to gas reactors that incorporate vented fuel. The work was separated into three different workscopes:

1. Quantitatively determine fission gas release from uranium carbide in a representative helium cooled fast reactor.
2. Model the fission gas behavior, transport, and collection in a Fission Product Vent System.
3. Perform a safety analysis of the Fission Product Vent System.

Each task relied on results from the previous task, culminating in a limited scope Probabilistic Risk Assessment (PRA) of the Fission Product Vent System. Within each task, many key parameters lack the fidelity needed for comprehensive or accurate analysis. In the process of completing each task, the data or methods that were lacking were identified and compiled in a Gap Analysis included at the end of the report.

The most fundamental question regarding the Safety and Feasibility of Vented Fuel Systems is "How much fission gas gets out of the fuel?" This is an essential input into the Fission Product Vent System loading, and ultimately determines the resulting consequences from the safety analysis. Unfortunately, this is also the most difficult problem to tackle. The hostile environment of a reactor core reduces nearly all experimental data to post irradiation measurements. This is further compounded by the lack of available uranium carbide data, the representative fuel form used for the current work.

There are two approaches to modeling the fission gas release from fuel pellets. The first is through experimentally determining a R/B, or Release Rate over Birth Rate line. This method condenses all of the complexity involved with fission gas release into a single relationship that produces a release rate as a function of isotope half-life. While this method is simple to implement, it quickly loses validity as the reactor design and irradiation parameters diverge from the original conditions the R/B line was formulated from.

The second approach is through mechanistic modeling of the behavior of the gas atoms themselves. This requires a even larger set of experimental data in order to validate the vast applicable time and space scales. While a model of such depth seems to work well for uranium oxide fuels for which an immense library of irradiation data is available, carbide fuel release models have yet to capture the true phenomena.

We initially started with a simple R/B model based on the previously operating commercial Peach Bottom gas reactor. This model was used to develop the initial systems modeling discussed in Section 4. A temperature dependent R/B model was eventually implemented to provide better data for the PRA modeling discussed in Section 3.3. Simultaneously, a more robust mechanistic model was developed to try and model the fission gas release phenomena. This involved the creation of BUCK (Basic Uranium Carbide Kernels), a fuel performance code that builds on Idaho National Lab's BISON code. While this code handled the macro-scale fuel behavior such as swelling, creep, and thermal conduction, it lacked the microscopic data necessary to track fission gas bubble behavior.

In order to capture some of the microscopic behavior of fission gas release, a rate equation type model that tracks the bubble size distribution is necessary to determine the behavior of the small and large bubbles present in uranium carbide. A Binary Collision Approximation code 3DOT was created to model the re-solution event in uranium carbide. The re-solution rate as a function of bubble radius was determined for uranium carbide fuels to a fidelity not previously modeled. The work with 3DOT has been accepted for publication in the Journal of Nuclear Materials [1].

Despite the success with the calculation of the re-solution rate and the ability of BUCK to model the macroscale phenomena, the final linkage between the two codes was not achieved within the scope of this project. Ultimately the R/B relationships were utilized in the systems modeling and the PRA analysis.

Although a vented fuel design directly changes the fuel pin design, the biggest safety concerns focus on the ability of the Fission Product Vent System to capture and contain the radioactive fission products. As such, the bulk of the safety analysis for this project focused on the helium purification system design and performance. The vented fission gases must be collected in a system that not only cools the vented purge stream to temperatures that will allow condensation of the gases, but also must provide enough space for the shear volume of vented gases.

In order to model the Fission Product Vent System, a model was created in the system analysis software STELLA that was able to track gas concentrations throughout a representative Fission Product Vent System (FPVS). This required a massive network of individual isobaric decay chain models to capture the expansive list of volatile isotopes. This work was initially completed by Wesley Deason, culminating in his Master's Defense in 2013 [2]. His original model was then extended to a more complex fission release model based on Modular High Temperature Gas Reactor (MHTGR) data, with a reduced number of tracked isotopes based on more recent temperature data. These updated values were then passed into the PRA modeling efforts described in Section 5.

Finally, the last task resulted in the completion of a limited scope Level 1, 2, and 3 PRA model. This work was completed by Renae Lenhof, culminating in her Master's Defense in 2014 [3]. Taking the mass accumulations calculated in the STELLA model, the failure mechanisms and their consequences were analyzed using modern PRA tools to determine the ultimate

risk involved with the current design of the representative reactor model used for this study, General Atomic's (GA) Energy Multiplier Module (EM^2). A Level 2 PRA analysis was applied to the vented fuel system using the PRA software SAPHIRE to understand how the accident progresses for each system damage state. To characterize the quantity of release for each damage state, the STELLA model was used to describe the time-dependent fission product transport in the vented fuel system. Attenuation factors were applied to the STELLA model results to account for the various fission product barriers and retention mechanisms in place to prevent or mitigate a release. Lastly, a Level 3 PRA analysis was applied to the vented fuel system using the atmospheric transport tool GENII. The acute transport model is used to determine the resulting dose and risk consequences associated with each source term group with a frequency that merits further analysis.

The present work found several vulnerabilities that require further assessment to ensure the safety of the vented fuel system. This is typical for new systems undergoing PRA for the first time. Based on the results of the present analysis, additional design and analysis of the vented fuel system is required. It should be noted that the present work operates under several highly conservative assumptions. Consequently, the vented fuel system, as modeled, may be safely operated without design changes pending the refinement of the models used to determine source term estimates and atmospheric transport. Specifically, the conservative modeling assumptions that have the potential to greatly reduce the estimated consequences if refined include the fraction of the activity within the adsorber beds that is released under accident conditions, the specific attenuation factors applied to the various fission product boundaries, and the atmospheric conditions selected for the atmospheric transport model. In addition, design changes such as an increase in the Exclusion Area Boundary or placement of the entire vented fuel system within the containment building may further reduce the consequences of a release.

Note: The term Helium Purification System (HPS) is used interchangeably with Fission Product Vent System (FPVS). Traditionally, the HPS has the primary function of maintaining the coolant chemistry and the FPVS has the primary function of removing and storing volatile fission gases from a purge stream. While these two systems differ in their primary function, they are often combined into a single system due to their similar function and components. For the purposes of this work, HPS and FPVS will refer to the same system that filters volatile fission gases out of the purge stream exiting the fuel directly.

2.2. Fission Products

Due to the inherent nature of heavy element fission, an accumulation of amazingly varied elements constantly keeps the fuel in chemical and mechanical imbalance. Along with several neutrons, a single uranium atom splits into two highly energetic fission fragments (FF) during fission. As these fragments bounce around within the fuel lattice, they eventually come to rest, becoming fission products (FP) and leaving a zone of displaced atoms in their wake. Most of these FP are relatively benign and can form varied chemical compounds within the fuel. Others, such as xenon-135 and samarium-149 are neutronically problematic and can cause issues during reactor restarts.

The path of gaseous fission products within the fuel is complicated (Figure 2.1. While most

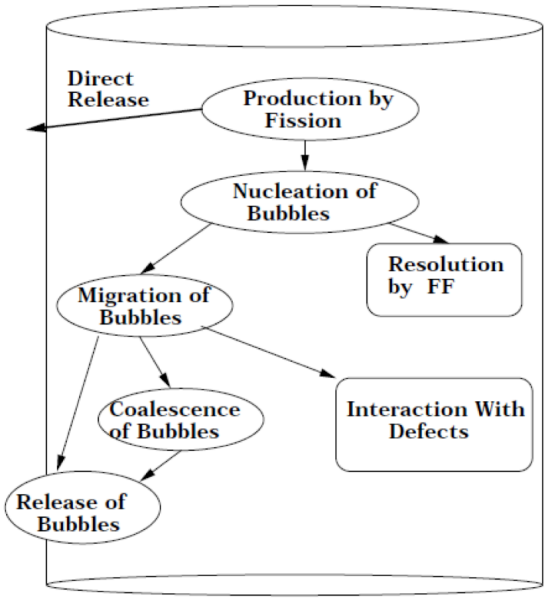

Figure 2.1.: Cartoon of fission gas behavior [4]

atoms remain stationary after becoming FP, volatile elements by definition will not stay in solution within the fuel lattice and will tend to thermally diffuse, forming bubbles or percolating as single gas atoms towards the grain boundaries. Furthermore, the highly energetic FF constantly streaming through the fuel can knock fission gas atoms out of the bubbles, resulting in a bubble population that is dependent on both material properties (ie. thermal conductivity, diffusivity) and state properties (ie. temperature, fission rate). In high burn-up fuels, such as those required in fast breeder reactors, both inter-granular and grain-boundary bubbles made up of these fission gases (FG) define the microstructure of the fuel. Figure 2.2 displays the stark contrast between the colder fuel pellet regions (III and IV) and the hotter central zones (I and II): The highly temperature-dependent diffusivity of FG results in little bubble formation at colder temperatures and a highly porous structure near the hot interior. Since bubble interconnectivity is directly related to how much of the FG escapes from the fuel, understanding of the FG atom and bubble behavior is essential in determing the total fission gas release.

2.3. Extending Fuel Lifetime

In order to make fast reactors more economic, the fuel is required to stay in the reactor for extended periods of time; the longer the fuel stays within the core, the more fertile material is converted into useable fissile material. Two strategies can be used to extend fuel lifetime. The first process involves removing fuel from the core after 3-7 years, reprocessing to remove the fissile material, refabrication of new fuel rods, and reinsertion into the core. Due to the high radioactivity of nuclear fuel after irradiation, reprocessing requires shielding and limited handling of the fuel during the process which can be reduced by cool-down times, requiring a

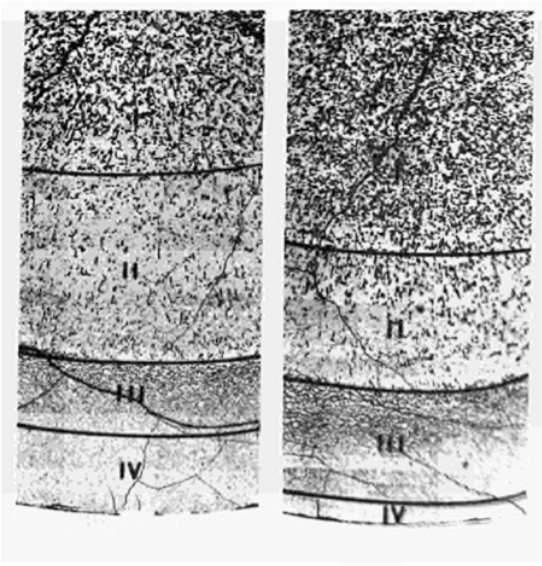

Figure 2.2.: Cross-section of two irradiated UC fuel pins [4]

large time and money investment in fuel rods waiting in spent fuel pools.

The second strategy to extend fuel lifetime is to simply leave the fuel in the core for long periods of time. This can include dynamic or static fuel locations, but ultimately results in the fuel remaining in the core for the lifetime of the reactor, around 30 years, requiring robust cladding that will maintain structural integrity. One of the limiting factors to fuel pin lifetime is strain on the cladding; as the fuel fissions, fission gas is continually released into the gap between the fuel and the cladding, creating a pressure differential between the interior of the clad and the reactor coolant. The strain on the cladding results in creep deformation, causing the clad to bulge that can ultimately lead to cladding failure. The high temperature and in-pile irradiation environment accelerates the creep rate even further. The implementation of a large internal pin plenum can help extend the fuel lifetime slightly by increasing the internal pin volume.

One solution to extend the lifetime of fuel cladding has been to permit venting of the fuel pin; by allowing an escape path for the fission gas, either directly to the coolant or into a separate collection system, the differential pressure across the cladding is able to remain low. This concept has been successfully implemented in the US in the now decommissioned Peach Bottom 1 reactor. Several other reactor designs have proposed to use vented fuel, such as the Gas Cooled Fast Reactor (GCFR) and GA's Energy Multiplier Module (EM^2) modular reactor [5].

The primary safety goal in nuclear reactors is containment of both the nonvolatile and gaseous FP. This has primarily been achieved in the US with the "Defense in Depth" philosophy, in which the use of independent, redundant, and diverse barriers prevents FP release. The first of these barriers is considered to be the fuel itself: most fuels are ceramic and do a fair job of retaining solid and some gaseous FP [6]. The second barrier is typically the cladding of the fuel. The cladding physically isolates the fuel from the coolant, and is the primary containment mechanism in the Defense in Depth concept. Other barriers include the coolant, pressure vessel, and the outer containment building. By design, vented fuels remove the ability of the fuel pin to

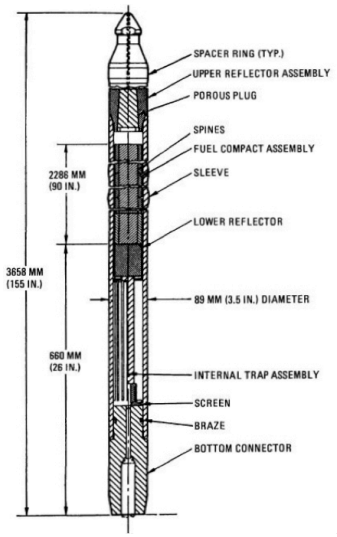

Figure 2.3.: Peach Bottom fuel element [7].

completely retain the fission products. Although this diverges from the traditional application of Defense in Depth, redundant collection systems still maintain control of the radioactive fission products, retaining the safety benefits of the Defense in Depth philosophy. Although secondary systems may complicate the safety analysis of the reactor, removal of activated products from the core may help reduce the emission of radioactive materials during reactor accidents. Regardless of the impact a vented fuel system has on the safety of the reactor, accurate release rates from the fuel are necessary to help quantify the source term and understand its behavior.

2.4. Previous Vented Fuel Designs

2.4.1. Peach Bottom Unit 1

Though design consideration of vented fuel in nuclear reactor systems has a long and varied history, the actual application of vented fuel in operating reactors has been quite limited. The only commercial gas reactor to have used vented fuel was the Peach Bottom Unit 1 Reactor [7]. Operating from June 1, 1967 to October 31, 1974, the reactor generated 40 MWe (115.3 MWt) of electrical power with an impressive 74% capacity factor. Unlike contemporary Light Water Reactor (LWR) designs, Peach Bottom used helium as a coolant and a carbon-based fuel with graphite cladding. To counter the poor barrier provided by the graphite cladding to fission product release, the core featured a purge stream which removed fission products from the inner cladding wall and carried them to an HPS.

The Peach Bottom core featured 804 pin type fuel elements with a 3.5 inch diameter, a 12 foot length, and a graphite cladded region of approximately 10 foot (Figure 2.3. The fuel elements were arranged in a triangular array and featured lower and upper connectors, lower and upper graphite reflectors, a 7.5 foot active fuel region, an internal fission product trap, and a low permeability graphite cladding (sleeve) which separated the fuel element internals from the primary

coolant. The uranium and thorium carbide (UC^2 and ThC^2) annular fuel contained in the active fuel region was stacked on a graphite center spine which, depending on the fuel element, may or may not have contained burnable poison.

During operation, helium for the fission product purge stream entered the fuel element at the hot end (top) of the core through a hole in the top reflector and flowed through the gap between the graphite sleeve and the annular fuel. It collected gaseous and volatile fission products from the fuel and was filtered by pin-internal fission product traps composed of silver-impregnated activated charcoal. After leaving the internal fission product trap, the fuel element purge stream flowed into a manifold in the core bottom and through a collective purge line to the HPS located outside the core pressure vessel and core primary containment. The pressure of the purge stream at this stage was 6 psi below the surrounding main coolant and the flow rate through each fuel element was 1.1 lb/hr of helium.

2.4.2. Gas-Cooled Fast Reactor

The Gas-Cooled Fast Reactor (GCFR), an unconstructed General Atomics design concept from the 1960's and 70's, was a 300 MWe (826 MWt) helium cooled fast reactor [8]. Unlike Peach Bottom Unit 1, it was design to use vented fuel primarily for relieving pressure on cladding produced by both the high pressure coolant and the gaseous fission product buildup, limiting the release of activity from failed fuel pins. For these reasons, the vented fuel system in the GCFR is often referred to as the "Pressure Equalization System."

The GCFR reactor core featured 265 hexagonal elements arranged in a triangular pitch; 91 of the elements were fuel elements (Figure 2.4), 147 were blanket elements and 27 were control elements. Each fuel element contained 270 stainless steel clad fuel pins of 0.282 inch diameter containing uranium oxide and plutonium oxide (UO^2 and PuO^2) in pellet form and each blanket element contained 126 stainless steel clad fuel pins of 0.504 inch diameter containing ThO2 in pellet form. Control elements were similar to fuel elements, but only contained 232 fuel pins, with the center region containing a guide tube for control rod insertion. Fuel and control elements were arranged in the core center, and the blanket elements were arranged in the radial outer region. Additionally, all fuel pins contained top and bottom axial blankets of depleted uranium.

In the GCFR, helium entered the vented fuel pin through suction holes in the core lower region, then driven past the fuel pellets and up into a header at the top of the fuel element by a pressure differential. From here, the helium traveled to the edge of the fuel element, through an internal fission product trap, and exited the core from this connection. Finally, the helium stream flowed to the HPS where fission product gases were removed. Testing and analysis showed that even if minor leaks were present through suction holes, cracks in fuel pin cladding, and vent tube connection points, release of volatiles into the GCFR plant primary coolant would be minimal [8].

2.4.3. Gen-IV Gas-Cooled Fast Reactor

The Gen-IV Gas-cooled Fast Reactor (GFR) was an unconstructed reactor design concept to consider vented fuel. It was a helium-cooled fast reactor developed under the United States De-

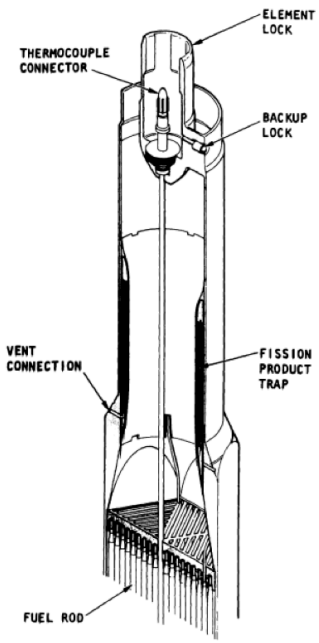

Figure 2.4.: GCFR fuel element [9].

partment of Energy's Generation IV reactor program, and was designed to be safe, proliferation resistant, and economically attractive [10]. It had two unit sizes, 600 MWt and 2400 MWt, and was built upon the pin core design of the GCFR. The Gen-IV GFR modified the GCFR design by replacing the stainless steel cladding with silicon carbide (SiC) ceramic cladding to better handle the Gen-IV GFR's higher outlet coolant temperature (850° C vs. 510° C). Additionally, the design considered using uranium carbide fuel (UC) over UO^2. The vented pin design using either monolithic SiC or Hexoloy SiC cladding was considered as a backup design option out of necessity to handle fission gas pressure which would overcome the weaker SiC cladding during a primary coolant depressurization scenario. The competing option for the Gen-IV GFR fuel pin design was the use of a traditional fission product plenum. Designers were wary that long lengths of strong SiC/SiC composite tubing could not be readily produced in time for application in the Gen-IV GFR. Due to the limited development of the vented fuel design option for the Gen-IV GFR, no fission product removal or helium purification system was studied which could accommodate the vented fuel design.

2.4.4. Energy Multiplier Module

The Energy Multiplier Module, or EM^2, is a 500 MWt helium-cooled fast reactor design by General Atomics that is currently in development [11]. The EM^2 design includes SiC clad and a UC fueled core with extended refueling intervals projected to be greater than thirty years. The higher burnup for the EM^2 is its largest defining characteristic, reaching a projected fuel burnup of 145 GWd/t, compared to the 100 GWd/t achieved by a SFR and the 30 GWd/t achieved by a

LWR , [11, 12]. Consequently, venting of fission product gases is necessary to relieve cladding internal pressure to utilize the full breeding potential of the fuel. The vented fuel system design for the EM^2 differs from those discussed previously by placing the first fission product trap outside of the core. Additionally, the EM^2 design separates the functions of maintaining the coolant chemistry and the removal of fission products from the coolant into two subsystems, the HPS and FPVS, respectively. Thus, in the EM^2 the HPS operation is independent of the FPVS.

2.4.5. Other gas-cooled reactors

The Advanced Gas Reactor (AGR) is a British graphite moderated, CO_2 cooled reactor developed from the Magnox reactor. Hartlepool, Dungeness B, Torness, Hinkley Point B, and Heysham AGR power stations are currently operating in the UK utilizing vented fuel [13]. Additionally, vented fuel has been considered for application to a Supercritical CO_2-Direct Cycle GFR using a variant of MIT's Tube-In-Duct (TID), or inverted fuel, design [14]. The TID design was driven by the need to reduce stress on the metal cladding and to employ a high volume fraction fuel to achieve a sustainable unity conversion ratio in a blanket-free core [15]. The TID design consists of an array of inverted unit cells with fuel outside of the coolant tubes. The design incorporates a long vent path from the small top plenum between coolant tubes, down the entire length of the assembly into a larger lower plenum/debris trap at the colder coolant inlet. Two venting options were considered, which include venting into the core grid plate to a collection/purification system (similar to the GA approach) or venting directly to the CO_2 reactor coolant. The later was ultimately identified as the optimal approach and was implemented in the final design.

2.4.6. Sodium Fast Reactors

In addition to gas-cooled reactor designs, a few projects pursuing Sodium Fast Reactors (SFR) designs have also considered the use of vented fuel, however its initial purpose differed from early gas-cooled reactors. When applied in the first SFR designs, the purpose of vented fuel was more similar to that of the EM^2, i.e. to extend the lifetime of the fuel and enable more economic operation.

In the early-to-mid 1960's, General Electric was one of the first companies to discuss the use of vented fuel in sodium fast reactors [16]. Specifically, their work looked at venting methods for the Fast Ceramic Reactor (FCR) development program. The most notable contribution of their work was the development of the "diving- bell" venting concept (Figure 2.5) through which a pressure equalized plenum prevented liquid sodium from entering the fuel pin, yet allowed gaseous fission products to leak out [17]. Other vented-to-coolant concepts were considered, but the diving bell design was the only concept to undergo significant economic analysis by General Electric.

At the same time, work done by Euratom pursued a different route for venting fission product gases to the primary coolant [18]. In their concept, gases were vented through a porous and sintered metal plug. Preliminary tests were done; however, issues arose with in-leakage of sodium into the fuel pin. Economic analysis showed a 2% cost savings through the use of vented fuel and safety analysis showed that the largest benefit gained in using vented fuel was

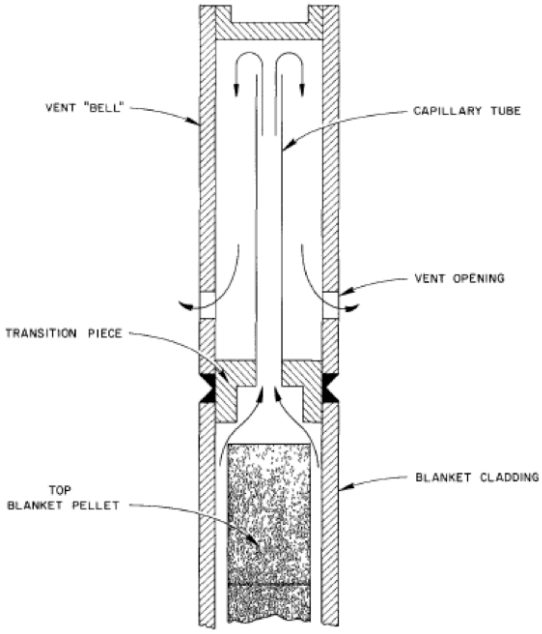

Figure 2.5.: Diving Bell vent concept [17].

the prevention of sudden blasts of fission product gases, an issue for SFRs due to their positive coolant void coefficient.

While pursuing a sodium-cooled reactor in the late 1960's, Westinghouse evaluated the economics and feasibility of using vented fuel in their designs as well. Economic analysis showed no significant difference between a vented and non-vented design, despite a 53 inch height difference due to the inclusion of a large fission gas plenum in the fuel pin [19]. It was also suggested that due to the control of fission product gas release from the fuel assemblies, a higher level of safety could be possible. In the case that a cladding leak occurred within a closed fuel pin, a situation more likely to occur in a non-vented fuel pin, fission products and possibly even fuel material could be released into the primary coolant. With a vented fuel pin design, the number of fuel element failures, and thus the overall circulating reactivity could possibly be reduced [17].

More recently, the TerraPower Travelling Wave Reactor (TWR) design, a pool-type, sodium-cooled fast reactor, requires a vented fuel system to accommodate the projected operations of 40 years without refueling [20]. The proposed venting methodology is to vent fission product gases to the primary sodium coolant in a controlled manner. Although no detailed system design is openly available, it was stated that the noble gases are collected in shielded carbon beds and Cs-137 is removed from the primary coolant via reticulated carbon traps.

Though not much more discussion will be given to vented fuel designs for SFRs, it is important to understand that the economic pressures placed on both liquid metal and gas cooled fast reactors forced each design toward higher burn-up and higher specific powers [19]. In a 1969 report by Oak Ridge National Laboratory, the use of vented fuel elements was mentioned as being in need of further evaluation, but could become standard practice for SFR designs [17]. Though

the specific venting methods (vented-to-coolant vs. vented-to-stream) are not comparable, the conclusions reached about the application of vented fuel should be considered as significant in future discussions.

2.5. Previous Helium Purification System Designs

Like all fission-based reactors, control of fission products in helium-cooled reactors is of upmost importance. While the basic strategies employed to achieve this goal vary between helium-cooled reactor types, the methods of fission product removal from helium remain essentially the same through utilization of a Helium Purification System. In the following subsections, a general comparison between previous HPS designs will be presented, followed by a more in-depth discussion of HPSs used in vented fuel designs.

The five HPS systems discussed below are compared in a document published by Idaho National Laboratories called the Coolant Chemistry Study [21]. These systems were from the Peach Bottom Unit 1, Fort St. Vrain, HTTR, HTR-10, and MHTGR power plants. Of these, the MHTGR was the only concept not to be constructed. The study determined there to be five different components traditionally used to remove impurities in an HTGR. These were a filter/absorber, an oxidizer, a molecular sieve, a charcoal bed, and hydrogen gettering material. A table was provided in the report, enabling the HPS system components to be directly compared. This table is reproduced in Table 2.1.

2.5.1. Peach Bottom Unit 1

In the HPS (also called Fission Product Trapping System) for Peach Bottom Unit 1, the purge stream flows through a series of contaminant trapping components. These components included a condensables trap, water-cooled delay beds, refrigerated delay beds, and a liquid-nitrogen-cooled trap. A process flow sheet for the external fission product removal system is shown in Figure 2.6.

Although the traps were expected to last the entire lifetime of the plant, they were designed to be removed in the case that a malfunction occurred. In this situation, the reactor would be shut down and the trap could be purged with clean helium and vented to a low pressure tank. Chemical impurities that were present in the primary coolant such as nitrogen, argon, hydrogen, carbon monoxide, and water vapor, were removed through a separate purification system.

2.5.2. Gas-Cooled Fast Reactor

The HPS designed for the GCFR was very similar to that used in Peach Bottom, with major differences attributed to the addition of completely separate backup trains, rather than just components. Two helium purification trains were used to maintain control over fission product release from the GCFR, each with their own backup, as is shown in Figure 2.7. Unit 1 processed helium from the reactor coolant stream and Unit 2 processed helium from the pressure equalization system. The arrangement of Unit 2 matched the design of Peach Bottom's Fission Product Trapping System very closely, which Unit 1 served a purpose similar to Peach Bottom's Chemical Cleanup System.

Table 2.1.: HPS operating parameters [21].

Reactor Name	Component or Subsystem	Operation Performed	Reaction Type	Temperature of Operation	Bypass Flow Rate	% of Bypass Flow in HPS	Location in the Plant
HTTR	Particle Filter	Mechanically Remove Debris	Filter & Plateout	< 280°C	200 kg/h	10%/h	Primary Circuit
	Pre-Charcoal Trap	Gaseous Fission Products	Adsorption	280°C	200 kg/h	10%/h	Primary Circuit
	Copper-Oxide Catalyst Beds	H and CO are converted to H_2O and CO_2	Oxidation	280°C	200 kg/h	10%/h	Primary Circuit
	Molecular Sieve Trap	Captures H_2O and CO_2	Adsorption	< 280°C	200 kg/h	10%/h	Primary Circuit
	Cold Charcoal Trap	Noble Gases, methane, nitrogen, and hydrogen	Adsorption	-195°C	50 kg/h	~2.5%/h	Primary Circuit
	Particle Filter	Mechanically Remove Debris	Filter & Plateout	< 280°C	200 kg/h	—	Secondary Circuit
	Copper-Oxide Catalyst Beds	H and CO are converted to H_2O and CO_2	Oxidation	—	200 kg/h	—	Secondary Circuit
HTR - 10	Cartridge Filter	Particles larger than 5 microns	Filter & Plateout	250°C	—	—	—
	Copper-Oxide Catalyst Beds	H and CO are converted to H_2O and CO_2	Oxidation	250°C	10.5 kg/h	5%/h	Primary Circuit
	Molecular Sieve Adsorber	Captures H_2O and CO_2	Adsorption	~ room temperature	10.5 kg/h	5%/h	Primary Circuit
	Low-Temperature Adsorber	methane, oxygen, nitrogen, noble gases	Adsorption	-160°C	10.5 kg/h	5%/h	Primary Circuit
Peach Bottom Unit 1	Water-Cooled Active Charcoal Traps (independent)	Noble gases, methane, nitrogen, and hydrogen	Adsorption	—	340 kg/h	80%/h	Primary Circuit — Fission Product Trapping System, Taken from Core
	Freon-cooled delay beds	Fission gases, hydrogen, nitrogen, carbon monoxide, methane	Adsorption	-80°C	340 kg/h	80%/h	Primary Circuit — Fission Product Trapping System, Taken from Core
	Liquid-nitrogen-cooled carbon bed	Removes all gas impurities especially argon, nitrogen, methane, krypton-85, and doesn't remove hydrogen and neon	Adsorption	—	22-45 kg/h	10.6%/h	Primary Circuit — Fission Product Trapping System, Taken from Core
	Copper-oxide bed	H and CO are converted to H_2O and CO_2	Oxidation	—	79 kg/h	20%/h	Primary Circuit — Chemical purification system, Taken from SG
	Molecular Sieve Trap	Captures H_2O and CO_2	Adsorption	—	79 kg/h	20%/h	Primary Circuit — Chemical purification system, Taken from SG
Fort St. Vrain	High-Temperature filter, potassium impregnated charcoal adsorber	Fission Products, Noble Gases	Filter & Plateout	400°C	1.85E5 kg/h	12%/h	Primary Circuit
	Cooler/ Water Separator	H_2O	—	48°C	1.85E5 kg/h	12%/h	Primary Circuit
	Dryer/ Molecular Sieve	H_2O and CO_2	Adsorption	48°C	1.85E5 kg/h	12%/h	Primary Circuit
	Cooled Nitrogen Trap	Noble gases, carbon monoxide, nitrogen, methane, hydrogen	Adsorption	Entered at -295°C and cooled to -310°C	1.85E5 kg/h	12%/h	Primary Circuit
	Particle Filter	Mechanically remove debris	Filter & Plateout	40°C	1.85E5 kg/h	12%/h	Primary Circuit
	Hydrogen Sponge	—	—	315°C	1.85E5 kg/h	12%/h	Primary Circuit
	Filter	Mechanically remove debris	Filter	78°C	1.85E5 kg/h	12%/h	Primary Circuit
MHTGR	High-temperature adsorber	Removes iodine, bromine, and other metallic fission products	Filter & Plateout	107°C	386 kg/h	~0.07%/h	Primary Circuit
	CuO, oxidizer	H and CO are converted to H_2O and CO_2	Oxidation	—	386 kg/h	~0.07%/h	Primary Circuit
	Water Cooler	—	Adsorption	38°C	386 kg/h	~0.07%/h	Primary Circuit
	Low-temperature adsorber	Fission Products, Noble Gases	Adsorption	-196°C	386 kg/h	~0.07%/h	Primary Circuit

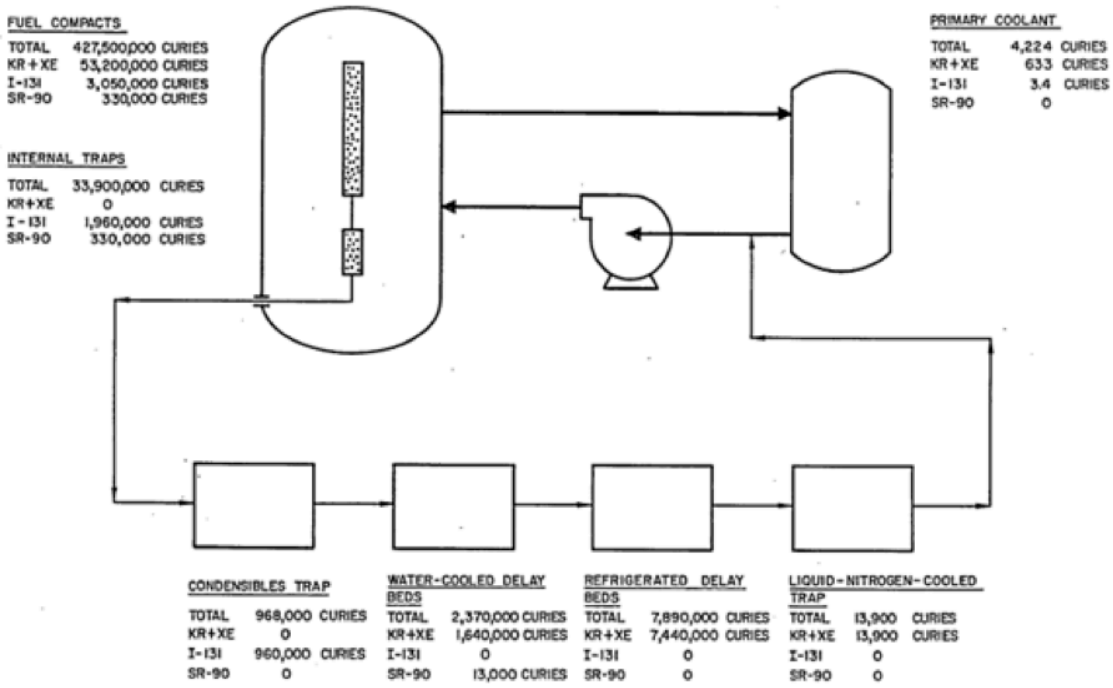

Figure 2.6.: Process flow sheet for Peach Bottom external fission product removal system [22].

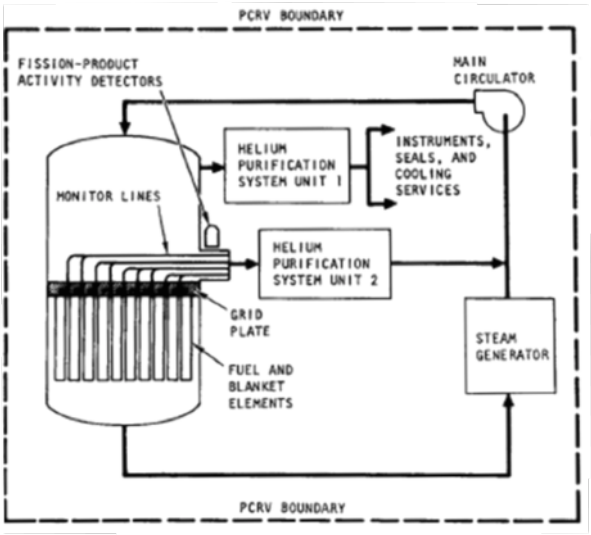

Figure 2.7.: GCFR helium purification system layout [8].

2.5.3. EM^2

As the EM^2 design is still in development, the purification and trapping system is continually undergoing revision; However the base design is well enough defined and understood and thus can be discussed here. The EM^2 HPS base design is a relatively simple arrangement, in comparison to the Peach Bottom Unit 1 and GCFR designs. Unlike the previously discussed designs, the EM^2 HPS does not include in-element fission product traps or noble gas delay beds prior to final adsorption in the low temperature adsorber. The EM^2 HPS base design is derived from the MHTGR HPS design, likely attributing to the observed differences [23].

As a result of the association of the EM^2 design to the present work, the HPS as described previously has undergone a series of modifications and evolutions. Although the system continues to be revised and refined, the following description of the EM^2 purification and trapping system reflects the most current state of the system that is analyzed in the present work. The current EM^2 purification and trapping systems complement both the Peach Bottom and GCFR HPS designs (Section 2.5) in the sense that the process of maintaining coolant chemistry and the process of trapping fission products are separated. In fact, the EM^2 design completely separates the two processes into two independent systems, the HPS and the FPVS.

The HPS, as the title suggests, serves the primary function of controlling the coolant chemistry whereas the FPVS serves the function of venting and trapping fission products from the EM^2. As the present work is focused on the venting of fission products, no further discussion of the EM^2 HPS design is included. The FPVS is further subdivided into a fission product transport system (FPTS) and the fission product retention system (FPRS). The portion of the system which collects the fission products from the fuel elements and transports the purge stream to the FPTS is generally referred to as the fuel system.

The FPTS receives helium and volatile fission products from the fuel system and transfers the purge stream to the FPRS. Additionally, the FPTS provides pressure regulation to maintain the proper pressure differential between the fuel bundle and the primary system. There are three redundant 100% trains of the FPTS which lead out to the FPRS. The FPRS serves to remove the fission products from the purge stream by means of filtration and adsorption at both high and low temperatures. The FPRS features three redundant 100% High Temperature Adsorber modules (HTAs), four redundant 50% Low Temperature Adsorber modules (LTAs), and two redundant compressor modules, as indicated in Figure 2.8.

2.6. Previous Vented Fuel Subsystems Safety Analyses

2.6.1. Peach Bottom Unit 1

Although fairly extensive safety analyses were performed for the Peach Bottom Unit 1 reactor, no modern probabilistic safety analyses were conducted, as the implementation of PRA in the nuclear industry was not yet established prior to the construction and operation of the reactor. Nonetheless, various safety analysis considerations for the fission product trapping system of the Peach Bottom plant were taken into consideration in the Final Hazards Summary Report (FHSR) [7]. The FHSR noted the rupture of the doubly contained fission product purge line as the most severe accident involving two independent failures in the reactor system. The potential

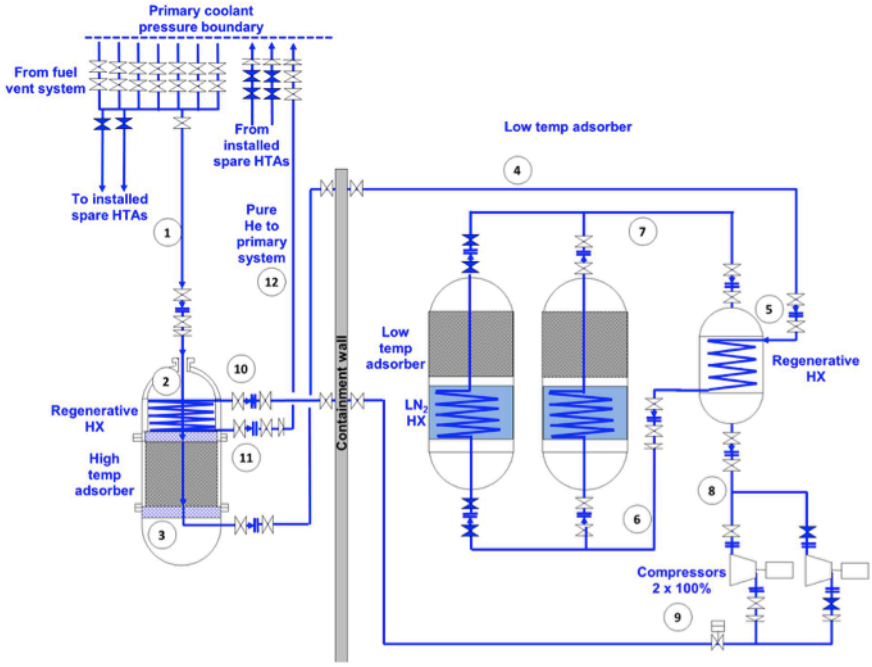

Figure 2.8.: EM^2 fission product vent system [24].

doses from this accident during an inversion for the first two hours at the site boundary were calculated to be 0.003 rem for whole body gamma and 0.9 rem to the thyroid. Moreover, the most severe accident involving a single failure in the reactor system was determined to be a large break in the primary loop which causes backflow of the purge gas inside the fuel elements to the coolant loops and through the rupture into containment. The potential doses from this accident during an inversion for the first two hours at the site boundary were calculated to be 0.001 rem whole body gamma and 0.02 rem to the thyroid.

The designed safety features for the external fission product trapping system included fuel backflow protection systems to prevent leakage of fission products during a large break and emergency cooling systems. The accidents considered in the FHSR were separated into three distinct categories: (1) loss of full cooling capability, (2) loss of fission product trapping system integrity, and (3) change in feed. The comprehensive list of accidents considered in the FHSR includes:

1. Loss of Full Cooling Capability
   a) Loss of Purge Flow
   b) Loss of Purified Helium Compressors
   c) Primary System Depressurization
   d) Loss of Refrigeration (in FPTS)
2. Loss of Fission Product Trapping System Integrity
3. Change in Feed

a) Increase in Fission Product Concentration

b) Increase in H2O Concentration (in purge flow inlet)

c) Increase in Chemical Impurity Concentration (in purge flow inlet)

In order to bound all accidents involving the FPTS, irrespective of credibility, the calculations assumed a total release of the entire fission product inventory of the trapping system into the secondary containment. The FHSR report indicated the resulting integrated doses for a person at the site boundary during the first two hours following the accident during an atmospheric inversion with a containment leakage of 0.2% per day would be less than 25 rem to the thyroid and 0.1 rem whole-body gamma radiation.

Moreover, the Peach Bottom Preliminary Hazards Summary Report (PHSR) provides a detailed description of the FPTS, insight into the design considerations of the system, and expected radiation levels within each portion of the system[18]. The portions of the system with listed specific radioactivity values for I-131, Sr-90, and Kr + Xe are the fuel compacts, internal traps, condensable trap, water-cooled delay beds, refrigerated delay beds, liquid-nitrogen-cooled trap, and the primary coolant. In addition, the heat loads within the purification system and the fission product concentrations in the purge stream are given in table form. Furthermore, the PHSR contains a description of the expected gaseous effluents released from Peach Bottom Unit 1 reactor during normal operating conditions. The potential sources of gaseous effluents listed in the report are leakage from the primary coolant system to the containment stack, leakage from the helium purification system to the containment stack, neutron activation of the containment atmosphere, and the purging and flushing gases from maintenance and refueling operations. The estimated concentrations for gaseous effluents at the site boundary are listed in the report and were shown to be well below the maximum permissible concentration allowed by 10 CFR 20, the governing document for public dose limits.

2.6.2. Other gas-cooled reactors

Minor safety analysis studies were performed on the GCFR helium purification system. Testing and analysis of the GCFR design showed that the occurrence of minor leaks present through suction holes, cracks in fuel pin cladding, and vent tube connection points would result in a minimal release of volatiles into the GCFR primary coolant system [8]. The MHTGR design did not include a vented fuel system; however a HPS is incorporated to necessarily purify the helium coolant. The safety considerations of the HPS discussed in the report are strictly related to the failure mode of HPS pumpdown, used to depressurize the reactor in the event of a small primary coolant leak [25]. HPS pumpdown was automatically initiated when a leak was detected by a drop in primary coolant pressure and increased radiation levels in the reactor building. A fault tree with the top event failure of HPS pumpdown was included in the analysis, however the reliability and failure modes of components of relevance to the current work were not discussed in detail. Limited analysis has been completed on the EM^2 vented fuel concept. Preliminary calculations on mass flow, fission product release and fission product diffusion, transport, and plate-out were completed [13] [24].

3. Fuel Modeling

3.1. Introduction

3.2. Fission Gas Behavior

As described in Section 2.2, fission gases (FG) are insoluble and tend to thermally diffuse through the fuel. As a single FG atom moves through the fuel, it will combine with other FG atoms to form energetically favorable bubbles within the fuel grain. The behavior of these single atoms and bubbles within the fuel grain comprise the inter-granular domain. As fission gas atoms reach the grain edge, they will combine to create large, lenticular bubbles in the spacing between the grains. As these bubbles grow larger, they will eventually interconnect with each other until a pathway is established with an exterior surface fuel pellet and the fission gas is vented into the fuel pellet plenum. The grain boundary bubbles and their interconnectivity comprise the intra-granular domain. Cartoons of these two models are displayed in Figure 3.1.

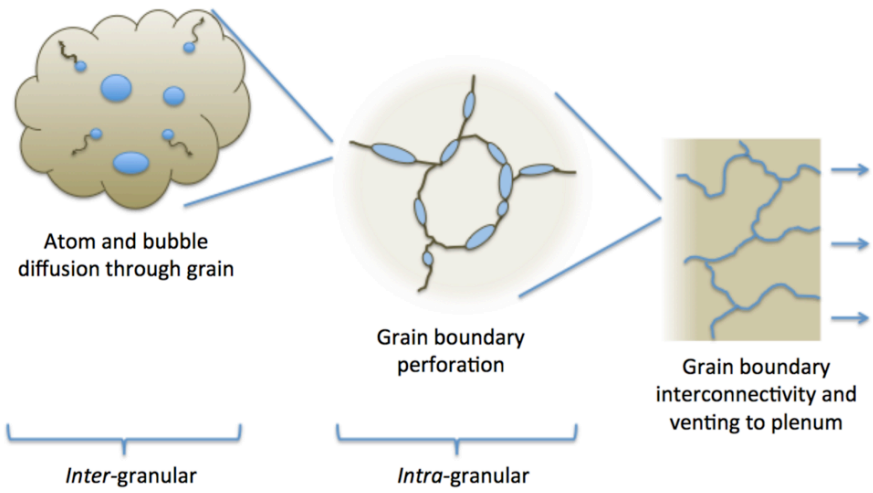

Figure 3.1.: Schematic of fission gas behavior in nuclear fuel.

Fission gas (FG) is continually created during the fission process, and is primarily comprised of xenon and krypton with smaller amounts of other volatiles such as cesium and iodine. The fission gas can either be created directly from the fission process, or result from transmutation of parent precursors to gaseous elements through beta-decay.

Since each fission fragment (FF) travels about 6 μm in the fuel material, if the fission event occurs near an exterior fuel surface, the FF can recoil directly into the plenum. While this

"athermal release" results in a geometrically-dependent release pathway, the vast majority of the fission fragments come to rest within the fuel's granular structure and can be described using the inter- and intra-granular models.

The crystal structure of uranium-carbide fuel is a NaCl type arrangement as a cubic lattice with alternating uranium and carbon atoms. Gas atom defects tend to be large, thus they exist in the combined defect of a uranium and carbon vacancy. As the fission gas diffuses through the fuel, the atoms can combine to form more energetically favorable bubbles. These bubbles will have reduced movement, and are typically assumed to be stationary within the lattice [26], effectively acting as traps for the fission gas. During irradiation fission fragments can strike the bubbles and knock fission gas back into the lattice, thus equilibrium bubble size depends on the competing processes of fission gas absorption through thermal diffusion and loss through fission re-solution.

If an inter-granular bubble is in equilibrium with the surrounding material, the pressure p within the bubble is related to the radius of the bubble r as,

$$p = \frac{2\gamma}{r} + \theta \tag{3.1}$$

where γ is the surface tension of the solid and θ is the hydrostatic stress in the solid. Although noble gases can be treated as ideal gases in most cases, for bubbles below $\sim$10 nm the van der Waals Equation of State (EOS) is more applicable [27]:

$$p\left(\frac{1}{\rho_g} - B\right) = kT \tag{3.2}$$

where ρ_g is the atomic density of the gas at temperature T and k is Boltzman's constant. B is a constant related to the volume occupied by the atoms, typically defined as 8.5×10^{-29} m^3/atom [27]. Combination of Equations 3.1 and 3.2 gives,

$$\frac{1}{\rho_g} = B + \left[\left(\frac{2\gamma}{kT}\right)\frac{1}{r} + \frac{\sigma}{kT}\right]^{-1} \tag{3.3}$$

Figure 3.2 plots the density as a function of bubble radius. In a stress free solid, the atomic density for bubbles with radius < 1 nm goes to a constant related to the inverse of B. For large radii > 100 nm, the gas density in the bubble reduces to the ideal gas law:

$$\rho_g = \left(\frac{2\gamma}{kT}\right)\frac{1}{r} \tag{3.4}$$

The atomic density is not very sensitive to temperature or surface temperature. However in the presence of compressive hydrostatic stress the bubble is able to maintain a higher atom density for larger bubble radii (Figure 3.2).

In stress free solids, the number of atoms in a bubble m is generally calculated using the Van der Waals equation of state. However, the high temperature and stress involved with very small bubbles in nuclear fuel results in an underestimation of atomic density, thus the EOS values calculated by Ronchi were utilized at small bubble radii [28]. Although more recent evaluations

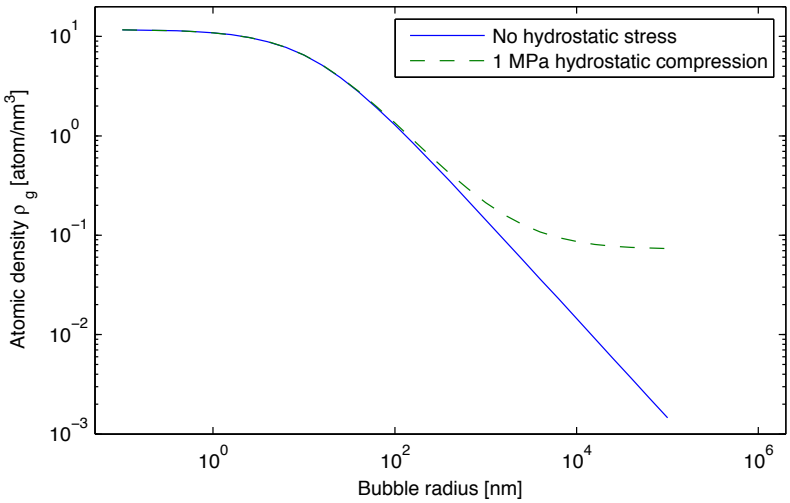

Figure 3.2.: Atom density in bubbles as a function of radius for a stress free solid and a solid with 1 MPa compressive stress.

show that the atomic density may actually be higher in very small bubbles [29], a smooth transition from Ronchi's data for small bubble sizes to values calculated using Equation 3.2 is utilized to calculate the atom density in the bubble due to the large spread of bubble radii, giving the "Combined" model types, as displayed in Figure 3.3.

The number of gas atoms m within a bubble is calculated from ρ_g by,

$$m = \left(\frac{4\pi r^3}{3}\right)\rho_g \tag{3.5}$$

At the lower bubble limit, the number of atoms in a bubble goes by r^3, as expected with a constant density. At the higher bubble limits, the number of atoms goes by r^2,

$$m = \left(\frac{8\gamma\pi}{3kT}\right)r^2 \tag{3.6}$$

Since the volume of the bubble goes by r^3, the combination of two identical bubbles with m number of gas atoms into a single bubble with $2m$ gas atoms, results in a local swelling increase of 40%. This means as bubbles get larger and combine, the swelling will increase drastically.

3.2.1. Bubble types

In general, four types of bubble concentrations are defined in UC fuels (Table 3.1). Although bubble concentrations exist in all irradiated nuclear fuel, carbide based fuels have much larger bubbles as opposed to oxide fuels. This is due to the much lower re-solution rate in carbide fuels due to the superior thermal properties (i.e. thermal conductivity and thermal diffusivity). The behavior of the re-solution rate is expanded on in Section 3.6.

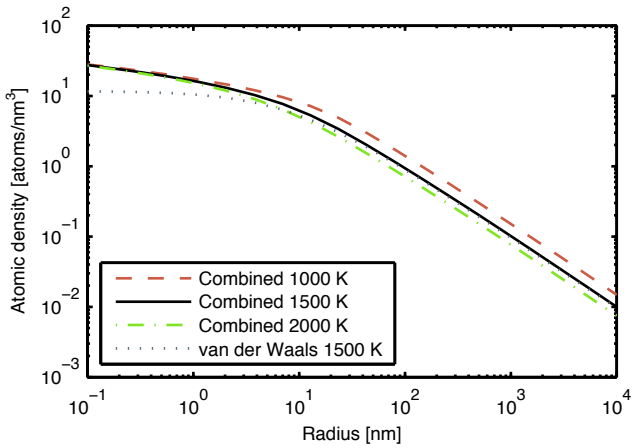

Figure 3.3.: Atomic densities calculated from different EOS models.

Table 3.1.: Bubble Types

Type	Size [nm]	Concentration [m^3]	Behavior
P_1	1-30	10^{21}	Nearly constant after some initial incubation time
P_2	30-400	10^{18} - 10^{20}	Dependent on temperature
P_3	50-1000	-	Increases until interconnection
P_0	10^3	-	Dependent on initial structure, decreases due to sintering
UO_2	1	10^{23}	

The P_1 bubbles are similar to the bubbles found in UO_2 fuel. It is unclear as to whether the P_2 bubble population is formed from its own unique population or through growth of P_1 bubbles. Although P_2 bubbles have a lower concentration, their size is highly temperature dependent and can cause problems with swelling, as will be discussed later. Both the P_1 and P_2 bubbles are included in the inter-granular model discussed above. The P_3 bubbles consist of grain-face bubbles that grow as a result of single fission gas atoms reaching the grain boundary. Once a P_3 bubble reaches an exterior fuel surface it releases, or "vents" its gas content to the plenum and is assumed to maintain its shape for the remainder of the irradiation time. Any additional gas that reaches a "vented" P_3 bubble is typically assumed to be instantaneously vented to the plenum. To model release, a saturation point is typically calculated for the each fuel grain. Venting saturation coverage is typically set to 50% of the total grain boundary area [30], but some authors claim higher coverage fractions [31].

Any future fission gas that reaches the grain boundary is typically assumed to be immediately vented to the plenum.

P_0 are voids or flaws introduced into the bulk during fabrication. As the P_2 and P_3 bubbles grow, they will eventually connect with each other and P_0 bubbles.

Due to their extremely small size, few studies have been completed on the P_1 concentration. Ray and Blank performed transmission electron microscopy (TEM) to measure bubble sizes and

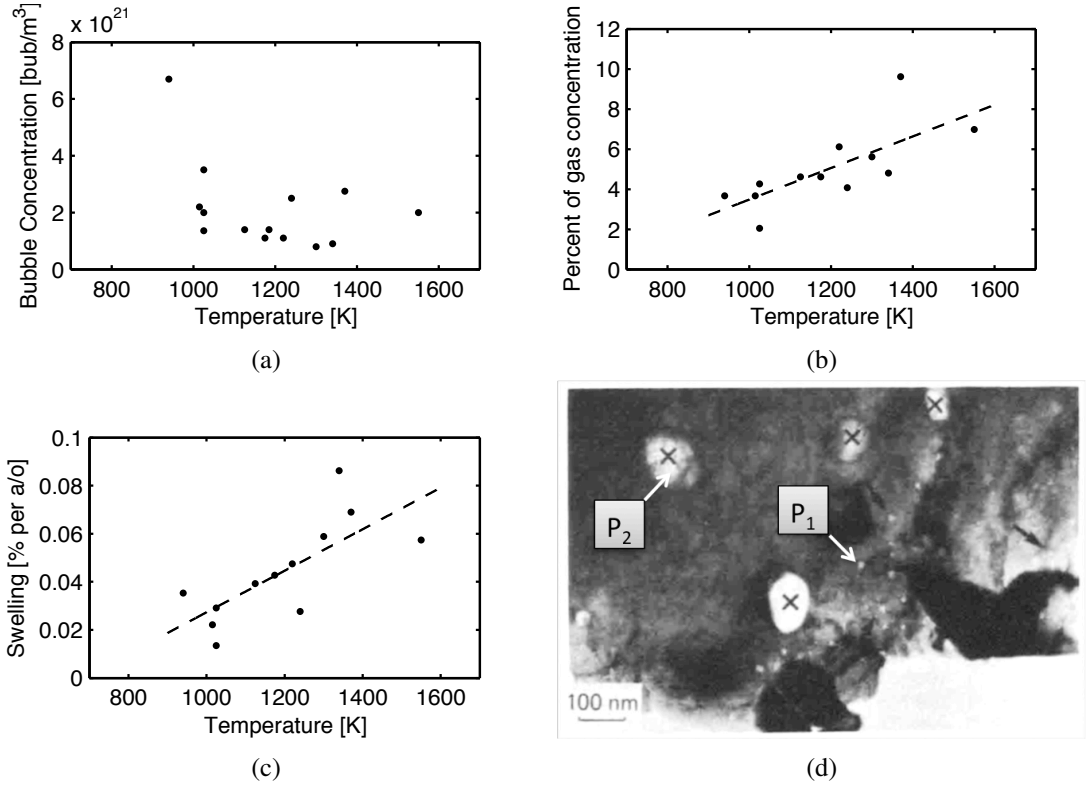

Figure 3.4.: P_1 bubble behavior: (a) concentration as a function of temperature, (b) percentage of the total gas concentration, (c) percentage of swelling per atom percent burn up, and (d) micrograph of P_1 bubbles.

form histogram data for both sodium and helium bonded UC fuel pins [32]. Their results showed that the bubble concentrations are relatively independent of temperature (Figure 3.4). While the P_1 swelling contribution and gas content is slightly dependent on temperature, both remain so low that the P_1 population is often ignored in simulations.

The small size of P_1 bubbles ensures that interactions remain only between single bubbles and diffusing gas atoms in the bulk, however as P_2 bubbles grow larger, they can combine. As discussed in Section 3.2, the combination of two equal sized bubbles results in a 40% volume increase, thus a considerable amount of swelling can occur once bubbles are large enough to interact with one another. This behavior has been observed in UC fuels, and in fact causes a sharp decrease in bubble concentration as well as breakaway swelling at a characteristic temperature, T_2 (Figure 3.5).

The swelling trend due to P_2 bubbles can be divided into low and high temperature domains: at low temperatures < 1100K, the swelling is nearly linear, while at higher temperatures the swelling follows a bell-shape curve. The low temperature behavior can be attributed to bubble size increase from single atom absorption. As temperature increases crosses the threshold T_2, a sharp increase in swelling occurs. Blank believes this sudden behavior is specifically due to a dumbbell coalesce of bubbles that occurs near the given temperature [26] and was captured in a

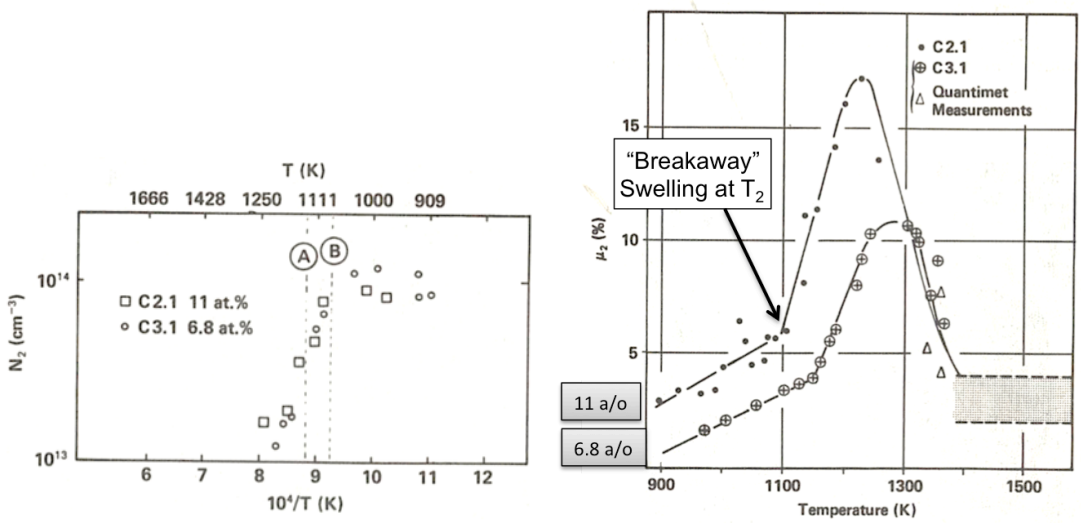

(a) (b)

Figure 3.5.: (a) Concentrations and (b) swelling caused by P_2 bubbles as a function of temperature. The breakaway swelling occurs at the point T_2 and peaks roughly at temperatures (T_2+200K). The decrease in the swelling is the result of the P_2 bubbles combining with the P_3 and P_0 bubble populations..

UC micrograph (Figure 3.6).

As the P_2 bubbles get larger and larger, they tend to combine with both the P_3 and P_0 bubbles, resulting in the decrease in swelling contribution at high temperatures in Figure 3.5, and forming a highly porous structure in the central regions of the pin. The different regions of P_2 bubble behavior results in a 4-zone structure that has been adopted in describing irradiated carbide fuels (Figure 2.2). The different regions are described in Table 3.2. Since most of the fission gas released originates from the interior zones of the fuel pin, the larger the fraction of pellet that remains as zone IV, the lower the fission gas release and swelling.

Figure 3.5b compares the difference in P_2 swelling from two irradiation tests, showing a slight dependence on burnup: as burnup increases, T_2 decreases. By comparing many different experiments, the so-called T_2 curve can be plotted as a function of burnup (Figure 3.7). The cause of this behavior is not explicitly understood. One cause may be that the earlier breakaway swelling is due to a higher concentration of fission gas at higher burnups. A second cause may be due to a change in fission gas diffusivity, and is discussed below.

3.2.2. Diffusivity dependence

The growth of bubbles is dependent on the ease of which fission gas atoms can diffuse through the fuel, or the diffusivity D:

$$D = D_0 \exp\left(\frac{-Q}{RT}\right) \tag{3.7}$$

Table 3.2.: Structural Zones in UC Fuel

Zone	Properties	Required Conditions
IV	*Zone of low swelling and base release:* As-build structure Slight densification Small P_1, P_2, P_0 bubbles	T <T Typically below 1100-1300K
III	*Transition from low to high:* Sudden change to high rate of swelling Grain Growth Increasing release up to 70% Increasing P_3 bubbles P_3 interlinkage in hotter regions	T $>T_2$ Width of zone 200K
II	*Pseudo columnar grain zone:* Not always present Fuel densification Possible columnar grain growth High gas release Low swelling	High T *and* high ΔT Typically only for >120 kW/m
I	*Porous structure:* Usually present Highly porous High gas release Low swelling Central hole possible Pore size equals grain size	High T Central part of pin

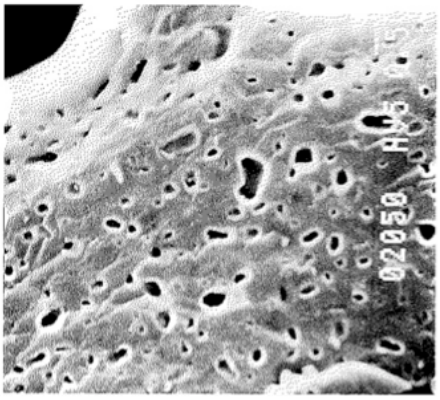

Figure 3.6.: SEM micrograph of dumbbell coalescence in uranium carbide fuel [26]

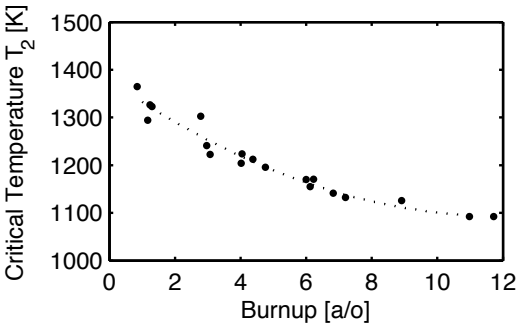

Figure 3.7.: Critical temperature vs. burn up for several irradiation tests [4, 33–35]

where D_0 is the intrinsic diffusivity, Q is the activation energy and R is the ideal gas constant. Because of the temperature dependence of D, larger bubbles are more prevalent at higher temperatures as single atoms move through the bulk easier and combine with bubbles more often.

The diffusivity can also be modifying the chemistry of the system. The GOCAR irradiation tests studied fuel with various ratios of nitrogen, oxygen, and carbon [34]. In general, the atomic mobility in nitride fuel is slower than carbide fuels [6], thus as the nitrogen/carbon ratio increases, the FG diffusivity lowers, resulting in smaller bubbles and an increase in the critical temperature, exactly what was measured in the GOCAR experiments; the higher the ratio of nitrogen in the fuel, the higher the critical temperature (Figure 3.8). Conversely, the increase of oxygen in the fuel increases diffusivity, resulting in a lower T_2. The GOCAR irradiation results repeated in Figure 3.8 compared UC fuel with a 3% oxygen impurity content to UCO fuel with 8% oxygen content. Although oxygen was present in only a small fraction, the critical temperature dropped by nearly 80 K at 2.2 a/o burnup (Figure 3.8. Extending this behavior to the concept of structural zones above, the higher the oxygen content or lower the nitrogen content, the smaller zone IV will be, thus more fission gas will be released.

The dependence on fission gas release on oxygen is also evident by examining fission gas release data from several irradiation tests (Figure 3.9). It was originally thought that fuel form,

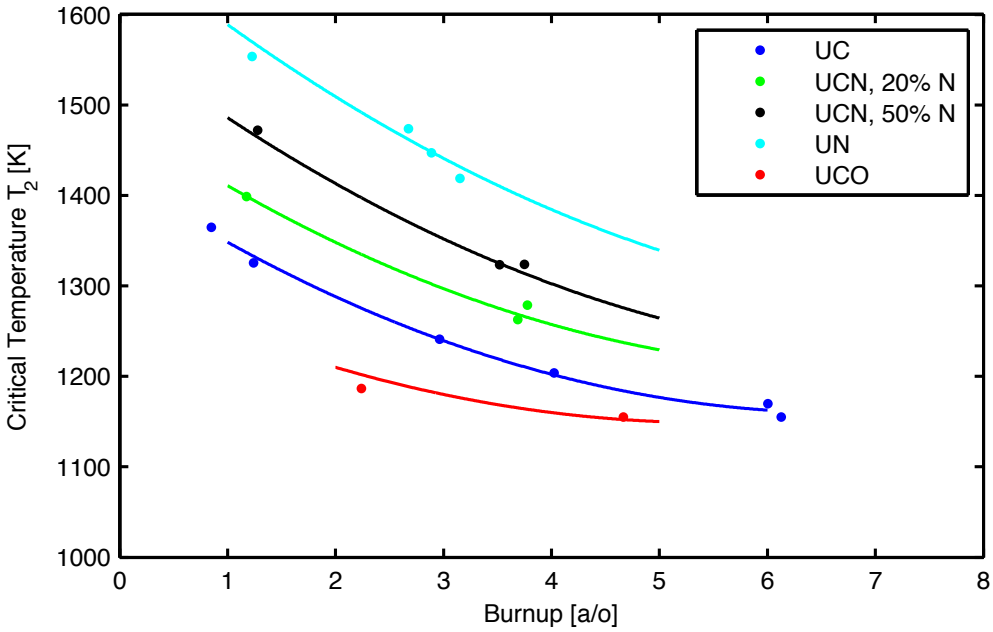

Figure 3.8.: Critical Temperatures of MX fuels [34].

both in diameter and type, played the primary role in curbing fission gas release through direct control of centerline temperatures [36]. However, fuel irradiated in the 1980s as part of the AC-3 test experienced extremely low fission gas release despite similar irradiation conditions as previous tests [37], with the primary difference being low oxygen impurities. Although temperature will always be the driving factor of fission gas release, the low oxygen concentration in the AC-3 tests raised the critical temperature threshold, avoiding the breakaway swelling and the bubble interconnectivity that often results in high fission gas release.

3.3. R/B curves

For many of the fission gas release calculations, a Release over Birth (R/B) curve can be used to compartmentalize all of the effects relating to fission gas release (Figure 3.10). This plot contains an estimated release rate over birth rate as a function of isotope half-life.

3.3.1. Peach Bottom

Figure 3.10 displays R/B curve used in the Peach Bottom Final Hazards Summary Report (Figure A-9 in [22]). The data for the curve was taken from linear accelerator experiments on uncoated (Th,U)C_2 fuel particles. The curve was then conservatively multiplied 3-fold for use in concentration estimations. This R/B curve was calculated at a non-specified temperature for sole application to the Peach Bottom reactor design. No burnup corrections, nor differences between

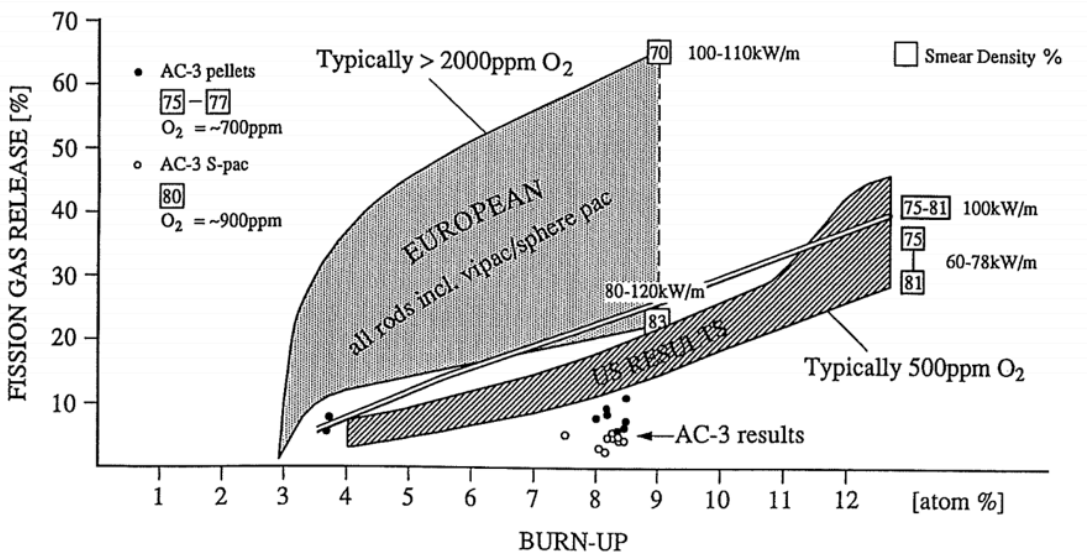

Figure 3.9.: Fission gas release from several UC irradiation tests [26].

gas species diffusivities is included. This figure was used in Wesley Deason's thesis work [2] with sufficient warning that a better calculation of fission gas release was necessary.

3.3.2. MHTGR model

A more complicated calculation of the R/B release curve for carbide fuel can be found in the 1993 MHTGR model database compiled by Martin [38]. Coefficients for R/B calculations were provided for $UCO_{1.6}$, $UCO_{1.1}$, ThO_2, UC_2, and UO_2 fuels. In general, the diffusive behavior of gas was reduced to xenon-like and krypton-like behavior. It is assumed that iodine and tellurium release is similar to xenon, and selenium and bromine release is similar to krypton.

The general model equation for unhydrolyzed fuel is given as:

$$(R/B) = \frac{(R/B)_0 \cdot f(T) + f_s(T)}{1 + f_s(T)}, \tag{3.8a}$$

$$(R/B)_0 = 3\left(\frac{\xi_{jk}}{\lambda_i}\right)^n, \tag{3.8b}$$

$$f(T) = c + (1-c)\exp(Q_{jk}/RT)\exp(-Q_{jk}/RT_0), \tag{3.8c}$$

$$f_s(T) = \exp(a[T - T_s]), \tag{3.8d}$$

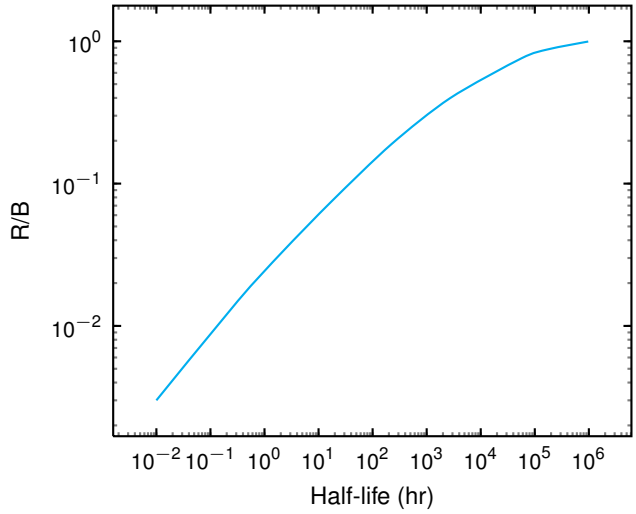

Figure 3.10.: Peach Bottom's R/B curve

(R/B)	=	calculated release rate over birth rate as a function of isotope i,
$(R/B)_0$	=	steady-state fractional release at reference temperature T_0,
$f(T)$	=	correction factor based on temperature,
$f_s(T)$	=	correction factor based on structural changes at high temperature,
T	=	temperature [K],
T_0	=	reference temperature (T_0=1373 K),
T_s	=	reference temperature for high temperature structural correction [K],
ξ_{jk}	=	reduced diffusion coefficient for element j (i.e. Xe or Kr) and fuel type k [1/s],
λ_i	=	decay constant of isotope i [1/s],
n	=	constant (a=0.5),
c_j	=	constant for element j (i.e. Xe or Kr),
Q_{jk}	=	activation energy for steady state fission gas release for element j and fuel type k [J/mol],
R	=	ideal gas constant (8.314 J/mol/K),
a_k	=	constant for fuel type k.

Table 3.3.: Parameters for Equation 3.8 [38]

Parameter	$UCO_{1.6}$		$UCO_{1.1}$		UC_2	
	Kr	Xe	Kr	Xe	Kr	Xe
ξ_{jk} [1/s]	$1.31\text{x}10^{-10}$	$1.35\text{x}10^{-11}$	$1.62\text{x}10^{-10}$	$1.67\text{x}10^{-11}$	$1.23\text{x}10^{-10}$	$1.26\text{x}10^{-11}$
c_j	0.073	0.21	0.073	0.21	0.073	0.21
Q_{jk} [J/mol]	$5.131\text{x}10^4$	$4.52\text{x}10^4$	$5.131\text{x}10^4$	$4.52\text{x}10^4$	$5.131\text{x}10^4$	$4.52\text{x}10^4$
a_k [1/K]	0.0128		0.0128		0.0133	
T_s [K]	1800		1800		1700	

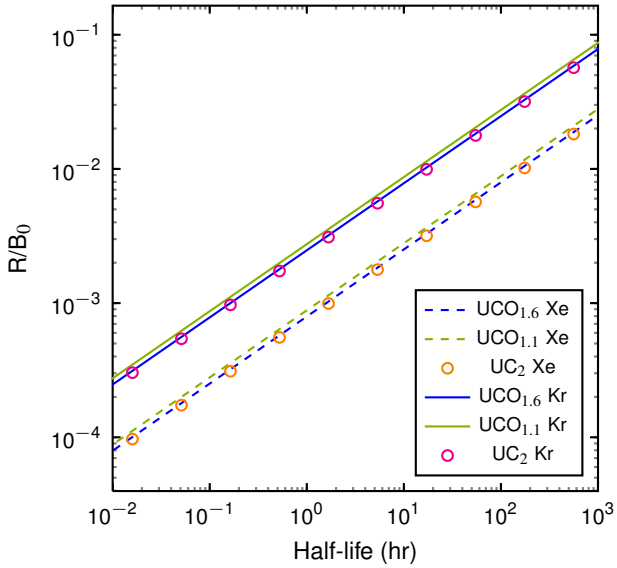

Figure 3.11.: $(R/B)_0$ plotted for several fuel types and for each diffusive element

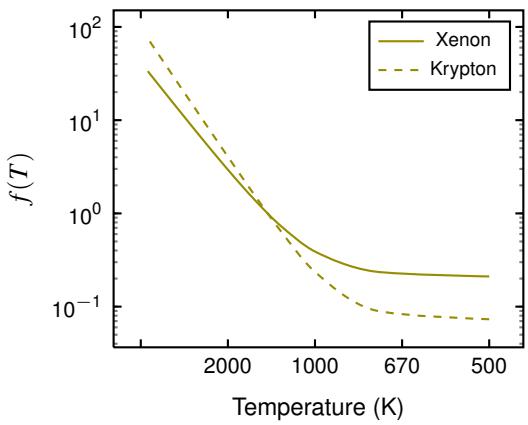

Figure 3.12.: Arrhenius plot of the temperature correction $f(T)$ for Xe and Kr. The same values apply for all fuel types.

The parameters used for Equation 3.8 are displayed in Table 3.3. According to the original documentation, $(R/B)_0$ is roughly related to the vacancy motion, $f(T)$ to the athermal release mechanism and overall temperature dependence, and $f_s(T)$ to the high temperature diffusion of gas atoms in grains and any possible bubble diffusion [38]. Missing from the above formulation is any burnup dependence; A correction function for oxide fuel types was included in [38], however since the focus of the current work is on carbide fuel types, any R/B calculations for the oxide fuels, and thus burnup dependence has been dropped from Equation 3.8.

The $(R/B)_0$ term depends purely on the decay constant of the isotope of interest, and varies for fuel type k and element behavior j. $(R/B)_0$ is plotted in Figure 3.11 for several fuel types and for Xe and Kr diffusive properties. The UC_2 and $UCO_{1.6}$ curves are nearly identical, while the

$UCO_{1.1}$ $(R/B)_0$ values are slightly higher. In general, the R/B values for Kr tend to be an order of magnitude higher than Xe.

The temperature correction function $f(T)$ is somewhat sensitive to temperature (Figure 3.12). The exponential behavior of the structure correction function $f_s(T)$ provides the greatest modification to the R/B values, especially for species with small half-lives. Figure 3.13 displays the corrected R/B calculated from Equation 3.8. Although the $f(T)$ correction is included, the $f_s(T)$ dominates the deviation from $(R/B)_0$. Due to differences between fuels in the $f_s(T)$ coefficients, the corrected R/B curve for UC_2 is higher than the corresponding UCO curves.

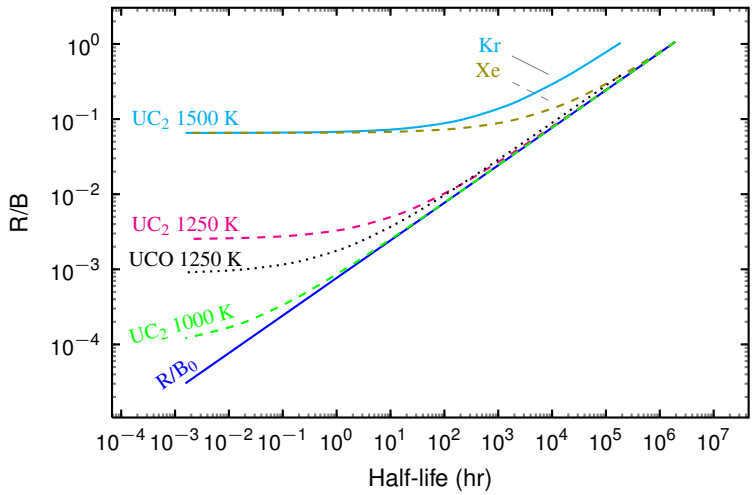

Figure 3.13.: MHTGR Xe R/B values compared to the uncorrected R/B_0 curve. Here, UCO corresponds to $UCO_{1.6}$. $UCO_{1.1}$ is omitted since it is rougly same as $UCO_{1.6}$. The UC_2 Kr R/B curve at 1500 K is included for comparison.

In order to correctly apply the MHTGR model, knowledge of the fuel temperature distribution is necessary to accurately estimate R/B since the exponential behavior of the $f_s(T)$ makes an ordinary volume averaged temperature inappropriate. Figure 3.14 displays some preliminary fuel temperatures for Beginning of Life (BOL) and End of Life (EOL) of a typical EM^2 fuel cycle. The peak/average fuel temperatures are 1700/990° C for BOL and 1400/1000° C for EOL.

The temperature distribution weighted MHTGR R/B curves for the estimated EM^2 BOL and EOL behavior is displayed in Figure 3.15. The parameters for UC_2 fuel were assumed for the EM^2 uranium mono-carbide fuel. Although a large number of fuel elements at BOL are relatively cold (<600° C), the R/B curve is actually higher due to the few high temperature fuel elements. The narrow EOL temperature distribution helps keep the fuel out of the high temperature region.

The R/B curves in Figure 3.15 can be represented as a two term power model. The R/B for diffusive behavior j (i.e. Kr or Xe) and isotope i can be estimated by:

$$R/B = a + \left(\frac{b}{\lambda_i}\right)^{1/2}, \tag{3.9}$$

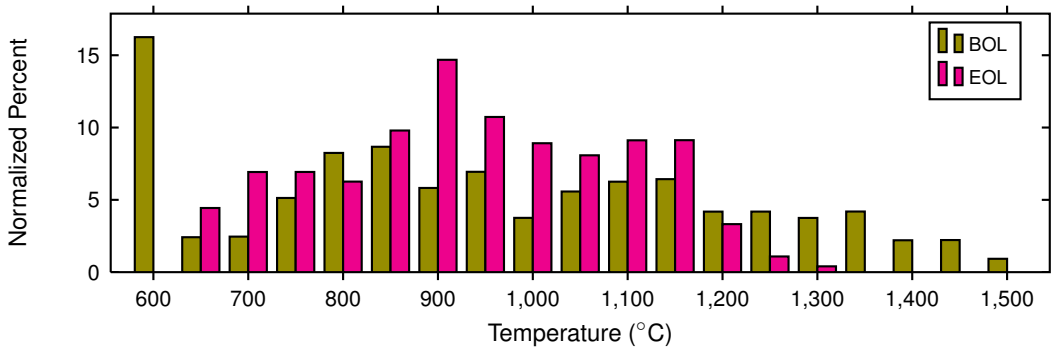

Figure 3.14.: Estimated fuel temperatures in EM^2 for Beginning of Life (BOL) and End of Life (EOL) [39]

.

where λ_i is the decay constant of the the isotope in [1/s], a is a constant that depends on the temperature distribution (a_{bol} = 0.0543 or a_{eol} = 0.0078), and b is a constant that depends on the diffusive behavior (b_{Xe} = 5.74e-11 [s] or b_{Kr} = 4.71e-10 [s]). In this way, the R/B can be simply calculated for each temperature distributions.

3.3.3. R/B model discussion

Initially, it was believed that the complexities present in the newer MHTGR model would result in lower fission gas release than the single Peach Bottom curve. While the narrow EOL temperature distribution does result in less release of gaseous fission products, the release actually increases for the BOL temperature distribution: a small percentage of hot fuel rods at BOL cause an increase in fission gas release, especially of isotopes with short half-lives. In general, the Peach Bottom curve lies between the BOL and EOL. The uncertainties involved affect both models equally (i.e. similar but different fuel types, thermal vs. fast reactor design, close packed vs. graphite dispersed particles), thus neither model is fully adequate. Regardless, the temperature dependence of the MHTGR allows for potentially more interesting calculations.

Even though there is a higher complexity level included in the MHTGR model, there are still many assumptions and uncertainties involved:

- the R/B curve was formulated from release rates of short-lived isotopes (half-life <5.3 days), although Martin claims that it is also applicable to long lived isotopes [38]. While this seems true, the curve would most likely asymptotically approach a release of 1.0, similar to the behavior of the Peach Bottom curve (Figure 3.10). Since the MHTGR R/B curve linearly approaches 1.0, it will tend to overestimate the release of long-lived isotopes.

- The MHTGR model only supplies R/B curves for Xe, Kr, I, Te, Br, and Se. Other species are assumed to follow a diffusion type models.

- The formulated R/B curves are for UC_2, not for the UC fuel present in the EM^2 core. There is some evidence that UC_2 has diffusion rates an order of magnitude slower than

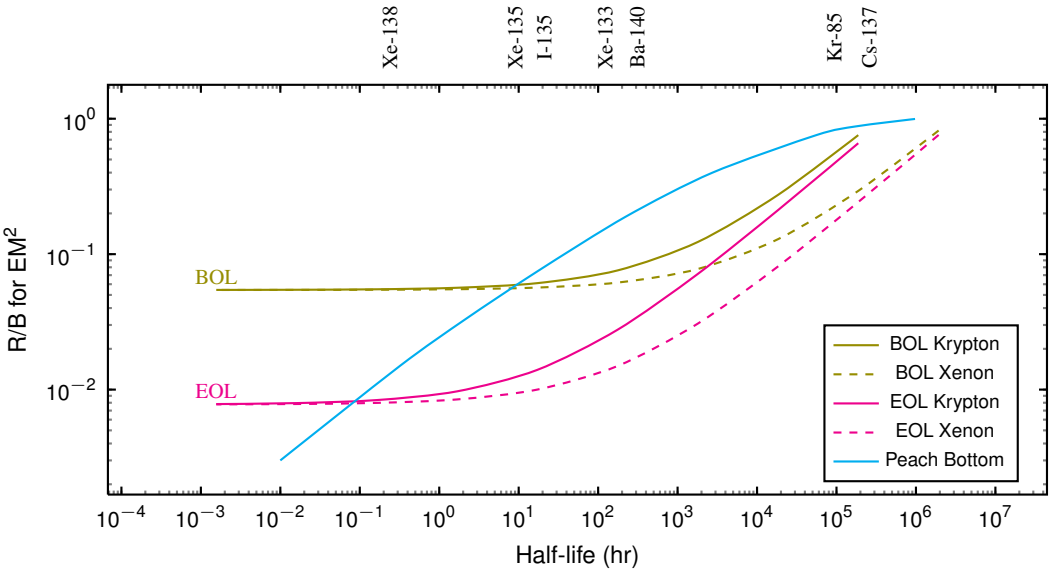

Figure 3.15.: R/B values for EM^2 estimated fuel temperatures [39].

UC [6, p. 493].

- The MHTGR model was based on release rates from failed coated particles (diameter = 200 μm) in thermal reactor designs. There is some evidence that the release mechanism is primarily from recoil events [40]. In MHTGR fuel designs, the fuel particles are embedded in a graphite matrix in which recoiling atoms can be trapped before entering a neighboring particle. The close-packed graphite-free kernels required for fast reactor fuel designs will result in a reduction of recoil release as knocked out atoms will have a high chance of reentering an adjoining fuel particle.

It should also be mentioned that Martin includes a model for diffusion of metallic fission products (i.e. Ag, Cs, Rb, Sr, Eu, Ce, Sm, and Ba) [38]. Models are included for oxide fuels, however due to the low oxygen potential in carbide fuels, complete release is conservatively assumed for carbide fuels. Metallic diffusion through UCO fuel is estimated by weighting the release based on the fraction of carbide and oxide present in the bi-phase material. An ambiguous sentence is included that mentions the MHTGR model can be used with a higher value of the constant n. Unfortunately, Martin fails to clarify the remaining constants, thus a release of 1 is assumed for stable metallic isotopes, and the MHTGR model with Xe parameters are assumed for Xe, I, and Te, and Kr parameters are assumed for all other radioactive isotopes (Section 4.5.2).

3.4. UC Material Property Database

The following attempts to collect material data primarily for uranium monocarbide fuels. However, data information will be included for $(U_w,Pu_x)_yC_z$ for various values of w, x, y, and z, when it is available. All combinations will now be labeled generically as MC fuels.

Table 3.4.: Relations between fuel behavior and fuel conditions. + indicates slight dependence, ++ indicates strong dependence, (+) indicates importance only at high temperatures, ? indicates incomplete understanding of behavior.

Condition	Density	Thermal Conductivity	Heat Capacity	Thermal Expansion	Fission Gas Diffusion	Fission Gas Venting
Temperature		+	+	+	++	++
Porosity	+	++			+	+
Burnup		?			+	+
Restructuring	+	+			?	+
M/C ratio	+	+	(+)	(+)	?	+
Pu/U ratio	+	+	(+)		?	?
Impurities		?			++	++

Table 3.4 displays some of the relationships between the fuel behavior vs. fuel conditions. The last two columns deal with the behavior of fission gas through the fuel, and indicate diffusion on a microscopic level, while venting indicates gross loss of fission gas to the exterior of the fuel.

The primary resources utilized for this Database are as follows:

• H. Matzke, Science of Advanced LMFBR Fuels. (1986) [6]: This extensive monograph touches on all topics of MC fuels up to the publishing date. Matzke himself contributes his own data to most topics. The book emphasizes the spread of sparse material data, and tries to give recommendations on the best practice, although it does not make explicit recommendations

• H. Blank, "Nonoxide ceramic nuclear fuels," in Materials science and technology: a comprehensive treatment Vol 10a, (1994) [26]: This summary is extensive in the material data up to the publishing date. It contains much of the same data as Matzke.

• T. Preusser, "Modeling of carbide fuel rods," Nuclear Technology, vol. 57, pp. 343-371, 1982 [41]: This article contains the relations used in the fuel performance code URANUS. A review of thermo-mechanical properties of UC and (U,Pu)C is used to backup the choices for the program. Also included is the physical model used for the fission gas release module in URANUS. Due to the complexity of the material data, much of the URANUS relations are simplistic.

• P. Petkevich, "Development and Application of an Advanced Fuel Model for the Safety Analysis of the Generation IV Gas-cooled Fast Reactor," (2008) [42]: This dissertation contains material properties compiled from several sources. The thermomechanical properties are taken from generic material property sources rather than MC specific sources, however hard to find swelling and creep relations are included.

In addition, choices used by General Atomics (GA) are noted, with references when available.

3.4.1. Density

The densities given by Matzke in Table 3.5 will be utilized. One interesting note is that $(U_0.8,Pu_0.2)C$ has a lower density than both UC and PuC.

Table 3.5.: Density for MC from several sources.

Compound	Density kg/m^3	
	From Matzke [6]	*Other values*
UC	13,630	13,630 [41, 42]
UC2	11,680	
U2C3	12,880	
PuC	13,600	
Pu2C3	12,700	
Pu3C2	15,300	
(U0.8,Pu0.2)C	13,580	13,600 [41]

3.4.2. Melting point

The melting points for several MC compounds are listed in Table 3.6.

Table 3.6.: Melting points for several MC species [43].

Compound	Temperature [K]
UC	2780 ± 25
PuC	1875 ±25
U_2C_3	2100
Pu_2C_3	2285
$(U_{0.8}Pu_{0.2})C$	2750 ± 30
$(U_{0.8}Pu_{0.2})_2C_3$	2480 ± 50

3.4.3. Specific Heat Capacity

Although steady state calculations are relatively insensitive to the heat capacity, accurate relations for C_p may be necessary for transient models. The heat capacity is dependent primarily on temperature [41]. Blanck claims the first studies of MC heat capacity did not take into account a strong upward trend in C_p at temperatures above 60% of the melting temperature [26]. This improper data was reproduced in the ANL collection on thermodynamic data for MC fuels [44]. Blanck believes the most accurate assessment of the heat capacity was completed by Holley in 1984 [45]. The heat capacity for MC is typically cast into a form as,

$$c_p(T) = a + bT + cT^2 + dT^3 + eT^{-2} \tag{3.10}$$

C_p = heat capacity [J/mol/K],
T = temperature [K].

Since simple relations are adequate for steady-state calculations, Preusser uses a linear trend for the heat capacity of UC given as,

$$C_p(T) = 54.4 + (0.00962)T \tag{3.11}$$

Table 3.7.: Coefficients for the heat capacities for several MC species.

Fuel	a	b	c	d	e	Trange (K)	Ref.
UC	50.98	2.57E-02	-1.87E-05	5.72E-09	-6.19E+05	298-2780	[2]
UC1.5	5.354	-2.39E-02	2.07E-05	0	-1.45E+06	298-1670	[2]
UC2	49	8.25E-02	-7.82E-05	3.03E-08	-5.93E+05	298-2000	[1]
U2C3	150.7	-4.79E-02	4.13E-05	0	-2.91E+05	360-1700	[1]
PuC0.84	57.876	-1.45E-02	7.71E-06	8.62E-09	-6.55E+05	298-1875	[2]
PuC1.5	78.0375	-4.00E-02	3.52E-05	0	-1.09E+06	298-2285	[2]

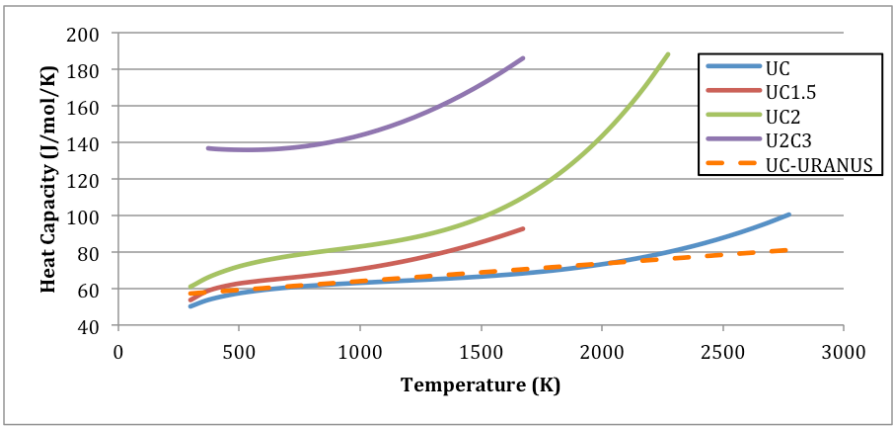

Figure 3.16.: Heat capacities for several uranium carbide compounds.

The heat capacities for uranium carbides are plotted in Figure 3.16, with plutonium carbides plotted in Figure 3.17.

As the M/C ratio decreases, the heat capacity tends to increase. The largest deviation occurs in the U2C3 composition, resulting in nearly a factor of 2 increase. At 1100K, the transition occurs for hyperstoichiometric fuels as (UC+C) transitions into (U_2C_3 + C) this phase change is visible in the heat capacity curves $UC_{1.5}$ and especially UC_2 transitions from following the UC heat capacity curve, to following the slope of U_2C_3.

The heat capacities given by Blank will be utilized as the standard. Deviation in stoichiometry and plutonium content will be ignored for the present. A relationship based on M/C or U/Pu ratio may be possible, perhaps even as simple as a linear relation.

3.4.4. Thermal Conductivity

The thermal conductivity is heavily dependent on temperature, porosity, and stoichiometry of MC. Any imperfections, such as Pu content, fission product, and deviations in stoichiometry serve to decrease the thermal conductivity [41].

GA is using thermal conductivity values given in Table 3.8. The values below 233° C were taken from a 1964 report that was primarily concerned with UO_2 fuel, but contained a brief mention of 95% dense UC and UC2 values. The stoichiometry of the specimens is unknown.

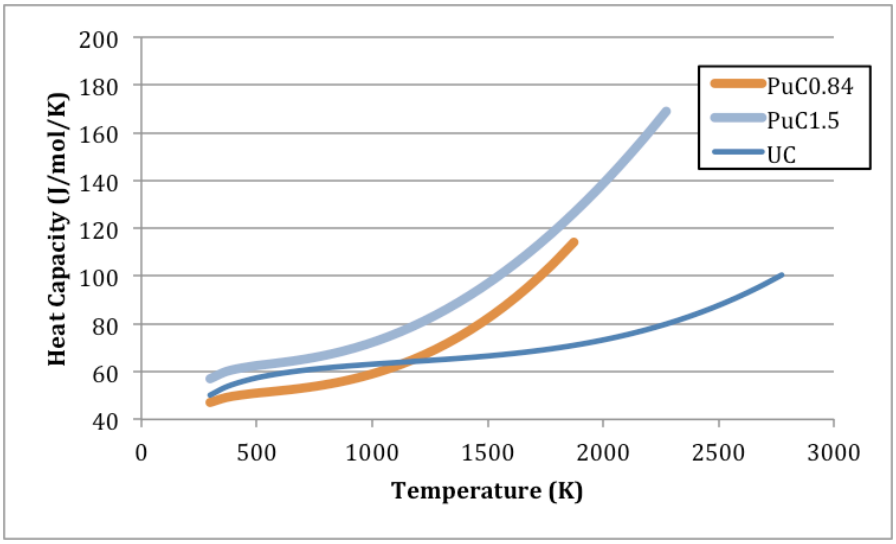

Figure 3.17.: Heat capacities for several plutonium carbide compounds.

Table 3.8.: Thermal conductivity values used by GA for 95% dense UC fuel

Temperature [° C]	Thermal Conductivity W/m/K
124	20.52
193	18.42
220	15.91
233	17.17
300	16.33
400	15.91
1530	20

The thermal conductivities from 300° C to 1530° C are from an unknown source.

The Preusser uses a much simpler relation [41]:

$$\lambda = \begin{cases} 20 & \text{for } T \leq 773 \text{ K} \\ 20 + (1.3 \cdot 10^{-3})T & \text{for } T > 773 \text{ K} \end{cases} \tag{3.12}$$

λ = thermal conductivity [W/m/K],
T = temperature [K].

Porosity corrections are typically given in the form:

$$\phi = \phi'(1-P)^n \tag{3.13}$$

ϕ = Property of sub-dense material,
ϕ' = Property of fully-dense material,
P = Fractional porosity,
n = correction factor.

The most basic approximation is for n=1, and usually applies to material in which the microstructural information is not known, namely the shape and orientation of the pores. Lower and upper third order bounds for a porous isotropic material with closed porosity are typically $n = 3$ and $n = 3/2$ respectively. Both $n = 3/2$ and a second type of correction,

$$\phi = \phi' \left(\frac{1-P}{1+P} \right) \tag{3.14}$$

have been used to for (U, Pu)C specifically. The latter will be utilized for now due to the fact it seems to split the difference between n=3 and n=3/2 lower and upper bounds. This same porosity correction is implemented in [46].

Figure 3.18 shows that the thermal conductivity is heavily dependent on C/U ratio. If the fuel is slightly hypostoichiometric, the extra uranium atoms will form a metallic phase along the grain boundaries, increasing the thermal conductivity. However, the extra carbon atoms incorporated in the crystal in hyperstoichiometric fuels will result in a decreased thermal conductivity. Note, UC fuels are typically kept at hyperstoichiometric levels to avoid the swelling issues caused by uranium metal. From a presentation from GA [47], we can take the fuel to be hypostochiometric, possibly as high as $UC_{1.3}$, thus the thermal conductivity lays beyond right edge of Figure 3.18.

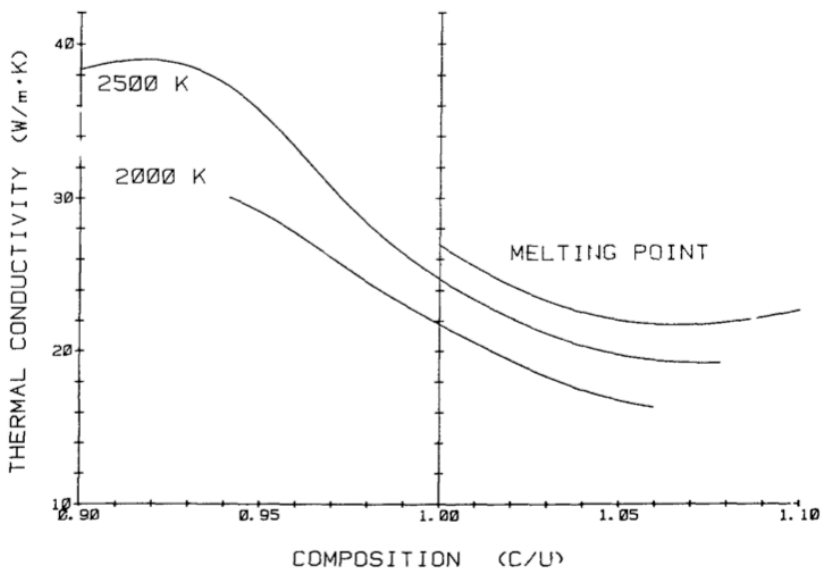

Figure 3.18.: Heat capacities for several plutonium carbide compounds.

By taking into account the C/M ratio, Storms [48] was able to isolate the effect of the U/Pu ratio on the thermal conductivity. For hyperstochiometric fuel, a plutonium ratio of 20% results in a very slight decrease in λ. Increasing the Pu ratio to 40% markedly decreases the conductivity. However, hypostochiometric fuel experiences decrease in thermal conductivity of about 20% up to 1000° C, at which point the UC and $(U_{0.8},Pu_{0.2})C$ have similar thermal conductivities.

Blank includes a summary on studies on the thermal conductivity of $(U_{0.8}Pu_{0.2})C_{1+x}$ with artificially mixed fission products Ce, Zr, and Mo. Table 3.9 displays the ratio of the thermal conductivities between the pure and FP mixed samples, λ/λ_{mod}.

Table 3.9.: Thermal conductivity ratios due to artificial additions of fission products. The change in the ratio is nearly constant for 5-10% molar introduction of MoC. Reproduced from [26].

Species	Atomic radius [μm]	Molar addition	λ/λ_{mod} at 700 K	λ/λ_{mod} at 1200 K
U	175	-	-	-
Ce	185	10%	1.15	1.087
Zr	155	10%	1.21	1.16
Mo	145	5%	1.25	1.186

Since the decrease in thermal conductivity is higher at lower temperatures, it can be expected that the outer ring of the fuel pellet will experience a greater change in thermal conductivity as a function of fission product addition.

From Table 3.9, it is clear that the addition of the Ce results in the lowest modification in the thermal conductivity, while Mo results in the highest. By plotting λ/λ_{mod} by the percentage difference in atomic radius of each FP with uranium, a nearly linear trend is obvious (Figure 3.19).

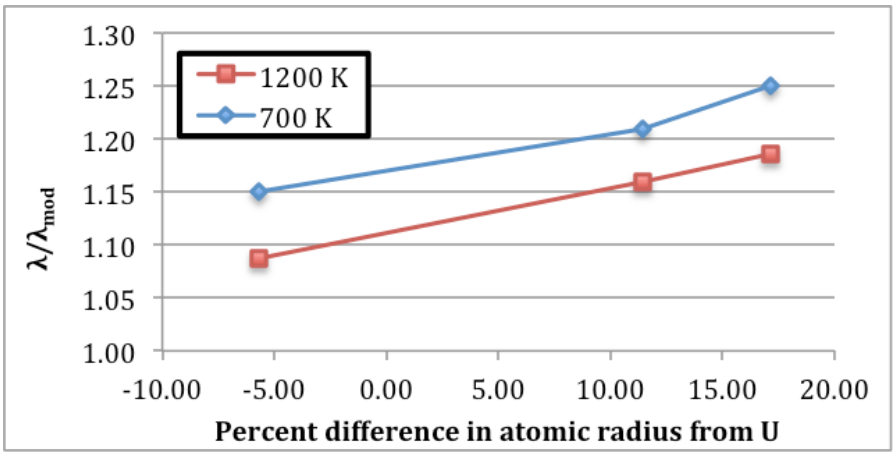

Figure 3.19.: λ/λ_{mod} vs. percent difference between the atomic radius of a given FP and U.

Although a trend might be drawn from the above, Matzke claims that even though the thermal conductivity has a slight dependence on the FP concentration, it is a smaller effect when compared to porosity, C/M ratio, and restructuring [6].

From the previous discussion, we can see that the thermal conductivity varies as a function of C/M and U/Pu ratios. What was not discussed was the even wider deviations between thermal conductivity reports. Matzke attributes the difficulty in determining an accurate value of λ (and many other physical properties) on the poor characterization of the material before measurement.

As a result of the inconsistency between results, no one set of values can be deemed better than the rest, thus the simple correlation in Equation 3.12 will be utilized, with the porosity correction in Equation 3.14.

3.4.5. Thermal Expansion

Most thermal expansion relations are given in the linear form:

$$\lambda_m = a + bT \tag{3.15}$$

λ_m = mean thermal expansion coefficient, [1/K]
T = temperature, [K]

Table 3.10.: Some coefficients for thermal expansion

Reference	a	b
General Atomics	1E-5	0.9E-9
Matzke [6]	1E-5	1.2E-9
Preusser [41]	1.007E-5	1.17E-9

Preusser claims that the above relation utilized in URANUS is highly representative of the values in literature, as well as conforming well to experimental data [41].

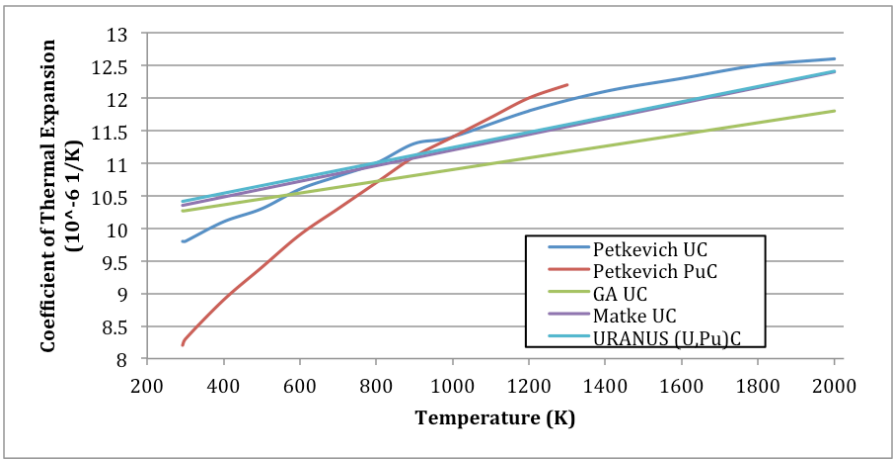

Figure 3.20.: Thermal expansion from several sources [6, 41, 49].

The coefficient of thermal expansion seems to be independent of the stoichiometry up to 800° C [6]. Above this temperature, hypostochiometric UC behaves differently than stoichiometric UC due to the phase changes of the free uranium present at the grain boundaries [41]. The decomposition temperature $U_2C_3 \rightarrow UC + UC_2$ occurs at 1780° C, and is accompanied with a large volume change [6]. Differences in the thermal expansion between UC and U_2C_3 should lead to noticeable internal stresses in two-phase structures [26].

Matzke claims that the U/Pu mixture does not exhibit great deviations. In addition, the URANUS code utilizes the same coefficient of thermal expansion for both UC and PuC.

In a thorough explanation of thermal expansion data, Blank claims that in principle, the porosity does not affect the thermal expansion, with data from dense arc-melted UC producing nearly the same results as 86% sub-dense hot-pressed UC.

The coefficient of thermal expansion used in URANUS will be adopted as the standard for this study for all Pu/C and M/C ratios. Further determination of stoichiometric effects may be beneficial, especially in hypostochiometric samples.

3.4.6. Young's Modulus

Table 3.11 displays the elastic moduli at room-temperature.

Table 3.11.: Elastic moduli at room-temperature [6]

Material	Young's [10^6 Pa]	Shear [10^6 Pa]	Bulk [10^6 Pa]	Poisson's
UC, $(U_{0.85}Pu_{0.15})C$	225	87.3	176.8	0.228
$UC_1$0.96	211	82.9	157.5	0.28
UC	210	81.3	167.8	0.291
$(U_{0.8}Pu_{0.2})C$	202	78.5	160.3	0.29

Preusser implements a temperature and porosity dependent thermal conductivity of the form,

$$E(T,p) = 2.15 \cdot 10^{11} \left(1 - a \cdot P\right) \left(1 - 0.92x10^{-4} \left[T - 273\right]\right) \tag{3.16}$$

E = Young's modulus, [Pa],
P = fractional porosity, $P \leq 30$,
T = temperature, [K],
a = porosity correction coefficient.

A porosity correction coefficient of a = 2.3 is typically used [6, 41], with a value of a = 1.54 for fuel with 20% Pu. The porosity correction does not consider the shape of the pores which may be important for highly porous material.

Matthews [50] claims both stoichiometry and grain radius does not significantly modify Young's Modulus. Matzke references several studies of Young's Modulus after the introduction of several fission products, and claims they have little affect [6].

The relationship from Preusser (Equation 3.16) will be utilized.

3.4.7. Poisson's Ratio

Preusser [41] utilizes a porosity corrected υ:

$$\upsilon = 0.288 - 0.286P, \quad \text{for } 0.05 \leq P \leq 0.27 \tag{3.17}$$

Preusser acknowledges other papers use fixed values, namely the first value given in Table 3.11. However, since the URANUS code utilizes values for Young's moduolus and Poisson's ratio from the same resource. Matzke claims that Poisson's ratio does not change as a function of temperature due to similar temperature dependencies for the moduli [6].

3.4.8. Thermal Creep

For fuel rod analysis, only primary and secondary creep is applicable as tertiary creep regions lie out of the time span of the rod lifetime. However, due to the complexity of primary creep, typically only secondary creep is modeled. In general, thermal creep begins at 1300 [K], and dominates radiation creep, although both are important to reducing stress in the fuel [41].

Preusser claims that the following relationship is the most applicable for thermal creep:

$$\dot{\varepsilon}_{cr}^{th} = c_{th} \cdot \sigma^{2.44} \exp(-63200/T) \tag{3.18}$$

$\dot{\varepsilon}_{cr}^{th}$ = thermal creep rate, [1/s],
c_{th} = coefficient, $c_{th} = 9.48 \cdot 10^{-9}$
σ = effective stress, [Pa],
T = temperature, [K].

The above equation only accounts for temperature and pressure dependence. The grain size will also affect creep since the speed of grain boundary sliding increase as grain size decreases. This results in different creep rates between coarse-grained arc-melted fuel and fine-grained sintered fuel.

The effect of impurities can be considerable to the creep rate. This is especially true with the addition of the sintering aid nickel, with an Ni addition to 0.05% resulting in 2-3 orders of magnitude increase in the creep rate. Similar behavior is observable with higher concentrations of carbon, however, additions of Pu, Zr, or O have little effect. Free mixed metal (U,Pu) in hypostoichiometric fuel can result in phases with low melting point eutectics that can lead to low creep resistance [41].

Although there is evidence that more parameters than just temperature and stress modify the creep rate, a lack in clear experimental data makes higher fidelity models inappropriate. The equation used in URANUS (Equation 3.18) will be utilized.

3.4.9. Irradiation Creep

As a result of the relatively low irradiation temperatures of carbide fuel, irradiation creep is more significant than similar behavior in oxide fuels where thermal creep dominates. Regardless, irradiation creep behavior is similar in the two types of fuel, most likely due to the linear relationship between creep and the number of point defects resulting from neutron dose. Preusser utilizes the following relationship for irradiation creep:

$$\dot{\varepsilon}_{cr}^{irr} = c_{irr} \dot{F} \sigma \tag{3.19}$$

$\dot{\varepsilon}_{cr}^{irr}$ = irradiation creep rate, [1/s],
c_{irr} = coefficient, $1 \cdot 10^{-37}$ [1/Pa·s·$\dot{F}$],
σ = effective stress, [Pa],
$\dot{F}$ = fission rate density, [fsn/m^3·s].

3.4.10. Fission products

Fission products (FP) are created on the order of 500 ppm per day, thus FP quickly overtake the number of as-fabricated impurities which are on the order of 1000 ppm for technological-grade samples. Table 3.12 displays a sample distribution of fission products after fissioning of 100 atoms of Pu-239. Of particular interest is the decrease free carbon as a function of burnup; At a burnup of 10% at, the C/M will decrease approximately 0.01 (ie. $UC_{1.10} \rightarrow UC_{1.09}$).

Table 3.12.: Sample distribution from fissioning of 100 atoms of Pu-239 [26].

Atom	Yield (at. %)	Compounds
Noble gases		
Xe	22.7	
Kr	2.5	
Volatiles		
Cs	19.2	
Rb, Te, I	5.8	
Earth Alkalines		
Sr, Ba	10.1	BaC_2, SrC_2
4d metals and Ag		
Zr	19.4	Mono, di, and
Mo	22.4	sesqueicarbides
Ru	21.9	
Pd	13.0	
Y, Nb, Tc, Rh, Ag	15.0	
Lanthanides and La		
Ce	12.8	Mono, and
Nd	13.8	sesqueicarbides
La, Pr, Pm, Sm, Eu, Gd, Tb	16.3	

3.4.11. Irradiation induced swelling and densification

Since the swelling of uranium carbide fuel is based on the total number of fissions, it can be approximated using a stepwise approach with the burnup, B:

$$V(B+\Delta B) = (1+V(B))\left[\frac{\partial(\Delta V/V)}{\partial B}\right]\Delta B \tag{3.20}$$

In this way, the swelling rate can be defined for given timestep. Although an approximation, the above equation is valid if the volume increase is small relative the the volume, which can be controlled by the timestep size.

3.4.11.1. Solid fission product swelling

Most authors quote a swelling rate of around 0.5% per % burnup in atom percent (a/o). This is derived from a very simplistic model: Given 100 fission events, 200 fission products are created. 50 of these fission products will be volatile and will not contribute to the solid swelling factor. 100 of the remaining 150 atoms can be assumed to occupy the original actinide location, thus 50 atoms create a new site in the lattice. If these atoms are assumed to take the same space as the actinide atoms, then each fission will cause the bulk to swell by the 0.5 per fission per initial metal (U, Pu) atom (FIMA).

Preusser uses the following relationship for swelling due to solid fission products [41]:

$$\frac{\partial(\Delta V/V)_{ss}}{\partial B} = c_{ss} \tag{3.21}$$

$\Delta(\Delta V/V)_{ss}$	=	fractional volume change,
c_{ss}	=	solid swelling factor, 0.417,
ΔB	=	change in burnup over timestep, [FIMA].

Although the above solid swelling factor is slightly less than the typical 0.5, the lower value is included with the same gaseous swelling formulation presented in [41].

3.4.11.2. Gaseous fission product swelling

The swelling due to gaseous fission products is one of the most complex behaviors in mixed carbide fuels. As discussed in Section 3.2, the bubble behavior in UC fuels is very complex and highly dependent on temperature, burnup, impurities, and microstructure.

The swelling due to gaseous fission products can be divided into two contributions. The first is the inclusion of single gas atoms which mimics the behavior of solid fission product swelling. At low temperatures when atomic diffusion is nearly absent, the gas atoms will remain isolated as point defects. However, at high temperatures, the gas atoms will tend to group together and form bubbles. These bubbles themselves can interconnect and form larger bubbles, resulting in a less efficient use of space (Section 3.2). As a result, the bulk fuel will swell as the concentration and sizes of bubbles increase.

Ideally, the swelling caused by gaseous fission products would be calculated using a bubble concentration distribution function. However, the complexity of such a model has typically forced empirical relationships to be used to describe the swelling behavior.

Preusser uses a volume swelling model that accounts for porosity, temperature, burnup, and contact pressure:

$$\frac{\partial(\Delta V/V)_{gs}}{\partial B} = \begin{cases} c_{gs} f_{por} f_{cont} & \text{for } T \leq 973 \text{ K} \\ (c_{gs} + f_{temp} f_{Bu}) f_{por} f_{cont} & \text{for } T > 973 \text{ K} \end{cases} \tag{3.22}$$

$$\frac{\partial(\Delta V/V)_{gs}}{\partial B} \leq 3.653 \qquad \text{for all } T \tag{3.23a}$$

$$f_{por} = \exp(0.04 - P) \qquad \text{for } P > 0.04 \tag{3.23b}$$

$$f_{cont} = \exp\left(-\frac{pc}{pc_0}b\right) \qquad \text{for } f_{cont} \leq 1 \tag{3.23c}$$

$$f_{temp} = 12.95 - (0.0281)T + (1.520 \cdot 10^{-5})T^2 \tag{3.23d}$$

$$f_{Bu} = \frac{B}{B_0} - a \qquad \text{for } f_{Bu} \geq 0 \tag{3.23e}$$

$\Delta(\Delta V/V)_{gs}$	=	fractional volume change,
c_{ss}	=	gaseous swelling factor, $c_{ss} = 1.528$,
f_{por}	=	porosity correction,
f_{cont}	=	contact pressure correction,
f_{temp}	=	temperature correction,
f_{Bu}	=	burn correction,
P	=	fractional porosity,
pc	=	cladding contact pressure, [Pa]
pc_0	=	constant, $pc_0 = 1 \cdot 10^6$ [Pa],
T	=	temperature, [K],
B	=	burnup, [FIMA],
B_0	=	threshold burnup, $B_0 = 0.0112$ [FIMA],
a	=	model fitting parameter, $a = 2.0$,
b	=	model fitting parameter, $b = 0.1$.

The model is Equation 3.22 combines the complexity of the gas bubble distribution into one experimentally derived equation. At low temperatures, the swelling rate dependent only on the porosity of the fuel and contact pressure with the cladding. At high temperatures, the swelling rate is much higher, simulating the run-away swelling above the threshold temperature, similar to the behavior discussed in section 3.2. The high temperature growth is also limited by the burnup correction, and is constrained only above the threshold burnup value B_0. The model parameters a and b were used to tune the model the the experimental data, resulting in a correlation that is somewhat limited.

3.4.11.3. Densification

Densification of the fuel occurs as a result of the high temperatures and irradiation environment in fuel rods. Carbide fuel pins have been observed to have an approximate volume fractional densification rate of $\Delta V/V = 0.67[\text{FIMA}]^-1$, with a maximum densification of about 90% of the theoretical density (TD). Creep tests on 85% TD $(U_{0.85}Pu_{0.15})C$ pellets showed a densification behavior of [51],

$$\Delta P = \Delta P_{max}[1 - \exp(-B/B_c)] \tag{3.24}$$

ΔP = porosity decrease,
ΔP_{max} = maximum porosity decrease, $\Delta P_{max} = -0.034$,
B = burnup, [FIMA],
B_c = burnup constant, $B_c = 0.006$ [FIMA].

Despite the difference in fuel forms, the relationship in Equation 3.24 will be used to model densification.

3.4.12. Fission gas release

Although the R/B model discussed in Section 3.3 was used for the STELLA model, other models were investigated for implementation within BUCK. As previously discussed, the fission gas release is a highly complex phenomena that relies on many different properties (Section 3.2). Regardless, some simple models can be built from careful consideration of experimental data. The model Preusser utilized for fission gas release is dependent on the temperature and burnup of the fuel, and is given as:

$$f_{rel} = f_{rel}^{temp}(1 - \exp[-1.5(B - B_{free})]) \qquad \text{for } B > B_{free} \tag{3.25a}$$

$$B_{free} = (-2.576 \cdot 10^{-6})T_c + 6.696 \cdot 10^{-3} \qquad \text{for } 0 \leq B_{free} \leq 0.00224 \tag{3.25b}$$

$$f_{rel}^{temp} = \begin{cases} 0, & \text{for } T_c \leq 1273 \text{ K} \\ 4.67 \cdot 10^{-4})T_c - 0.594, & \text{for } 1273 \text{ K} < T_c \leq 2343 \text{ K} \\ 0.7419 \cdot \ln[0.7675 \cdot (T_c - 273)] - 4.9685, & \text{for } T_c > 2343 \text{ K} \end{cases} \tag{3.26}$$

f_{rel} = fractional fission gas release rate,
f_{rel}^{temp} = temperature correction,
B = burnup, [FIMA],
B_{free} = burnup threshold,
T_c = centerline temperature, [K].

The temperature behavior of fission gas release is captured in the f_{rel}^{temp} term, with no release occurring for low centerline temperature fuels in which the diffusivity is too slow to allow transport to the grain boundaries. Similarly, the burnup correction takes into account the fact that no fission gas release occurs for low burnup fuels where the concentration of fission gas is too small to result in large releases.

Preusser uses an incremental model to calculate fission gas production, g_{gen} using the fission rate of the fuel, $\dot{F}$ and the total fission gas yield, γ_{gas}:

$$g_{gen}(t + \Delta t) = g_{gen}(t) + \Delta g_{gen} \tag{3.27a}$$

$$\Delta g_{gen} = \dot{F}\gamma_{gas} \tag{3.27b}$$

The increase and decrease in temperature is handled through incremental stepping as well, depending on the comparison between the average fission gas release ratio, g_{rel}/g_{gen} and the

fractional fission gas release rate, f_{rel}:

$$g_{rel}(t+\Delta t) = \begin{cases} g_{rel}(t) + \Delta g_{gen} f_{rel}, & \text{for } f_{rel} < g_{rel}(t)/g_{gen}(t) \\ g_{gen}(t+\Delta t) f_{rel}, & \text{for } f_{rel} > g_{rel}(t)/g_{gen}(t) \end{cases} \tag{3.28}$$

Equation 3.28a ensures that if a decrease in temperature occurs, then all the fission gas that was previously released, stays released. Equation 3.28 models the breakaway fission gas release that can occur during high temperature ramps by ensuring not only Δg_{gen} is released, but some fraction of fission gas already within the fuel is released as well.

3.5. The BUCK Fuel Performance Code

BUCK (Basic Uranium Carbide Kernels) is a fuel performance code built that is being developed at OSU within the MOOSE (Multiphysics Object Oriented Software Environment) software environment. Due to the similarities between uranium-carbide and oxide fuels, BUCK is essentially an extension of the BISON [52] software package already implemented in the MOOSE framework [53] for fuel performance modeling of UO_2 fuels.

3.5.1. BUCK software classes

Within the MOOSE framework, custom C++ classes are used to implement all necessary parts of the problem such as the specific physics, material properties, functions, postprocessors, etc. Following the testing standards set by the MOOSE team, each piece of code is then isolated and verified against a hand calculation to ensure that the code has been implemented correctly. Output files containing these verified results are retained such that BUCK can be compared against these "gold" standards. Modifications to BUCK, BISON, or MOOSE can be ensured to remain constant throughout implementation of BUCK development.

BUCK implements the following models, based on the relationships presented in Section 3.4:

- Thermal: The thermal conductivity and specific heat is calculated as a function of temperature and evolving porosity. While the specific heat is not very important for the near steady state analysis conducted within BUCK, the temperature distribution in the fuel pin is highly dependent on the thermal conductivity, thus accurate estimations are important.

- Mechanical: Young's modulus and Poisson's ratio are calculated based temperature and initial porosity. The strength of the material is important as the fuel pellet comes in contact with the cladding wall, thus models that account for temperature and porosity are implemented. In addition, temperature dependent thermal expansion is included.

- Creep: Both thermal and irradiation creep models are included to account for the relaxation of internal stresses of the fuel pin. The relatively low temperature of carbide fuel rods elevates the importance of a fission-rate dependent creep term, although both enhance the stress relaxation within the pellet.

- Swelling: Volumetric swelling is an important phenomenon to model for any nuclear fuel, and includes swelling due to solid fission products, swelling due to gaseous fission products and bubbles, and densification due to the high temperature irradiation environment. All three models are incorporated within BUCK, however the swelling due to gaseous fission products model is limited and requires a bubble distribution model to accurately capture the bubble behavior in carbide fuels.

- Fission gas release: The release of fission gas was the primary goal of the BUCK models, but it also affects other simulated parameters such as gap conductivity and internal pin pressure. Similar to the gaseous fission product swelling model, the fission gas release model currently incorporated is simplistic and relies heavily on experimental data. A bubble distribution model is required to accurately capture the bubble behavior in carbide fuels.

The simplicity introduced by the empirical swelling and fission gas release models is the largest source of error in the BUCK calculations. As discussed in Section 3.2, there tends to be distinct radial zones in the fuel, described primarily by the amount of porosity. This behavior requires a bubble distribution model and is not currently implemented within BUCK. Such a model would allow the evolving bubble population to not only impact the fission gas release and swelling, but could allow the changing porosity to feed back into the thermal and mechanical models. As it stands now, the swelling due to gaseous fission products is also used to calculate the increase the porosity. The evolving porosity is utilized in the thermal models to update the thermal conductivity.

3.5.2. Representative pin model

Despite the limitation in the current implementation of BUCK, representative cases can be simulated to show the behavior of carbide fuel. Figures 3.21, 3.22, and 3.23 shows the temperature and Von Mises stress behavior of a fuel rodlet based on the K7 helium-bonded carbide fuel tests [54]. At the initial heat up, the central fuel temperature peaks at about 2066 K, close to the estimated value of 2100 K. Also of interest is the quick decrease in internal stress in the fuel due to the combination of thermal and radiation creep. Finally, the severe drop in fuel temperature is evident as the fuel swelling causes the gap between the fuel and clad to close and heat is conducted between the fuel and clad, rather than across the gas gap. This same behavior is clear in Figure 3.23. The slight increase in fuel temperature near the beginning of the simulation is a result of the release of fission gas into the plenum, which in turn causes a decrease in the gap conductivity.

3.5.3. Representative sphere model

The EM^2 design consists of many spherical particles sintered together into one fuel form. It was unclear how best way to model the fuel, be it through a full pin simulation, or through explicit tracking of each fuel kernel. Ultimately, the pin simulation is the simplest and should be utilized for fuel modeling, but a simplistic representation of an interaction between two kernels was

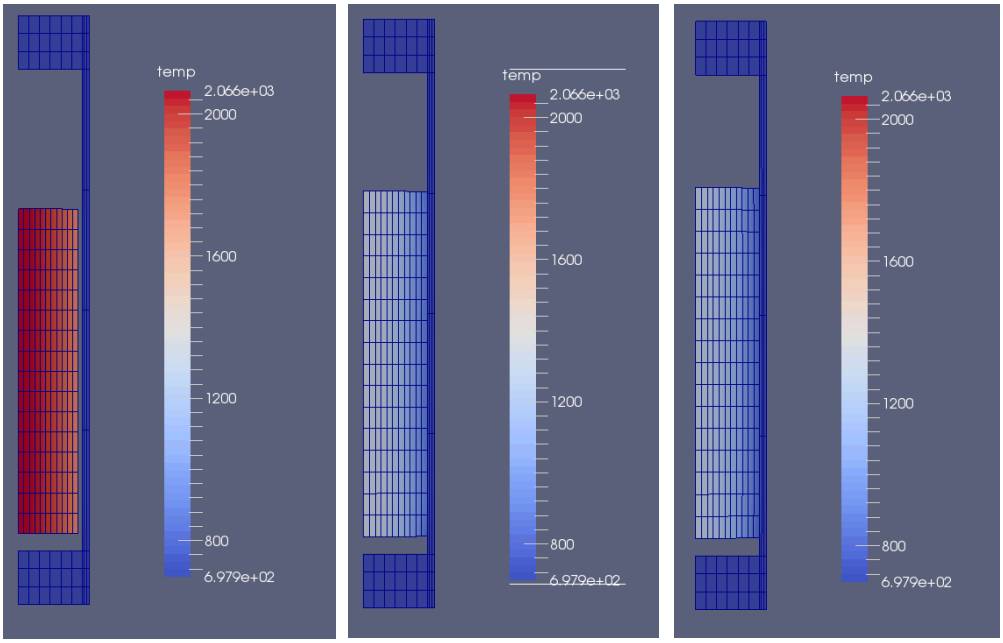

(a) (b) (c)

Figure 3.21.: Simulation of K7 fuel pin after initial heat up showing (a) BOL temperature profile; (b) at 0.8 FIMA showing the temperature decrease as the fuel comes into contact with cladding; (c) and at EOL at 1.5 FIMA.

run to try and picture the behavior between two adjacent kernels. Missing in this model is the appropriate distortion size, and necking between the two sintered particles.

With the EM^2 design, the voids between the kernels are assumed to maintain throughout the 30-year irradiation. Depending on the level of cladding restraint, swelling due to fission products may reduce the porosity, while swelling due to fission gas will contribute to the overall fuel swelling, but will reach a saturation point once the inter-granular bubbles become interconnected. Regardless, after about 0.1 FIMA, the two spheres will grow together, producing very high internal stress and forming some sort of porous single particle (Figure 3.24). The simple models that are utilized in BUCK are ill-equipped to handle this sort of behavior, and a different modeling technique is necessary if kernel-kernel behavior is to be analyzed. What is clear is that the as-built fuel form composed of individual kernels can be expected to growth together into a single solid.

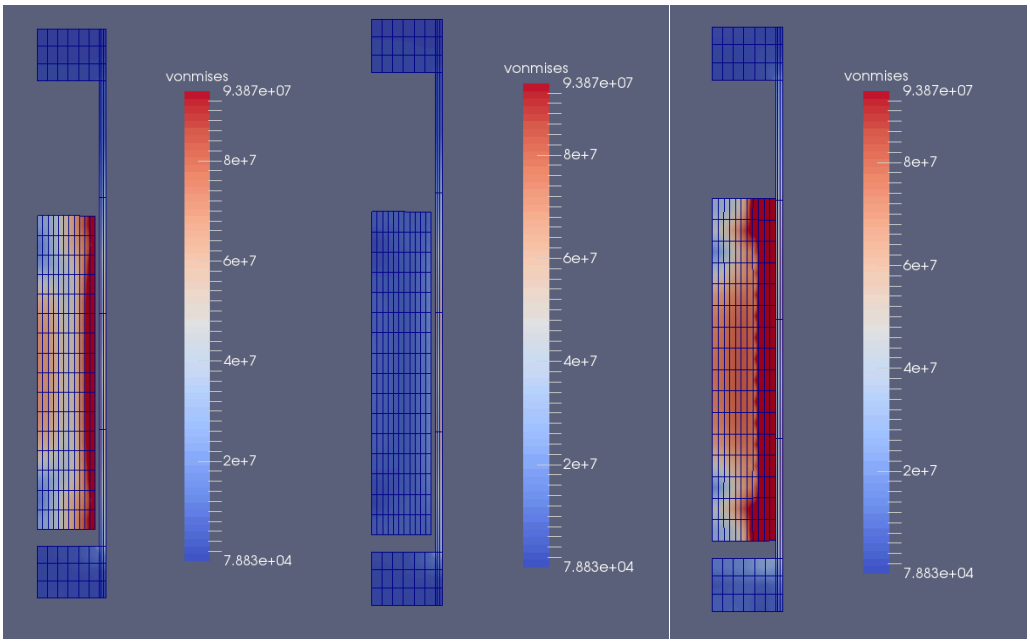

(a) (b) (c)

Figure 3.22.: Simulation of K7 fuel pin after initial heat up showing (a) BOL stress profile; (b) after several hours showing stress relaxation; and (c) at 0.8 FIMA showing the stress increase as the fuel comes into contact with cladding.

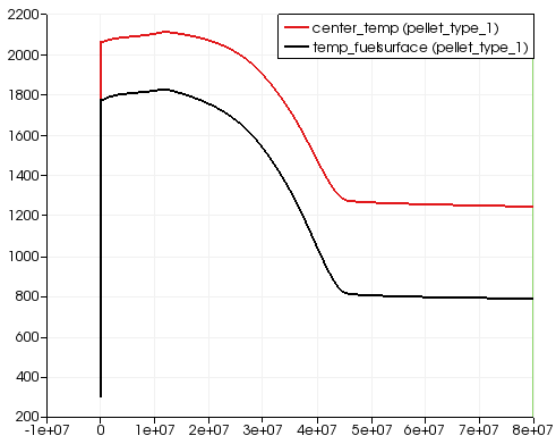

Figure 3.23.: Center and surface temperatures for the K7 test.

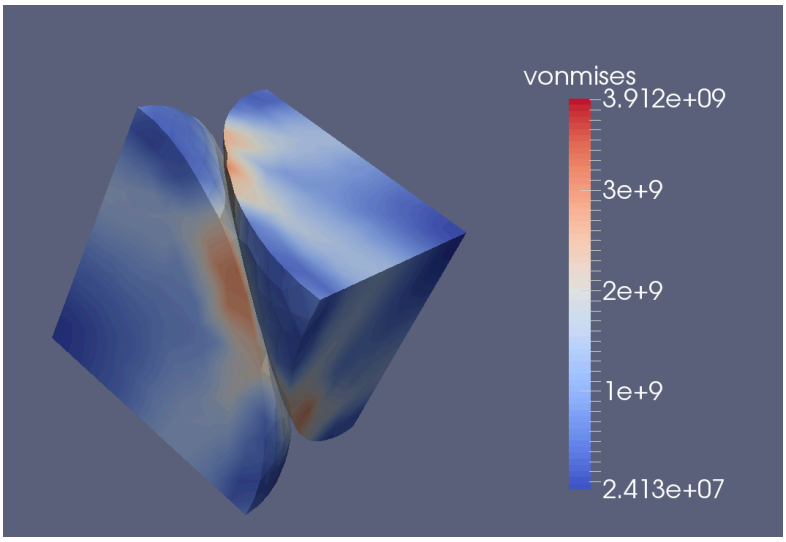

Figure 3.24.: Representative kernel-kernel sphere model at 0.1 FIMA.

3.6. Re-solution Rate Calculation

In the simplest of terms, the fission gas release can be calculated using a spherical grain model which solves for the grain and grain boundary concentrations using empirical diffusivity values. Complicating this simple model is the tendency of the insoluble fission gas to collect and form bubbles within the fuel grain before reaching the grain boundary. In addition, highly energetic fission fragments can strike the intra-granular bubbles, resulting in re-solution of gas atoms back into the fuel lattice. Many models account for these different trapping and re-solution behaviors by tuning the diffusivity [6,30,55,56]. However, estimation of fission gas in its different physical forms may result in more accurate calculation of fission gas release [57].

The re-solution event has been described as either a collisional atom-by-atom loss or though a complete destruction process (see Olander and Wongsawaeng [58] for a recent review). The latter theory first developed by Turnbull [59], termed "heterogenous" re-solution by Olander and Wongsawaeng, assumes a bubble is destroyed if it lies within a destruction zone of approximately a nanometer around a given fission track. A second "homogenous" theory originally presented by Nelson [60] assumes that individual gas atoms are knocked out of bubbles through direct collisions with fission fragments or from fuel cascades produced in the fuel. Many previous studies have looked at one or both of these theories in UO_2 [55, 57, 61–65]. In general, the homogenous theory tends to underestimate the re-solution rate in UO_2, while success has been achieved with the heterogenous theory [57, 65, 66]. Although fewer studies have looked at re-solution in non-oxide fuels, a study by Ronchi and Elton showed the homogenous theory produces favorable results in uranium carbide (UC) fuels [65].

The ability of the heterogenous re-solution model to accurately estimate re-solution in oxide fuels, while homogenous re-solution seems more applicable to uranium carbide fuel, lies in the inherent differences between the two materials; uranium carbide is bonded by a mix of covalent and metallic contributions [26], resulting in different energy transport properties such as higher thermal conductivity and diffusivity when compared to UO_2. Fission fragments are well known to create displacement spikes in materials [27]. Following the lattice disorder, a local temperature increase on the order of 2000° C occurs in UO_2, along with a mechanical shock that moves through the lattice as a result of rapid thermal expansion [65, 67]. However, theoretical calculations have shown that considering the higher electrical conductivity and thermal diffusivity present in uranium carbide which permits rapid dispersal of energy, the temperature increase is on the order of only 50° C [65]. As a result, the thermoelastic stress field caused by a thermal spike is nearly absent in UC [68, 69].

In light of the differences between UC and UO_2, it is understandable that the bubble destruction model has seen success in oxide fuels, while the atom-by-atom knockout microscopic model is applicable to carbide fuels [65]. Because of this, the typically used, albeit computational expensive, Molecular Dynamics (MD) fission spike models of determining re-solution can be avoided in favor of Binary Collision Approximation (BCA) models.

In his original 1969 formulation, Nelson estimated the re-solution rate of a 5 nm xenon gas bubble in UO_2 by assuming Rutherford potential for fission fragment collisions and a hard-sphere potential for all other collisions, with no electronic losses [60]. An atom was assumed to be implanted back into the fuel if a gas atom located within a critical distance of 1 nm from the surface of the bubble was struck by an ion and transferred a minimum implantation energy

E_{min} = 300 eV [60]. The critical distance limit assumed that all centrally located fission gas atoms would suffer a large angle collision before reaching the bubble surface, while atoms close to the bubble surface result in a re-solution event if struck with sufficient energy. Ronchi and Elton extended the calculation by allowing E_{min}, as well as the radius of the bubble, to be a variable parameter of the calculation in oxide and carbide fuels [65]. Ronchi and Elton utilized the critical distance criterion for re-solution as well, ignoring the centrally located atoms in the bubble. However, due to the larger bubble sizes in their study, the critical distance was not held constant, but rather allowed to increase in order to compensate for the lower atomic densities present in larger bubbles.

While re-solution in oxide fuels has been studied experimentally, the lack of specific experiments to measure the re-solution parameter in uranium carbide makes direct verification difficult [65]. Many UC irradiations focused on bubble populations as a function of temperature and burnup [34, 35, 70–72]. Through the use of rate-equation type models, it may be possible to correctly simulate the bi-modal behavior that exists in UC fuel irradiated at high temperature [73].

An important link in such a rate-equation model is the bubble loss term, thus motivating the current work to develop a radius dependent re-solution parameter for use in fission gas bubble simulations. By using BCA to calculate the trajectory of fission fragments and their subsequent cascades, the fraction of atoms that escaped the bubble and became implanted in the surrounding fuel was tracked, resulting in a re-solution parameter that can be used to calculate the total re-solution rate. We will show that the re-solution parameter decreases as a function of radius up to a threshold. In addition, we will show that by accounting for electronic losses and through replacement of the hard-sphere potential with the more realistic Ziegler-Biersack-Littmark (ZBL) universal potential, knocked uranium atoms have a much greater role in implanting gas atoms than previously thought.

3.6.0.1. Methodology

The BCA code 3DOT [74] was used for all calculations in the current work. 3DOT is based on Schwen's 3DTrim [75] which utilizes the previously published TRIM algorithm [76] to track ion cascades in non-Cartesian geometry. The TRIM algorithm utilizes the ZBL universal potential to model the interactions between moving ions and stationary samples, and calculates the electronic stopping power by scaling proton stopping powers using the Brandt-Kitagawa theory [76, 77]. Due to the nature of TRIM calculations, each ion interacts with an undamaged, 0 K amorphous target.

Each 3DOT simulation model consisted of a fuel cube with an implanted sphere of xenon. Owing to the small computation expense of BCA and the wide spread of bubble sizes present in uranium carbide [26], the simulated bubble radii ranged from 0.5 nm to 500 nm with periodic boundary conditions enforced on all box sides. As the current study was focused on intragranular bubbles, grain boundary effects were not considered and the theoretical density of 13.63 g/cm^3 was assumed for uranium carbide. Fission fragments were randomly created based on the probability distribution functions of typical fission fragment mass and energies.

For these calculations, a fission gas atom was considered implanted if it exited the bubble surface with an implantation energy greater than E_{min}. The value of E_{min} = 300 eV first utilized by Nelson has been implemented in many re-solution studies [60, 65, 66]. More recently, a study

aimed at determining the implantation energy in UO_2 fuels determined that while re-solution did occur for atoms with implantation energies less than the 300 eV, the original implantation energy of 300 eV resulted in a 85% probability of re-solution [78]. In light of this, the value of E_{min} = 300 eV will be utilized unless otherwise specified, although model sensitivity to this value will be explored.

The total re-solution rate at which atoms are knocked back into the fuel can be calculated by,

$$R\left[\text{atom}/(\text{s}\cdot\text{m}^3)\right] = \int \dot{F} b(r) m(r) \rho(r) dr, \tag{3.29}$$

where r is the bubble radius, $\dot{F}$ is the fission rate, b is the re-solution parameter, m is the number of atoms in a bubble, and ρ is the bubble concentration distribution function,

$$N\left[\text{bub}/\text{m}^3\right] = \int \rho(r) dr. \tag{3.30}$$

Here, N is the total concentration of bubbles in the sample.

Considering the many combinations of bubble radii and box sizes, any dependence on simulation volume must be removed. Due to the periodic boundary conditions, the approximately 6 μm fission fragment path will wrap around the model many times. Due to the relatively low density within the bubble, as the porosity increases, the total fission fragment path will also increase. In order to avoid a bubble concentration dependent path length, comparative studies of various bubble and box sizes showed that the artificial lengthening of the fission fragment path was minimized when the cube length was at least 10 times the bubble radius. In this way, a value for b can be calculated independent of the bubble concentration.

3.6.0.2. Applicability of BCA

The ability of 3DOT to quickly analyze ion trajectories lies in the basic BCA simplification in which each collision is modeled as a single two-body collision. While this approximation is physically appropriate for high ion energies (typically above 1 keV), multi-body collisions tend to occur at lower ion energies. Several publications have attempted to quantify the limits of BCA with limited success [79–82].

The error introduced by BCA must be quantified in order to justify its use within this study. Fortunately, the use of a threshold implantation energy allows all ions below E_{min} to be ignored. Above this limit, the error introduced by ignoring multi-body collisions can be estimated by calculating the maximum deviation that can occur from the next nearest-neighor atom. If the angular and energy difference from the otherwise ignored atom has minimal effect on the re-solution rate, then the use of BCA is appropriate in this study for ions down to E_{min}.

In general, the kinematics of two body collisions can be described by the angle of deflection of the ion, θ. The energy transfer T can then be calculated as,

$$T = \Lambda E_0 \sin^2(\theta/2), \tag{3.31}$$

where $\Lambda = 4m_1m_2/(m_1+m_2)^2$, and E_0 is the initial ion energy. In 3DOT, the value $\sin^2(\theta/2)$ is calculated using the ZBL potential with the ion and target atomic attributes, and the impact

parameter p. As with all potentials, the smaller the impact parameter, the larger the angular deflection. Using Equation 3.31, large angle deflections correspond to high energy transfer. The greatest effect a second body can have on an ion, and thus the smallest impact parameter, is exactly between two atoms. The deviation caused by a target atom at this minimum impact parameter will estimate the angular deviation that is ignored by the BCA approximation in the worst case scenario.

In general, the fission gas escape process can be separated into two events. First, a fission gas atom must be hit by either a fission fragment or by a fuel atom that has been knocked out of its lattice site by a fission fragment. Due to the random nature of fission fragment creation in 3DOT, any error introduced to the fission fragment scatter angle can be ignored as long as all fission fragments are treated similarly. The same is also true for lattice atom (uranium and carbon) collisions. However, since the energy of knocked fission gases needs to be explicitly tracked, fission fragment and lattice ion energies must be correctly tracked for all ion energies above E_{min}. Uranium carbide has a simple cubic NaCl crystal structure with a lattice parameter of roughly 0.5 nm, resulting in $p_{min} = 0.125$ nm as an ion travels between a uranium and carbon atom. Due to the Λ factor included in the energy transfer equation, uranium-uranium collisions result in the highest energy transfer. Using the minimum impact parameter, the maximum energy transferred in a uranium-uranium collision is 60 eV for all initial ion energies. This value quickly diminishes as the impact parameter increases, reducing to less than 3 eV when the impact parameter is 0.2 nm. In the worst possible case, a lattice atom with energy 300 eV will overestimate the ion energy after a collision by 20%. However, the probability of such an event is small enough that BCA accurately represents fission fragment and lattice collisions for the purposes of this work.

The second event that must occur to create an implanted atom is the transport of a fission gas atom from the interior to the surface of the bubble. As opposed to the fuel lattice, both fission gas ion energy transfer and angular deflection are both important to track, as a knocked fission gas atom can receive a large-angle deflection very near the bubble surface. In the amorphous bubble region, the distance between fission gas atoms in the bubble d can be approximated by,

$$d = 2\,p_{min} = 2\,(3/4\pi m)^{1/3}\,. \tag{3.32}$$

Using the Combined EOS described previously, the density in a 1 nm bubble at 2000 K is 15.3 atoms/nm^3. Since the minimum impact parameter occurs directly between two atoms, $p_{min} =$ 0.25 nm. At this large of an impact parameter, the direction of the ion in a representative Xe-Xe collision deviates by only 2° with an initial ion energy of 300 eV. The ion energy must be reduced below 10 eV to result in a deviation of greater than 30°. In addition, such small deflections result in negligible energy transfer. Since these deviations occur during the most conservative atomic densities and smallest impact parameters, reduction of collisions within the bubble to single collisions was deemed appropriate for this work.

3.6.0.3. Results

Figure 3.25 shows the re-solution parameter b as a function of radius r for different EOS models, where b represents the number of escaped atoms per bubble atoms for a single fission and single bubble. A quick decrease initially occurred, reducing b nearly 60% as the bubble radius increases from 1 to 50 nm, beyond which the re-solution parameter became nearly constant. Since b was

calculated on a per bubble atom basis, it represents the average probability of any given bubble atom to be implanted. As the bubble radius increases, interior atoms have further to travel before becoming implanted, resulting in the quick decrease in b as a function of radius. However, as r becomes larger than 10 nm, the atomic density exponentially decreases as a function of radius (Figure 3.3), boosting the probability of a struck interior atom reaching the surface and flattening b as a function of radius. If the bubble sizes increase past the radii of interest present here, the low atomic density will eventually serve to create a positive slope in the re-solution parameter at very large radii.

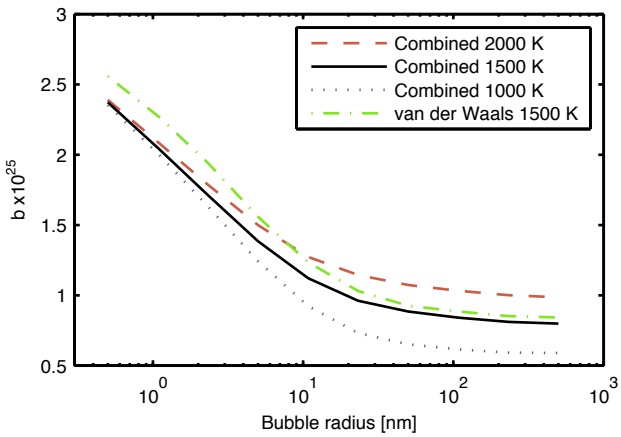

Figure 3.25.: Calculated b for several atomic density calculation methods.

Figure 3.25 also includes the re-solution parameter using different EOS methods: combined at 1000 K, 1500 K, and 2000 K, and van der Waals at 1500 K. In general, b was inversely proportional to the atomic density, producing fewer implanted ions at higher atomic densities.

As discussed previously, there is some uncertainty on the value of E_{min}. Figure 3.26 displays b for various values of E_{min} at 1500 K. Previous studies have shown that E_{min} may be less than 300 eV [78]. By reducing the assumed E_{min} to 150 eV, the re-solution parameter only increases by 30%, without much variation in the shape of the curve.

A gas atom can be knocked out of the bubble after first being struck by either a fission fragment or indirectly through a fuel cascade. Figure 3.27 displays the fraction of implanted gas atoms that were a result of either a fuel cascade or solely through a direct fission fragment hit in a 5 nm bubble at 1500 K. Roughly 90% of all implanted ions were a result of a cascade started within the fuel, showing the overall importance of fuel cascades over direct fission fragment collisions.

As ions propagate through the material, they produce additional "daughter" ions by knocking atoms from their lattice site. Figure 3.28 displays the probability of each type of "parent" as a function of bubble radius. For nearly all bubble radii, the direct fission fragment contribution remained near 10% due to the low cross-section of small bubbles and low interaction probabilities for low density, large radii bubbles. Due to their small mass and Λ factor, the relative importance of carbon atoms was insignificant. For very small bubble sizes, the majority of all collisions were a result of uranium atoms directly knocking out fission gas atoms. The increase

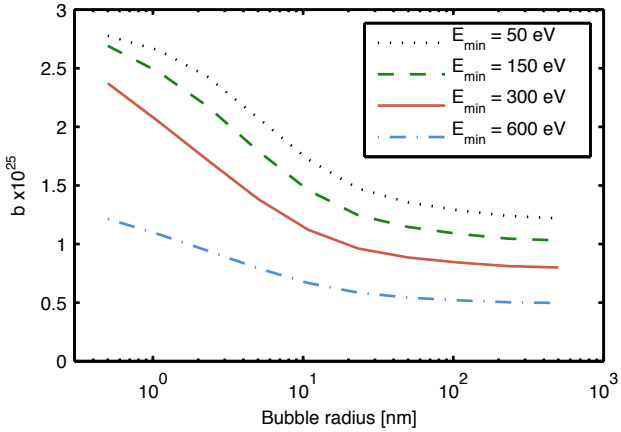

Figure 3.26.: Calculated b for various E_{min} thresholds.

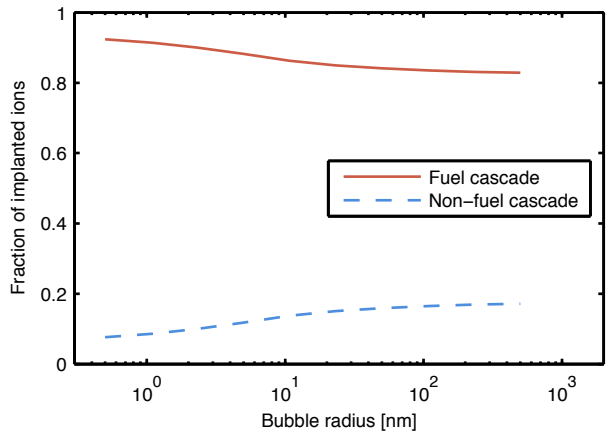

Figure 3.27.: Probability of a direct fission fragment implantation or fuel cascade implantation.

in fission gas parents indicates that as the bubble size enlarged, a knock-on effect occurred, resulting in implanted atoms different than the original struck gas atoms.

As shown in Figure 3.27, the importance of fission fragment collisions were relatively minor compared with the importance of fuel cascades. However, it can be expected that the highly energetic fission fragments create daughter ions with relatively high energies, thus resulting in more energetic and more deeply implanted atoms. This phenomenon can be shown by plotting the re-solution parameter in a 1500 K 5 nm bubble as a function of E_{min}, (Figure 3.29). For low E_{min} energies, fuel cascades have a much higher importance in the total re-solution parameter than fission fragments, similar to what was displayed in Figure 3.28. However at a crossover energy of about 40 keV, fission fragment interactions produced more implanted atoms than fuel cascades.

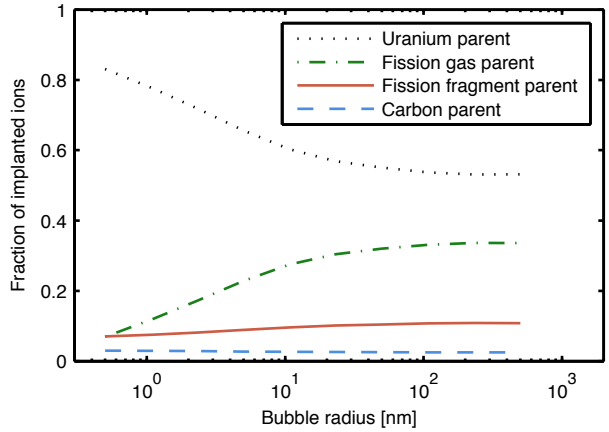

Figure 3.28.: Parent fractions as a function of bubble radius.

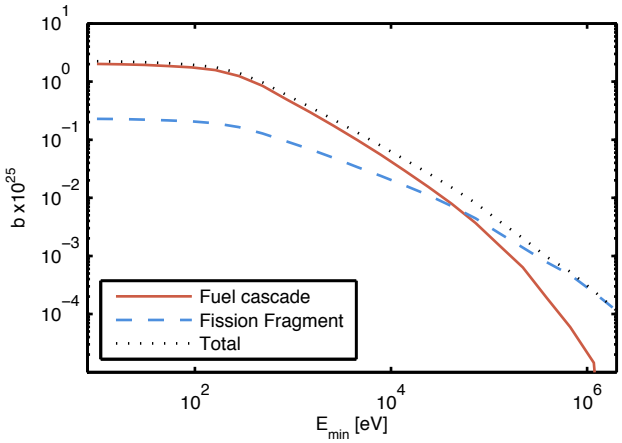

Figure 3.29.: Re-solution in a 5 nm bubble due to fission fragment and fuel cascades as a function of E_{min}.

3.6.0.4. Discussion and conclusions

When comparing the current work to the previous calculations, two results seem to conflict. The first is that for a bubble radius of 5 nm, we found the re-solution parameter to be $1.4 \cdot 10^{-25}$ atoms/(fsn·m^3), an order of magnitude less than the previously calculated value of $b = 3 \cdot 10^{-24}$ atoms/(fsn·m^3) [60, 65]. In addition, the previous re-solution parameter vs. E_{min} results showed the cascade/fission fragment importance cross-over occurring at 5 keV, while our calculations show a cross-over at 50 keV. The reasons for these differences are rooted in differences between the models used in each study and warrant discussion.

By tallying energy losses in a 3DOT simulation, we found the amount of energy dissipated due to electronic losses accounted for about 90% of the original fission fragment energy. In light of this, it can be expected that by ignoring these losses, the fission fragment range, and thus b, will increase by an order of magnitude. This was verified by running 3DOT simulations without

accounting for electronic losses in which we calculated the re-solution parameter for a 5 nm bubble at 1500 K to be $b = 4.8 \cdot 10^{-24}$ atoms/(fsn·m^3), within 50% of the previously calculated value [65].

One of the largest improvements over the previous studies is the use of the ZBL potential for all atoms and energies, as opposed to the Rutherford potential for fission fragment collisions, and the hard-sphere potential for all other collisions. The Rutherford potential is an adequate representation of high energy ion collisions, and in fact is utilized in 3DOT at high ion energies [76]. Conversely, the hard-sphere approximation is adequate for very low ion energies. However, at intermediate energies, neither approximation is appropriate [83].

The hard-sphere potential calculates the scattering angle for use in Equation 3.31 from the geometry of the problem, thus each scatter is independent of the ion's energy. This results in a much higher probability of high angle collisions and ultimately an underestimation of an ion's range. When applied to lattice atoms, the hard-sphere potential ensures that an entering ion will only penetrate a short distance into the bubble. Likewise, gas atoms far from the bubble surface have a low probability of re-solution due to an enhanced probability of large-angle scatter events. With the more physical ZBL potential, the scattering cross-section is inversely proportional to the ion's energy, thus uranium atoms are allowed to penetrate to more realistic depths. In addition, all atoms in the bubble become "available" for re-solution, albeit with a frequency less likely for atoms near the center of the bubble. Since the ZBL potential is well approximated by the Rutherford potential, similar behavior is not reproduced in the highly energetic fission fragments that were originally treated with a purely Coulombic potential. All of this resulted in a higher probability of the less energetic lattice cascades, shifting the fuel cascade contribution to b to higher E_{min} values in Figure 3.29, and increasing the cross-over point to 50 keV.

One final note about the previous studies must be addressed; one of the most interesting results from Ronchi and Elton was a positive slope in the re-solution parameter at high radii and high E_{min} [65]. It should be noted that the value plotted is actually the combination of the product of the re-solution parameter and critical distance, thus the positive slope is heightened by an increasing critical distance as a function of radius. Although similar phenomenon can be achieved with the results from 3DOT, they were not nearly as drastic without the inclusion of the critical distance.

In conclusion, due to the relatively high energy transfer material properties in uranium carbide, fission gas re-solution can be modeled using the homogeneous, atom-by-atom loss model. We found a re-solution parameter that was an order of magnitude lower than previous studies due to the inclusion of electronic ion energy losses in this study. A decrease in the re-solution parameter as a function of radius occurred for low radii, with a nearly constant re-solution parameter for radii above 50 nm. The BCA approximation allowed the computationally cheap analysis of many different types of bubbles, and it was shown that the fundamental BCA assumption is appropriate for use in the simulations presented here. Through comparative studies on the re-solution parameter for various values of implantation energy and atomic density in the bubble, we found that while the re-solution parameter did change, the overall shape did not. The re-solution parameter calculated here can be used in rate-equation type simulations to model fission gas bubble behavior, and ultimately fission gas release.

4. Systems Modeling

In order to model the Helium Purification System (HPS), a STELLA model was created that was able to track gas concentrations throughout a representative HPS. This required a massive network of individual isobaric decay chain models to capture the expansive list of volatile isotopes. This work was initially completed by Wesley Deason, culminating in his Master's Defense in 2013 [2]. His original model was then extended to a more complex fission release model based on MHTGR data (see Section 3.3), with a reduced number of tracked isotopes based on more recent temperature data. These updated values were then passed into the PRA modeling efforts described in Section 5.

4.1. Theory

The identification of fission product transport phenomena present in helium-cooled GFRs is important to understand the behavior of fission gas in the helium purification system. While much of the phenomena identified is common in all helium-cooled reactors (and in general, fission-based nuclear reactors), some of the identified phenomena vary dramatically between reactor types. In cases where details do become important during this discussion, the GFR reactor type using vented fuel will be used as the relevant reactor type.

Note: The term Helium Purification System (HPS) is used interchangeably with Fission Product Vent System (FPVS). Traditionally, the HPS has the primary function of maintaining the coolant chemistry and the FPVS has the primary function of removing and storing volatile fission gases from a purge stream. While these two systems differ in their primary function, they are often combined into a single system due to their similar function and components. For the purposes of this work, HPS and FPVS will refer to the same system that filters volatile fission gases out of the purge stream exiting the fuel directly.

4.1.1. Fission Product Transport Phenomena

4.1.1.1. Fission product generation and decay in fuel

Fission product generation in nuclear reactors is the result of the energetic splitting of uranium and plutonium nuclei in nuclear fuel. The rate at which this occurs can be directly correlated to the reactor's thermal power through the fission product yield fraction. For a 500 MWth reactor using uranium-235 based fuel, assuming 95% of released energy is converted to heat and 200 MeV of energy is released per fission [84], the fission rate is approximately $1.56 \cdot 10^{19}$ fissions per second. The fission product generation rate is the product of the fission rate and the fission production yield curve. Figure 4.1 shows a typical "double-hump" fission yield curve for fission products along isobaric chains. Since two fission products are produced per fission, if the

fission yields shown in Figure 4.1 were summed, the total yield would be 2. As is also seen in Figure 4.1, variation in the fission yield is dependent upon the fissioning nuclide, as well as the incident neutron energy.

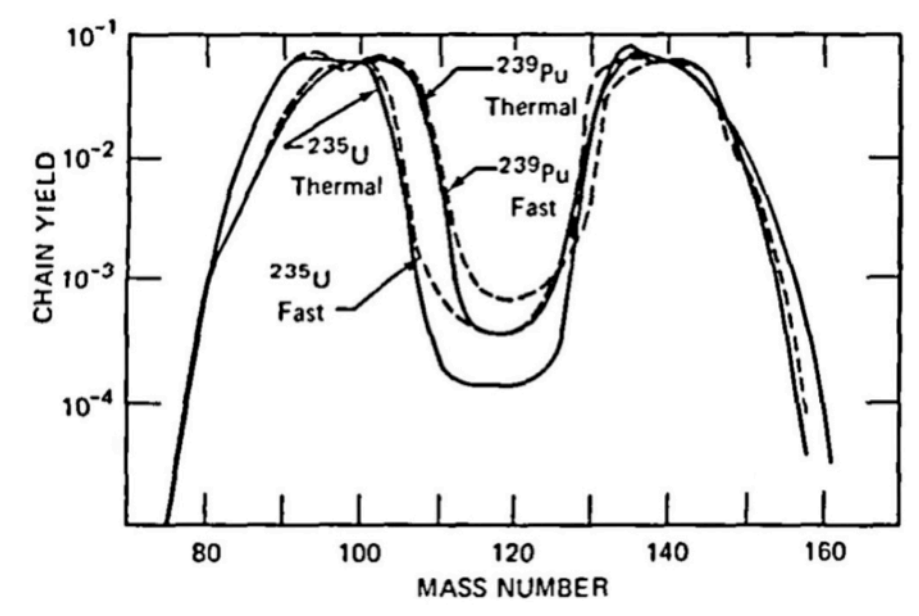

Figure 4.1.: Fission yields by isotope [27].

At the nuclide level, fission product yield can be split into two categories: independent and cumulative fission yield. Independent yield is the yield per fission for a particular nuclide while cumulative is the independent yield of a nuclide summed with the independent yields of its decay precursors. As will be seen later, both values are useful for modeling fission product behavior in fuel. Lastly, neutron absorption can cause values of fission product yield to vary in reactors. While this is significant in reactors with a thermal neutron energy spectrum, reactors with a fast neutron energy spectrum, such as helium-cooled GFRs, are unaffected due to the lower neutron absorption cross-sections present in fission products bombarded with at higher neutron energies [27].

Since fission products are neutron heavy, their most probable action will be β^- decay until the line of stability is reached. Generally, the more neutron heavy a nucleus is, the shorter its half-life and smaller its fission yield. Due to this relation, it is rare to find a decay chain longer than 3 significantly long-lived fission products.

Decay of any radioactive isotope will follow the radioactive decay law:

$$A(t) = \lambda N(t) \tag{4.1}$$

where A is the time-dependent activity of the radionuclide, λ is the decay constant, and N is the time-dependent quantity of the radionuclide. The concentration of a decaying nuclide can reduced to:

$$N(t) = N_0 \exp(-\lambda t) \tag{4.2}$$

It is also possible to solve decay chain systems, though they become increasingly complex with the addition of production and loss terms. The purpose of the present work is to utilize numerical methods to solve very complicated decay chain systems with many production, loss, and decay terms.

4.1.1.2. Volatile fission product chemistry

Nuclear fuel present in its initial form is purely sintered (shaped under heat and pressure) mixtures of uranium and/or plutonium in oxide or carbide form. The oxide or carbide form serves the purpose of increasing the melting temperature of the fuel and making it chemically stable, allowing the nuclear reactor to operate at a higher power. When the reactor is initially brought to power, fission products begin to be generated according to the reactor's fission rate and will begin to form chemical bonds, achieving the lowest energy state possible. This process is described using the Gibb's Free Energy of the chemical system G:

$$G = H - TS \tag{4.3}$$

where H is the enthalpy, S is the entropy, and T is the temperature of the system [85].

4.1.1.3. Fission product diffusion and release in fuel

During the fission reaction, fission products are expelled in opposite directions from the point where they were born. Their kinetic energy is quickly transferred to the surrounding fuel lattice in the form of heat in a process called "fission product recoil". After recoiling, the fission product nuclide is free to interact and move within the fuel lattice. The time rate of change of the concentration of a nuclide C in a spherical fuel particle, can be described in spherical coordinates as,

$$\frac{\partial C}{\partial t} = \frac{1}{r^2}\frac{\partial}{\partial r}\left(D\frac{\partial C}{\partial r}\right) - \lambda C + \dot{B}, \tag{4.4}$$

where D is the diffusion coefficient, or diffusivity, of an isotope through the fuel, and $\dot{B}$ is the birth rate of the given nuclide. Assuming a constant birth rate, time-indepdent properties, and a boundary condition of $C(a) = 0$, where a is the radius of the spherical fuel particle, Equation 4.4 can be rearranged to,

$$R/B(t) = \left[-\frac{4D\pi r^2 \frac{\partial C}{\partial r}}{4/3\pi r^3 B}\right]_{r=a}, \tag{4.5}$$

$$R/B(\infty) = 3\left(\frac{D}{\lambda a^2}\right)^{1/2}\left[coth\left(\frac{\lambda a^2}{D}\right)^{1/2} - \left(\frac{D}{\lambda a^2}\right)^{1/2}\right]. \tag{4.6}$$

Finally, the diffusion coefficient, D, is often defined by two constants,

$$D = D_0 \exp(-Q/RT) \tag{4.7}$$

where D_0 is a correlation factor with units of inverse time and Q is the activation energy for the diffusing species. While the use of the diffusion coefficient is necessary for determining diffusion rates for any medium, geometry, and temperature, it is not commonly used when measuring and inventorying release rates of fission product gases in carbide fuel. In nearly all resources found for this project, information on the release of fission product gases were given in terms of the experimentally derived R/B curve. An example of this is given in Figure 4.2, where the R/B for krypton and xenon are compared between the first Peach Bottom Unit 1 core and Fort St. Vrain. While information is commonly only available for xenon and krypton release rates, iodine and tellurium release rates can be assumed to be released in similar fractions to xenon, bromine and selenium can be assumed to be released similarly to krypton [38].

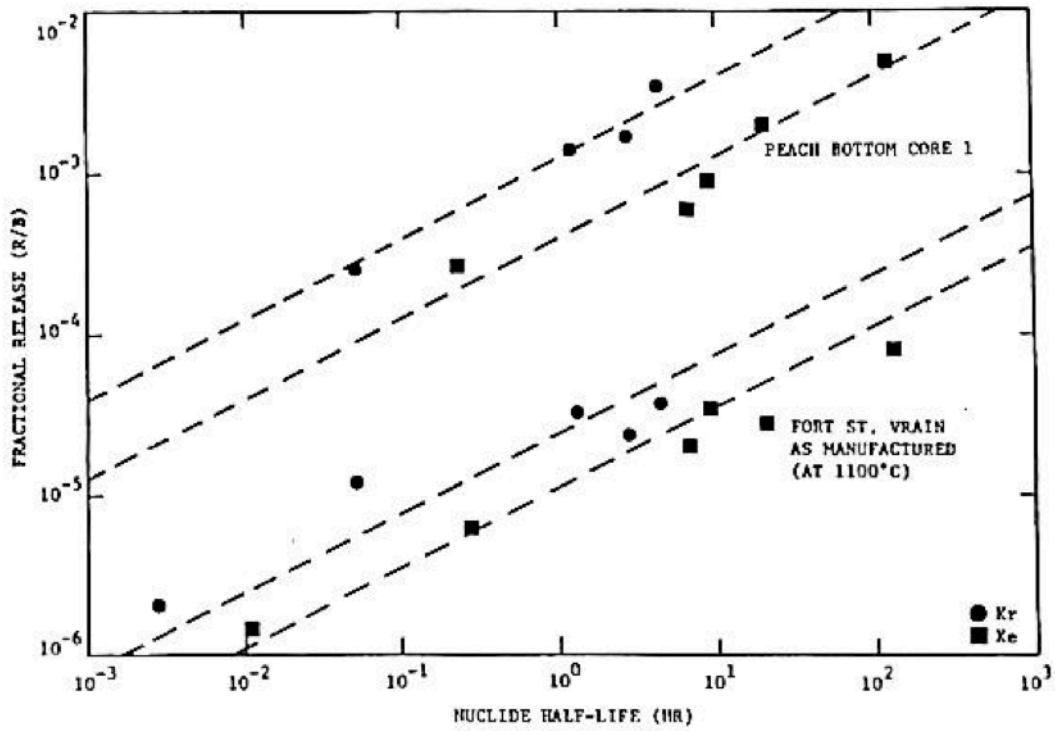

Figure 4.2.: R/B for xenon and krypton fission products released from Peach Bottom and Fort St. Vrain [38].

For release of volatile fission product metals, however, release is studied through the use of the diffusion coefficient. Modeling this diffusive release often become more complicated due to the large effect of chemical bonds on the diffusivity of the element and diffusion data for release of fission product metals from carbide fuel is available but harder to find [86]. Modern sources characterizing fission product release in HTGR fuel will assume that the fission metal is immediately released from the fuel kernel up until the kernel coating. Some data was found characterizing fission metal release from uncoated carbide fuel and in instances where data is hard to come by for fission product release from carbide fuel that samarium can be assumed to

diffuse like barium, that europium can be assumed to diffuse like strontium, and rubidium can be modeled to diffuse like cesium [87, 88].

4.1.1.4. Fission product leakage through non-fuel components

Information on fission product leakage from a system is particularly difficult to determine as it depends upon the specific design and construction of the plant. For helium-cooled GFRs using vented fuel, maintaining a negative pressure on the purge stream relative to its core inlet can minimize or even eliminate leakage of gaseous fission products into the primary coolant. Values of condensable fission product release are even more difficult to predict as the fission products may chemisorb to the inside of the fuel element during diffusive release. Lastly, the rate of fission product release from a fuel element is affected by the material choice of cladding and core components. In more recent designs of helium-cooled GFRs, silicon carbide cladding has been chosen in place of graphite or stainless steel cladding due to its performance under high temperatures and neutron fluences [10].

4.1.1.5. Fission product plate-out

After release from the fuel, fission products will travel throughout the system depending upon its design. In helium-cooled GFRs utilized vented fuel, the fission products will most likely travel in the direction of the fission product purge stream. While most fission products will travel into the HPS to be filtered out and delayed, some may leak out and enter the primary coolant stream. Additionally, there is a probability, albeit, very small, that some of the fission products are not filtered out by the purge stream. What is the journey like for these "missed" fission products?

For non-noble gas fission products released into the primary coolant, their end destination is often "plateout" along the surfaces in the primary system. Fission product plateout is the general term used for the many different deposition processes which occur in the primary coolant, such as chemisorption, adsorption, and condensation onto piping and component surfaces and attachment to plated dust and other contaminants. Plateout is an important issue to study due to its impact on operation and maintenance efforts in the plant, particularly in direct-cycle plants where the turbine contacts the primary coolant directly [89]. Additionally, in the case of an accident, radioactive fission products may "liftoff" and contribute to on and off site doses. The modeling of fission product plateout and liftoff is therefore a quite complicated task due to its dependence upon the local chemical composition of the fission products and the primary coolant surfaces throughout the system. Extensive computer codes have been developed for modeling plateout by German, American, and Japanese researchers but the contribution to plateout related to the presence of dust in the primary coolant remains poorly quantified [90]. Additionally, many theoretical phenomena related to plateout and liftoff in helium-cooled reactors remains to be properly understood, such as plateout effects in complex flows, particulate bounce-off (contacting but not adhering to a surface), surface geometry effects, and liftoff during normal operation effects [91].

Proper modeling of plateout within helium-cooled reactors relies on prior modeling of fission product release into and removal from the primary coolant, as well as determination of its chemical and thermodynamic state. If these values can be quantitatively evaluated, or at-least

assumed, then calculation of fission product plateout in the primary coolant can commence.

4.1.2. Helium purification system design

The Helium Purification System (HPS) plays a crucial role in insuring the safety of GFRs and HTGRs. HPSs used in both reactor types serve the same general purpose: to control the movement of contaminants within the plant. However, an important distinction between vented and non-vented systems is the crucial role of the helium purification system to maintain the primary fission product barrier. Whereas this is accomplished through cladding and fuel particle coatings in non-vented designs, in vented designs, the helium purification system becomes the primary fission product barrier. Traditional HTGRs use particle fuel called TRISO, specifically designed to hold fission products in and prevent their release during the fuel's lifetime. Reactors with vented fuel do not employ these barriers and thus require more robust purification systems to handle the increased radionuclide load. If precautions are taken to ensure that the design and operation of the plant can handle the increased load through sizing, then the components necessary for helium purification are equivalent between vented and non-vented systems.

4.1.2.1. Choice of helium purification system components

The first objective of HPSs used in conjunction with vented fuel is purification of the fission product purge stream. Carrying fission products released directly from the fuel, the purge stream is highly radioactive and of particularly great safety concern. After leaving the fuel region under low pressure conditions (relative to primary coolant pressure) the purge stream has accomplished its primary purpose of removing pressure from the cladding and the fission products present in the purge stream must be removed as soon as possible to reduce any risk of environmental release. With the high level of radioactivity present in the purge stream, it is desirable that traps collect as many fission products as possible, and as close to their source as possible, to reduce the chance for them to be released from the system into the environment. The most commonly used material for fission product sorption is activated charcoal. Activated charcoal is chosen due to its ability to operate at many temperatures (charcoal has a very high melting temperature) and capability for capturing and delaying radioactive noble gases which are famously inert. Additionally, the choice of activated charcoal for use as an adsorbent is attractive due to its cheapness, large capacity, and non-hygroscopic nature (ability to hold water) [92]. For collection of noble gases, activated charcoal uses the principle of adsorption, or collection of a particle on a surface, as opposed to the more commonly known principle of absorption, which is collection of a particle in a volume. For other fission products the charcoal bed can be used to invoke condensation (if the temperature of the bed is below the boiling point of the element) and chemisorption, or the process of sorbing an element by chemical bonding with the carbon or an impregnated element or molecule.

Activated charcoal is capable of capturing all fission products released from the core, though the adsorption characteristics of activated charcoal vary drastically depending upon the temperature and the element of the adsorbed contaminant. For volatile metals and non-metals released from the fuel, decent adsorption can be accomplished at higher temperatures, but for noble gases and halogens, proper adsorption can only be done at lower temperatures [92]. This process is

completely reversible for noble gases and recharging the system is as simple as allowing the temperature of the bed to increase and capturing the released noble gases.

The process of physical adsorption or "physisorption" is properly described by the Langmuir Isotherm relationship,

$$Q = \frac{k_1 p}{1 + k_1 k_2 p}, \tag{4.8}$$

where Q is the number of moles of a gas absorbed per unit volume of charcoal bed, p is the partial pressure of the gas over the bed, and k_1 and k_2 are constants. Q can described graphically by the plot shown in Figure 4.3. At low partial pressures, it can be seen that adsorption follows a linear relationship described by k_1. If there is more than one species of noble gas present in the flow stream, then Q can be described by,

$$Q_A = \frac{(k_1 p)_A}{1 + (k_1 k_2 p)_A + (k_1 k_2 p)_B + ...} \tag{4.9}$$

where Q is in units of moles per [cm^3], T is temperature in [K], and p is partial pressure in units of [mm Hg]. Q can then be used to define the adsorption coefficient as,

$$\phi = \frac{22400 \cdot 760 \cdot QT}{273 \cdot p} \tag{4.10}$$

where ϕ is in terms of mols per cm^3 of charcoal bed over mols per cm^3 of gas phase.

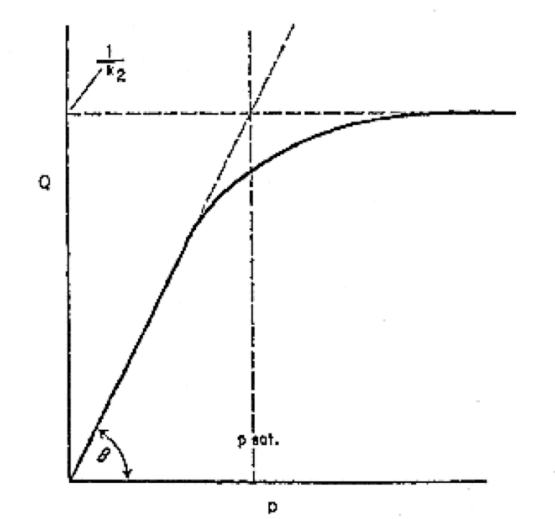

Figure 4.3.: Graphical representation of the Langmuir Isotherm [92].

When evaluating these parameters, it may be necessary to consider the effect of decay heating due to the decay of the adsorbed nuclides. Increased temperature of the charcoal bed, particularly in regions geometrically distant from the cooling surface, will decrease its adsorptive capability and affect the volume needed for proper contaminant collection.

To understand the application of the adsorption coefficient in realistic scenarios, it is necessary to define several modes of operation for the charcoal bed for noble gas contaminants. When the size of the charcoal bed is appreciably small or the temperature of the bed is appreciably high, the noble gas contaminants will "breakthrough" the charcoal bed, causing a reduction of the purification stream activity. This phenomena can be characterized by an average "delay time" in which newer incoming species will replace older adsorbed species. At low partial pressures, as is normally found in helium purification streams [93], $Q = k_1 p$ and the delay time can be calculated by,

$$t = \frac{V(\phi + \alpha)}{F} \tag{4.11}$$

where V is the volume of the charcoal bed, α is a voidage fraction (usually negligible), and F is the volumetric flow rate. This time can be input into the time dependent radionuclide equation (Equation 4.2) to calculate the exiting nuclide concentration of the bed.

Alternatively, when the size of the charcoal bed is appreciably large or the temperature is appreciably small, the charcoal bed can collect the contaminant for a length of time which exceeds the time it takes for breakthrough to occur. Obtaining this point usually requires temperatures only obtainable through cooling by liquid nitrogen, which is particularly energy intensive. Because of this, it is economical to use delay beds to reduce the activity of the purification stream, thus reducing the quantity of long lived noble gases which must be collected by the HPS. Additional constraints on the cold bed design will be the amount of radioactive source term desired on site and the economy and risk of recharging of the system at regular intervals. Determination of these source term limits will depend upon the risk of release and regulatory standards imposed on the location of the cold side of the HPS.

4.1.2.2. Helium purification system component layout

An ideal HPS would be able to collect all fission product contaminants from the helium purge stream in one trap and keep them from leaving containment in the case of an accident scenario. Unfortunately, the decay heat makes maintaining the traps at low temperatures a difficult task. Thus, it is necessary to split the system into at least two regions. In its simplest form, a hot region used for the collection of volatile metals and non-metals, and a cold region is used for collection of halogens and noble gases. This design configuration attempts to remove as many contaminants as possible before reaching the cold region of the HPS in order to reduce its required cooling load.

The first place to start when considering proper placement of the components in the helium purification is historical design. While Peach Bottom and the GCFR used in-element charcoal traps for their designs, the EM^2 considers placing the first fission product trap outside the core. There are benefits and drawbacks to both location choices and it is beneficial to consider both options and their impact on a specific system.

The first benefit to placing a trap in the core is that it allows the to be cooled by the primary coolant, rather than through a separate cooling system, as would be required in a core-external fission product trap. A core-internal fission product trap also negatively affects the size of the

core and thus the cost of the reactor vessel and fuel elements and the neutronic performance of the core.

However, placing the first fission product trap outside of the core allows the trap to be cooled to lower temperatures than the primary coolant, increasing the adsorption capability of the charcoal. Additionally, placing the first fission product trap outside the coolant allows the trap to be larger and more complex. Drawbacks to the core-external trap are the additional cooling burden which could become of issue during an accident scenario, as well as the increased chance for radioactive release as a consequence of almost all the volatile radioactive material produced being carried outside the core through piping and valves.

One compromise could include placement of the first fission product trap as a manifold or piece of the pressure vessel, limiting the amount of radioactivity carried into primary containment. If arranged properly, the primary coolant could be used for cooling during accident scenarios, removing the risk of improper cooling. Additionally, integrating the first fission product trap into the pressure vessel would remove the added cost to the core, as well as the neutronic effect of a core-internal fission product trap. There will be an increased cost to the pressure vessel, but if it was possible to integrate a large enough trap within, then cost may be able to be picked up from other parts of the system.

4.1.2.3. Removal of tritium and other contaminants

Though it is not discussed in depth in this thesis, another contaminant produced in the core is radioactive tritium. In GFRs, tritium is produced most commonly through the phenomenon of tertiary fission. In HTGRs, tritium is also produced through the thermal absorption of a neutron in helium-3, however this is not expected in GFRs due to the fast neutron spectrum. Tritium can be removed from the system through two methods, cold charcoal adsorption or a oxidizer/molecular sieve combination. Since the use of an oxidizer/molecular sieve combination does not require cooling to subfreezing conditions, it is the preferred method for tritium capture. Because of its radioactivity, tritiated water collected by the molecular sieve must be removed at a regular interval to prevent buildup of the source term outside of the primary containment. It is also necessary to strike a balance with the quantities of other contaminant present in the primary coolant. In the NGNP Coolant Chemistry Study [21], this balance is considered in appreciable depth, however it will not be considered in the present work.

4.2. System Model

To begin the safety and feasibility analysis of vented fuel systems, it is necessary to build a digitized system model through which the transport and diffusion of fission products could be understood under various scenarios and system configurations. Options to accomplish the goal included building a model from the ground up using a computer programming language like FORTRAN and C++ or using a chemical engineering program such as ASPEN which is capable of modeling steady state chemical systems to aid in understanding the chemical reactions which may occur in the system. However, after discussion and consideration within fellow researchers, it was decided to use the system modeling program STELLA (Systems Thinking for Education

and Research) [94]. STELLA is currently used in the OSU NERHP department to study the movement of fission products through environmental systems, which led to its investigation for use in this project. Due to its graphical interface the program can seem to be overly simplistic, leading to skepticism about it capabilities, but the first test model laid these fears to rest as the program performed superbly.

STELLA was first tested to see if it was capable of solving the many coupled differential equations that describe the transport of volatile elements through a complex vented fuel system. Its graphical interface allowed for the quick construction of a working system and due to its flexibility of input types, it showed to be capable of modeling all components of a vented fuel system. The first system to be put into STELLA was the Peach Bottom model for krypton-85 production and transport through the reactor plant, shown in Figure 4.4. The model output matched closely the numbers provided in the Peach Bottom Final Hazards Safety Analysis report [7] and allowed for tracking of the radionuclide from birth in the fuel or delay beds to decay. The experience gained in building the test model helped in understanding the preparations necessary before a representative vented fuel system could be attempted.

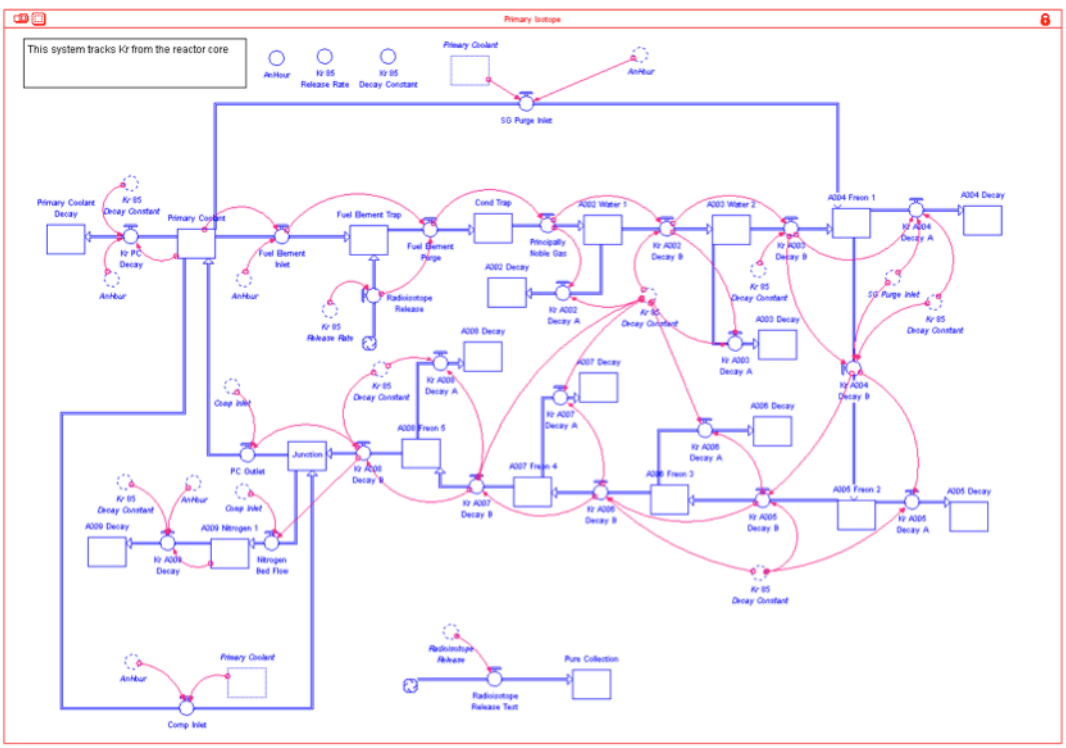

Figure 4.4.: STELLA model for krypton-85 transport and decay. Kr-85 generation is purely due to fission purge flow stream concentration and does not include Kr-85m decay.

4.2.1. Selection of radionuclides

In determining a reasonable scope for the fission product transport modeling, it was necessary to understand what was being modeled. Many fission products are non-volatile and will never leave the fuel in significant quantities. Alternatively, of those fission products which are volatile, some may be produced in insignificant quantities or activities.

The first step for determining the model scope was the selection of which fission product elements (and eventually the isotopes of those elements) should be considered for analysis. This is a particularly important step, as each element contains its fair share of highly radioactive isotopes. After review of papers and reports discussing the experimental release of radionuclides from coated and uncoated uranium carbide fuel particles, it was decided that the first distinction between a volatile and non-volatile element would be its boiling temperature. This conservative choice insures that every volatile element which could possibly be gaseous within the fuel is considered. The cutoff temperature for this choice was decided upon to be 1500° C. Next, a review of the literature provided a list of elements whose volatility increased due to the formation of carbides or compounds with uranium [95]. Both of these conditions yielded a list of elements which would be assumed to be released during the operation of a reactor utilizing vented fuel. Elements not chosen in this selection process are assumed to be non-volatile and not leave the fuel in any substantial amount. The list of volatile elements chosen is shown in Table 4.1.

Table 4.1.: Selected elements

Element	Type	Boiling Temperature [K]	Forms carbide?
Tritium (H)	Nonmetal	-252.87	No
Arsenic (As)	Metalloid	602.8	No
Selenium (Se)	Nonmetal	684.8	No
Bromine (Br)	Halogen	58.7	No
Krypton (Kr)	Noble Gas	-243.8	No
Rubidium (Rb)	Alkali Metal	687.8	No
Strontium (Sr)	Alkaline Earth Metal	1382	Yes
Cadmium (Cd)	Transition Metal	766.8	No
Tellurium (Te)	Metalloid	988	No
Iodine (I)	Halogen	184.4	No
Xenon (Xe)	Noble Gas	-108	No
Cesium (Cs)	Alkali Metal	670.8	No
Barium (Ba)	Alkaline Earth Metal	1897	Yes
Samarium (Sm)	Inner Transition Metal	1794	Yes
Europium (Eu)	Inner Transition Metal	1529	Yes

Isotopes of these elements which were stable or had a half-life greater than ten minutes were selected to be tracked. Previously, a half-life of one hour was used as a cutoff, but after application of the R/B curve shown in Figure 4.5, it became apparent that short-lived nuclides between ten minute and one hour half-lives were released in low, but significant, activity quantities. To evaluate the 30 year accumulation of fission products in the system, independent of reactor power, the concentration of radioactive isotopes N_i were determined using,

$$N_i = (R/B)\frac{\gamma_i}{\lambda_i}[1 - \exp(-\lambda_i t_{end})] \tag{4.12}$$

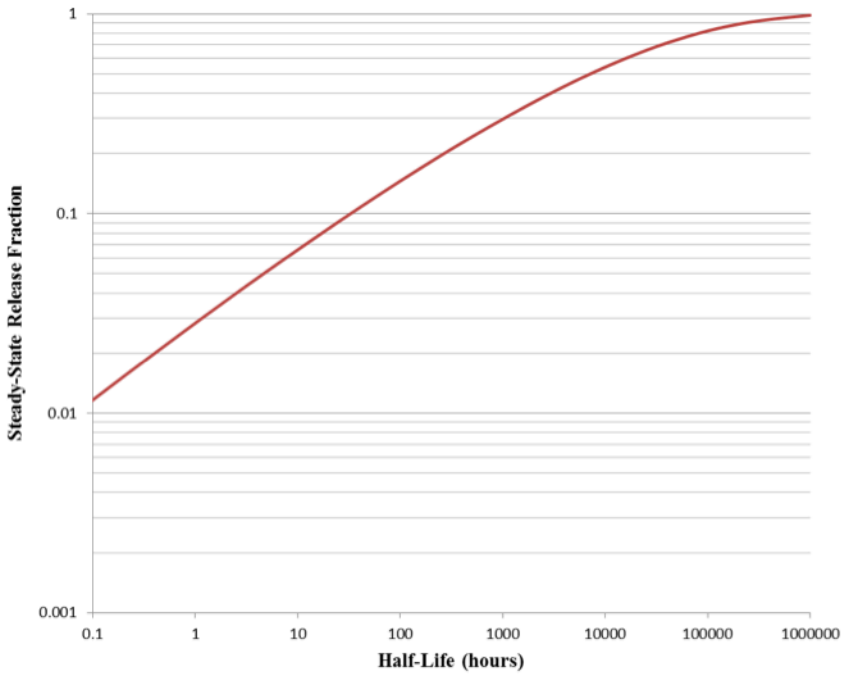

Figure 4.5.: Peach Bottom HTGR design release curve for volatile radioactive fission products [7].

where R/B is the steady state release fraction from Figure 4.5, γ_i is the 500 keV plutonium/uranium average cumulative fission yield, and $t_{end} = 30$ years. The concentration of stable isotopes, N_j, can be calculated from,

$$N_j = \gamma_j t_{end} \tag{4.13}$$

The 500 keV plutonium/uranium average cumulative fission yield was chosen for this calculation over the equivalent independent yield in order to capture the importance of short-lived precursors. After applying Equations 4.12 and 4.13, two lists were made which ranked accumulated mass after thirty years and accumulated activity after thirty years by percentage. The top 99% of both lists were chosen, producing a much more compact picture of volatile fission product production in a reactor. Lastly, the non-volatile daughters of each isobaric chain were added until a stable nuclide was reached, producing a complete picture of each isobaric decay chain and encompassing any production of radioactive non-volatiles in the system model.

A design yield for each fission product nuclide was also calculated. This design yield is either the 500 keV plutonium-239/uranium-235 average cumulative yield or the 500 keV plutonium-239/uranium-235 average independent yield. Nuclides which lie at the beginning of their isobaric chain use their associated cumulative yield while nuclides which lie after use their individual yield. Additionally, yields for intermediate nuclides were added to the yields of their daughters to insure all fission product production pathways are covered. The final set of nuclides chosen for tracking totaled at 88 nuclides contained within 39 isobaric decay chains, and is shown in Table 4.2.

Table 4.2.: Final Set of Tracked Nuclides for Study in the Representative Radionuclide Removal System Model

Number	Nuclide	Z	A	Half-life [h]	Design Yield	Yield Type	Branch
1	Selenium - 80	34	80	stable	1.342E-03	Cumulative	1
2	Bromine - 81	35	81	stable	1.849E-03	Cumulative	1
3	Selenium - 82	34	82	stable	2.789E-03	Cumulative	1
4	Krypton - 83	36	83	stable	4.460E-03	Cumulative	1
5	Krypton - 84	36	84	stable	7.647E-03	Cumulative	1
6	Krypton - 85m	36	85	4.480E+00	9.776E-03	Cumulative	0.214
7	Krypton - 85	36	85	9.432E+04	6.280E-05	Independent	1
8	Rubidium - 85	37	85	stable	5.770E-07	Independent	1
9	Krypton - 86	36	86	stable	1.368E-02	Cumulative	1
10	Krypton - 87	36	87	1.270E+00	1.790E-02	Cumulative	1
11	Rubidium - 87	37	87	stable	3.940E-05	Independent	1
12	Krypton - 88	36	88	2.840E+00	1.368E-02	Cumulative	1
13	Rubidium - 88	37	88	2.950E-01	4.815E-04	Independent	1
14	Strontium - 88	38	88	stable	1.880E-06	Independent	1
15	Rubidium - 89	37	89	2.600E-01	3.047E-02	Cumulative	1
16	Strontium - 89	38	89	1.215E+03	2.940E-05	Independent	1
17	Yttrium - 89	39	89	stable	n/a	n/a	1
18	Strontium - 90	38	90	2.525E+05	3.757E-02	Cumulative	1
19	Yttrium - 90m	39	90	3.190E+00	n/a	n/a	1
20	Yttrium - 90	39	90	6.406E+01	n/a	n/a	1
21	Zirconium - 90	40	90	stable	n/a	n/a	1
22	Strontium - 91	38	91	9.500E+00	4.124E-02	Cumulative	1
23	Yttrium - 91m	39	91	8.283E-01	n/a	n/a	1
24	Yttrium - 91	39	91	1.404E+03	n/a	n/a	1
25	Zirconium - 91	40	91	stable	n/a	n/a	1
26	Strontium - 92	38	92	2.610E+00	4.430E-02	Cumulative	1
27	Yttrium - 92	39	92	3.540E+00	n/a	n/a	1
28	Zirconium - 92	40	92	stable	n/a	n/a	1
29	Cadmium - 111	48	111	stable	1.998E-03	Cumulative	1
30	Tellurium - 126	52	126	stable	1.822E-03	Cumulative	1
31	Tellurium - 127m	52	127	2.544E+03	6.457E-04	Cumulative	0.976
32	Tellurium - 127	52	127	9.400E+00	3.000E-09	Independent	1
33	Iodine - 127	53	127	stable	0.000E+00	Independent	1
34	Tellurium - 128	52	128	stable	6.917E-03	Cumulative	1
35	Tellurium - 129m	52	129	8.064E+02	1.899E-03	Cumulative	0.63
36	Tellurium - 129	52	129	1.160E+00	7.110E-07	Independent	1
37	Iodine - 129	53	129	stable	1.140E-12	Independent	1
38	Tellurium - 130	52	130	stable	2.123E-02	Cumulative	1
39	Tellurium - 131m	52	131	3.264E+01	6.722E-03	Cumulative	0.222
40	Tellurium - 131	52	131	4.200E-01	1.643E-03	Independent	1
41	Iodine - 131	53	131	1.926E+02	1.059E-04	Independent	1
42	Xenon - 131	54	131	stable	1.820E-07	Ind. + Metastable	1
43	Tellurium - 132	52	132	7.680E+01	4.907E-02	Cumulative	1
44	Iodine - 132	53	132	2.280E+00	8.650E-04	Ind. + Metastable	1
45	Xenon - 132	54	132	stable	7.200E-05	Ind. + Metastable	1
46	Tellurium - 133m	52	133	9.200E-01	3.206E-02	Cumulative	0.175
47	Tellurium - 133	52	133	2.100E-01	1.922E-02	Independent	1
48	Iodine - 133	53	133	2.080E+01	8.572E-03	Ind. + Metastable	1
49	Xenon - 133m	54	133	5.256E+01	2.544E-04	Independent	1

Table 4.2.: Final Set of Tracked Nuclides for Study in the Representative Radionuclide Removal System Model

Number	Nuclide	Z	A	Half-life [h]	Design Yield	Yield Type	Branch
50	Xenon - 133	54	133	1.258E+02	8.650E-05	Independent	1
51	Cesium - 133	55	133	stable	1.090E-07	Independent	1
52	Tellurium - 134	52	134	7.000E-01	5.678E-02	Cumulative	1
53	Iodine - 134	53	134	8.800E-01	1.704E-02	Ind. + Metastable	1
54	Xenon - 134	54	134	stable	5.273E-04	Ind. + Metastable	1
55	Iodine - 135	53	135	6.570E+00	6.189E-02	Cumulative	1
56	Xenon - 135m	54	135	2.500E-01	5.366E-03	Independent	0.994
57	Xenon - 135	54	135	9.100E+00	3.668E-03	Independent	1
58	Cesium - 135	55	135	stable	3.180E-05	Independent	1
59	Xenon - 136	54	136	stable	6.577E-02	Cumulative	1
60	Cesium - 137	55	137	2.636E+05	6.403E-02	Cumulative	1
61	Barium - 137	56	137	stable	2.800E-05	Ind. + Metastable	1
62	Xenon - 138	54	138	2.350E-01	5.361E-02	Cumulative	1
63	Cesium - 138	55	138	5.400E-01	9.400E-03	Ind. + Metastable	1
64	Barium - 138	56	138	stable	1.010E-03	Ind. + Metastable	1
65	Barium - 139	56	139	1.396E+00	5.977E-02	Cumulative	1
66	Lanthanum - 139	57	139	stable	n/a	n/a	1
67	Barium - 140	56	140	3.060E+02	5.650E-02	Cumulative	1
68	Lanthanum - 140	57	140	4.027E+01	n/a	n/a	1
69	Cerium - 140	58	140	stable	n/a	n/a	1
70	Barium - 141	56	141	3.100E-01	5.511E-02	Cumulative	1
71	Lanthanum - 141	57	141	3.900E+00	n/a	n/a	1
72	Cerium - 141	58	141	7.800E+02	n/a	n/a	1
73	Praseodymium - 141	59	141	stable	n/a	n/a	1
74	Barium - 142	56	142	1.800E-01	4.995E-02	Cumulative	1
75	Lanthanum - 142	57	142	1.540E+00	n/a	n/a	1
76	Cerium - 142	58	142	stable	n/a	n/a	1
77	Samarium - 147	62	147	stable	2.065E-02	Cumulative	1
78	Samarium - 149	62	149	stable	1.139E-02	Cumulative	1
79	Samarium - 151	62	151	7.889E+05	5.985E-03	Cumulative	1
80	Europium - 151	63	151	stable	3.870E-11	Independent	1
81	Samarium - 152	62	152	stable	4.488E-03	Cumulative	1
82	Samarium - 153	62	153	4.627E+01	2.964E-03	Cumulative	1
83	Europium - 153	63	153	stable	2.250E-08	Independent	1
84	Samarium - 154	62	154	stable	1.698E-03	Cumulative	1
85	Europium - 155	63	155	4.164E+04	1.241E-03	Cumulative	1
86	Gadolinium - 155	64	155	stable	n/a	n/a	1
87	Europium - 156	63	156	3.648E+02	8.750E-04	Cumulative	1
88	Gadolinium - 156	64	156	stable	n/a	n/a	1

4.2.2. Evaluation of the chemical state of fission products

Once all nuclides and elements were chosen, the next step was to determine the chemical form of the volatile nuclides when leaving the fuel and when produced throughout the system. Due to effects in the way a nuclide interacts with filters and components throughout the system it is important to track its chemical state. The fuel type in this calculation was assumed to be a U/Pu Carbide.

There are a few methods by which the resulting chemical makeup of the fission products can be determined. The first and most complete method is to conduct an experimental study where vented carbide fuel is analyzed and the chemical makeup of release fission products is tracked. Such an experiment is unfortunately outside the scope of the current work, thus the solution must be found theoretically. To determine the theoretical equilibrium chemical composition requires knowledge of the concentrations of each element in the fuel and all associated chemical reactions which are possible. Then, using the specific thermodynamic properties of each chemical reaction, the system of equations related to each chemical reaction can be solved. This solution is equivalent to the system configuration with the lowest minimum Gibb's free energy, as discussed within the Theory section. It is possible to do hand calculations for 2 or 3 different chemical reactions but larger, more accurate calculations requires much more complicated modeling. Additionally, accessing thermodynamic properties for reactions between rare earth metals is particularly difficult and requires an extensive library to handle all reactions considered. There are a few programs that have been used in the past to conduct these calculations, specifically HSC chemistry and SOLGASMIX-PV [96, 97]. HSC Chemistry provides the benefit of an extensive thermodynamic library for conducting these calculations while SOLGASMIX-PV requires the thermodynamic properties to be known.

Though no analysis has been found which examines the transient inventory of chemicals in vented carbide fuel, some research has been conducted on non-vented carbides. For example, in research conducted at the Bhabha Atomic Research Centre in India, SOLGASMIX-PV has been used to calculate the transient equilibrium buildup of fission products in non-vented carbide fuels [96]. While the goal of the paper was to determine if fission products would cause the formation of a metallic fuel phase by forming carbides, the analysis proved useful for the present work. By using the cumulative fission yield, the R/B curve shown in Figure 4.5, and the results from the previously cited work, a design chemical form was determined for each volatile nuclide. Table 4.3 shows the design chemical form of each fission product element before interaction with the first fission product trap in the system. While a fission product may bond easily with others in the fuel, after the first fission product trap, many will no longer be present in the helium purge stream. If an element is produced anywhere in the system due to radioactive decay, it is assumed to be in its elemental form. The chemical forms shown in Table 4.3 are assumed to be sufficient for the present analysis. If it proves necessary, HSC Chemistry or a similar program can be utilized in the future to perform more refined calculations on the chemical makeup of fission products in uranium carbide fuel.

4.2.3. Discussion of an appropriate model

Once the number and arrangement of nuclides and their chemical configuration is identified, it is now possible to build a system model to analyze them. The goals of the model are to be able to track the production, decay, and accumulation of each fission product decay chain throughout the system. Due to the dependence of each nuclide on the behavior of its decay precursor, decay chains must be modeled together. By examining the set of tracked nuclides shown in Table 4.2 it can be seen that the longest decay chain to be modeled is the 133 isobar, with 6 nuclides, meaning the model must be able to handle a decay chain 6 nuclides long. Additionally, some of the metastable states present in krypton, tellurium, and xenon have branching ratios, meaning

Table 4.3.: Design chemical forms for fission products interacting within the fuel, HPS, and elsewhere in the system

Volatile	Element	Z	Vented Yield Fraction	Interaction before first trap
Yes	Selenium	34	0.52%	BaSe
Yes	Bromine	35	0.23%	CsBr
Yes	Krypton	36	3.68%	Elemental
Yes	Rubidium	37	3.64%	Elemental
Yes	Strontium	38	9.16%	SrC2
No	Yttrium	39	0.00%	n/a
No	Zirconium	40	0.00%	n/a
Yes	Cadmium	48	0.25%	Elemental
Yes	Tellurium	52	5.31%	BaTe
Yes	Iodine	53	4.45%	CsI
Yes	Xenon	54	22.47%	Elemental
Yes	Cesium	55	25.20%	Elemental
Yes	Barium	56	18.18%	BaC2
No	Lanthanum	57	0.00%	n/a
No	Cerium	58	0.00%	n/a
No	Praseodymium	59	0.00%	n/a
Yes	Samarium	62	5.62%	SmC2
Yes	Europium	63	1.27%	EuC2
No	Gadolinium	64	0.00%	n/a

that when the metastable state undergoes decay, there is a possibility that it will decay though beta emission rather than isomeric transition. In this process, the decay effectively skips the next nuclide in the chain. It is desired that the model reflect this decay phenomena appropriately as well.

Lastly, it is necessary for the model to be capable of simulating the many various configurations which are possible for vented and non-vented systems. It must contain features for analyzing phenomena associated with plateout, decay, trapping, noble gas delay, and system recirculation. To model this, the arrangement shown in Figure 4.6 was constructed.

Starting from left to right, fission products enter the purge stream where they are given the option for plateout, leak to the cold leg of the primary coolant (compressor to reactor), or continue to the first fission product trap. Inlets to the purge stream are from the fuel, the cold leg of the primary coolant, and from the nuclide decay precursor. The reason for connecting the inlet for the purge stream to the primary coolant cold leg is that the purge stream begins in the reactor, which occurs at the end of the cold leg. When plating out in the "In-Core Purge Stream", fission products will collect and decay according to their decay constant. Any decays from the plateout will reenter the In-Core Purge Stream through the next nuclide's model, where its next destination will be decided based on the parameters of that nuclide. This action is similar to all decays occurring in the STELLA model. Additionally, no decay is assumed to occur due to residence time in the purge stream, nor any of the other regions of the HPS other than the delay beds, which purposely cause their contents to decay.

Next, the purge stream carries fission products to the First Fission Product Trap. To model

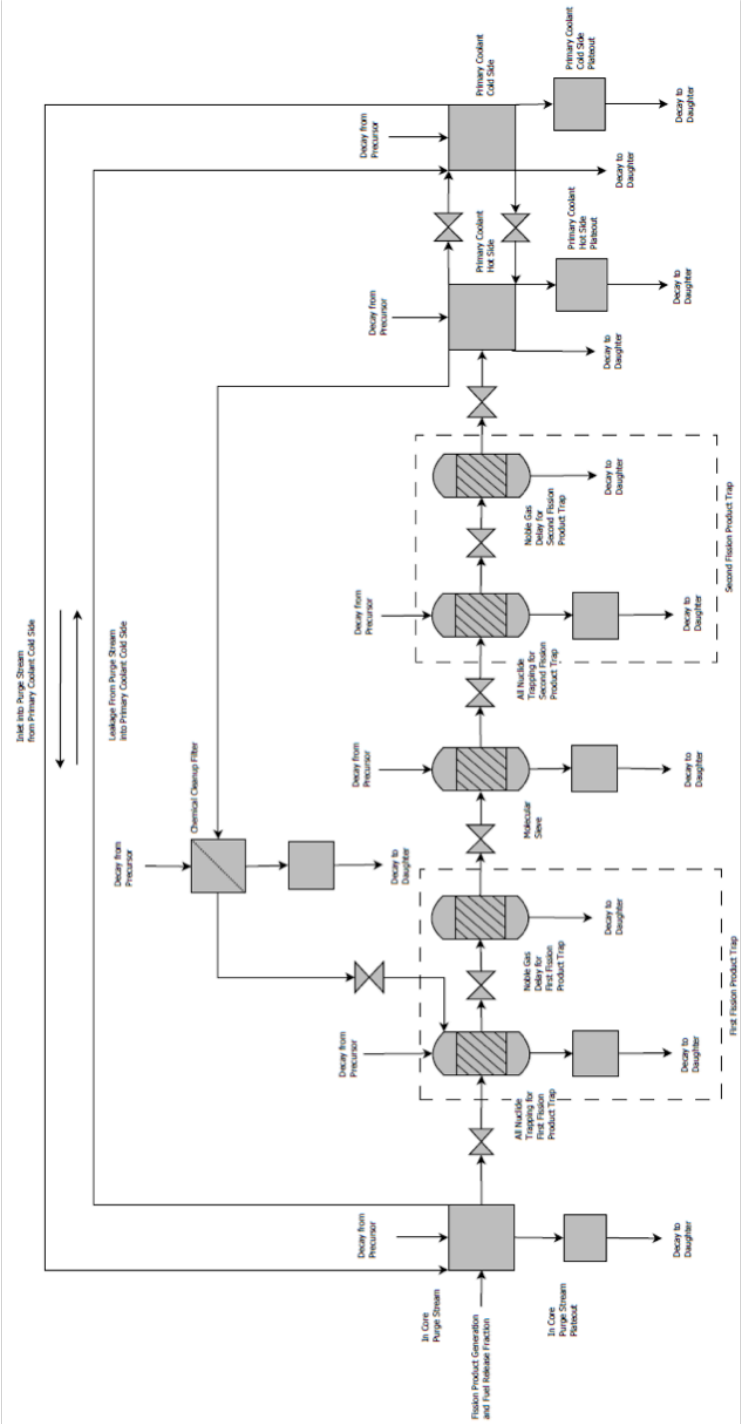

Figure 4.6.: Test configuration for the STELLA model

the trap properly, it has been split into two sections: a trapping section and a delay section. The trapping section removes a fraction of the incoming contaminant while the delay section allows for the simulation of a decay time for a radioactive nuclide. Like plateout in the In-Core Purge Stream, trapping collects the trapped fission products and allows them to decay to their daughter.

Other than the Second Fission Product Trap, which mirrors the capabilities of the First Fission Product Trap exactly, the only component left in the purification stream is the Molecular Sieve. The reason for its placement here is to maintain flexibility in modeling a HPS or a FPVS. In older designs, the HPS was responsible for cleanup of the primary coolant as well as collection of gaseous fission products [7]. More recently, the EM^2 design includes a separate FPVS with the sole purpose of collecting the gaseous fission products from a dedicated purge stream [98]. As discussed previously, the Molecular Sieve functions as a catch for oxidized carbon monoxide and oxidized hydrogen (likely tritium), and will be absent in a dedicated FPVS. Finally, it can also be used to simulate a third fission product trap for the purification stream, though it lacks the delay bed feature of the other two traps.

After leaving the Second Fission Product Trap, any fission products remaining in the purification stream will be dumped into the Primary Coolant Hot Leg (reactor to compressor). Entering the Primary Coolant Hot Leg, the fission product may have many different destinations depending upon its element type. The inlets to the Primary Coolant Hot Leg are from precursor decay, from the HPS, or from the Primary Coolant Cold Leg. The outlets are the Chemical Cleanup system, nuclide plateout, and nuclide decay, with any remainder being sent into the Primary Coolant Cold Leg. The connection for the Chemical Cleanup system was placed in the Primary Coolant Hot Leg due to its intake being present in the compressor (or the end of the hot leg) on the Peach Bottom Unit 1 reactor [7]. In comparison to the hot leg, the Primary Coolant Cold Leg features nearly the same inlets and outlets, with differences attributed to the intake for the In-Core Purge Stream and the lack of an input from the HPS.

The last feature in the model is the Chemical Cleanup system. In Peach Bottom, the Chemical Cleanup system was essentially just an oxidizer, molecular sieve and filter, though in the model, it can be used for any purpose. One possibility is its use to test placement of other traps, including the cold charcoal trap, outside of the main purification stream. Within the EM^2 desgin, the Chemical Cleanup system will be absent.

4.2.4. Analytical treatment of vented fuel and HPS components

A STELLA model is constructed through the graphical connection of variables, called “convertors”. Convertors can be assigned a numerical value by the user, or be assigned a value based on other components of the model.

In Figure 4.7, the convertor, “Nuclide Generation Rate”, can be seen to depend on the two convertors “Fission Rate units of fissions per hour” and “Design Yield Fraction”. Once STELLA is given the dependencies for Nuclide Generation Rate, it will not let the user run the model until the relation is defined, as shown in Figure 4.8. The convertor can now be used in other parts of the model to define flows, or other convertors. An example of this application is shown in Figure 4.9, where convertors are used to define “flows” and their connections to “stocks”. It is possible to directly connect components directly, however, the use of convertors allows for cleaner, more organized models. In the next few subsections, the basis for and application of

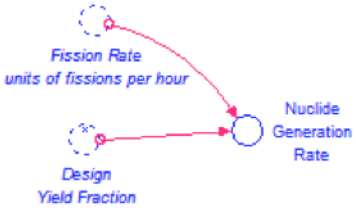

Figure 4.7.: Example of Converter Connection in STELLA model.

recurring or otherwise significant phenomena applied in the model will be discussed.

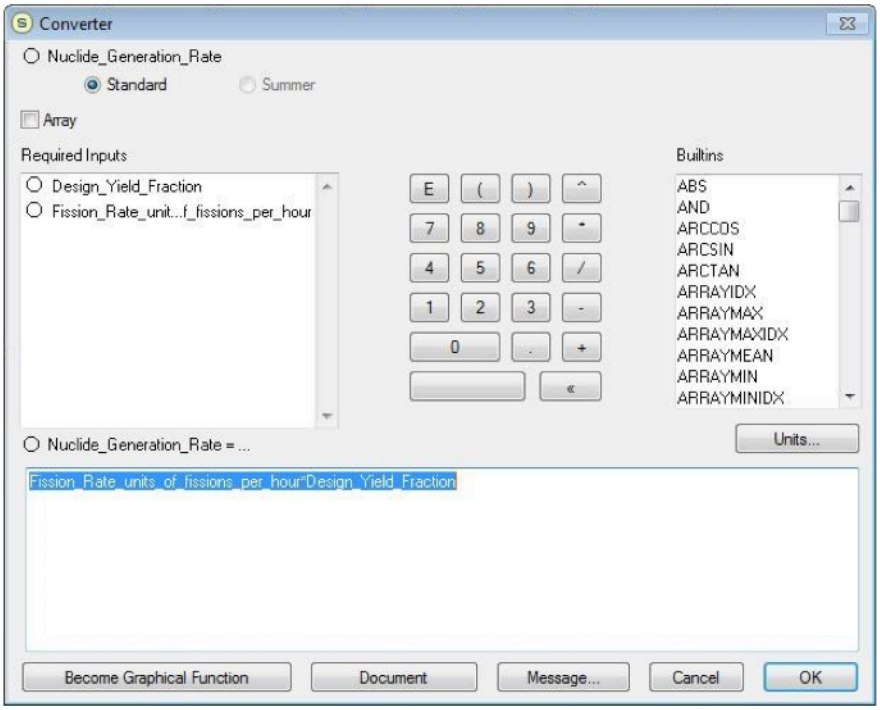

Figure 4.8.: Defining Convertor Relationships in STELLA model.

4.2.4.1. Release of fission products from fuel

The birth rate of a given isotope $\dot{B}_i$ can be calculated from the fission rate, $\dot{F}$ by,

$$\dot{B}_i = \dot{F}\gamma_i, \tag{4.14}$$

γ_i is the isotopic specific fission yield. After generation in fuel, the volatile nuclide will do one of two things. Either leave the fuel due to diffusion or decay to its daughter. Easily enough, both of these phenomena are controlled by the R/B of the nuclide in the fuel. Assuming that the

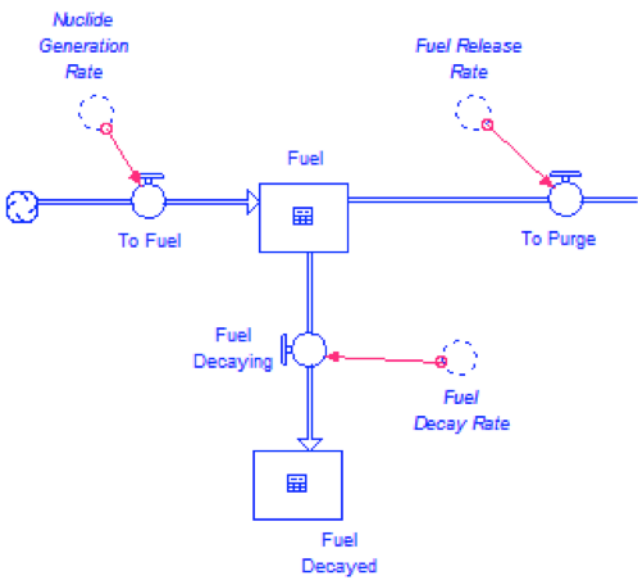

Figure 4.9.: Use of Convertors to Define "Flows" in STELLA Model.

release rate has reached a steady state value and is constant over burnup, then any nuclide which is not released, must decay to its daughter. Using any R/B desired, the release rate $\dot{R}_i$, or decay rate $\dot{D}_i$ in the fuel can be described by,

$$\dot{R}_i = \dot{B}_i \cdot (R/B), \tag{4.15}$$

$$\dot{D}_i = \dot{B}_i(1 - R/B). \tag{4.16}$$

4.2.4.2. Purge stream trapping, plateout, and leakage fractions

After leaving the fuel, the fission product will enter the purge stream and begin to be carried through the HPS. Along the way toward an eventual release into the primary coolant, it will be subject to several phenomena which can be most easily described through the use of fractions. For example, when fission product enters a charcoal trap, a certain fraction of the entering contaminant will be trapped, while the remainder continues in the purification stream. This concept can also be applied to the phenomena of plateout and leakage in the stream as well, assuming that data can be found to support the fraction used. The trapping rate $\dot{T}_i$ can be modeled using,

$$\dot{T}_i = \varepsilon f_i, \tag{4.17}$$

where ε is the component inflow rate and f_i is the trapping fraction. The component out flow rate and then be calculated by,

$$\dot{O}_i = \varepsilon - \dot{T}_i. \tag{4.18}$$

4.2.4.3. Radioactive noble gas delay in the HPS delay beds

As discussed previously, at low temperatures, charcoal beds can function either as final traps or as a delay to the life of the fission product. To simulate this phenomenon, the delay bed components of a fission product trap were modeled by calculation of the exponential decay over the user defined delay period by,

$$\dot{D}_i^{DB} = \varepsilon(1 - \exp(-\lambda_i t_{delay}), \tag{4.19}$$

where $\dot{D}_i^{DB}$ is the decay rate of isotope i in the delay bed, and t_{delay} is the delay time. The delay bed outflow rate can then be calculated by

$$\dot{O}_i^{DB} = \varepsilon - \dot{D}_i^{DB}. \tag{4.20}$$

4.2.4.4. Primary coolant decay, plateout, and removal fractions

After leaving the HPS or through leakage from the in-core purge stream, released fission products begin to accumulate in the HPS. According to their type, they may either plateout or decay and a fraction of all nuclides in the Primary Coolant will removed by the chemical cleanup system or the in-core purge stream. While at first it may seem as though plateout, decay, and removal can be modeled like other components in the system, if done so it would create a circular relationship, causing the system to be insolvable. The primary coolant must serve as a source for the rest of the model as well as a sink, meaning prior knowledge of the flow rate must be input. Thankfully, this is possible by applying plateout, decay, and removal to the primary coolant in units of fractions per time. The resulting product is a source for the system and prevents the occurrence of a circular relationship. Another way to consider the need for this source is that it allows helium purification to occur through the in core purge stream and the chemical cleanup system even if the reactor is no longer releasing any fission products.

The decay rate of isotope i in the primary coolant can be modeled by,

$$\dot{D}_i^{PC} = \chi_{PC}\lambda_i, \tag{4.21}$$

where q_{PC} is the quality of the primary coolant.

The primary coolant plateout rate can be modeled by,

$$\dot{P}_i^{PC} = \chi_{PQ}\rho_i, \tag{4.22}$$

where ρ_i is the plateout fraction per hour.

Finally, the chemical cleanup or purge stream intake rate can be modeled using,

$$\dot{I}_i = \chi_{PQ}\kappa_i, \tag{4.23}$$

where κ_i is the intake fraction per hour.

4.2.5. System model verification and validation

Within the model itself, there were two main sections, one lacking decay precursors and one inclusive of decay precursors, both of which needed to be verified and validated to insure they are modeling what is intended. To do this properly, each connection in the model was tested for proper behavior and inputs and outputs of the model were recorded. The results of these tests are shown in the Appendix B.2.

4.3. Results and Discussion

In this section, recommendations for the reduction of uncertainties related to vented fuel systems will be presented alongside recommended design and operational conditions for GFRs. For reference, the assumed fission rate used in all simulations is that of a 500 MWth reactor, the same thermal reactor power as the EM^2 concept reactor [5]. Supplemental results for the simulations run in Cases 1 through 7 can be found in the AppendixB.1.

Important Note: Since the current system does not model the transport of tritium throughout the vented fuel system, the molecular sieve has been re-purposed to create a total of three fission product traps in the HPS of the model. This allows more flexibility in the number of cases which may be simulated and provide clarity in the presentation of their results. In the following cases, the "Second Fission Product Trap" will refer to what was previously known as the "Molecular Sieve" in Figure 4.6 and the "Third Fission Product Trap" will refer to what was previously known at the "Second Fission Product Trap".

For clarification:

- FFPT = First fission product trap.
- SFPT = Second fission product trap (previously labeled as "Molecular Sieve").
- TFPT = Third fission product trap.
- CC = Chemical cleanup.
- PC = Primary coolant.
- Purge = Fuel element purge stream.

4.3.1. Helium purification system significance

The first question to be answered in the design of a vented fuel system is "Why is a helium purification system needed?" To answer this, two simulation cases, Case 1 and Case 2, were used to compare the difference between a helium-cooled system with and without a HPS.

Case 1 and Case 2 represent both extremes of the design spectrum achievable in a vented fuel system. Case 1 provides an ideal example of a vent-to-stream strategy, while Case 2 provides an extreme example of the vent-to-coolant strategy (normally a vent-to-coolant strategy would include the addition of an HPS). By comparing these two cases, the differences and similarities present will provide characteristics of general systems, as well as those unique to their specific venting strategy.

4.3.1.1. Case 1: An ideal system

The first simulation to be conducted was that of an ideal vent-to-stream system. In an ideal system, fission product nuclides will be captured immediately after they are carried from the fuel by the purge stream and no leakage will occur from the purge stream into the primary coolant. To simulate this, the capture fraction for the first fission product trap has been set to 1 for all nuclides and the leakage fraction from the purge stream set to 0. Table 4.4 describes all model parameters used in the simulation.

Table 4.4.: Case 1: Parameters.

Parameter	Noble Gases	Halogens	Chalcogens & Metals	Plateout (I, Cs, Sr)
FFPT - trapping Fraction	1	1	1	Mixed
SFPT - trapping fraction	0	0	0	Mixed
TFPT - trapping fraction	0	0	1	Mixed
CC - trapping fraction	0	0	0	Mixed
FFPT - delay time [hr]	0	0	0	Mixed
TFPT - delay time [hr]	0	0	0	Mixed
Purge - plateout fraction	0	mixed	mixed	0.1
PC Cold - plateout fraction	0	mixed	mixed	0.1
PC Hot - plateout fraction	0	mixed	mixed	0.1
CC - Intake fraction	0.01	0.01	0.01	0.01
Purge - Intakte fraction	0.01	0.01	0.01	0.01
Purge - leakage fraction	0.01	0.01	0.01	0.01
Fission rate [fsn/hr]	5.80E+22	5.80E+22	5.80E+22	5.80E+22

4.3.1.2. Case 2: An open system

Next, to provide perspective for the ideal system, a simulation was evaluated for a system lacking the inclusion of both a purge stream and HPS. All trapping fractions and intake fractions were set to 0 and plateout fractions (except for the purge stream) were kept the same as in Case 1. All model parameters used in the simulation are shown in Table 4.5

4.3.1.3. Case 1 and 2 analysis

When reviewing the data from Case 1 and 2, the first noticeable characteristic of both systems is that the quantity of material removed from the core during operation is very large. Both cases accumulate approximately 200 kg of volatile fission product from the core after a 25,000 hour (2.85 yr) operation period. A large portion of this amount is composed of stable or long lived nuclides, with Cs-137 (30.07 yr half-life) and Sr-90 (28.78 yr half-life), being the only long-lived nuclides to appear in the top ten mass nuclides of Table 4.6. However, above all nuclides shown in columns 1 and 2 of Table 4.6, the “other” category contains nearly twice the amount of the top nuclide, Xe-134. While the content of the “other” category is very complicated, its behavior can be observed in Figure 4.10.

Table 4.5.: Case 2: Parameters.

Parameter	Noble Gases	Halogens	Chalcogens & Metals	Plateout (I, Cs, Sr)
FFPT - trapping Fraction	0	0	0	Mixed
SFPT - trapping fraction	0	0	0	Mixed
TFPT - trapping fraction	0	0	0	Mixed
CC - trapping fraction	0	0	0	Mixed
FFPT - delay time [hr]	0	0	0	Mixed
TFPT - delay time [hr]	0	0	0	Mixed
Purge - plateout fraction	0	mixed	mixed	0.1
PC Cold - plateout fraction	0	mixed	mixed	0.1
PC Hot - plateout fraction	0	mixed	mixed	0.1
CC - Intake fraction	0	0	0	0
Purge - Intakte fraction	0	0	0	0
Purge - leakage fraction	0	0	0	0
Fission rate [fsn/hr]	5.80E+22	5.80E+22	5.80E+22	5.80E+22

Figure 4.10 demonstrates the time dependence of the top ten nuclides ranked by mass. The "other" category can be seen to behave similar to a long-lived or stable nuclide. This behavior is described by the linear accumulation of a nuclide over time, as opposed to reaching a maximum equilibrium value. Over a period of 2.85 years, the "other" category is nearly linear, demonstrating that the mass which accumulates is driven by stable or relatively long-lived nuclides.

When reviewing the activity accumulated in the first fission product trap from Case 1, it can be seen that it is also has quite a large value. Over a period of 2.85 years, nearly 76 MCi of activity has accumulated in the fission product trap. Similarly, the power generated by the decay of these nuclides has reached a value of 841 kW or approximately 0.17% of the operating reactor power. Neither of these are small values when handling radioactivity or heat production and must be handled appropriately in the design of an HPS. Both cooling and shielding will be required to handle the heat load. As opposed to the top ten mass accumulated nuclides in the fission product trap, the list of top ten activity and power generating nuclides is composed nearly entirely of short-lived nuclides. Sr-89 is an outlier with a half-life of 50.52 days; the next longest lived nuclide on the list is Ba-140 with a half-life of 12.75 days.

A visual inspection of Figure 4.11 shows that all top ten power generating nuclides reach equilibrium after around 7000 hrs or about 292 days with Sr-89 taking by far the longest time to reach equilibrium. By examining the y-intercept of the "other" line in Figure 4.11, it can be seen that the majority of fission products which comprise the "other" group are short lived and have already reached equilibrium value. The slope of the "other" line shows power generation will continue to rise due to long lived nuclides. To provide a conservative estimate for accumulation beyond the 25,000 hr time limit of the model, the slope of this line can be extrapolated towards the operational lifetime of the reactor, approximately thirty years. Using the average slope of the line between 20,000 and 25,000 hours yields a power generation rate increase of 1.2 W/hr. Calculating this increase over 27.15 years and summing with the current power generation rate of 841 kW yields a power generation rate of 1127 kW. Given the conservative values used for

Table 4.6.: Case 1: First fission product trap accumulations.

Isotope	Mass [g]	Isotope	Activity [Ci]	Isotope	Power [W]
xenon-134	2.40E+04	xenon-133	9.56E+06	barium-139	1.25E+05
xenon-136	2.15E+04	barium-139	9.11E+06	lanthanum-140	1.25E+05
barium-138	2.12E+04	xenon-133m	6.00E+06	iodine-132	9.52E+04
cesium-135	2.10E+04	lanthanum-140	5.60E+06	iodine-133	5.56E+04
cesium-133	1.79E+04	barium-140	5.60E+06	iodine-134	4.07E+04
cesium-137	1.67E+04	strontium-89	4.28E+06	strontium-89	3.79E+04
xenon-132	1.59E+04	iodine-132	3.83E+06	barium-140	3.48E+04
samarium-147	7.30E+03	xenon-135	3.82E+06	cesium-138	3.37E+04
tellurium-130	6.64E+03	tellurium-132	3.11E+06	xenon-135	2.61E+04
strontium-90	6.41E+03	iodine-133	2.76E+06	xenon-133	2.42E+04
other	4.27E+04	other	2.23E+07	other	2.42E+05
total	2.01E+05	total	7.59E+07	total	8.41E+05

the fuel release fraction and the assumptions made using the slope of the "other" line, this can be considered a conservative prediction of the heat load limit which will be imposed upon the system. The methodology can also be extended to the activity and mass of the system (using the total value), yielding a value of approximately 2105 kg and 123.5 MCi at 30 years. These values provide bounding estimates to be used when designing a vented fuel system.

Comparing the values of nuclides accumulated in the open system (Case 2) with the ideal system (Case 1) reveals several differences with how the two systems accumulate fission products. The main difference is the effect of decay between the hot and cold sides of the primary coolant. By examining Figures 4.12 and 4.13, it can be seen that the short lived nuclides which compose the majority of the activity present in the "other" line decay significantly over the 1 hour time-step difference between the two sides.

Additionally, for the long lived and stable nuclides which comprise most of the fission product mass deposited in the system, the influence of plateout can be seen to contribute significantly to the removal of fission products from the primary coolant. The time dependent values of accumulated mass in the primary coolant, shown in Figure 4.14 , can be compared with the accumulated mass in Case 1, shown in Figure 4.11 . Specifically, the value of the "other" group at 25,000 can be seen to be significantly decreased due to the removal of the high yield cesium nuclides from circulation in the primary coolant. The accumulation of these cesium nuclides can observed in Table 4.7.

As can be gathered from the previous two cases, the inclusion of an HPS is required for the prevention of accumulation and plateout of radioactive fission products in the primary coolant. Additionally, it can be gathered from Table 4.7 that the activity generated from plated out elements can be substantial, generating nearly 8 MCi of activity in the hot side, and slightly less in the cold side, as is demonstrated in Table 4.8.

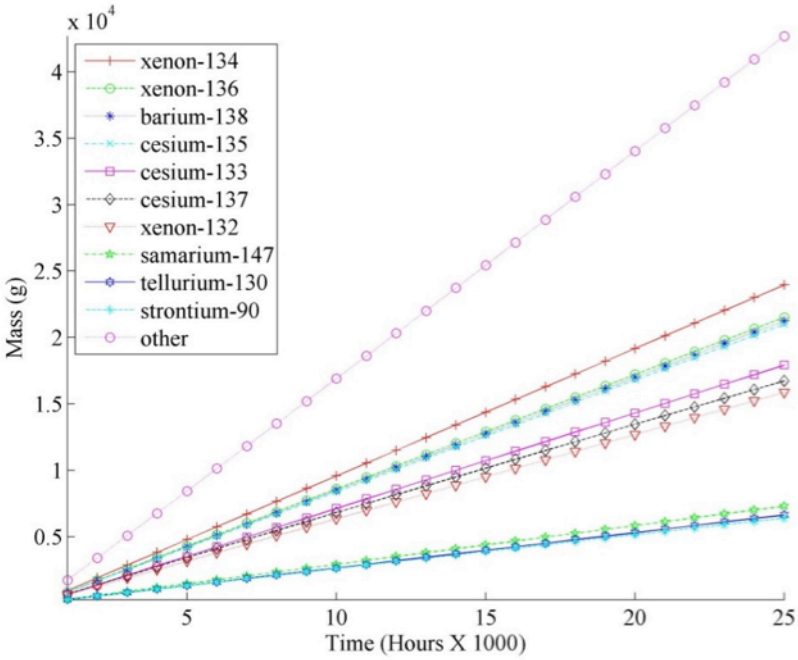

Figure 4.10.: Case 1: First fission product trap mass accumulation

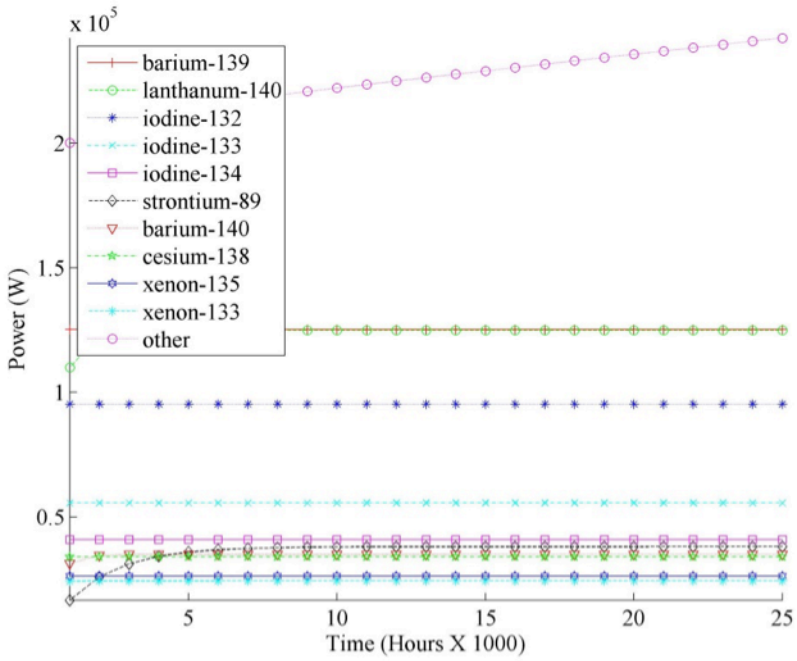

Figure 4.11.: Case 1: First fission product trap power accumulation

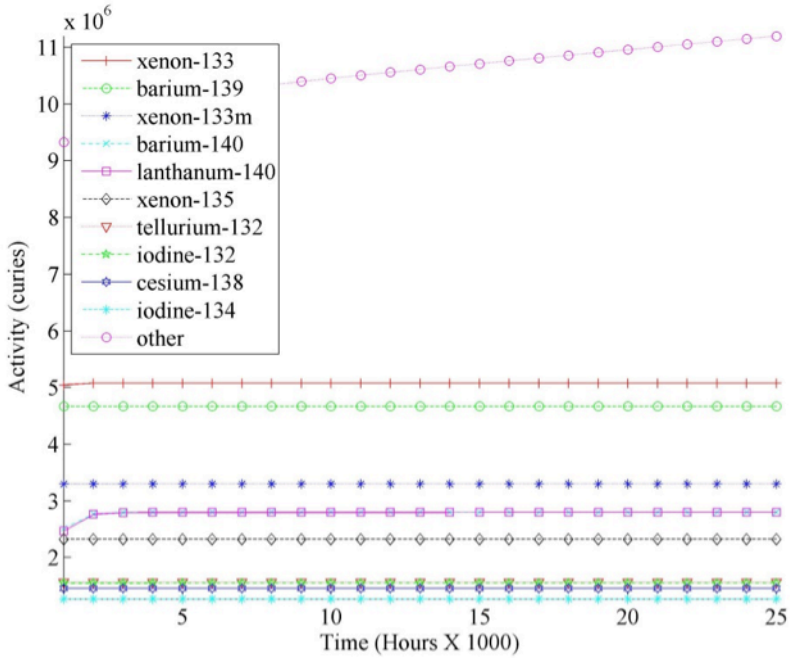

Figure 4.12.: Case 2: Activity accumulation in the hot side of the primary coolant trap

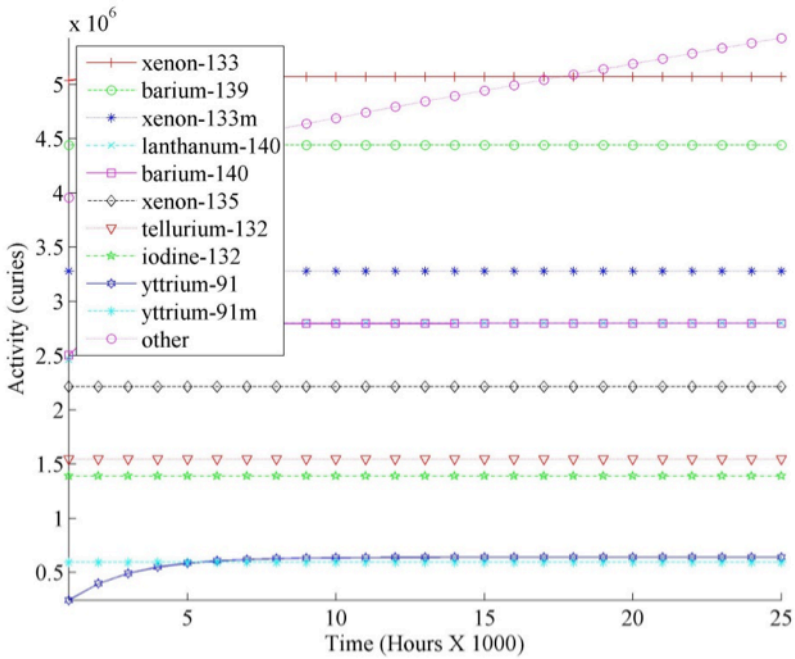

Figure 4.13.: Case 2: Activity accumulation in the cold side of the primary coolant trap

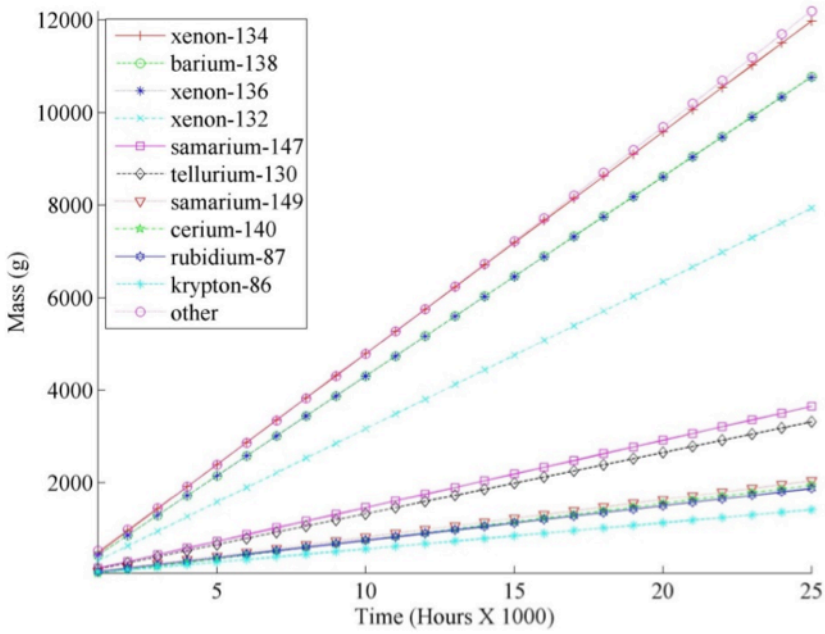

Figure 4.14.: Case 2: Mass accumulation in the hot side of the primary coolant trap

Table 4.7.: Case 2: Hot side of the primary coolant accumulations.

Isotope	Mass [g]	Isotope	Activity [Ci]	Isotope	Power [W]
cesium-135	1.12E+04	strontium-89	2.48E+06	iodine-133	2.89E+04
cesium-133	9.45E+03	iodine-133	1.43E+06	strontium-89	2.19E+04
cesium-137	8.80E+03	cesium-137	9.26E+05	iodine-132	1.27E+04
strontium-90	3.37E+03	strontium-90	5.64E+05	iodine-135	7.11E+03
strontium-88	1.53E+03	iodine-131	5.38E+05	cesium-137	6.46E+03
iodine-129	2.80E+02	iodine-132	5.09E+05	strontium-91	6.43E+03
iodine-127	9.00E+01	iodine-135	4.53E+05	iodine-134	4.36E+03
strontium-89	7.03E+01	strontium-91	4.02E+05	cesium-138	4.01E+03
iodine-131	3.69E+00	iodine-134	1.60E+05	iodine-131	3.63E+03
iodine-133	1.01E+00	strontium-92	1.43E+05	strontium-90	1.82E+03
other	2.25E-01	other	1.05E+05	other	1.62E+03
total	3.48E+04	total	7.71E+06	total	9.89E+04

Table 4.8.: Case 2: Cold side of the primary coolant accumulations.

Isotope	Mass [g]	Isotope	Activity [Ci]	Isotope	Power [W]
cesium-135	1.12E+04	strontium-89	2.48E+06	iodine-133	2.89E+04
cesium-133	9.45E+03	iodine-133	1.43E+06	strontium-89	2.19E+04
cesium-137	8.80E+03	cesium-137	9.26E+05	iodine-132	1.27E+04
strontium-90	3.37E+03	strontium-90	5.64E+05	iodine-135	7.11E+03
strontium-88	1.53E+03	iodine-131	5.38E+05	cesium-137	6.46E+03
iodine-129	2.80E+02	iodine-132	5.09E+05	strontium-91	6.43E+03
iodine-127	9.00E+01	iodine-135	4.53E+05	iodine-134	4.36E+03
strontium-89	7.03E+01	strontium-91	4.02E+05	cesium-138	4.01E+03
iodine-131	3.69E+00	iodine-134	1.60E+05	iodine-131	3.63E+03
iodine-133	1.01E+00	strontium-92	1.43E+05	strontium-90	1.82E+03
other	2.25E-01	other	1.05E+05	other	1.62E+03
total	3.48E+04	total	7.71E+06	total	9.89E+04

4.3.2. Benefits of a complex helium purification system

Now that a basic understanding has been gained on the necessity of a helium purification system in GFRs using vented fuel, analysis can be conducted on more complex system arrangements. This will allow the system to be optimized towards a lower operation cost. The first step in that direction is made by capturing the metal, chalcogen, and halogen fission products at higher temperatures and the noble gas fission products at low temperatures. As discussed previously, to achieve the proper removal of noble gas contaminants from the purge stream, cooling to low temperatures is required. By splitting the HPS into two separate regions, it is hypothesized that the required heat removal rate in the low temperature region can be greatly decreased.

4.3.2.1. Case 3: A two region system

A basic two-region system was composed using the first fission product trap as the hot adsorption bed and the third fission product trap as the cold one. In Case 3, the hot adsorption bed is assumed to be capable of trapping most fission product contaminant, excluding noble gases, while the cold adsorption bed traps all remaining contaminant. This provides a baseline for determining the total load placed on a system due to noble gas fission products. All model parameters used in the simulation are shown in Table 4.9.

Table 4.9.: Case 3: Parameters.

Parameter	Noble Gases	Halogens	Chalcogens & Metals	Plateout (I, Cs, Sr)
FFPT - trapping Fraction	0	0.99	1	mixed
SFPT - trapping fraction	0	0	0	mixed
TFPT - trapping fraction	1	1	1	mixed
CC - trapping fraction	0	0	0	mixed
FFPT - delay time [hr]	0	0	0	mixed
TFPT - delay time [hr]	0	0	0	mixed
Purge - plateout fraction	0	mixed	mixed	0.1
PC Cold - plateout fraction	0	mixed	mixed	0.1
PC Hot - plateout fraction	0	mixed	mixed	0.1
CC - Intake fraction	0	0	0	0
Purge - Intakte fraction	0	0	0	0
Purge - leakage fraction	0	0	0	0
Fission rate [fsn/hr]	5.80E+22	5.80E+22	5.80E+22	5.80E+22

4.3.2.2. Case 4: A delayed two region system

As discussed previously, one possibility for reducing the cooling load on the coldest fission product trap is through the utilization of activated charcoal delay beds. To understand the effect that this has on the system, a semi-optimal HPS design was modeled the current model configuration. The goal of the design was to reduce the cooling load required for the cold region of the system. Through a visual inspection of released noble gas isotopes, it can be seen that it is not possible to

delay the transport of krypton-85 (10.76 yr half-life), but it is possible to delay the transport of all other nuclides. By assuming a 600 hr xenon (about 3 hr for krypton) delay on the first fission product trap, most of the radioactive xenon present in the purge stream can be removed (600 hr is about 5 times the half-life of Xe-133). Additionally, by placing a 25 hour krypton (about 5000 hr for xenon) delay on the second fission product trap, most of the radioactive krypton present in the purge stream can be removed, excluding Kr-85 (25 hr is about 5 times the half-life of Kr-85m). The multiplier for delay of 200 between krypton and xenon decay was taken from the delays used in the Peach Bottom Unit 1 Final Hazards Summary Report [7]. To allow utilization of all three fission product traps and full use of two representative delay beds, the delay times listed previously have been converted to trapping fractions, as shown in Table 4.11. All model parameters used in the simulation are shown in Table 4.10 and Table 4.11.

Table 4.10.: Case 4: Parameters.

Parameter	Noble Gases	Halogens	Chalcogens & Metals	Plateout (I, Cs, Sr)
FFPT - trapping Fraction	Table 4.11	1	1	mixed
SFPT - trapping fraction	Table 4.11	1	1	mixed
TFPT - trapping fraction	1	1	1	mixed
CC - trapping fraction	0	0	0	mixed
FFPT - delay time [hr]	Applied as Trapping Fraction	0	0	Mixed
TFPT - delay time [hr]	Applied as Trapping Fraction	0	0	Mixed
Purge - plateout fraction	0	mixed	mixed	0.1
PC Cold - plateout fraction	0	mixed	mixed	0.1
PC Hot - plateout fraction	0	mixed	mixed	0.1
CC - Intake fraction	0	0	0	0
Purge - Intakte fraction	0	0	0	0
Purge - leakage fraction	0	0	0	0
Fission rate [fsn/hr]	5.80E+22	5.80E+22	5.80E+22	5.80E+22

4.3.2.3. Case 3 and 4 analysis

After reviewing the results of the basic two region system, it is interesting to compare the difference between the three different accumulation values shown in Tables 4.12 and 4.13. Comparison between the total values of the hot trap and the cold region trap reveals that noble gases and their daughters compose approximately 40% of accumulated mass, approximately 29% of accumulated activity and approximately 13% of power generation due to decay. Despite being only 13% of the total power generation rate due to decay, the cold region still produces over 100 kW, assumedly causing difficulty for cooling to low temperatures.

Further analysis of the time dependent results shown in Figure 4.15 reveals that the vast majority of power generation in the cold region is due to short-lived nuclides, with the longest lived being Xe-133 with a 5.2 d half-life. It is interesting to see the large contribution to the power generation rates by Cs-138 and Rb-88, daughters to Xe-138 and the difficult-to-delay Kr-88 nuclides.

Table 4.11.: Case 4: Trapping fractions.

Nuclide	Half-life	First Fission Production Trap (Xe-600 hr; Kr-3 hr)	Second Fission Production Trap (Xe-5000 hr; Kr-25 hr)
Kr - 83	stable	0	0
Kr - 84	stable	0	0
Kr - 85m	4.48 hr	0.371	0.979
Kr - 85	10.8 yr	0	0
Kr - 86	stable	0	0
Kr - 87	1.27 hr	0.806	1
Kr- 88	2.84 hr	0.519	0.998
Xe - 131	stable	0	0
Xe - 132	stable	0	0
Xe - 133m	52.56 hr	1	1
Xe - 133	125.8 hr	0.963	1
Xe - 134	stable	0	0
Xe - 135m	0.255 hr	1	1
Xe - 135	9.1 hr	1	1
Xe - 136	stable	0	0
Xe - 138	0.235 hr	1	1

One issue that can be seen arise is due to accumulation of stable noble gases in the cold region of the HPS. Because the HPS must rely on adsorption techniques for removal of radioactive fission product gases, the accumulation of stable noble gases will over time reduce the effectiveness of the traps. This accumulation over time is demonstrated in Figure 4.16. Due to this effect, it may be necessary to regenerate the cold region of the HPS at regular intervals, preventing breakthrough of purge stream contaminants into the primary coolant. However, this result can be avoided if the system is built large enough to accommodate all the accumulated gases. All radioactive noble gases and their daughters are relatively short-lived (excluding Kr-85) and will not require additional cooling over time. Additionally, regeneration of the cold region requires a system built in parallel, allowing purification of the helium during maintenance operations. However, if a backup/secondary system is already planned to be included in the design of the plant, it may be more economical to design for regeneration, reducing the size requirement of the last adsorption bed. If no regeneration is assumed to occur in the last adsorption bed, then the amount of noble gases will eventually reach a value of 757 kg, which is significant even when compared to the total mass of released fission product, 2105 kg, calculated for Case 1.

In the end, whether or not regeneration is chosen as the optimum operation strategy, cooling to low enough temperatures to prevent breakthrough of the last adsorption bed drives the system design to one which removes as much radioactivity through delay as possible.

Case 4 attempted to use the tools available in the fission product transport model to simulate a system which was as close to optimum as possible. Without attempting to optimize the size, material, or operational requirements, a system was simulated by assuming delay times for xenon and krypton radionuclides. The third fission product trap was assumed to stop all gases and prevent breakthrough of noble gas fission products into the primary coolant. The results of the simulation showed that, for the most part, the assumed design worked in achieving its intended

Table 4.12.: Case 3: First fission product trap accumulations.

Isotope	Mass [g]	Isotope	Activity [Ci]	Isotope	Power [W]
barium-138	2.10E+04	barium-139	9.11E+06	barium-139	1.25E+05
cesium-135	1.84E+04	lanthanum-140	5.60E+06	lanthanum-140	1.25E+05
cesium-137	1.67E+04	barium-140	5.60E+06	iodine-132	9.43E+04
cesium-133	1.15E+04	strontium-89	4.28E+06	iodine-133	5.51E+04
samarium-147	7.30E+03	iodine-132	3.79E+06	iodine-134	4.03E+04
tellurium-130	6.64E+03	tellurium-132	3.11E+06	strontium-89	3.79E+04
strontium-90	6.41E+03	iodine-133	2.73E+06	barium-140	3.48E+04
samarium-149	4.08E+03	cesium-137	1.58E+06	iodine-135	2.33E+04
cerium-140	3.89E+03	iodine-135	1.49E+06	cesium-138	2.28E+04
rubidium-87	3.64E+03	iodine-134	1.48E+06	yttrium-92	1.84E+04
other	2.24E+04	other	1.53E+07	other	1.61E+05
total	1.22E+05	total	5.40E+07	total	7.38E+05

Table 4.13.: Case 3: Third fission product trap accumulations.

Isotope	Mass [g]	Isotope	Activity [Ci]	Isotope	Power [W]
xenon-134	2.40E+04	xenon-133	9.56E+06	xenon-135	2.61E+04
xenon-136	2.15E+04	xenon-133m	6.00E+06	xenon-133	2.42E+04
xenon-132	1.59E+04	xenon-135	3.82E+06	cesium-138	1.87E+04
cesium-133	6.37E+03	cesium-138	4.88E+05	rubidium-88	8.55E+03
krypton-86	2.83E+03	xenon-135m	4.16E+05	xenon-133m	8.28E+03
xenon-131	2.66E+03	xenon-138	3.48E+05	krypton-87	6.07E+03
cesium-135	2.61E+03	krypton-88	2.72E+05	xenon-138	5.71E+03
krypton-84	1.54E+03	rubidium-88	2.71E+05	krypton-88	4.69E+03
krypton-83	8.90E+02	krypton-87	2.63E+05	xenon-135m	1.32E+03
krypton-85	3.32E+02	krypton-85m	2.29E+05	krypton-85m	1.15E+03
other	7.12E+02	other	2.47E+05	other	2.79E+03
total	7.93E+04	total	2.19E+07	total	1.08E+05

purpose and using delay times as the primary design condition appears to be a good methodology for design of the cold region in an HPS. The comparative results between the results between Case 3 and Case 4, shown below in Tables 4.14, 4.15, and 4.16, reveal that a 600 hr xenon delay can reduce the heating load on the last two adsorption beds by a factor of 11 to approximately 9.75 kW. Additionally, the combination of a 600 hr xenon delay and a 25 hr krypton delay can reduce the heating load on the last adsorption bed by a factor of 172 to approximately 600 W, which almost entirely comes from the decay of Kr-85 (10.8 yr halflife), as is shown in Table 4.16. While it is true that no matter how it is arranged, a total of 841 kW (Case 1) of decay heat must be removed from the system, it appears that it may be better to do so at as high a temperature as possible to improve system efficiency.

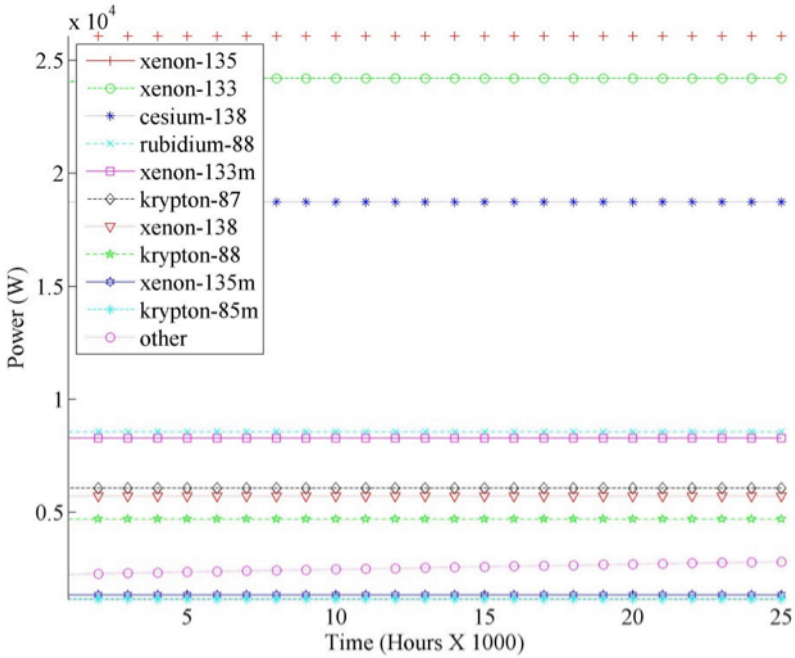

Figure 4.15.: Case 3: Power accumulation in the third fission product trap.

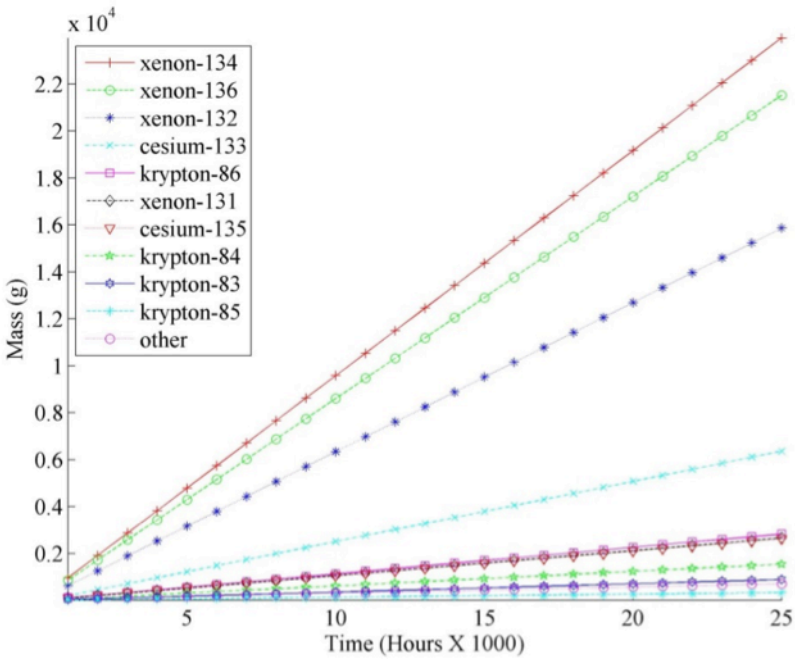

Figure 4.16.: Case 3: Mass accumulation in the third fission product trap.

Table 4.14.: Case 4: First fission product trap accumulations.

Isotope	Mass [g]	Isotope	Activity [Ci]	Isotope	Power [W]
barium-138	2.12E+04	xenon-133	9.21E+06	barium-139	1.25E+05
cesium-135	2.10E+04	barium-139	9.11E+06	lanthanum-140	1.25E+05
cesium-133	1.77E+04	xenon-133m	5.99E+06	iodine-132	9.52E+04
cesium-137	1.67E+04	lanthanum-140	5.60E+06	iodine-133	5.56E+04
samarium-147	7.30E+03	barium-140	5.60E+06	iodine-134	4.07E+04
tellurium-130	6.64E+03	strontium-89	4.28E+06	strontium-89	3.79E+04
strontium-90	6.41E+03	iodine-132	3.83E+06	barium-140	3.48E+04
samarium-149	4.08E+03	xenon-135	3.82E+06	cesium-138	3.37E+04
cerium-140	3.89E+03	tellurium-132	3.11E+06	xenon-135	2.61E+04
rubidium-87	3.73E+03	iodine-133	2.76E+06	iodine-135	2.36E+04
other	2.26E+04	other	2.17E+07	other	2.33E+05
total	1.31E+05	total	7.50E+07	total	8.31E+05

Table 4.15.: Case 4: Second fission product trap accumulations.

Isotope	Mass [g]	Isotope	Activity [Ci]	Isotope	Power [W]
cesium-133	2.35E+02	xenon-133	3.53E+05	rubidium-88	4.10E+03
strontium-88	5.80E+01	krypton-85m	1.41E+05	krypton-88	2.25E+03
rubidium-85	4.77E+01	krypton-88	1.30E+05	krypton-87	1.18E+03
rubidium-87	2.26E+01	rubidium-88	1.30E+05	xenon-133	8.93E+02
xenon-133	1.73E+00	krypton-87	5.12E+04	krypton-85m	7.06E+02
krypton-85	6.10E-02	xenon-133m	2.19E+03	xenon-133m	3.03E+00
krypton-85m	1.57E-02	krypton-85	2.60E+01	krypton-85	1.06E-01
krypton-88	9.51E-03	N/A	0.00E+00	N/A	0.00E+00
xenon-133m	4.48E-03	N/A	0.00E+00	N/A	0.00E+00
krypton-87	1.65E-03	N/A	0.00E+00	N/A	0.00E+00
other	9.88E-04	other	0.00E+00	other	0.00E+00
total	3.65E+02	total	8.08E+05	total	9.14E+03

Table 4.16.: Case 4: Third fission product trap accumulations.

Isotope	Mass [g]	Isotope	Activity [Ci]	Isotope	Power [W]
xenon-134	2.40E+04	krypton-85	1.42E+05	krypton-85	5.77E+02
xenon-136	2.15E+04	krypton-85m	3.01E+03	krypton-85m	1.51E+01
xenon-132	1.59E+04	krypton-88	2.92E+02	rubidium-88	9.21E+00
krypton-86	2.83E+03	rubidium-88	2.92E+02	krypton-88	5.05E+00
xenon-131	2.66E+03	krypton-87	5.12E-02	krypton-87	1.18E-03
krypton-84	1.54E+03	N/A	0.00E+00	N/A	0.00E+00
krypton-83	8.90E+02	N/A	0.00E+00	N/A	0.00E+00
krypton-85	3.32E+02	N/A	0.00E+00	N/A	0.00E+00
rubidium-85	3.24E+01	N/A	0.00E+00	N/A	0.00E+00
strontium-88	1.30E-01	N/A	0.00E+00	N/A	0.00E+00
other	3.81E-04	other	0.00E+00	other	0.00E+00
total	6.96E+04	total	1.45E+05	total	6.06E+02

4.3.3. Evaluation of system uncertainties

In any theoretical system design, previously compiled data is used to develop models of physical phenomena. These models are then used to determine what is thought to be the best system possible based on predetermined design constraints. It is advantageous for the engineer to use the best data available for the development of his or her models, but oftentimes resources are limited and not all necessary data is able to be acquired. The engineer must choose which data is most important for the design process. This next section will seek to determine what data is most important for the design of vented fuel systems using the developed system model. The uncertainties examined will be those due to leakage from the purge stream, plateout in the primary coolant, and the fuel release fraction.

4.3.3.1. Case 5: Influences of purge stream leakage

A large uncertainty in the evaluation of the safety and feasibility of vented fuel is the release of fission products to the primary coolant through purge stream leakage. The uncertainty in the determination of the purge stream leakage rate is due mainly to the difficulty in estimating a value for any reactor design before extensive testing is completed. To understand the significance of the purge stream leakage rate on primary coolant and plateout inventories, a parametric simulation has been conducted Other than augmentation of the purge stream leakage fraction, the model parameters used are identical to those previously used in Case 3 (the basic two region system). All model parameters used in the simulation are shown in Table 4.17.

Table 4.17.: Case 5: Parameters.

Parameter	Noble Gases	Halogens	Chalcogens & Metals	Plateout (I, Cs, Sr)
FFPT - trapping Fraction	0	0.99	1	mixed
SFPT - trapping fraction	0	0	0	mixed
TFPT - trapping fraction	1	1	1	mixed
CC - trapping fraction	0	0	0	mixed
FFPT - delay time [hr]	0	0	0	mixed
TFPT - delay time [hr]	0	0	0	mixed
Purge - plateout fraction	0	mixed	mixed	0.1
PC Cold - plateout fraction	0	mixed	mixed	0.1
PC Hot - plateout fraction	0	mixed	mixed	0.1
CC - Intake fraction	0	0	0	0
Purge - Intakte fraction	0.002	0.002	0.002	0.002
Purge - leakage fraction	[1E-4; 1E-5]	[1E-4; 1E-5]	[1E-4; 1E-5]	[1E-4; 1E-5]
Fission rate [fsn/hr]	5.80E+22	5.80E+22	5.80E+22	5.80E+22

4.3.3.2. Case 6: Influences of primary coolant plateout

In addition to the determination of the purge stream leakage fraction, large uncertainties remain in prediction of plateout rates for volatile, non-noble gas fission products in the primary coolant.

To understand the significance of the primary coolant plateout rate, a parametric simulation has been run between two different values for the primary coolant plateout fraction in the hot and cold sides of the primary coolant All model parameters used in the simulation are shown in Table 4.18.

Table 4.18.: Case 6: Parameters.

Parameter	Noble Gases	Halogens	Chalcogens & Metals	Plateout (I, Cs, Sr)
FFPT - trapping Fraction	0	0.99	1	mixed
SFPT - trapping fraction	0	0	0	mixed
TFPT - trapping fraction	1	1	1	mixed
CC - trapping fraction	0	0	0	mixed
FFPT - delay time [hr]	0	0	0	mixed
TFPT - delay time [hr]	0	0	0	mixed
Purge - plateout fraction	0	mixed	mixed	0.1
PC Cold - plateout fraction	0	mixed	mixed	[0.2; 0.3]
PC Hot - plateout fraction	0	mixed	mixed	[0.2; 0.3]
CC - Intake fraction	0	0	0	0
Purge - Intakte fraction	0.002	0.002	0.002	0.002
Purge - leakage fraction	0.0001	0.0001	0.0001	0.0001
Fission rate [fsn/hr]	5.80E+22	5.80E+22	5.80E+22	5.80E+22

4.3.3.3. Case 7: Influences of fuel release fraction

Finally, the fuel release fraction represents a very large uncertainty present in the design of vented fuel systems. Its value directly affects radioactivity levels in the primary coolant, as well as stored inventories in the HPS. While it is possible to analyze the effect of fuel release fraction on all aspects of the system, it is most important to observe its effect on the HPS, as the design of an efficient and economical HPS relies on an accurate understanding of fuel release rates. To provide comparison for the worth of the fuel release fraction, a simulation has been conducted with a release fraction of 1 for all volatile nuclides, allowing comparison with all previously conducted simulations. All model parameters used in the simulation are shown in Tables 4.19 and 4.20.

4.3.3.4. Case 5, 6, and 7 analysis

When comparing the relative importance of uncertainties present in any system, it is first necessary to define what is meant by “importance”. In general, it is important in the design of a vented fuel system to enable a GFR to operate safely and economically for many years. More specifically, activities within the primary coolant must be maintained at appropriate levels, allowing for safe operation and maintenance of the plant. Additionally, in the case of an accident scenario, it is necessary to understand the inventory and distribution of radioactive material in the plant in order to conduct a proper safety analysis. The three uncertainties discussed in this section will be judged using this definition of “importance”.

Table 4.19.: Case 7: Parameters.

Parameter	Noble Gases	Halogens	Chalcogens & Metals	Plateout (I, Cs, Sr)
FFPT - trapping Fraction	Table 4.20	1	1	mixed
SFPT - trapping fraction	Table 4.20	1	1	mixed
TFPT - trapping fraction	1	1	1	mixed
CC - trapping fraction	0	0	0	mixed
FFPT - delay time [hr]	Applied as Trapping Fraction	0	0	Mixed
TFPT - delay time [hr]	Applied as Trapping Fraction	0	0	Mixed
Purge - plateout fraction	0	mixed	mixed	0.1
PC Cold - plateout fraction	0	mixed	mixed	0.1
PC Hot - plateout fraction	0	mixed	mixed	0.1
CC - Intake fraction	0	0	0	0
Purge - Intakte fraction	0	0	0	0
Purge - leakage fraction	0	0	0	0
Fission rate [fsn/hr]	5.80E+22	5.80E+22	5.80E+22	5.80E+22

The first uncertainty to be evaluated is the leakage fraction from the purge stream. Results from Case 5 are shown in Table 4.21, and reveal the significant impact of the purge stream release fraction on the level of activity present in the primary coolant. Assuming that the HPS is properly designed to handle the released fission product load, the only pathways for fission products to enter the primary coolant is through leakage from the purge stream or as a result of fuel cladding failure.

It is recommended that the during vented fuel system design, the maximum desired activity level in the primary coolant is used to determine the maximum allowable purge stream leakage fraction. This fraction can then be used as a design constraint to determine the amount of negative pressure required to operate the HPS. Due to its direct impact on the safety of the system, the determination of the purge stream leakage fraction is of crucial importance in the design of a GFR using vented fuel.

The next uncertainty to be examined was the amount of plateout per pass of an element present in the primary coolant. The results of Case 6 are shown in Tables 4.22 and 4.23, and reveal that the plateout fraction in the primary coolant has a relatively small impact on the amount of plateout which occurs in the system as long as the plateout fraction is large compared to the purge intake fraction. To further explain, if the intake fraction for the purge stream is small relative to the plateout fraction, and if the nuclide is not short-lived, it will eventually plateout whether it takes just one pass or many passes.

However, changing the plateout fraction in the primary coolant does have an interesting effect on the distribution of the plated out element. At higher plateout fractions, an isotope is more likely to plate out closest to the region where it first entered the primary coolant. This can be seen as plateout fraction increases, the relative plateout present between the hot side and the cold side of the primary coolant increases. The level of plateout in the cold side is higher due to the flow structure of the model, which transfers fissions products from the purge stream directly into the primary coolant cold side.

Table 4.20.: Case 7: Trapping fractions.

Nuclide	Half-life	First Fission Production Trap (Xe-600 hr; Kr-3 hr)	Second Fission Production Trap (Xe-5000 hr; Kr-25 hr)
Kr - 83	stable	0	0
Kr - 84	stable	0	0
Kr - 85m	4.48 hr	0.371	0.979
Kr - 85	10.8 yr	0	0
Kr - 86	stable	0	0
Kr - 87	1.27 hr	0.806	1
Kr- 88	2.84 hr	0.519	0.998
Xe - 131	stable	0	0
Xe - 132	stable	0	0
Xe - 133m	52.56 hr	1	1
Xe - 133	125.8 hr	0.963	1
Xe - 134	stable	0	0
Xe - 135m	0.255 hr	1	1
Xe - 135	9.1 hr	1	1
Xe - 136	stable	0	0
Xe - 138	0.235 hr	1	1

Because it has little effect on the safety and economy of the system, it is not of the upmost importance to determine with high certainty the plateout rate of fission products within the system. This of course relies on the condition that the plate out fraction per cycle is large relative to the purge stream intake fraction per cycle. It is important, however, to know whether or not a fission product plates out, as it will decide its ultimate fate in the system.

Out of the three uncertainties discussed in this section, it can be seen conceptually that the one with the broadest effect on the system is the fuel release fraction. The fuel release fraction directly impacts the results of the other two uncertainties, as well as impacting the necessary size of the purification system. Without a good grasp on the value of the fuel release fraction for each significant volatile nuclide, it is not possible to optimize the design for the most economical system. One way to estimate the upper bound of gaseous fission product release is to assume 100% for all volatile fission product. To understand the impact of this assumption, the results of Case 7 are displayed in Tables 4.24, 4.25, and 4.26.

By inspecting the data presented in Tables 4.24, 4.25, and 4.26, it can be seen that the amount of fission product accumulated in the HPS is higher than calculated in Case 1 and Case 4, as is expected. To provide a broader scope for the impact of a fuel release fraction of 1, discussion will focus on comparisons with Case 1. The total mass accumulated in Case 7 after a 25,000 hr operation time is approximately 300 kg, compared with 200 kg in Case 1. Additionally, the amount of radioactivity accumulated in the HPS has increased to 981 MCi and the power generation rate has increased to 14.2 MW (approximately 2.8% of the reactor's assumed 500 MWth operating power). These values can be compared to the values of 76 MCi and 841 kW calculated in Case 1. The reason for the much higher increase of accumulated activity and power generation rate relative to accumulated mass is mostly due to the influence of stable, volatile nuclides, which already had a fuel release fraction of 1 in Case 1 and comprise the majority of

Table 4.21.: Case 5: Primary coolant activity comparisons

Isotope	PC activity [Ci]		Isotope	PC plateout activity [Ci]	
	1E-4 leakage	*1E-5 leakage*		*1E-4 leakage*	*1E-5 leakage*
barium-139	4.35E+02	4.35E+01	strontium-89	2.39E+02	2.39E+01
xenon-133	4.17E+02	4.17E+01	iodine-133	1.24E+02	1.24E+01
xenon-133m	3.14E+02	3.14E+01	cesium-137	8.24E+01	8.24E+00
xenon-135	2.28E+02	2.28E+01	strontium-90	5.02E+01	5.02E+00
barium-140	1.94E+02	1.94E+01	iodine-131	4.87E+01	4.87E+00
lanthanum-140	1.83E+02	1.83E+01	iodine-132	4.19E+01	4.19E+00
tellurium-132	1.39E+02	1.39E+01	iodine-135	3.57E+01	3.57E+00
iodine-132	1.27E+02	1.27E+01	strontium-91	3.30E+01	3.30E+00
yttrium-91m	6.03E+01	6.03E+00	strontium-92	9.00E+00	9.00E-01
yttrium-90m	5.71E+01	5.71E+00	iodine-134	1.77E+00	1.77E-01
other	5.36E+02	5.36E+01	other	0.00E+00	0.00E+00
total	2.69E+03	2.69E+02	total	6.66E+02	6.66E+01

accumulated mass in the system. Among those affected most by the fuel release fraction were the short-lived nuclides, as they had very small release fractions in prior cases.

The two main impacts of these results are the increased heat load placed on the HPS, as well as the increased activity in the primary coolant due to leakage of the purge stream. First, the very high heat output rate of 14.2 MW makes cooling of the HPS nearly impossible. Thus, to allow for the construction of a reasonably sized HPS, the fuel release fraction must be known. Second, since the amount of activity present in purge stream depends directly upon the fuel release rate, the amount of activity leaked into the primary coolant cannot be determined, along with the negative system pressure required to keep the purge stream leakage fraction at a reasonably low level. Therefore, due to its direct impact on the safety and economics of the system, the determination of the fuel release fraction is of crucial importance in the design of a GFR using vented fuel.

Table 4.22.: Case 6: Primary coolant hot-side activity comparisons

Isotope	PC activity [Ci]		Isotope	PC plateout activity [Ci]	
	0.2 plateout	*0.3 plateout*		*0.2 plateout*	*0.3 plateout*
barium-139	4.35E+02	4.35E+02	strontium-89	2.26E+02	2.10E+02
xenon-133	4.17E+02	4.18E+02	iodine-133	1.34E+02	1.30E+02
xenon-133m	3.15E+02	3.15E+02	iodine-132	7.77E+01	8.04E+01
xenon-135	2.28E+02	2.28E+02	cesium-137	6.58E+01	7.21E+01
barium-140	1.94E+02	1.94E+02	iodine-135	4.78E+01	4.58E+01
lanthanum-140	1.83E+02	1.83E+02	iodine-131	4.73E+01	4.58E+01
tellurium-132	1.39E+02	1.39E+02	strontium-90	4.46E+01	4.39E+01
iodine-132	9.98E+01	8.14E+01	strontium-91	3.89E+01	3.91E+01
yttrium-90m	5.76E+01	5.66E+01	strontium-92	1.27E+01	1.36E+01
yttrium-91m	5.70E+01	5.44E+01	iodine-134	3.36E-01	1.54E-01
other	4.69E+02	4.40E+02	other	0.00E+00	0.00E+00
total	2.59E+03	2.54E+03	total	6.95E+02	6.81E+02

Table 4.23.: Case 6: Primary coolant cold-side activity comparisons

Isotope	PC activity [Ci]		Isotope	PC plateout activity [Ci]	
	0.2 plateout	*0.3 plateout*		*0.2 plateout*	*0.3 plateout*
barium-139	4.58E+02	4.58E+02	strontium-89	2.84E+02	3.01E+02
xenon-133	4.19E+02	4.19E+02	iodine-133	1.72E+02	1.91E+02
xenon-133m	3.17E+02	3.18E+02	cesium-137	9.74E+01	1.03E+02
cesium-138	2.43E+02	2.43E+02	iodine-132	7.67E+01	9.80E+01
xenon-135	2.40E+02	2.40E+02	iodine-135	6.43E+01	7.73E+01
barium-140	1.95E+02	1.95E+02	strontium-90	5.93E+01	6.29E+01
lanthanum-140	1.84E+02	1.84E+02	iodine-131	5.58E+01	6.26E+01
tellurium-132	1.41E+02	1.41E+02	strontium-91	5.37E+01	5.85E+01
barium-142	1.35E+02	1.35E+02	iodine-134	3.17E+01	3.29E+01
iodine-134	1.25E+02	1.25E+02	strontium-92	2.38E+01	3.15E+01
other	1.39E+03	1.36E+03	other	0.00E+00	0.00E+00
total	3.85E+03	3.82E+03	total	9.18E+02	1.02E+03

Table 4.24.: Case 7: First fission product trap accumulations.

Isotope	Mass [g]	Isotope	Activity [Ci]	Isotope	Power [W]
cesium-135	2.30E+04	barium-139	2.84E+08	barium-139	3.90E+06
barium-138	2.22E+04	iodine-134	3.43E+07	cesium-138	9.65E+05
lanthanum-139	2.00E+04	xenon-135	3.36E+07	iodine-134	9.30E+05
cerium-142	1.88E+04	xenon-138	3.28E+07	lanthanum-142	7.34E+05
cesium-133	1.87E+04	xenon-133m	2.92E+07	lanthanum-140	5.99E+05
cerium-140	1.87E+04	iodine-133	2.87E+07	iodine-132	5.89E+05
cesium-137	1.84E+04	xenon-133	2.82E+07	iodine-133	5.79E+05
praseodymium-141	1.78E+04	lanthanum-142	2.75E+07	xenon-138	5.39E+05
zirconium-92	9.80E+03	tellurium-134	2.70E+07	barium-141	4.99E+05
zirconium-91	8.28E+03	lanthanum-140	2.69E+07	yttrium-92	4.54E+05
other	5.09E+04	other	4.17E+08	other	4.17E+06
total	2.27E+05	total	9.69E+08	total	1.40E+07

Table 4.25.: Case 7: Second fission product trap accumulations.

Isotope	Mass [g]	Isotope	Activity [Ci]	Isotope	Power [W]
strontium-88	1.39E+03	krypton-88	3.12E+06	rubidium-88	9.82E+04
rubidium-85	9.66E+02	rubidium-88	3.12E+06	krypton-88	5.38E+04
rubidium-87	7.28E+02	krypton-85m	2.85E+06	krypton-87	3.81E+04
cesium-133	7.21E+02	krypton-87	1.65E+06	krypton-85m	1.43E+04
xenon-133	5.30E+00	xenon-133	1.08E+06	xenon-133	2.74E+03
krypton-85m	3.17E-01	xenon-133m	1.07E+04	xenon-133m	1.47E+01
krypton-88	2.28E-01	krypton-85	3.11E+01	krypton-85	1.27E-01
krypton-85	7.29E-02	N/A	0.00E+00	N/A	0.00E+00
krypton-87	5.34E-02	N/A	0.00E+00	N/A	0.00E+00
rubidium-88	2.36E-02	N/A	0.00E+00	N/A	0.00E+00
other	2.18E-02	other	0.00E+00	other	0.00E+00
total	3.81E+03	total	1.18E+07	total	2.07E+05

Table 4.26.: Case 7: Third fission product trap accumulations.

Isotope	Mass [g]	Isotope	Activity [Ci]	Isotope	Power [W]
xenon-134	2.40E+04	krypton-85	1.72E+05	krypton-85	6.99E+02
xenon-136	2.15E+04	krypton-85m	6.09E+04	krypton-85m	3.05E+02
xenon-132	1.58E+04	krypton-88	6.99E+03	rubidium-88	2.20E+02
krypton-86	2.83E+03	rubidium-88	6.99E+03	krypton-88	1.21E+02
xenon-131	2.63E+03	krypton-87	1.65E+00	krypton-87	3.81E-02
krypton-84	1.54E+03	N/A	0.00E+00	N/A	0.00E+00
krypton-83	8.90E+02	N/A	0.00E+00	N/A	0.00E+00
krypton-85	4.02E+02	N/A	0.00E+00	N/A	0.00E+00
rubidium-85	5.87E+01	N/A	0.00E+00	N/A	0.00E+00
strontium-88	3.11E+00	N/A	0.00E+00	N/A	0.00E+00
other	8.07E-03	other	0.00E+00	other	0.00E+00
total	6.97E+04	total	2.46E+05	total	1.34E+03

4.4. System Modeling Conclusions

The goal of the system modeling work was to increase the current understanding of fission product transport in helium-cooled GFRs using vented fuel and to provide a toolset for determining issues which may arise during normal and abnormal operating conditions. To meet this goal, several research objectives were defined accordingly:

1. Determine all significant fission product transport phenomena present in helium-cooled GFRs.
2. Develop a model to compute time-dependent inventories of fission products in the reactor and HPS system for normal and abnormal operating conditions.
3. Using the developed model, determine design and operational conditions necessary for the construction of safe and feasible helium-cooled GFRs using vented fuel.

To meet the first objective, the Theory section discussed six different significant transport phenomena which affect the transport of fission products within a helium-cooled GFR plant. These phenomena were:

1. Fission product generation and decay in fuel,
2. Volatile fission product chemistry,
3. Fission product diffusion and release in fuel,
4. Fission product diffusion and leakage through non-fuel components,
5. Fission product plateout,
6. Collection of gaseous fission products through adsorption.

To meet the second objective, a time-dependent fission product transport model of a helium-cooled GFR plant was developed using the systems modeling program STELLA. The STELLA model contained analytical equations describing all applicable phenomena and a system was put together with an aim for flexibility and completeness.

Lastly, to meet the third objective, the system model was used to test seven case scenarios, ranging from a completely open system with no HPS, to an attempt at a system with a slightly optimized HPS. These results revealed that the following design constraints and considerations are necessary for implementation of vented fuel within a helium-cooled GFR:

1. The quantity of fission products accumulated in the HPS is likely very large. The system must be designed to accommodate the fission product load or be regenerated at regular intervals to prevent breakthrough into the primary coolant from occurring in the last fission product trap.
2. The activity and power generation rate of fission products collected in the HPS is also very large. Cooling the purge stream to temperatures necessary for the adsorption of noble gas fission products may present a large power requirement for the helium-cooled

GFR plant. Additionally, extensive shielding systems will be required to allow operations and maintenance to occur in the vicinity of the HPS.

3. Safety systems will be necessary to prevent overheat and release of the contents of a HPS in an accident scenario. Use of defense-in-depth strategies to reduce the impact of a possible release of gaseous fission products is recommended.

4. Determination of the purge stream leakage rate is of crucial importance for predicting the level of radioactivity in the primary coolant.

5. Determination of the fuel release rate is of crucial importance for predicting the level of radioactivity in all areas of the plant and for the design of a safe and economical HPS.

4.5. Updated Values using MHTGR model

4.5.1. R/B model comparison

The Peach Bottom and MHTGR models were compared for a representative STELLA model, similar to Wesley Deason's Case 3 [2]. The model consists of a hot and cold fission product trap in serial, with plate-out of Cs, I, and Sr occurring in the pipe section between the fuel and the first hot fission product trap. The hot trap is assumed to capture everything but the noble gases, while the cold trap collects everything. The equation displayed in Equation 3.9 will be used for the MHTGR results, while Figure 3.10 will be used to determine the Peach Bottom R/B. Xe behavior is assumed for I, Te and Xe, with all remaining isotopes behaving like Kr. Table 4.27 displays a summary of the accumulated power, activity, and masses at the end of a 2.85 year run. Appendix B contains tables of the power, activity, and mass by isotope.

In general, the the BOL MHTGR model calculates powers 30-50% higher than the Peach Bottom model, while the EOL model predicts about 1/4 of the Peach Bottom values. The accumulated masses are roughly the same for each model. Although the results are only for 2.85 years, the power and activity in the traps reach equilibrium within the first simulated hour, while the plate-out power and activity only slightly increases over time. However, since the accumulated mass in each element is primarily stable elements, it will linearly increase throughout the operating time.

4.5.2. Tracked fission product list update

For the safety analysis of the FPVS, the STELLA design has been set to one hot and one cold fission product trap in series. The hot fission product trap is assumed to catch any isotope other than the noble gases Xe and Kr, while the second cold fission product trap will catch everything. Besides the fuel, the only other place fission products reside is in the piping between the fuel and the first hot trap. Plate out of Cs, I, and Se can occur on these pipes, and depending on the temperature, condensation of other non-noble elements. Figure 4.17 displays a possible configuration. The fuel purge stream (green arrows) flows up through the fuel, and back down in a downcomer between the fuel rods. The purge streams connect through headers that then travel

Table 4.27.: STELLA results comparing PB and MHTGR model with original tracked elements list at the end of 2.85 years.

	Peach Bottom R/B	MHTGR BOL R/B	MHTGR EOL R/B
Hot Fission Product Trap Power (kW)	377.9	454.3	97.1
Cold Fission Product Trap Power (kW)	54.9	86.6	14.3
Plateout Power (kW)	10.9	15.5	2.7
Hot Fission Product Trap Activity (MCi)	54.2	59.8	16.3
Cold Fission Product Trap Activity (MCi)	21.8	19.4	3.6
Plateout Activity (MCi)	1.7	1.6	0.5
Hot Fission Product Trap Mass (kg)	122	136.6	121.8
Cold Fission Product Trap Mass (kg)	79.3	77.6	71
Plateout Mass (kg)	6.2	6.3	6.8

through the pressure vessel to the hot and cold traps. After passing through the compressor, the purge stream mixes with the primary coolant and is re-injected back into the core.

While the primary coolant temperature can be characterized by an assumed inlet and outlet temperature of 550° C and 830° C, with a peak temperature of 1000° C, the temperature of the purge stream may be handled differently depending on its travel path. At the first extreme, if the purge stream exits the fuel and directly connects to the first hot trap, no cool-down of the purge stream will occur and it will enter the hot trap at the same temperature when it left the fuel. In this case, any fission product that is volatile at the peak purge stream temperature will be collected at the hot trap, and no condensation will occur in the piping. Conversely, if the purge stream connection remains in the core long enough for the purge gas to come to equilibrium with the coolant cold leg, the purge stream temperature can decrease to the inlet coolant temperature. While the noble gases and halogens will be unaffected by a temperature drop to 550° C, it is possible that the other volatile fission products will collect in the piping between the fuel and first hot trap.

Both extremes present two cases:

1. Purge stream exits fuel at 1000° C. Plateout of Cs, I, and Se occurs in piping. Purge stream enters hot trap at 1000° C. Trapping of everything but Xe and Kr occurs in first hot trap. Purge stream containing only Xe and Kr travels to cold trap where Xe, Kr, and their daughters are collected.

2. Purge stream exits fuel at 1000° C. Purge stream cools to 550° C. Condensation of everything but noble gases and halogens occurs in piping. Plateout of I occurs in piping. Purge stream enters hot trap at 550° C. Trapping of everything but Xe and Kr occurs in first hot trap. Purge stream containing only Xe and Kr travels to cold trap where Xe, Kr, and their daughters are collected.

The assumption in both cases is that the purge stream leaves the fuel at the peak coolant temperature 1000° C. The condensation location of each element is displayed in the last column of Table 4.28.

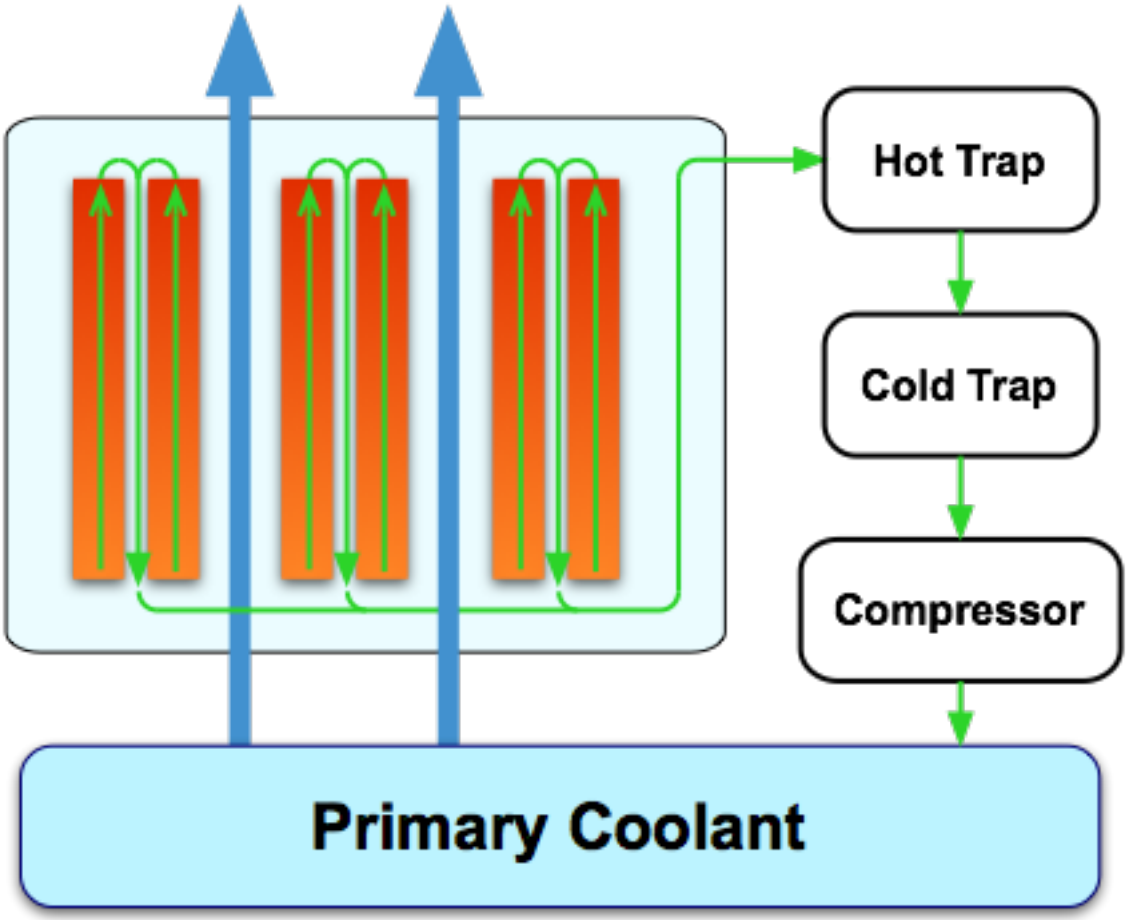

Figure 4.17.: Potential model of Fission Product Vent Stream.

In order to further down select elements that will remain volatile upon exiting the fuel, a cut-off temperature must be assigned. Wesley Deason assumed a threshold temperature of 1500° C based on the average temperature of the hottest fuel pin [2] . While a cut-off based on the fuel temperature includes all elements that will transport through the fuel, some of the elements with high melting temperature will condense on the exterior of the fuel pellet or the interior of the cladding, thus remaining within the fuel pin. In order for an element to travel out of the fuel and to the first fission trap, it must have a boiling temperature below the coolant temperature to remain entrained in the helium flow. Tracking of elements that remain gaseous at coolant temperatures will provide more realistic accumulation of atoms at different points of the system. Typical inlet and outlet temperatures are 550° C and 830° C respectively, with a peak coolant temperature of 1000° C. Although the average coolant temperature may be more realistic, the peak coolant temperature has been conservatively chosen as the new cut-off temperature. The element selection is displayed in Table 4.28.

For the final element selection for modeling in STELLA, those elements that will leave the fuel form are tracked. From these elements, isotopes with with a half-life greater than 10 minutes

Table 4.28.: List of elements tracked in STELLA model. († Assumed volatile in Wesley Deason's Thesis.)

Z	Element	Design Yield	Boiling Point [K]	# isotopes tracked	Condensation Location
34	Selenium (Se)	$3.19 \cdot 10^{-3}$	958	2	Piping
35	Bromine (Br)	$2.82 \cdot 10^{-3}$	331	1	Hot trap
36	Krypton (Kr)	$5.4 \cdot 10^{-2}$	120	7	Cold trap
37	Rubidium (Rb)	$1.43 \cdot 10^{-2}$	974	4	Piping
38	Strontium (Sr)	$6.87 \cdot 10^{-2}$	1,640	2	Fuel†
39	Yttrium (Y)	–	3,500	1	Fuel
40	Zirconium (Zr)	–	4,650	–	Fuel
41	Niobium (Nb)	–	5,200	–	Fuel
42	Molybdenum (Mo)	–	5,100	–	Fuel
43	Technetium (Tc)	–	4,900	–	Fuel
44	Ruthenium (Ru)	–	4,000	–	Fuel
45	Rhodium (Rh)	–	4,000	–	Fuel
46	Palladium (Pd)	–	3,400	–	Fuel
47	Silver (Ag)	0	2,450	–	–
48	Cadmium (Cd)	$2.02 \cdot 10^{-3}$	1,038	1	Piping
49	Indium (In)	0	2,320	–	–
50	Tin (Sn)	–	2,960	–	Fuel
51	Antimony (Sb)	–	1,910	–	Fuel
52	Tellurium (Te)	$4.14 \cdot 10^{-2}$	1,260	13	Piping
53	Iodine (I)	0.11	456	7	Hot trap
54	Xenon (Xe)	0.15	165	9	Cold trap
55	Cesium (Cs)	0.19	958	4	Piping
56	Barium (Ba)	0.13	1,910	2	Fuel†
57	Lanthanum (La)	–	3,640	–	Fuel
58	Cerium (Ce)	–	3,200	–	Fuel
59	Praseodymium (Pr)	–	3,290	–	Fuel
60	Neodymium (Nd)	–	3,360	–	Fuel
61	Promethium (Pm)	–	3,000	–	Fuel
62	Samarium (Sm)	$4.59 \cdot 10^{-2}$	1,860	–	Fuel†
63	Europium (Eu)	$2.97 \cdot 10^{-3}$	1,700	–	Fuel†

were selected for individual tracking. Furthermore, some non-volatile elements are included in order to complete isobaric chains or otherwise radioactive daughters. These final selected isotopes are displayed in Table 4.29.

The tables below list the elements and isotopes to be tracked using the updated methodolgy described in Section 4.5.2. The isotopes tracked in Wesley Deason's original STELLA model can be found in his thesis [2].

Table 4.29.: List of isotopes tracked in STELLA model. Type describes whether isotope yield is calculated based on cumulative (C), individual (I), or individual plus metastable (I+MS) yield data.

Nuclide	Half-life (hr)	Design Yield	Type	Peach Bottom R/B	MHTGR BOL R/B	MHTGR EOL R/B
Selenium-80	–	$1.34 \cdot 10^{-3}$	C	1	1	1
Bromine-81	–	$1.85 \cdot 10^{-3}$	C	1	1	1
Selenium-82	–	$2.79 \cdot 10^{-3}$	C	1	1	1
Krypton-83	–	$4.46 \cdot 10^{-3}$	C	1	1	1
Krypton-84	–	$7.65 \cdot 10^{-3}$	C	1	1	1
Krypton-85m	4.48	$9.78 \cdot 10^{-3}$	C	0.049	0.058	0.011
Krypton-85	94,319.58	$6.28 \cdot 10^{-5}$	I	0.816	0.535	0.488
Rubidium-85	–	$5.77 \cdot 10^{-7}$	I	1	1	1
Krypton-86	–	$1.37 \cdot 10^{-2}$	C	1	1	1
Krypton-87	1.27	$1.79 \cdot 10^{-2}$	C	0.031	0.056	0.01
Rubidium-87	–	$3.94 \cdot 10^{-5}$	I	1	1	1
Krypton-88	2.84	$1.37 \cdot 10^{-2}$	C	0.042	0.057	0.01
Rubidium-88	0.3	$4.82 \cdot 10^{-4}$	I	0.018	0.055	0.009
Strontium-88	–	$1.88 \cdot 10^{-6}$	I	0	0	0
Rubidium-89	0.26	$3.05 \cdot 10^{-2}$	C	0.017	0.055	0.009
Strontium-89	1,214.64	$2.94 \cdot 10^{-5}$	I	0	0	0
Yttrium-89	–	–	–	0	0	0
Cadmium-111	–	$2 \cdot 10^{-3}$	C	1	1	1
Tellurium-126	–	$1.82 \cdot 10^{-3}$	C	1	1	1
Tellurium-127m	2,544	$6.46 \cdot 10^{-4}$	C	0.386	0.133	0.087
Tellurium-127	9.4	$3 \cdot 10^{-9}$	I	0.065	0.059	0.013
Iodine-127	–	–	I	0	0	0
Tellurium-128	–	$6.92 \cdot 10^{-3}$	C	1	1	1
Tellurium-129m	806.4	$1.9 \cdot 10^{-3}$	C	0.28	0.099	0.052
Tellurium-129	1.16	$7.11 \cdot 10^{-7}$	I	0.03	0.056	0.009
Iodine-129	–	$1.14 \cdot 10^{-12}$	I	1	1	1
Tellurium-130	–	$2.12 \cdot 10^{-2}$	C	1	1	1
Tellurium-131m	32.64	$6.72 \cdot 10^{-3}$	C	0.1	0.063	0.017
Tellurium-131	0.42	$1.64 \cdot 10^{-3}$	I	0.02	0.055	0.009
Iodine-131	192.55	$1.06 \cdot 10^{-4}$	I	0.18	0.076	0.03
Xenon-131	–	$1.82 \cdot 10^{-7}$	I+MS	1	1	1
Tellurium-132	76.8	$4.91 \cdot 10^{-2}$	C	0.134	0.068	0.022
Iodine-132	2.28	$8.65 \cdot 10^{-4}$	I+MS	0.039	0.057	0.01
Xenon-132	–	$7.2 \cdot 10^{-5}$	I+MS	1	1	1
Tellurium-133m	0.92	$3.21 \cdot 10^{-2}$	C	0.027	0.056	0.009
Tellurium-133	0.21	$1.92 \cdot 10^{-2}$	I	0.015	0.055	0.009
Iodine-133	20.8	$8.57 \cdot 10^{-3}$	I+MS	0.086	0.061	0.015
Xenon-133m	52.56	$2.54 \cdot 10^{-4}$	I	0.118	0.066	0.019
Xenon-133	125.83	$8.65 \cdot 10^{-5}$	I	0.157	0.072	0.025
Cesium-133	–	$1.09 \cdot 10^{-7}$	I	1	1	1
Tellurium-134	0.7	$5.68 \cdot 10^{-2}$	C	0.025	0.056	0.009
Iodine-134	0.88	$1.7 \cdot 10^{-2}$	I+MS	0.027	0.056	0.009
Xenon-134	–	$5.27 \cdot 10^{-4}$	I+MS	1	1	1
Iodine-135	6.57	$6.19 \cdot 10^{-2}$	C	0.057	0.058	0.012
Xenon-135m	0.26	$5.37 \cdot 10^{-3}$	I	0.017	0.055	0.009
Xenon-135	9.1	$3.67 \cdot 10^{-3}$	I	0.064	0.059	0.013

Table 4.29.: List of isotopes tracked in STELLA model. Type describes whether isotope yield is calculated based on cumulative (C), individual (I), or individual plus metastable (I+MS) yield data.

Nuclide	Half-life (hr)	Design Yield	Type	Peach Bottom R/B	MHTGR BOL R/B	MHTGR EOL R/B
Cesium-135	–	$3.18 \cdot 10^{-5}$	I	1	1	1
Xenon-136	–	$6.58 \cdot 10^{-2}$	C	1	1	1
Cesium-137	$2.64 \cdot 10^{5}$	$6.4 \cdot 10^{-2}$	C	0.91	0.857	0.811
Barium-137	–	$2.8 \cdot 10^{-5}$	I+MS	0	0	0
Xenon-138	0.24	$5.36 \cdot 10^{-2}$	C	0.016	0.055	0.009
Cesium-138	0.54	$9.4 \cdot 10^{-3}$	I+MS	0.022	0.055	0.009
Barium-138	–	$1.01 \cdot 10^{-3}$	I+MS	0	0	0

4.5.3. Updated case study results

Two cases were run in the STELLA model based on the two extremes presented in Section 4.5:

- Case 8: Elements with $T_{melt} < 1000°$ C leave fuel and enter hot trap. Plateout of Cs, I, and Se occurs in piping. Xe and Kr bypass hot trap and are collected in the cold trap.
- Case 9: Elements with $T_{melt} < 550°$ C leave fuel and enter hot trap. Condensation of everything but noble gases and halogens occurs in piping. Plateout of Cs, I, and Se occurs in piping. Xe and Kr bypass hot trap and are collected in the cold trap.

The cases retained the same parameters as Case 3 (Section 4.3.2.1), with the updated tracked isotope list (Table 4.29) and the MHTGR R/B model given in Equation 3.8 will be used Equation 3.9. The *b* values for Xe will be utilized for I, Te and Xe, with all remaining isotopes behaving like Kr.

The results of each case study is displayed in Table 4.30, while isotope specific results are displayed in Appendices B and B. There is no difference in the cold trap concentrations between the two cases as would be expected. The plate-out power, activity, and mass is roughly an order of magnitude higher if condensation is assumed to take place, resulting in 230 kW of heat from 72 kg worth of condensed fission products. The power and activity in the hot fission product trap is about half as much for Case 9. However, the total mass drops by a factor of 70. Although the results are only for 2.85 years, the power and activity in the traps reach equilibrium within the first simulated hour, while the plate-out power and activity only slightly increases over time. However, since the accumulated mass in each element is primarily stable elements, it will linearly increase throughout the operating time.

What is not included in the studies here is the actual location of the condensation. If the majority of the condensation occurs very near the fuel element, then the heat loading is no different than the decay heating present in freshly irradiated nuclear fuel which is cooled during normal operation and accident conditions by the fuel cooling systems. However, if the condensation is taking place at location where cooling is not readily available, some sort of special heat removal system may be required. Furthermore, the design of the piping must be able to accommodate the extra accumulated mass.

Table 4.30.: Case study results with MHTGR model and updated tracked elements at the end of 2.85 years.

	BOL		**EOL**	
	Case 8	Case 9	Case 8	Case 9
Hot Fission Product Trap Power (kW)	220.7	116.6	34.8	19.7
Cold Fission Product Trap Power (kW)	86.6	86.6	14.3	14.3
Plateout/Condensation Power (kW)	12.9	117	1.9	16.9
Hot Fission Product Trap Activity (MCi)	19.5	9.2	4.2	1.6
Cold Fission Product Trap Activity (MCi)	17.8	17.8	3.3	3.3
Plateout/Condensation Activity (MCi)	1	11.3	0.3	2.9
Hot Fission Product Trap Mass (kg)	67.9	1.1	69.9	1.1
Cold Fission Product Trap Mass (kg)	77.6	77.6	71	71
Plateout/Condensation Mass (kg)	5.4	72.2	5.8	74.6

5. Safety Analysis

A limited scope Probabilistic Risk Assessment (PRA) of a vented nuclear fuel system for a Generation IV Gas-Cooled Fast Reactor Plant was performed. The goal of the study was to better understand the safety and licensing implications of vented fuel technology. A Level 1 PRA was performed to determine the possible and probable failure mechanisms of the vented fuel fission product collection and auxiliary systems. A Level 2 PRA was performed to determine the possible releases from the vented fuel collection system under normal and abnormal operating conditions. Finally, a Level 3 PRA was performed to understand the consequence of a release of fission products from the vented fuel collection system to the population and environment.

5.1. Background

5.1.1. History of safety analysis in commercial nuclear power

Prior to the publication of WASH-1400 [99] in 1975, the nuclear safety regulations in the US were determined from conservative deterministic margins and models based on operating experience, expert judgment, and test results. WASH-740, issued by Brookhaven National Laboratory in 1957, was the first report addressing the risk associated with Nuclear Power Plants (NPPs) [100]. The report estimates the maximum possible damage from a reactor core meltdown with no containment building at a large nuclear reactor. The results of the study yielded unacceptable, and unrealistic results. The report estimated 45,000 deaths, 100,000 injuries, and $17 billion in property damage, encouraging further investigation of a more detailed and realistic evaluation of NPP risk.

5.1.1.1. WASH-1400

The completion of WASH-1400 in 1975 marked a pivotal event in the evaluation of NPP risk, establishing the pattern for future nuclear power plant PRAs, introducing fault trees and event trees to a large audience. WASH-1400, or the Reactor Safety Study (RSS), provided comparison with other non-nuclear risks, identified transients (loss of flow, rod withdrawal, etc.) and small break loss of coolant accidents (SB LOCA) as major risk contributors [99]. Furthermore, it showed the impact of testing and maintenance, common mode interactions, and human error contributions. The RSS showed that radiological risks from NPPs were small when compared to other societal risks. Although the report was criticized, it was a good first attempt at applying fault tree and event tree analysis to a nuclear reactor to determine the overall probability and consequence of an accident [101].

5.1.1.2. Post WASH-1400

Following the publication of WASH-1400, the Energy Reorganization Act of 1974 created the Nuclear Regulatory Commission (NRC) and the Department of Energy out of what was previously the Atomic Energy Commission (AEC). The NRC appointed the Risk Assessment Review Group to assess the quality of WASH-1400, whose findings are documented in the Lewis Committee Report published in 1977 [101]. The committee concluded that the Reactor Safety Study was performed with an inadequate database, poor statistical treatment, an inconsistent propagation of uncertainties throughout the calculation. The committee did note, however, that the fault-tree/event-tree methodology is sound and both can and should be more widely used by the NRC. Furthermore, the committee stated the implementation of the methodology in WASH-1400 was a pioneering step.

In response to the Three Mile Island (TMI) accident in 1979, the nuclear industry and regulators made several changes in regards to safety assessment of NPPs. Prior to the accident, only design basis accidents (DBAs) were considered in the licensing process. DBAs are postulated accidents that a facility is designed to withstand without exceeding the offsite exposure guidelines defined in 10CFR100. TMI prompted the industry to take a closer look at severe, or beyond design basis accidents, which usually involves multiple simultaneous failures; by definition, they include any unplanned accident resulting in significant core damage. Although the TMI release did not exceed the 10CFR100 limits, the outraged public prompted the NRC to determine "how safe is safe enough?" and published NUREG-880 documenting suggested qualitative and quantitative nuclear reactor safety goals [102]. A formal statement was issued in 1986, Federal Register 51.162, defining two qualitative and two quantitative goals [103].

5.1.1.3. NUREG-1150

In 1988, the NRC requested that each plant expressly assess its severe accident vulnerabilities. The Individual Plant Examination (IPE) would ultimately supplement the NRC's own reassessment of severe accident risks. As an update to WASH-1400, NUREG-1150 was published, documenting the severe accident risks of five nuclear power plants: Surry Power Station, Peach Bottom Station, Zion Nuclear Power Station, Sequoyah Nuclear Generation Station, and Grand Gulf Nuclear Generating Station [104]. The assessments included a variety of designs, including three- and four-loop Westinghouse PWRs (PWR, W3 & W4) and four- and six-loop BWRs (BWR - 4 & 6).

5.1.1.4. Post NUREG-1150

NUREG-1150 was further built upon with the NRC publication of the State-of-the-Art Reactor Consequence Analyses (SOARCA) report [105]. The SOARCA report includes an analysis of two plants believed to be representative of the two basic types of U.S. commercial nuclear power plants. These include the Peach Bottom Atomic Power Station Unit 2 and the Surry Power Station, a BWR - 4 and PWR W3 respectively, which were both analyzed in NUREG-1150. The goal of the SOARCA project is to develop updated and more realistic analyses of severe reactor accidents using computer modeling techniques to understand how a reactor might behave under severe accident conditions and furthermore how a release of radioactive material from the plant

might impact the public. Specifically, MELCOR (an integral severe accident analysis code) is used to model accident scenarios within the plant and MACCS2 (a consequence assessment code) is used to model the offsite health consequences resulting from atmospheric releases of radioactive material.

5.1.1.5. Risk-Informed regulation

Risk-informed regulation is an approach to regulation taken by the NRC, which incorporates an assessment of safety significance or relative risk. This approach ensures that the regulatory burden imposed by an individual regulation or process is appropriate to its importance in protecting the health and safety of the public and the environment. As stated in 10CFR52, all next generation (Gen III+ and beyond) reactors are required to include a PRA in the original license application. Interestingly, there are no PRA requirements for the current generation of LWRs. However, Regulatory Guide 1.174 requires the use of PRA for risk-informed decisions regarding changes to the plant's Licensing Basis (LB). By definition, LB changes are modifications to the plant's design, operation, or other activities that require NRC approval. Arguably, one can safely assume all plants will have LB changes at some point throughout their lifetime, thereby requiring all current generation LWRs to possess an updated PRA.

5.1.2. Probabilistic Risk Assessment

PRA, synonymous with Probabilistic Safety Assessment (PSA), is a systematic methodology for investigating the strengths and weaknesses of the design and operation of complex systems, such as a nuclear power plant. PRA is used extensively in the nuclear industry to estimate risk by addressing three fundamental questions, commonly referred to as "the set of triplets", which are:

1. What can go wrong?
2. How likely is it?
3. What are the consequences?

PRA is a method of identifying, characterizing, quantifying probabilistically, and evaluating hazards [106]. It should be noted the most significant result of the PRA is not the bottom line value of the risk computed, but the determination of the system elements that substantially contribute to the risks of that system, the uncertainties associated with such estimates, and the effectiveness of various available risk reduction strategies [107].

5.1.2.1. PRA Levels 1, 2, and 3

PRA is subdivided into three levels of analysis which each estimate a different level of risk. A Level 1 PRA estimates the frequency of accidents that cause damage to the nuclear reactor core. This level of analysis begins with an initiating event (i.e. station black-out or loss of coolant accident) and continues until the reactor core reaches a damaged state, determined by the success criteria for assuring adequate core cooling. Through the use of event/fault trees, scenarios

leading to core damage are defined resulting in an estimation of plant damage state frequencies. Thus, the output of a Level 1 PRA is an estimation of plant damage state frequencies, which combined give an overall core damage frequency (CDF). In comparison to the other levels of PRA, Level 1 is a relatively quick and inexpensive method of providing risk insight.

Level 2 PRA expands on the Level 1 PRA results by beginning with core damage accidents and continues the analysis until containment is breached or bypassed. This level of analysis includes accident progression, containment loadings, and structural response analysis combined with radioactive materials transport analysis. Event/fault trees address phenomenological events which challenge the integrity of the containment under specific accident scenarios. Accidents are quantified by the severity of the release of radioactive material, and ultimately grouped into plant damage states with similar conditions. The progression of a given accident differs for a given plant damage state (PDS), requiring accident progression analysis to be performed for each PDS. Thus, a Level 2 PRA estimates the frequency of accidents that release radioactivity from the nuclear power plant and the resulting radioactivity release, or source term.

Level 3 PRA expands on the Level 2 PRA results starting with a radioactive release outside of containment and continues the analysis to estimate the consequences of a given release by way of estimating the health effects from radiation doses to the surrounding population and land contamination from released radioactive material. The quantification of these effects is dependent on several factors. For example, the health effects from radiation dose are dependent on the population in the vicinity of the plant, evacuation conditions, and the path of the radioactive plume. Additionally, the plume is dependent on wind speed and direction and the presence of rain or snowfall. Likewise, land contamination is dependent on the characteristics of the release of radioactive material and how the land surrounding the plant is used. Thus, the Level 3 PRA estimates the final measure of risk combining consequence analysis with frequency estimations [108].

5.1.2.2. Event and fault trees

Fault trees are a deductive process by means of which an undesirable event, called a top event, is postulated and the possible ways for this event to occur are systematically deduced. The fault tree graphically represents the various combinations of component failures that lead to the occurrence of the top event. Thus, a fault tree does not necessarily contain all possible failure modes of the system, merely those failure modes which contribute to the occurrence of the top event [107].

For example, a simple pumping system, shown in Figure 5.1, can be analyzed using the fault tree methodology for the top event “no water delivered”. The system consists of five valves, two pumps, a water source, and a sensing and control system, which operate on AC power. There are two parallel trains in the system, meaning the failure of one train doesn’t dictate the failure of the entire system. However, failure of the water source (T-1), the shared isolation valve (V-1) to remain open, the sensing and control system, or the AC power would result in water delivery failure.

The fault tree is constructed by first identifying the top event, “no water delivered.” Next, the paths by which the top event may be achieved are determined and described by logical statements. For instance, there are four immediate paths to failure: either there is no water at V-

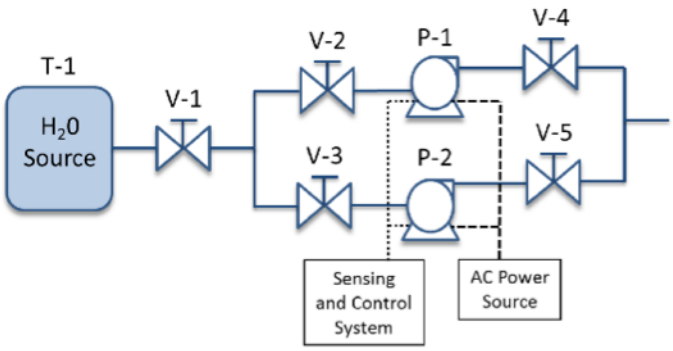

Figure 5.1.: Example pumping system [107].

1, the AC power fails, the sensors fail, or no water is delivered from the two pumping branches. This logic is depicted in the example fault tree shown in Figure 5.2, where basic events are represented as circles, intermediate events are represented by rectangles, undeveloped events are shows as diamonds, and logic gates are represented by their standard symbols (AND gates have a straight bottommost line whereas OR gates are concave). Since any of the four paths would lead to the top event, no water delivered, an OR gate is used to represent that condition.

There are underlying causes of failure of the AC power system and the sensing and control system, however in this analysis they are not considered, as indicated by the diamonds signifying an undeveloped event. In contrast, the methods by which no water is delivered to V-1 and the pumping branches fail is further analyzed, thus these two events are designated as intermediate events represented by a rectangle. There are only two paths that result in no water being delivered from V-1: either tank T-1 ruptures or V-1 fails to close. As either of these would result in such an event, an OR gate is chosen to logically represent this occurrence. For the upper pumping branch to fail to deliver water, the pump P-1 would have to fail to function or the valves V-2 or V-4 would have to fail closed. Similarly, for the lower pumping branch to fail to deliver water, the pump P-2 or the valves V-3 or V-5 would have to fail. A fault tree such as this enables system designers to better understand the system's strengths and weaknesses by detailing the possible ways by which an undesirable end state may be realized. Developing a simple fault tree requires only a minimum understanding of the overall system functionality; however developing a more compact version, preferable for computational efficiency, requires a much better understanding of the overall system logic.

The evaluation of fault trees involves two distinct aspects: logical or qualitative evaluation and probabilistic or quantitative evaluation. Qualitative evaluation involves the determination of the logic tree cut sets, which represent a single path that leads to an occurrence of the top event. A minimum cut set thus represents the minimum path that leads to an occurrence of the top event. Top event probability determination from cut sets involves the use of simple Boolean logic. An OR gate represents the union of the input events, denoted by the symbol $\cup$ and mathematically equivalent to the $+$ symbol. An AND gate represents the intersection of the input events, denoted by the symbol $\cap$ and mathematically equivalent to the $\cdot$ symbol. Determining the probability of the top event can be arduous, especially when the number of cut sets is large. Generally, there

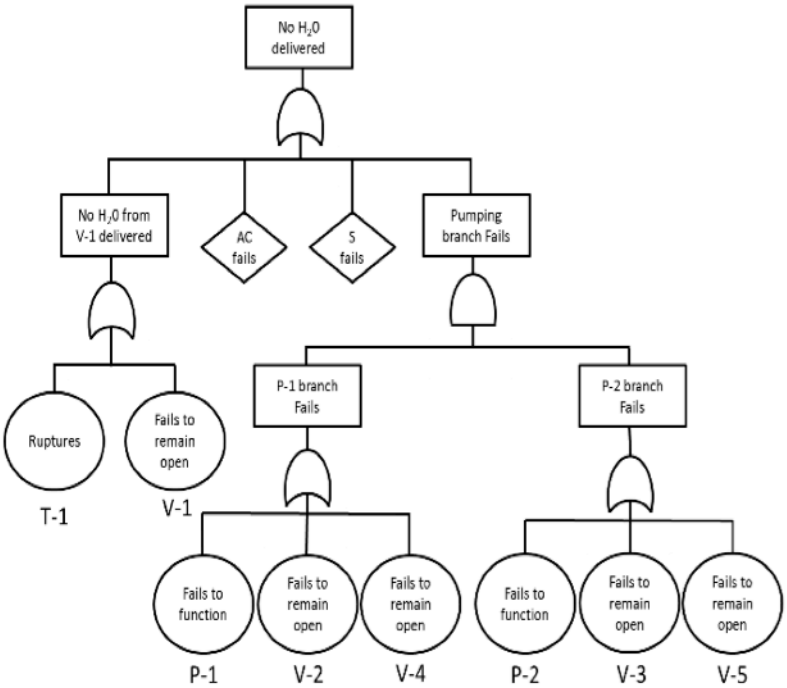

Figure 5.2.: Fault Tree for Top Event "No Water Delivered" [107].

are $2n-1$ such terms in cut sets, where n is the number of cut sets. For example, in the 13 cut sets generated for the pumping example in Figure 5.1 there are 8191 such terms [107]. For larger event trees, this can be a daunting task even for the most powerful computers, making software tools such as SAPHIRE [106] invaluable for organizing data and quantifying top events.

Event trees, similar to fault trees, are used to help deduce the logical chronological sequence of events leading to a failure. Event trees are horizontally built configurations that begin with an initiating event on the left side and proceeds chronologically to the right passing through various branch points, or points where systems succeed or fail, ultimately leading to a variety of end states. At each branch point, the upper branch represents success of the event heading, and the lower branch represents a failure. An example event tree is given in Figure 5.3. The qualitative evaluation of event trees is obtained through the use of Boolean algebra. The components are shown in failure mode while their compliments, represented with a bar, $\overline{AC}$, illustrate the probability of the system not failing.

5.1.2.3. Accident Progression Event Trees (APET)

The logical structure for modeling of the progression of an accident in the reactor system and in the containment can be provided by event trees. The Accident Progression Event Trees (APETs) used in NUREG-1150 were a major improvement over the Containment Event Tree (CET) ap-

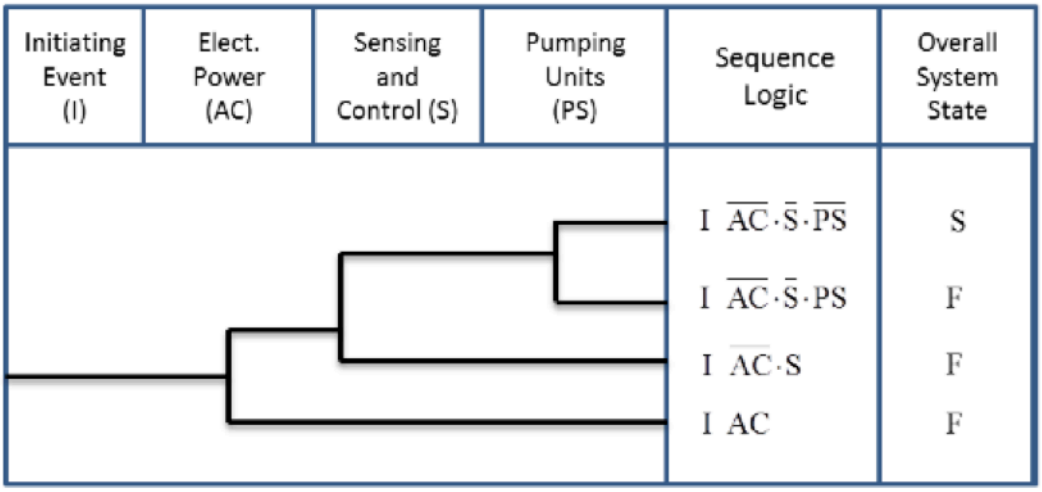

Figure 5.3.: Fault Tree for Top Event "No Water Delivered" [107].

proach used in WASH-1400. APETs are developed as a means of tracing the significant interdependent physical-chemical processes impacting accident progression and containment behavior. An APET identifies the ways by which containment failure or bypass may occur in addition to the various severe accident processes that affect the mode of failure, timing of failure, and magnitude of environmental radioactive material release [109]. Unlike the WASH-1400 event trees, where branch points are based on the failure or success of safety systems in demand, APETs address questions such as "Amount of hydrogen released in-vessel during core damage?" and "Type of vessel breach?" that represent various complicated processes occurring in the containment as the accident progresses. Each question in an APET analysis has two or more answers, creating two or more subsequent branches to follow after each branch point, or node, in the tree [110].

To initiate an APET, prior analysis is necessary to provide information about the PDS. PDS information includes a detailed description of the status of the plant operation and safety systems, containment safety systems, and support systems immediately before the core damage begins. This information is considered to be the initial condition of the plant for a given APET.

Branching point probabilities are typically determined for APETs by comparing physical conditions obtained in the severe accident scenario with branching criteria. However, there is not a deterministic outcome of "failure" or "no failure" for a given scenario because of the uncertainties (epistemic and aleatory) in the analysis. Consequently, uncertainty analysis is necessary to determine failure probability by performing several accident progression calculations using different modeling or input assumptions.

5.1.2.4. SAPHIRE

SAPHIRE (Systems Analysis Programs for Hands-on Integrated Reliability Evaluations) is a PRA software tool designed for reliability assessment and risk/safety assessment [106]. SAPHIRE

is used by the Nuclear Regulatory Commission (NRC), National Aeronautics and Space Administration (NASA), and the Department of Energy (DOE) for risk informed analyses. SAPHIRE can be used for Level 1 PRA analysis to model a plant's response to initiating events, quantify resulting core damage frequencies, and identify important contributors to core damage. Additionally, SAPHIRE can be used for Level 2 PRA severe accident analyses starting with a core damage state and evaluating containment failure and/or release models. SAPHIRE's capabilities include:

- Graphical event/fault tree construction;
- Rule-based fault tree linking;
- Fast cut set generation;
- Fault tree flag sets;
- Failure data;
- Uncertainty analysis;
- Cut set editor, slice, display, and recovery analysis tools;
- Cut set path tracing;
- Cut set comparison;
- Cut set and end-state partitioning;
- End-state analysis; and
- User-defined analysis types.

SAPHIRE is primarily used for generating minimal cut sets, the minimum combination of failures needed to result in the occurrence of the event of interest, for extremely large and complex event/fault tree logic models. Individual cut set probabilities are determined by adding the probabilities of the applicable basic events:

$$C_i = q_1 + q_2 + ... + q_n, \tag{5.1}$$

where C_i is the probability of cut set i and q_k is the probability of the k-th basic event in the i-th cut set.

After determination of the dominant cut sets, they are used to quantify the overall probability of basic events. Cut sets may be generated in SAPHIRE in three ways. The first method is the rare event approximation in which cut set values are simply summed:

$$S = \sum_{i=1}^{m} C_i, \tag{5.2}$$

where S is the minimal cut set upper bound for the system unavailability, C_i is the probability of the i-th cut set, and m is the number of minimal cut sets in the fault tree. The rare event

approximation is accurate when the cut set probabilities are small and the cut sets do not share many of the same basic events.

The second method is the minimal cut set upper bound approximation, which is the default method in SAPHIRE. The minimal cut set upper bound approximation is an approximation of the probability of the union of the minimal cut sets"

$$S = 1 - \prod_{i=1}^{m}(1 - C_i), \tag{5.3}$$

where S is the minimal cut set upper bound for the system unavailability, C_i is the probability of the i-th cut set, and m is the number of minimal cut sets in the fault tree.

The third method is the exact calculation method, entitled the inclusion approach, in cases where the rare event and minimal cut set upper bound approximations provide too conservative a result. The exact calculation is the sum of the probability of the individual sets, minus the sum of the probability of all possible pairs, plus the sum of the probabilities of all possible combinations of three, minus the probabilities of all possible combinations of four, plus the probability of intersection of all five minimal cut sets, etc. After cut sets are generated, they may be used to obtain standard importance measures and to propagate the epistemic uncertainty.

Uncertainty analysis in SAPHIRE provides information regarding the variability of a fault tree top event (or sequence) probability resulting from uncertainties in the basic event probabilities. Two sampling methods are provided: Monte Carlo or Latin Hypercube sampling. The Monte Carlo random number generator sampling technique was chosen for this analysis. In this methodology, repeated quantifications of the system cut sets are made using each random variable sampled from the basic event uncertainty distributions.

Similarly, importance measures in SAPHIRE provide information regarding reliability worth about basic events appearing in the cut sets of a given fault tree. Components with high relative importance may merit close monitoring of component degradation over time or design changes to increase component reliability. There are essentially three types of importance measures: ratio, interval, and uncertainty. The ratio importance measures include Fussell-Vesely Importance (FV), Risk Reduction Ratio (RRR), and Risk Increase Ratio (RIR). The interval importance measures include Brinbaum Importance (B), Risk Reduction Interval (RRI), and Risk Increase Interval (RII). The uncertainty importance measures are expressed through the probability distribution as a standard deviation. FV is an indication of the fractional contribution of the basic event to the minimal cut set upper bound. Both the RRR and RRI indication how much the minimal cut set upper bound would decrease if the basic event probability were reduced to a probability of 0 (i.e. never failed). The RIR and RII indicate how much the minimal cut set upper bound would increase if the basic event probability were increase to a probability of 1. Finally, B indicates the sensitivity of the minimal cut set upper bound with respect to a change in the basic event probability.

5.1.3. Atmospheric transport modeling

Modeling the release of radioactive material outside of a nuclear power plant is a complicated process, and is based on empirical models that account for the distribution and dilution in air,

surface water, ground water, and terrestrial ecosystems. The goal of atmospheric transport modeling is to determine the quantity of radionuclides reaching the population or environment. This is calculated by estimating quantities such as external submersion dose from a contaminated cloud, external dose from contaminated soil deposition, internal inhalation dose from the cloud, and internal dose from ingestion of contaminated water and or foodstuff. Atmospheric releases of a pollutant are usually assumed to originate from a source that can reasonably be approximated as a point emitting material at a steady rate.

5.1.3.1. Gaussian Puff/Plume modeling

The most commonly used diffusion model is the Gaussian Plume/Puff model (GPM). A plume is defined as a continuous release from a point source for an arbitrarily long amount of time (Figure 5.4). Gaussian-distributed plumes represent most releases from point sources because the free atmosphere is not confined [111].

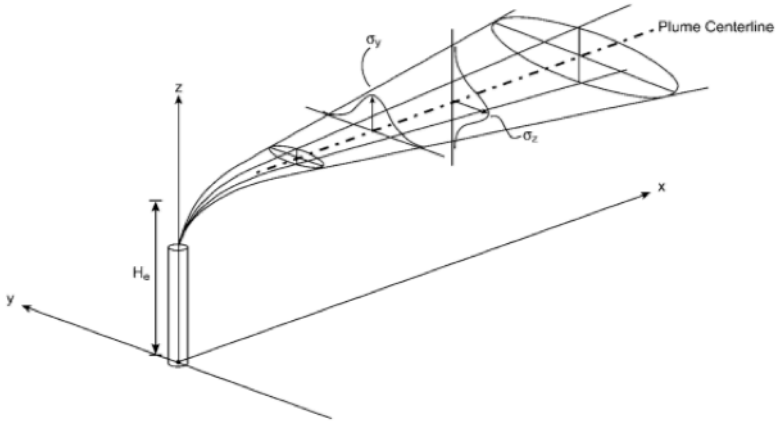

Figure 5.4.: Gaussian Plume Model [111].

The general equation for the concentration of the contaminant using the GPM model is

$$\chi(x,y,z,H) = \frac{Q(pers)}{2\pi\bar{u}\sigma_y\sigma_z}\exp\left(-\frac{y^2}{2\sigma^2{}_y}\right)\left[\exp\left(-\frac{(z-H_{eff})^2}{2\sigma^2{}_z}\right)+\exp\left(-\frac{(z+H_{eff})^2}{2\sigma^2{}_z}\right)\right] \tag{5.4}$$

$$H_{eff} = H + d\left(\frac{v_s}{\bar{u}}\right)^{1.4}\left(1+\frac{T_s-T_a}{T_s}\right) \tag{5.5}$$

χ	=	concentration of the contaminant,
x	=	distance downwind,
y	=	horizontal distance from the plume centerline,
z	=	height above ground,
Q	=	release rate of contaminants,
$\overline{u}$	=	mean wind speed,
σ_y	=	horizontal dispersion coefficient,
σ_z	=	vertical dispersion coefficient,
H_{eff}	=	effective stack height,
H	=	actual stack height [m],
d	=	inside diameter of stack [m],
ν_s	=	exit velocity of the stack [m/s],
$\overline{u}$	=	mean wind speed at top of the stack [m/s],
T_s	=	temperature in stack [K],
T_a	=	temperature of atmosphere [K].

For the case of ground contamination (z=0), the concentration is effectively doubled by combining the exponential terms inside the brackets. This can be thought of as accounting for the reflection of the plume from the ground, where the plume essentially folds over on itself to double the ground-level concentration [111]. The effective stack height term, H_{eff}, accounts for the temperature differential of the gas, momentum effects due to the velocity of the discharged effluent, and the horizontal translation due to the wind field.

A puff is defined as a single discrete point source release modeled with respect to time and position. The Gaussian Puff Model is commonly used for a single, instantaneous release (Figure 5.5.

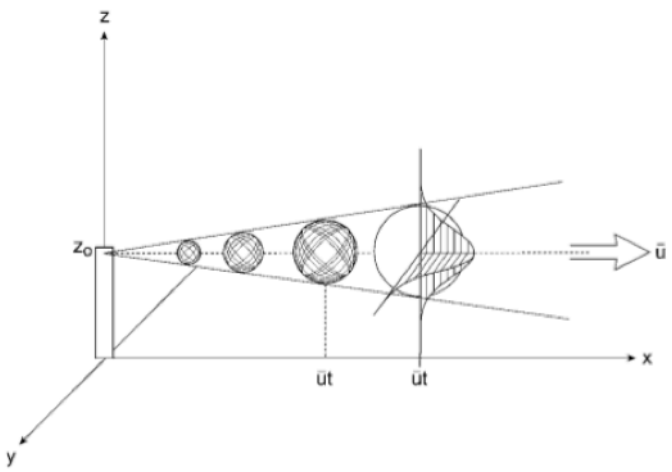

Figure 5.5.: Gaussian Plume Model [111].

The general equation for the concentration of the contaminant using the puff model is:

$$\chi(x,y,z,t) = \frac{Q_p}{(2\pi)^{\frac{3}{2}}\sigma'_x\sigma'_y\sigma'_z} \exp\left\{-\frac{1}{2}\left[\left(\frac{x-\overline{u}t}{\sigma'_x}\right)^2 + \left(\frac{y}{\sigma'_y}\right)^2 + \left(\frac{z-H_{eff}}{\sigma'_z}\right)^2\right]\right\} \quad (5.6)$$

χ	=	concentration of the contaminant at a point and time,
Q_p	=	total release of material,
$\overline{u}$	=	mean wind speed,
H_{eff}	=	effective stack height,
σ'_x	=	horizontal dispersion coefficient,
σ'_y	=	crosswind dispersion coefficient,
σ'_z	=	vertical dispersion coefficient.

5.1.3.2. Atmospheric stability classes

Various turbulence conditions affect the rise and dispersion of plumes. Classes of turbulence are classified in terms of the temperature profile with height and variations in wind speed and direction, each of which affects the turbulence field. The Stability Classes range from A-F, where A represents the least stable conditions and F represents the most stable conditions.

- Class A: Extremely unstable conditions (bright sun, daytime)
- Class B: Moderately unstable conditions (sunny, daytime)
- Class C: Slightly unstable conditions (light cloudiness, daytime)
- Class D: Neutral conditions (overcast sky, brisk wind, day or night)
- Class E: Slightly stable conditions (early evening, light winds, relatively clear sky)
- Class F: Moderately stable conditions (late night, light wind, clear sky)
- Class G: Very stable conditions (predawn, very light wind, clear sky)

These general conditions in terms of wind speed and the amount of sunshine or cloudiness are shown in Table 5.1. The representative stability class establishes the dispersion coefficients, σ_y and σ_z, for the period under consideration, using curves of dispersion coefficient verses distance for stability classes A-F.

5.1.3.3. GENII

GENII is a computer code developed for the Environmental Protection Agency (EPA) at the Pacific Northwest National Laboratory (PNNL) which incorporates state-of-the-art internal and external dosimetry models into updated versions of environmental pathway analysis models [112]. GENII is primarily used for calculating radiation doses for individuals and populations following chronic or acute releases. This is accomplished by modeling radionuclide transport via air, water, or biological activity. The air transport modeling options include puff and plume models, calculation of effective stack height, plume rise from buoyant or atmospheric releases, and

Table 5.1.: Atmospheric Stability Classes.

Wind Speed (m/s at 10m)	Daytime Incoming Sunlight *Strong*	*Moderate*	*Slight*	Nighttime Cloud Cover *>50%*	*<50%*
<2	A	A-B	B	E or F	F or G
2-3	A-B	B	C	E	F
3-5	B	B-C	C	D	E
5-6	C	C-D	D	D	D
>6	C	D	D	D	D

building wake effects. GENII is run through a user interface using the Framework for Analysis in Multimedia Environmental Systems (FRAMES).

5.1.4. Past PRAs of gas-cooled reactors

5.1.4.1. Modular High-Temperature Gas-Cooled Reactor (MHTGR)

The DOE submitted a MHTGR PRA to the NRC as part of the pre-application review process in 1987. The MHTGR PRA documentation was submitted in two volumes; Volume 1 contains the majority of the overall discussion related to methodology, plant description, accident initiators, plant response, consequences, and results [113]. Volume 2 contains the majority of the technical information pertinent to the PRA such as the data base, event tree construction and quantification, and release category description and dose quantification [25]. The basis for the PRA assessment is the standard MHTGR design as presented in the Preliminary Safety Information Document (PSID) [113]. The MHTGR PRA includes:

- MHTGR-specific initiating events, event sequences, and end states sufficient for integrated plant risk assessment;
- event sequences involving release from single and multiple reactor modules;
- fault tree models and data to estimate event sequence frequencies;
- plant transient response analysis for each event sequence;
- mechanistic source terms for each event sequence involving a release of radioactive material; and
- offsite dose consequences for each MHTGR-specific release category.

The PRA utilized a combined event tree-fault tree approach to define risk-related sequences and their frequencies. Initiating event groupings were established for primary coolant leaks, loss of heat transport system (HTS) cooling, earthquakes, loss of offsite power, transient, control rod withdrawal and steam generator leak. Event trees were developed describing sequences associated with the failure of functions provided to mitigate the effects of these initiators.

Systems and functions included in the event trees defined which fault tree models were developed. The fault tree and event tree models addressed support system interactions on an assumed set of high-level functional intersystem dependencies, but did not utilize linked fault tree or support state methodologies in the process [114]. Sequences were completely developed only in cases where the sequence frequency was greater than 1E-8 1/yr, for which release categories were defined and used to describe plant risk.

5.1.4.2. Pebble Bed Modular Reactor (PBMR)

Exelon submitted a proposed approach to the PBMR PRA to the NRC in 2002 to support licensing decisions as part of the documentation of the proposed licensing approach for the PBMR in the US [115]. Since there is no counterpart for the Light Water Reactor (LWR) core damage end-state, the splitting up of event sequences into Level 1-2-3 does not apply to the PBMR. The NRC provided feedback supporting the development of a full-scope, detailed PRA. It was acknowledged that while the PBMR PRA does not fit the mold of the Level 1-2-3 framework, equivalent information regarding radiological consequences can be provided.

Furthermore, the NRC staff recognized a belief that further development of standards was necessary because current ASME standards focus on Large Early Release Frequency (LERF) analysis for Level 2 PRAs and does not address Level 3 PRAs. Finally, it was acknowledged that the PBMR PRA results will have relatively large uncertainties stemming from the lack of operating experience [116]. PBMR licensing project activities were discontinued due to a lack of funding and no further development of the PRA is documented.

5.1.4.3. Next Generation Nuclear Plant (NGNP)

A PRA has yet to be fully developed for the proposed NGNP project designs; however a white paper was published describing the scope and objectives for the PRA for use in the NGNP Combined Operating License Application (COLA) and subsequent HTGRs [117]. The approach is applied to a single reactor module with the capability to extend later to multi-module plant designs. It was noted that the NGNP HTGR PRA will take into account insights from the Exelon PBMR pre-application review and build upon the approach applied to the MHTGR as part of the pre-application review. In addition to discussion of PRA methodology, the paper outlines the relevant regulatory policy and guidance for the proposed HTGR PRA. Furthermore, it was acknowledged that the PRA will necessarily account for the risk of multiple modules.

Similar to the PBMR PRA approach, the NGNP PRA would not calculate CDF or LERF metrics but rather would calculate HTGR-specific plant state frequencies that correspond with the Licensing Basis Events (LBEs). Certain intermediate plant states may be defined to describe intermediate risk metrics, typically involving pressurized and depressurized conduction cooldown events, where the capability for forced circulation core cooling by active systems is lost.

The proposed PRA model structure would consist of a continuous event sequence spanning the initiation of events to the release categories for which mechanistic source terms and radiological consequences are calculated. Thus, the integral HTGR PRA approach encompasses the functions of a full scope Level 1-2-3 LWR PRA. A comparison of the HTGR PRA structure for

Table 5.2.: Comparison of HTGR PRA with LWR PRA Model Structure [117].

PRA Model Attributes	PRA Outputs	LWR Level 1	LWR Level 2	LWR Level 3	HTGR
Assessment of accident frequencies	Core Damage Frequency (CDF)	Yes	Yes	Yes	No, however a range of selected risk metrics consider releases from the fuel.
	Plant Damage State (PDS) frequencies	Not necessary but sometimes included	Yes, all PDSs are variations of LWR core damage state	Yes, all PDSs are variations of LWR core damage state	Yes, NGNP plant states defined as event sequence families for LBEs; some intermediate states may be defined.
	Release category frequencies	No	Yes, all involve core damage and are LWR specific	Yes, all involve core damage and are LWR specific	Yes, however NGNP HTGR-specific release categories are not tied to a core damage state
	Frequencies of site meteorological conditions and emergency planning responses	No	No	Yes	Yes, conservative bounding treatment is expected to meet COLA requirements
Assessment of accident consequences	Source Terms	No	Yes, mechanistic source terms for each LWR release category quantified	Yes, mechanistic source terms for each LWR release category quantified	Yes, mechanistic source terms for each NGNP HTGR release category quantified.
	Consequences to the Public	No	No	Yes, early and latent health effects (QHOs).	Yes, but doses would be assessed at the exclusion area boundary.

the NGNP COLA with that of the Level 1-2-3 framework for an LWR was provided in the white paper and is duplicated in Table 5.2.

5.1.5. Recent PRAs of gas-cooled reactors

5.1.5.1. CEA Gas-Cooled Fast Reactor (CEA GFR)

The CEA developed a Level 1 probabilistic model to support the design of the 2400 MWth gas-cooled fast reactor [118]. The GFR design is helium cooled with a core outlet temperature of about 850-900° C and an operating pressure of 7 MPa. The top events for the Event Trees (ETs) are mostly related to the mission of the front line systems. Fourteen Initiating Event (IE) families were selected using the Master Logic Diagram (MLD) approach. The frequencies of the IEs are based on similar data for various reactor types (LWR, SFR, HTGR, PBMR) and expert judgment with uncertainties described by lognormal distributions and assumed a low Error Factor (EF) of

3. The EF is calculated by taking the square root of the ratio of the 95th percentile to the 5th percentile. The Level 1 PSA, equivalent to PRA, model assumes a mission time of 7 days, where the mission time refers to the time that a system or component is required to operate in order to successfully perform its function.

Component failure rates were obtained from three databases: EIREDA (French PWRs), T-BOOK 6 (Scandinavian LWRs), and EG&G-gas (related to gas-cooled reactors). A simplified methodology for creating the component reliability database was executed under the assumption that components belonging to GFR gaseous circuits are affected by failure rates consistent with the EG&G-gas database, whereas for GFR water circuits the EIRDA database is preferred. In cases where a value is not obtainable, the assumed values of 10E-3 for a failure on demand and 10E-6 per hour for a failure to run are applied. Uncertainties in failure rate data are described by lognormal distributions with an EF of 3 indicating "good" confidence and an EF of 10 indicating "poor" confidence. Furthermore, the Multiple Greek Letter (MGL) model was selected to describe Common Cause Failures (CCF). Neither Human Reliability Assessment (HRA) nor component unavailability due to repair actions were accounted for in the model, driven by the early design stage of the reactor. CDFs are provided for each IE, with a total core damage frequency of 1.47E-06 per year.

5.1.5.2. Very High-Temperature Reactor (VHTR)

The VHTR currently in development in Korea is a gas-cooled graphite reactor with Tristructural-Isotropic (TRISO) fuel assembled in either block or pebble form [119]. Similar to the PBMR PSA approach, the VHTR PSA approach diverts from the traditional Level 1-2-3 approach. A two level procedure is approached which consists of a sequence level PSA, analyzing the accident sequence and containment performance, and a consequence level PSA, for consequence analysis. Sixteen radiation release categories are identified, stemming from five plant damage states and two core heat-up states. IE selection is based on the MLD method, identifying the accident initiators having a radiological potentiality according to the conceptual design of the VHTR; twenty two IEs were selected for the analysis.

IE frequencies were assigned in a subjective manner due to the lack of information, and will necessarily be continually refined. Event tree models are used for accident sequences and supporting logic models are used to estimate functional heading events in the main event trees, as opposed to fault tree models which require more depth. Documented preliminary results for the unfavorable core heat-up estimate 4.27E-05 per year. No specific component reliability database, HRA, or reliability of the digital instrumentation and Controls (I&C) system, or source terms are currently assessed due to the insufficient level of depth of the VHTR design development. The VHTR PSA is expected to develop concurrently with the development of the VHTR design.

5.1.5.3. High Temperature Gas-Cooled Reactor- Pebble Bed Module (HTR-PM)

The internal initiating event PSA under the power operation mode for the HTR-PM has been completed [120]. PSA models for the extended scope such as low power and shutdown mode, internal hazards (fire and flood), and external events (seismic) are under development. The typical CDF and LERF risk metrics are replaced by the HTR-PM specific risk metric representing

the cumulative frequency of all the beyond design basis accident sequences which may cause the off-site individual effective dose at the site boundary to exceed 50mSv. The estimated value of 3.7E-7 per reactor year is calculated for the cumulative frequency of the accident sequences which may exceed the 50mSv consequence limit.

As expected, the HTR-PM PSA does not follow the traditional Level 1-2-3 framework, instead electing an integrated framework which combines the level 1 and 2 PSA. The eighteen categories of IEs were selected using deductive methods such as the MLD method and Failure Mode and Effect Analysis (FMEA). IE frequency quantification is determined under the assumption that transient initiating events similar to those found in LWRs can be determined based on world-wide operating experience and LOCA and support system failure initiating events are quantified specifically using expert judgment and consolidated operating experience where applicable.

Component reliability data for the HTR-PM PSA is based on generic sourced due to insufficient relevant operation information. Reference databases include Jul-Spez-388 (German HTR), URD database (EPRI LWR), NUREG/CR-6928 (US LWR), and NUREG/CR-2728 (US LWR). Conservative choices are made if obvious differences exist among the databases. Although disparities among databases exist, sensitivity studies of component data revealed the fact that the problem of component reliability data is much less severe than conceived. It was noted that the unique design conception and functional features of the reactors can influence the results more significantly than the component reliability data of new reactor concepts.

5.2. Vented Fuel System Design

In order to perform a PRA, specifics of the system such as component types, component layout, system redundancies, and operator interaction are necessary inputs. As stated previously, the present work utilizes the GA EM^2 vented fuel design as the representative system for the PRA due to the sufficient state of the design and collaboration with GA. The following sections discuss the components of the fission product vent system and their arrangement in greater detail.

5.2.1. Choice of fission product vent system components

The purpose of the FPVS system is to transport fission products from the core to a collection system for long term safe keeping in order to achieve the projected extensive core life without over-pressurizing the fuel. The purge stream, which carries fission products directly from the fuel, is highly radioactive, requiring safety considerations during transport. One such safety feature is a negative pressure differential (relative to the primary coolant inlet pressure) that is maintained to prevent leakage of gaseous fission products into the primary coolant. With the high level of radioactivity present in the purge stream, it is desirable to trap as many fission products as possible, as close to their source as possible to reduce the risk of environmental release. Consequently, the specific configuration of the system must be optimized to safely remove and store the majority of the fission products in the beginning portion of the system.

The most commonly used material for fission product sorption is activated charcoal. Activated charcoal is often chosen due to its high melting temperature, permitting operation at high operating temperatures concomitant of GFRs, and its capability for capturing and delaying ra-

dioactive noble gases that are markedly inert. Activated charcoal is an attractive adsorbent due to its large capacity, non-hygroscopic nature (ability to not hold water) [92], and is relatively inexpensive. The process of collecting noble gasses using activated charcoal relies on the principle of adsorption (collection of a particle on a surface) rather than the more familiar principle of absorption (collection of a particle in a volume). To trap additional fission products, the activated charcoal bed can be used to exploit the principles of condensation (if the temperature of the bed is below the boiling point of the element) and chemisorption (the process of sorbing an element by chemical bonding with the carbon or an impregnated element or molecule).

Activated charcoal is capable of trapping all fission products released from the fuel, however the adsorption characteristics of activated charcoal vary considerably as a function of temperature and the elemental properties of the adsorbed contaminant. For instance, volatile metals and non-metals released from the core can be adequately adsorbed at higher temperatures however for noble gases and halogens, satisfactory adsorption can only be achieved at lower temperatures [92]. Naturally, this process is completely reversible for noble gases by simply allowing the temperature of the charcoal bed to increase. This ability is desirable for recharging the system under controlled settings, however can be deleterious if unintentional reversal occurs under accident conditions.

5.2.2. Fission product vent system component layout

As discussed previously, the configuration of the system must be designed in order to ensure effective removal and retention of the fission products quickly and efficiently. Thus, it is desirable to remove as many fission products as possible as close to the source as conceivable. In an ideal situation, a single trap would be employed to collect all fission product contaminants from the helium purge stream immediately after exiting the core, however the presence of decay heat and the variation of fission products present in the purge stream makes this task impractical. Thus, the system is essentially divided into two regions based on temperature. First, the purge stream passes through a hot region, which is designed for the collection of volatile metals and non-metals, and next a cold region which is intended for the collection of halogens and noble gases. By configuring the system with the hot region first, the required cooling load is reduced by removing as many contaminants as possible before reaching the cold region.

The FPVS is subdivided into the FPTS and the FPRS. The FPTS consists of a series of manifolds, pipes, and valves, which transport the purge stream from the fuel elements to the FPRS via three 100% redundant trains. The FPTS is additionally responsible for regulating the pressure to ensure a negative pressure differential between the fuel bundle and the primary system to prevent leakage of gaseous fission products into the primary coolant. The FPRS is designed to remove and retain the fission products from the purge stream via filtration and adsorption at both high and low temperatures. The FPRS features three 100% HTAs located outside of the pressure vessel and inside of containment. The placement of the first fission product trap outside of the fuel element deviates from the Peach Bottom and GCFR systems which utilize in-element charcoal traps.

By placing a trap in the core it can be cooled by the primary coolant, rather than a separate cooling system required of a core-external fission product trap. However, the internal placement of the trap negatively impacts the size of the core and consequently the cost of the reactor vessel

and fuel elements in addition to diminishing the neutronic performance of the core. Conversely, placing the first trap outside of the core allows the trap to be cooled to lower temperatures than the primary coolant, increasing the adsorption capability of the charcoal bed. Moreover, this placement allows the trap to be larger and more complex without the inherent restrictions of an in-core configuration. The disadvantages of a core-external trap are the additional cooling burden, which could potentially become an issue during an accident scenario, and the increased risk of radioactive release as a consequence of almost all the volatile radioactive material produced in the core being carried outside of the core through piping and valves. Keeping this in mind, the EM^2 design places the first fission product trap in containment, removing the majority of the fission products prior to exiting containment via dual redundant containment isolation valves.

The remainder of the system, which includes four redundant 50% LTAs and two redundant compressor modules, is located in the reactor auxiliary building. Placement of these components in the auxiliary building allows for easy access for maintenance and precludes an increase of containment sizing necessary to house additional components. Although this placement does introduce some risk of release from the reactor auxiliary building, the magnitude of fission products in the purge stream is significantly decreased after passing through the HTA. Additionally, dual redundant automatic isolation valves are in place for system piping entering and exiting the containment. Thus, in the event of an accident scenario, the portion of the system located in the auxiliary building can be isolated.

As stated previously, the EM^2 design has undergone a series of modifications and evolutions in association with the present work. In addition to the determination of valve and flange types and locations, it was decided to remove the dependency of the HPS from the FPVS. Early in the design process, the LTA and compressor modules were shared between the HPS and FPVS as a means of reducing capital cost by eliminating duplicate components that could be otherwise shared between the two systems. It was determined that little, if any, reduction in capital costs resulting from the elimination of independent LTA and compressor modules for the HPS, both relatively low-cost components, would be at least partially offset by the cost of additional piping and valves required for a shared component interface. Furthermore, the interfaces between the HPS and FPVS add complexity to the safety analysis and increase the probability of potential containment bypass scenarios. The functions of the HPS, in addition to maintaining proper coolant chemistry, are to provide purified helium to various purges and buffers in the plant and purify the helium inventory before sending it to the helium storage tanks. By sharing the LTA with the FPVS, which provides a relatively large fission product inventory, there is an increased potential of inadvertently distributing radioactivity around the plant via the HPS. Although a PRA of the shared HPS and FPVS configuration was not completed, preliminary work on the PRA model for this configuration proved overly complicated, requiring an assessment of the HPS system in its entirety due to the dependence of the two systems. Furthermore, the HPS functions providing purified helium to various purges and buffers in the plant added complexity to the analysis, broadening the scope of the PRA to an impractical level given the time and resources available. The vented fuel system, as modeled in the subsequent analyses, is shown in Figure 5.6.

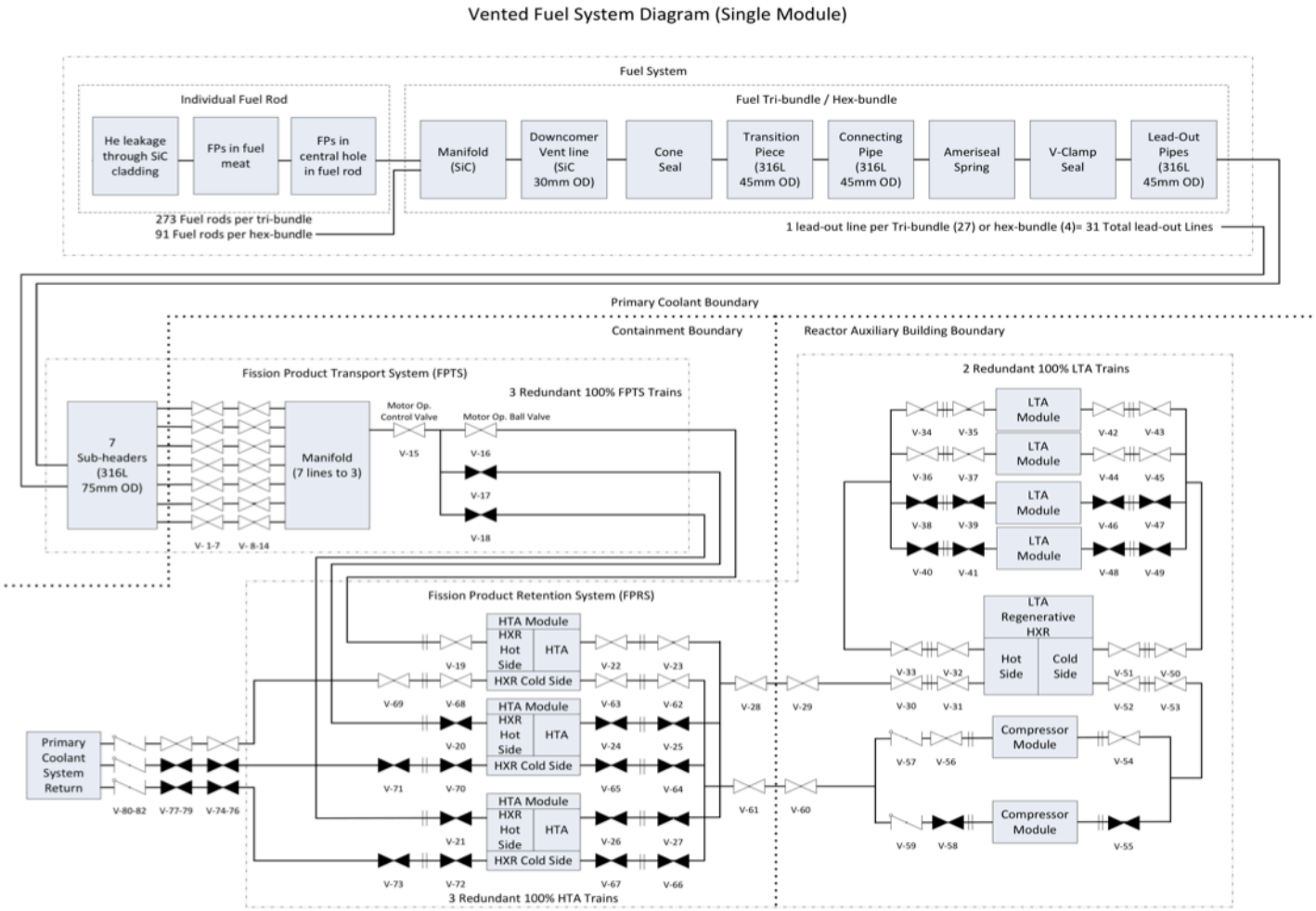

Figure 5.6.: Vented fuel system diagram.

5.3. Probabilistic Risk Assessment Modeling Assumptions

The present work aims at understanding the safety implications and feasibility of the FPVS. As such, it is necessary to define the scope of the PRA performed in the present work and the subsequent assumptions necessary. In order to determine the risk associated with a failure of the FPVS to retain fission products under accident conditions, the FPVS is treated as an isolated system. The following analyses are performed under the assumption that the FPVS is isolated from the effects of a failure of surrounding plant systems, with the exception of the integrity of the reactor pressure boundary, containment, reactor building, and auxiliary building. Furthermore, it is assumed that the systems not analyzed in the PRA operate perfectly. The pathways by which fission products may escape the FPVS and lead to an environmental release are shown in Figure 5.7.

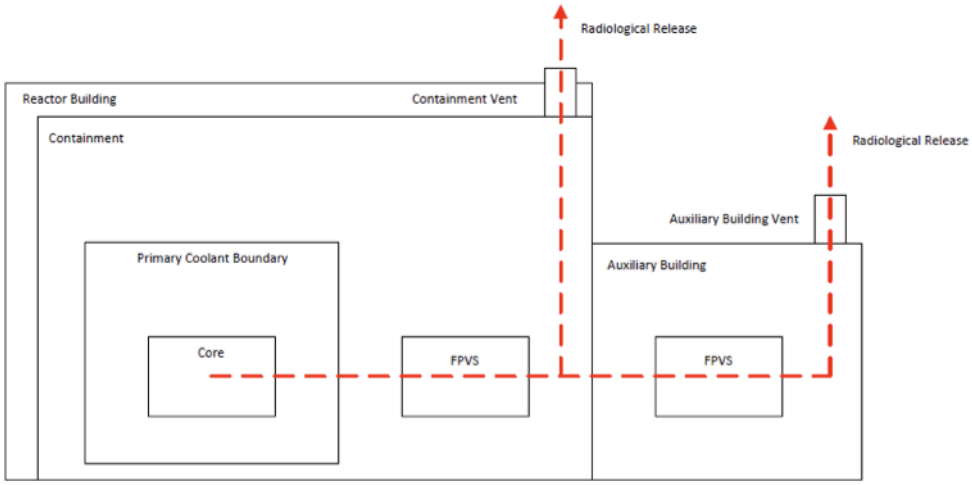

Figure 5.7.: FPVS potential pathways to environmental release.

5.4. Probabilistic Risk Assessment Inputs

To perform a PRA, it is necessary to quantify the frequency of a given initiating event and the probability of component failure, human failure, and common cause failures. Furthermore, these frequencies and probabilities serve as input into a graphical representation of system and accident progression failure through the use of fault tree, event tree, and accident progression event tree analysis. Additionally, specifics of the quantity and distribution of fission products throughout the system and the capacity of various fission product barriers to limit the release to the environment are necessary input in calculating the source term. Finally, in order to determine the environmental consequences, additional information regarding the location and type of release and atmospheric dispersion conditions must be quantified. The following sections discuss the various inputs to the vented fuel system PRA.

5.4.1. Initiating event frequency

Every accident analysis begins with an initiating event, thus the first node of an event tree is the initiating event frequency. The initiating event frequency is the numerical value (in units of 1/year) assigned to reflect the estimated frequency of occurrences of a given accident type for a given plant design and location. When available, initiating event frequencies are determined based on operating experience data spanning several decades. In the U.S., the extent of our operating experience data is primarily for BWR and PWR plants; this data is analyzed, continually updated and made available to the general public by the NRC [121]. Unfortunately, the lack of operational experience for advanced gas reactors makes it difficult to determine both initiating event scenarios and their corresponding frequencies. The method commonly employed for advanced gas reactor PRAs in determining initiating event frequencies is to integrate the limited gas reactor specific data, relevant LWR data, and expert engineering judgment. Similar methodology will be used for the vented fuel system PRA.

5.4.2. Component reliability

When analyzing the reliability of a system, the system is broken down to the component level and analyzed using fault tree analysis [107]. The reliability of a component refers to the component's ability to successfully perform an intended function. There are two basic types of components, those that operate continuously (fails when operating) and those that operate on demand (fails to start or while operating after start). The probability of component failure is determined using component failure rate data, a statistical model (typically exponential), and a set mission time. The unreliability of a component is defined as,

$$\Pr(T \leq t) = \int_0^t f(t')dt', \quad t \geq 0 \tag{5.7}$$

which represents the probability that the component will fail sometime up to time t: T represents the time-to-failure of the component and $f(t)$ is the probability distribution function (PDF). The hazard rate of a component shows the changes in the probability of failure over the lifetime of the component; the shape of the hazard curve exhibits a bathtub shape and is commonly referred to as the bathtub curve, as shown in Figure 5.8.

The exponential distribution is the most commonly used PDF in reliability analysis, corresponding to a constant hazard rate model representative of the chance failure region of the bathtub curve. The exponential distribution is given as,

$$f(t) = \lambda \exp(-\lambda t) \tag{5.8}$$

where λ is the instantaneous failure rate. Similar to the determination of initiating event frequencies, the failure rate for a given component is determined by operational experience data and is readily available for LWR environments [121]. Conversely, component data unique to gas reactors is limited requiring an assessment method of integrating failure rate data from various reliability databases and exercising engineering judgment. Thus, the component reliability database for the vented fuel system is assembled by selectively merging failure data from several applicable reliability databases.

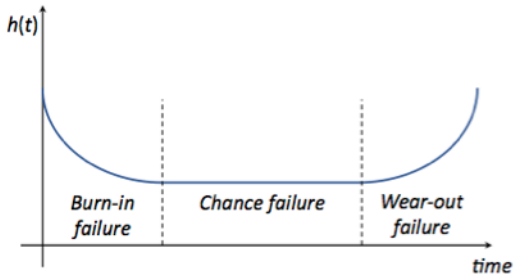

Figure 5.8.: Typical Bathtub Curve [107].

5.4.3. Common Cause Failure (CCF)

Dependent failures are defined as events in which the probability of each failure is dependent on the occurrence of other failures [107]. In reliability analysis, dependent failures must be given adequate treatment in order to minimize overestimation of reliability. These failures may be caused by internal events (internal challenges, intersystem or inter-component dependencies) or external events (natural or man-made environmental events). Several major causes of dependence can be explicitly described and modeled, however the remainder of the causes can be collectively modeled using the concept of CCF. CCFs are defined as a subset of dependent events in which two or more component fault states exist at the same time, or in a short time interval, and are direct results of the same cause. These dependencies of CCFs are not known and difficult to model explicitly. Consequently, several parametric models have been developed to quantify the probability of CCF.

These models include the beta factor, MGL, alpha factor, and binomial failure rate models. The beta factor model is the most common single parameter model, which assumes whenever a common cause event occurs all components of the redundant component system are assumed to fail instantaneously. This method is commonly used for its simplicity, but at higher levels of redundancy other multiple parameter models should be used.

One such multiple parameter method is the MGL model. This model utilizes additional parameters (γ, δ, etc.) to distinguish among common cause events affecting different numbers of components in a higher level of redundancy. In this model, (β, γ, δ) represent the conditional probability to have at least (2, 3, 4) components belonging to the same CCF group failing by the same cause knowing that (1, 2, 3) components failed. The probability Q_k represents the probability of CCF among k specific components in a component group of size m, such that $1 < k < m$. Q_k for the MGL model can be calculated by,

$$Q_k = \frac{1}{\binom{m-1}{k-1}} (1 - \rho_{k+1}) \left(\prod_{i=1}^{k} \rho_i \right) Q_t \tag{5.9}$$

$k = 1, ..., m$

$\rho_1 = 1, \quad \rho_2 = \beta, \quad \rho_3 = \gamma, \quad ... \quad , \quad \rho_{k+1} = 0$

where Q_t represents the total probability of failure accounting both for common cause and independent failures.

5.4.4. Human reliability

The method of quantifying the reliability of human interaction is called human reliability analysis. The assumptions, mechanisms, and approaches used by any one specific human model cannot be applied to all human activities [107]. Human performance can be affected by social, environmental, psychological, organizational, and physical factors that are difficult to quantify. Human error may occur in any phase of the design, manufacturing, construction, and operation of a complex system, however human reliability during system operation is generally of primary concern in PRA. In instances where operator action is required, such as switching trains for testing and maintenance, it is important to properly model the probability associated with the reliability of a given operator to successfully perform the task at hand.

The MHTGR PRA operator response model was based on cognitive error as opposed to procedural [122]. It was identified that accident timing and operating systems differ from those of PWRs, requiring a different operator response model. Furthermore, reliance on computer controlled systems during normal operation conditions and on passive safety systems during accident conditions removed dependencies on operator interaction in several instances. The MHTGR operator response model assigns a human error probability as a function of time, based on the 1982 generic data base for data models chapter of National Reliability Evaluation Program (NREP) guide [123].

Several more modern HRA methodologies have since been applied to industry reliability assessments. These include: Technique for Human Error Rate Prediction (THERP) [124], Accident Sequence Evaluation Program (ASEP) HRA Procedure [125], Cause Based Decision Tree (CBDT) Method [126], Human Cognitive Reliability (HCR)/Operator Reliability Experiments (ORE) Method [126], Standardized Plant Analysis Risk HRA (SPAR-H) method [127], and A Technique for Human Event Analysis (ATHEANA) Method [128]. All of the previously mentioned methods have strengths and weaknesses; the chosen method for a specific application is dependent on the application and importance of the breadth and depth of the analysis [129].

The THERP Method is resource intensive and lacks guidance leading to an increased potential for analyst-to-analyst variability in the results [129]. The generic Time/Reliability Correlation (TRC) for addressing diagnostic errors is an over-simplification for addressing cognitive causes and failure rates for diagnosis errors when used by itself. Inputs besides time availability may impact the error rate and are not accounted for in this method. The ASEP method is a simplified and easy to use version of the THERP method, which similarly uses a generic TRC for addressing diagnosis errors, which leads to over-simplification. The CBDT method uses decision tress, similar to fault trees, to provide an initial set of failure mechanisms and influencing factors to be considered, offering flexibility. However, this flexibility leads to potential variability among analysts and was not intended to address time-limited conditions.

The HCR/ORE method uses empirical data and results in a reasonable and reliable quantification, however there is no systematic approach to identify causal factors that could affect diagnosis for actions modeled and the associated limitations to this method questions the consistency and appropriate application of this method [129]. The SPAR-H method is relatively simple

to use and results are traceable. The eight Performance-Shaping Factors (PSFs) included cover many situations where more detailed analysis is not required and the effect of the time dependence is considered in this method. The resolution of the PSFs is inadequate for detailed analysis, however this is considered inconsequential for systems with limited information available for the system. The ATHEANA method is among the most thorough context developing HRA methods considering a reasonable range of different conditions as part of the context. However, this method is both time and resource intensive offering flexibility and detailed analysis with a cost.

5.4.5. Fault tree analysis

As described in Section 5.1.2.2, fault trees are used to determine the various combinations of component failures that lead to the occurrence of the top event. Fault trees are developed by breaking down the system into constituent components and modeling their dependence accordingly. Fault trees can be developed for subsystems within a larger system for simplicity and transferred into the larger system's fault tree accordingly. This methodology was applied to the vented fuel system PRA, where fault trees were developed for the individual modules which together constitute the FPTS and FPRS, which ultimately form the FPVS. Thus, fault trees were developed for in-service and stand-by HTAs, LTAs, compressor modules, and the regenerative heat exchanger and were transferred into the fault trees for the FPTS and FPRS.

5.4.6. Event tree analysis

As described in Section 5.1.2.2, event trees are developed to model an initiating event and the chronological demand of each subsequent system in response to the initiating event. At each branch point, the demand on the postulated system is either a success or failure, leading to an eventual end state where the core is either damaged or OK. Pathways that lead to core damage end states are qualitatively evaluated resulting in a PDS frequency. PDSs are scenarios leading to core damage, thus the summation of the calculated PDS frequencies results in an overall CDF, the traditional output of a Level 1 PRA analysis.

As the present work is limited to the evaluation of the vented fuel system explicitly, an end state of a vented fuel system Level 1 PRA event tree resulting in a system failure is defined as a System Damage State (SDS), in lieu of a PDS. Likewise, the summation of SDSs results in a System Failure Frequency (SFF), in lieu of a CDF, as the SFF more accurately integrates the definition of failure for this analysis. A system failure for this analysis is defined as the release of radioactivity from the vented fuel system, thus failure modes resulting in leakage from the vented fuel system are analyzed.

5.4.7. Accident progression event tree analysis

As described in Section 5.1.2.3, PDS information is considered to be the initial condition of the plant for the APET. In a typical LWR Level 2 PRA, APETs are used to identify the ways by which containment failure or bypass may occur in addition to the various severe accident processes that affect the mode of failure, timing of failure, and magnitude of environmental

radioactive material release. As the present work is limited to the evaluation of the vented fuel system safety implications explicitly, the APET is developed to analyze the progression of the accident in the vented fuel system and containment.

The top events of the APET incorporate the effects of changes to the system in response to the initiating event beyond leakage from the system. These top events incorporate the additional possible failure modes of the vented fuel system and associated systems that have the potential to alter the progression of the accident via the timing of a failure or the magnitude of the radioactive release. The top events are categorized to describe failures related to pressure control, availability of cooling systems, change in adsorption capabilities, status of pressure boundary and containment isolation, and the status of the integrity of containment itself. The end states of the various sequences of the APET are categorized into release categories of similar significance, identified as Source Term Groups (STGs). Thus, the output of the Level 2 APET analysis is ultimately a frequency of occurrence for the various STGs.

5.4.8. Source term analysis

The source term calculations for the GA MHTGR [130] and NGNP HTGR [106, 131] identify two distinct components to the source term: a prompt term which can be released immediately and a delayed term whose timing is dictated by the slow heatup of the core. The prompt source term is comprised of both circulating and plateout inventories. The delayed source term is a larger fraction of the total fission products and consists of the release from fuel particles which have manufacturing defects, including heavy metal contamination, released by transients or chemical attack from water ingress events. Due to the assumptions and limitations of the modeling tools currently developed for the system, only the prompt source term is considered in the present work.

Similar to LWRs, gas reactors employ several fission product barriers to limit the release of radionuclides to the environment. The functional containment of many gas reactor designs includes the fuel particle and coating, the graphite core, the pressure boundary, the containment, the reactor building, and the auxiliary building. As the vented fuel system is designed to remove fission product gases from the core, the present work focuses on the barriers outside of the core, which include the pressure boundary, containment, and reactor building. The ability of these fission product barriers to limit the release of radionuclides is characterized by way of Attenuation Factors (AFs).

Numerous analytical tools are used to model and calculate fission product generation, transport, and release to the environment. Frequently, these include computer codes specific to the reactor designer [131]. In general, separate sets of codes are used to calculate the distribution of fission products in the core and in the primary cooling system during normal operations and the behavior of the fission products during accident sequences, including incremental, additional fuel failure and fission product transport and release. The present work employs a fission product transport model developed using the software tool STELLA for the vented fuel system.

5.4.9. Consequence analysis

Consequence analysis is often performed using MELCOR Accident Consequence Code (MACCS) software as a continuation of the integral severe accident analysis code MELCOR frequently used for Level 2 analysis. Due to the limited scope of the present work, a more general industry standard release model code was selected. The present work utilizes the software tool GENII version 2.10 for calculation of radiation dose and risk from radionuclides released to the environment from the vented fuel system under accident conditions [112].

The MHTGR PRA includes a consequence assessment for forced convection cooldown events under dry and wet conditions [132]. Since the EM^2 does not employ a steam generator, only dry accident scenarios are considered further. Forced convection cooldowns under dry conditions are assumed to be imitated by primary coolant leaks. Several sub categories are considered within the forced convection cooldown dry condition scenario, which differ in consequence dependent on the size of the leak. The fission product transport in the reactor building, subsequent release to the atmosphere, and resultant dose calculations were performed using the TDAC computer code, based on coupled linear differential equations governing the activity in the different volumes representing the reactor vessel, reactor building, and the environment over time.

The assumption of instantaneous homogeneous mixing is used to calculate the activity in each volume. The dose calculations are based on the semi-infinite cloud approximation. The parameters and site data used in the TDAC model include a settling rate of 0.32 h^{-1}, plateout rate of 1.0 h^{-1}, leak rate of 1 volume/day, Exclusion Area Boundary (EAB) distance of 425 m, atmospheric dispersion factor at the EAB (including building wake effect) from 0 to 8 hours of 1.22 x 10-4 s/m^3, and a breathing rate from 0 to 8 hours of 3.47 x 10-4 s/m^3. The atmospheric dispersion factors used in the nominal analysis were derived in accordance with the methodology of Regulatory Guide 1.4 [133], including the effect of the building wake. Ten percent of the Regulatory Guide 4.2 [134] atmospheric dispersion factors are used for the median values, in accordance with Regulatory Guide 4.2, since it results in typical values for any potential site and is expected to envelope about 85% of U.S. sites. The breathing rates used in the analysis are taken directly from the Regulatory Guide 1.4. The nominal does consequence for each of the release categories analyzed is given for 30-day EAB thyroid, lung, bone, and whole body gamma doses.

More recently, a NGNP scoping analysis of source term and functional containment attenuation study was performed in which a simplified model of representative reactor configurations was used to estimate potential source terms and consequences. Atmospheric dispersion and deposition values are determined using the methodology and meteorological information identified in the report, "Engineering Evaluation of X/Q Values Consistent with Regulatory Guide 1.145" [135]. Dose calculations were performed for distances of 400 m, 800 m, 1600 m, 3200 m, and 8000 m. Distance-weighted dose conversion factors are calculated in MACCS.

Atmospheric dispersion factors (X/Q values) were determined at the specified downwind distances for a hypothetical ground-level release using meteorological data form a site with the worst case average annual dispersion coefficients. Building wake-effects were not included, since the building wake acts to increase diffusion and lower the X/Q's, this assumption is conservative. For DBA analyses, 95% values for X/Q were used and for PAG analyses average X/Q values were used. The standard dose conversion factors listed in the EPA Federal Guidance

Table 5.3.: NGNP 95% X/Q Values for 400 m EAB

Release Assumption	0-2 hours	0-8 hours	8-24 hours
95% Ground Level	3.35E-03	1.91E-03	1.49E-03
95% Elevated (100m)	6.17E-06	3.33E-06	2.54E-06

Technical Reports (FGRs) 11 and 12 were used and the computer code MACCS generated a set of distance-weighted dose conversion factors for each exposure scenario. Five scenarios were modeled for a receptor located at 400 m for plume exposures and at all analyzed distances for the ingestion pathway.

The report "Engineering Evaluation of X/Q Values Consistent with Regulatory Guide 1.145" [135] was developed to aid the progression of the NGNP by way of evaluating site specific atmospheric dispersion estimates that will be established during subsequent design development. In the evaluation, the atmospheric dispersion model PAVAN was used to calculate X/Q values at defined downwind distances from hypothetical ground-level and elevated releases using meteorological data from 18 nuclear sites.

Basic model input requirements include release type and height, building dimensions to calculate wake effects, and downwind X/Q evaluation distances (i.e. the EAB or LPZ distances). Both a ground-level and an elevated release height of 100 meters are simulated in PAVAN to provide bounds on the estimates of X/Q at downwind distances, including 400, 800, 1600, 3200, and 8000 meters. The NGNP model assumes no building wake effects to be conservative, ground-level and elevated to 100m release types, flat terrain, and evaluation distances of 400, 800, 1600, 3200, and 8000 meters. Additionally, PAVAN requires meteorological data in the form of a joint frequency distribution (JFD) of wind direction, wind speed, and atmospheric stability. The JFD's summarize wind information using 16 sectors based on standard cardinal compass directions and wind speed binds. Vertical temperature difference is used to estimate the Pasquill stability classes.

The calculated maximum X/Q values correspond well to LWR values obtained from Design Certification Documents (DCDs) for currently approved or undergoing review Generation III LWRs. Similar to the MHTGR approach, the 50th and 95th percentiles form the basis of environmental and safety evaluations, respectively. The 95% X/Q value for a distance of 400 meters was chosen as a reasonable value for NGNP scoping calculations based on the 18 different nuclear sites considered. The resulting X/Q values are summarized in Table 5.3.

The Total Effective Dose Equivalent (TEDE) for each isotope is calculated by,

$$TEDE_i = C_i(DCF_i^{WB} + DCF_i^{In} \cdot BR)\frac{\chi}{Q} \tag{5.10}$$

i	=	isotope index
BR	=	Breathing rate [3.5E-04 m^3/s]
Ci	=	Activity of isotope i [Ci]
$TEDE_i$	=	TEDE Dose for isotope i [rem]
DCF_i^{WB}	=	Whole Body Air Immersion DCF for isotope i [rem-m^3/(Ci·s))
DCF_i^{In}	=	Inhalation Effective DCF for isotope i [rem/Ci]
χ/Q	=	Atmospheric Dispersion Factor (s/m^3)

The atmospheric transport code GENII performs essentially the same calculation in addition to calculating the atmospheric dispersion factors given meteorological data for the site of interest. Dose calculations were performed using this method for one source term group as a means of validating the GENII model.

5.5. Vented Fuel System PRA Integration

As discussed in the previous section, a Level 1, 2 and 3 PRA entails the use of several software tools in varying levels of detail and application. To better understand how the various components of the vented fuel system PRA are combined, the integration methodology applied to the present work is graphically summarized in Figure 5.9.

5.6. Level 1 PRA Model

To begin the PRA of the vented fuel system, it is necessary to build a Level 1 system model using a software program with the ability to quantify the SDSs and resulting cumulative SFF. The industry standard software tool SAPHIRE version 8.1.0.0 was chosen for this analysis. In order to complete the Level 1 PRA model, it is necessary to select initiating events and their associated frequencies, establish a component reliability database, select a methodology for quantifying CCF and HRA, and finally to build fault trees and event trees to model system failure and the system response to a given initiating event. The following sections discuss the components of the vented fuel system Level 1 PRA development in greater detail.

5.6.1. Selection of initiating event frequencies

The lack of operational experience with advanced gas reactors makes it difficult to determine IE scenarios and frequencies, thus the method of identifying and quantifying initiating event frequencies is similar to the method executed in assigning component reliability data from several database sources. The accident sequences to be analyzed were chosen based on the contents of advanced gas reactor safety analyses and PRA reports, while incorporating LWR initiating events that are independent of reactor type. The safety analysis and PRA reports considered include the Peach Bottom (PB) Unit 1 [7,136] GCFR [118], and HTGR [25,113] and PBMR [137] safety analysis and PRA reports.

The PB FHSR identifies a rupture of the doubly contained fission product purge line as the most severe accident involving two independent failures [7]. A large break in the primary loop

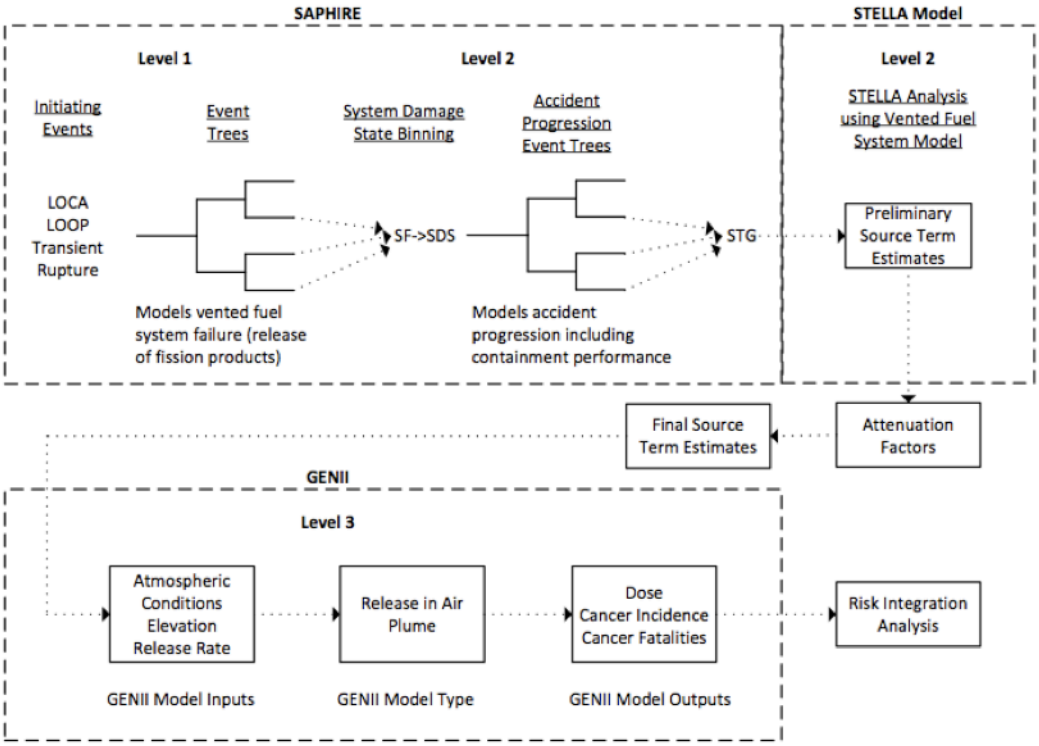

Figure 5.9.: Vented Fuel System Level 1, 2 and 3 PRA Integration.

causing backflow of purge gas was identified as the most severe accident involving a single failure. The PB PHSR identifies three types of accident scenarios related to the helium purification system, namely loss of cooling capability, rupture of the trapping system, and changes in purge flow contents [136]. The accidents identified within the loss of cooling capability category are the following: loss of purge flow, loss of purification compressors, primary system depressurization, loss of cooling water, and loss of refrigeration. The accidents within the changes in purge flow contents category are the following: increase in fission product concentration, increase in water content, and an increase in chemical impurities. In addition to the failure scenarios included in these analyses, a station blackout event is considered in response to the industry wide efforts to prevent and understand the effects of a Fukushima-like event.

Furthermore, a NGNP HTGR lessons learned report documents moisture problems occurring in the FSV HPS [138]. Moisture bypassed the chiller that was used to precipitate water from the helium purification system. The excessive moisture in the system caused the operating helium purification train to ice up, causing problems with the purification system during a moisture ingress event. Although the EM^2 design does not incorporate a steam generator, alternative water sources are available in the design. Nonetheless, it was determined that water ingress event is extremely unlikely and therefore omitted from the present work. The initiating events considered in the aforementioned sources were incorporated in the present work by inclusion

Table 5.4.: Events and Failure Modes Challenging the FPVS.

Accident Scenario	Relevance	Comments	Conclusion
Rupture of doubly contained fission product purge line	PB FHSR	Rupture or breach of FPVS inlet, highest fission product concentration.	Initiating Event – Rupture/Breach at FPVS Inlet
Large break in primary loop causing backflow of purge gas	PB FHSR	Large break in primary loop not analyzed in subsystem fault trees.	Initiating Event – Large Break Loss of Coolant Accident (LB LOCA)
Loss of purge flow	PB PHSR	Blockage, valve failure, rupture.	Fault Tree Failure Mode
Loss of purification compressors	PB PHSR	Compressor failure.	Fault Tree Failure Mode
Primary system depressurization	PB PHSR	Compressor failure.	Initiating Event – LB LOCA (Primary system rupture)
Loss of cooling water	PB PHSR	Heat exchanger failure.	Fault Tree Failure Mode
Loss of refrigeration	PB PHSR	Liquid nitrogen cooling system failure.	Fault Tree Failure Mode
Rupture of trapping system	PB PHSR	Pipe/valve/seal failure.	Fault Tree Failure Mode
Increase in fission product concentration	PB PHSR	Transient.	Initiating Event – Reactive Excursion/Transient
Increase in water content	PB PHSR/ FSV	Water ingress, SG tube rupture (not applicable to all systems).	Initiating Event – Water Ingress (SG Tube Rupture)
Increase in chemical impurities	PB PHSR	Filter failure.	Fault Tree Failure Mode
Station Blackout (SBO)	Fukushima	IE of Loss of off-site power (LOOP) followed by loss of on-site power.	Initiating Event – Station Blackout

as either a failure mode in the fault tree or a subsystem of the HPS or as an initiating event. A description of the accident scenarios considered, their relevance, and conclusion is included in Table 5.4.

Generally, transient initiating events similar to those in LWRs can be determined based on LWR operation experience [120]. However, LOCA and support system failure initiating events unique to advanced gas reactors are quantified specifically using frequency values available in gas reactor PRA literature wherever possible. A lognormal uncertainty distribution was assumed with an error factor chosen based on the availability and applicability of the data. A summary of the initiating events selected to be analyzed, associated frequencies, and error factor is included in Table 5.5.

5.6.2. Selection of component reliability data

The availability of reliability data for components unique to gas reactors is both limited and dated. A 1976 MIT PhD dissertation [9] documents a probabilistic analysis of the GCFR demonstration plant. As this study was an extension of the Reactor Safety Study, WASH-1400 [99], failure data from the 1974 study was used in the GCFR analysis. The GCR Reliability Data Bank

Table 5.5.: Initiating Event Frequencies

Number	Initiating Event	Frequency/yr	Error Factor
1	Rupture/Breach at FPVS Manifold	8.76E-05	10
2	LB LOCA	1.00E-04	10
3	Reactivity Excursion/Transient	7.00E-01	10
4	LOOP (Leading to SBO)	6.14E-02	3

Status Report [139], published in 1978, is a component and system reliability database developed by GA. The data bank resulted from extraction of several sources of data that were synthesized into generic failure rate estimates with variability ranges for GCR components. WASH-1400 was one of several reliability data sources which served as inputs to the creation of the GCR Reliability Data Bank. The 1987 GA MHTGR PRA Database [25] extensively references the GCR Reliability Data Bank as the primary source of reliability data. The failure rate data found in the MHTGR PRA Database are extremely similar to those found in the GCR Data Bank. Additionally, the 1989 Failure Rate Screening Data for Fusion Reliability and Risk Analysis (EGG-GAS) [140] references WASH-1400 and the GCR Reliability Data Bank as inputs into the fusion database among fission plant data sources.

More recent advanced gas reactor PRA literature references the 1988 MHTGR PRA Database as a primary source of data. This includes a 2001 document describing the licensing approach for the PBMR in the US [115]. It is noted within this document that the process is based on methods developed for the MHTGR and modified to reflect advances that have been made since. Specifics regarding the database used for the PBMR are not openly available; however there are extensive references to MHTGR documentation, including the MHTGR PRA, which suggests the incorporation of the HTGR database to that of the PBMR. A 2011 article discussing the reliability database for the CEA 2400 MWth GFR identifies the GCR Reliability Data Bank as the main source for components of the primary circuit [141]. EGG-GAS, a LWR and SFR database referred to as EGG-SSRE [142], and several other LWR and electronic databases serve as input to the CEA GFR database. A more recent publication documenting the reliability database for the CEA GFR [118] indicates the EGG-GAS database was used as the main source for gaseous circuits as opposed to the GCR Reliability Databank previously chosen. There is no specific indication as to why this is the case. The gas-cooled system data within the EGG-GAS database, published 11 years after the GCR databank, is derived directly from the GCR databank. Therefore, there is no observable difference in the values indicated, merely an updated database source which is likely the context behind the change.

Moreover, a 2012 article discussing the PSA for the HTR-PM demonstration plant in China references the MHTGR PRA, although not specifically related to the component reliability data [120]. Due to insufficient operation information, the HTR-PM component reliability data is based on generic sources similar to the CEA GFR database. The first specifically referenced source is the 1987 German reliability database Jul-Spez-388, which was used for the risk analysis of the German HTR design that is regarded as the prototype for the HTR-PM. Moreover, several LWR databases including NUREG/CR-6928 [121] are referenced as inputs. NUREG/CR-6928

Table 5.6.: FPVS database input reliability data.

Database Name	Application Field	Publication Year
GCR Reliability Data Bank [139]	GCR	1976
MHTGR PRA Database [113]	MHTGR	1987
EGG-GAS [140]	Fusion	1989
EGG-SSRE [142]	LWR/SFR	1990
INEEL Fusion [144]	Fusion	1998
NUREG/CR-6928 2010 Update [143]	PWR/BWR	2010
CEA GFR PRA Database [145]	GCFR	2010

is superseded by updated data in 2010 that is available on the NRC website in spreadsheet form [143]. The EGG-GAS database was essentially updated in 1998 to form a new INEEL Fusion database [144] written by L.C. Cadwallader, a co-author of EGG-GAS.

In addition, a 2011 NGNP PRA white paper [117] discusses the development of a PRA database for the NGNP. It was noted that the amount of relevant HTGR and GCR experience available to support the PRA is comparatively small, yet comparable to the amount of experience that existed with LWRs when the WASH-1400 study was performed in the mid-1970s. Existing generic data for LWRs will be used for many components, however, unique HTGR components for which there are little or no service data available to derive failure rates from will rely upon engineering judgment. Consequently, the limited availability of service data will be reflected in larger uncertainties for such components.

As documented in the more modern gas-cooled reactor PRA literature, the common approach to establishing a reliability database is to obtain reliability data from gas reactor studies to the extent possible and use reliability data for fusion, LWR, SFR, and electronic fields to fill in the gaps as deemed appropriate. This approach is executed in the development of the reliability database for the vented fuel system. A list of component reliability database documents that were used as inputs to the FPVS database is included in Table 5.6.

Due to the narrow scope of the vented fuel system PRA, reliability data for components within each subsystem is essential. As this type of study has not yet been performed, reliability data for components unique to the FPVS are not included in the reactor databases listed in Table 5.6. These components include the charcoal adsorption beds and the liquid nitrogen cooling system. In order to assign reliability data for these unique components with a basis, alternative sources such as fusion and tritium processing laboratory component reliability data were examined. Tritium Processing Laboratory (TPL) component data was chosen based on the similarities in both environment and system components required. Reliability data specific to adsorber bed failure was particularly difficult to find. The only documented reference to adsorber failure rates found was included in a PNNL Carbon Capture System reliability analysis [146]. Although a failure rate was determined for the study, it was omitted from the reliability assessment due to the high failure rate dominating the reliability measures in an unrealistic manner. As a result, the adsorber failure rate for the present work was assigned a target value using engineering judgment. The additional sources utilized in determining the failure rate of unique HPS components are listed

Table 5.7.: FPVS database input unique to FPVS component reliability data.

Database Name	Application Field	Publication Year
EFDA - Fusion [147]	Fusion	2004
JAERI - Tritium Processing Lab [148]	Fusion/TPL	2002
INEEL - Tritium Component Data [149]	Fusion/TPL	2005

in Table 5.7.

The process of selectively merging the data to create the FPVS database is based on the process documented for the CEA GCFR PSA [141] and shown graphically in Figure 5.10. A FPVS database is built based on the degree of analogy of components in existing databases to those of the FPVS. For each component and failure mode, three database relevance tests are performed to determine the appropriateness among available data. These tests determine the relevance of the component data regarding the function, failure mode(s), and environment. Components are divided into three categories distinguishing the degree of similarity of the HPS component to that included in the reference database. These categories are "identical," "similar," and "not referenced" components.

"Identical" components are defined as components which are included in at least one database which meets the three relevance tests in their entirety having the same function, failure mode, and environment of that included in the reference database. A "similar" component is defined as having only partial analogy to the component included in the reference database, generally differing in environment. Finally, the "not referenced" component category is for components where no comparable data exists. This category is further separated into two subcategories, namely "innovative" and "not innovative." A component deemed "not innovative" is assigned a target value common for industry reliable components. The suggested mean industry target value is 10-6/h for random failure under operation and 10-3/d for random failure per demand. An "innovative" component is a component for which no data corresponds to that component and a challenging numerical value is proposed instead of a target value. At this point in time, no innovative components are included in the FPVS database.

Once categorized, data is selected among several choices, according to the relevance of information, the database specificity and its homogeneity. Components belonging to gaseous circuits are assigned failure rates as indicated in the MHTGR PRA database whenever possible. When data is unavailable in a gas reactor database, fusion and TPL reliability data is considered. Likewise, components belonging to environments identical to that of a PWR are assigned failure rates as indicated in the NUREG/CR-5486 2010 update whenever possible. In instances where component data is not included in gas reactor or LWR databases, alternative sources such as fusion, SFR, and TPL reliability data is used to assign a best estimate value. Furthermore, if there is no available component reliability data in any of the input data sources, a target value is assigned. The distribution associated with the data is transferred with the value for identical components. Engineering judgment is exercised in assessing the degree of applicability of the distribution associated with the reliability data for components that are designated as similar. For components with no previously allocated distribution, a lognormal distribution is applied

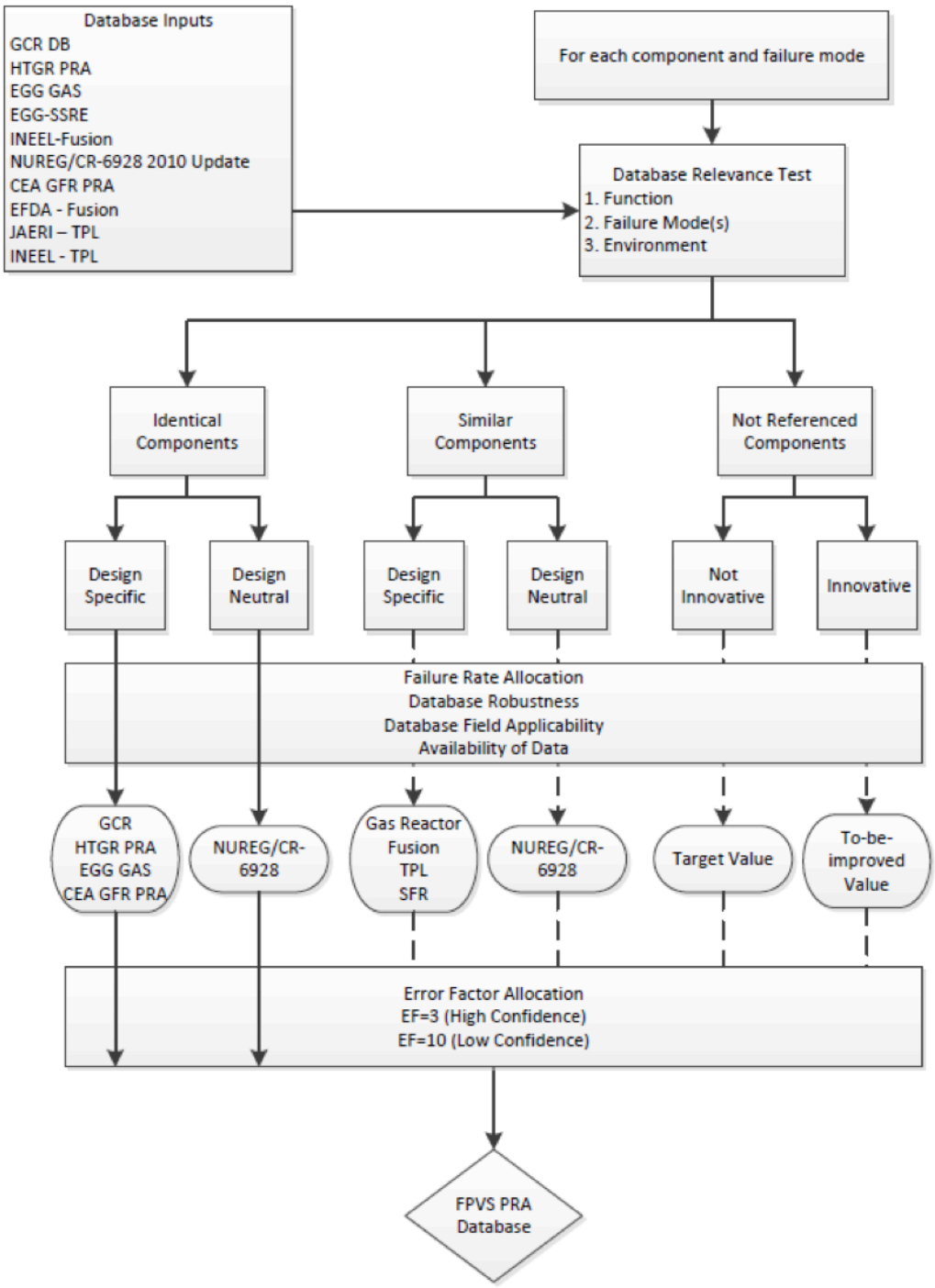

Figure 5.10.: FPVS component reliability database flowchart.

Table 5.8.: Generic CCF Parameters for MGL Model

Components in CCF Group	β	γ	δ
2	0.05	-	-
3	0.08	0.25	-
4	0.10	0.40	0.25

and error factor values are assigned based on the degree of uncertainty associated with the data. The overall approach is outlined in Figure 5.10.

It is important to acknowledge that the lack of component reliability data specific for advanced gas reactor environments requires the use of generic data sources in differing environments, suggesting a negative impact on the validity of the results. Literature pertaining to the PSA of the HTR-PM in China [120] states that the results of a sensitivity study of the component data reveal the effect from the lack of reliability data is far less severe than previously perceived. The unique functional features and design of the advanced reactors can influence the results more significantly than the component reliability data. The redundancy and diversity of design components contribute to a situation where the component reliability data is less sensitive to the overall risk. Although this statement applies to a full plant PRA, similar results are expected for the FPVS PRA. Nonetheless, a sensitivity study is performed for components of the FPVS PRA with higher uncertainty to understand their effect on overall risk of the system. The FPVS component reliability database is included in Appendix C.1.

5.6.3. Selection of a Common Cause Failure (CCF) model

With the combination of limited reliability data and the preliminary nature of the EM^2 design, the generic multiple parameter MGL model was chosen to quantify CCF probabilities. This method is applied to cut sets containing the same failure mode for sample component type. The MGL method is used in the 2010 Level 1 PRA analysis of the CEA GFR [145] and the proposed PBMR PRA [137]. The MGL model is identified as a popular multi-parameter model in NUREG-CR-5485 [150], Guidelines on Modeling Common-Cause Failures in Probabilistic Risk Assessment. In this model, (β, γ, δ) represent the conditional probability to have at least (2, 3, 4) components belonging to the same CCF group failing by the same cause knowing that (1, 2, 3) components failed. The parameters required to calculate CCF probabilities are included in Table 5.8.

5.6.4. Selection of a Human Reliability Assessment (HRA) model

Considering the strengths and weaknesses and appropriateness of the various HRA methodologies discussed in Section 5.4.4, the SPAR-H method was chosen for this analysis. This method was selected due to its simplicity, traceable results using the worksheets provided, generic application, and inclusion of multiple PSFs covering several situations of importance addressing both diagnosis and execution aspects of human events. Due to the lack of specific information related to human interaction with the system available at this time, the nominal value of 1.1E-2 is used

for control room operator actions in this analysis. As the design is finalized further, aspects of the worksheet may be modified and updated appropriately. The SPAR-H worksheets used to obtain this value are included in Appendix C.2.

5.6.5. Level 1 fault tree development

Fault trees are created for the FPVS subsystems for both normal operating conditions and accident conditions. The analysis of the vented fuel system operating under normal conditions offers insight regarding the potential and probable failure mechanisms which may inhibit the system's ability to successfully remove and retain fission products from the purge stream and return the filtered helium to the primary system. Although it is possible that a series of failures of FPVS components during normal operation could potentially lead to an undesirable event with safety repercussions, the probability of such a failure is reasonably small. Furthermore, analysis conducted on the Peach Bottom HPS regarding expected failure modes of the system during normal operations determine the consequences to be fairly insignificant with the exception of a loss of cryogenic cooling of the LTA or a rupture of the doubly contained purge line.

The bounding failure mode of the EM^2 vented fuel system during normal operations is a rupture of the FPVS manifold at the primary coolant boundary, equivalent to the rupture of the doubly contained purge line, releasing purge stream gas prior to any filtering or adsorption treatment. This bounding failure mode is further evaluated as part of the accident scenario, further exacerbated with the failure of the liquid nitrogen cooling system as analyzed in the Level 2 analysis. Thus, the normal operation event tree analysis of the system does not offer additional insight regarding the safety implications of the vented fuel system and is dismissed at this stage.

To analyze the safety implications of the system under accident conditions, the first step is to analyze how fission products could potentially escape the vented fuel system. Thus, fault trees are developed for the various components of the vented fuel system with the top event of release of fission products. In addition, a fault tree was developed for the on-site emergency power system in order to model the failure of on-site power leading to a station blackout event.

5.6.5.1. Normal Operation fault trees

The goal of the normal operation fault tree analysis is to understand how the system might fail to remove and retain fission products from the purge stream and return the filtered helium to the primary system. Therefore, failure modes resulting in unavailability of a train or module, breaches in the system, a disruption in the flow path, flow rate, or temperature are considered. For clarity, the system is broken down into the fuel system and the FPVS, which consists of the FPTS and FPRS. Individual fault trees are created for the various modules and are transferred into the main fault trees for their respective system (FPTS or FPRS) which are in turn transferred in to the overall vented fuel system fault tree.

The fault tree for the fuel system consists of failure modes resulting in leakage or clogging of the piping. The FPTS fault tree consists of failure modes resulting in leakage from the system, failure to maintain the pressure differential (via single control valve), and unavailability of the three trains of the FPTS due to operator error and valve failures. The FPRS fault tree consists

of failure modes resulting in leakage from the system, and inaccessibility and failure of the various modules. Failure modes for the modules consist of failure of individual components such as filters, adsorbers, compressors, and cooling systems. The LTA modules are considered to collectively fail if three of the four available modules fail or are unavailable since each is a 50% train, thus a minimum of two modules is required at a given time.

For operational component failure modes, a standard mission time of 24 hours was used. The SAPHIRE default cut set solve package was used with the minimal cutset quantification method and a cut set truncation value of 1E-15. For uncertainty analyses, the Monte Carlo method was used with 5000 iterations. The fault trees for the vented fuel system under normal operation are included in Appendix C.3.

5.6.5.2. Accident Condition fault trees

Recalling that failure for this analysis is defined as a release of radioactivity from the vented fuel system, the fault trees developed for the vented fuel system under accident conditions consist of failure modes resulting in leakage from the vented fuel system. Likewise, the failure modes of interest include breaches of vessels, manifolds and piping and leakage and spurious operation of valves. For operational component failure modes, a standard mission time of 24 hours was used.

The vented fuel system is broken down into three primary fault tree components based on their location within the plant and the fission product barriers in place to inhibit a release to the environment. A fault tree was developed with the top event of release from the vented fuel system from within the primary coolant boundary, within the containment boundary, and within the auxiliary building. The decision to divide the system in such a way naturally leads to an easier determination of the end state of the system given a specific sequence of failures.

The primary coolant boundary release fault tree, containment boundary release fault tree, auxiliary building release fault tree, and in the case of the LOOP event tree, the loss of on-site power fault tree, are the only fault trees directly transferred in to the Level 1 event trees. All remaining fault trees consist of constituents of the three primary fault trees which were analyzed separately in order to create a more readable and manageable model. Recalling that the FPVS consists of the FPTS and the FPRS, the FPTS solely consists of piping, manifolds, and valves necessary to transfer the purge stream to the retention portion of the system. In contrast, the FPRS consists of several modules, both in-service and stand-by, which can be further broken down into constituent components. Thus, each in-service and stand-by module of the FPRS is analyzed in a distinct fault tree which is individually transferred in to the relevant containment or auxiliary building release fault tree, dependent on the location of the module.

The majority of the components of the FPTS are contained within the containment boundary, thus the majority of the FPTS is modeled in a single FPTS fault tree that is transferred into the containment boundary release fault tree. The remaining portion of the FPTS that lies within the primary coolant boundary (seven sub-header piping trains) along with the entirety of the fuel system fault tree comprise the basic events of the primary coolant boundary release fault tree. The FPVS components are subdivided into two groups, those located in containment and those located in the auxiliary building. Portions of the FPVS that are located inside the containment boundary naturally are included in the containment release fault tree. Likewise, components of the FPVS that are located in the auxiliary building are included in the auxiliary building release

fault tree. Minor modifications to these fault trees are necessary for the initiating event of a rupture of the manifold to ensure that the failure of the manifold is not counted twice.

The FPVS is designed to operate on Class 1E emergency backup AC power in the event that normal AC power is otherwise unavailable [24]. The EM^2 emergency electrical power architecture is not yet finalized, thus the analysis assumes a similar structure to that of the MHTGR. The MHTGR emergency power system consists of an Uninterruptable Power Supply (UPS) [122]. The UPS is capable of providing emergency power pending the availability of a power supply via several sources as well as reliable operation of the various electrical components required to manipulate and transfer the power. The MHTGR UPS is capable of providing power via four redundant channels each powered by two redundant buses which are fed from unit power, off-site power, battery power, or one of two cross tied backup generators. For comparison purposes, the vast majority of the U.S. operating fleet of nuclear power plants relies on one of two backup diesel generators to provide backup emergency power [151].

A station blackout event is defined in 10 CFR 50.2 as a complete loss of Alternating Current (AC) electric power to the essential and nonessential switchgear buses in a nuclear power plant (i.e., loss of offsite electric power system concurrent with turbine trip and unavailability of the onsite ac power system). It was further stated that a SBO does not include the loss of available AC power to buses fed by station batteries through inverters or by alternate AC [152]. Accordingly, the fault tree representative of the loss of on-site power consists of the failure of two safety class backup diesel generators, as the failure of emergency battery power is not included and is thereby omitted from the loss of on-site power fault tree.

The SAPHIRE default cut set solve package was used with the minimal cutset quantification method and a cut set truncation value of 1E-15. For uncertainty analyses, the Monte Carlo method was used with 5000 iterations. The fault trees for the vented fuel system under accident conditions are included in Appendix C.4.

5.6.6. Level 1 event tree development

Event trees for this analysis consist of an initiating event, specified in Table 5.5, with subsequent nodes representing a release of fission products from the vented fuel system inside the primary coolant boundary, a release from inside the containment boundary, and a release inside the auxiliary building, as indicated in Figure 5.11. Furthermore, the event tree for the LOOP initiating event contains an additional node immediately following the initiating event representing the loss of on-site power in order to analyze the system under SBO conditions. Physically, a reactor trip follows each of the specified initiating events. However, under the stated assumption that all supplementary systems operate perfectly, the reactor trip is assumed to have a 100 percent probability of success, therefore this top event is excluded from the event trees. The end state of each sequence consisting of at least one failure of a top event results in a radiological release by definition. Thus, the SFF is the summation of all end states resulting in a radiological release.

Note that the top events have been specifically divided into failures of the vented fuel system within a specified location. As a result, the various end states can be further subdivided into categories based on the location of release, representative of a specific SDS category. Therefore, the various SDS sequences can be grouped (or binned) into SDS frequencies for subsequent accident progression analysis in the Level 2 APET. The event trees for the vented fuel system

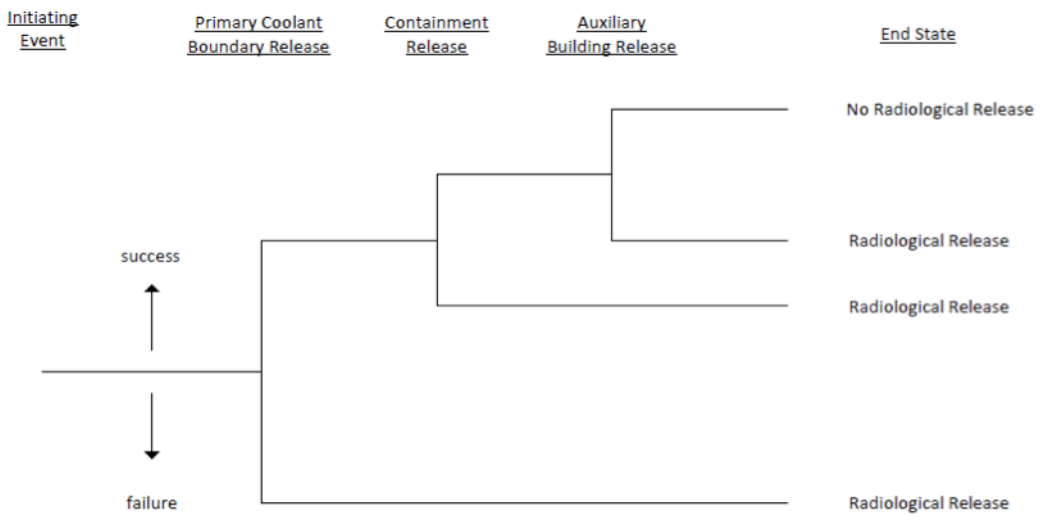

Figure 5.11.: FPVS event tree.

are included in Appendix C.5.

5.6.7. Level 1 system damage state determination

To proceed in the analysis in a concise manner, it is necessary to assign each end state resulting in radioactive release a SDS category. Ideally a detailed analysis of the entire system would be performed such that the accident progression would be largely dependent on the initiating event. However, due to the limitations of the source term model and limited scope of the present work, it is assumed that all other systems operate perfectly. As defined in 10 CFR 50.2, a SBO does not include the loss of available AC power to buses fed by station batteries through inverters or by alternate AC sources. Therefore, assuming perfect operation of the Class 1E power supply, sourced by emergency battery power, the SBO has no effect on the availability of power in this analysis. Consequently, it is assumed that the progression of the accident is unaffected by the initiating event.

The organization of system damage states are determined based on the location and combination of releases for a given sequence. Since we are interested in the safety implications of the system by way of a release of fission products to the environment, there is a natural separation of SDSs based on the location of the release relative to the location and number of remaining fission product barriers in place. Consequently, SDSs have been defined for the various combinations of sequences resulting in a release in the Primary Coolant Boundary (PCB), containment boundary, auxiliary building, or any combination thereof. For clarity, the SDS categories are presented in Table 5.9.

Each SDS category is manually binned in SAPHIRE to calculate the cumulative frequency and uncertainty information for each SDS. The SDS frequency is transferred into the Level 2

Table 5.9.: System Damage State Categories

num	SDS ID	SDS Description
1	PCB-REL	Primary coolant boundary release.
2	CONT-REL	Containment release.
3	AUX-REL	Auxiliary building release.
4	PCB-CONT-REL	Primary coolant boundary and containment release.
5	PCB-AUX-REL	Primary coolant boundary and auxiliary building release.
6	CONT-AUX-REL	Containment and auxiliary building release.
7	PCB-CONT-AUX-REL	Primary coolant boundary, containment, and auxiliary building release.

analysis as the initiating event for subsequent accident progression analysis. As each SDS is unique, the APET top events for each SDS differ slightly in response to the location and type of system failure. To conserve information regarding the specific location of the release within the system, split fractions are utilized in the APET to identify the fraction of the time that a release occurs between essential component barriers, effecting the source term calculations.

5.7. Level 2 PRA Model

The Level 2 model in SAPHIRE analyzes the progression of the failure of the system to retain fission products by way of incorporating the additional failure modes of the vented fuel system and associated systems that have the potential to alter the timing or magnitude of the radioactive release. To incorporate these failure modes in a SAPHIRE model, an APET was developed. As stated previously, the accident progression is dependent on the state of failure of the system. Therefore, a unique APET is created for each SDS category in order to address the distinctive challenges presented by a given accident scenario. A total of thirteen APETs were developed to analyze the accident progression and resulting source term. Although only seven SDSs were identified, the APETs for SDS 6 (release in the containment and auxiliary building) and SDS 7 (release in the PCB, containment, and auxiliary building) were split into four separate trees due their size. The fractional probability of containment release for the location of interest for the SDS 6 and SDS 7 APETs is quantified via the containment release location top event specific to the APET. A description of the APET model and the corresponding SDS is given in Table 5.10. The Level 2 event trees for the vented fuel system are included in Appendix C.7.

5.7.1. Level 2 Accident Progression Event Tree (APET) development

In order to develop an APET it is necessary to understand how the system is expected to respond to the various accident sequences. The EM^2 is designed to achieve a stable state following an initiating event by tripping the reactor and establishing residual heat removal via the Primary Coolant System (PCS) or Direct Reactor Auxiliary Cooling System (DRACS). The shutdown core heat removal modes are turbo-compressor coast-down after load shedding, two 100% passive cooling loops of the DRACS, two 100% forced helium circulators, and passive heat removal

Table 5.10.: APET Model Descriptions

num	SDS ID	SDS Description
1	APET-1	SDS 1 PCB Release
2	APET-2	SDS 2 Containment Release
3	APET-3	SDS 3 Auxiliary Building Release
4	APET-4	SDS 4 PCB and Containment Release
5	APET-5	SDS 5 PCB and Auxiliary Release
6	APET 6-1	SDS 6 Containment and Auxiliary Release (Before HTA)
7	APET 6-2	SDS 6 Containment and Auxiliary Release (HTA Module)
8	APET 6-3	SDS 6 Containment and Auxiliary Release (After HTA)
9	APET 6-4	SDS 6 Containment and Auxiliary Release (HTA Return)
10	APET 7-1	SDS 7 PCB, Containment, and Auxiliary Release (Before HTA)
11	APET 7-2	SDS 7 PCB, Containment, and Auxiliary Release (HTA Module)
12	APET 7-3	SDS 7 PCB, Containment, and Auxiliary Release (After HTA)
13	APET 7-4	SDS 7 PCB, Containment, and Auxiliary Release (HTA Return)

through the containment liner. In addition, the containment is sealed, leak-tight, below grade, and maintained at 20 psig (0.14 MPa) with an inert gas [153]. The current containment design does not include venting through a filter to relieve over pressurization of the containment, however preliminary analysis indicates that this feature is desirable and will likely be implemented. It is assumed for this analysis that the containment filter allows filtered venting of the containment. The vented fuel system response modes of primary interest are isolation status, pressure control, temperature control, and primary coolant boundary and containment integrity.

Following a reactor trip or breach in the FPVS, the FPVS isolation valves are automatically initiated via the Reactor Protection System (RPS). Again, it is assumed that the RPS operates perfectly, and the failure of the isolation valves lies solely on their ability to close. Thus, the first and second nodes of the accident progression event tree indicate the successful isolation of the primary coolant boundary and containment, respectively.

The pressure differential driving the fission product purge stream is controlled by the motor operated control valve, V-15. The control valve continually maintains a slightly negative pressure differential from the primary system to suppress fission product counter-diffusion through cracks and pinholes in the cladding [24]. In the event of a system depressurization, the control valve is designed to reach pressure equilibration within sixty seconds. However, the control valve is located outside the primary coolant redundant isolation valves, thus if the primary coolant boundary is successfully isolated, this function of the control valve function will be lost. Failure to maintain the pressure differential would result in counter-diffusion of fission products through the cladding into the primary coolant. The current system model is not capable of accurately modeling the behavior of the fission products that counter diffuse incorporating their ability to plateout inside the core and pressure vessel. As this failure is more applicable to core analysis and is a limitation of the current system model, the effects on the vented fuel system are not further considered.

The compressor module provides the driving force for the flow through the FPVS. In addition, the compressor module functions to raise the helium pressure in the purge stream to that needed for return to the primary coolant system helium inventory. The compressor module does require power and the effect of a SBO must be considered. The FPVS operates using Class 1E power from the electrical system and is designed to operate on emergency backup AC power when necessary. As stated in 10 CFR 50.2, a SBO does not include the loss of available AC power to buses fed by station batteries [152]. Under the assumption that the station batteries successfully provide AC power to the backup AC power buses a loss of power to the compressor module is not a possible failure mode. Consequently, the failure of the compressor module is quantified by unavailability and failure to run or start. A loss of purge stream flow would likely increase the temperature a few degrees since the purge stream itself provides some cooling via regenerative heat exchangers, possibly resulting in failure of a HTA or LTA module to retain trapped fission products [7]. However, the effects of a failure of the compressor are inconsequential in the event the system is successfully isolated, thereby obstructing the purge stream flow path. Thus, the function of the compressor is not of importance under accident conditions and is not included in the accident progression analysis.

Furthermore, the loss of liquid nitrogen cooling to the LTA would clearly increase the temperature of the LTA module, resulting in failure of the LTA module to retain trapped fission products increasing the quantity of noble gases in the purge stream. In addition, the purge stream exiting the LTA modules acts as the heat sink in the HTA regenerative heat exchanger prior to return to the primary coolant inventory. Therefore, an increase in the temperature of the LTA module will in turn increase the temperature of the HTA module, potentially resulting in a release of the contents of both the HTA and LTA. The failure of the liquid nitrogen cooling system is a bounding event having the potential to significantly increase the radioactive release should the contents of the adsorber beds desorb in response to the temperature increase.

Assuming the liquid nitrogen cooling system is similar to that used in the MHTGR, the liquid nitrogen is held at low pressure, flowing by a combined gravity-thermal siphon effect and vaporizing on the shell side of the heat exchanger [154]. Assuming the cryogenic cooling system is representative of systems commercially available, the system requires a compressor, which consequently requires power. Under the stated assumption that Class 1E power is available to the system under all accident scenarios for this analysis via the safety class battery power. Thus, the failure of the liquid nitrogen cooling system is quantified by unavailability and failure to function.

Intuitively, should the vented fuel system be breached, the operator would actively determine the source of the breach and isolate the system components as necessary. For instance, if the piping between the HTA module and containment is breached, the HTA module outgoing isolation valves and containment isolation valves would be closed to prevent the release of additional fission products. Thus, the isolation of the HTA and LTA are included as top events.

Finally, the integrity of both the reactor coolant boundary and the containment impact the release and are consequently included as top events in the APETs. In an accident scenario, the primary coolant boundary and containment will likely be challenged by the success or failure of several other plant systems. As stated previously, the present work assumes perfect operation of other systems thereby removing dependent failures of associated systems which are not taken into consideration in this analysis. Therefore, it is assumed that all primary coolant boundary

and containment engineered safety systems operate perfectly.

To further refine the source term information, it is important to understand where the breach lies within the containment or auxiliary building. It would be a gross overestimate to assume all releases within containment result in a release of the entire HTA bed contents or purge stream prior to any treatment. For example the return line, which generally may contain a minute amount of activity, is included in the containment release fault. Since the potential release differs at various points within the system, it is important to include information regarding the location of the release in the APET. Thus, the top events for primary coolant boundary and containment release location utilize multiple branches to assign the appropriate probability of failure for the various points of interest within the containment and auxiliary building which effect the potential source term.

Finally, in a depressurization event the primary coolant boundary is breached, thereby significantly reducing the retention capabilities of the primary coolant boundary. It is assumed the LOCA and manifold rupture initiating event sequences entail a breach of the primary coolant boundary, whereas the transient and LOOP initiating event sequences assume the primary coolant boundary remains intact. This information is transferred from the Level 1 results by way of assigning fractional values to the primary coolant boundary status top event based on the cut set results from the SDS sequences. The output of the APET is a set of STGs and their associated frequencies.

A series of linkage rules, in the form of if-then statements, are utilized to quantify multiple branch events for each APET. For example, the containment and auxiliary release location top events contain multiple branches representing a release before the adsorber module, in the adsorber module, after the adsorber module, and in the case of the containment release the return line. This information is required to properly identify the resulting release form a given sequence. Furthermore, basic event process flags and calculation types were adjusted for each APET top event to ensure success (upper branch) events were included in the cut sets, as these successes may still lead to a release and require further analysis.

5.7.2. Selection of APET top event probabilities

The APET top event failure probabilities are assigned depending on the resulting SDS for each system failure sequence. For several SDS analyses, the probability is the same for all APETs (i.e., independent of the SDS). Top events are assigned probabilities through the use of fault tree analyses and when specific system information is unavailable engineering judgment is exercised in order to assign a probability. For top events with insufficient information to assign probabilities directly, a probability is based on a verbal descriptor and corresponding likelihood. The verbal descriptor is based on information gathered from literature and previous studies combined with an understanding of the characteristics of each SDS. The assignment of numerical values to verbal descriptors is summarized in Table 5.11. The resulting top event probabilities for the APET are summarized in Table 5.12.

Table 5.11.: Numerical Values Assigned to Verbal Descriptors

Verbal Descriptor	Likelihood
Certain	1.0
Almost Certain	0.99;0.999
Likely	0.9
Intermediate	0.5
Unlikely	0.1/0.01
Remotely Possible	0.001
Impossible	0.0

5.7.3. Selection of Source Term Groups (STGs)

The end state for each APET sequence is a unique source term group. The source term groups are determined based on the location and combination of releases for a given sequence, dependent on the location of the failure, type of failure, and the ability of the various top events in the APET to successfully constrain the progression of the accident sequence. Thus, the source term for each sequence is a combination of the estimated activity that could potentially be released (as calculated in the STELLA model) as well as the appropriate application of attenuation factors dependent on the systems response by way of isolation and integrity of the PCB and containment boundaries.

To reduce the number of STGs, a few generalized assumptions were applied in determining the source term components. First, it was assumed that the contents of the purge stream after the HTA are the same as the contents of the purge stream before the LTA. Second, it was assumed that a breach in the FPVS after the LTA does not result in a release since the contents of the purge stream after the LTA normally should have little to no activity present. Furthermore, if activity was introduced into the purge stream as a result of a failure of the LTA, multiple isolation valves would coincidently have to fail to result in a release, thus a release is unlikely. Finally, it was assumed that a breach in the return lines of the FPVS inside containment does not result in a release since the purge stream in the return line normally should have little to no activity present and such an event is unlikely.

Thus, depending on the sequence, the source term may be composed of any combination of activity estimates within the FPVS STELLA model, which include plateout on the piping in the PCB, the purge stream from the core to the HTA, the HTA bed contents, the purge stream from the HTA to the LTA, and the LTA bed contents. Furthermore, the application of the attenuation factors for the PCB, containment, reactor building, and containment filter are determined by the accident progression. In instances where the specific source term component has the potential to be released in two or more locations, the more conservative location (fewest fission product barriers) is chosen.

Due to the large number of STGs possible, IDs rather than names are given to each source term group. The STG IDs are composed of combinations of alphabetic characters identifying the potential released activity from the STELLA model and the attenuation factors to be applied for each sequence. The STG ID alphabetic characters are presented in Table 5.13.

Table 5.12.: Accident Progression Event Tree Top Event Probabilities.

Top Event	Description	Probability
CONT_REL_LOC	Release Location from Level 1 fault trees.	-
	Before HTA Module	6.30E-01
	HTA Module	1.90E-01
	After HTA Module	4.00E-02
	Return Line	1.40E-01
AUX_REL_LOC	Release Location from Level 1 fault trees.	-
	Before LTA Module	2.60E-01
	LTA Module	3.00E-01
	After LTA Module	4.40E-01
PCB_ISO_STATUS	Pressure boundary isolation valves closed.	Fault Tree
CONT_ISO_STATUS	Containment boundary isolation valves closed.	Fault Tree
LNC_STATUS	LTA temperature functional to retain FPs.	7.20E-05
LTA_ISO	LTA module isolation valves closed.	Fault Tree
HTA_ISO	HTA module isolation valves closed.	Fault Tree
PCB _STATUS	Reactor pressure boundary intact.	-
	APET-1 SDS 1	1.00E-04
	APET-2 SDS 2	5.58E-02
	APET-3 SDS 3	0.00E+00
	APET-4 SDS 4	5.58E-02
	APET-5 SDS 5	0.00E+00
	APET-6 SDS 6	5.67E-02
	APET-7 SDS 7	6.75E-02
CONT _STATUS	Containment intact.	3.00E-02

The source terms can be grouped into three catagories, with attenuation factors applied based on their location. The source term A occurs within the primary vessel, and physically represents the source due to plateout of fission products from leakage into the primary coolant. The attenuation factors H (PCB) and K (Reactor building) are always applied to the A source term, while the attenuation factor F is applied only if the PCB is intact. The source terms B and C are located outside of the PCB, but still within the containment building. The attenuation factors J (Containment) and K (Reactor building) are always applied to the source terms B and C, while the attenuation factor G is applied to the source terms B and C only if the containment is intact and the flow path is constrained through the filter. Lastly, the source terms D and E are located outside the reactor building where it is conservatively assumed that no attenuation credit is given to the auxiliary building. Attenuation credit is still given to the delay beds in the event of a release from the source terms C or E, as displayed in Table 5.16.

Group source term IDs are formulated using the following order: Reactor building source terms, attenuation factors, then Auxiliary building source terms. As an example, the source term group ID BCGJKXD represents a release of B and C within the reactor building, with attenuation credit given to G, J, and K. The source term D is released within the auxiliary building, and is separated from the previous attenuation factors by the marker X.

5.7.4. Estimating source terms using STELLA model of FPVS

5.7.4.1. Producing source terms

Source term estimates are obtained using a system model developed using the modeling program STELLA, which solves coupled differential equations describing the transport of volatile

Table 5.13.: Source Term Group character definitions. † All IDs to the right of the X are assumed to release in the auxiliary building with no additional attenuation.

ID	Description
A	Source Term: PCB Plateout
B	Source Term: Core to HTA Purge Stream
C	Source Term: HTA
D	Source Term: HTA to LTA Purge Stream
E	Source Term: LTA
F	Attenuation Factor: Intact PCB
G	Attenuation Factor: Containment Filter
H	Attenuation Factor: PCB (failed or intact)
J	Attenuation Factor: Containment (failed or intact)
K	Attenuation Factor: Reactor Building (failed or intact)
X	Auxiliary Building Release Marker†

elements through the vented fuel system. The original STELLA model was developed by Wesley Deason and is documented thoroughly in his thesis [2] and presented in Section 4. The graphical interface of the model allows flexibility of input types providing the capability of modeling various configurations of the vented fuel system representative of a given accident scenario. To validate STELLA, the software was used to model the Peach Bottom Helium Purification System for Krypton-85 production and transport though the reactor plant. The model output matched closely to the numbers provided in the Peach Bottom Final Hazards Safety Analysis report and allowed for tracking of the radionuclide from birth in the fuel or delay beds to decay, confirming its proper use for modeling the representative vented fuel system [7].

The immense number of isotopes found in nuclear fuel spans over 37 elements from zinc to dysprosium. The low yield of elements at the far edges of this spectrum simplifies the model and allows the elements Zn, Ga, Ge, As, Gd, Tb, and Dy to be ignored. Furthermore, the elements in the middle of the double hump fission yield, Ag and In, can also be ignored. Of the remaining 28 elements, over half are considered nonvolatile or form carbides with relatively high stability and are assumed to diffuse negligibly slow through the fuel; these include: Y, Zr, Nb, Mo, Tc, Ru, Rh, Pd, Sn, La, Ce, Pr, Nd, and Pm. The remaining 14 elements are assumed to be volatile within the helium system and will be released from the fuel. After the final selection, a total of 19 elements were chosen to be included in the STELLA model, with a total of 88 tracked isotopes and 39 isobars. Despite their previous exclusion, the elements Y, In, La, Ce, and Gd are included in the STELLA model due to radioactive daughter products resulting from the decay of volatile elements. However, it was determined that these four additional species do not contribute appreciably to the fission gas release from the fuel. Of the 88 tracked isotopes, Sr-90, Cs-137, Ba-140, I-131, and Xe-135 warrant special attention due to safety reasons, their impact on maintenance activities, and a large neutron cross section in the case of Xe-135.

The original STELLA model was updated to reflect the EM^2 vented fuel system as analyzed in the SAPHIRE PRA models (Section 4.5). Additionally, the Release over Birth (R/B) release curve was updated to reflect the MHTGR R/B model, as opposed to the Peach Bottom R/B

curve that was previously utilized. The Peach Bottom R/B curve was taken from linear accelerator experiments on uncoated $(Th,U)C_2$ fuel particles and later multiplied 3-fold for safety calculations. The R/B curve was calculated for a specific non-identified temperature for application to the Peach Bottom design; furthermore, no burnup corrections nor differences between gas species diffusivities is included. This curve was used in the original analysis with sufficient warning that it would be important to develop a better calculation of fission gas release in the future. Note a reactor power of 500 MWth, equivalent to the EM^2 design, was assumed for all STELLA analyses.

After updating Deason's original work with updated system design considerations, three principal cases were developed:

1. The purge stream exits the fuel at 1000° C. Plateout of Cs, I, and Se occurs in piping. Purge stream enters hot trap at 1000° C. Trapping of everything but Xe and Kr occurs in first hot trap. Purge stream containing only Xe and Kr travels to cold trap where Xe and Kr, and their daughters are collected.

2. Purge stream exits the fuel at 1000° C and cools to 550° C. Condensation of everything but noble gases and halogens occurs in piping. Plateout of I occurs in piping. Purge stream enters hot trap at 550° C. Trapping of everything but Xe and Kr occurs in first hot trap. Purge stream containing only Xe and Kr travels to cold trap where Xe, Kr, and their daughters are collected.

3. Same parameters as Case 2 above except reactor shutdown after 3000 hours.

Case 1 and 2 are identical to Cases 8 and 9 in Section 4.5.3. The Case 2 model includes condensation in the piping prior to the HTA, thereby reducing the contents of the HTA. Similarly, the Case 3 model after shutdown would exhibit a decrease in the activity present in the fission product traps and purge stream. Furthermore, the piping prior to the HTA module will be heated such that limited condensation occurs. Thus, the Case 1 model was chosen as the most applicable and conservative system model for the present work.

The STELLA model results include fission product activity, power, and mass accumulation for plateout in the piping within the primary coolant boundary, the purge stream contents between the core and the HTA module, the HTA bed contents, the purge stream contents between the HTA module and the LTA module, and the LTA bed contents. These individual activities are summed as appropriate to determine the resulting source term for each of the source term groups identified in the Level 2 APET.

5.7.4.2. Application of Attenuation Factors

The STELLA model calculations provide source terms from the vented fuel system, however additional fission product barriers, such as the pressure boundary, containment, and reactor building, and containment filter are in place that may limit the release of radioactivity. Conservatively, the retention capabilities of the auxiliary building are ignored in the present work. In order to integrate the retention capability of each of these barriers of release to the environment in the source term calculations, an attenuation factor is applied. An attenuation factor, also known as a Decontamination Factor (DF) or Retention Factor (RF), accounts for the reduction in radiation

release sourcing from fission product barriers such as vessels, buildings, cooling systems, etc. A representative equation of the AF was used:

$$AF = \frac{\text{Radiation level before attenuation}}{\text{Radiation level after attenuation}} \tag{5.11}$$

The corrected release can then be calculated by,

$$\text{Corrected Release} = \frac{\text{Calculated Release}}{AF} \tag{5.12}$$

Since the release limits from plants are very stringent, most of the advanced containments give credit to decontamination factors for the radionuclides that escape the primary containment [155]. For example, in the European Pressurized Reactor (EPR) calculations credit is given for a grace period of several hours to the secondary containment for collection, deposition, and hold up of fission products leaked through the primary containment shell. The Simplified Boiling Water Reactor (SBWR) and Advanced PWR (AP-600) calculations adopt the strategy of purely static and passive partial secondary envelopes, reasonably tight, in which credit is given for only hold up and deposition, and no filtering is available. Unlike LWRs, whose coolant system and containment building serve as ultimate barriers to fission product release, the MHTGR relies significantly less on the attenuation of the helium pressure boundary and reactor building and relies significantly more on retention in the fuel, TRISO coatings, and graphite. For advanced gas reactor source term analyses, credit is merited in the form of a decontamination factor. A MHTGR source term study documents DFs for filters incorporated in the reactor pressure boundary vent line, containment vent line, and reactor building vent line [130].

A more recent NGNP study documents AFs for the fission product barriers of the various proposed NGNP MHTGR designs. The AFs were estimated by an expert panel based on HTGR fuel testing results and radionuclide predictions developed for previous HTGR designs such as the MHTGR and PBMR [106]. Unlike LWRs, the fission product barriers which form the functional containment of the MHTGR include the fuel, graphite in the core, helium pressure boundary, and the reactor building. Compared to the fuel and graphite in the reactor core, the helium pressure boundary and the reactor building play a minor role in overall retention of fission products in a MHTGR.

Condensable fission products in the helium pressure boundary can plate out on cool metallic surfaces and/or interact with dust in the system [156]. Additionally, the HPS continually removes impurities and some fission products from a fraction of the primary coolant. A small fraction of the helium leaks into the reactor building during normal operation, however the majority remain within the primary coolant boundary. In a depressurization event, however, the circulating activity in the coolant can be transported to the reactor building, thus the retention capabilities of the primary coolant boundary decrease dramatically. In the reactor building structure, venting, building leakage, condensation, deposition, and settling can influence the magnitude and timing of the release.

The attenuation behavior anticipated in the helium pressure boundary and the reactor building differs under dry and wet conditions for a break in the helium pressure boundary. In dry conditions, the fission product behavior depends, in the short term, on the ability of the shear forces induced by the blowdown associated with the break to liftoff fission products. In the longer term

Table 5.14.: NGNP dry scenario attenuation factors for helium pressure boundary (HPB) or reactor building [156].

Fission Product Class	**Normal Operations**		**Depressurization Accident Conditions**			
	HPB		HPB		Reactor Building	
Confidence Limit	*AF 50%*	*AF 95%*	*AF 50%*	*AF 95%*	*AF 50%*	*AF 95%*
Noble gases	1	1	1	1	1	1
I, Br, Se, Te	10^6	10^6	200	20	2	1
Cs, Rb	10^6	10^6	200	20	2	1
Sr, Ba, Eu	10^6	10^6	200	20	2	1
Ag, Pd	10^6	10^6	200	20	2	1
Sb	10^6	10^6	200	20	2	1
Mo, Ru, Rh, Tc	10^6	10^6	200	20	2	1
La, Ce	10^6	10^6	200	20	2	1
Pu, actinides	10^6	10^6	200	20	2	1

following pressure equilibration after the blowdown, the fission product behavior is dominated by the expansion and contraction of the gas phase as the reactor vessel slowly heats up and then cools down, along with potential for density-driven exchange flows between the reactor and the cavity. In wet conditions, it is conservative to assume that there is sufficient moisture available to wash off all of the plated out fission products. It is anticipated that the steam will condense in the much cooler reactor building, thus trapping the fission products in the condensate. Overall, the differing behaviors tend to result in a slightly greater source term in the wet scenario than in the dry scenario. Since the initiating event of water ingress was found to be extremely unlikely and henceforth removed from the analysis, the dry conditions will be of primary importance.

The EM^2 reactor produces 500 MWth and is cooled by helium coolant pressurized to 1900 psia (13.1 MPa) with an average core inlet and outlet temperature of 500°C and 850°C, respectively [153]. Thus, the NGNP 600 MWth prismatic design with a Reactor Outlet Temperature (ROT) of 900°C most closely corresponds to the EM^2 reactor design. The estimated AFs are not associated with any specific fission product retention mechanism or leak tightness of the reactor building, rather with the driving force to transport the gas through the reactor building to the environment. The short-term AF estimates are conservative by nature under the strong influence of an early depressurization state.

AFs are estimated for a 50% and 95% upper bound value. The 50% value is the median value and the 95% upper bound is the value above which there is a 5% chance of exceeding in the case of a one-sided distribution applied to the AFs. Additionally, AFs for fission product barriers are assumed to be lognormally distributed with median and N-sigma values. The median values will be applied to the source term estimates obtained from the STELLA model. The normal operation and short-term accident condition attenuation factors for the dry scenario are given in Table 5.14.

Since the EM^2 design includes containment in addition to the reactor building, an additional attenuation factor is applied to source term sequences where the containment barrier remains intact; the attenuation factor is based on the expected leak rate of 0.1% per day. In addition to the

Table 5.15.: HTGR Alternative Design Strategy Attenuation Factors

Strategy Description	Option	Decontamination Factors		
		Noble Gas	*Halogens*	*Particulates*
Provide He relief valve blowdown filter	1	1	10	10
	2	1	100	100
	3	1	100	1000
Provide reactor building flow path with filter	1	1	3	3
	2	1	30	30

estimated attenuation of radioactivity provided by the pressure boundary and reactor building, the EM^2 design will likely implement vented filters for containment and auxiliary building release pathways as a result of preliminary safety analyses performed by GA. To be conservative, the auxiliary building filter is not applied in the present work. A NGNP reactor building design assessment identified the addition of passive and active filtering for the reactor building atmosphere to be essential under limiting accident scenarios to ensure site boundary dose limits are not exceeded and may be used to depressurize the primary system and the reactor building [157].

Moreover, a GA HTGR source term and containment report examines the benefit of providing a filtered release pathway from the reactor building and pressure boundary; sand or gravel and packed glass fiber filter mediums are considered to be capable to withstand the expected temperatures and to remain suitably inert over a long standby period [130]. Generally, the decontamination factor of the filter increases as the length of the flow path (filter bed depth) increases and is inversely proportional to the flow velocity through the filter bed. The various attenuation factors used in the scoping studies of alternative design strategies for reducing off-site exposure are given in Table 5.15, where the options refer to filter types of increasing effectiveness; The particulates group includes all remaining nuclides (i.e. anything but noble gases and halogens).

In addition to the attenuation factors applied to the primary coolant boundary, containment, reactor building, and containment filter, it is necessary to apply an attenuation factor to the event tree sequences resulting in an adsorber bed release. As the temperature of the bed increases in response to a loss of cooling, rupture in the system, or loss of purge flow, the radioactivity contained in the adsorber bed may desorb and be released. The STELLA model is limited in its ability to model desorbing radionuclides however an assumption that all adsorber bed activity is released in the event of a failure is overly conservative and may lead to a misrepresentation of the safety implications of the vented fuel system.

An analysis of the Peach Bottom vented fuel system was performed for an accident involving a rupture in the trapping system which determined that less than 20% of the activity contained in the trapping system is released [136]. A more detailed model of the FPVS response in such accidents should be developed to address this constraint. It is assumed for the present work that a failure of the HTA or LTA module results in a release of 25% of the activity contained in the bed. The attenuation factors credited in the present work are summarized in Table 5.16.

Table 5.16.: Vented Fuel System PRA Attenuation Factors

Fission Product Barrier	Attenuation Factors			
	ID	*Noble Gas*	*Halogens*	*Particulates*
PCB (Intact)	F	1	10^6	10^6
Containment (Intact)	G	1	10^3	10^3
Containment Filter	G	1	10	10
PCB (Compromised or Intact)	H	1	200	200
Containment (Compromised or Intact)	J	1	2	2
Reactor Building	K	1	2	2
HTA/LTA Adsorber Bed Retention	-	1	4	4

5.8. Level 3 PRA Model

5.8.1. Building an atmospheric transport model in GENII

The source term estimates, after applying the appropriate AFs, are used as input to the atmospheric dispersion model. In addition, the dispersion model requires various other inputs such as release exit area, elevation, medium, and atmospheric conditions. The inputs required for the dispersion model are summarized in Table 5.17.

The timing of the model determines whether an acute or chronic exposure is analyzed. Acute exposure refers to exposures over a short period of time (hours to days) whereas chronic exposure refers to exposure from routine releases [158]. For this analysis, acute exposure is appropriate since we are concerned with an unexpected release due to an accident rather than chronic releases due to normal operations, as appropriate for modeling accidental releases. The scenario type for far-field is selected as the generally applicable safety analysis scenario type. The receptor dose is selected for an individual and the individual type input is selected for maximum individual to be conservative. The selected transport pathway is airborne, since the atmospheric release is considered to diffuse in the air rather than surface water. The exposure pathways include inhalation, direct shine from the plume, and ground shine from deposited material; ingestion exposures are not considered.

The inventory radionuclides are specified for each radionuclide released as calculated using the STELLA model and adjusting for attenuation as appropriate in units of curies. The inventory of radionuclides source terms are specified as activity rates for either a gas (Xe, Kr, and I) or particle. The assumed nonreactive fraction applied to the noble and non-noble gases is 1.0 and 0.10, respectively. It is assumed that the gas density is 4.0 g/cm^3, the particle radius is 0.5 μm and the density is 3.0 g/cm^3.

Plume rise from momentum and buoyancy effects can result in separation of the plume centerline from the ground thereby lowering the plume concentration observed at ground level. The input parameters for plume rise calculations are the source exit velocity, source exit temperature, and ambient air temperature. The exit velocity should be conservatively estimated on the low side. The plume rise from buoyancy effects decrease with increasing ambient air temperature and should consequently be conservatively estimated on the high side. Plume rise from buoy-

Table 5.17.: Atmospheric Dispersion Model Inputs

Input	Value/Selection
Model Basis	Gaussian Plume
Release Timing	Acute
Scenario Type	Far-Field
Receptor Does	Individual
Individual Type	Maximum Individual
Transport Pathway	Airborne
Exposure Pathway	Inhalation and External
	(direct plume shine and ground shine deposited material)
Inventory Radionuclides	Source Term Activity (Ci)
	(released over the period specified for the plume duration)
X/Q Value	NGNP 95th percentile (Pre-calculated)
EAB	400 m, 800 m, 1600 m, 3200 m, 8000 m
Release Type	Point
Exit Area of Source	0.785 m^2 (Assumes 1.0 m Diameter Vent/Breach)
Source Height	0.0 m (Ground-level release)
Adjacent Structure Height	0.0 m(No building wake effects)
Source Exit Velocity	0.0 m/s (No momentum effects)
Source Exit Temperature	Texit = Tair = 0°C (Ignore buoyancy effects)
Ambient Air Temperature	Texit = Tair = 0°C (Ignore buoyancy effects)
End of Intake Period	1 year (Lowest possible entry)
Dose Commitment Period	50 years (Average adult remaining lifetime)
Soil Contamination Exposure	2 hours
Inhalation Exposure	2 hours
Deposition Velocity	Default
	Particles: 0.001 m/s
	Iodine: 0.01 m/s
	Noble gases: 0.0 m/s
Breathing Rate	3.3E-04 m3/s (default)

ancy effects increase with increasing effluent temperature, therefore exit temperatures should be conservatively estimated on the low side. Since the site location is unidentified, the temperatures are not available however buoyant plume rise can be ignored by setting the source exit temperature equal to the ambient temperature.

The cloud of released material undergoes dilution during atmospheric transport and diffusion that is characterized by the X/Q value, which represents the time-integrated concentration at a specific downwind location. GENII allows the use of pre-calculated atmospheric dispersion factors (X/Q) as user-defined values for converting chronic releases into air concentration or acute release into time-integrated air concentration and total deposition. Separate values are needed for gases and particles. Two options were considered for the calculation of the representative X/Q value. The first was to use the meteorological data from any one representative site for a specific period of time readily available. The meteorological data would first need to be converted into a form acceptable for use with GENII to provide time dependent information regarding wind speed, wind direction, and atmospheric stability for calculation of X/Q values in GENII. The other option is to enter user-defined atmospheric dispersion factors from a pre-calculated source representative of the 95th percentile X/Q value. The 95th percentile X/Q value utilized for the NGNP scoping analyses is selected for the vented fuel system atmospheric transport model. The X/Q values calculated in the NGNP scoping analysis represent an aggregate value for 18 representative site locations [106]. Since the specific site is not yet known, the generic X/Q value was considered most appropriate. The source height is conservatively specified to be ground-level while taking no credit for plume rise effects from either momentum or buoyancy. Plumes from elevated discharges can be drawn downward and entrained into the wake in the wind field caused by the building (building wake). To be conservative, the adjacent structure height is specified to be zero for a ground-level release with no initial momentum or buoyancy.

The end of intake period is the time step for the GENII computer simulations in integer years. The intake for an acute release will be much less than one year, however one year is the minimum specification for such a release. When a radioactive particle is inhaled, it will cause long-term damage to the body as it remains in the body and continues to disintegrate and irradiate organs and tissues; the predicted dose from internal exposures over the remaining life of the individual is normally taken to be 50 years for adults. Consequently, the dose commitment period is selected to be 50 years. The period of time for soil contamination exposure is recommended not to exceed 8 hours and to ignore prolonged effects such as resuspension. The recommended period of time for inhalation exposure is not to exceed 2 hours or 8 hours for slow developing release scenarios. If the scenario involves a release duration that is shorter than 2 hours, the scenario specific release duration should be specified instead.

Furthermore, there are several default parameters preset in GENII. Several of which are recommended for safety analysis applications to not be changed except for compelling reasons. One such default parameter is the deposition velocity. The deposition velocity represents the ratio of the ground surface contamination rate from deposition to the contaminant concentration in the plume above. Larger solid particles released in a plume will fall to the ground due to gravitational settling while smaller particles, and even some gases, will deposit on ground surface elements such as vegetation through a variety of processes including chemical, biological, and physical interactions. The recommended default deposition velocity for particles is 0.001 m/s, for Iodine is 0.01 m/s, and 0.0 m/s for noble gases. These values are reasonable and should

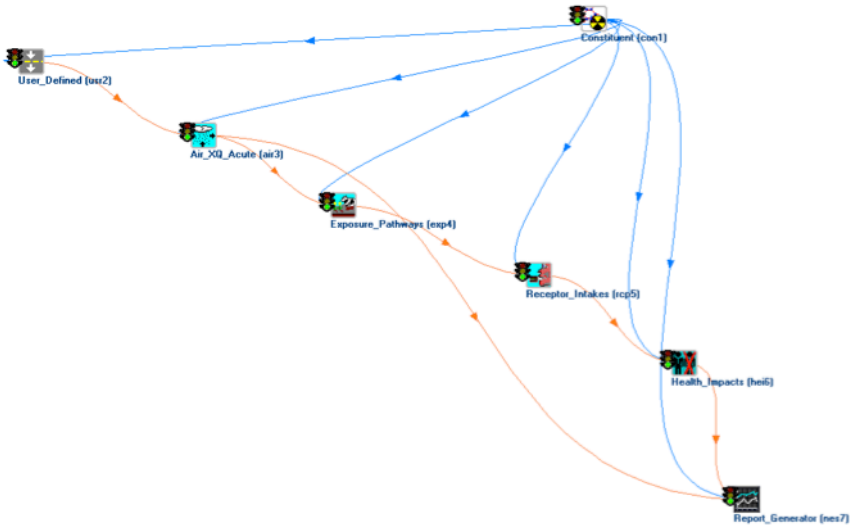

Figure 5.12.: GENII atmospheric transport model.

be generally used for safety analysis applications. The breathing rate should be set equal to the default value of 3.3E-04 m^3/s for acute releases. The inhalation dose conversion factors for external radiation should be based on Federal Guidance Technical Report 12 (FGR-12) and for internal radiation should be based on FGR-11.

The model includes several separate modules connected sequentially with one another, as indicated in Figure 5.12. The constituent source term radionuclides are input in the Constituent module. Next, the source term isotopic specific activity rate, time-dependent release rates, and composition (gas or particle) are entered in the User Defined module. The atmospheric transport module is selected based on pre-calculated dispersion and deposition coefficients in the Air Module. The various exposure pathways such as inhalation, external and ingestion are selected in the Exposure Pathways module. The specific exposure and age group information is selected for the individual pathways in the Intake Module. The method of calculating radiation dose and risk is selected in the Health Impacts Module. Finally, the results are generated using the Report Generator Module. Additionally, a sensitivity module may be added after running all constituent models and connecting the appropriate modules together.

5.9. Level 1 PRA Results

The results for the Level 1 PRA for both normal operations and accident conditions are given in the following section. The strengths and weaknesses of the system may be determined by analyzing the failure frequency, cut sets, importance measures, and uncertainty analysis for the various fault trees and event trees.

Importance measures provide reliability-worth information about basic events appearing in the cut sets of a given fault tree. Several importance measures are calculated, however only the FV, RRR, and uncertainty are included here. Recall that the FV indicates that the factional contributions of the basic event to the minimal cut set upper bound. The RRR indicates how much the minimal cut set upper bound would decrease if the basic event probability were reduced. Finally, the uncertainty importance measure quantifies the contribution of the individual basic event's uncertainty to the total output uncertainty.

The Monte Carlo sampling approach was used for uncertainty analysis. In this approach repeated quantifications are made of the system cut sets using each random variable sampled from the basic event uncertainty distributions. A sample size of 5000 was used for each of the uncertainty analysis runs. In addition to the point estimate SFF, the mean, median, 5th percentile, 95th percentile, standard deviation, skewness and kurtosis coefficients for each fault tree and event tree are calculated. The coefficients of skewness and kurtosis are often used in comparison to the normal distribution. Skewness is a measure of the symmetry of the distribution about the center point where a value of zero indicates perfect symmetry, negative values indicate a long left tail and positive values indicating a long right tail. Kurtosis is a measure of whether the data is peaked or flat, where values greater than three are more peaked than the normal distribution and values less than three are flatter than the normal distribution having more weight in the tails.

As the information produced in SAPHIRE is rather extensive, tables and graphs summarizing the most pertinent results are given here. All remaining results may be found in Appendix C.6. All frequency values presented are in units of inverse years.

5.9.1. System Evaluation: Normal Operations

5.9.1.1. Fault tree failure probability

The overall reliability of the vented fuel system is summarized by the "Vented Fuel System Fail" fault tree. All subsequent fault trees are sub-trees which are transferred in to the overall fuel system failure fault tree. The resulting failure probabilities and uncertainty for the various normal operation fault tree models are given in Table 5.18 and Figure 5.13.

The standby modules (HTA 2, HTA 3, LTA 3, LTA 4, and COMP 2) each exhibit a relatively large point estimate of failure largely due to the operator failure to switch trains, conservatively estimated to be a nominal value of 1.1E-02. This failure clearly dominates in the standby modules and should be refined further when operator system interactions are more clearly defined. Overall, the failure mechanisms resulting in a breach of the system are comparable to the failure mechanisms resulting in a functional failure of the module due to unavailability of the module or a component failure to perform its function. The fault tree modeling the 2 out of 4 operating LTA module requirement is a clear outlier with a significantly lower failure probability. This makes

Table 5.18.: Normal Operations: Fault tree results

Fault Tree	Point Estimate	Mean	Median	Standard Deviation
AUX RELEASE	1.94E-03	1.94E-03	1.76E-03	8.88E-04
COMP1 FAIL	1.47E-03	1.56E-03	7.43E-04	3.90E-03
COMP1 RELEASE FPS	2.16E-04	2.19E-04	1.44E-04	2.59E-04
COMP2 FAIL	2.44E-02	2.50E-02	1.78E-02	2.98E-02
COMP2 RELEASE FPS	1.44E-04	1.44E-04	8.98E-05	2.05E-04
CONT RELEASE	1.95E-03	1.95E-03	1.76E-03	8.99E-04
FPRS CONT RELEASE	7.21E-04	7.28E-04	5.93E-04	5.37E-04
FPRS FAIL	3.57E-03	3.58E-03	3.35E-03	1.22E-03
FPTS BREACH	1.23E-03	1.23E-03	1.06E-03	7.06E-04
FPTS FAIL	2.37E-03	2.37E-03	2.16E-03	9.75E-04
FPTS RELEASE FPS	1.23E-03	1.22E-03	1.06E-03	6.75E-04
FUEL SYSTEM FAIL	2.56E-05	2.41E-05	1.06E-05	5.05E-05
HTA1 FAIL	8.16E-04	8.28E-04	6.90E-04	5.70E-04
HTA1 RELEASE	4.32E-04	4.29E-04	3.15E-04	4.03E-04
HTA2 FAIL	5.24E-02	5.24E-02	4.61E-02	2.38E-02
HTA2 RELEASE FPS	1.56E-08	1.53E-08	5.24E-09	4.50E-08
HTA3 FAIL	4.68E-02	4.60E-02	4.03E-02	2.23E-02
HTA3 RELEASE FPS	1.56E-08	1.60E-08	5.29E-09	8.62E-08
LTA HXR FAIL	5.76E-04	5.69E-04	4.44E-04	5.15E-04
LTA HXR RELEASE FPS	5.76E-04	5.68E-04	4.42E-04	4.49E-04
LTA MODULES 2OF4	1.27E-06	1.28E-06	8.66E-07	2.78E-06
LTA1 FAIL	5.04E-04	5.00E-04	3.97E-04	4.19E-04
LTA1 RELEASE FPS	2.88E-04	2.85E-04	1.96E-04	3.17E-04
LTA2 FAIL	5.04E-04	5.10E-04	4.08E-04	5.17E-04
LTA2 RELEASE FPS	2.88E-04	2.86E-04	1.93E-04	3.42E-04
LTA3 FAIL	3.47E-02	3.52E-02	2.84E-02	2.73E-02
LTA3 RELEASE FPS	1.44E-04	1.40E-04	7.76E-05	2.08E-04
LTA4 FAIL	3.47E-02	3.49E-02	2.83E-02	2.49E-02
LTA4 RELEASE FPS	1.44E-04	1.41E-04	7.48E-05	2.15E-04
PCB ISO SPO	1.01E-03	1.00E-03	8.52E-04	6.40E-04
PCB RELEASE	2.74E-06	2.76E-06	1.74E-06	3.73E-06
VENTED FUEL SYSTEM FAIL	5.95E-03	5.98E-03	5.70E-03	1.60E-03

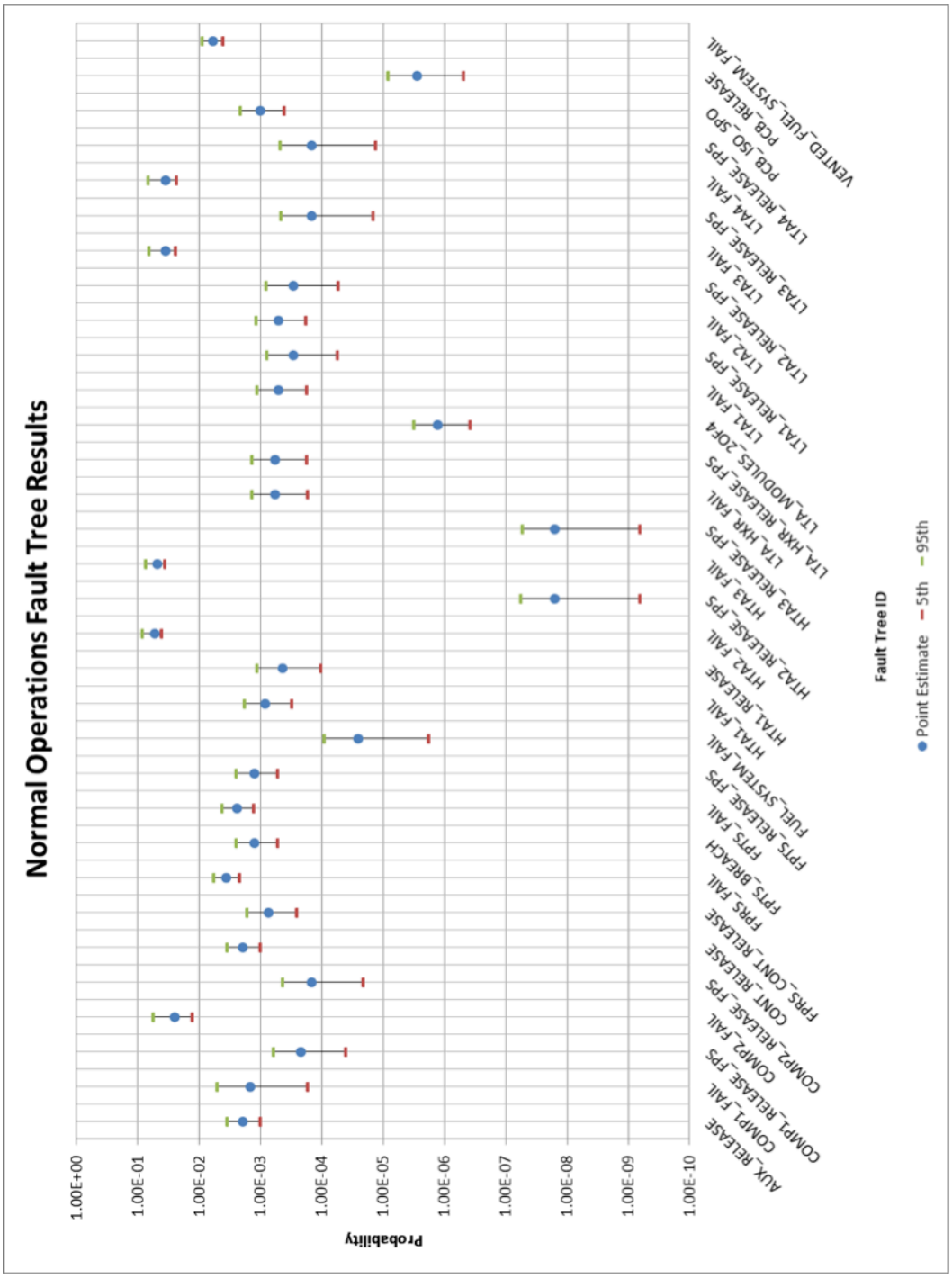

Figure 5.13.: Normal Operation: Fault tree results.

logical sense as the successful operation of any two of the 4 modules in place would result in a success; this flexibility increases the reliability of the system.

5.9.1.2. Cut set analysis

A full list of cut set data is impractical to include due the sheer number of cut sets generated (reaching well beyond 5,000 for the Vented Fuel System fault tree alone). Therefore, a summary of the cut set results is provided here. The failure of the system, for this analysis, is defined as a breach in the system or failure of a component to perform its function; consequently, there are several cut sets with a single component failure contributing largely to the overall probability of failure for the various fault trees. Failure modes such as a valve leak, vessel breach, pipe breach, unintentional valve closure, etc. require only a single failure leading to a failure of the system as a whole, thus the reliability, and consequently quantification of reliability, of these components are of greatest importance.

Spurious operation of the motor operated isolation valves for the primary coolant boundary and containment (V-1 through V-14, V-28, V-29, V-60, and V-61), spurious operation of the LTA regenerative heat exchanger isolation valves and the pressure control valve V-15, and leakage of all valves in contact with the purge stream under normal operations contribute equally to the total probability of system failure, each holding a 1.21% contribution toward overall system failure. Additionally, failure of V-15 to control contributes 1.05%, a plug in the fuel system piping contributes 0.40%, and failure of the in-service compressor coincident with the unavailability of the standby compressor via operator failure or valve failure contributes 0.22% and 0.12%, respectively. All remaining failure modes contribute less than 0.05%.

Markedly, the motor operated control valve (V-15) is a single point failure of extreme importance. This valve is the only control valve available to maintain the pressure differential in the purge stream. Additionally, each of the three 100% FPVS trains may be made unavailable by the inadvertent closure of V-15. There are several other instances of single point failures due to leakages and failure to remain open when necessary, however V-15 is clearly an important component that should be evaluated further.

5.9.1.3. Importance measures

A summary of the resulting Fussell-Vesely (F-V), Risk Reduction Ratio (RRR), and uncertainty importance measures for the vented fuel fault tree model is given in Table 5.19. The maximum value for each importance measure is presented for the vented fuel system fault tree below.

As indicated in the importance measures presented here, the failure of the valves in the system holds the highest importance. Thus, it is important to refine the failure rate data for these components and ensure adequate reliability of the system. To improve the reliability of the system, valves with superior reliability could be selected. Although testing and maintenance is not included in this analysis due to the preliminary nature of the system, reducing the interval between testing of these components may also improve the reliability of the system.

Table 5.19.: Normal Operations: Maximum Importance Measures.

Importance measure	F-V	RRR	uncertainty
V-1 to V-14 Leak	0.0121	1.01	1.77E-04
V-1 to V-14 SPO	0.0121	1.01	1.77E-04
V-15 SPO	0.0121	1.01	1.77E-04
V-15 Control Pressure	0.0121	1.01	-
V-16 to V-19 Leak	0.0121	1.01	1.77E-04
V-22 to V-23 Leak	0.0121	1.01	1.77E-04
V-28 to V-38 Leak	0.0121	1.01	1.77E-04
V-28 to V-33 SPO	0.0121	1.01	1.77E-04
V-40 Leak	0.0121	1.01	1.77E-04
V-42 to V-45 Leak	0.0121	1.01	1.77E-04
V-47 Leak	0.0121	1.01	1.77E-04
V-49 to V-57 Leak	0.0121	1.01	1.77E-04
V-50 to V-53 SPO	0.0121	1.01	1.77E-04
V-59 Leak	0.0121	1.01	-
V-60 to V-63 Leak	0.0121	1.01	1.77E-04
V-60 to V-61 SPO	0.0121	1.01	1.77E-04
V-74 Leak	0.0121	1.01	1.77E-04
V-77 Leak	0.0121	1.01	1.77E-04
V-80 Leak	0.0121	1.01	-

Table 5.20.: Normal Operations: Uncertainty analysis.

Event	Uncertainty
Nominal Probability	5.95E-03
MOV SPO	1.12E-02
Vessel Breach	5.97E-03
MOV Leak	2.57E-02
MOVI Leak	1.88E-02
Operator Reliability	6.13E-03

5.9.1.4. Uncertainty analysis

In addition to the uncertainty importance measure analysis, which quantifies the contribution of the individual basic event's uncertainty to the total output uncertainty, a scoping assessment was performed in which failure rates for basic events of interest were increased by an order of magnitude to better understand how the system reliability would ultimately change. The spurious operation (SPO) of a motor operated valve (MOV), vessel breach, and leak rate of a motor operated valve (MOV) and motor operated isolation valve (MOVI) were chosen for this analysis. The resulting uncertainty analysis for the vented fuel system fault tree model is given in Table 5.20.

As indicated in the table, an increase in the leakage failure rate of the motor operated valve clearly has the greatest overall impact on the failure probability of the system, significantly increasing the failure frequency. Similarly, the increase in the leakage failure rate and spurious

Table 5.21.: Accident Conditions: Fault tree results

Fault Tree	Point Estimate	Mean	Median	Standard Deviation
AUX RELEASE	1.94E-03	1.94E-03	1.75E-03	8.64E-04
COMP1 RELEASE FPS	2.16E-04	2.17E-04	1.44E-04	3.17E-04
COMP2 RELEASE FPS	1.44E-04	1.40E-04	8.94E-05	1.79E-04
CONT RELEASE	1.95E-03	1.94E-03	1.74E-03	9.56E-04
CONT RELEASE MAN	1.95E-03	1.95E-03	1.74E-03	9.26E-04
FPTS RELEASE FPS	1.23E-03	1.21E-03	1.06E-03	7.16E-04
FPTS RELEASE FPS MAN	1.23E-03	1.22E-03	1.06E-03	6.79E-04
FUEL SYSTEM RELEASE FPS	1.56E-06	1.57E-06	9.18E-07	2.50E-06
HTA1 RELEASE	4.32E-04	4.36E-04	3.27E-04	4.08E-04
HTA2 RELEASE FPS	1.56E-08	1.62E-08	5.30E-09	5.38E-08
HTA3 RELEASE FPS	1.56E-08	1.66E-08	5.20E-09	1.02E-07
LOSS OF ONSITE POWER	6.82E-03	6.69E-03	5.03E-03	5.70E-03
LTA1 RELEASE FPS	2.88E-04	2.89E-04	1.93E-04	3.44E-04
LTA2 RELEASE FPS	2.88E-04	2.93E-04	1.96E-04	4.31E-04
LTA3 RELEASE FPS	1.44E-04	1.46E-04	7.68E-05	2.49E-04
LTA4 RELEASE FPS	1.44E-04	1.44E-04	7.57E-05	2.11E-04
LTA HXR RELEASE FPS	5.76E-04	5.67E-04	4.53E-04	4.57E-04
PCB RELEASE	2.74E-06	2.76E-06	1.73E-06	3.91E-06

operation of the motor operated isolation valve and noticeably increase the failure probability. The operator reliability increases the failure frequency albeit to a lesser degree. The effects of increasing the vessel breach failure rates are relatively insignificant. Logically, these results make sense as the large number of valves present in the system contributes to several potential release pathways. Similarly, there are fewer vessels in the system that could be breached. The spurious operation of any number of motor operated valves in the system could result in the unavailability of a component or entire train, leading to a large overall increase in the failure probability. Additionally, operator error has been shown to dominate the failure of the standby modules as indicated in the fault tree results, thus we would expect an increase. Although the nominal value of operator error is conservative, the sensitivity analysis shows that the variation of an order of magnitude of the failure probability only slightly increases the overall system failure probability.

5.9.2. System Evaluation: Accident Conditions

5.9.2.1. System failure probability and frequency

The resulting failure probabilities for the various fault tree models are given in Table 5.21 and Figure 5.14. Note that several of the fault trees are inputs into the three main fault trees for a release from the auxiliary building, containment, and primary coolant boundary. The three main fault trees, in addition to the fault tree for loss of onsite power, are the only fault trees directly transferred into the event trees. All subsequent fault trees are transferred in to one of the four main fault tree models.

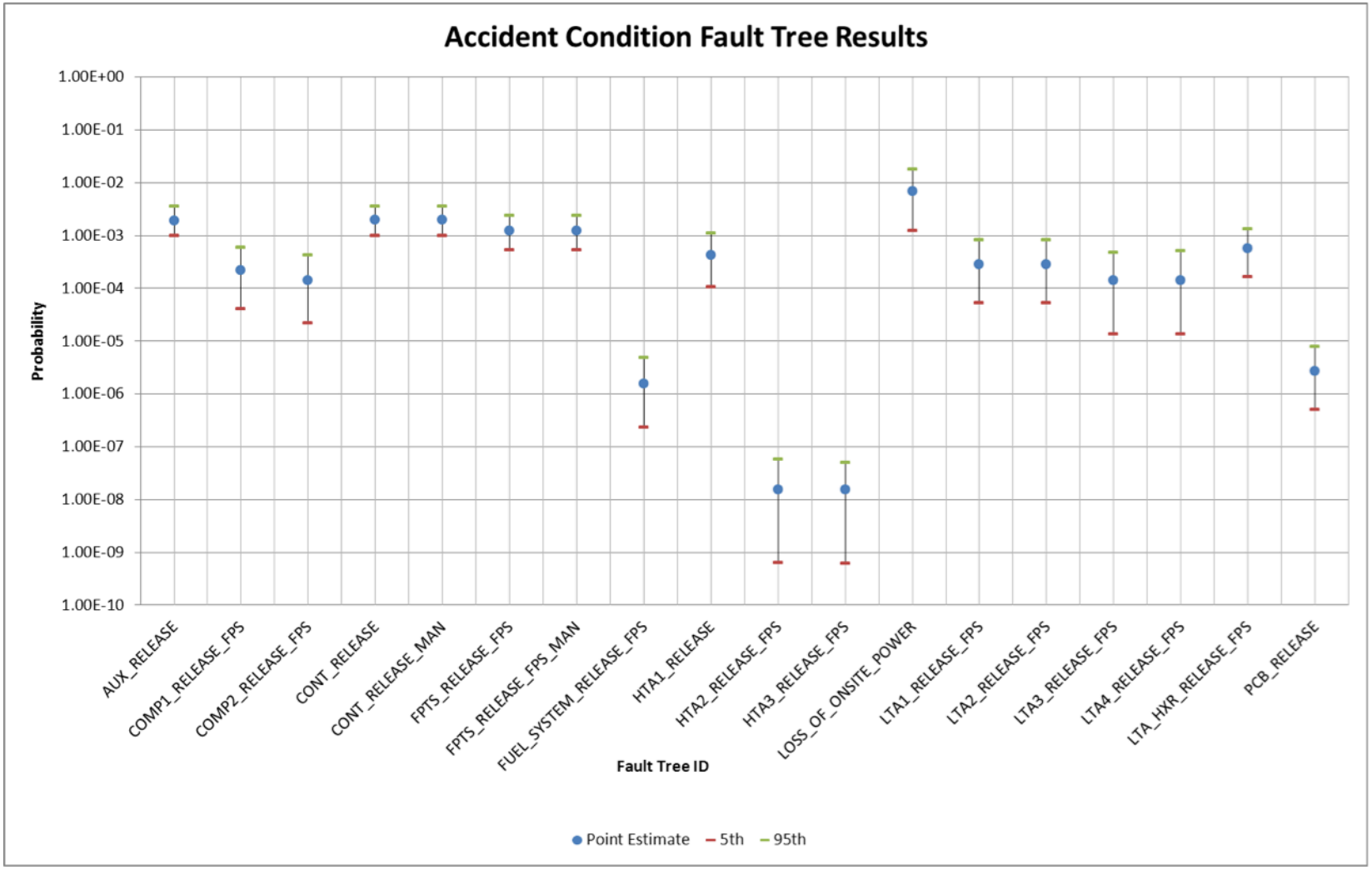

Figure 5.14.: Accident Condition: Fault tree results.

Table 5.22.: LOCA Event Tree results with Standard Deviation (SD).

Sequence ID	End State	Point Estimate (Per Year)	Mean (Per Year)	Median (Per Year)	SD (Per Year)
Total	N/A	3.90E-07	3.95E-07	1.39E-07	9.48E-07
LOCA:2	AUX-REL	1.94E-07	1.88E-07	6.79E-08	4.67E-07
LOCA:3	CONT-REL	1.95E-07	1.99E-07	6.82E-08	4.59E-07
LOCA:4	AUX-CONT-REL	3.79E-10	3.99E-10	1.20E-10	1.45E-09
LOCA:5	PCB-REL	2.74E-10	2.45E-10	6.36E-11	7.63E-10
LOCA:6	PCB-AUX-REL	5.33E-13	5.79E-13	1.23E-13	2.76E-12
LOCA:7	PCB-CONT-REL	5.33E-13	5.53E-13	1.22E-13	2.40E-12
LOCA:8	PCB-CONT-AUX-REL	0.00E+00	0.00E+00	0.00E+00	0.00E+00

A release in containment is estimated as more probable than a release in the auxiliary building or primary coolant boundary. Logically, we expect the failure frequency to be larger for a release in the containment and auxiliary building in comparison to the primary coolant boundary due to the fact the majority of the vented fuel system is located in those two regions. Likewise, we expect the failure frequency within containment to be larger than that for the auxiliary building largely due to the numerous pathways for failure stemming from the large number of valves and piping located within containment. However, the failure frequencies are relatively similar, likely due the large number of valves and piping also located within the auxiliary building.

On an individual system level, the compressor modules and in-service HTA module (HTA 1) have the largest failure frequencies. In contrast, the stand-by HTA modules (HTA 2 and HTA 3) have the lowest failure frequencies. This is expected as the failure here is defined as a release from the system, thus the more avenues through which radioactive material may be released, the larger the probability. By definition, stand-by modules have fewer opportunities for failure since a release of radioactive material from the vessel would first require a failure of the module isolation valves on either side. The compressor modules only have one isolation valve on the incoming side, thus a single valve failure could introduce purge stream gas into the stand-by module; in contrast two isolation valve failures are required of all other stand-by modules in the system. Similarly, a release from either of the standby HTA modules is least likely since this would require a breach of the train isolation valves and module isolation valves. Fortunately, should a release occur from a HTA module, the containment boundary will reduce the risk of any release to the environment. Furthermore, the purge stream entering the compressor module has already been treated, having already passed through the HTA and LTA modules which remove the vast majority of fission products under normal operating conditions.

The resulting event tree failure frequencies for the various event tree models are given in Tables 5.22 through Table 5.25. Note that the probability truncation was set to 1.00E-15, thus the results in the following tables displaying a point estimate of 0.00E+00 fall below this cut off value and are assumed to be zero in the quantification of overall system failure frequency. A graphical summary of the event tree results is given in Figure 5.15.

The system failure frequency is the summation of the sequences of a given event tree resulting in a system failure, defined here as a release of fission products. The resulting system failure frequencies for the various event tree models are summarized in Table 5.26, given in units of

Table 5.23.: Manifold Rupture Event Tree results with Standard Deviation (SD).

Sequence ID	End State	Point Estimate (Per Year)	Mean (Per Year)	Median (Per Year)	SD (Per Year)
Total	N/A	8.79E-05	9.05E-05	3.21E-05	2.78E-04
RUPTURE:1	CONT-REL	8.76E-05	8.51E-05	3.36E-05	1.83E-04
RUPTURE:2	AUX-REL	1.70E-07	1.70E-07	5.91E-08	4.42E-07
RUPTURE:3	CONT-REL	1.71E-07	1.71E-07	5.84E-08	4.25E-07
RUPTURE:4	AUX-CONT-REL	3.32E-10	2.98E-10	1.05E-10	7.01E-10
RUPTURE:5	PCB-REL	2.40E-10	2.28E-10	5.88E-11	8.61E-10
RUPTURE:6	PCB-AUX-REL	4.67E-13	4.79E-13	1.11E-13	1.59E-12
RUPTURE:7	PCB-CONT-REL	4.67E-13	4.35E-13	1.07E-13	1.86E-12
RUPTURE:8	PCB-CONT-AUX-REL	0.00E+00	0.00E+00	0.00E+00	0.00E+00

Table 5.24.: Transient Event Tree results with Standard Deviation (SD).

Sequence ID	End State	Point Estimate (Per Year)	Mean (Per Year)	Median (Per Year)	SD (Per Year)
Total	N/A	2.73E-03	2.69E-03	9.67E-04	6.49E-03
TRANSIENT:2	AUX-REL	1.36E-03	1.31E-03	4.61E-04	3.47E-03
TRANSIENT:3	CONT-REL	1.36E-03	1.38E-03	4.86E-04	3.28E-03
TRANSIENT:4	AUX-CONT-REL	2.65E-06	2.83E-06	8.86E-07	9.46E-06
TRANSIENT:5	PCB-REL	1.92E-06	1.97E-06	4.54E-07	8.77E-06
TRANSIENT:6	PCB-AUX-REL	3.73E-09	3.47E-09	8.61E-10	9.92E-09
TRANSIENT:7	PCB-CONT-REL	3.74E-09	4.22E-09	8.23E-10	4.56E-08
TRANSIENT:8	PCB-CONT-AUX-REL	6.57E-12	5.84E-12	1.20E-12	2.05E-11

Table 5.25.: Station Black-Out (SBO) Event Tree results with Standard Deviation (SD).

Sequence ID	End State	Point Estimate (Per Year)	Mean (Per Year)	Median (Per Year)	SD (Per Year)
Total	N/A	2.41E-04	2.41E-04	1.83E-04	2.00E-04
SBO:02	AUX-REL	1.19E-04	1.17E-04	8.70E-05	1.08E-04
SBO:03	CONT-REL	1.20E-04	1.19E-04	8.80E-05	1.06E-04
SBO:04	CONT-AUX-REL	2.33E-07	2.36E-07	1.57E-07	2.98E-07
SBO:05	PCB-REL	1.68E-07	1.71E-07	8.68E-08	3.05E-07
SBO:06	PCB-AUX-REL	3.27E-10	3.30E-10	1.59E-10	6.57E-10
SBO:07	PCB-CONT-REL	3.28E-10	3.44E-10	1.56E-10	8.15E-10
SBO:08	PCB-CONT-AUX	0.00E+00	0.00E+00	0.00E+00	0.00E+00
SBO:10	AUX-REL	8.17E-07	8.00E-07	4.57E-07	1.12E-06
SBO:11	CONT-REL	8.18E-07	8.09E-07	4.42E-07	1.23E-06
SBO:12	CONT-AUX-REL	1.59E-09	1.56E-09	7.96E-10	2.56E-09
SBO:13	PCB-REL	1.15E-09	1.10E-09	4.42E-10	2.17E-09
SBO:14	PCB-AUX-REL	2.08E-12	2.13E-12	6.85E-13	8.31E-12
SBO:15	PCB-CONT-REL	2.08E-12	1.99E-12	6.80E-13	4.84E-12
SBO:16	PCB-CONT-AUX-REL	0.00E+00	0.00E+00	0.00E+00	0.00E+00

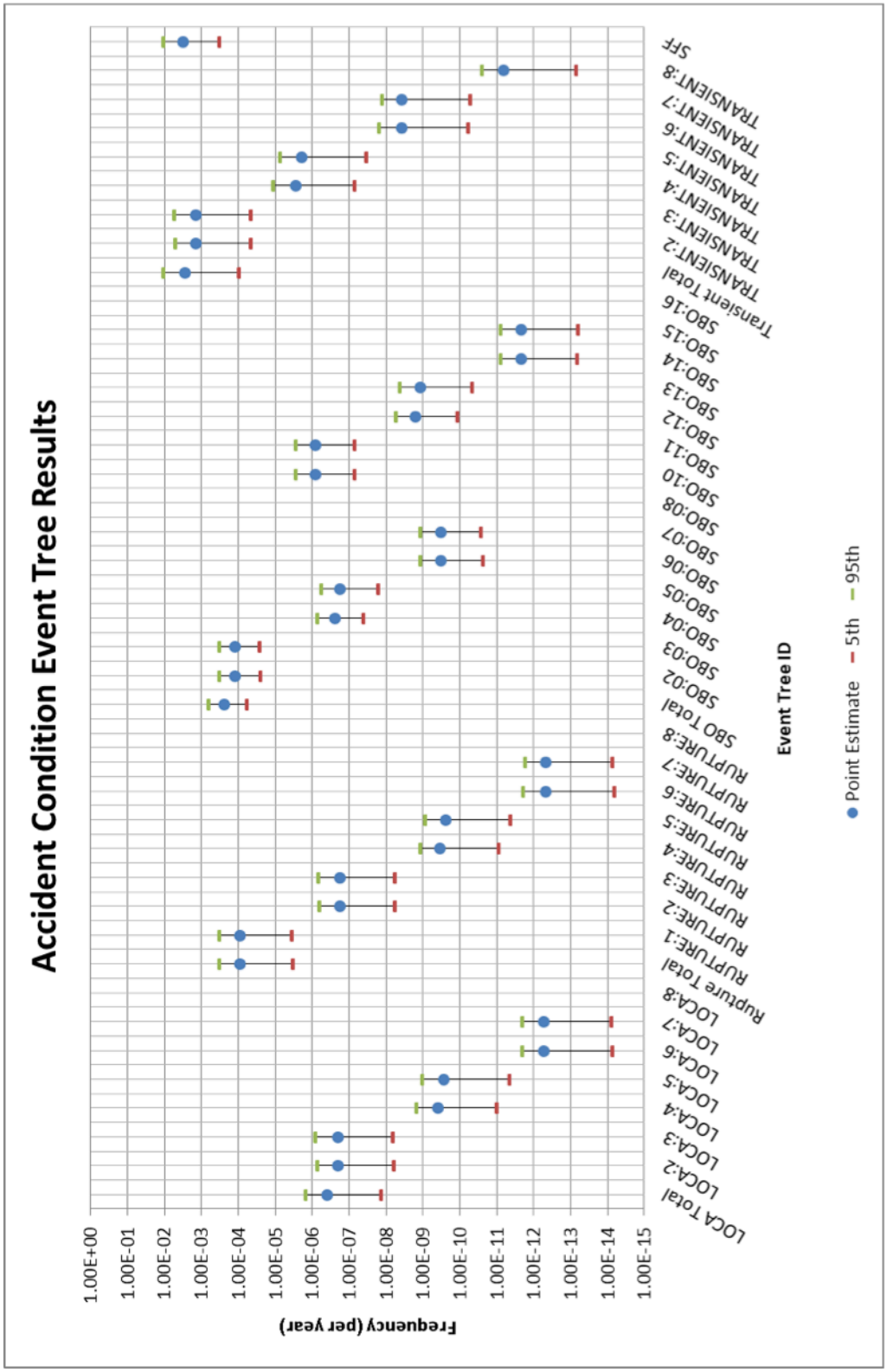

Figure 5.15.: Accident Condition: Event tree results.

Table 5.26.: System Failure Frequency

Initiating Event	System Failure Frequency (Per Year)	5th Percentile (Per Year)	95th Percentile (Per Year)
LOCA	3.90E-07	1.34E-08	1.47E-06
LOOP	2.41E-04	5.62E-05	6.18E-04
Transient	2.73E-03	9.33E-05	1.04E-02
Rupture in FPVS Manifold	8.79E-05	3.27E-06	3.08E-04
Total	3.06E-03	3.10E-04	1.04E-02

inverse years. For example, it is estimated that there are 3.90E-07 occurrences per year that a LOCA will lead to a failure of the vented fuel system, releasing radioactive material from the vented fuel system. The SFF uncertainty is represented by a confidence interval where the 95th percentile value represents the value at which 95% of the distribution is less than or equal to, thereby representing an upper bound value. Similarly, the 5th percentile value represents the value at which 5% of the distribution is less than or equal to, thereby representing a lower bound value.

The range of system failure frequencies stem primarily from the large range of initiating event frequency values, as indicated in the importance measures which will be discussed further in the next section. Similarly, the event trees for each event contain the same input probabilities (with the exception of the minor changes necessary for the rupture in the FPVS manifold initiating event) for the nodes related to the vented fuel system. Thus, the primary differences in the results are directly attributed to the initiating event frequency, and in the case of the LOOP analysis the loss of on-site power required for an SBO analysis. The calculated SFF values are all relatively small, however large enough to merit further analysis.

5.9.2.2. Cut set analysis

A full list of cut set data is impractical to include here due to the sheer number of cut sets generated (reaching well beyond 11,000 for the SBO event tree alone). Therefore, a summary of the cut set results is provided here. By definition of a failure of the system being a release of radiation, there are several cut sets with a single component failure contributing largely to the overall probability of failure for the various fault trees. The largest contributor to the overall failure probability for the primary coolant boundary release fault tree is a failure of the 7 FPTS sub-header pipes, contributing 43.2%. The containment release fault tree dominant cut sets are valve leaks for all valves in contact with the purge stream under normal operations, each equally contributing 3.7% to the total failure probability; all remaining cut sets contribute 0.12% or less.

Similarly, the leakage of all valves in contact with the purge stream under normal conditions are the dominant cut sets for the auxiliary building release fault tree, each equally contributing 3.7%; all remaining cut sets contribute 0.02% or less. For the LOCA, SBO, and transient event trees a valve leak failure is clearly the dominant contributor to the overall failure frequency. The manifold rupture event tree differs of course due to the initiating event being a rupture of the system, thus the initiating event itself contributes 99.6% to the failure frequency. Failure modes such as a valve leak, vessel breach, pipe breach, manifold breach, etc. require only a single

Table 5.27.: Accident Operations: Maximum Importance Measures.

Fault/Event Tree	FV	RRR	Uncertainty
Primary Coolant Boundary Release	4.32E-01 *7 Sub-headers*	1.76E+00 *7 Sub-headers*	2.92-06 *7 Sub-headers*
Containment Release	3.70E-02 *V-1 to V-14 Leak* *V-16 to V-19 Leak* *V-22 to V-23 Leak* *V-28 Leak* *V-61to V-63 Leak* *V-74 Leak* *V-77 Leak* *V-80 Leak*	*1.04E+00* *V-1 to V-14 Leak* *V-16 to V-19 Leak* *V-22 to V-23 Leak* *V-28 Leak* *V-61to V-63 Leak* *V-74 Leak* *V-77 Leak* *V-80 Leak*	1.77E-04 *V-1 to V-14 Leak* *V-16 to V-19 Leak* *V-22 to V-23 Leak* *V-28 Leak* *V-61to V-63 Leak* *V-74 Leak* *V-77 Leak* *V-80 Leak*
Containment Release (Rupture in Manifold)	3.70E-02 *V-1 to V-14 Leak* *V-16 to V-19 Leak* *V-22 to V-23 Leak* *V-28 Leak* *V-61to V-63 Leak* *V-74 Leak* *V-77 Leak* *V-80 Leak*	*1.04E+00* *V-1 to V-14 Leak* *V-16 to V-19 Leak* *V-22 to V-23 Leak* *V-28 Leak* *V-61to V-63 Leak* *V-74 Leak* *V-77 Leak* *V-80 Leak*	1.77E-04 *V-1 to V-14 Leak* *V-16 to V-19 Leak* *V-22 to V-23 Leak* *V-28 Leak* *V-61to V-63 Leak* *V-74 Leak* *V-77 Leak* *V-80 Leak*
Auxiliary Building Release	3.70E-02 *V-29 to V-38 Leak* *V-40 Leak* *V-42 to V-45 Leak* *V-47 Leak* *V-49 to V-57 Leak* *V-59 to V-60 Leak*	1.04E+00 *V-29 to V-38 Leak* *V-40 Leak* *V-42 to V-45 Leak* *V-47 Leak* *V-49 to V-57 Leak* *V-59 to V-60 Leak*	1.77E-04 *V-29 to V-38 Leak* *V-40 Leak* *V-42 to V-45 Leak* *V-47 Leak* *V-49 to V-57 Leak* *V-59 to V-60 Leak*
LOCA	1.00E+00 *IE-LOCA*	1.90E+38 *IE -LCOA*	9.61E-07 *IE -LCOA*
Rupture in Manifold	1.00E+00 *IE-Rupture*	1.90E+38 *IE-Rupture*	2.16E-04 *IE-Rupture*
SBO	1.00E+00 *IE-LOOP*	1.90E+38 *IE -LOOP*	1.80E-04 *IE -LOOP*
Transient	1.00E+00 *IE-Transient*	1.90E+38 *IE -Transient*	6.73E-03 *IE -Transient*

failure leading to a failure of the system, thus the reliability, and consequently quantification of reliability, of these components are of greatest importance. As indicated in these results, it is essential to refine the reliability analysis of the various valves in the system as they contribute greatly to the overall probability of failure of the system.

5.9.2.3. Importance measures

A summary of the resulting FV, RRR, and uncertainty importance measures for the various fault tree models are given in Table 5.27. The maximum value for each importance measure is presented for each of the four main fault trees and event trees with the corresponding basic event(s) or top event(s) listed directly below.

As stated previously, the initiating event frequency is of high importance for the event tree calculations, as indicated by the FV and RRR, and uncertainty importance measures, having the ability to drastically increase or reduce the calculated SFF. The values for the maximum RRR importance measures for the event trees are extremely large as a direct consequence of the RRR

Table 5.28.: System Failure Probability Uncertainty.

Event	**Failure Probabiliy Uncertainty**		
	AUX RELEASE	*CONT RELEASE*	*PCB RELEASE*
Nominal Probability	1.94E-03	1.95E-03	2.74E-06
MOV SPO	1.94E-03	1.95E-03	2.74E-06
Vessel Breach	1.95E-03	1.95E-03	4.90E-06
MOV Leak	1.67E-02	7.11E-03	2.74E-06
MOVI Leak	3.24E-03	1.35E-02	2.74E-06
Operator Reliability	1.94E-03	1.95E-03	2.74E-06

Table 5.29.: System Failure Frequency Uncertainty.

Event	**Failure Frequency Uncertainty (1/year)**				
	LOCA	*LOOP*	*Transient*	*Rupture*	*Total*
Nominal Probability	3.90E-07	2.41E-04	2.73E-03	8.79E-05	3.06E-03
MOV SPO	3.90E-07	2.41E-04	2.73E-03	8.79E-05	3.06E-03
Vessel Breach	3.91E-07	2.42E-04	2.74E-03	8.79E-05	3.07E-03
MOV Leak	2.39E-06	1.48E-03	1.68E-02	8.97E-05	1.84E-02
MOVI Leak	1.68E-06	1.04E-03	1.18E-02	8.91E-05	1.29E-02
Operator Reliability	3.90E-07	2.41E-04	2.73E-03	8.79E-05	3.06E-03

equation used in SAPHIRE. The RRR is calculated by dividing the nominal minimal cut set upper bound by the calculated minimal cut set upper bound value after setting the basic event of interest to zero. Since the basic event of interest for the event trees is the initiating events, the RRR calculation essentially divides the nominal minimal cut set upper bound by zero, resulting in an excessively large value.

In regards to the four primary fault trees, the importance measures are dominated primarily by valve leakage failures of motor operated valves, with the exception of the sub-header piping in the case of the primary coolant boundary release fault tree, which consists of mostly pipe breach failures. Thus, the reliability of the motor operated valves is of utmost importance to ensure safe and reliable operation of the vented fuel system. Furthermore, accurate failure rate data for these components is of greatest importance to ensure accurate quantification of the reliability of the system.

5.9.2.4. Uncertainty analysis

In addition to the uncertainty importance measure analysis, which quantifies the contribution of the individual basic event's uncertainty to the total output uncertainty, a scoping assessment was performed in which failure rates for basic events of interest were increased by an order of magnitude to better understand how the individual fault tree failure probabilities and overall SFF would ultimately change. The SPO of a MOV, vessel breach, and leak rate of a MOV and MOVI, and human reliability were chosen for this analysis. The results are given in Table 5.28, Table 5.29 and Figure 5.16.

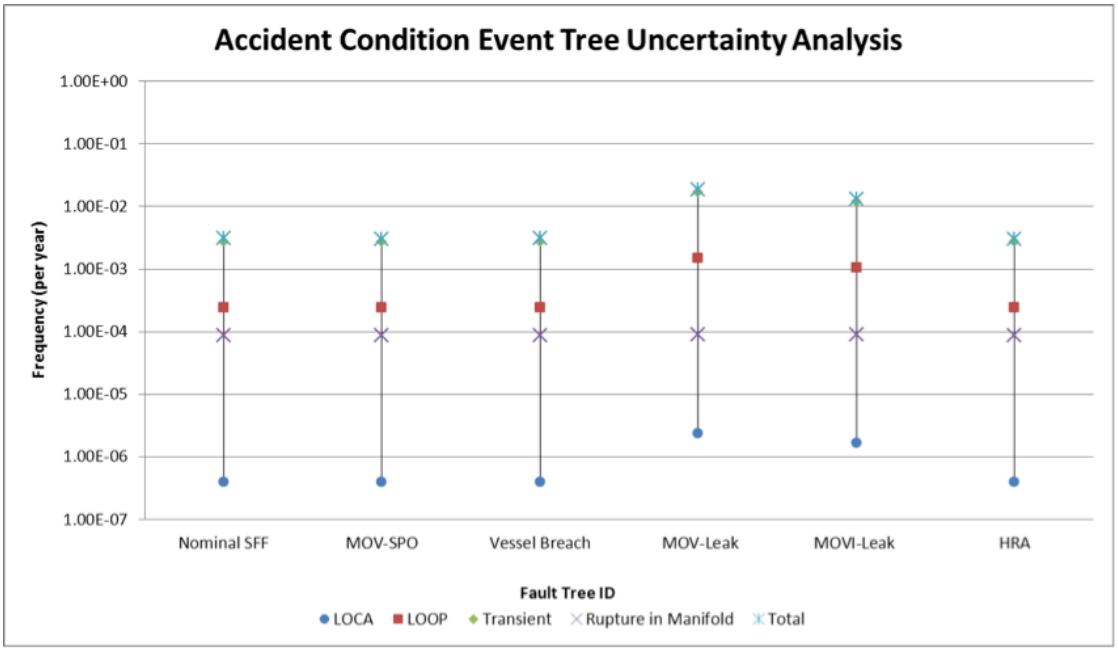

Figure 5.16.: Accident condition event tree uncertainty analysis.

As indicated in the table, an increase in the leakage failure rate of the motor operated valve clearly has the greatest overall impact on the SFF, significantly increasing the failure frequency. Similarly, the increase in the leakage failure rate of the motor operated isolation valve noticeably increases the failure frequency albeit to a lesser degree. The effects of increasing the vessel breach and motor operated valve spurious operation, and HRA failure rates are relatively insignificant. Logically, these results make sense as the large number of valves present in the system contributes to several potential release pathways. Similarly, there are fewer vessels in the system that could be breached and fewer yet motor operated valves whose spurious operation or operator error would lead to a leakage since an additional failure would be required. Moreover, the event tree for the rupture in the FPVS manifold does not display the same overall trend as the remainder of the event trees. This is likely due to the dominant nature of the initiating event itself being a rupture of the manifold within the FPVS, thus the effect of an increase in the failure rate of any subsidiary component is overshadowed.

5.9.3. System damage states

To proceed with the Level 2 analysis, the end states of the Level 1 accident condition fault trees were binned into System Damage State groups of similar failure modes. Each SDS group is transferred as the initiating event for the Level 2 APETs. Thus, initiating events were created for each SDS group assuming a lognormal distribution utilizing the calculated failure frequency and uncertainty results from Level 1. The EF is calculated by taking the square root of the ratio of the 95th percentile to the 5th percentile. The results are summarized in Table 5.30.

According to these results an estimated 2.09E-06 occurrences per year radioactive material

Table 5.30.: System Damage State results.

Description	SDS ID	Frequency (1/year)	Error Factor
PCB-REL	SDS 1	2.09E-06	12.78
CONT-REL	SDS 2	1.57E-03	8.15
AUX-REL	SDS 3	1.48E-03	8.68
PCB-CONT-REL	SDS4	4.30E-09	11.45
PCB-AUX-REL	SDS 5	4.06E-09	13.55
CONT-AUX-REL	SDS 6	3.06E-06	8.91
PCB-CONT-AUX-REL	SDS 7	7.04E-12	15.78

will be released from the vented fuel system within the primary coolant boundary. The estimated number of occurrences per year radioactive material is released from the vented fuel system within the primary coolant boundary, containment, and auxiliary building concurrently is extremely small and the least likely of all system damage states considered, as expected due to the large number of component failures required. In contrast, the estimated number of occurrences per year that radioactive material is released from the vented fuel system within containment or within the auxiliary building is larger, as expected due to the majority of the FPVS being located in either of those two locations.

5.10. Level 2 PRA Results

5.10.1. Accident progression event tree results

The results for the Level 2 PRA are given in the following section. The strengths and weaknesses of the system response under accident conditions may be determined by analyzing the failure frequency, cut sets, importance measures, and uncertainty analysis for the various event trees. The Monte Carlo sampling approach was used for uncertainty analysis with a sample size of 5000. All frequency values presented are in units of inverse years. A truncation value of 1.00E-15 was used to reduce the resulting source term groups.

5.10.1.1. Source term group frequency

The resulting release frequency for each APET is not included here as the values are identical to the SDS frequency that acts as the initiating event for each SDS specific APET. Nonetheless, the results can be used to validate proper utilization of the logic in SAPHIRE for partitioning the various accident progression sequences into source term groups. Although some of these sequences do not result in a release to the environment, the sum of source term group frequencies (including no release) should equal the sum of the SDS release frequency; inspection of the APET results indicate proper partitioning of the source term groups. The resulting release frequencies from the various APET models are given in Table 5.31 for the source term groups with an estimated release frequency larger than 1.00E-10.

The resulting release frequencies of primary interest are the higher frequency releases including source term components from the HTA module or LTA module (Source Term IDs C and

Table 5.31.: Source Term Group Release Frequencies.

Source Term Group ID	Release Frequency (1/yr)	5th Percentile (1/yr)	95th Percentile (1/yr)
BGJK	9.60E-04	5.46E-05	3.63E-03
DE	4.44E-04	2.25E-05	1.58E-03
D	3.85E-04	1.80E-05	1.41E-03
BCGJK	2.90E-04	1.64E-05	1.00E-03
DGJK	6.09E-05	3.39E-06	2.29E-04
BJK	2.97E-05	1.56E-06	1.13E-04
BCJK	8.96E-06	4.96E-07	3.27E-05
ABFGHJK	2.03E-06	5.29E-08	7.84E-06
DJK	1.94E-06	1.30E-07	6.49E-06
BGJKXDE	5.61E-07	2.66E-08	2.13E-06
BGJKXD	4.86E-07	2.31E-08	1.64E-06
BCGJKXDE	1.69E-07	8.05E-09	5.98E-07
BCGJKXD	1.47E-07	7.08E-09	5.56E-07
ABFHJK	6.28E-08	1.51E-09	2.20E-07
BJKXDE	1.74E-08	7.88E-10	6.21E-08
BJKXD	1.50E-08	7.17E-10	5.54E-08
BCJKXDE	5.23E-09	2.36E-10	1.98E-08
BCJKXD	4.54E-09	2.08E-10	1.70E-08
ABFGHJKXDE	1.18E-09	2.58E-11	4.26E-09
ABFGHJKXD	1.03E-09	2.38E-11	3.85E-09
ABCFGHJK	7.49E-10	2.17E-11	2.80E-09
ABGHJK	4.50E-10	5.48E-11	1.35E-09
ABDFGHJK	1.58E-10	4.50E-12	5.99E-10

E, respectively). Additionally, of particular concern are the source term groups which include source term components from the adsorber modules and do not benefit from attenuation via fission product barriers (Source Term IDs F, G, H, J, and K). It is important to note that the cumulative SFF from the Level 1 results was 3.06E-03 in smaller in comparison to the cumulative Level 2 STG frequency of 2.18E-03; consequently, it can be stated that about 70% of the releases from the vented fuel system result in an environmental release. This stems from the assumption that a release in the system after the LTA module or in the HTA return line does not contribute to a release of radioactivity due to the multiple isolation mechanisms available and the expected low level of radioactivity at this point within the system.

The release frequencies for all source term groups greater than the 1.00E-15 truncation threshold are given in Figure 5.17 in descending order. The majority of the source term group frequencies exhibit a plateau like trend which physically corresponds to the unlikely failure of a fission product barrier affecting the retention capabilities. For example, the source term ID ABFGHJKXDE represents a release from the primary coolant boundary and the purge stream before the HTA module in containment with the primary coolant boundary intact, containment intact, and attenuation from the PCB, containment, and reactor building. The XDE portion represents an additional release from within the auxiliary building of the purge stream contents before the LTA module in addition to the LTA module contents. Failure of any one of these

fission product barriers, while unlikely (as indicated in the small decrease in frequency) results in allocation to a source term group with identical contents with the exception of the removal of the failed fission product barrier; for instance, if the containment failed the representative attenuation factor ID G would be removed and the source term ID would be ABFHJKXDE.

5.10.1.2. Cut set analysis

A full list of cut set data is impractical to include here due to the vast number of cut sets generated. Therefore, a summary of the cut set results is provided. The largest contributor to the overall APET sequences is a release from within the containment (SDS 2) before the HTA module with successful isolation of the PCB and containment and intact liquid nitrogen cooling and containment boundary, contributing 31%. The second largest contributor, 21.3%, stems from a release form within the auxiliary building downstream of the LTA. As stated previously, it is assumed a release downstream of the LTA does not result in a release due to the large number of isolation valves available to mitigate the release. Likewise, the same assumption is applied to releases from the HTA return line, which contributes 7.17% to the overall APET frequency. These two sequences alone are primarily responsible for the roughly 30% of SFF sequences that do not result in a release to the environment. Furthermore, the cut sets reveal a release in the auxiliary building (SDS 3) and in the containment building (SDS 2) to be a major contributors to release, resulting in 48.4% and 51.2% of the releases, respectively. Consequently, all other SDSs have a much lesser impact on the overall outcome.

5.10.1.3. Importance measures

A summary of the resulting Fussell-Vesely, Risk Reduction Ratio, and uncertainty importance measures for the various fault tree models are given in Table 5.32. The maximum value for each importance measure is presented for each of the accident progression event trees with the corresponding top event(s) listed directly below.

As indicated in the results, the initiating event frequencies for each SDS input to the APET are of greatest importance. Although this is expected, it fails to provide much insight into the importance of the elements of the APET with the largest overall impact. Generally, the importance measures for the second largest top event are related to the release location within the containment or auxiliary building. Since the APET for SDS 1, a release in the primary coolant boundary does not include these top events the second largest top event importance measures correspond to the containment status.

5.10.2. Source term estimation results

The large number of source term combinations possible precludes the possibility of including each isotopic specific source term here. However, a summation of released activity for each source term group with a release frequency larger than the 1.00E-10 cut off value are provided in Table 5.33. Recalling that the R/B values differ for BOL and EOL, both values are provided for comparison. For additional reference, the bounding source term value, assuming a release from all FPVS source term components with no attenuation, is also provided in Table 5.33. The

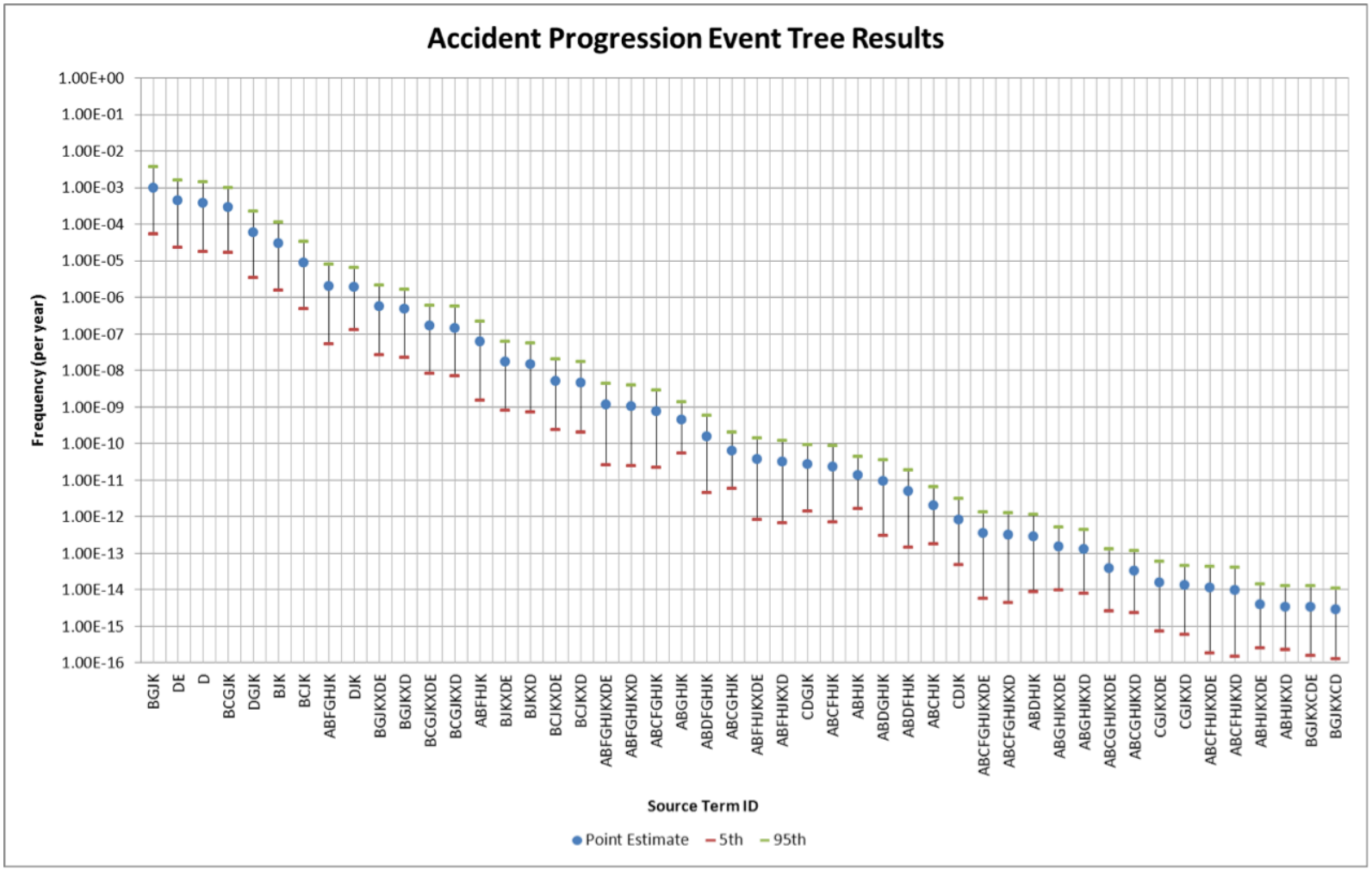

Figure 5.17.: Accident Progression Event Tree Results.

Table 5.32.: Accident Progression: Maximum Importance Measures.

Event Tree	FV	RRR	Uncertainty
APET-1	1.00E+00 *INIT-SDS-1*	1.90E+38 *INIT-SDS-1*	6.42E-06 *INIT-SDS-1*
APET-2	1.00E+00 *INIT-SDS-2*	1.90E+38 *INIT-SDS-2*	2.63E-03 *INIT-SDS-2*
APET-3	1.00E+00 *INIT-SDS-3*	1.90E+38 *INIT-SDS-3*	2.63E-03 *INIT-SDS-3*
APET-4	1.00E+00 *INIT-SDS-4*	1.90E+38 *INIT-SDS-4*	8.88E-09 *INIT-SDS-4*
APET-5	1.00E+00 *INIT-SDS-5*	1.90E+38 *INIT-SDS-5*	9.63E-09 *INIT-SDS-5*
APET-6-1	1.00E+00 *INIT-SDS-6*	1.90E+38 *INIT-SDS-6*	4.65E-06 *INIT-SDS-6*
APET-6-2	1.00E+00 *INIT-SDS-6*	1.90E+38 *INIT-SDS-6*	4.69E-06 *INIT-SDS-6*
APET-6-3	1.00E+00 *INIT-SDS-6*	1.90E+38 *INIT-SDS-6*	4.49E-06 *INIT-SDS-6*
APET-6-4	1.00E+00 *INIT-SDS-6*	1.90E+38 *INIT-SDS-6*	5.93E-06 *INIT-SDS-6*
APET-7-1	1.00E+00 *INIT-SDS-7*	1.90E+38 *INIT-SDS-7*	1.91E-11 *INIT-SDS-7*
APET-7-2	1.00E+00 *INIT-SDS-7*	1.90E+38 *INIT-SDS-7*	2.35E-11 *INIT-SDS-7*
APET-8-3	1.00E+00 *INIT-SDS-7*	1.90E+38 *INIT-SDS-7*	2.68E-11 *INIT-SDS-7*
APET-7-4	1.00E+00 *INIT-SDS-7*	1.90E+38 *INIT-SDS-7*	2.45E-11 *INIT-SDS-7*

estimated isotopic specific source term components for Case 1, before applying the appropriate AFs, are summarized in Appendix C.8. In addition, the isotopic specific source term after applying the appropriate AFs for the source term groups with a release frequency larger than the 1.00E-10 cut off value are provided in Appendix C.8.

In general, the source term estimates for the purge stream between elements is relatively small. The dominant source term components are clearly the HTA and LTA modules, as we would expect as their function is to collect and retain the fission products in the system. Additionally, the plated out fission products in the primary coolant boundary attribute a relatively large fraction of the activity present in the system, albeit an order of magnitude less than the HTA and LTA modules.

Out of the isotopes contributing to the source term of the vented fuel system, several warrant special attention:

- Cs-137 (30 yr half-life, 6% cumulative yield): May impact maintenance activities due to its long half-life and high yield.
- I-131 (8 day half-life, 4% cumulative yield): Important for safety reasons due to accumulation in the thyroid gland. Other iodine isotopes are less important due to their shorter half-lives.

Table 5.33.: Source Term Group Activities.

Source Term Group ID	Release Frequency (1/yr)	BOL Released (Ci)	EOL Released (Ci)	BOL % of Total	EOL % of Total
BGJK	9.60E-04	4.54E+03	4.54E+03	0.01%	0.06%
DE	4.44E-04	1.64E+07	3.10E+06	42.85%	39.56%
D	3.85E-04	4.13E+03	4.13E+03	0.01%	0.05%
BCGJK	2.90E-04	4.66E+03	4.56E+03	0.01%	0.06%
DGJK	6.09E-05	4.13E+03	4.13E+03	0.01%	0.05%
BJK	2.97E-05	6.90E+03	6.90E+03	0.02%	0.09%
BCJK	8.96E-06	1.23E+06	2.71E+05	3.20%	3.47%
ABFGHJK	2.03E-06	4.54E+03	4.54E+03	0.01%	0.06%
DJK	1.94E-06	4.13E+03	4.13E+03	0.01%	0.05%
BGJKXDE	5.61E-07	1.64E+07	3.10E+06	42.86%	39.62%
BGJKXD	4.86E-07	8.67E+03	8.67E+03	0.02%	0.11%
BCGJKXDE	1.69E-07	1.64E+07	3.10E+06	42.86%	39.62%
BCGJKXD	1.47E-07	8.79E+03	8.69E+03	0.02%	0.11%
ALL FPVS	N/A	3.83E+07	7.83E+06	100.00%	100.00%

- Xe-135 (9 hr half-life, 7% cumulative yield): Important due to its large neutron cross section, effectively acting as a poison in the core.

The effects of a release of these specific isotopes from the vented fuel system will be considered further in the Level 3 consequence analysis.

5.11. Level 3 PRA Results

The risk of a system is defined as the summation of the products of identified consequences and their frequencies. The STG frequency in combination with the estimated dose and cancer risks associated with each specific STG provide insight into the overall risk profile for a failure of the vented fuel system. The output of the atmospheric transport model developed using GENII is a series of dose estimates for the STGs with a frequency greater than 5.0E-7, representative of the lower bound of the Beyond Design Basis Event (BDBE) region of the frequency-consequence curve for NGNP [117]. To validate the GENII model, simplified calculations were performed.

5.11.1. Overall risk profile

The risk associated with the vented fuel system is enveloped by the STG frequencies and their resulting consequences in the form of dose and cancer risks at the Exclusion Area Boundary (EAB) for an instantaneous release and two hour exposure period using the BOL source term. For comparison, several different EAB values were analyzed. The TEDE dose, cancer incidence and fatal cancers risk are calculated by GENII using effective dose equivalents and a dose-to-risk conversion factor using ICRP-60 FGR 12 and 13 and EPA risk factors. The results are given in Appendix C.9 and summarized graphically in Figure 5.18 through Figure 5.20. Note the source term ID's are defined in Table 5.13.

Table 5.34.: STELLA Estimates for Activity.

Activity (Ci) in the Fission Product Vent System										
Location	Plateout in PCB		Piping from core to HTA		HTA Contents		Piping from HTA to LTA		LTA Contents	
Nuclide	BOL	EOL	BOL	EOL	BOL	EOL	BOL	EOL	BOL	EOL
Krypton - 85m	-	-	3.35E+01	3.35E+01	-	-	2.97E+01	2.97E+01	2.45E+05	4.72E+04
Krypton - 85	-	-	2.72E-03	2.72E-03	-	-	2.72E-03	2.72E-03	8.82E+04	7.77E+04
Krypton - 87	-	-	2.11E+02	2.11E+02	-	-	1.87E+02	1.87E+02	4.37E+05	7.45E+04
Krypton - 88	-	-	7.31E+01	7.31E+01	-	-	6.48E+01	6.48E+01	3.39E+05	6.21E+04
Rubidium - 88	-	-	6.10E+02	6.10E+02	3.32E+05	6.37E+04	6.42E-02	6.42E-02	3.39E+05	6.21E+04
Rubidium - 89	-	-	1.74E+03	1.74E+03	7.31E+05	1.14E+05	-	-	-	-
Strontium - 89	-	-	3.71E-04	3.71E-04	7.32E+05	1.14E+05	-	-	-	-
Tellurium - 127m	-	-	5.54E-03	5.54E-03	2.30E+04	9.95E+03	-	-	-	-
Tellurium - 127	-	-	8.15E-01	8.15E-01	3.65E+04	1.22E+04	-	-	-	-
Tellurium - 129m	-	-	4.38E-02	4.38E-02	5.77E+04	1.93E+04	-	-	-	-
Tellurium - 129	-	-	1.25E+01	1.25E+01	6.30E+04	1.64E+04	-	-	-	-
Tellurium - 131m	-	-	3.15E+00	3.15E+00	1.68E+05	3.20E+04	-	-	-	-
Tellurium - 131	-	-	9.44E+01	9.44E+01	1.10E+05	1.82E+04	-	-	-	-
Iodine - 131	2.13E+04	5.60E+03	5.59E-01	5.59E-01	4.32E+05	9.34E+04	-	-	-	-
Tellurium - 132	-	-	1.01E+01	1.01E+01	1.26E+06	2.69E+05	-	-	-	-
Iodine - 132	1.13E+05	1.85E+04	2.50E+02	2.50E+02	2.28E+06	4.36E+05	-	-	-	-
Tellurium - 133m	-	-	5.07E+02	5.07E+02	7.66E+05	1.16E+05	-	-	-	-
Tellurium - 133	-	-	1.53E+03	1.53E+03	6.13E+05	9.17E+04	-	-	-	-
Iodine - 133	1.40E+05	2.66E+04	3.41E+01	3.41E+01	2.65E+06	4.49E+05	-	-	-	-
Xenon - 133m	-	-	1.59E+01	1.59E+01	-	-	1.59E+01	1.59E+01	4.15E+06	7.77E+05
Xenon - 133	-	-	5.76E+00	5.76E+00	-	-	5.76E+00	5.76E+00	5.50E+06	1.13E+06
Tellurium - 134	-	-	1.18E+03	1.18E+03	1.35E+06	2.04E+05	-	-	-	-
Iodine - 134	1.69E+05	2.65E+04	9.71E+02	9.71E+02	2.87E+06	4.43E+05	-	-	-	-
Iodine - 135	1.50E+05	2.48E+04	1.30E+02	1.30E+02	1.35E+06	2.23E+05	-	-	-	-
Xenon - 135m	-	-	7.88E+02	7.88E+02	-	-	7.88E+02	7.88E+02	6.33E+05	1.00E+05
Xenon - 135	-	-	9.67E+01	9.67E+01	-	-	9.67E+01	9.67E+01	3.49E+06	5.92E+05
Cesium - 137	1.52E+05	1.44E+05	5.14E-02	5.14E-02	1.37E+06	1.29E+06	-	-	-	-
Xenon - 138	-	-	3.31E+03	3.31E+03	-	-	2.94E+03	2.94E+03	1.07E+06	1.58E+05
Cesium - 138	2.55E+05	2.39E+04	2.39E+03	2.39E+03	2.29E+06	2.15E+05	1.60E+00	1.60E+00	1.50E+06	2.21E+05

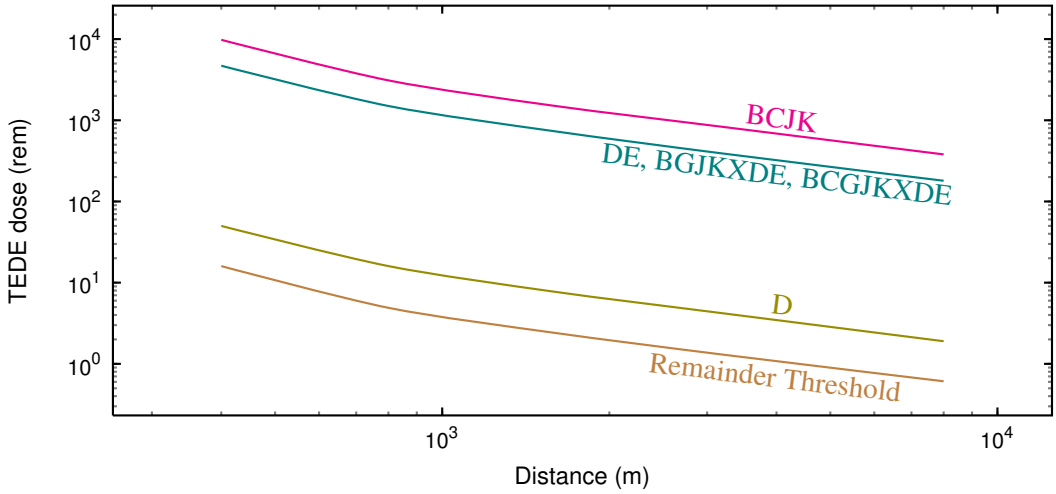

Figure 5.18.: TEDE Dose (rem) as a function distance for BOL.

The TEDE and cancer incidence and fatalities risk curves have the same shape and differ only in magnitude. This makes logical sense because the applied risk/dose coefficient differs for each risk scenario. The source term groups BCJK, DE, BGJKXDE, and BCGJKXDE contribute to the largest overall consequences, with the remaining groups having consequences below the remainder threshold. Although other source term groups may have high risk (Figures 5.18 and 5.19), when coupled with the frequency, only these four present a significant concern. As indicated by the source term IDs, each of these release categories represents a release directly from the auxiliary building with no attenuation (DE, BGJKXDE, and BCGJKXDE) or a bypass of the containment and filter (BCJK). It is clear that the dose and risk decrease with increasing EAB distance. This information may be of use in determining how to ensure compliance with the various radionuclide control requirements represented by the solid black line in Figure 5.20.

There are evidently three (D, DE, and BCJK), nearly five (BGJK and BGJKXDE), release sequences that result in unacceptable dose consequences with respect to their frequency, assuming an EAB of 400m. This is unacceptable for commercial operation and will need to be addressed. Noting that the source term and atmospheric transport model estimates are generally conservative and result in a larger dose, a more refined model of the system may remove this concern, especially those groups very near the regulatory limits. Often the specific containment type and choice to add filtered venting is a direct result of the consequence analyses. Therefore, although the vented fuel system as modeled in this analysis does not comply with the radionuclide control requirements in its entirety, this does not necessarily indicate that the use of vented fuel is not possible in a regulated environment. This merely suggests the need to better understand the system components, the dependency of the vented fuel system on core accident events, and to pursue the consequence analysis further. One potential solution to these unfavorable results would be to maintain the entirety of the vented fuel system within containment, thereby taking credit for radiation barriers in the event of a LTA module failure, thus reducing the D and DE source risk. It should be noted that in this analysis in which the noble gases are conservatively assumed to have no attenuation, the results would not change; however, in refined analysis and physical

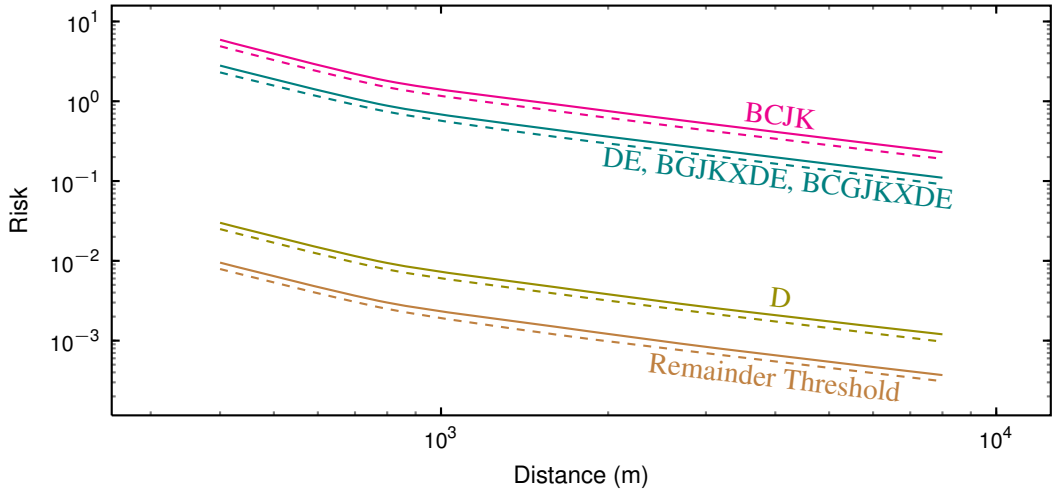

Figure 5.19.: Cancer Incidence (solid) and Cancer Fatalities (dashed) as a function distance for BOL.

reality, additional fission product barriers would undoubtedly decrease the magnitude of release to the environment. This however may have a negative impact on the cooling requirements of the LTA system, increasing the power input to the compressor necessary to maintain cryogenic refrigeration temperatures. A simple calculation of the power contained in the LTA module and the maximum efficiency of the refrigerator yields an estimated input power of roughly 380 kW. Nevertheless, solutions for reducing the estimated dose rate from the vented fuel system and their corresponding effects on the system performance should be considered further. In order to take credit for the attenuation of noble gases within the containment (nearly all of the contents of the LTA), more accurate estimates are needed to update Table 5.14. For this study, it was conservatively assumed that no attenuation factors could be applied to noble gases.

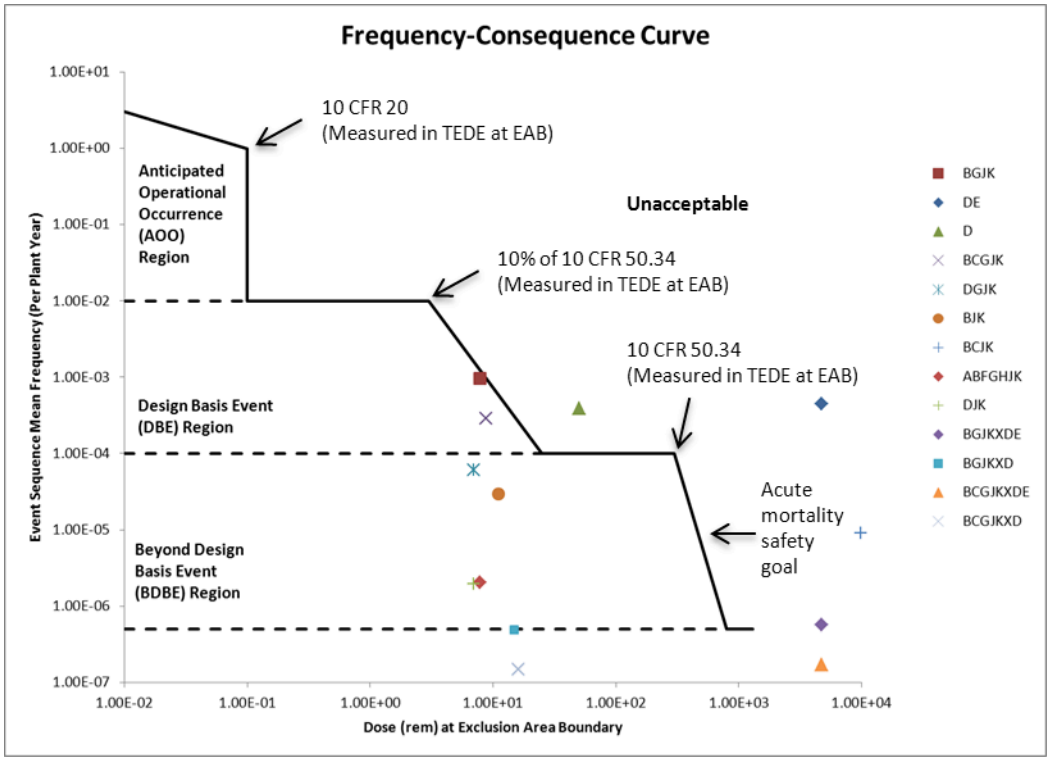

Figure 5.20.: Frequency-Consequence Curve assuming an EAB of 400m.

5.12. Conclusions

The goal of the present work was to increase the understanding of the possible and probable failure mechanisms and the resulting implications of utilizing a vented fuel system in a helium-cooled GFR which may arise during both normal and abnormal operating conditions. To meet this goal the following research objectives were defined:

1. Determine the possible and probable failure mechanisms of the vented fuel system during normal operation.
2. Determine the possible and probable failure mechanisms of the vented fuel system during abnormal operation.
3. Develop a model to characterize the frequency of vented fuel system failure.
4. Develop a model to characterize the frequency and quantity of release from a failure of the vented fuel system.
5. Develop a model to characterize the frequency and associated potential consequences to the environment and the public from a release from the failure of the vented fuel system.
6. Using the developed models, determine the safety and licensing implications of vented fuel which require further investigation.

To meet the first, second, and third objectives, fault tree and event tree Level 1 PRA analysis was applied to the vented fuel system using the software tool SAPHIRE. The SAPHIRE model contains a logical breakdown of the system failure modes during both normal and abnormal operating conditions, providing insight into the weaknesses of the system and the associated probability of failure for individual components and subsystems as well as the cumulative system failure frequency. The end states for the various failure sequences were categorized into system damage states and used as input into the accident progression analysis.

To meet the fourth objective a Level 2 PRA analysis was applied to the vented fuel system using SAPHIRE to understand how the accident progresses for each system damage state. The ability of the vented fuel system to respond to challenges imposed under abnormal conditions differs for each system damage state. The resulting frequencies of failure sequences resulting in similar radiological releases are binned together to form source term groups. To characterize the quantity of release for each source term group, the STELLA model was used to describe the time-dependent fission product transport in the vented fuel system. Attenuation factors were applied to the STELLA model results to account for the various fission product barriers and retention mechanisms in place to prevent or mitigate a release.

To meet the fifth objective a Level 3 PRA analysis was applied to the vented fuel system using the atmospheric transport tool GENII. The acute transport model is used to determine the resulting dose and risk consequences associated with each source term group with a frequency that merits further analysis.

Finally, to meet the sixth objective information provided by the Level 1, 2, and 3 PRA analyses was collectively evaluated to determine the safety implications of the vented fuel system and which aspects of the analysis require continue research.

The present work found several vulnerabilities that require further assessment to ensure the safety of the vented fuel system. This is typical for new systems undergoing PRA for the first time.

First, the motor operated isolation control valve, identified as V-15, is a single point failure having the sole ability to maintain the pressure differential required to ensure the purge stream does not counter diffuse into the primary coolant. In addition, each of the three 100% FPVS trains may be made unavailable by an inadvertent closure of V-15. Although the consequences of such an event were not further analyzed in the present work, a failure of the valve to function is shown in the Level 1 PRA to be an important component, contributing largely to the failure of the vented fuel system to function under normal conditions. The current system model is unable to analyze the effects of a failure of V-15 to maintain the required pressure differential resulting in counter diffusion of fission products into the primary system however this modeling deficiency needs to be addressed in future safety analyses.

Of the individual modules comprising the vented fuel system, the in-service HTA module was found to have the largest failure probability under accident conditions. Uncertainty analysis shows the reliability of the motor operated valves in the system to have the greatest overall impact on the performance of the system, therefore a better understanding of failure rate data for these critical components needs to be considered.

System failures initiated by transient events dominate the overall system failure frequency as a direct consequence of the larger initiating event frequency. The most probable system damage states are a release from the vented fuel system within the containment building and within the auxiliary building. It is assumed for the present analysis that the containment building has a leak rate of 0.1% per day and is equipped with a filter allowing filtered venting of the containment whereas no retention capabilities of the auxiliary building are credited. As a result of the reduced fission product boundaries present in the event of a release within the auxiliary building, consequences of these events prove to be more severe.

The most probable STG is a release of the contents of the fission product purge stream prior to the HTA module with containment intact, releasing less than 0.01% of the activity present in the vented fuel system at an estimated frequency of 9.60E-04 instances per year. The conservatively estimated dose for 2 hours at the 400m EAB was found to be within the acceptable limits for a DBE, however the result of this analysis is very close to the edge of being considered unacceptable. Three source term groups were found to have exceedingly high dose consequences with respect to their estimated frequencies assuming a 400m EAB. Two of these high-consequence STG releases fall within the DBE frequency category. Both of these event sequences appear to have relatively large consequences as a result of the release stemming from the auxiliary building where no attenuation from the building is credited. These include a release of the purge stream entering the LTA and a release of the purge stream entering the LTA combined with a fraction of the activity present in the LTA bed without attenuation, source term IDs of D and DE respectively. The third inordinately high release event sequence falls under the BDBE category with a release of the purge stream contents and a fraction of the HTA bed activity coincident with containment failure, source term ID BCJK. Although unlikely, the resultant dose is well outside the radionuclide control limits.

Based on the results of the present analysis, additional design and analysis of the vented fuel system is required. It should be noted that the present work operates under several highly

conservative assumptions. Consequently, the vented fuel system, as modeled, may be safely operated without design changes pending the refinement of the models used to determine source term estimates and atmospheric transport. Specifically, the conservative modeling assumptions that have the potential to greatly reduce the estimated consequences if refined include the fraction of the activity within the adsorber beds that is released under accident conditions (100% for noble gases and 25% for halogens and particulates, Section 5.8), the specific attenuation factors applied to the various fission product boundaries, and the atmospheric conditions selected for the atmospheric transport model. In addition, design changes such as an increase in the EAB or placement of the entire vented fuel system within the containment building may further reduce the consequences of a release.

6. Conclusions

6.1. Summary

The present work progressed the understanding of the feasibility and safety issues related to gas reactors that incorporate vented fuel. The work was separated into three different work-scopes:

1. Quantitively determine fission gas release from uranium carbide in a representative helium cooled fast reactor.

2. Model the fission gas behavior, transport, and collection in a Fission Product Vent System.

3. Perform a safety analysis of the helium purification system.

Each task relied on results from the previous task, culminating in a limited scope PRA of the Fission Product Vent System. Within each task, many key parameters lack the fidelity needed for comprehensive or accurate analysis. In the process of completing each task, the data or methods that were lacking were identified and compiled in a Gap Analysis at the end of the report.

Although a vented fuel design directly changes the fuel pin design, the safety concerns primarily focuses on the ability of a Fission Product Vent System (FPVS) to capture and contain the radioactive fission products. As such, the bulk of the safety analysis for this project focused on the FPVS design and performance. The vented fission gases must be collected in a system that not only cools the vented purge stream to temperatures that will allow condensation of the gases, but also must provide enough space for the shear volume of vented gases.

The volume of fission products that escape the fuel defines the mass, activity, and heat loading on the FPVS. Unfortunately, this is also the most difficult problem to tackle. The hostile environment of a reactor core reduces nearly all experimental data to post irradiation measurements. This is further compounded by the lack of available uranium carbide data, the representative fuel form used for the current work.

A simple Release rate over Birth rate, or R/B model, based on the previously operating commercial Peach Bottom gas reactor, was initially utilized to estimate the release of fission gas. This model was used to develop the initial systems modeling discussed in section 4. Responding to recommendations made by General Atomics, a more refined R/B model that accounts for temperature was implemented to estimate release rates of volatile fission products from the fuel. The newer model comes from a 1993 document [38] that compiles all of the MHTGR calculation models. The calculation includes an exponential temperature correction factor, necessitating application of the MHTGR model to a temperature distribution rather than an average. Estimated Beginning of Life (BOL) and End of Life (EOL) fuel temperature distributions provided by GA allowed calculation of R/B at two contrasting operating conditions. Initially, it was believed that the complexities present in the new model would result in lower fission gas release than

the single Peach Bottom curve. While the narrow EOL temperature distribution does result in less release of gaseous fission products, the release actually increases for the BOL temperature distribution: a small percentage of hot fuel rods at BOL cause an increase in fission gas release, especially of isotopes with short half-lives. In general, the Peach Bottom curve lies between the BOL and EOL. The uncertainties involved affect both models equally (i.e. similar but different fuel types, thermal vs. fast reactor design, close packed vs. graphite dispersed particles), thus neither model is fully adequate. Regardless, the temperature dependence of the MHTGR allows for potentially more interesting calculations.

Along with the release rates from the fuel, the list of volatile elements that escape from the fuel has a high impact on the fission gas loading. A cut-off boiling temperature of 1500° C was initially implemented that based the volatility of fission products on the peak fuel temperatures. However, a cut-off temperature based on coolant temperatures has been deemed more appropriate. Even still, it is unclear what elements actually reach the Fission Product Vent System.

A more robust mechanistic model was developed to try and model the fission gas release phenomena. This involved the creation of BUCK, a fuel performance code that builds on Idaho National Lab's BISON code. While this code handled the macro-scale fuel behavior such as swelling, creep, and thermal conduction, it lacked the microscopic data necessary to track fission gas bubble behavior. Regardless, macro-scale simulations were conducted that modeled representative uranium carbide fuel pins. The simulations incorporated the important phenomena in a fully coupled non-linear solve. Behavior such as porosity, thermomechanical properties, and creep were captured. Simple models to account for volume swelling and fission gas release were also incorporated, but failed to accurately capture the complex behavior resulting from the accumulation of fission gas bubbles.

In order to capture some of the microscopic behavior of fission gas release, a rate equation type model that tracks the bubble size distribution is necessary to determine the behavior of the small and large bubbles present in uranium carbide. As a first step, the Binary Collision Approximation code 3DOT was created to model the re-solution event in uranium carbide, an important loss term necessary for bubble size distribution simulations. The re-solution rate as a function of bubble radius was determined for uranium carbide fuels to a fidelity not previously modeled. Due to the relatively high energy transfer material properties in uranium carbide, fission gas re-solution can be modeled using the homogeneous, atom-by-atom loss model. We found a re-solution parameter that was an order of magnitude lower than previous studies due to the inclusion of electronic ion energy losses in this study. A decrease in the re-solution parameter as a function of radius occurred for small bubble radii, with a nearly constant re-solution parameter for radii above 50 nm. The BCA approximation allowed the computationally inexpensive analysis of many different types of bubbles, and it was shown that the fundamental BCA assumption is appropriate for use in the simulations presented here. Through comparative studies on the re-solution parameter for various values of implantation energy and atomic density in the bubble, we found that while the re-solution parameter did change, the overall shape did not. The re-solution parameter calculated here can be used in rate-equation type simulations to model fission gas bubble behavior, and ultimately fission gas release. The work with 3DOT has been accepted for publication in the Journal of Nuclear Materials [1].

In order to model the Helium Purification System (HPS), a STELLA model was created that was able to track gas concentrations throughout a representative Fission Product Vent System

(FPVS). This required a massive network of individual isobaric decay chain models to capture the expansive list of volatile isotopes. This work was initially completed by Wesley Deason, culminating in his Master's Defense in 2013 [2]. The system model was used to test seven case scenarios, ranging from a completely open system with no FPVS, to an attempt at a system with a slightly optimized FPVS. These results revealed that the following design constraints and considerations are necessary for implementation of vented fuel within a helium-cooled GFR:

1. The quantity of fission products accumulated in the FPVS is likely very large. The system must be designed to accommodate the fission product load or be regenerated at regular intervals to prevent breakthrough into the primary coolant from occurring in the last fission product trap.

2. The activity and power generation rate of fission products collected in the FPVS is also very large. Cooling the purge stream to temperatures necessary for the adsorption of noble gas fission products may present a large power requirement for the helium-cooled GFR plant. Additionally, extensive shielding systems will be required to allow operations and maintenance to occur in the vicinity of the FPVS.

3. Safety systems will be necessary to prevent overheat and release of the contents of a FPVS in an accident scenario. Use of defense-in-depth strategies to reduce the impact of a possible release of gaseous fission products is recommended.

4. Determination of the purge stream leakage rate is of crucial importance for predicting the level of radioactivity in the primary coolant.

5. Determination of the fuel release rate is of crucial importance for predicting the level of radioactivity in all areas of the plant and for the design of a safe and economical FPVS.

The original STELLA model was then extended to a more complex fission release model based on MHTGR data (see Section 3.3). In general, the the BOL MHTGR model calculates powers 30-50% higher than the Peach Bottom model, while the EOL model predicts about 1/4 of the Peach Bottom values. The accumulated masses are roughly the same for each model. The updated tracked element list was updated to reflect a more accurate purge stream temperature, resulting in a roughly 50% reduction in mass, power, and activity loading in the hot fission product trap.

The STELLA results utilized in the safety analysis were developed using the MHTGR model with a representative BOL temperature distribution, with a 1000° C cut-off boiling temperature. The power loading is relatively high, with a steady state output of 220 kW in the hot fission product trap, and 97 kW in the cold fission product trap.

The mass accumulations calculated in the STELLA model, the failure mechanisms and their consequences were analyzed using modern PRA tools to determine the ultimate risk involved with the current design. A Level 1 PRA analysis was completed to determine the failure mechanisms associated with the FPVS. A Level 2 PRA analysis was applied to the vented fuel system using SAPHIRE to understand how the accident progresses for each system damage state. To characterize the quantity of release for each damage state, the STELLA model was used to describe the time-dependent fission product transport in the vented fuel system. Attenuation factors

were applied to the STELLA model results to account for the various fission product barriers and retention mechanisms in place to prevent or mitigate a release. Lastly, a Level 3 PRA analysis was applied to the vented fuel system using the atmospheric transport tool GENII. The acute transport model is used to determine the resulting dose and risk consequences associated with each source term group with a frequency that merits further analysis.

The present work found several vulnerabilities that require further assessment to ensure the safety of the vented fuel system. This is typical for new systems undergoing PRA for the first time. First, the motor operated isolation control valve, identified as V-15, is a single point failure having the sole ability to maintain the pressure differential required to ensure the purge stream does not counter diffuse into the primary coolant. In addition, each of the three 100% FPVS trains may be made unavailable by an inadvertent closure of V-15. Although the consequences of such an event were not further analyzed in the present work, a failure of the valve to function is shown in the Level 1 PRA to be an important component, contributing largely to the failure of the vented fuel system to function under normal conditions. The current system model is unable to analyze the effects of a failure of V-15 to maintain the required pressure differential resulting in counter diffusion of fission products into the primary system however this modeling deficiency needs to be addressed in future safety analyses.

System failures initiated by transient events dominate the overall system failure frequency as a direct consequence of the larger initiating event frequency. The most probable system damage states are a release from the vented fuel system within the containment building and within the auxiliary building. It is assumed for the present analysis that the containment building has a leak rate of 0.1% per day and is equipped with a filter allowing filtered venting of the containment whereas no retention capabilities of the auxiliary building are credited. As a result of the reduced fission product boundaries present in the event of a release within the auxiliary building, consequences of these events prove to be more severe.

Based on the results of the present analysis, additional design and analysis of the vented fuel system is required. It should be noted that the present work operates under several highly conservative assumptions. Consequently, the vented fuel system, as modeled, may be safely operated without design changes pending the refinement of the models used to determine source term estimates and atmospheric transport. Specifically, the conservative modeling assumptions that have the potential to greatly reduce the estimated consequences if refined include the fraction of the activity within the adsorber beds that is released under accident conditions, the specific attenuation factors applied to the various fission product boundaries, and the atmospheric conditions selected for the atmospheric transport model. In addition, design changes such as an increase in the Exclusion Area Boundary or placement of the entire vented fuel system within the containment building may further reduce the consequences of a release.

6.2. Gap Analysis

As with many advanced reactor concepts, there is a large gap between the analysis required for licensing, and the data, techniques, and methods to allow accurate analysis to be completed. While completing the work for the current project, holes in the current state of the art were compiled to provide to provide a list of workscopes to further the knowledge-base on the array

of subjects touched on during this project. This section compiles some of these gaps along with a short discussion.

6.2.1. Fuel modeling

No topic within this project is hampered as much as the ability to accurately estimate fission gas behavior. The phenomena that drives the movement and growth of gas atoms and bubbles determines not only the fission gas release, but the swelling of the fuel as bubbles begin to populate the fuel grains. There are two approaches to modeling the fission gas release from fuel pellets. The first is through experimentally determining a R/B, or Release Rate over Birth Rate line. This empirical method condenses all of the complexity involved with fission gas release into a single relationship that produces a release rate as a function of isotope half-life, temperature, and burnup. The second approach is through mechanistic modeling of the behavior of the gas atoms themselves. This requires an even larger set of experimental data in order to validate the vast applicable time and space scales.

For the present project, a R/B model based on the MHTGR irradiation data [38] was utilized to produce the mass loadings for the STELLA model. Although this model was deemed the most appropriate, it had many limitations:

- the R/B curve was formulated from release rates of short-lived isotopes (half-life <5.3 days), although Martin claims that it is also applicable to long lived isotopes [38]. While this seems true, the curve would most likely asymptotically approach a release of 1.0, similar to the behavior of the Peach Bottom curve (Figure 3.10). Since the MHTGR R/B curve linearly approaches 1.0, it will tend to overestimate the release of long-lived isotopes.

- The R/B curve only explicitly models Xe, Kr, I, Te, Br, and Se. No other accounts of possibly volatile elements is included.

- The formulated R/B curves are for UC_2, not for the UC fuel present in the EM^2 core. There is some evidence that UC_2 has diffusion rates an order of magnitude slower than UC [6, p. 493].

- The MHTGR model was based on release rates from failed coated particles in thermal reactor designs. There is some evidence that the release mechanism is primarily from recoil events [40]. In MHTGR fuel designs, the fuel particles are embedded in a graphite matrix in which recoiling atoms can be trapped before entering a neighboring particle. The close-packed graphite-free kernels required for fast reactor fuel designs will result in a reduction of recoil release as knocked out atoms will have a high chance of reentering an adjoining fuel particle.

Despite the issues with the currently implemented R/B curve, fission gas release estimations based on R/B curves in general would be the easiest to obtain and utilize, requiring only irradiation data to obtain release rates. While expensive, fueled irradiation capsules would provide the most accurate data. The major drawback of such models is that each test is integral, meaning the models may lose validity for designs or conditions deviate from the reactor type, fuel design,

and irradiation conditions used to initially create the model. A broad experimental matrix may allow for interpolation between variables, improving the robustness of the model. Regardless, R/B curves could provide release rates with high confidence if licensability is necessary for only a small range of fuel types or irradiation conditions.

In order to move away from fission gas release estimates hindered by the available data, a mechanistic model that captures the relevant physics of fission gas behavior is necessary. Such a model requires several layers of complexity [159]:

- Macroscopic: Full pin modeling in a fuel performance code. This has been rudimentary achieved before done in the current project for BISON, and previously for FRAPCON [49]. This level of modeling handles the heat transfer within the pin, cladding, and across the cladding gap. Creep models are also necessary to correctly estimate the internal stresses introduced in the fuel and cladding due to thermal gradients and swelling. Many of the models that are necessary for this level of modeling exist to an appropriate level of complexity, aside from swelling and fission gas release which relies on lower-scale models.

- Microstructure: This level of modeling deals with fuel structure and behavior on the granular level and aims to model phenomena such as bubble and grain growth. This level of modeling captures the most important physical phenomena to estimate the swelling and fission gas release in uranium carbide fuel. Unfortunately, this has also been the most complex area to produce a model due difficulty in obtaining experimental data at this scale such as atom diffusivity and atomic behavior. These limitations may eventually be overcome by using microscopic models as a enhancement to empirical data. Models for oxide fuels have seen success at this level by relying on the broad assumption that intra-granular bubbles are mono-sized and temperature independent. This assumption does not transfer over to carbide fuels due to the 1-400 nm sized bubbles that occur in UC.

- Microscopic: This level of modeling has seen recent success, but is still heavily hampered by the physical models. Simulations at this data deal with the quantum mechanics of a given problem, solving terms such as diffusivity, surface energy, and defect energy through so called "first-principles" methods. Although difficult to produce, data at this level may circumvent a need for separate effects tests needed to support microstructure level modeling.

Within this project, a Macroscopic model was created to model the bulk phenomena in uranium carbide fuels, however an appropriate microstructural code that can model the bubble population distribution is really necessary to capture the swelling and fission gas release. An example model can be composed of many coupled rate-equations of the form:

$$\frac{\partial c_1}{\partial t} = \beta + \sum_{k=2}^{I} f^R_{k\to 1} R(c_k) - \sum_{i=2}^{I} K(c_i) \tag{6.1a}$$

$$\frac{\partial c_i}{\partial t} = -R_{c_i} - K(c_i) + \sum_{k=i+1}^{I} f^R_{k\to i} R(c_k) + \sum_{k=1}^{i} f^K_{k\to i} K(c_k) \tag{6.1b}$$

where c_1 is the concentration of single gas atoms within the matrix, c_i is the concentration of bubbles with i gas atoms, I is the largest bubble size, and β is the production term of gaseous fission products from fission. The remaining terms deal with the resolution rate R or absorption rate K. For single gas atoms, the re-solution rate R acts as a source term that produces single gas atoms from bubbles with a probability described by f^R. For bubbles, the re-solution rate acts as a loss term as atoms are knocked out, and as a source term as larger bubbles enter the c_i concentration as their atoms are knocked out. For single gas atom, the absorption rate K results in a decrease in the single gas atom concentration, while for bubbles, absorption acts as a loss term as bubbles absorb single gas atoms or other bubbles to form larger bubbles, as well as a source term as smaller bubbles absorb atoms until reaching i gas atoms.

Within this project, the re-solution rate was calculated as a function of bubble radius. Due to the relatively high energy transfer material properties in uranium carbide, fission gas re-solution can be modeled using the homogeneous, atom-by-atom loss model. We found a re-solution parameter that was an order of magnitude lower than previous studies due to the inclusion of electronic ion energy losses in this study. A decrease in the re-solution parameter as a function of radius occurred for low radii, with a nearly constant re-solution parameter for radii above 50 nm.

The absorption term K is another important term that contains many uncertainties. Although theoretical diffusion studies provides easy analytical solutions to absorption in bubbles, the diffusivity term that describes the mobility of fission gas atoms remains to be one of the most elusive parameters in fuel modeling. A comparison of the available data up to 1986 showed a scatter over several orders of magnitude between various experiments trying to determine the fission gas atom diffusivity [6].

A second complication to the simple model presented above is the question of bubble nucleation. Although it is clear that heterogenous nucleation dominates in carbide fuel [26], it is unclear how the large bubble population forms. Micrograph studies have shown that the smaller P_1 bubbles are nearly always associated with local defect clusters in the fuel lattice, while P_2 bubbles are typically found attached to larger precipitates in the fuel [32], but it is uncertain if the two bubble populations interact with each other or grow out of the same original population of small bubbles.

The steps necessary to accurately model fission gas release in carbide fuel can be summarized as follows:

1. In order to estimate fission gas release only from a standardized fuel form, a R/B model should be adequate. Many irradiations are necessary across a carefully chosen number of parameters to ensure that the variations in design can be captured by an R/B model. Although potentially costly, the R/B model presents a brute-force method that will provide adequate results within an operating envelope. Empirical models for fuel swelling due to gas bubbles are also necessary in order to correctly predict the behavior of the fuel-cladding contact.

2. In order to estimate fission gas beyond normal designs or normal operation, a mechanistic model of the fission gas release phenomena is necessary. This method requires a much more thorough understanding of the physics at hand, but will allow modeling of the fuel during off-normal events. Such a model could predict both gas release and swelling due

to gas bubbles. While many macro-scale models exist, microstructural models that adequately capture bubble behavior need to be created. A broad supporting experimental database is also necessary.

3. An intermediate solution combining an R/B-type model with a fuel performance model may capture the advantages of both. Although somewhat limited by the experimental data used to produce the R/B model, gas release calculations may benefit from higher fidelity results from fuel performance models such as temperature and stress distributions.

6.2.2. Fission Product Vent System

Several limiting factors became clear during the current study, and may motivate future work in this subject. The first is in the accurate determination of fission product behavior in the reactor and Fission Product Vent System. This requires comprehensive knowledge of the operating parameters of the reactor itself, such as temperature distributions, pressures, and core materials, as well as knowledge of how fission products behave at those conditions.

One of the biggest gaps is the accurate estimation of the fission product trap's ability to trap and hold onto fission gases. This is important not only at their standard operating temperature, but as a function of temperature and time for determination of gas release during accident conditions.

In addition to the delay beds, plateout of certain elements will occur on all of the Fission Product Vent System piping. The concentration of the plateout and its behavior to temperature is important to estimate the activity levels of these pipes so as to adequately shield them during repairs.

An important design parameter that is necessary to calculate in order to determine the primary coolant activity is the purge stream leakage fraction. Though the purge stream leakage fraction is very specific to the plant design that it refers to, research into techniques which would decrease the probability of release of fission products into the primary coolant would be valuable. One purge stream design which may be of worthy pursuit is the use of a helium stream which operates completely separate from the primary coolant, though still at a lower pressure, allowing a possibly large reduction in the amount of leaked fission products [14].

Another issue of concern that could be addressed is the development of a more complex and more precise system model of a helium-cooled GFRs plant utilizing vented fuel. With a more complex and precise model, many more delay bed arrangements in the Fission Product Vent System could be tested and the plateout distribution in the primary coolant and behavior of short-lived fission products in the system could be better understood.

The last issue of concern which requires future work is the impact of pressure transients, such as breaks in the pressure boundary and the breathing phenomena [14], on the behavior of the vented fuel system in a helium-cooled GFR. Some work has been done on the analysis of pressure transients on a direct cycle supercritical CO_2 plant utilizing vented fuel, but little to none has been done for a helium-cooled plant. The presence of pressure transients in the vented fuel system could have a significant impact on the transport of volatile fission products from the core and throughout the plant. If possible, these pressure transients should be evaluated in an in-pile fuel test that is also capable a measuring fission product plateout and adsorption to

properly verify the analytical models of the system behavior.

The steps necessary to accurately model a Fission Product Vent System can be summarized as follows:

1. Accurate determination of fission product behavior leaving the fuel: This requires better estimation of core parameters such as temperature and pressure, as well as better knowledge of how elements behave in those conditions.

2. More suitable models to estimate fission product traps contain and ultimately release fission products: This is necessary so as to limit the amount of break-through in an inadequately sized or cooled trap.

3. Better estimation of fission product plateout in the Fission Product Vent System piping, including liftoff during abnormal operating conditions.

4. Transient modeling: Better understanding of transient conditions is necessary in order to prevent inadvertent release during accident conditions.

6.2.3. PRA

The breadth of analysis conducted in the present project revealed several avenues by which the safety implications of using vented fuel might be better understood. The first is in establishing a more detailed software tool capable of analyzing the transient effects of an accident scenario which challenge the vented fuel system. STELLA has inherent limitations requiring conservative assumptions regarding source term attenuation factors and the retention capabilities of the adsorber modules under various accident conditions. While some conservatism is good practice, failure to address such deficiencies in the analysis may lead to a misguided understanding of the risks associated with the application of a vented fuel system for advanced gas reactor concepts. A more refined and precise model including pressure and temperature feedback from accident progression could assist in a more accurate, and likely less conservative, assessment of the safety significance of a release from the vented fuel system. This includes an improved method for determining fuel release fractions.

Another issue of concern that could be addressed is the general lack of gas reactor component reliability data, which increases the uncertainty associated with the reliability of several important components whose failure directly impacts the potential source term and associated consequences. The Level 1 results indicate that the failure of the motor operated valves in the system hold the highest importance. As the design matures, an effort to refine the component reliability database, specifically for components with high importance factors such as valves, should be pursued to ensure adequate reliability of the system. The relevance and value of the PRA analysis conducted in the present project ultimately depends on the quality of component reliability data and initiating event frequency data input into the analysis.

Additionally, a concern that could be addressed at a later date is the integration of more detailed system modeling as the design matures. In several instances assumptions were made based on legacy General Atomics designs and current gas reactors of comparable functionality. To truly assess the reliability of the system, consideration of systems in close association with

the FPVS must be considered for a more physical representation of the interdependence of the vented fuel system with the remainder of the plant. Due to the limited scope of the present project, the assumption of perfect operation of outside systems precluded the need to analyze the remainder of the plant systems. This however is unphysical and should be addressed further. In addition, the consequences of a failure of V-15 to maintain the pressure differential required to prevent counter diffusion of fission products into the primary coolant was not explored further due to limitations of the current system model. This failure has potential safety implications and should be addressed in future analyses.

Finally, to better understand the cost-benefit ratio of utilizing a vented fuel system, a full plant wide PRA should be performed to assess the risks related to a release of fission products for a base design utilizing vented fuel and a design which elects to increase the plenum volume to allow for storage of fission gas accumulation over the extended operating life. Although there is risk introduced by removing the fission products from the core, there is also a benefit of isolating these fission products from the effects of a challenging event in the reactor core. The risks identified in the present project may be of less concern than the risks associated with choosing to preserve the fission products in the core for the full projected thirty year core life.

The steps necessary to accurately produce a PRA analysis of the Fission Product Vent System can be summarized as follows:

1. Appropriate models for fission product loading: In general, conservative choices assumed while modeling the release of fission products and the ability of the Fission Product Vent System to contain these products decreases the overall analyzed safety of such a system. By improving the fuel and fission product trap models, it can be expected that the analyzed consequence of a release will decrease, reducing the risk and enhancing the licensability of vented fuel systems.

2. Component reliability data: the Level 1 PRA showed failure of motor operated valves to be a major component to the reliability of a Fission Product Vent System. More accurate data predicting the reliability of such valves is needed to capture the chance of failure. One particular model that needs to be updated is the Human Reliability data.

3. Incorporation of related systems to the Fission Product Vent System: Failure mechanisms of the core, containment structure, and auxiliary building may hamper the ability of the Fission Product Vent System to contain the fission products. Incorporation of these other systems into a broader PRA analysis will help clarify the interaction between them.

6.3. Recommended Experiments

The primary uncertainty in the current project is due to the limited predictability of fission gas release from uranium carbide fuel. The combination of highly coupled complex phenomena, as seen in Figure 6.1, and the prohibitive cost of irradiation tests allows for only a limited understanding of fission gas release [26].

Two potential paths to develop an adequate understanding of uranium carbide fuel fission gas release is through either an array of integral tests or through targeted separate effects tests with

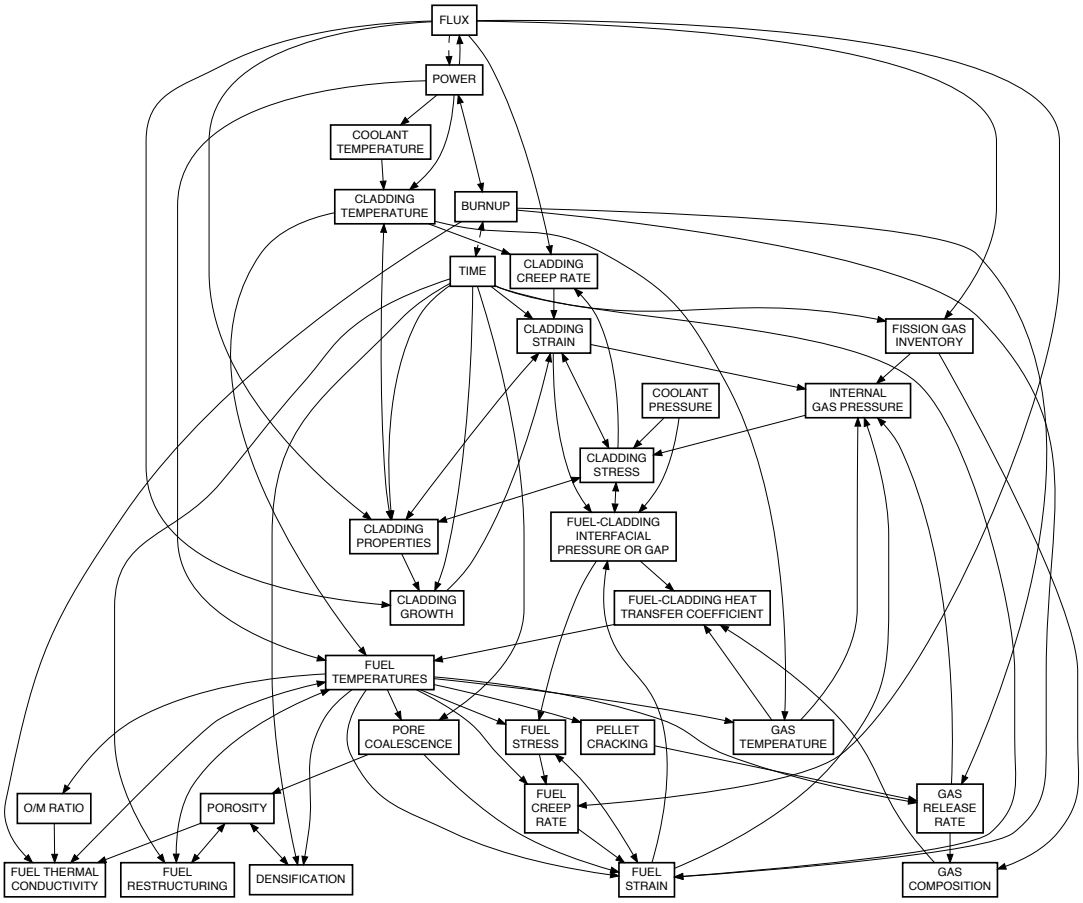

Figure 6.1.: Schematic showing interconnectivity of physical phenomena that must be accounted for in order to sufficiently model nuclear fuel [160].

supporting simulation models, as demonstrated in Figure 6.2. Both methods produce essentially the same thing: fuel modeling software that can be used to estimate the fission gas release. In addition, it is clear that fission gas release is dependent on temperature and mechanical stress. In order to estimate the temperature and stress profile in the fuel pin, adequate models of basic thermo-mechanical behavior such as thermal conductivity, thermal creep, and cladding interaction, are needed for both integral and separate effects tests.

It should be emphasized that much of the previous irradiation data holds limited applicability due to the inadequate characterization of the fuel before irradiation. Either method described here will clearly benefit from the improved methods and instruments that come with any modern analysis.

One of the simplest experimental plans to determine fission gas release is through a brute force completion of a vast array of fuel irradiations. This method is possible if the operating conditions are known and stay within a predefined window. In addition, an adequate understanding of the conditions present during accident scenarios is also necessary to try and predict the behavior of the fuel during off-normal events. Luckily, such a test matrix only requires limited Post Irradi-

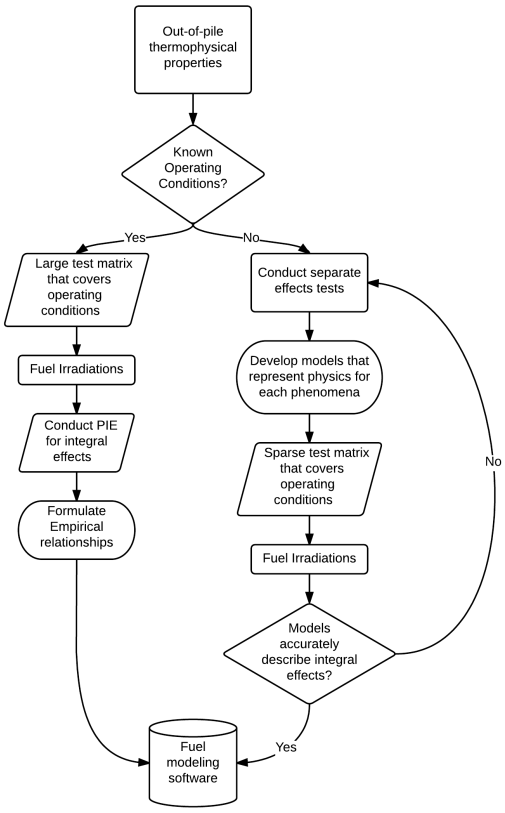

Figure 6.2.: Flowchart of two possible paths towards fuel modeling.

ation Examination (PIE). In the case of fission gas release, the amount of fission gas released to an irradiation capsule can be measured by piercing the cladding wall in an enclosed environment and analyzing the escaped gas. Cladding interaction can be determined through visual inspection of pin cross-sections. Unfortunately, the limitations of one time measurements requires an extensive set of pins to be irradiated, thus the test matrix must include adequate samples across the temperatures, burnups, and pressures that the fuel is expected to encounter.

One possible advanced irradiation experiment that could capture the relevant release data as a function of time would be an online monitoring system similar to that used for qualification of Advanced Gas Reactor (AGR) fuel [161]. In the case of the AGR-1 experiment [162], TRISO fuel compacts were placed in the Advanced Test Reactor (ATR) at Idaho National Lab (INL). Since the ATR utilizes pressurized water as both the coolant and moderator, the fuel was placed in a capsule with a gas gap so as to generate the high temperature environments the AGR fuel was expected to reach. The pin fill gas was maintained in a loop to detectors out of the pressure vessel. A combination of radiation detectors and mass spectroscopy instruments allowed for direct determination of the quantity and composition of released fission gas. Constant manipulation of the return fill gas composition ensured that the fuel was maintained at the appropriate temperature determined by online monitoring of implanted thermocouples.

Due to the differences between the AGR and EM^2 fuel, several parameters must be modified in order to capture the correct behavior of future EM^2 fuel. First, the thermal spectrum of the ATR may have to be shielded using cadmium lined irradiation capsules to more closely represent the fast spectrum required by the breeding behavior of the EM^2. Second, the amount of fission gas released from the fuel pellets will be significantly higher than those that were collected in the AGR-1 experiment due to the uncoated particle release vs. TRISO particle release. As such, smaller fewer fuel compacts can be tested at the same time, or accommodations for the larger volume of fission gas must be made.

Whichever method is used to determine the fission gas release, integral tests such as those described above are confined to the narrow window enclosed by their tested irradiation conditions. This limitation is especially limiting when applied to the expected in-core residence time of 30 years in the EM^2. Although similar burnups can be achieved if the fuel is maintained in a high flux environment, there are few reactors that can provide the space and fluence necessary to simulate extremely high burnup fuel.

A second method to determining fission gas release is through a spectrum of separate effects tests with corresponding models. The physical phenomena necessary to test includes the diffusivity of fission gas, determination of the re-solution rate, movement of fission gas bubbles, and swelling due to fission gas bubbles. Unlike the previous path discussed above, each experiment sub-set may not provide enough information to produce valid models, thus iterations may be required to ensure the phenomena is modeled appropriately. The primary hindrance of such a test program is the large amount of microscopic PIE that is necessary. However, recent microscopic sample preparation and analysis may allow the radioactivity of each sample to be small enough to be more easily handled.

From this project, it became clear that the fission gas bubble behavior drives the total fission gas release and swelling. The smaller bubbles accumulate in the dislocation networks, while the larger bubbles tend to be associated with solid precipitates. The precipitates are most likely a grouping of solid fission products, although the exact concentration has not been completely determined. The formation of these larger precipitates, as well as how and why the larger bubbles attach themselves to their surfaces would help support the development of a fission gas release simulation.

Beyond experiments that deal with the fuel, the recommended experiments deal with the behavior of fission gas within the cleanup system. One large uncertainty is how the fission gas will plateout on the piping systems of the Fission Product Vent System. This is important in order to estimate what fraction of released gases will actually reach the traps, to estimate the activity of the pipes in order to protect the workers, and to be protect against re-volatilization of the gases during accident scenarios. Since the plateout of the gases on the piping is primarily based on the chemical behavior, non-radioactive species could be used in plateout experiments. However, it is important that the temperature dependence is accurately captured.

Obviously, the ability of the hot and cold traps to capture and retain fission gases is also important to understand. Similar to plateout, the temperature dependence is extremely important to capture, as the amount of volatile gas available for release during cooling failure directly impacts the source term input into the current PRA analysis.

References

[1] C. Matthews, D. Schwen, A. C. Klein, Radiation re-solution of fission gas in non-oxide nuclear fuel, Journal of Nuclear Materials 456 (2015) 273–278. doi:10.1016/j.jnucmat.2014.11.108 .

[2] W. Deason, Characterization of Fission Product Transport in a Gen. IV Gas-Cooled Fast Reactor Plant Utilizing Vented Fuel, Ph.D. thesis, Oregon State University (2013).

[3] R. Lenhof, Probabilistic risk assessment of a vented fuel system utilized in a generation IV gas-cooled fast reactor nuclear power plant, Ph.D. thesis, Oregon State University (2014).

[4] H. Blank, I. Ray, C. Walker, A coherent description of fission gas swelling in the structural zones III and IV of advanced fuels Part I: Properties of Bubble Populations P2 and the Critical Temperature Burn-up Relation in Carbide Fuel Under the Conditions of Free Swelling, European Applied Research, Nuclear Science and Technology 4 (5) (1983) 1223–1274.

[5] R. W. Schleicher, T. C. Bertch, A. S. Shenoy, P. K. Gupta, K. R. Schultz, EM^2: An Innovative Approach to U.S. Energy Security and Nuclear Waste Disposition, in: Nuclear Power International 2010 Conference, no. May, 2010.

[6] H. Matzke, Science of Advanced LMFBR Fuels, North-Holland, 1986.

[7] Philadelphia Electric Company, APPLICATION OF PHILADELPHIA ELECTRIC COMPANY FOR Construction Permit and Class 104 License; PART C Final Hazards Summary Report Peach Bottom Atomic Power Station (Annexes A and B) (1964).

[8] U.S. Department of Energy, Preliminary Safety and Environmental Information Document Volume V: Gas-Cooled Fast Reactors, Tech. rep., DOE, Washington, D.C. (1980).

[9] P. De Laquil III, An accident probability analysis and design evaluation of the gas-cooled fast breeder reactor demonstration plant, Ph.D. thesis, Massachusetts Institute of Technology (1976).

[10] M. T. Farmer, E. A. Hoffman, P. F. Pfeiffer, I. U. Therios, T. Y. C. Wei, Generation IV Nuclear Energy System Initiative Pin Core Subassembly Design, Tech. Rep. ANL-GenIV-070, Argonne National Lab, Argonne, Illinois (2006). doi:ANL-GenIV-070 .

[11] H. Choi, R. Schleicher, Design Characteristics of the Energy Multiplier Module (EM2).

[12] R. Knief, Nuclear Engineering: Theory and Practice of Commercial Nuclear Power, Hemisphere, Washington, 1992.

[13] R. Schleicher, Presentation to Oregon State Nuclear Engineering Department: EM2 Update, Tech. rep., General Atomics, Corvallis, Oregon (2011).

[14] S. McKee, Implementation of vented fuel assemblies in the supercritical CO2-cooled fast reactor, Ph.D. thesis (2008).

[15] M. Driscoll, Optimized, Competitive Supercritical-CO2 Cycle GFR for Gen IV Service, Tech. rep., Massachusetts Institute of Technology (2008). doi:MIT-GFR-045 .

[16] G. O'Neill, F. Knight, F. Leitz, D. Sherer, Safety and Economic Aspects of Vented Fuel in Sodium-Cooled Reactors, in: Proceedings of the Conference on Safety, Fuels, and Core Design in Large Fast Power Reactors, no. 1965, Argonne National Laboratory, Illinois, 1965, pp. 540–548.

[17] G. W. Keilholtz, G. C. Battle Jr, Fission product release and transport in liquid metal fast breeder reactors, Tech. rep., Oak Ridge National Laboratories (1969).

[18] D. Smidt, W. Sommer, Application of the vented fuel concept to a sodium cooled power breeder with 1000 MWe, in: Conference on Safety, Fuels and Core Design in Large Fast Power Reactors, no. 1965, Karlsruhe, Argonne, Illinois, 1965.

[19] A. J. Lipps Jr, 1000 MWe LMFBR Follow-on Study: Topical Report Vvaluation of Vented-to-Coolant Design for Sodium-Bonded Carbide Fuel Rods, Tech. Rep. WARD-2000-31, Westinghouse Electric Corporation (1968).

[20] Terra Power, Conceptual Design of a 500 MWe Traveling Wave Demonstration Reactor Plant (2011).

[21] B. Castle, NGNP Reactor Coolant Chemistry Study, Tech. Rep. 2010, Idaho National Laboratory (2010). doi:INL/EXT-10-19533 .

[22] Philadelphia Electric Company, Final Hazards Summary Report Peach Bottom Atomic Power Station: Volume V - Plant Description and Safeguards Analysis (Annexes), Tech. rep. (1961).

[23] B. Buckingham, EM^2 Helium Purification System: Models and Concepts (2011).

[24] General Atomics, Energy Multiplier Module Conceptual Technical Description: Volume IV Fission Product Control, Tech. rep. (2013).

[25] General Atomics, Tritium distribution in the mhtgr, Tech. Rep. May, Department of Energy (1988).

[26] H. Blank, Nonoxide ceramic nuclear fuels, in: Materials science and technology: a comprehensive treatment Vol 10a, Wiley-VCH, 1994.

[27] D. R. Olander, Fundamental Aspects of Nuclear Reactor Fuel Elements, Tech. Rep. TID-26711-P1, DOE (1976).

[28] C. Ronchi, Extrapolated equation of state for rare gases at high temperatures and densities, Journal of Nuclear Materials 96 (1981) 314–328.

[29] K. Nogita, K. Une, High resolution TEM observation and density estimation of Xe bubbles in high burnup UO_2 fuels 141 (1998) 481–486.

[30] G. Pastore, L. Luzzi, V. Di Marcello, P. Van Uffelen, Physics-based modelling of fission gas swelling and release in UO_2 applied to integral fuel rod analysis, Nuclear Engineering and Design 256 (2013) 75–86. doi:10.1016/j.nucengdes.2012.12.002 .

[31] P. Prajoto, A. Wazzan, D. Okrent, Computer Modeling of Steady State Fission Gas behavior in Carbide Fuels, Nuclear Engineering and Design 48 (1978) 461–495.

[32] I. Ray, H. Blank, Microstructure and fission gas bubbles in irradiated mixed carbide fuels at 2 to 11 a/o burnup, Journal of Nuclear Materials 124 (1984) 159–174.

[33] M. Colin, M. Coquerelle, I. Ray, C. Ronchi, C. T. Walker, H. Blank, The Sodium-bonding pin concept for advanced fuels Part I: Swelling of carbide fuel up to 12% burnup, Nuclear Technology 63 (1983) 442–460.

[34] C. Ronchi, M. Campana, M. Coquerelle, J. V. de Laar, Reactor Performance of MC, MN, MCN and MCO: Results of the comparative irradiation experiments GOCAR, European Applied Research, Nuclear Science and Technology 6.

[35] C. Ronchi, I. Ray, H. Thiele, J. V. de Laar, Measurements and observations on microscopic swelling in MX-type fuels, Tech. Rep. EUR 5907 EN, Institue for Transuranium elements (1978).

[36] R. B. Matthews, R. J. Herbst, Uranium-plutonium carbide fuel for fast breeder reactors, Nuclear Technology 63 (1) (1983) 9–22.

[37] G. Bart, F. Botta, C. Hoth, G. Ledergerber, R. Mason, R. Stratton, AC-3-irradiation test of sphere-pac and pellet (U, Pu)C fuel in the US Fast Flux Test Facility, Journal of Nuclear Materials 376 (1) (2008) 47–59.

[38] R. Martin, Compilation of Fuel Performance and Fission Product Transport Models and database for MHTGR Design, Tech. Rep. ORNL/NPR-91/6, ORNL (1993). doi:ORNL/NPR-91/6 .

[39] J. Saurwein, Fission Product Vent System (FPVS) (Apr. 2014).

[40] B. Myers, N. Baldwin, W. Bell, R. Burnette, The behavior of fission product gases in HTGR Fuel Material, Tech. Rep. 17, GA (1977).

[41] T. Preusser, Modeling of Carbide Fuel Rods, Nuclear Technology 57 (1982) 343–371.

[42] P. Petkevich, Development and Application of an Advanced Fuel Model for the Safety Analysis of the Generation IV Gas-cooled Fast Reactor, Ph.D. thesis, Ecole Polytechnique Federale de Lausanne (2008).

[43] IAEA, Status and Trends of Nuclear Fuels Technology for Sodium Cooled Fast Reactors, Tech. rep., IAEA, Vienna, Austria (2009).

[44] M. Tetenbaum, A. Sheth, W. Olson, A Review of the Thermodynamics of the U-C, Pu-C, and U-Pu-C Systems, Tech. Rep. ANL-AFP-8, ANL (1975).

[45] C. Holley, Jr., M. Rand, E. Storms, The Actinide Carbides, in: Chemical Thermodynamics, IAEA, 1984, Ch. 6.

[46] S. Govindarajan, P. Puthiyavinayagam, S. Clement Ravi Chandar, S. Chetal, S. Bhoje, Performance of FBTR Mixed Carbide Fuel, in: Influence of high dose irradiation on core structural and fuel materials in advanced reactors, 1997, pp. 47–56.

[47] O. Izhvanov, EM2 Fuel Irradiatoin Test Planning (2011).

[48] E. Storms, An Analytical Representation of the Thermal Conductivity and Electrial Resistivity of UC, PuC, and (UPu)C, Tech. Rep. LA-9524, LANL (1982).

[49] P. Petkevich, K. Mikityuk, P. Coddington, R. Chawla, Development and benchmarking of a 2D transient thermal model for GFR plate-type fuel, Annals of Nuclear Energy 34 (9) (2007) 707–718. doi:10.1016/j.anucene.2007.03.009 .

[50] J. Matthews, Mechanical Properties and Diffusion Data for Carbide and Oxide Fuels, Tech. rep., UK Atomic Energy Authority (1974).

[51] W. Dienst, Swelling, Densification and Creep of (U, Pu)C Fuel under irradiation, Journal of Nuclear Materials 124 (1984) 153–158.

[52] R. Williamson, J. Hales, S. Novascone, M. Tonks, D. Gaston, C. Permann, D. Andrs, Multidimensional multiphysics simulation of nuclear fuel behavior, Journal of Nuclear Materials 423 (2012) 149–163.

[53] D. Gaston, C. Newman, G. Hansen, D. Lebrun-Grandie, D. Lebrun-Grandié, MOOSE: A parallel computational framework for coupled systems of nonlinear equations, Nuclear Engineering and Design 239 (10) (2009) 1768–1778. doi:10.1016/j.nucengdes.2009.05.021 .

[54] D. L. Y. Louie, Characterization of Fuel Swelling in Helium-bonded carbide fuel pins, Tech. Rep. LA-11051-T, LANL (1987).

[55] R. White, M. Tucker, A new fission-gas release model, Journal of Nuclear Materials 118 (1983) 1–38.

[56] M. Speight, A calculation on the migration of fission gas in material exhibiting precipitation and re-solution of gas atoms under irradiation, Nuclear Science and Engineering 37 (1969) 180–185.

[57] K. Govers, C. Bishop, D. Parfitt, S. Lemehov, M. Verwerft, R. Grimes, Molecular dynamics study of Xe bubble re-solution in UO_2, Journal of Nuclear Materials 420 (2012) 282–290. doi:10.1016/j.jnucmat.2011.10.010 .

[58] D. R. Olander, D. Wongsawaeng, Re-solution of fission gas - A review: Part I. Intragranular bubbles, Journal of Nuclear Materials 354 (2006) 94–109.

[59] J. Turnbull, The distribution of intragranular fission gas bubbles in UO_2 during irradiation, Journal of Nuclear Materials 38 (1971) 203–212.

[60] R. Nelson, The stability of gas bubbles in an irradiation environment, Journal of Nuclear Materials 31 (2) (1969) 153–161. doi:10.1016/0022-3115(69)90189-5 .

[61] G. Pastore, Modelling of Fission Gas Swelling and Release in Oxide Nuclear Fuel and Application to the TRANSURANUS Code, Ph.D. thesis (2012).

[62] H. Blank, H. Matzke, The effect of fission spikes on fission gas re-solution, Radiation Effects 17 (1973) 57–64.

[63] J. Turnbull, A review of irradiation induced re-solution in oxide fuels, Radiation Effects 53 (1980) 243–250.

[64] K. Govers, S. Lemehov, M. Verwerft, In-pile Xe diffusion coefficient in UO_2 determined from the modeling of intragranular bubble growth and destruction under irradiation, Journal of Nuclear Materials 374 (2008) 461–472. doi:10.1016/j.jnucmat.2007.10.005 .

[65] C. Ronchi, P. Elton, Radiation re-solution of fission gas in uranium dioxide and carbide, Journal of Nuclear Materials 140 (1986) 228–244.

[66] D. Schwen, M. Huang, P. Bellon, R. Averback, Molecular dynamics simulation of intragranular Xe bubble re-solution in UO_2, Journal of Nuclear Materials 392 (2009) 35–39.

[67] C. Ronchi, T. Wiss, Fission-fragment spikes in uranium dioxide, Journal of Applied Physics 92 (10) (2002) 5837. doi:10.1063/1.1513192 .

[68] H. Blank, Properties of Fission Spikes in UO_2 and UC Due to Electronic Stopping Power, Physica Status Solidi (a) 10 (1972) 465.

[69] C. Ronchi, H. Matzke, J. van de Laar, H. Blank, Fission Gas Behaviour in Nuclear Fuels, European Applied Research Reports - Nuclear Science and Technology 1 (1) (1979) 1–350.

[70] C. Ronchi, H. Matzke, Calculations on the in-pile behavior of fission gas in oxide fuels, Journal of Nuclear Materials 45 (1972) 15–28.

[71] C. Ronchi, I. Ray, H. Thiele, J. V. de Laar, Swelling analysis of highly-rated MX-type LMFBR fuels: II. Microsopic swelling behaviour, Journal of Nuclear Materials 74 (1978) 193–211.

[72] C. Ronchi, C. Sari, Swelling analysis of highly rated MX-type LMFBR fuels. I. Restructuring and Porosity Behaviour, Journal of Nuclear Materials 58 (2) (1975) 140–152.

[73] C. Ronchi, J. van de Laar, H. Blank, The sodium-bonding pin concept for advanced fuels. Part III: calculation of the swelling performance, Nuclear Technology 68 (1985) 48–65.

[74] C. Matthews, 3DOT Source.
URL: https://github.com/tophmatthews/3DOT

[75] D. Schwen, 3DTrim Source.
URL: http://groups.mrl.illinois.edu/averback/3dtrim/

[76] J. F. Ziegler, J. Biersack, U. Littmark, The stopping and range of ions in solids: Volume 1, Pergamon, New York, 1985.

[77] W. Brandt, M. Kitagawa, Effective stopping-power charges of swift ions in condensed matter, Physical Review B 25 (9).

[78] D. Parfitt, R. Grimes, Predicting the probability for fission gas resolution into uranium dioxide, Journal of Nuclear Materials 392 (2009) 28–34. doi:10.1016/j.jnucmat.2009.03.046 .

[79] M. Posselt, Comparison of BC and MD simulations of low-energy ion implantation 102 (1995) 236–241.

[80] V. Ferleger, I. Wojciechowski, On non-binary nature of the collisions of heavy hyperthermal particles with solid surfaces, Nuclear Instruments and Methods in Physics Research Section B: Beam Interactions with Materials and Atoms 164-165 (2000) 641–644. doi:10.1016/S0168-583X(99)01043-5 .

[81] G. Hobler, G. Betz, On the useful range of application of molecular dynamics simulations in the recoil interaction approximation, Nuclear Instruments and Methods in Physics Research Section B: Beam Interactions with Materials and Atoms 180 (2001) 203–208. doi:10.1016/S0168-583X(01)00418-9 .

[82] I. Chakarov, R. Webb, An investigation of collision propagation in energetic ion initiated cascades in copper, Nuclear Instruments and Methods in Physics Research B 102 (1995) 145–150.

[83] G. S. Was, Fundamentals of radiation materials science: Metals and alloys, Springer Berlin Heidelberg, 2007.

[84] N. E. Todreas, Nuclear Systems Volume I: Thermal Hydraulic Fundamentals, Taylor and Francis, New York, 1989.

[85] M. J. Moran, H. N. Shapiro, Fundamentals of engineering thermodynamics, Wiley, New York, 2000.

[86] D. Hanson, A Review of Radionuclide Release from HTGR Cores During Normal Operation, Tech. Rep. 3 (2004).

[87] W. Bell, A national program plan for work to establish fission-product behavior in HTGR systems, Tech. rep., GA (1970).

[88] L. Zumwalt, P. E. Gethard, E. E. Anderson, Fission-Product Release from Monogranular UC2 Particles, Nuclear Engineering and Design 21 (1965) 1–12.

[89] EPRI, Plateout Phenomena in Direct-Cycle High Temperature Gas-Cooled Reactors, Tech. Rep. 1003387 (2002). doi:1003387 .

[90] IAEA, Fuel performance and fission product behaviour in gas cooled reactors, Tech. Rep. IAEA-TECDOC-978, IAEA (1997). doi:IAEA-TECDOC-978 .

[91] R. Wichner, Fission Product Plateout and Liftoff in the MHTGR Primary System: A Review, Tech. rep., ORNL (1991).

[92] J. Antill, D. Bradley, R. Flowers, N. Hodge, The Purification of helium in high temperature reactors, Progress in Nuclear Energy in Nuclear Energy 4 (1961) 63–101.

[93] R. Burnette, W. Graham, D. Morse, The removal of radioactive krypton and xenon from a flowing helium stream by fixed-bed adsorption, Tech. rep., GA, Gatlinberg (1962).

[94] ISEE Systems, STELLA Modeling and Simulation Software (2013).
URL: http://www.iseesystems.com/softwares/Education/StellaSoftware.aspx

[95] F. Vanslager, W. Bell, O. Sisman, M. T. Morgan, Fission product transport in HTGR systems - A summary, Tech. Rep. GA-100073, Gulf General Atomic (1970). doi:GA-10073 .

[96] R. Agarwal, V. Venugopal, Chemical states of fission products in irradiated (U0.3Pu0.7)C1+x fuel at high burn-ups, Journal of Nuclear Materials 359 (1) (2006) 122–131. doi:dx.doi.org/10.1016/j.jnucmat.2006.08.005 .

[97] S. McKee, M. J. Driscoll, An Evaluation of Vented Gas Cooled Fast Reactor Fuel (1) (1980) 58–60.

[98] R. W. Schleicher, EM2 Update - Presentation to Oregon State Nuclear Engineering Dept. (2011).

[99] U.S. Nuclear Regulatory Commission, Reactor Safety Study - An Assessment of Accident Risks in U.S. Commercial Nuclear Power Plants, Tech. Rep. WASH-1400 (1975). doi:WASH-1400(NUREG-75/014) .

[100] U.S. Atomic Energy Commission, Theoretical Possibilities and Consequences of Major Accidents in Large Nuclear Power Plants, Tech. Rep. 1957, U.S. Research and Development Administration (1957). doi:WASH-740 .

[101] H. Lewis, R. Budnitz, H. Kouts, W. Loewenstein, Risk Assessment Review Group Report to the U.S. Nuclear Regulatory Commission, Tech. Rep. 1978, Ad Hoc Risk Assessment Review Group (1978).

[102] U.S. Nuclear Regulatory Commission, Discussion Paper on Safety Goals of Nuclear Power Plants, Tech. Rep. 1983 (1983). doi:NUREG-880 .

[103] U.S. Nuclear Regulatory Commission, Safety Goals for the Operation of Nuclear Power Plants: Policy Statement, Tech. Rep. 1986 (1986). doi:51FR30028 .

[104] U.S. Nuclear Regulatory Commission, Severe Accident Risks: An Assessment for Five U.S. Nuclear Power Plants, Tech. rep., NRC (1990). doi:NUREG-1150 .

[105] U.S. Nuclear Regulatory Commission, State-of-the-Art Reactor Consequence Analysesdoi:NUREG-1935 .

[106] Idaho National Laboratory, SAPHIRE 8 Basics: An Introduction to Probabilistic Risk Assessment via the Systems Analysis Program for Hands-On Integrated Reliability Evaluations (SAPHIRE) Software, Tech. Rep. 2012 (2012).

[107] M. Modarres, M. Kaminskiy, V. Krivtsov, Reliability Engineering and Risk Analysis: A Practical Guide 2nd Edition, 2nd Edition, Vol. 1, CRC Press, Boca Raton, Florida, 2010.

[108] U.S. Nuclear Regulatory Commission, NRC Website: Probabilistic Risk Assessment (PRA).
URL: http://www.nrc.gov/about-nrc/regulatory/risk-informed/pra.html

[109] A. Hakobyan, T. Aldemir, R. Denning, S. Dunagan, D. Kunsman, B. Rutt, U. Catalyurek, Dynamic Generation of Accident Progression Event Trees, Nuclear Engineering and Design.

[110] A. Hakobyan, Severe Accident Analysis Using Dynamic Accident Progression Event Trees, Ph.D. thesis, Ohio State University (2006).

[111] J. Martin, Physics for Radiation Protection, 2nd Edition, Vol. 1, Wiley-VCH, Weinheim, Germany, 2006.

[112] B. Napier, GENII Version 2 Users Guide, Tech. Rep. PNNL-14583 (2012). doi:PNNL-14583 .

[113] U.S. Department of Energy, Preliminary Safety Information Document for Standard MHTGR, Tech. Rep. DOE-HTGR-86-024 (1988). doi:DOE-HTGR-86-024 .

[114] Science Applications Internal Corporation, Draft Review of the Standard Modu lar High Temperature Gas Cooled Reactor Probabilistic Risk Assessment, Tech. rep. (1987).

[115] Exelon Generating Company, Proposed Licensing Approach for the Pebble Bed Modular Reactor in the United States, Tech. Rep. 2002 (2002).

[116] U.S. Nuclear Regulatory Commission, NRC Staff's Preliminary Findings Regarding Exelon Generating Company's Proposed Licensing Approach for the Pebble Bed Modular Reactor, Tech. Rep. 2002 (2002).

[117] Idaho National Laboratory, Next Generation Nuclear Plant Probabilistic Risk Assessment White Paper, Tech. Rep. INL/EXT-11-21270, INL (2011). doi:INL/EXT-1121270 .

[118] C. Bassi, P. Azria, M. Balmain, Level 1 probabilistic safety assessment to support the design of the CEA 2400MWth gas-cooled fast reactor, Nuclear Engineering and Design 240 (11) (2010) 3758–3780. doi:10.1016/j.nucengdes.2010.09.003 .

[119] S. Han, Overview of VHTR's PSA Approach in Korea, Tech. rep. (2012).

[120] J. Tong, J. Zhao, T. Liu, D. Xue, Development of Probabilistic Safety Assessment with respect to the first demonstration nuclear power plant high temperature gas cooled reactor in China, Nuclear Engineering and Design 251 (2012) 385–390.

[121] U.S. Nuclear Regulatory Commission, Industry-Average Performance for Components and Initiating Events at U.S. Commercial Nuclear Power Plants, Tech. Rep. NUREG/CR-6928 (2007). doi:NUREG/CR-6928 .

[122] General Atomics, Probabilistic Risk Assessment for the Standard Modular High Temperauter Gas-Cooled Reactor Volume 1 Revision 5, Tech. Rep. DOE-HTGR-86011 (1988).

[123] EG&G Idaho, Generic Data Base for Data and Models: Chapter of National Reliability Evaluation Program (NREP) Guide, Tech. Rep. EGG-EA-5887 (1982). doi:EGG-EA-5887 .

[124] A. Swain, Accident Sequence Evaluaiton Program Human Reliability Analysis Procedure, Tech. Rep. NUREG/CR-4772/SAND86-1996, Sandia National Laboratories (1987). doi:NUREG/CR-4772/SAND86-1996 .

[125] A. Swain, H. Guttmann, Handbook of Human Reliability Analysis with Emphasis on Nuclear Power Plant Applications, Tech. Rep. NUREG/CR-1278/SAND80-0200, Sandia National Laboratories (1983). doi:NUREG/CR-1278/SAND80-200 .

[126] G. Parry, An Approach to the Analysis of Operator Actions in PRA, Tech. Rep. EPRI TR-100259, Electric Power Institute (EPRI) (1992). doi:EPRITR-100259 .

[127] D. Gertman, The SPAR-H Method, Tech. Rep. NUREG/CR-6883, U.S. Nuclear Regulatory Commission (2000). doi:NUERG/CR-6883 .

[128] U.S. Nuclear Regulatory Commission, Technical Basis and Implementation Guidelines for a Technique for Human Event Analysis (ATHEANA) Rev. 1, Tech. Rep. NUREG/CR-1624 (2000). doi:NUREG/CR-1624 .

[129] U.S. Nuclear Regulatory Commission, Evaluation of Human Reliability Analysis Methods Against Good Practices, Tech. Rep. NUREG-1842 (2006). doi:NUREG-1842 .

[130] D. Dilling, HTGR 450 MW(t) MHTGR Source Term and Containment Report, Tech. Rep. DOE-HTGR-90321, GA (1993).

[131] Idaho National Laboratory, Mechanistic Source Terms White Paper, Tech. Rep. INL/EXT-10-17997, INL (2010). doi:INL/EXT-10-17997 .

[132] General Atomics, Probabilistic Risk Assessment for the Standard Modular High Temperature Gas-Cooled Reactor: Version 2 Revision 3, Tech. Rep. DOE-HTGR-86011 (1988).

[133] U.S. Atomic Energy Commission, Regulatory Guide 1.4 - Assumptions Used for Evaluating the Potential Radiological Consequences of a Loss of Coolant Accident for Pressurized Water Reactors, Tech. Rep. 1974 (1974).

[134] U.S. Nuclear Regulatory Commission, Regulatory Guide 4.2- Preparation of Environmental Reports for Nuclear Power Reactors Rev. 2, Tech. Rep. NUREG-0099 Rev 2 (1976). doi:NUEG-0099 .

[135] S. Ross, J. Rishel, P. Lowry, Engineering Evaluations of X/Q Values Consistent with Regulatory Guide 1.145, Tech. Rep. PNNL-19217 (2010). doi:PNNL-19217 .

[136] Philadelphia Electric Company, Application of Philadelphia Electric Company for Construction Permit and Class 104 License; Part B Preliminary Hazards Summary Report Peach Bottom Atomic Power Station, Tech. rep. (1961).

[137] Pebble Bed Modular Reactor Ltd., Proposed PBMR Safety Analysis Report, Tech. Rep. 2002 (2002).

[138] Idaho National Laboratory, Summary of Planned Implementation for the HTGR Lessons Learned Applicable to the NGNP, Tech. Rep. INL/EXT=11-21545, Idaho National Laboratory (2011). doi:INL/EXT-11-21545 .

[139] G. Hannaman, GCR reliability data bank status report, Tech. Rep. GA-14839, General Atomics (1978).

[140] L. Cadwallader, S. Piet, The 1988 failure rate screening data for fusion reliability and risk analysis, Tech. Rep. EGG-FSP-8709, Idaho National Engineering Laboratory (Jan. 1988).

[141] P. Saignes, Reliability Database for PSA in Support to the Design of the Innovative CEA 2400 MW, in: Proceedings of the International Probabilistic Safety Assessment and Management Conference, Vol. 47, 2008.

[142] S. Eida, S. Chmielewski, T. Swantz, Generic Component Failure Data Base for Light Water and Liquid Sodium Reactor PRAs, Tech. Rep. EGG-SSRE-8875, EG&G (1990). doi:EGG-SSRE-8875 .

[143] NRC, U.S. Nuclear Regulatory Commission, Summary of SPAR Component Unreliability Data Results: 2010 Parameter Estimates Update (2010).
URL: http://nrcoe.inel.gov/resultsdb/AvgPerf/

[144] L. Cadwallader, Selected Component Failure Rate Values from Fusion Safety Assessment Tasks, Tech. Rep. INEEL/EXT-98-00892, Idaho National Engineering and Environmental Laboratory (1998). doi:INEEL/EXT-98-00892 .

[145] C. Bassi, P. Azria, M. Balmain, PBMR White Paper: PRA Approach, Tech. Rep. 2006, Pebble Bed Modular Reactor Ltd. (2006). doi:USDC20060613-1 .

[146] D. Engel, A. Dalton, C. Dale, E. Jones, Risk Analysis and Decision Making FY 2013 Milestone Report, Tech. Rep. PNNL-22563, Pacific Northwest National Laboratory (2013). doi:PNNL-22563 .

[147] T. Pinna, G. Cambi, S. Caittaglia, A. Bue, Collection and Analysis of Data Related to Fusion Machines (JET and TLK) Operating Experience or Component Failure, Fusion Engineering and Design 75 (2004) (2004) 119–1203.

[148] M. Yamada, T. Yamanishi, W. Shu, T. Suzuki, Operation Results on Safety Systems of Tritium Processsing Laboratory in Japan Atomic Energy Research Institute, Fusion Science and Technology 41 (2002) 593–597.

[149] L. Cadwallader, Comparison of Tritium Component Failure Rate Data, Fusion Science and Technology 47 (2005) 983–988.

[150] A. Mosleh, D. Rasmuson, F. Marshall, Guidelines on Model ing Common-Cause Failures in Probabilistic Risk Assessment, Tech. Rep. NUREG/CR-5485, Idaho National Engineering and Environmental Laboratory (1998). doi:NUREG/CR-5485 .

[151] U.S. Nuclear Regulatory Commission, Reevaluation of Station Blackout Risk at Nuclear Power Plants: Analysis of Station Blackout Risk, Tech. Rep. NUREG/CR-6890 (2005). doi:NUREG/CR-6890 .

[152] U.S. Nuclear Regulatory Commission, NRC Regualtions (10CFR) Part 50 - Domestic Licensing of Production and Utilization Facilities Sec. 50.2 Definitions, Tech. Rep. 2009 (2009).

[153] R. W. Schleicher, H. Choi, J. Rawls, The Energy Multiplier Module: Advancing The Nuclear Fuel Cycle Through Technology Innovations, Nuclear Technology 184 (2013) 169–180.

[154] General Atomics, Helium Purification Subsystem Design Description, Tech. Rep. DOE-HTGR-86-103, GA (1987). doi:DOE-HTGR-86-103 .

[155] IAEA, Status of advanced containment systems for next generation water reactors, Tech. Rep. IAEA-TECDOC-752, IAEA (1994). doi:IAEA-TECDOC-752 .

[156] D. Petti, R. R. Hobbins, P. Lowry, H. Gougar, I. Introduction, Representative source terms and the influence of reactor attributes on functional high-temperature gas-cooled reactors, Nuclear Technology 184 (2013) 181–197.

[157] Areva, NGNP Conceptual Design Studies Reactor Building Design, Containment Issues, and Embedment Effects, Tech. Rep. 12-19088427-001 (2008). doi:12-9088427-001 .

[158] U.S. Department of Energy, Interim Report: GENII Computer Code Application Guidance for Documented Safety Analysis, Tech. Rep. DOE-EH-4.2.1.4-Interim-GENII (Feb. 2003). doi:DOE-EH-4.2.1.4-Interim-GENII .

[159] M. Stan, Multi-Scale Models and Simulations of Nuclear Fuels, Nuclear Engineering and Technology 41 (1) (2009) 39–52.

[160] K. Lassmann, The structure of fuel element codes (1980). doi:10.1016/0029-5493(80)90221-6 .
URL: http://www.sciencedirect.com/science/article/pii/0029549380902216

[161] D. Petti, G. Bell, The DOE Advanced Gas Reactor (AGR) Fuel Development And Qualification Program, Tech. Rep. INEEL/CON-04-02416, INL (2005).

[162] P. Demkowicz, R. Morris, Post-Irradiation Examination of the AGR-1 Experiment: Plans and Preliminary Results, Tech. Rep. INL/CON-10-19184, INL (2010).

Appendices

A. Fuel modeling appendicies

Section purposely left blank.

B. System Design Appendicies

Appendix B.1: Charts of Nuclide Behavior in the Vented Fuel System

a. Case 1: An Ideal System

Table B.1-1: Significant Nuclides Plated Out in Purge Stream at 25,000 hours – Case 1

Top Ten Mass	g	Top Ten Activity	Ci	Top Ten Power	W
cesium-135	2.04E+03	strontium-89	4.49E+05	iodine-133	4.80E+03
cesium-137	1.86E+03	iodine-133	2.38E+05	strontium-89	3.98E+03
cesium-133	1.28E+03	cesium-137	1.76E+05	iodine-135	2.62E+03
strontium-90	7.12E+02	iodine-135	1.67E+05	cesium-138	2.54E+03
strontium-88	2.82E+02	strontium-91	1.27E+05	iodine-134	2.51E+03
iodine-129	4.17E+01	strontium-90	1.07E+05	strontium-91	2.03E+03
strontium-89	1.42E+01	iodine-134	9.25E+04	iodine-132	1.98E+03
iodine-127	1.14E+01	strontium-92	8.52E+04	cesium-137	1.23E+03
iodine-131	4.88E-01	iodine-132	7.95E+04	strontium-92	9.65E+02
iodine-133	1.92E-01	iodine-131	6.62E+04	iodine-131	4.47E+02
other	9.29E-02	other	6.61E+04	other	3.47E+02
total	**6.25E+03**	**total**	**1.65E+06**	**total**	**2.34E+04**

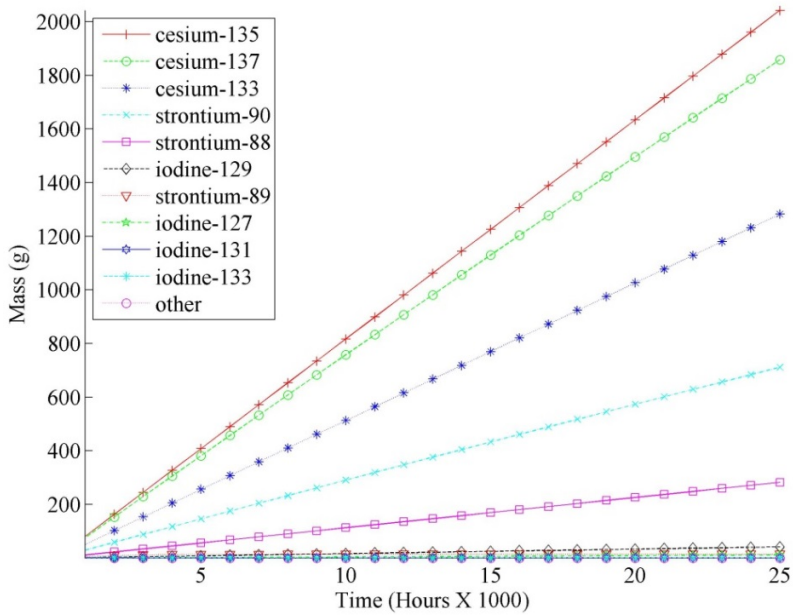

Figure B.1-1: Top Ten Mass Accum. Nuclides Plated Out in Purge Stream - Case 1

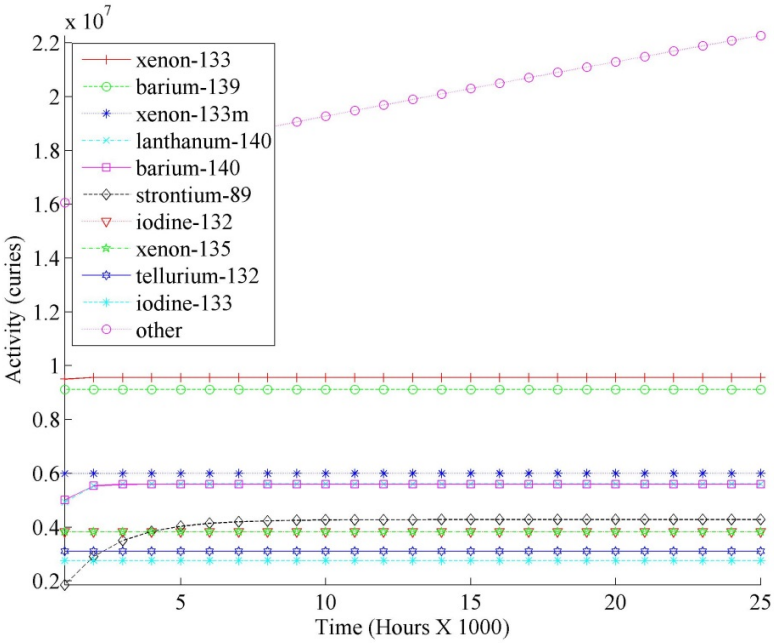

Figure B.1-2: Top Ten Activity Accum. Nuclides in First Fission Product Trap - Case 1

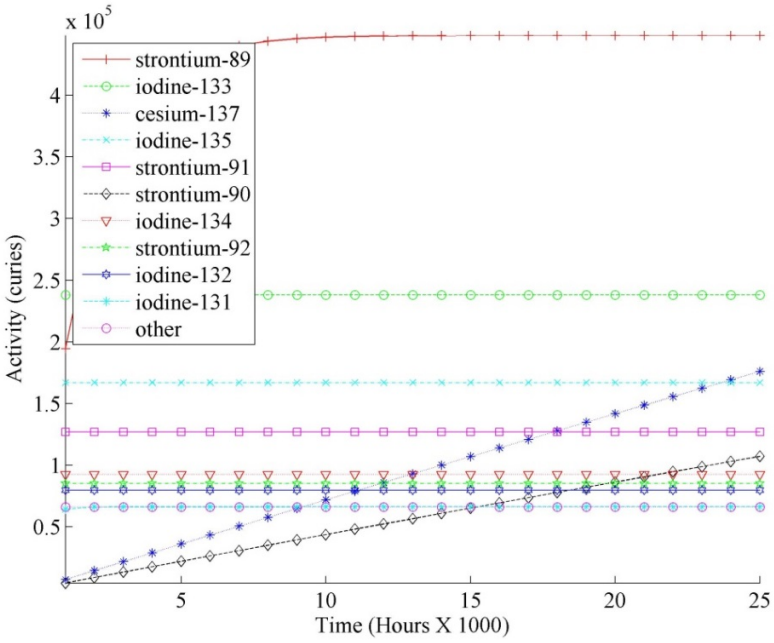

Figure B.1-3: Top Ten Activity Accum. Nuclides Plated Out in Purge Stream - Case 1

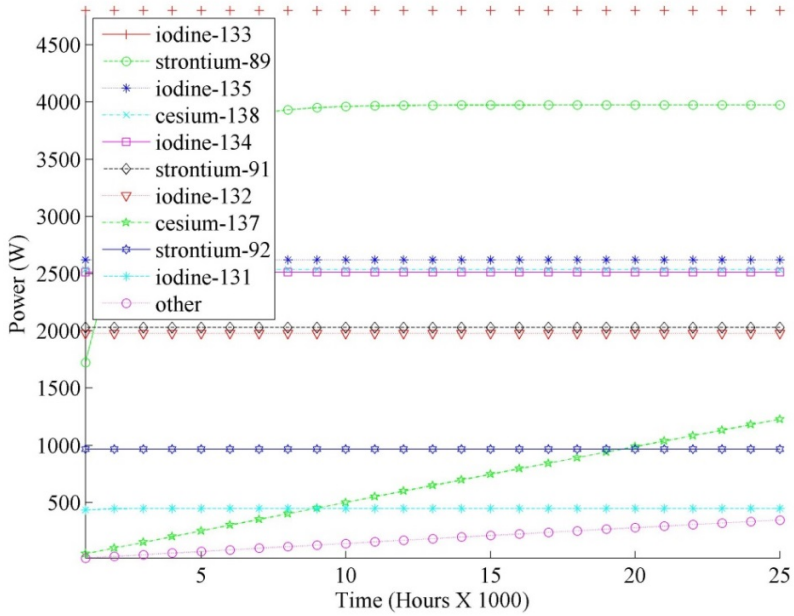

Figure B.1-4: Top Ten Power Generating Nuclides Plated Out in Purge Stream - Case 1

b. Case 2: An Open System

Table B.1-2: Significant Nuclides Collected in Primary Coolant Hot Side at 25,000 hours - Case 2

Top Ten Mass	g	Top Ten Activity	Ci	Top Ten Power	W
xenon-134	1.20E+04	xenon-133	5.08E+06	barium-139	6.42E+04
barium-138	1.08E+04	barium-139	4.67E+06	lanthanum-140	6.25E+04
xenon-136	1.08E+04	xenon-133m	3.30E+06	cesium-138	5.58E+04
xenon-132	7.94E+03	barium-140	2.80E+06	iodine-132	3.85E+04
samarium-147	3.65E+03	lanthanum-140	2.80E+06	iodine-134	3.45E+04
tellurium-130	3.32E+03	xenon-135	2.32E+06	rubidium-88	1.99E+04
samarium-149	2.04E+03	tellurium-132	1.56E+06	barium-140	1.74E+04
cerium-140	1.95E+03	iodine-132	1.55E+06	xenon-135	1.58E+04
rubidium-87	1.88E+03	cesium-138	1.45E+06	tellurium-133	1.39E+04
krypton-86	1.41E+03	iodine-134	1.27E+06	xenon-133	1.29E+04
other	1.22E+04	other	1.12E+07	other	1.27E+05
total	**6.79E+04**	**total**	**3.80E+07**	**total**	**4.63E+05**

Table B.1-3: Significant Nuclides Collected in Primary Coolant Cold Side at 25,000 hours - Case 2

Top Ten Mass	g	Top Ten Activity	Ci	Top Ten Power	W
xenon-134	1.20E+04	xenon-133	5.07E+06	lanthanum-140	6.25E+04
barium-138	1.08E+04	barium-139	4.44E+06	barium-139	6.10E+04
xenon-136	1.08E+04	xenon-133m	3.28E+06	iodine-132	3.47E+04
xenon-132	7.94E+03	lanthanum-140	2.80E+06	barium-140	1.74E+04
samarium-147	3.65E+03	barium-140	2.80E+06	xenon-135	1.51E+04
tellurium-130	3.32E+03	xenon-135	2.22E+06	xenon-133	1.28E+04
samarium-149	2.04E+03	tellurium-132	1.55E+06	yttrium-92	8.97E+03
cerium-140	1.95E+03	iodine-132	1.39E+06	rubidium-88	8.65E+03
rubidium-87	1.88E+03	yttrium-91	6.39E+05	iodine-133	8.42E+03
krypton-86	1.41E+03	yttrium-91m	5.91E+05	yttrium-90	7.22E+03
other	1.22E+04	other	5.43E+06	other	5.66E+04
total	**6.79E+04**	**total**	**3.02E+07**	**total**	**2.93E+05**

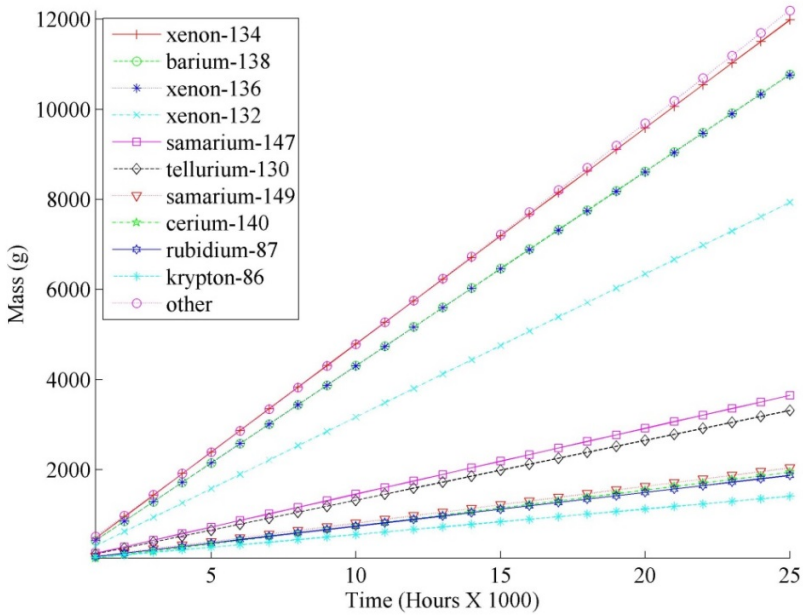

Figure B.1-5: Top Ten Mass Accum. Nuclides in PC Cold Side - Case 2

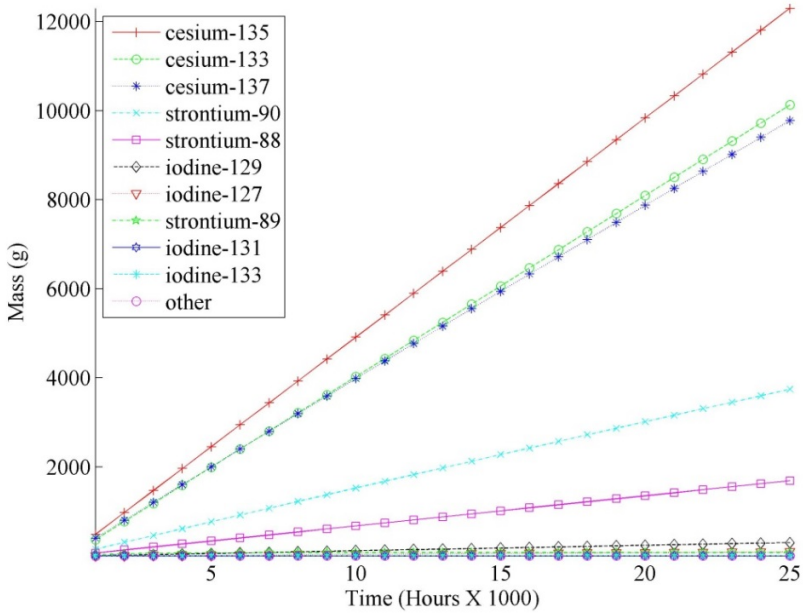

Figure B.1-6: Top Ten Mass Accum. Nuclides Plated Out in PC Hot Side - Case 2

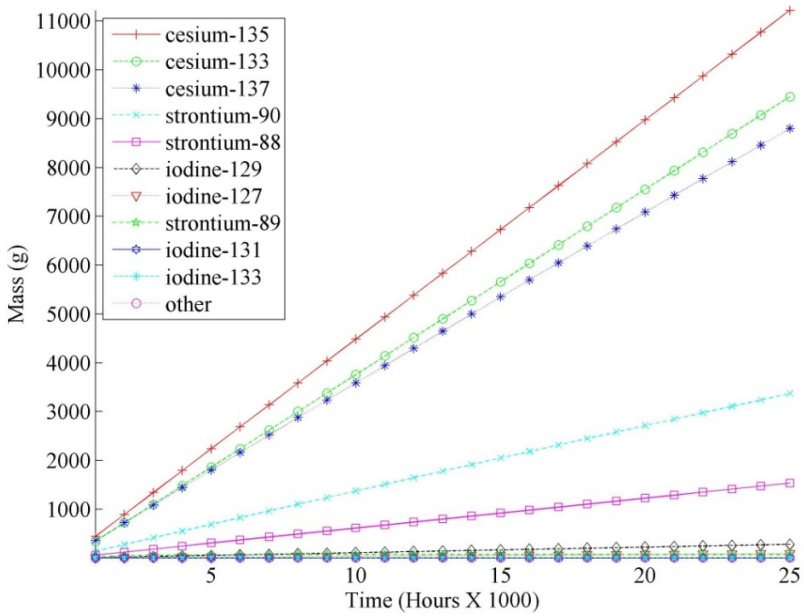

Figure B.1-7: Top Ten Mass Accum. Nuclides Plated Out in PC Cold Side - Case 2

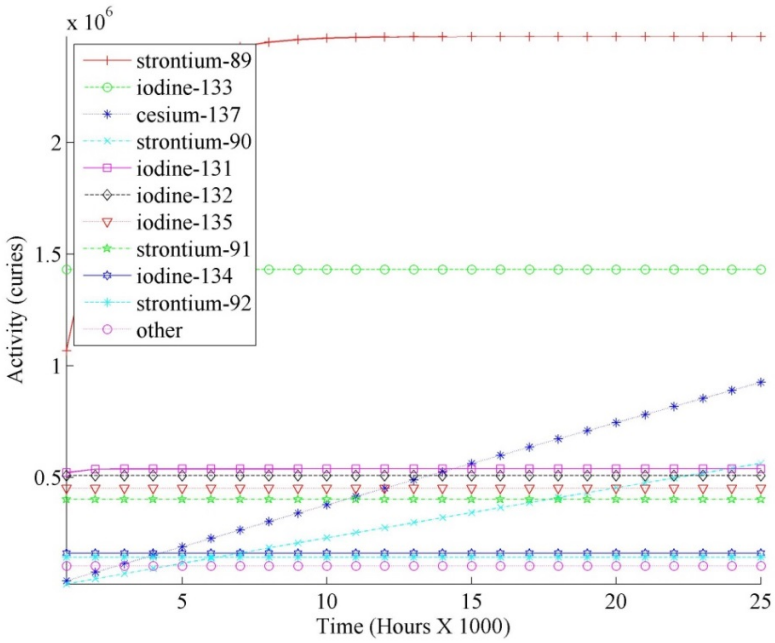

Figure B.1-8: Top Ten Activity Accum. Nuclides Plated Out in PC Hot Side - Case 2

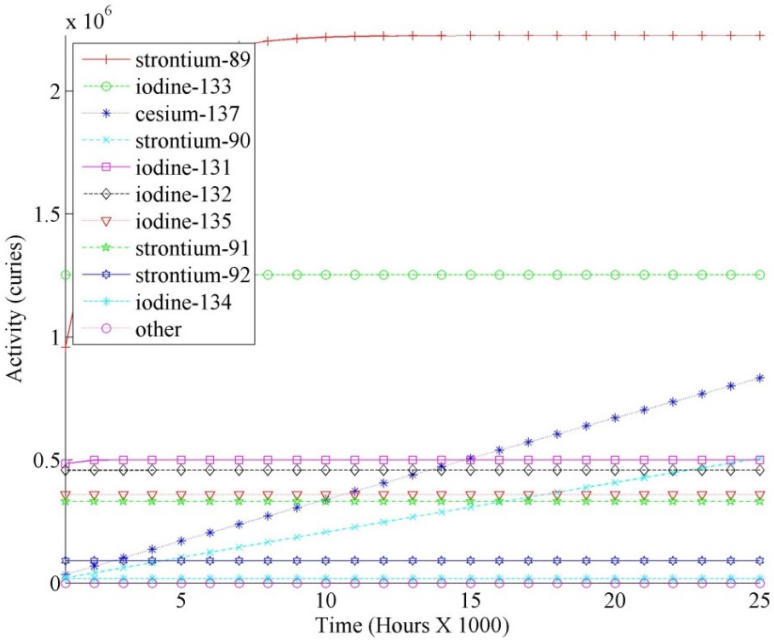

Figure B.1-9: Top Ten Activity Accum. Nuclides Plated Out in PC Cold Side - Case 2

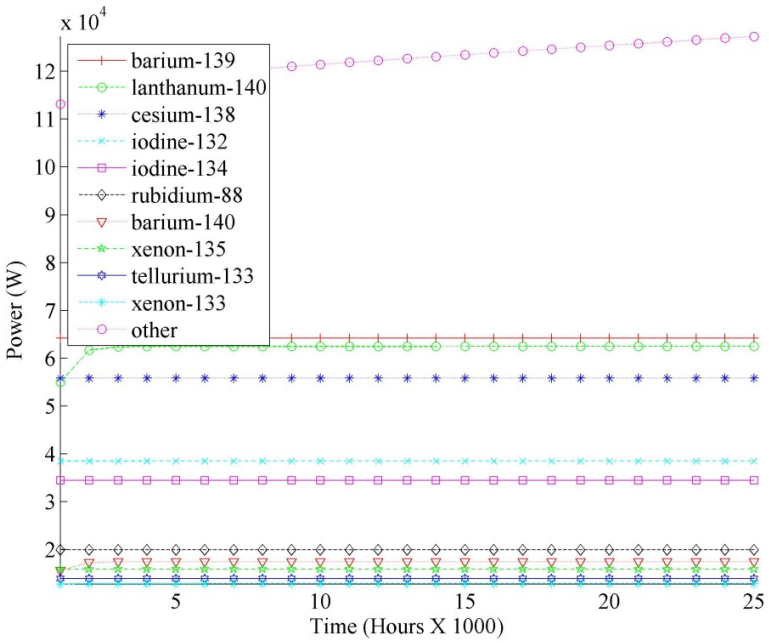

Figure B.1-10: Top Ten Power Generating Nuclides in PC Hot Side - Case 2

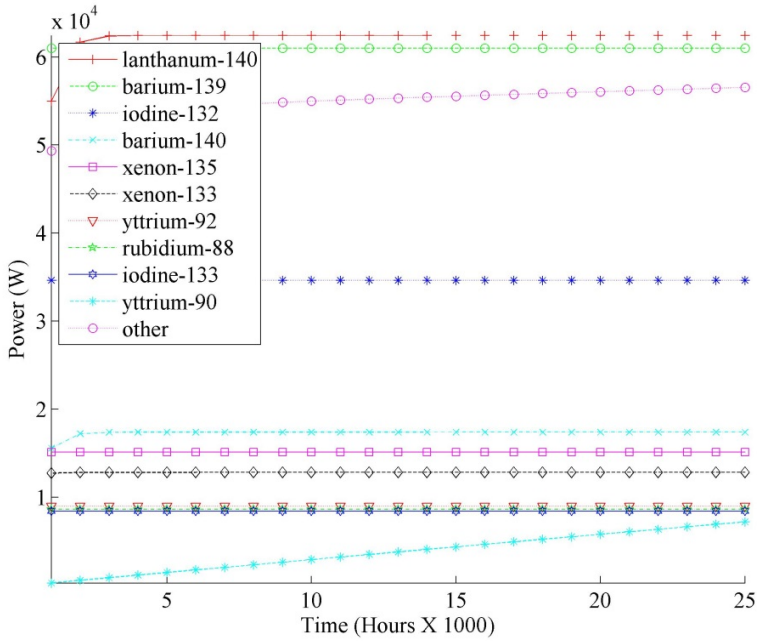

Figure B.1-11: Top Ten Power Generating Nuclides in PC Cold Side - Case 2

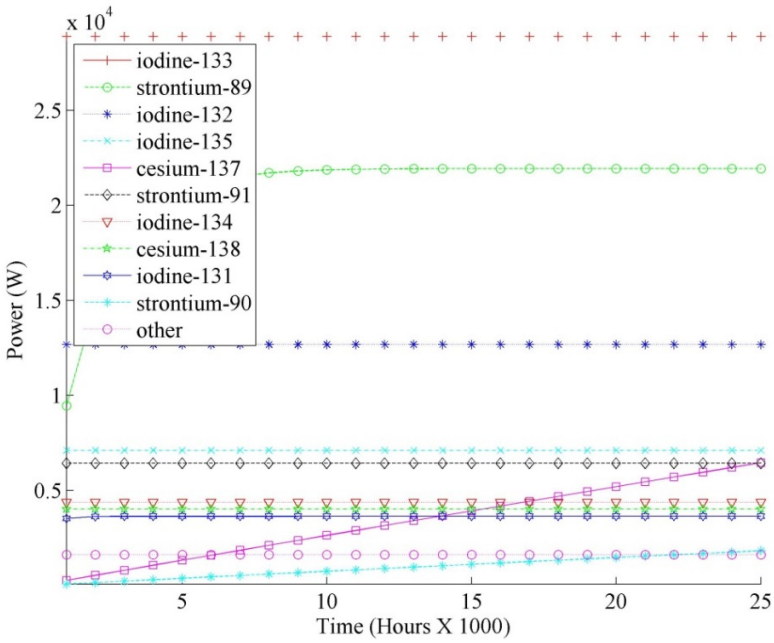

Figure B.1-12: Top Ten Power Generating Nuclides Plated Out in PC Hot Side - Case 2

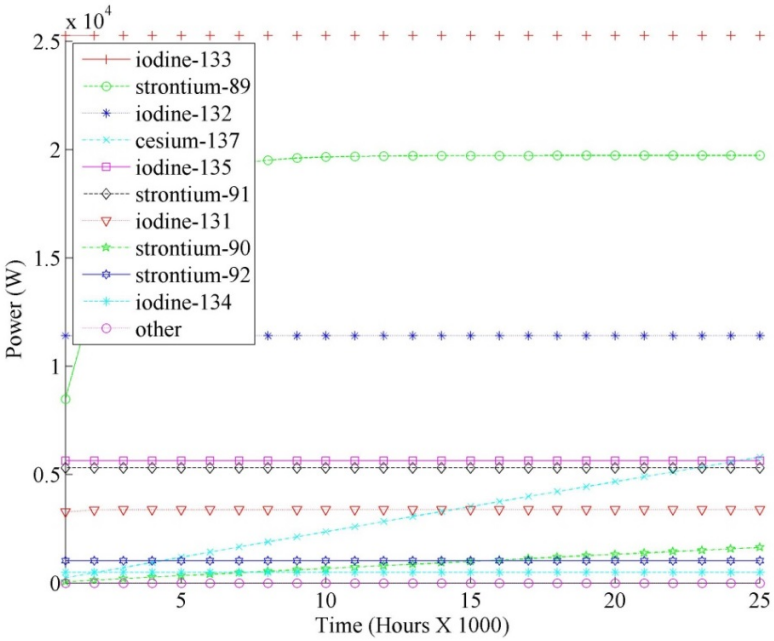

Figure B.1-13: Top Ten Power Generating Nuclides Plated Out in PC Cold Side - Case 2

c. Case 3: A Two Region System

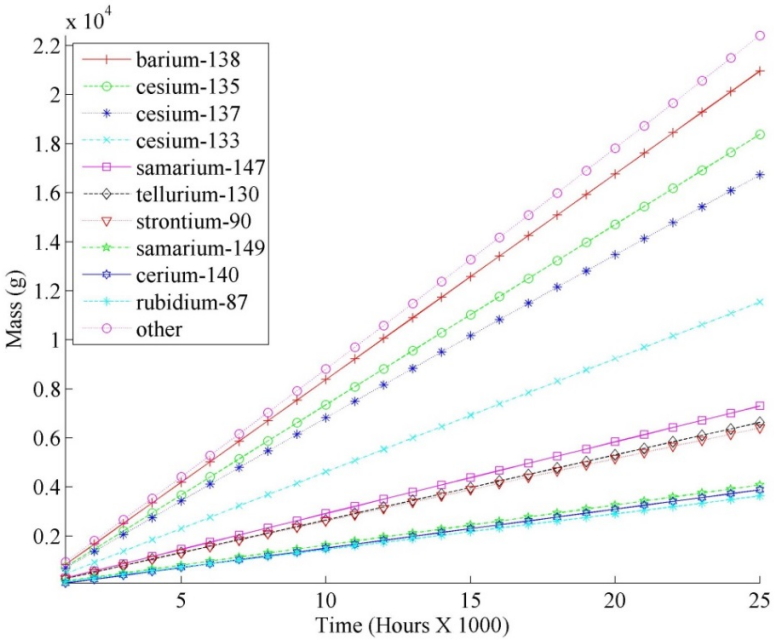

Figure B.1-14: Top Ten Mass Accum. Nuclides in First Fission Product Trap - Case 3

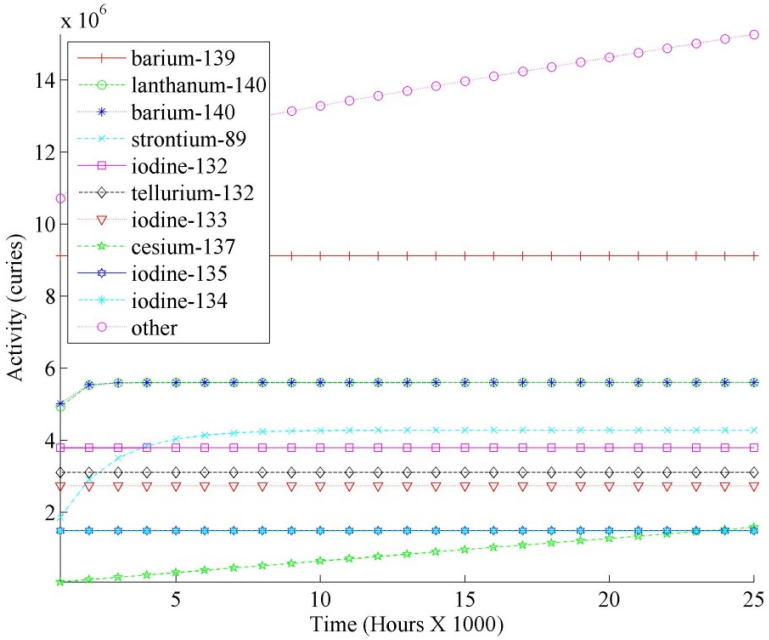

Figure B.1-15: Top Ten Activity Accum. Nuclides in First Fission Product Trap - Case 3

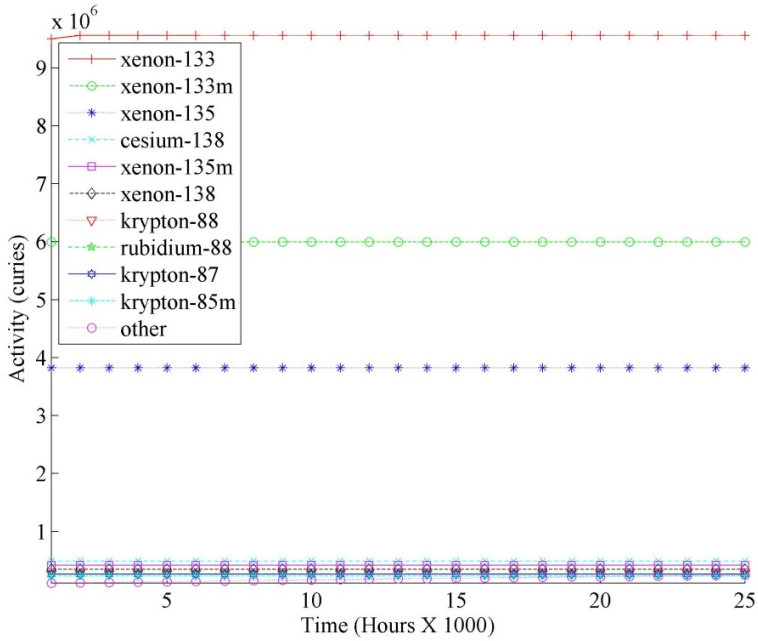

Figure B.1-16: Top Ten Activity Accum. Nuclides in Third Fission Product Trap - Case 3

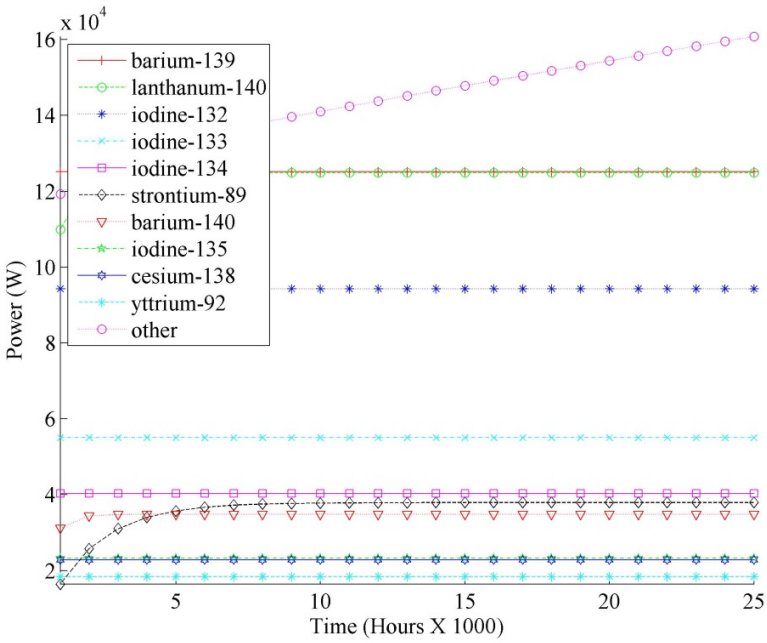

Figure B.1-17: Top Ten Power Generating Nuclides in First Fission Product Trap - Case 3

d. Case 4: A Delayed Two Region System

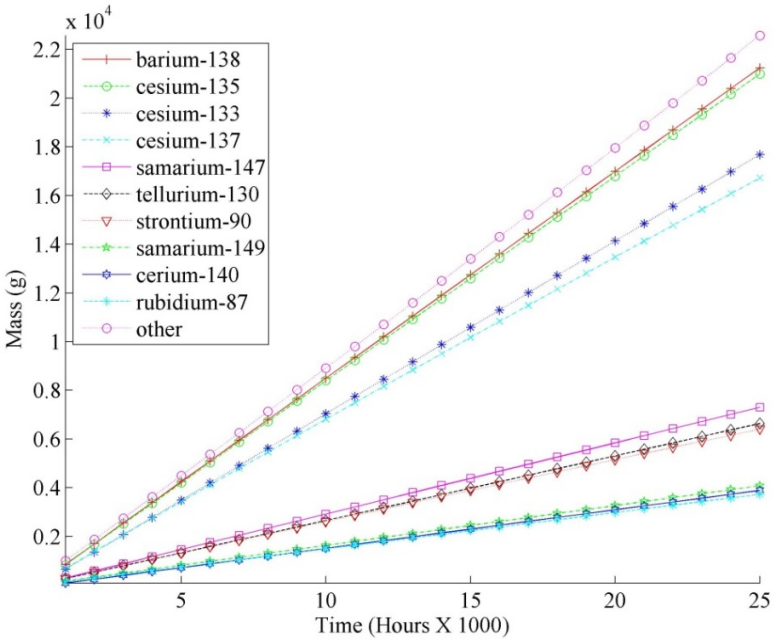

Figure B.1-18: Top Ten Mass Accum. Nuclides in First Fission Product Trap - Case 4

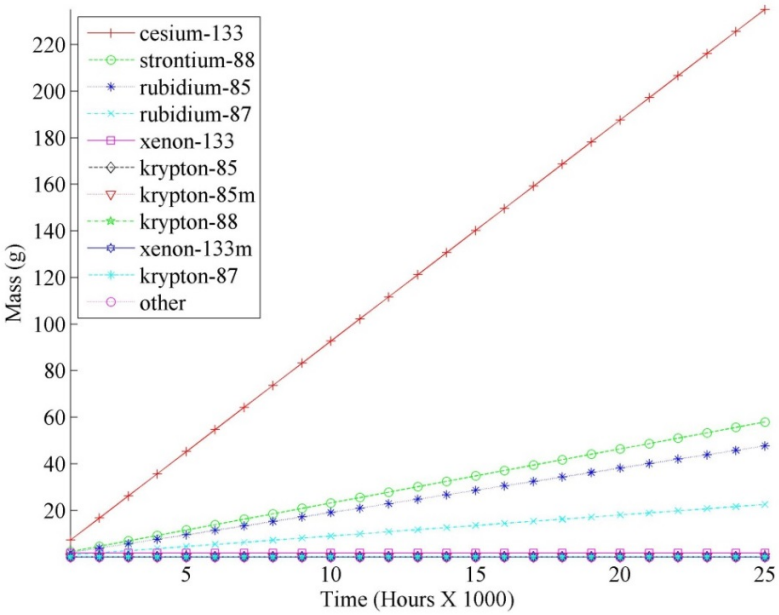

Figure B.1-19: Top Ten Mass Accum. Nuclides in Second Fission Product Trap - Case 4

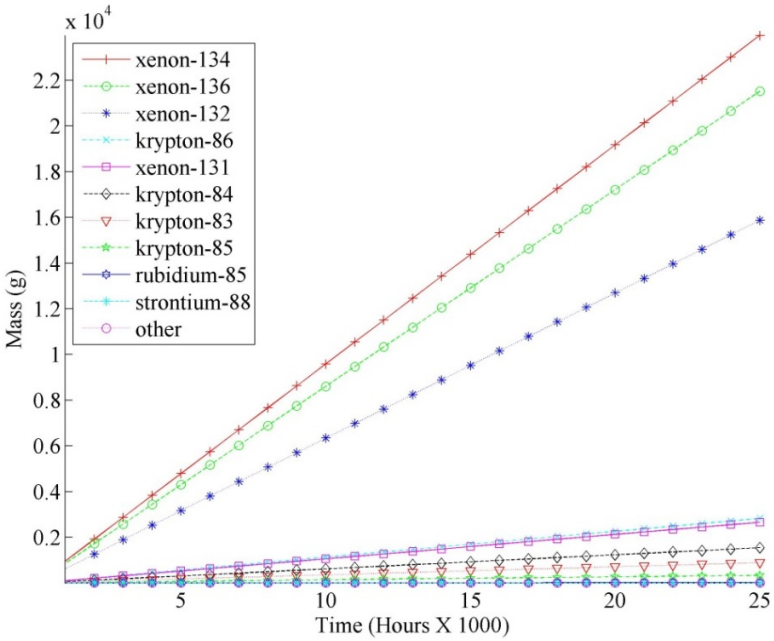

Figure B.1-20: Top Ten Mass Accum. Nuclides in Third Fission Product Trap - Case 4

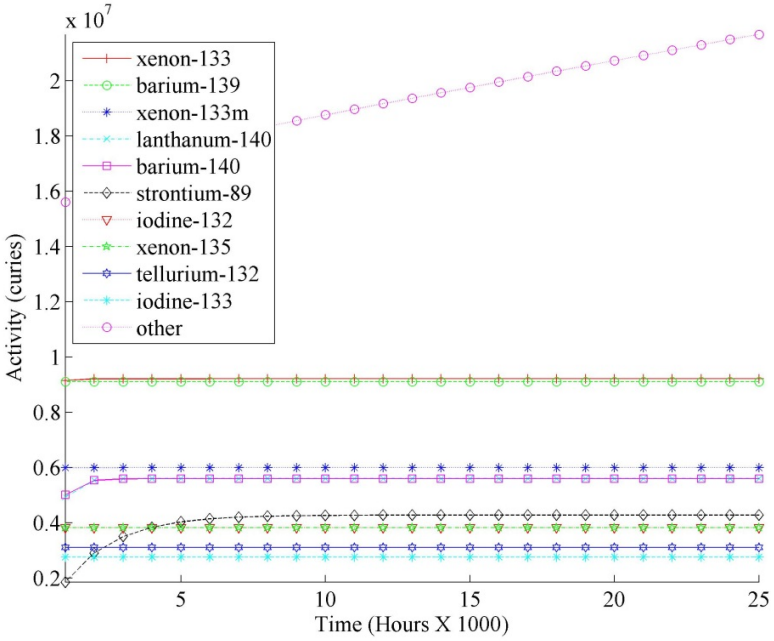

Figure B.1-21: Top Ten Activity Accum. Nuclides in First Fission Product Trap - Case 4

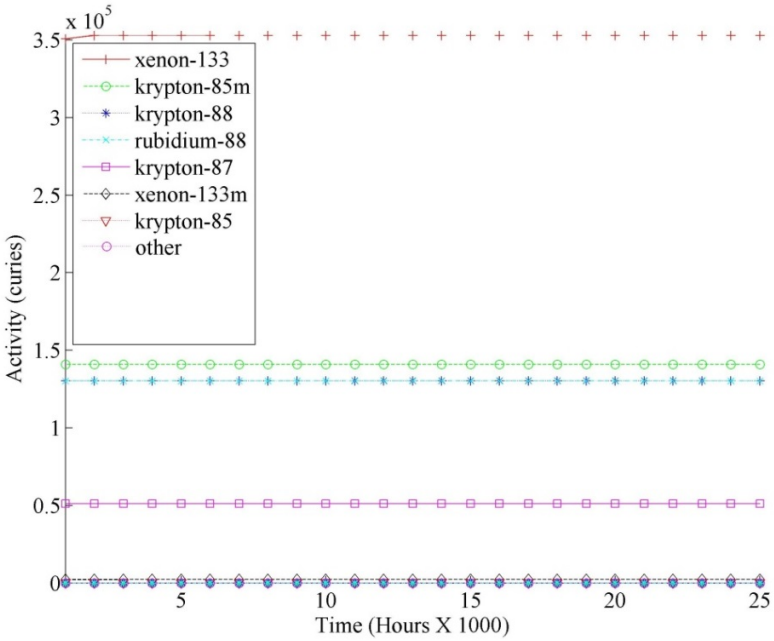

Figure B.1-22: Top Ten Activity Accum. Nuclides in Second Fission Product Trap - Case 4

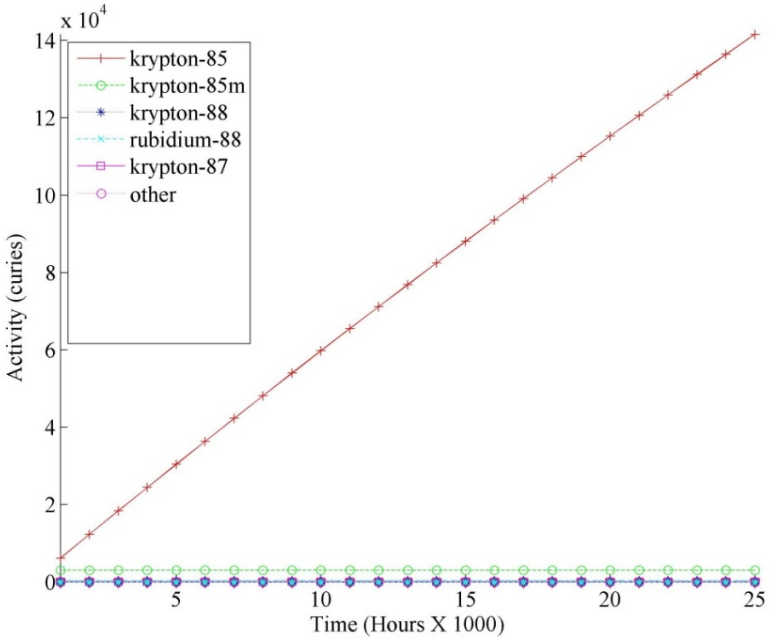

Figure B.1-23: Top Ten Activity Accum. Nuclides in Third Fission Product Trap - Case 4

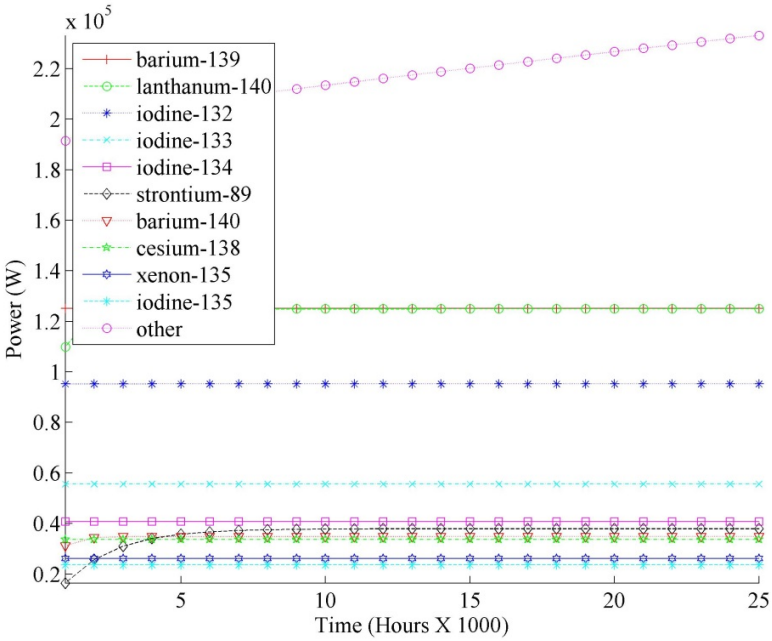

Figure B.1-24: Top Ten Power Generating Nuclides in First Fission Product Trap - Case 4

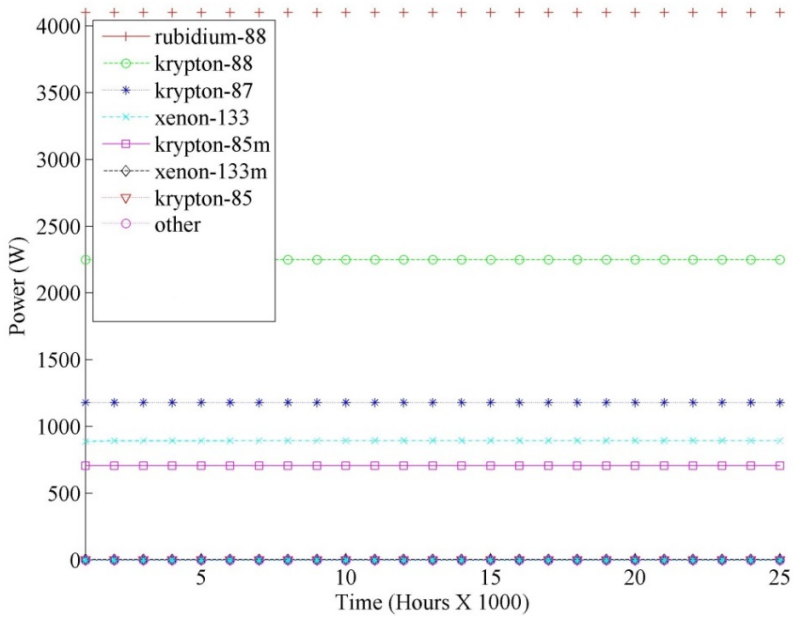

Figure B.1-25: Top Ten Power Generating Nuclides in Second Fission Product Trap - Case 4

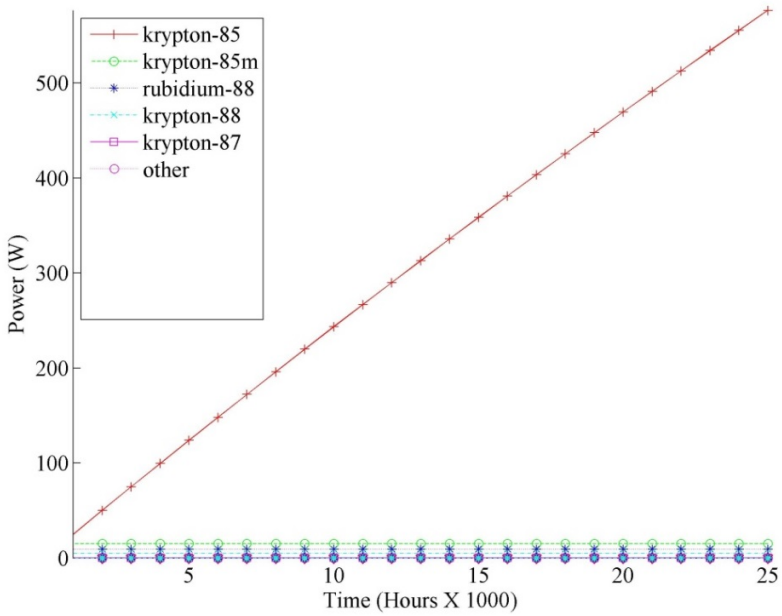

Figure B.1-26: Top Ten Power Generating Nuclides in Third Fission Product Trap - Case 4

e. Case 5: Influences of Purge Stream Leakage

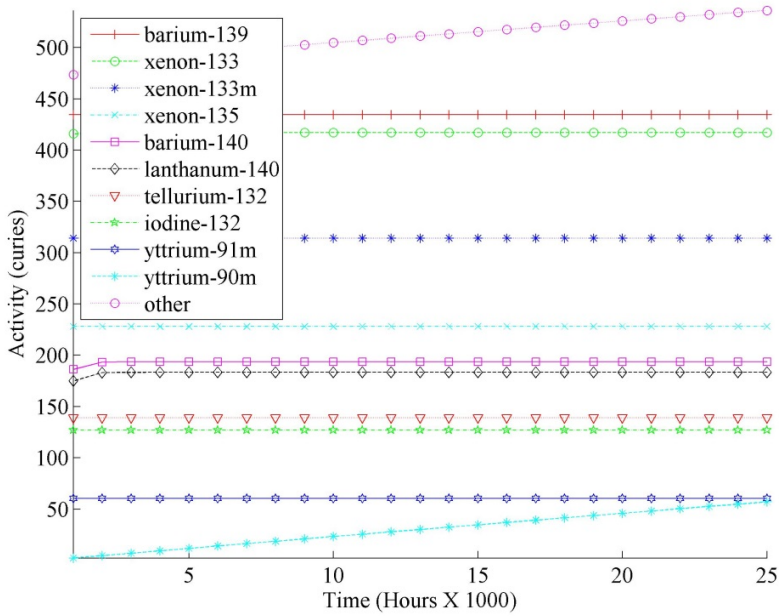

Figure B.1-27: Top Ten Activity Accum. Nuclides in PC Hot Side - Case 5 .0001 Purge Stream Leakage Fraction

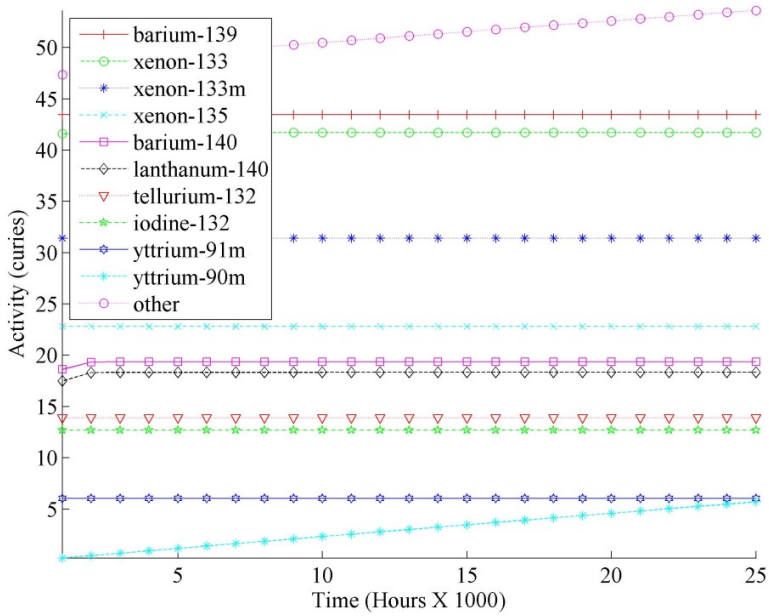

Figure B.1-28: Top Ten Activity Accum. Nuclides in PC Hot Side - Case 5 .00001 Purge Stream Leakage Fraction

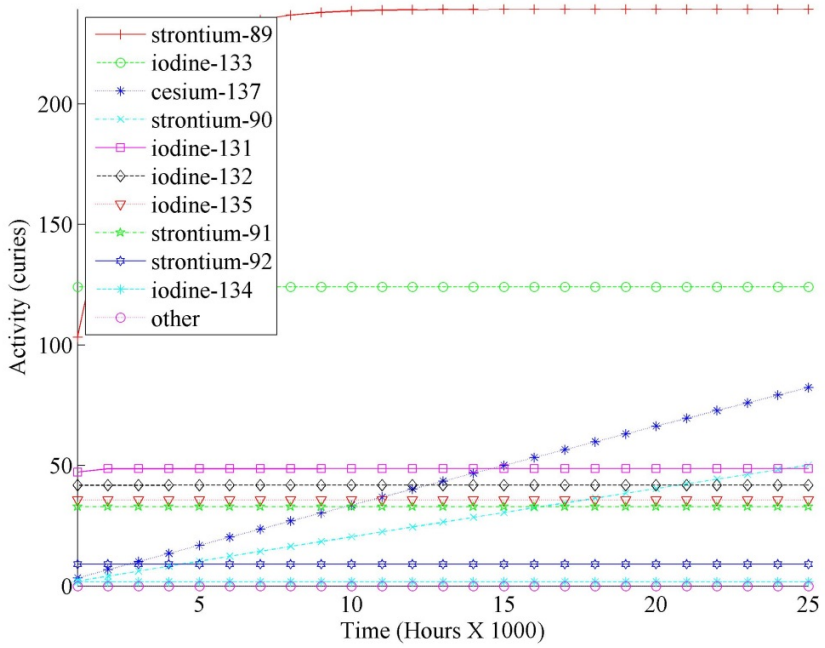

Figure B.1-29: Top Ten Activity Accum. Nuclides Plated Out in PC Hot Side - Case 5 .0001 Purge Stream Leakage Fraction

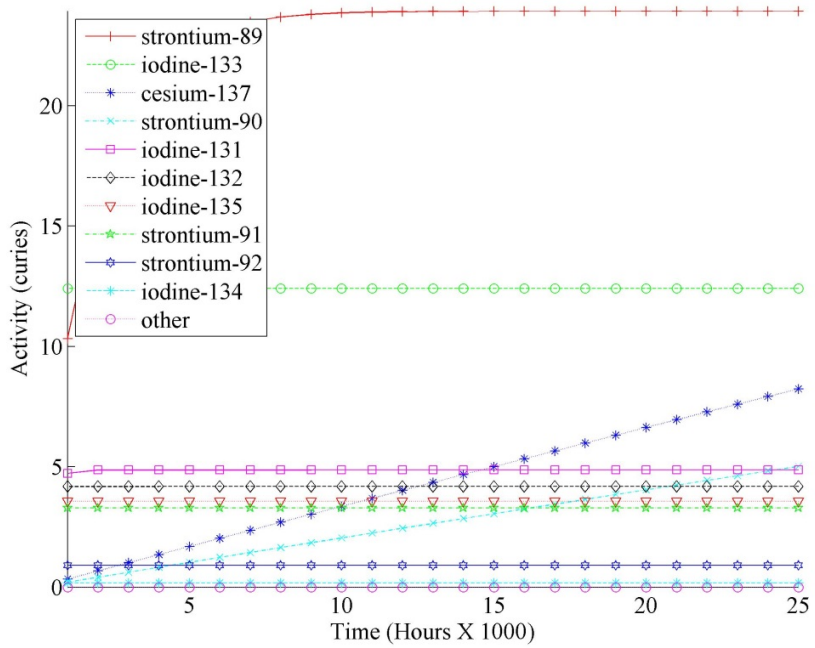

Figure B.1-30: Top Ten Activity Accum. Nuclides Plated Out in PC Hot Side - Case 5 .00001 Purge Stream Leakage Fraction

f. Case 6: Influences of Primary Coolant Plateout

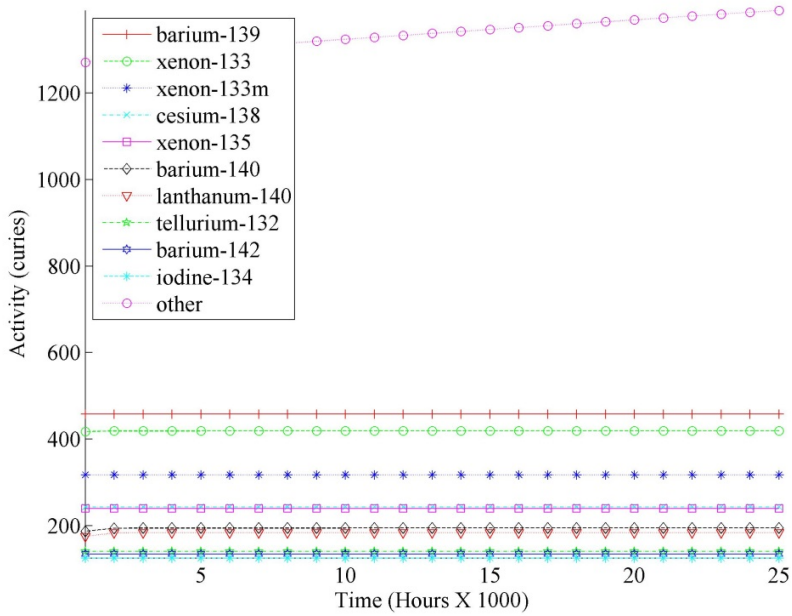

Figure B.1-31: Top Ten Activity Accum. Nuclides in PC Cold Side - Case 6 .2 Plateout Fraction

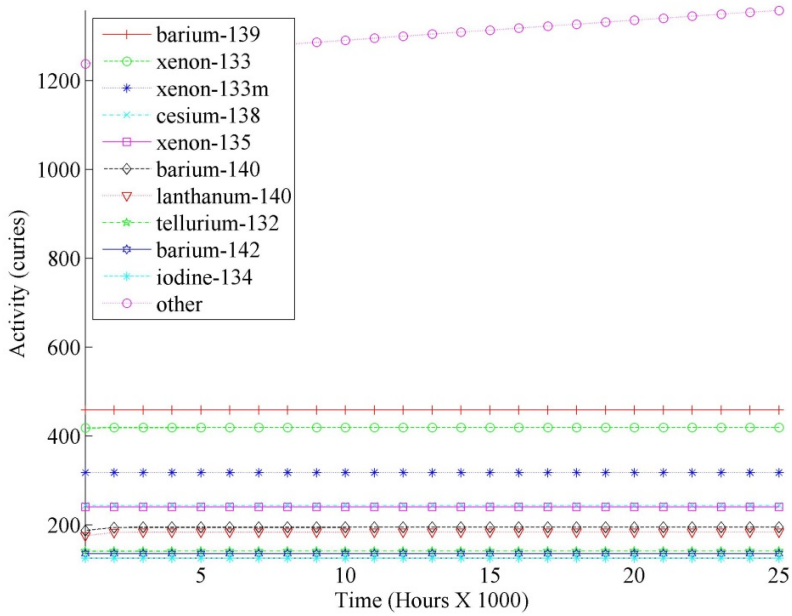

Figure B.1-32: Top Ten Activity Accum. Nuclides in PC Cold Side - Case 6 .3 Plateout Fraction

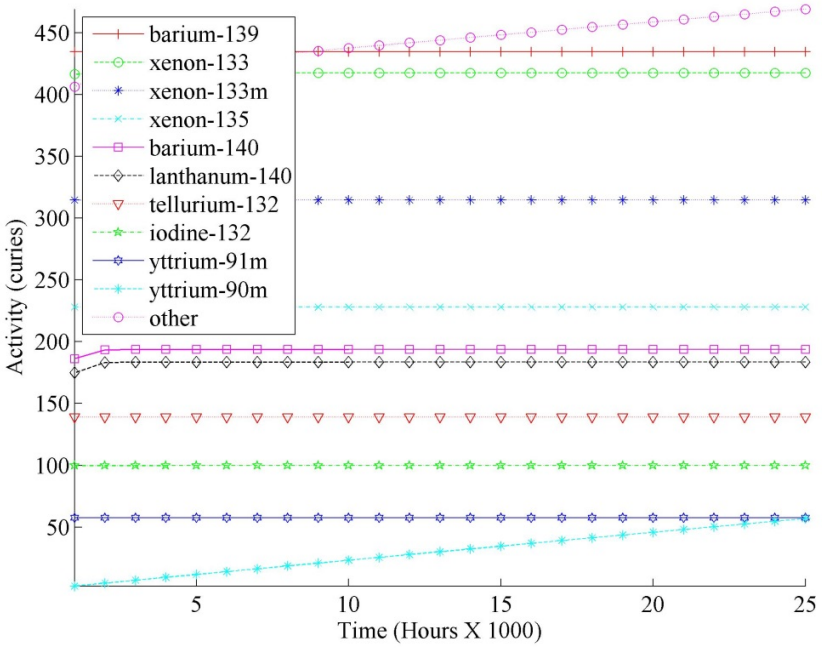

Figure B.1-33: Top Ten Activity Accum. Nuclides in PC Hot Side - Case 6 .2 Plateout Fraction

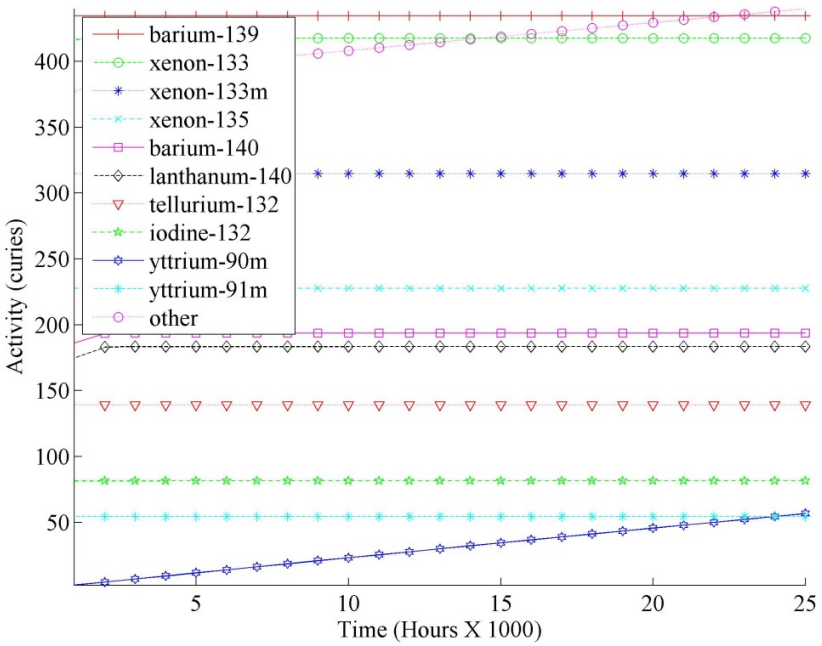

Figure B.1-34: Top Ten Activity Accum. Nuclides in PC Hot Side - Case 6 .3 Plateout Fraction

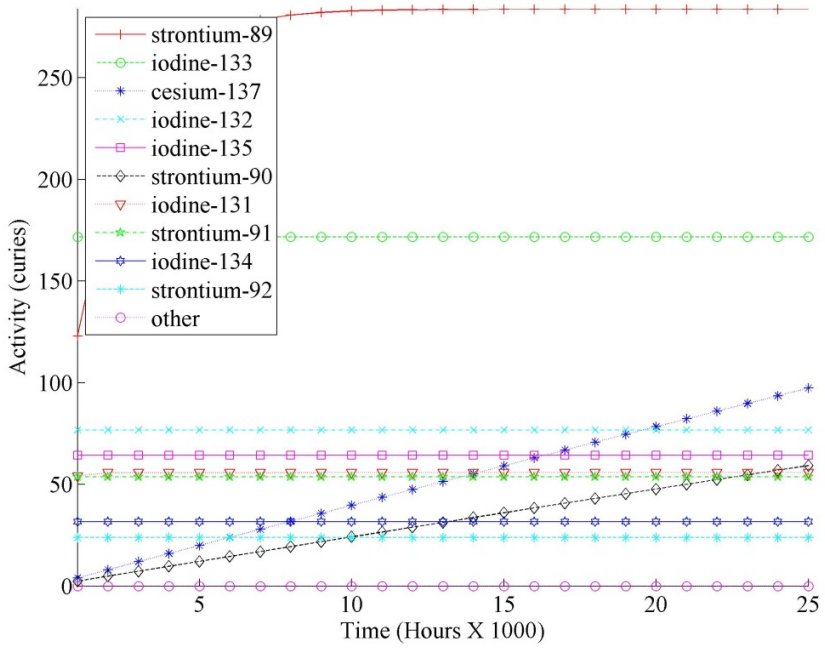

Figure B.1-35: Top Ten Activity Accum. Nuclides Plated Out in PC Cold Side - Case 6 .2 Plateout Fraction

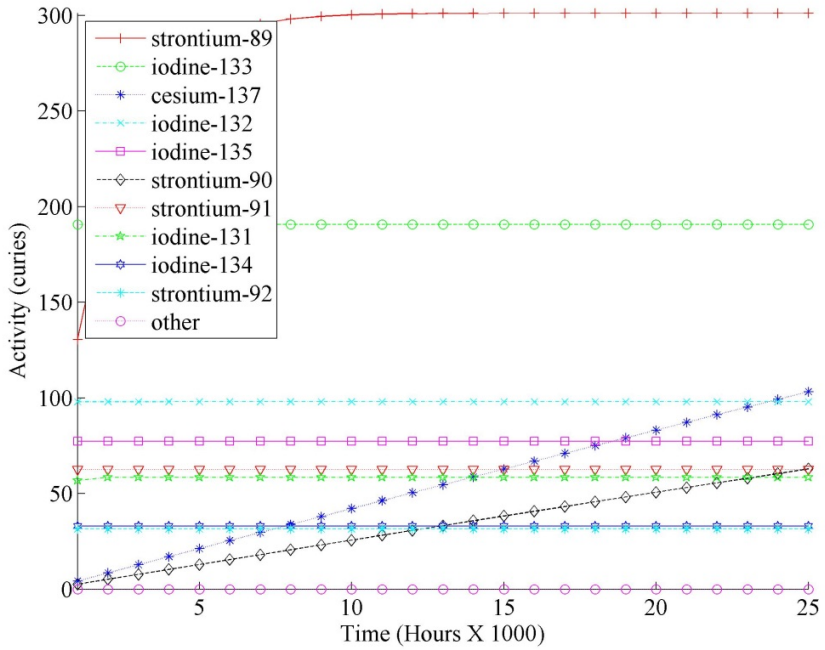

Figure B.1-36: Top Ten Activity Accum. Nuclides Plated Out in PC Cold Side - Case 6 .3 Plateout Fraction

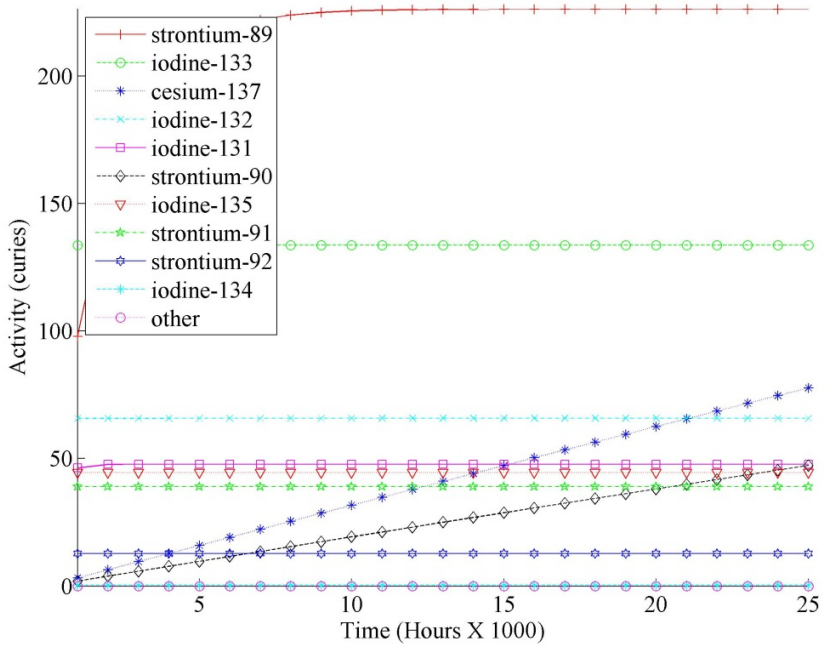

Figure B.1-37: Top Ten Activity Accum. Nuclides Plated Out in PC Hot Side - Case 6 .2 Plateout Fraction

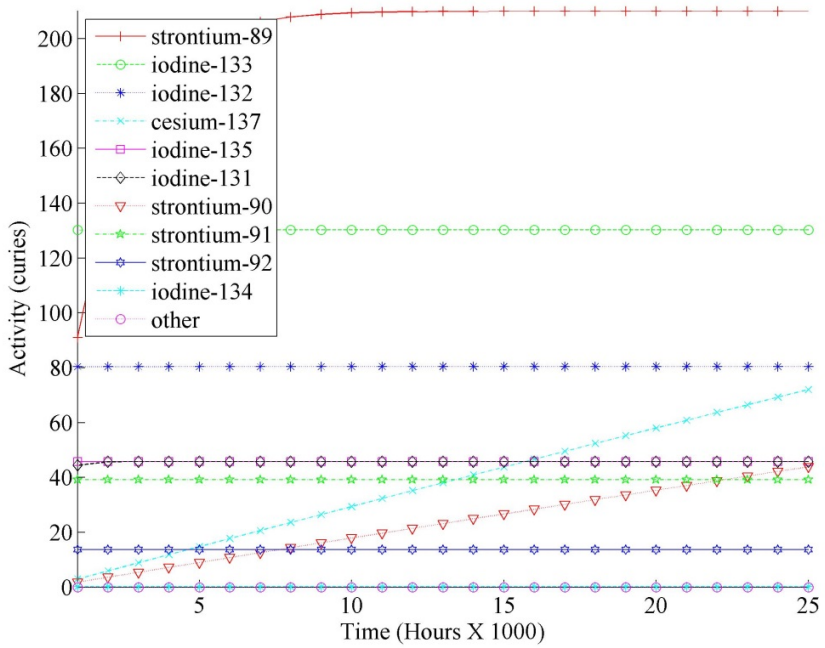

Figure B.1-38: Top Ten Activity Accum. Nuclides Plated Out in PC Hot Side - Case 6 .3 Plateout Fraction

g. Case 7: Influences of Fuel Release Fraction

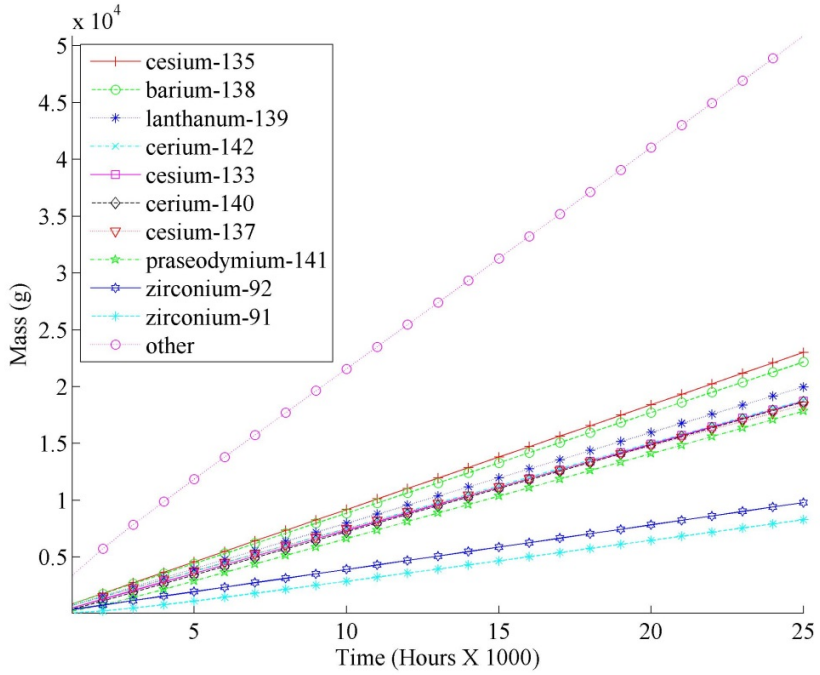

Figure B.1-39: Top Ten Mass Accum. Nuclides in First Fission Product Trap - Case 7

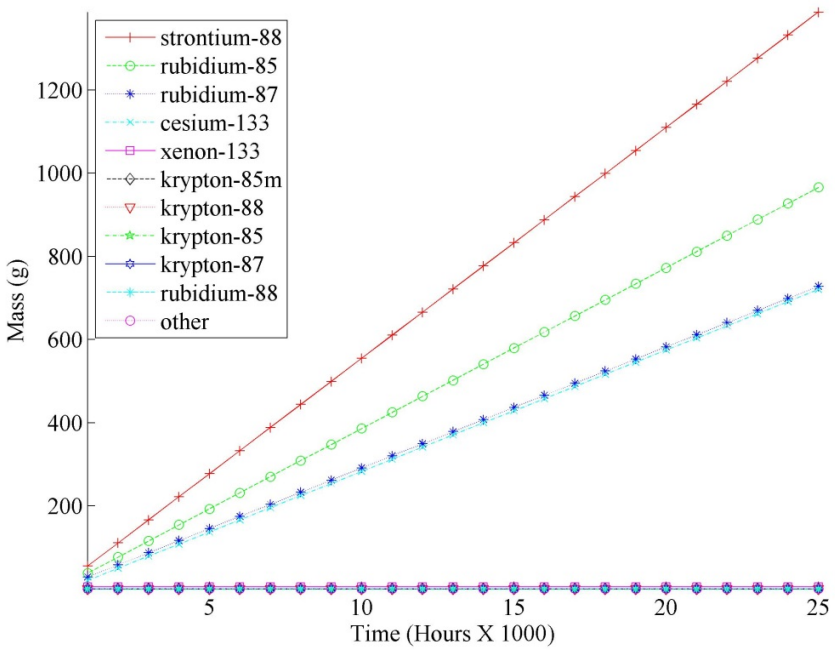

Figure B.1-40: Top Ten Mass Accum. Nuclides in Second Fission Product Trap - Case 7

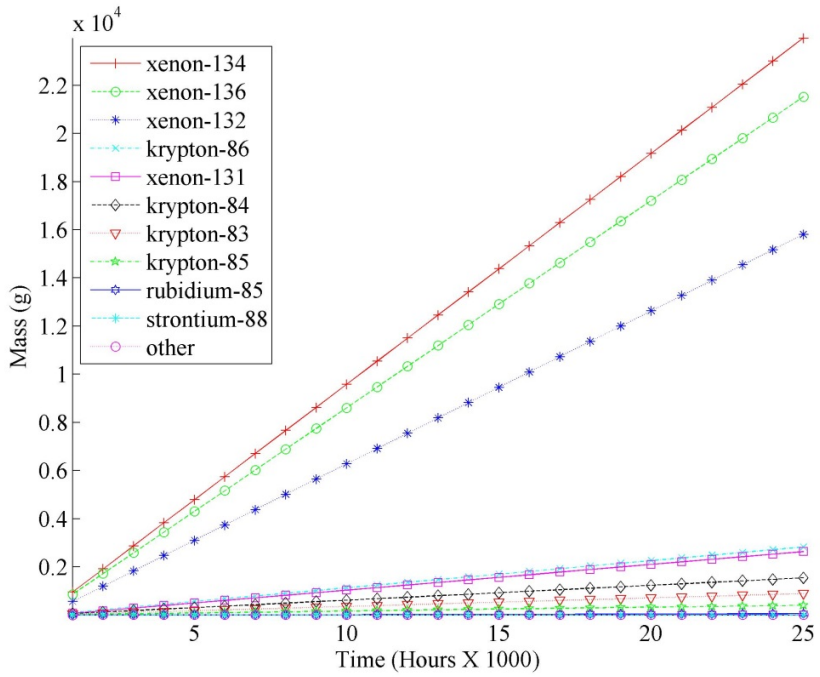

Figure B.1-41: Top Ten Mass Accum. Nuclides in Third Fission Product Trap - Case 7

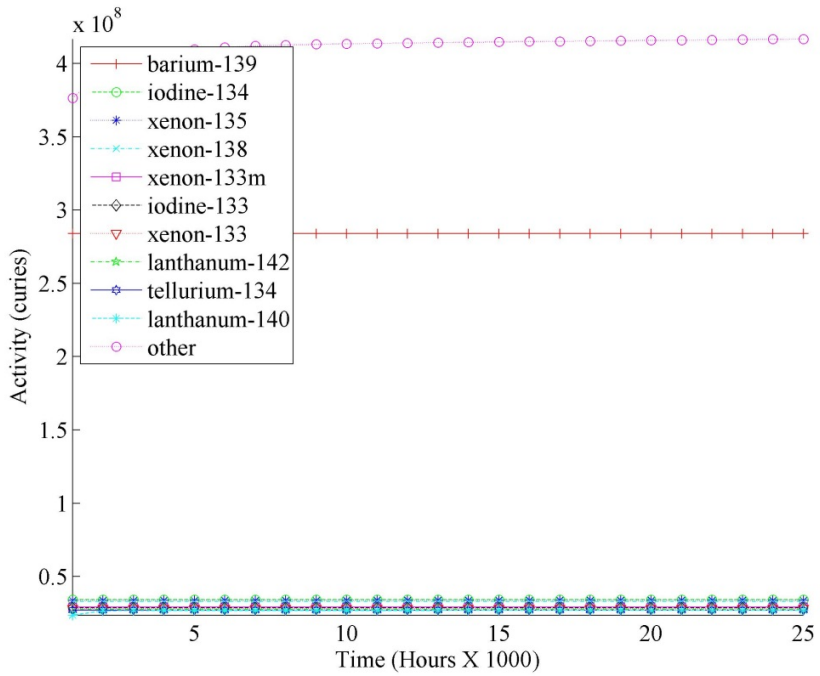

Figure B.1-42: Top Ten Activity Accum. Nuclides in First Fission Product Trap - Case 7

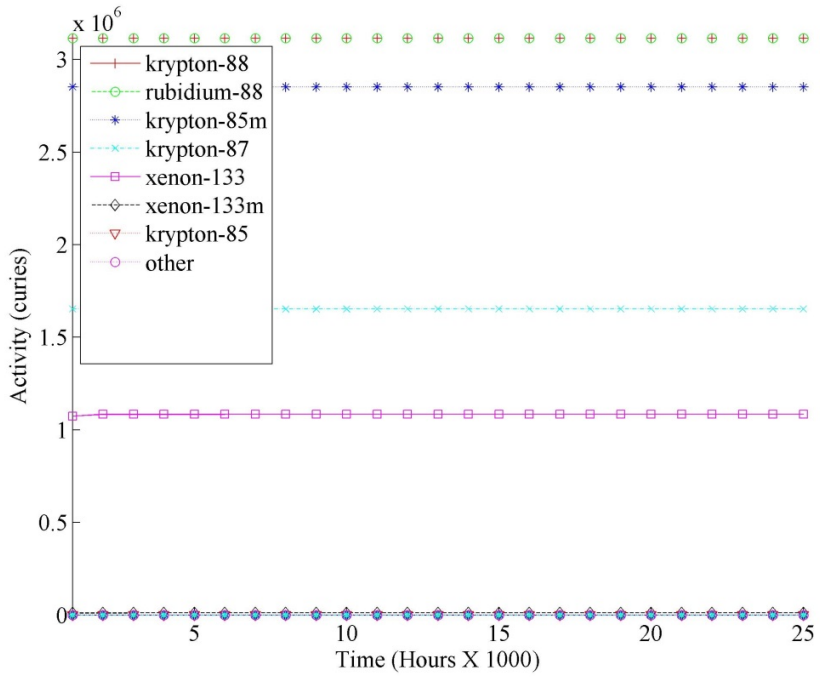

Figure B.1-43: Top Ten Activity Accum. Nuclides in Second Fission Product Trap - Case 7

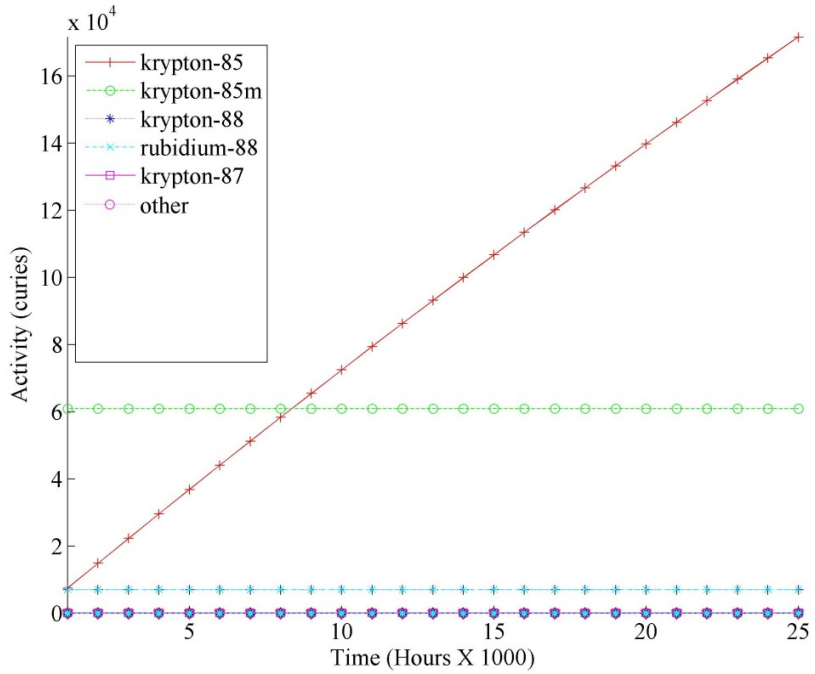

Figure B.1-44: Top Ten Activity Accum. Nuclides in Third Fission Product Trap - Case 7

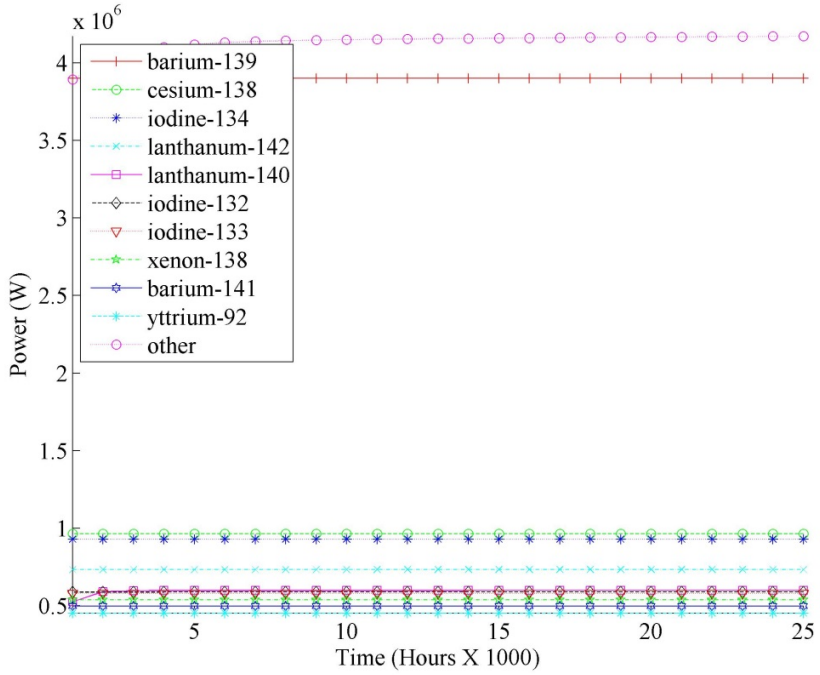

Figure B.1-45: Top Ten Power Generating Nuclides in First Fission Product Trap - Case 7

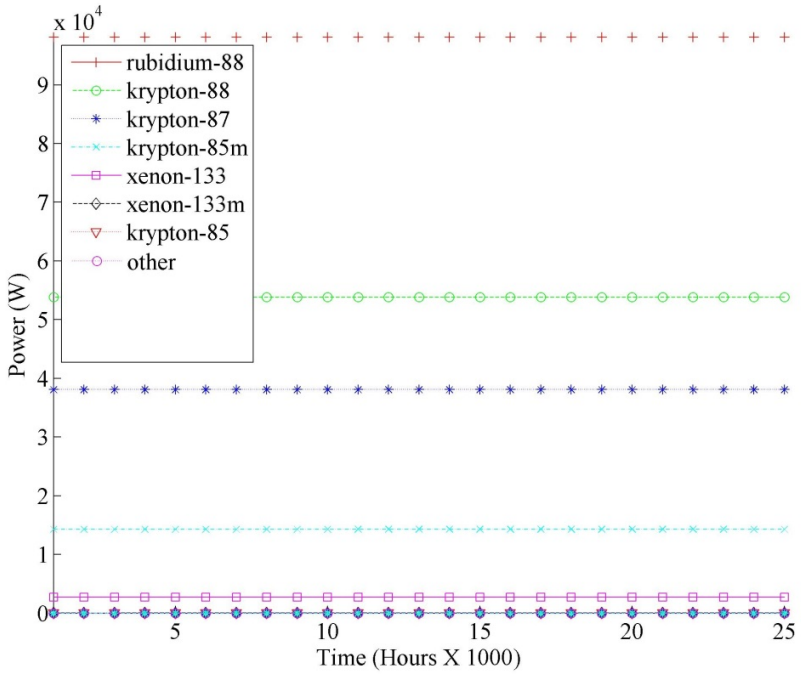

Figure B.1-46: Top Ten Power Generating Nuclides in Second Fission Product Trap - Case 7

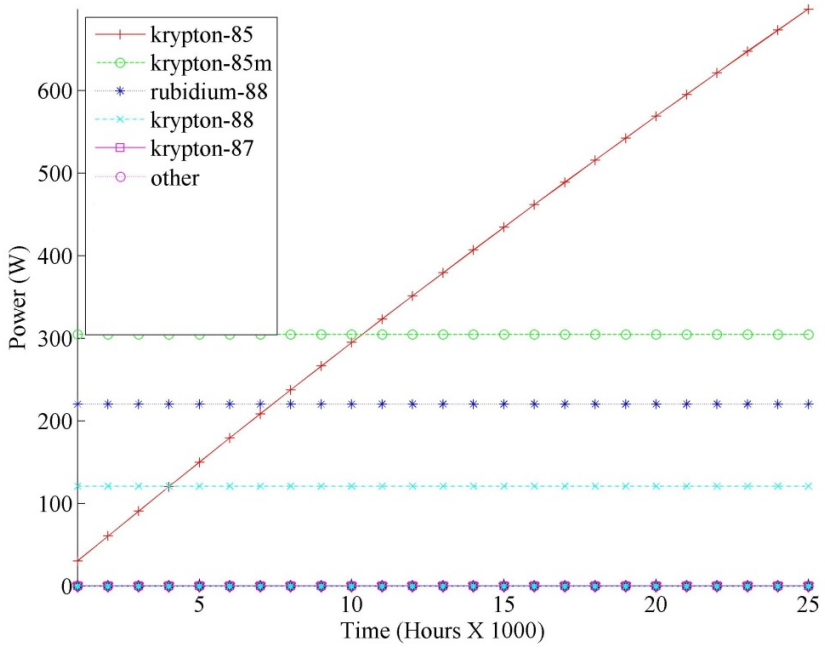

Figure B.1-47: Top Ten Power Generating Nuclides in Third Fission Product Trap - Case 7

a. Decays:

Most of the decays which are found in the STELLA model are what I will call ordinary decays. These ordinary decays work through the definition of radioactive decay, A=lambda*N. The best way to test these is by filling the previous reservoir (N) and letting it decay over time:

- CC Trapping
    - Initial
        - decay constant = .00693 inverse hours
        - length of simulation = 100 hours
        - dt = 1 hour
        - CC trapped = 100
    - Final
        - CC trapped = 49.89
        - CC trapped decayed = 50.11

- FFPT Trapping
    - Initial
        - decay constant = .00693 inverse hours
        - length of simulation = 100 hours
        - dt = 1 hour
        - FFPT Trapped = 100
    - Final
        - FFPT Trapped = 49.89
        - FFPT Trapped Decayed = 50.11

- MS Sieving
    - Initial
        - decay constant = .00693 inverse hours
        - length of simulation = 100 hours
        - dt = 1 hour
        - MS Sieved = 100
    - Final
        - MS Sieved = 49.89
        - MS Sieved Decayed = 50.11

- SFPT Trapping
    - Initial
        - decay constant = .00693 inverse hours
        - length of simulation = 100 hours
        - dt = 1 hour
        - SFPT Trapped = 100

- Final
    - SFPT Trapped = 49.89
    - SFPT Trapped Decayed = 50.11

- PCHS Decaying
    - Initial
        - decay constant = .00693 inverse hours
        - length of simulation = 100 hours
        - dt = 1 hour
        - Primary Coolant Hot Side = 100
        - To PCCS Switch = 0
    - Final
        - Primary Coolant Hot Side = 49.89
        - PCHS Decayed = 50.11

- PCHS Plateout Decaying
    - Initial
        - decay constant = .00693 inverse hours
        - length of simulation = 100 hours
        - dt = 1 hour
        - PCHS Plated Out = 100
    - Final
        - PCHS Plated Out = 49.89
        - PCHS Plated Out Decayed = 50.11

- PCCS Decaying
    - Initial
        - decay constant = .00693 inverse hours
        - length of simulation = 100 hours
        - dt = 1 hour
        - Primary Coolant Cold Side = 100
        - To PCHS Valve = 0
    - Final
        - Primary Coolant Cold Side = 49.89
        - PCCS Decayed = 50.11

- PCCS Plateout Decaying
    - Initial
        - decay constant = .00693 inverse hours
        - length of simulation = 100 hours
        - dt = 1 hour
        - PCCS Plated Out = 100
    - Final
        - PCCS Plated Out = 49.89

- PCCS Plated Out Decayed = 50.11

- ICPS Plateout Decaying
    - Initial
        - decay constant = .00693 inverse hours
        - length of simulation = 100 hours
        - dt = 1 hour
        - ICPS Plated Out = 100
    - Final
        - ICPS Plated Out = 49.89
        - ICPS Plated Out Decayed = 50.11

Fuel Decay is unique because it depends on the nuclide generation rate and the fuel release rate to determine the fuel decay rate. The fuel release rate must be set to 0 to cause all generated nuclides to decay. If we use a fission rate of 1 fission per hour and run the program for 100 hours, then the amount decayed should be 100 atoms.

- Fuel Decaying
    - Initial
        - length of simulation = 100 hours
        - dt = 1 hour
        - Fission Rate = 1 fission per hour
        - Design Yield Fraction = 1 atom per fission
    - Final
        - Fuel Decayed = 100

The delay beds (FFPT Delayed Decayed and SFPT Delayed Decayed) are also unique in that they calculate the amount of fission product decayed based on the input delay time. Since they depend upon the flow rates, fission products must be released from the fuel and travel to the delay beds where they are stopped. If the delay bed is set to delay the atoms for 100 hours and the valve to the next component is shut off, the half should decay, and half should build up in the specified delay section.

- FFPT Decaying
    - Initial
        - length of simulation = 100 hours
        - dt = 1 hour
        - Fission Rate = 1 fission per hour
        - Design Yield Fraction = 1 atom per fission
        - Fuel Release Fraction = 1
        - Decay Constant = .00693
        - To MS Valve = 0
        - FFPT Delay Time = 100 hours
    - Final

- FFPT Delay = 49.51
- FFPT Delayed Decayed = 49.49

- SFPT Decaying
  - Initial
    - length of simulation = 100 hours
    - dt = 1 hour
    - Fission Rate = 1 fission per hour
    - Design Yield Fraction = 1 atom per fission
    - Fuel Release Fraction = 1
    - Decay Constant = .00693
    - To Primary Coolant = 0
    - SFPT Delay Time = 100 hours
  - Final
    - SFPT Delay = 49.01
    - SFPT Delayed Decayed = 48.99

b. Plateouts, Traps, and Leakages:

Most of the plateout and trap rates within the STELLA model are modeled by the product of the input flow rate and the plateout or trap fraction. In order to test for their proper operation, a flow must be present in the system. To test each plateout and trap rate, a flow will travel to the desired component and fraction will be tested.

- ICPS Plated Out
  - Initial
    - length of simulation = 100 hours
    - dt = 1 hour
    - Fission Rate = 1 fission per hour
    - Design Yield Fraction = 1 atom per fission
    - Fuel Release Fraction = 1
    - Decay Constant = .00693
    - To Fission Product Removal Valve = 0
    - ICPS Plateout Fraction = .5
  - Final
    - In Core Purge Stream = 50.50
    - ICPS Plated Out = 49.50

- ICPS Leaking
  - Initial
    - length of simulation = 100 hours
    - dt = 1 hour
    - Fission Rate = 1 fission per hour

- Design Yield Fraction = 1 atom per fission
- Fuel Release Fraction = 1
- Decay Constant = .00693
- To Fission Product Removal Valve = 0
- ICPS Leakage Fraction = .5
- To PCHS Valve = 0
- To Fission Product Removal Valve = 0

- Final
  - In Core Purge Stream = 50.50
  - Primary Coolant Cold Side = 49.50

- FFPT Trapped
  - Initial
    - length of simulation = 100 hours
    - dt = 1 hour
    - Fission Rate = 1 fission per hour
    - Design Yield Fraction = 1 atom per fission
    - Fuel Release Fraction = 1
    - To FFPT Delay Valve = 0
    - FFPT Trapping Fraction = .5
  - Final
    - First FP Trap = 49.50
    - FFPT Trapped = 49.50
    - In Core Purge Stream = 1.00

- MS Sieved
  - Initial
    - length of simulation = 100 hours
    - dt = 1 hour
    - Fission Rate = 1 fission per hour
    - Design Yield Fraction = 1 atom per fission
    - Fuel Release Fraction = 1
    - To SFPT Valve = 0
    - MS Sieving Fraction = .5
  - Final
    - Molecular Sieve = 50.00
    - MS Sieved = 49.00
    - In Core Purge Stream = 1.00

- SFPT Trapped
  - Initial
    - length of simulation = 100 hours
    - dt = 1 hour

- Fission Rate = 1 fission per hour
- Design Yield Fraction = 1 atom per fission
- Fuel Release Fraction = 1
- To SFPT Delay Valve = 0
- SFPT Trapping Fraction = .5

- Final
  - SFPT Trapped = 49.00
  - Second FP Trap = 49.00
  - Molecular Sieve = 1.00
  - In Core Purge Stream = 1.00

Flows leaving the Primary Coolant are modeled differently than flows in other parts of the system. The reason for this is mainly for preventing circular logic from occurring in the system due to the dependence most flows on their inlet. Additionally, it allows flows to continue in the system even when there are no fission products being produced in the reactor core. To test flows connected directly to the primary coolant, it will be loaded with an initial value, then allowed to move in the system.

Because of the modeling methodology in the primary coolant, the plateout fraction will incur every time step (equivalent to a pass. To insure this is the case, the length of the simulation will only be 2 time steps.

- PCHS Plated Out
  - Initial
    - length of simulation = 2 hours
    - dt = 1 hour
    - To PCCS Valve = 0
    - Primary Coolant Hot Side = 100
    - PCHS Plateout Fraction per pass= .5
  - Final
    - Primary Coolant Hot Side = 25.00
    - PCHS Plated Out = 75.00

- PCCS Plated Out
  - Initial
    - length of simulation = 2 hours
    - dt = 1 hour
    - To PCHS Valve = 0
    - Primary Coolant Cold Side = 100
    - PCCS Plateout Fraction per pass= .5
  - Final
    - Primary Coolant Cold Side = 25.00
    - PCCS Plated Out = 75.00

Since the Primary Coolant should work on a "per pass" basis, a test should be done to insure that this is the case. After 1000 hours, all of the atoms should be plated out approximately the same on each side with a "per pass" fraction of .005.

- PCHS and PCCS Plated Out
    - Initial
        - length of simulation = 1000 hours
        - dt = 1 hour
        - Primary Coolant Hot Side = 100
        - PCHS Plateout Fraction per pass= .005
        - PCCS Plateout Fraction per pass= .005
    - Final
        - Primary Coolant Hot Side = .67
        - PCHS Plated Out = 49.79
        - PCCS Plated Out = 49.54

Finally, the flows leaving the Primary Coolant can be tested

- ICPS Intake Rate
    - Initial
        - length of simulation = 1 hours
        - dt = 1 hour
        - Primary Coolant Cold Side = 100
        - ICPS Intake Fraction = 1
        - To PCHS Valve = 0
    - Final
        - In Core Purge Stream = 100

- CC Trapping Fraction
    - Initial
        - length of simulation = 1 hours
        - dt = 1 hour
        - Primary Coolant Hot Side = 100
        - CC Intake Fraction = 1
        - CC Trapping Fraction = .5
        - To FFPT Valve = 0
    - Final
        - Chemical Cleanup = 50.0
        - CC Trapped = 50.0

c. <u>Rates adjusted to account for Precursor Decay Rate:</u>

Fuel Decay Rate 2 - changed

Fuel Release Rate 2 - changed

ICPS Leaving Rate 2 - changed
ICPS Plateout Rate 2 - changed
ICPS Leakage Rate 2 - changed

FFPT Leaving Rate 2 - changed
FFPT Trapping Rate 2 - changed

MS Leaving Rate 2 - changed
MS Sieving Rate 2 - changed

SFPT Leaving Rate 2 - changed
SFPT Trapping Rate 2 - changed

CC Leaving Rate 2 - changed
CC Trapping Rate 2- changed

Now that units have checked out, It is time to begin testing. All of the rated changed above need to be retested for the second nuclide system.

For the fuel precursor, decay is dependent upon the fuel release fraction. If that is set to 0, all incoming precursors should decay directly to fuel.

- Fuel Precursor Decaying 2
    - Initial
        - length of simulation = 100 hours
        - dt = 1 hour
        - Fission Rate = 1 fission per hour
        - Design Yield Fraction = 1 atom per fission
    - Final
        - Fuel Decayed = 100
        - Fuel Decayed 2 = 100

To test the non-fuel rates listed above, a decay rate and a flow will be used. This will test the flow due to decay and the flow from the previous component simultaneously.

- ICPS Plateout Rate 2 ***test 1***
    - Initial
        - length of simulation = 100 hours
        - dt = 1 hour
        - Decay Constant 1 = .693 inverse hours
        - Fission Rate 2 = 1 fission per hour
        - Design Yield Fraction 2 = 1 atom per fission

- Fuel Release Fraction 2 = 1
- To Fission Product Removal Valve 2 = 0
- ICPS Plateout Fraction 2 = .5
- ICPS Plated Out = 100

- Final
  - ICPS Plated Out 2 = 64.85
  - ICPS Plated Out Decayed = 100
  - In Core Purge Stream 2 = 135.15

*****So what we see here is an error created due to the short half-life of the precursor (1 hr) and the length of dt (1hr). Investigation of the integration methods provided in STELLA proved that use of the Runge-Kutta 4 integration method yielded the best results. From here out it will be the prefered method of integration. Additionally, increasing the half-life to a ratio half-life to dt of 10 to 1 proved to remove any additional significant error*****

- ICPS Plateout Rate 2 ***test 2***
  - Initial
    - length of simulation = 100 hours
    - dt = 1 hour
    - Decay Constant 1 = .0693 inverse hours
    - Fission Rate 2 = 1 fission per hour
    - Design Yield Fraction 2 = 1 atom per fission
    - Fuel Release Fraction 2 = 1
    - To Fission Product Removal Valve 2 = 0
    - ICPS Plateout Fraction 2 = .5
    - ICPS Plated Out = 100
  - Final
    - ICPS Plated Out = .1
    - ICPS Plated Out 2 = 98.65
    - ICPS Plated Out Decayed = 99.9
    - In Core Purge Stream 2 = 101.25

- FFPT Trapping Rate 2
  - Initial
    - length of simulation = 100 hours
    - dt = 1 hour
    - Decay Constant 1 = .0693 inverse hours
    - Fission Rate 2 = 1 fission per hour
    - Design Yield Fraction 2 = 1 atom per fission
    - Fuel Release Fraction 2 = 1
    - To FFPT Delay Valve 2 = 0
    - FFPT Trapping Fraction 2 = .5
    - FFPT Trapped = 100

- Final
    - FFPT Trapped = .1
    - FFPT Trapped 2 = 98.5
    - FFPT Trapped Decayed = 99.9
    - First FP Trap = 100.4

- MS Sieving Rate 2
    - Initial
        - length of simulation = 100 hours
        - dt = 1 hour
        - Decay Constant 1 = .0693 inverse hours
        - Fission Rate 2 = 1 fission per hour
        - Design Yield Fraction 2 = 1 atom per fission
        - Fuel Release Fraction 2 = 1
        - To SFPT Valve 2 = 0
        - MS Sieving Fraction 2 = .5
        - MS Sieved 2 = 100
    - Final
        - In Core Purge Stream 2 = 1
        - Molecular Sieve 2 = 97.95
        - MS Sieved = .1
        - MS Sieved 2 = 99.95
        - MS Sieved Decayed = 99.9

- SFPT Trapping Rate 2
    - Initial
        - length of simulation = 100 hours
        - dt = 1 hour
        - Decay Constant 1 = .0693 inverse hours
        - Fission Rate 2 = 1 fission per hour
        - Design Yield Fraction 2 = 1 atom per fission
        - Fuel Release Fraction 2 = 1
        - To SFPT Delay Valve 2 = 0
        - SFPT Trapping Fraction 2 = .5
        - SFPT Trapped = 100
    - Final
        - First FP Trap 2 = 1
        - In Core Purge Stream 2 = 1
        - Second FP Trap 2 = 97.95
        - SFPT Trapped = .1
        - SFPT Trapped 2 = 99.95
        - SFPT Trapped Decayed = 99.9

- CC Trapping Rate 2

- Initial
    - length of simulation = 100 hours
    - dt = 1 hour
    - Decay Constant 1 = .0693 inverse hours
    - Fission Rate 2 = 1 fission per hour
    - Design Yield Fraction 2 = 1 atom per fission
    - Fuel Release Fraction 2 = 1
    - To FFPT Valve 2 = 0
    - CC Trapping Fraction 2 = .5
    - CC Trapped = 100
    - CC Intake Fraction 2 = 1
- Final
    - CC Trapped = .1
    - CC Trapped 2 = 98.45
    - CC Trapped Decayed = 99.9
    - Chemical Cleanup 2 = 98.45
    - First FP Trap 2 = 1
    - In Core Purge Stream 2 = 1
    - Primary Coolant Hot Side 2 = 1

STELLA R/B curve Comparisons

The following tables show results from different R/B models, as described in Section 3.3. The three models are the Peach Bottom (PB), MHTGR at Beginning of Life (BOL), and MHTGR at EOL (EOL).

Table B.1.: Mass accumulation (g) in the fission product traps.

	Hot Fission Product Trap			**Cold Fission Product Trap**			**Plateout/Condensation**		
	PB	*MHTGR*		*PB*	*MHTGR*		*PB*	*MHTGR*	
Nuclide		BOL	EOL		BOL	EOL		BOL	EOL
selenium-80	258	258	258	–	–	–	–	–	–
bromine-81	360	360	360	–	–	–	–	–	–
selenium-82	550	550	550	–	–	–	–	–	–
krypton-83	–	–	–	890	890	890	–	–	–
krypton-84	–	–	–	1,545	1,545	1,545	–	–	–
krypton-85m	–	–	–	$3 \cdot 10^{-2}$	$3 \cdot 10^{-2}$	$6 \cdot 10^{-3}$	–	–	–
krypton-85	–	–	–	332	225	199	–	–	–
rubidium-85	1,570	1,673	1,776	109	112	36	–	–	–
krypton-86	–	–	–	2,828	2,828	2,828	–	–	–
krypton-87	–	–	–	$9 \cdot 10^{-3}$	$2 \cdot 10^{-2}$	$3 \cdot 10^{-3}$	–	–	–
rubidium-87	3,636	3,542	3,716	116	210	36	–	–	–
krypton-88	–	–	–	$2 \cdot 10^{-2}$	$3 \cdot 10^{-2}$	$5 \cdot 10^{-3}$	–	–	–
rubidium-88	$9 \cdot 10^{-4}$	$3 \cdot 10^{-3}$	$5 \cdot 10^{-4}$	$2 \cdot 10^{-3}$	$3 \cdot 10^{-3}$	$5 \cdot 10^{-4}$	–	–	–
strontium-88	2,592	2,564	2,672	121	165	30	282	267	293
rubidium-89	$2 \cdot 10^{-3}$	$5 \cdot 10^{-3}$	$8 \cdot 10^{-4}$	–	–	–	–	–	–
strontium-89	135	68	29	–	–	–	14	5	3
yttrium-89	1,979	958	427	–	–	–	–	–	–
strontium-90	6,405	5,932	5,603	–	–	–	712	659	623
yttrium-90m	$9 \cdot 10^{-2}$	$8 \cdot 10^{-2}$	$8 \cdot 10^{-2}$	–	–	–	–	–	–
yttrium-90	2	2	2	–	–	–	–	–	–
zirconium-90	245	227	214	–	–	–	–	–	–
strontium-91	$3 \cdot 10^{-1}$	$3 \cdot 10^{-1}$	$6 \cdot 10^{-2}$	–	–	–	$3 \cdot 10^{-2}$	$3 \cdot 10^{-2}$	$6 \cdot 10^{-3}$
yttrium-91m	$3 \cdot 10^{-2}$	$3 \cdot 10^{-2}$	$5 \cdot 10^{-3}$	–	–	–	–	–	–
yttrium-91	48	44	9	–	–	–	–	–	–
zirconium-91	537	490	105	–	–	–	–	–	–
strontium-92	$5 \cdot 10^{-2}$	$8 \cdot 10^{-2}$	$1 \cdot 10^{-2}$	–	–	–	$6 \cdot 10^{-3}$	$8 \cdot 10^{-3}$	$2 \cdot 10^{-3}$
yttrium-92	$8 \cdot 10^{-2}$	$1 \cdot 10^{-1}$	$2 \cdot 10^{-2}$	–	–	–	–	–	–
zirconium-92	397	557	101	–	–	–	–	–	–
cadmium-111	534	534	534	–	–	–	–	–	–
tellurium-126	552	552	552	–	–	–	–	–	–
tellurium-127m	11	2	1	–	–	–	–	–	–
tellurium-127	$4 \cdot 10^{-2}$	$1 \cdot 10^{-2}$	$5 \cdot 10^{-3}$	–	–	–	–	–	–
iodine-127	175	178	177	–	–	–	11	17	19
tellurium-128	2,130	2,130	2,130	–	–	–	–	–	–
tellurium-129m	8	2	$6 \cdot 10^{-1}$	–	–	–	–	–	–
tellurium-129	$7 \cdot 10^{-3}$	$3 \cdot 10^{-3}$	$8 \cdot 10^{-4}$	–	–	–	–	–	–
iodine-129	540	535	532	–	–	–	42	53	57
tellurium-130	6,640	6,640	6,640	–	–	–	–	–	–
tellurium-131m	$4 \cdot 10^{-1}$	$2 \cdot 10^{-1}$	$4 \cdot 10^{-2}$	–	–	–	–	–	–
tellurium-131	$2 \cdot 10^{-3}$	$2 \cdot 10^{-3}$	$3 \cdot 10^{-4}$	–	–	–	–	–	–
iodine-131	7	3	$8 \cdot 10^{-1}$	–	–	–	$5 \cdot 10^{-1}$	$2 \cdot 10^{-1}$	$5 \cdot 10^{-2}$
xenon-131	–	–	–	2,661	2,665	2,668	–	–	–
tellurium-132	9	4	$9 \cdot 10^{-1}$	–	–	–	–	–	–
iodine-132	$3 \cdot 10^{-1}$	$2 \cdot 10^{-1}$	$4 \cdot 10^{-2}$	–	–	–	$7 \cdot 10^{-3}$	$1 \cdot 10^{-2}$	$2 \cdot 10^{-3}$
xenon-132	–	–	–	15,871	15,877	15,880	–	–	–
tellurium-133m	$2 \cdot 10^{-2}$	$3 \cdot 10^{-2}$	$5 \cdot 10^{-3}$	–	–	–	–	–	–
tellurium-133	$2 \cdot 10^{-3}$	$5 \cdot 10^{-3}$	$8 \cdot 10^{-4}$	–	–	–	–	–	–
iodine-133	2	2	$4 \cdot 10^{-1}$	–	–	–	$2 \cdot 10^{-1}$	$1 \cdot 10^{-1}$	$2 \cdot 10^{-2}$

Table B.1.: Mass accumulation (g) in the fission product traps.

Nuclide	**Hot Fission Product Trap**			**Cold Fission Product Trap**			**Plateout/Condensation**		
	PB	*MHTGR*		*PB*	*MHTGR*		*PB*	*MHTGR*	
		BOL	EOL		BOL	EOL		BOL	EOL
xenon-133m	–	–	–	12	9	2	–	–	–
xenon-133	–	–	–	47	29	6	–	–	–
cesium-133	11,546	13,723	16,582	6,370	3,991	823	1,283	1,525	1,842
tellurium-134	$2 \cdot 10^{-2}$	$4 \cdot 10^{-2}$	$6 \cdot 10^{-3}$	–	–	–	–	–	–
iodine-134	$5 \cdot 10^{-2}$	$1 \cdot 10^{-1}$	$2 \cdot 10^{-2}$	–	–	–	$3 \cdot 10^{-3}$	$6 \cdot 10^{-3}$	$1 \cdot 10^{-3}$
xenon-134	–	–	–	23,966	23,965	23,966	–	–	–
iodine-135	$4 \cdot 10^{-1}$	$4 \cdot 10^{-1}$	$6 \cdot 10^{-2}$	–	–	–	$4 \cdot 10^{-2}$	$4 \cdot 10^{-2}$	$7 \cdot 10^{-3}$
xenon-135m	–	–	–	$4 \cdot 10^{-3}$	$7 \cdot 10^{-3}$	$1 \cdot 10^{-3}$	–	–	–
xenon-135	–	–	–	1	1	$2 \cdot 10^{-1}$	–	–	–
cesium-135	18,384	18,394	20,341	2,614	2,603	442	2,043	2,044	2,260
xenon-136	–	–	–	21,521	21,521	21,521	–	–	–
cesium-137	16,728	15,754	14,900	–	–	–	1,859	1,750	1,655
barium-137	2,519	3,601	4,551	–	–	–	–	–	–
xenon-138	–	–	–	$3 \cdot 10^{-3}$	$1 \cdot 10^{-2}$	$2 \cdot 10^{-3}$	–	–	–
cesium-138	$1 \cdot 10^{-2}$	$5 \cdot 10^{-2}$	$5 \cdot 10^{-3}$	$1 \cdot 10^{-2}$	$4 \cdot 10^{-2}$	$5 \cdot 10^{-3}$	$1 \cdot 10^{-3}$	$6 \cdot 10^{-3}$	$6 \cdot 10^{-4}$
barium-138	20,963	35,341	20,729	295	986	146	–	–	–
barium-139	$5 \cdot 10^{-1}$	$1 \cdot 10^{0}$	$2 \cdot 10^{-1}$	–	–	–	–	–	–
lanthanum-139	641	1,201	272	–	–	–	–	–	–
barium-140	70	27	12	–	–	–	–	–	–
lanthanum-140	9	4	2	–	–	–	–	–	–
cerium-140	3,891	1,523	656	–	–	–	–	–	–
barium-141	$6 \cdot 10^{-3}$	$2 \cdot 10^{-2}$	$3 \cdot 10^{-3}$	–	–	–	–	–	–
lanthanum-141	$8 \cdot 10^{-2}$	$2 \cdot 10^{-1}$	$4 \cdot 10^{-2}$	–	–	–	–	–	–
cerium-141	15	46	7	–	–	–	–	–	–
praseodymium-141	321	985	155	–	–	–	–	–	–
barium-142	$2 \cdot 10^{-3}$	$9 \cdot 10^{-3}$	$1 \cdot 10^{-3}$	–	–	–	–	–	–
lanthanum-142	$3 \cdot 10^{-2}$	$1 \cdot 10^{-1}$	$1 \cdot 10^{-2}$	–	–	–	–	–	–
cerium-142	274	1,033	159	–	–	–	–	–	–
samarium-147	7,305	7,305	7,305	–	–	–	–	–	–
samarium-149	4,084	4,084	4,084	–	–	–	–	–	–
samarium-151	2,090	2,149	2,149	–	–	–	–	–	–
europium-151	83	24	24	–	–	–	–	–	–
samarium-152	1,639	1,639	1,639	–	–	–	–	–	–
samarium-153	$3 \cdot 10^{-1}$	$2 \cdot 10^{-1}$	$5 \cdot 10^{-2}$	–	–	–	–	–	–
europium-153	1,090	1,090	1,090	–	–	–	–	–	–
samarium-154	629	629	629	–	–	–	–	–	–
europium-155	273	141	124	–	–	–	–	–	–
gadolinium-155	61	31	28	–	–	–	–	–	–
europium-156	2	$6 \cdot 10^{-1}$	$3 \cdot 10^{-1}$	–	–	–	–	–	–
gadolinium-156	71	27	12	–	–	–	–	–	–
sum	$1 \cdot 10^{5}$	$1 \cdot 10^{5}$	$1 \cdot 10^{5}$	79,298	77,622	71,016	6,246	6,320	6,753

Table B.2.: Power from each element (W) in the fission product traps.

	Hot Fission Product Trap			**Cold Fission Product Trap**			**Plateout/Condensation**		
	PB	*MHTGR*		*PB*	*MHTGR*		*PB*	*MHTGR*	
Nuclide		BOL	EOL		BOL	EOL		BOL	EOL
krypton-85m	–	–	–	1,146	1,337	258	–	–	–
krypton-85	–	–	–	577	392	345	–	–	–
krypton-87	–	–	–	6,067	10,978	1,873	–	–	–
krypton-88	–	–	–	4,690	6,388	1,171	–	–	–
rubidium-88	3,610	11,397	2,188	8,553	11,650	2,135	–	–	–
rubidium-89	6,485	21,267	3,317	–	–	–	–	–	–
strontium-89	37,938	18,965	8,250	–	–	–	3,976	1,322	794
strontium-90	3,122	2,891	2,731	–	–	–	347	321	303
yttrium-90m	4,332	4,012	3,790	–	–	–	–	–	–
yttrium-90	14,431	13,365	12,625	–	–	–	–	–	–
strontium-91	18,274	16,672	3,559	–	–	–	2,030	1,852	395
yttrium-91m	4,357	3,975	849	–	–	–	–	–	–
yttrium-91	11,702	10,677	2,279	–	–	–	–	–	–
strontium-92	8,689	12,191	2,215	–	–	–	965	1,355	246
yttrium-92	18,383	25,794	4,687	–	–	–	–	–	–
tellurium-127m	74	16	7	–	–	–	–	–	–
tellurium-127	527	165	55	–	–	–	–	–	–
tellurium-129m	986	246	82	–	–	–	–	–	–
tellurium-129	1,520	610	159	–	–	–	–	–	–
tellurium-131m	3,638	2,089	397	–	–	–	–	–	–
tellurium-131	1,319	1,585	262	–	–	–	–	–	–
iodine-131	6,371	3,185	688	–	–	–	447	157	41
tellurium-132	9,089	4,022	857	–	–	–	–	–	–
iodine-132	95,242	61,849	11,823	–	–	–	1,979	3,065	503
tellurium-133m	6,806	13,584	2,063	–	–	–	–	–	–
tellurium-133	3,771	11,578	1,732	–	–	–	–	–	–
iodine-133	55,619	58,374	9,877	–	–	–	4,803	3,090	586
xenon-133m	–	–	–	8,281	6,255	1,170	–	–	–
xenon-133	–	–	–	24,202	15,172	3,127	–	–	–
tellurium-134	6,120	13,567	2,046	–	–	–	–	–	–
iodine-134	40,705	85,098	13,125	–	–	–	2,513	4,999	786
iodine-135	23,585	23,128	3,820	–	–	–	2,621	2,570	424
xenon-135m	–	–	–	1,318	2,186	345	–	–	–
xenon-135	–	–	–	26,083	25,960	4,408	–	–	–
cesium-137	11,047	10,403	9,839	–	–	–	1,227	1,156	1,093
xenon-138	–	–	–	5,709	19,109	2,824	–	–	–
cesium-138	22,830	95,897	9,014	18,735	62,715	9,269	2,537	10,655	1,002
barium-139	$1 \cdot 10^5$	$2 \cdot 10^5$	53,193	–	–	–	–	–	–
barium-140	34,847	13,641	5,873	–	–	–	–	–	–
lanthanum-140	$1 \cdot 10^5$	48,903	21,055	–	–	–	–	–	–
barium-141	8,983	27,528	4,323	–	–	–	–	–	–
lanthanum-141	6,989	21,420	3,364	–	–	–	–	–	–
cerium-141	1,624	4,977	782	–	–	–	–	–	–
barium-142	4,010	15,095	2,324	–	–	–	–	–	–
lanthanum-142	10,715	40,336	6,209	–	–	–	–	–	–
samarium-151	27	28	28	–	–	–	–	–	–
samarium-153	758	437	124	–	–	–	–	–	–
europium-155	216	112	98	–	–	–	–	–	–
europium-156	1,330	508	227	–	–	–	–	–	–
sum	$7 \cdot 10^5$	$9 \cdot 10^5$	$2 \cdot 10^5$	$1 \cdot 10^5$	$2 \cdot 10^5$	26,925	23,445	30,542	6,174

Table B.3.: Isotope specific activities (Ci) in the fission product traps.

Nuclide	**Hot Fission Product Trap**			**Cold Fission Product Trap**			**Plateout/Condensation**		
	PB	*MHTGR*		*PB*	*MHTGR*		*PB*	*MHTGR*	
		BOL	EOL		BOL	EOL		BOL	EOL
krypton-85m	–	–	–	$2 \cdot 10^5$	$3 \cdot 10^5$	51,454	–	–	–
krypton-85	–	–	–	$1 \cdot 10^5$	96,245	84,742	–	–	–
krypton-87	–	–	–	$3 \cdot 10^5$	$5 \cdot 10^5$	81,276	–	–	–
krypton-88	–	–	–	$3 \cdot 10^5$	$4 \cdot 10^5$	67,784	–	–	–
rubidium-88	$1 \cdot 10^5$	$4 \cdot 10^5$	69,447	$3 \cdot 10^5$	$4 \cdot 10^5$	67,767	–	–	–
rubidium-89	$2 \cdot 10^5$	$8 \cdot 10^5$	$1 \cdot 10^5$	–	–	–	–	–	–
strontium-89	$4 \cdot 10^6$	$2 \cdot 10^6$	$9 \cdot 10^5$	–	–	–	$4 \cdot 10^5$	$1 \cdot 10^5$	89,609
strontium-90	$1 \cdot 10^6$	$9 \cdot 10^5$	$8 \cdot 10^5$	–	–	–	$1 \cdot 10^5$	99,258	93,764
yttrium-90m	$1 \cdot 10^6$	$1 \cdot 10^6$	$9 \cdot 10^5$	–	–	–	–	–	–
yttrium-90	$1 \cdot 10^6$	$1 \cdot 10^6$	$9 \cdot 10^5$	–	–	–	–	–	–
strontium-91	$1 \cdot 10^6$	$1 \cdot 10^6$	$2 \cdot 10^5$	–	–	–	$1 \cdot 10^5$	$1 \cdot 10^5$	24,718
yttrium-91m	$1 \cdot 10^6$	$1 \cdot 10^6$	$2 \cdot 10^5$	–	–	–	–	–	–
yttrium-91	$1 \cdot 10^6$	$1 \cdot 10^6$	$2 \cdot 10^5$	–	–	–	–	–	–
strontium-92	$8 \cdot 10^5$	$1 \cdot 10^6$	$2 \cdot 10^5$	–	–	–	85,227	$1 \cdot 10^5$	21,731
yttrium-92	$9 \cdot 10^5$	$1 \cdot 10^6$	$2 \cdot 10^5$	–	–	–	–	–	–
tellurium-127m	$1 \cdot 10^5$	25,122	10,851	–	–	–	–	–	–
tellurium-127	$1 \cdot 10^5$	39,862	13,309	–	–	–	–	–	–
tellurium-129m	$3 \cdot 10^5$	62,971	21,022	–	–	–	–	–	–
tellurium-129	$2 \cdot 10^5$	68,708	17,903	–	–	–	–	–	–
tellurium-131m	$3 \cdot 10^5$	$2 \cdot 10^5$	34,922	–	–	–	–	–	–
tellurium-131	99,630	$1 \cdot 10^5$	19,805	–	–	–	–	–	–
iodine-131	$9 \cdot 10^5$	$5 \cdot 10^5$	$1 \cdot 10^5$	–	–	–	66,194	23,258	6,111
tellurium-132	$3 \cdot 10^6$	$1 \cdot 10^6$	$3 \cdot 10^5$	–	–	–	–	–	–
iodine-132	$4 \cdot 10^6$	$2 \cdot 10^6$	$5 \cdot 10^5$	–	–	–	79,549	$1 \cdot 10^5$	20,205
tellurium-133m	$4 \cdot 10^5$	$8 \cdot 10^5$	$1 \cdot 10^5$	–	–	–	–	–	–
tellurium-133	$2 \cdot 10^5$	$7 \cdot 10^5$	$1 \cdot 10^5$	–	–	–	–	–	–
iodine-133	$3 \cdot 10^6$	$3 \cdot 10^6$	$5 \cdot 10^5$	–	–	–	$2 \cdot 10^5$	$2 \cdot 10^5$	29,036
xenon-133m	–	–	–	$6 \cdot 10^6$	$5 \cdot 10^6$	$8 \cdot 10^5$	–	–	–
xenon-133	–	–	–	$1 \cdot 10^7$	$6 \cdot 10^6$	$1 \cdot 10^6$	–	–	–
tellurium-134	$7 \cdot 10^5$	$1 \cdot 10^6$	$2 \cdot 10^5$	–	–	–	–	–	–
iodine-134	$2 \cdot 10^6$	$3 \cdot 10^6$	$5 \cdot 10^5$	–	–	–	92,522	$2 \cdot 10^5$	28,955
iodine-135	$2 \cdot 10^6$	$1 \cdot 10^6$	$2 \cdot 10^5$	–	–	–	$2 \cdot 10^5$	$2 \cdot 10^5$	27,041
xenon-135m	–	–	–	$4 \cdot 10^5$	$7 \cdot 10^5$	$1 \cdot 10^5$	–	–	–
xenon-135	–	–	–	$4 \cdot 10^6$	$4 \cdot 10^6$	$6 \cdot 10^5$	–	–	–
cesium-137	$2 \cdot 10^6$	$1 \cdot 10^6$	$1 \cdot 10^6$	–	–	–	$2 \cdot 10^5$	$2 \cdot 10^5$	$2 \cdot 10^5$
xenon-138	–	–	–	$3 \cdot 10^5$	$1 \cdot 10^6$	$2 \cdot 10^5$	–	–	–
cesium-138	$6 \cdot 10^5$	$3 \cdot 10^6$	$2 \cdot 10^5$	$5 \cdot 10^5$	$2 \cdot 10^6$	$2 \cdot 10^5$	66,104	$3 \cdot 10^5$	26,100
barium-139	$9 \cdot 10^6$	$2 \cdot 10^7$	$4 \cdot 10^6$	–	–	–	–	–	–
barium-140	$6 \cdot 10^6$	$2 \cdot 10^6$	$9 \cdot 10^5$	–	–	–	–	–	–
lanthanum-140	$6 \cdot 10^6$	$2 \cdot 10^6$	$9 \cdot 10^5$	–	–	–	–	–	–
barium-141	$5 \cdot 10^5$	$1 \cdot 10^6$	$2 \cdot 10^5$	–	–	–	–	–	–
lanthanum-141	$5 \cdot 10^5$	$1 \cdot 10^6$	$2 \cdot 10^5$	–	–	–	–	–	–
cerium-141	$5 \cdot 10^5$	$1 \cdot 10^6$	$2 \cdot 10^5$	–	–	–	–	–	–
barium-142	$3 \cdot 10^5$	$1 \cdot 10^6$	$2 \cdot 10^5$	–	–	–	–	–	–
lanthanum-142	$4 \cdot 10^5$	$2 \cdot 10^6$	$2 \cdot 10^5$	–	–	–	–	–	–
samarium-151	60,009	61,712	61,712	–	–	–	–	–	–
samarium-153	$2 \cdot 10^5$	91,306	25,925	–	–	–	–	–	–
europium-155	$1 \cdot 10^5$	74,877	65,553	–	–	–	–	–	–
europium-156	91,528	34,986	15,658	–	–	–	–	–	–
sum	$5 \cdot 10^7$	$6 \cdot 10^7$	$2 \cdot 10^7$	$2 \cdot 10^7$	$2 \cdot 10^7$	$4 \cdot 10^6$	$2 \cdot 10^6$	$2 \cdot 10^6$	$5 \cdot 10^5$

Case 8 Results

The following tables show results from Case 8, as described in Section 4.5.3, using the updated tracked isotope list from Table 4.29. The three R/B models are the Peach Bottom (PB), MHTGR at Beginning of Life (BOL), and MHTGR at EOL (EOL) as described in Section 3.3.

Table B.4.: Mass accumulation (g) in the fission product traps.

	Hot Fission Product Trap			**Cold Fission Product Trap**			**Plateout/Condensation**		
	PB	*MHTGR*		*PB*	*MHTGR*		*PB*	*MHTGR*	
Nuclide		BOL	EOL		BOL	EOL		BOL	EOL
selenium-80	258	258	258	–	–	–	–	–	–
bromine-81	360	360	360	–	–	–	–	–	–
selenium-82	550	550	550	–	–	–	–	–	–
krypton-83	–	–	–	890	890	890	–	–	–
krypton-84	–	–	–	1,545	1,545	1,545	–	–	–
krypton-85m	–	–	–	$3 \cdot 10^{-2}$	$3 \cdot 10^{-2}$	$6 \cdot 10^{-3}$	–	–	–
krypton-85	–	–	–	332	225	199	–	–	–
rubidium-85	1,570	1,673	1,776	109	112	36	–	–	–
krypton-86	–	–	–	2,828	2,828	2,828	–	–	–
krypton-87	–	–	–	$9 \cdot 10^{-3}$	$2 \cdot 10^{-2}$	$3 \cdot 10^{-3}$	–	–	–
rubidium-87	3,636	3,542	3,716	116	210	36	–	–	–
krypton-88	–	–	–	$2 \cdot 10^{-2}$	$3 \cdot 10^{-2}$	$5 \cdot 10^{-3}$	–	–	–
rubidium-88	$9 \cdot 10^{-4}$	$3 \cdot 10^{-3}$	$5 \cdot 10^{-4}$	$2 \cdot 10^{-3}$	$3 \cdot 10^{-3}$	$5 \cdot 10^{-4}$	–	–	–
strontium-88	51	161	31	121	165	30	–	–	–
rubidium-89	$2 \cdot 10^{-3}$	$5 \cdot 10^{-3}$	$8 \cdot 10^{-4}$	–	–	–	–	–	–
strontium-89	8	25	4	–	–	–	–	–	–
yttrium-89	102	334	52	–	–	–	–	–	–
cadmium-111	534	534	534	–	–	–	–	–	–
tellurium-126	552	552	552	–	–	–	–	–	–
tellurium-127m	11	2	1	–	–	–	–	–	–
tellurium-127	$4 \cdot 10^{-2}$	$1 \cdot 10^{-2}$	$5 \cdot 10^{-3}$	–	–	–	–	–	–
iodine-127	175	178	177	–	–	–	11	17	19
tellurium-128	2,130	2,130	2,130	–	–	–	–	–	–
tellurium-129m	8	2	$6 \cdot 10^{-1}$	–	–	–	–	–	–
tellurium-129	$7 \cdot 10^{-3}$	$3 \cdot 10^{-3}$	$8 \cdot 10^{-4}$	–	–	–	–	–	–
iodine-129	540	535	532	–	–	–	42	53	57
tellurium-130	6,640	6,640	6,640	–	–	–	–	–	–
tellurium-131m	$4 \cdot 10^{-1}$	$2 \cdot 10^{-1}$	$4 \cdot 10^{-2}$	–	–	–	–	–	–
tellurium-131	$2 \cdot 10^{-3}$	$2 \cdot 10^{-3}$	$3 \cdot 10^{-4}$	–	–	–	–	–	–
iodine-131	7	3	$8 \cdot 10^{-1}$	–	–	–	$5 \cdot 10^{-1}$	$2 \cdot 10^{-1}$	$5 \cdot 10^{-2}$
xenon-131	–	–	–	2,661	2,665	2,668	–	–	–
tellurium-132	9	4	$9 \cdot 10^{-1}$	–	–	–	–	–	–
iodine-132	$3 \cdot 10^{-1}$	$2 \cdot 10^{-1}$	$4 \cdot 10^{-2}$	–	–	–	$7 \cdot 10^{-3}$	$1 \cdot 10^{-2}$	$2 \cdot 10^{-3}$
xenon-132	–	–	–	15,871	15,877	15,880	–	–	–
tellurium-133m	$2 \cdot 10^{-2}$	$3 \cdot 10^{-2}$	$5 \cdot 10^{-3}$	–	–	–	–	–	–
tellurium-133	$2 \cdot 10^{-3}$	$5 \cdot 10^{-3}$	$8 \cdot 10^{-4}$	–	–	–	–	–	–
iodine-133	2	2	$4 \cdot 10^{-1}$	–	–	–	$2 \cdot 10^{-1}$	$1 \cdot 10^{-1}$	$2 \cdot 10^{-2}$
xenon-133m	–	–	–	12	9	2	–	–	–
xenon-133	–	–	–	47	29	6	–	–	–
cesium-133	11,546	13,723	16,582	6,370	3,991	823	1,283	1,525	1,842
tellurium-134	$2 \cdot 10^{-2}$	$4 \cdot 10^{-2}$	$6 \cdot 10^{-3}$	–	–	–	–	–	–
iodine-134	$5 \cdot 10^{-2}$	$1 \cdot 10^{-1}$	$2 \cdot 10^{-2}$	–	–	–	$3 \cdot 10^{-3}$	$6 \cdot 10^{-3}$	$1 \cdot 10^{-3}$
xenon-134	–	–	–	23,966	23,965	23,966	–	–	–
iodine-135	$4 \cdot 10^{-1}$	$4 \cdot 10^{-1}$	$6 \cdot 10^{-2}$	–	–	–	$4 \cdot 10^{-2}$	$4 \cdot 10^{-2}$	$7 \cdot 10^{-3}$
xenon-135m	–	–	–	$4 \cdot 10^{-3}$	$7 \cdot 10^{-3}$	$1 \cdot 10^{-3}$	–	–	–
xenon-135	–	–	–	1	1	$2 \cdot 10^{-1}$	–	–	–
cesium-135	18,384	18,394	20,341	2,614	2,603	442	2,043	2,044	2,260
xenon-136	–	–	–	21,521	21,521	21,521	–	–	–

Table B.4.: Mass accumulation (g) in the fission product traps.

Nuclide	**Hot Fission Product Trap**			**Cold Fission Product Trap**			**Plateout/Condensation**		
	PB	*MHTGR*		*PB*	*MHTGR*		*PB*	*MHTGR*	
		BOL	EOL		BOL	EOL		BOL	EOL
cesium-137	16,728	15,754	14,900	–	–	–	1,859	1,750	1,655
barium-137	617	581	550	–	–	–	–	–	–
xenon-138	–	–	–	$3 \cdot 10^{-3}$	$1 \cdot 10^{-2}$	$2 \cdot 10^{-3}$	–	–	–
cesium-138	$1 \cdot 10^{-2}$	$5 \cdot 10^{-2}$	$5 \cdot 10^{-3}$	$1 \cdot 10^{-2}$	$4 \cdot 10^{-2}$	$5 \cdot 10^{-3}$	$1 \cdot 10^{-3}$	$6 \cdot 10^{-3}$	$6 \cdot 10^{-4}$
barium-138	462	1,941	182	295	986	146	–	–	–
sum	64,881	67,880	69,870	79,298	77,622	71,016	5,238	5,389	5,834

Table B.5.: Power from each element (W) in the fission product traps.

	Hot Fission Product Trap			**Cold Fission Product Trap**			**Plateout/Condensation**		
	PB	*MHTGR*		*PB*	*MHTGR*		*PB*	*MHTGR*	
Nuclide		BOL	EOL		BOL	EOL		BOL	EOL
krypton-85m	–	–	–	1,146	1,337	258	–	–	–
krypton-85	–	–	–	577	392	345	–	–	–
krypton-87	–	–	–	6,067	10,978	1,873	–	–	–
krypton-88	–	–	–	4,690	6,388	1,171	–	–	–
rubidium-88	3,610	11,397	2,188	8,553	11,650	2,135	–	–	–
rubidium-89	6,485	21,267	3,317	–	–	–	–	–	–
strontium-89	2,157	7,072	1,103	–	–	–	–	–	–
tellurium-127m	74	16	7	–	–	–	–	–	–
tellurium-127	527	165	55	–	–	–	–	–	–
tellurium-129m	986	246	82	–	–	–	–	–	–
tellurium-129	1,520	610	159	–	–	–	–	–	–
tellurium-131m	3,638	2,089	397	–	–	–	–	–	–
tellurium-131	1,319	1,585	262	–	–	–	–	–	–
iodine-131	6,371	3,185	688	–	–	–	447	157	41
tellurium-132	9,089	4,022	857	–	–	–	–	–	–
iodine-132	95,242	61,849	11,823	–	–	–	1,979	3,065	503
tellurium-133m	6,806	13,584	2,063	–	–	–	–	–	–
tellurium-133	3,771	11,578	1,732	–	–	–	–	–	–
iodine-133	55,619	58,374	9,877	–	–	–	4,803	3,090	586
xenon-133m	–	–	–	8,281	6,255	1,170	–	–	–
xenon-133	–	–	–	24,202	15,172	3,127	–	–	–
tellurium-134	6,120	13,567	2,046	–	–	–	–	–	–
iodine-134	40,705	85,098	13,125	–	–	–	2,513	4,999	786
iodine-135	23,585	23,128	3,820	–	–	–	2,621	2,570	424
xenon-135m	–	–	–	1,318	2,186	345	–	–	–
xenon-135	–	–	–	26,083	25,960	4,408	–	–	–
cesium-137	11,047	10,403	9,839	–	–	–	1,227	1,156	1,093
xenon-138	–	–	–	5,709	19,109	2,824	–	–	–
cesium-138	22,830	95,897	9,014	18,735	62,715	9,269	2,537	10,655	1,002
sum	$3 \cdot 10^5$	$4 \cdot 10^5$	72,453	$1 \cdot 10^5$	$2 \cdot 10^5$	26,925	16,126	25,692	4,435

Table B.6.: Isotope specific activities (Ci) in the fission product traps.

	Hot Fission Product Trap			**Cold Fission Product Trap**			**Plateout/Condensation**		
	PB	*MHTGR*		*PB*	*MHTGR*		*PB*	*MHTGR*	
Nuclide		BOL	EOL		BOL	EOL		BOL	EOL
krypton-85m	–	–	–	$2 \cdot 10^5$	$3 \cdot 10^5$	51,454	–	–	–
krypton-85	–	–	–	$1 \cdot 10^5$	96,245	84,742	–	–	–
krypton-87	–	–	–	$3 \cdot 10^5$	$5 \cdot 10^5$	81,276	–	–	–
krypton-88	–	–	–	$3 \cdot 10^5$	$4 \cdot 10^5$	67,784	–	–	–
rubidium-88	$1 \cdot 10^5$	$4 \cdot 10^5$	69,447	$3 \cdot 10^5$	$4 \cdot 10^5$	67,767	–	–	–
rubidium-89	$2 \cdot 10^5$	$8 \cdot 10^5$	$1 \cdot 10^5$	–	–	–	–	–	–
strontium-89	$2 \cdot 10^5$	$8 \cdot 10^5$	$1 \cdot 10^5$	–	–	–	–	–	–
tellurium-127m	$1 \cdot 10^5$	25,122	10,851	–	–	–	–	–	–
tellurium-127	$1 \cdot 10^5$	39,862	13,309	–	–	–	–	–	–
tellurium-129m	$3 \cdot 10^5$	62,971	21,022	–	–	–	–	–	–
tellurium-129	$2 \cdot 10^5$	68,708	17,903	–	–	–	–	–	–
tellurium-131m	$3 \cdot 10^5$	$2 \cdot 10^5$	34,922	–	–	–	–	–	–
tellurium-131	99,630	$1 \cdot 10^5$	19,805	–	–	–	–	–	–
iodine-131	$9 \cdot 10^5$	$5 \cdot 10^5$	$1 \cdot 10^5$	–	–	–	66,194	23,258	6,111
tellurium-132	$3 \cdot 10^6$	$1 \cdot 10^6$	$3 \cdot 10^5$	–	–	–	–	–	–
iodine-132	$4 \cdot 10^6$	$2 \cdot 10^6$	$5 \cdot 10^5$	–	–	–	79,549	$1 \cdot 10^5$	20,205
tellurium-133m	$4 \cdot 10^5$	$8 \cdot 10^5$	$1 \cdot 10^5$	–	–	–	–	–	–
tellurium-133	$2 \cdot 10^5$	$7 \cdot 10^5$	$1 \cdot 10^5$	–	–	–	–	–	–
iodine-133	$3 \cdot 10^6$	$3 \cdot 10^6$	$5 \cdot 10^5$	–	–	–	$2 \cdot 10^5$	$2 \cdot 10^5$	29,036
xenon-133m	–	–	–	$6 \cdot 10^6$	$5 \cdot 10^6$	$8 \cdot 10^5$	–	–	–
xenon-133	–	–	–	$1 \cdot 10^7$	$6 \cdot 10^6$	$1 \cdot 10^6$	–	–	–
tellurium-134	$7 \cdot 10^5$	$1 \cdot 10^6$	$2 \cdot 10^5$	–	–	–	–	–	–
iodine-134	$2 \cdot 10^6$	$3 \cdot 10^6$	$5 \cdot 10^5$	–	–	–	92,522	$2 \cdot 10^5$	28,955
iodine-135	$2 \cdot 10^6$	$1 \cdot 10^6$	$2 \cdot 10^5$	–	–	–	$2 \cdot 10^5$	$2 \cdot 10^5$	27,041
xenon-135m	–	–	–	$4 \cdot 10^5$	$7 \cdot 10^5$	$1 \cdot 10^5$	–	–	–
xenon-135	–	–	–	$4 \cdot 10^6$	$4 \cdot 10^6$	$6 \cdot 10^5$	–	–	–
cesium-137	$2 \cdot 10^6$	$1 \cdot 10^6$	$1 \cdot 10^6$	–	–	–	$2 \cdot 10^5$	$2 \cdot 10^5$	$2 \cdot 10^5$
xenon-138	–	–	–	$3 \cdot 10^5$	$1 \cdot 10^6$	$2 \cdot 10^5$	–	–	–
cesium-138	$6 \cdot 10^5$	$3 \cdot 10^6$	$2 \cdot 10^5$	$5 \cdot 10^5$	$2 \cdot 10^6$	$2 \cdot 10^5$	66,104	$3 \cdot 10^5$	26,100
sum	$2 \cdot 10^7$	$2 \cdot 10^7$	$5 \cdot 10^6$	$2 \cdot 10^7$	$2 \cdot 10^7$	$4 \cdot 10^6$	$9 \cdot 10^5$	$1 \cdot 10^6$	$3 \cdot 10^5$

Case 9 Results

The following tables show results from Case 9, as described in Section 4.5.3, using the updated tracked isotope list from Table 4.29. The three models are the Peach Bottom (PB), MHTGR at Beginning of Life (BOL), and MHTGR at EOL (EOL) as described in Section 3.3 as described in Section 3.3.

Table B.7.: Mass accumulation (g) in the fission product traps.

	Hot Fission Product Trap			**Cold Fission Product Trap**			**Plateout/Condensation**		
	PB	*MHTGR*		*PB*	*MHTGR*		*PB*	*MHTGR*	
Nuclide		BOL	EOL		BOL	EOL		BOL	EOL
selenium-80	–	–	–	–	–	–	258	258	258
bromine-81	360	360	360	–	–	–	–	–	–
selenium-82	–	–	–	–	–	–	550	550	550
krypton-83	–	–	–	890	890	890	–	–	–
krypton-84	–	–	–	1,545	1,545	1,545	–	–	–
krypton-85m	–	–	–	$3 \cdot 10^{-2}$	$3 \cdot 10^{-2}$	$6 \cdot 10^{-3}$	–	–	–
krypton-85	–	–	–	332	225	199	–	–	–
rubidium-85	–	–	–	109	112	36	1,570	1,673	1,776
krypton-86	–	–	–	2,828	2,828	2,828	–	–	–
krypton-87	–	–	–	$9 \cdot 10^{-3}$	$2 \cdot 10^{-2}$	$3 \cdot 10^{-3}$	–	–	–
rubidium-87	–	–	–	116	210	36	3,636	3,542	3,716
krypton-88	–	–	–	$2 \cdot 10^{-2}$	$3 \cdot 10^{-2}$	$5 \cdot 10^{-3}$	–	–	–
rubidium-88	–	–	–	$2 \cdot 10^{-3}$	$3 \cdot 10^{-3}$	$5 \cdot 10^{-4}$	$9 \cdot 10^{-4}$	$3 \cdot 10^{-3}$	$5 \cdot 10^{-4}$
strontium-88	–	–	–	121	165	30	51	161	31
rubidium-89	–	–	–	–	–	–	$2 \cdot 10^{-3}$	$5 \cdot 10^{-3}$	$8 \cdot 10^{-4}$
strontium-89	–	–	–	–	–	–	8	25	4
yttrium-89	–	–	–	–	–	–	102	334	52
cadmium-111	–	–	–	–	–	–	534	534	534
tellurium-126	–	–	–	–	–	–	552	552	552
tellurium-127m	–	–	–	–	–	–	11	2	1
tellurium-127	–	–	–	–	–	–	$4 \cdot 10^{-2}$	$1 \cdot 10^{-2}$	$5 \cdot 10^{-3}$
iodine-127	167	175	177	–	–	–	19	19	20
tellurium-128	–	–	–	–	–	–	2,130	2,130	2,130
tellurium-129m	–	–	–	–	–	–	8	2	$6 \cdot 10^{-1}$
tellurium-129	–	–	–	–	–	–	$7 \cdot 10^{-3}$	$3 \cdot 10^{-3}$	$8 \cdot 10^{-4}$
iodine-129	524	529	530	–	–	–	58	59	59
tellurium-130	–	–	–	–	–	–	6,640	6,640	6,640
tellurium-131m	–	–	–	–	–	–	$4 \cdot 10^{-1}$	$2 \cdot 10^{-1}$	$4 \cdot 10^{-2}$
tellurium-131	–	–	–	–	–	–	$2 \cdot 10^{-3}$	$2 \cdot 10^{-3}$	$3 \cdot 10^{-4}$
iodine-131	7	3	$7 \cdot 10^{-1}$	–	–	–	$7 \cdot 10^{-1}$	$4 \cdot 10^{-1}$	$8 \cdot 10^{-2}$
xenon-131	–	–	–	2,661	2,665	2,668	–	–	–
tellurium-132	–	–	–	–	–	–	9	4	$9 \cdot 10^{-1}$
iodine-132	$3 \cdot 10^{-1}$	$2 \cdot 10^{-1}$	$4 \cdot 10^{-2}$	–	–	–	$3 \cdot 10^{-2}$	$2 \cdot 10^{-2}$	$4 \cdot 10^{-3}$
xenon-132	–	–	–	15,871	15,877	15,880	–	–	–
tellurium-133m	–	–	–	–	–	–	$2 \cdot 10^{-2}$	$3 \cdot 10^{-2}$	$5 \cdot 10^{-3}$
tellurium-133	–	–	–	–	–	–	$2 \cdot 10^{-3}$	$5 \cdot 10^{-3}$	$8 \cdot 10^{-4}$
iodine-133	2	2	$4 \cdot 10^{-1}$	–	–	–	$2 \cdot 10^{-1}$	$2 \cdot 10^{-1}$	$4 \cdot 10^{-2}$
xenon-133m	–	–	–	12	9	2	–	–	–
xenon-133	–	–	–	47	29	6	–	–	–
cesium-133	–	–	–	6,370	3,991	823	12,830	15,248	18,425
tellurium-134	–	–	–	–	–	–	$2 \cdot 10^{-2}$	$4 \cdot 10^{-2}$	$6 \cdot 10^{-3}$
iodine-134	$5 \cdot 10^{-2}$	$1 \cdot 10^{-1}$	$2 \cdot 10^{-2}$	–	–	–	$5 \cdot 10^{-3}$	$1 \cdot 10^{-2}$	$2 \cdot 10^{-3}$
xenon-134	–	–	–	23,966	23,965	23,966	–	–	–
iodine-135	$4 \cdot 10^{-1}$	$4 \cdot 10^{-1}$	$6 \cdot 10^{-2}$	–	–	–	$4 \cdot 10^{-2}$	$4 \cdot 10^{-2}$	$7 \cdot 10^{-3}$
xenon-135m	–	–	–	$4 \cdot 10^{-3}$	$7 \cdot 10^{-3}$	$1 \cdot 10^{-3}$	–	–	–
xenon-135	–	–	–	1	1	$2 \cdot 10^{-1}$	–	–	–
cesium-135	–	–	–	2,614	2,603	442	20,427	20,438	22,600

Table B.7.: Mass accumulation (g) in the fission product traps.

Nuclide	**Hot Fission Product Trap**			**Cold Fission Product Trap**			**Plateout/Condensation**		
	PB	*MHTGR*		*PB*	*MHTGR*		*PB*	*MHTGR*	
		BOL	EOL		BOL	EOL		BOL	EOL
xenon-136	–	–	–	–	21,521	21,521	21,522	–	–
cesium-137	–	–	–	–	–	–	18,587	17,505	16,555
barium-137	–	–	–	–	–	–	617	581	550
xenon-138	–	–	–	$3 \cdot 10^{-3}$	$1 \cdot 10^{-2}$	$2 \cdot 10^{-3}$	–	–	–
cesium-138	–	–	–	$1 \cdot 10^{-2}$	$4 \cdot 10^{-2}$	$5 \cdot 10^{-3}$	$1 \cdot 10^{-2}$	$6 \cdot 10^{-2}$	$6 \cdot 10^{-3}$
barium-138	–	–	–	295	986	146	462	1,941	182
sum	1,061	1,071	1,068	57,777	77,622	71,016	90,580	72,200	74,636

Table B.8.: Power from each element (W) in the fission product traps.

	Hot Fission Product Trap			**Cold Fission Product Trap**			**Plateout/Condensation**		
	PB	*MHTGR*		*PB*	*MHTGR*		*PB*	*MHTGR*	
Nuclide		BOL	EOL		BOL	EOL		BOL	EOL
krypton-85m	–	–	–	1,146	1,337	258	–	–	–
krypton-85	–	–	–	577	392	345	–	–	–
krypton-87	–	–	–	6,067	10,978	1,873	–	–	–
krypton-88	–	–	–	4,690	6,388	1,171	–	–	–
rubidium-88	–	–	–	8,553	11,650	2,135	3,610	11,397	2,188
rubidium-89	–	–	–	–	–	–	6,485	21,267	3,317
strontium-89	–	–	–	–	–	–	2,157	7,072	1,103
tellurium-127m	–	–	–	–	–	–	74	16	7
tellurium-127	–	–	–	–	–	–	527	165	55
tellurium-129m	–	–	–	–	–	–	986	246	82
tellurium-129	–	–	–	–	–	–	1,520	610	159
tellurium-131m	–	–	–	–	–	–	3,638	2,089	397
tellurium-131	–	–	–	–	–	–	1,319	1,585	262
iodine-131	6,136	3,007	656	–	–	–	682	334	73
tellurium-132	–	–	–	–	–	–	9,089	4,022	857
iodine-132	87,499	58,422	11,093	–	–	–	9,722	6,491	1,233
tellurium-133m	–	–	–	–	–	–	6,806	13,584	2,063
tellurium-133	–	–	–	–	–	–	3,771	11,578	1,732
iodine-133	54,380	55,318	9,416	–	–	–	6,042	6,146	1,046
xenon-133m	–	–	–	8,281	6,255	1,170	–	–	–
xenon-133	–	–	–	24,202	15,172	3,127	–	–	–
tellurium-134	–	–	–	–	–	–	6,120	13,567	2,046
iodine-134	38,896	81,087	12,520	–	–	–	4,322	9,010	1,391
iodine-135	23,585	23,128	3,820	–	–	–	2,621	2,570	424
xenon-135m	–	–	–	1,318	2,186	345	–	–	–
xenon-135	–	–	–	26,083	25,960	4,408	–	–	–
cesium-137	–	–	–	–	–	–	12,274	11,559	10,932
xenon-138	–	–	–	5,709	19,109	2,824	–	–	–
cesium-138	–	–	–	18,735	62,715	9,269	25,366	$1 \cdot 10^5$	10,015
sum	$2 \cdot 10^5$	$2 \cdot 10^5$	37,505	$1 \cdot 10^5$	$2 \cdot 10^5$	26,925	$1 \cdot 10^5$	$2 \cdot 10^5$	39,383

Table B.9.: Isotope specific activities (Ci) in the fission product traps.

Nuclide	**Hot Fission Product Trap**			**Cold Fission Product Trap**			**Plateout/Condensation**		
	PB	*MHTGR*		*PB*	*MHTGR*		*PB*	*MHTGR*	
		BOL	EOL		BOL	EOL		BOL	EOL
krypton-85m	–	–	–	$2 \cdot 10^5$	$3 \cdot 10^5$	51,454	–	–	–
krypton-85	–	–	–	$1 \cdot 10^5$	96,245	84,742	–	–	–
krypton-87	–	–	–	$3 \cdot 10^5$	$5 \cdot 10^5$	81,276	–	–	–
krypton-88	–	–	–	$3 \cdot 10^5$	$4 \cdot 10^5$	67,784	–	–	–
rubidium-88	–	–	–	$3 \cdot 10^5$	$4 \cdot 10^5$	67,767	$1 \cdot 10^5$	$4 \cdot 10^5$	69,447
rubidium-89	–	–	–	–	–	–	$2 \cdot 10^5$	$8 \cdot 10^5$	$1 \cdot 10^5$
strontium-89	–	–	–	–	–	–	$2 \cdot 10^5$	$8 \cdot 10^5$	$1 \cdot 10^5$
tellurium-127m	–	–	–	–	–	–	$1 \cdot 10^5$	25,122	10,851
tellurium-127	–	–	–	–	–	–	$1 \cdot 10^5$	39,862	13,309
tellurium-129m	–	–	–	–	–	–	$3 \cdot 10^5$	62,971	21,022
tellurium-129	–	–	–	–	–	–	$2 \cdot 10^5$	68,708	17,903
tellurium-131m	–	–	–	–	–	–	$3 \cdot 10^5$	$2 \cdot 10^5$	34,922
tellurium-131	–	–	–	–	–	–	99,630	$1 \cdot 10^5$	19,805
iodine-131	$9 \cdot 10^5$	$4 \cdot 10^5$	97,228	–	–	–	$1 \cdot 10^5$	49,495	10,803
tellurium-132	–	–	–	–	–	–	$3 \cdot 10^6$	$1 \cdot 10^6$	$3 \cdot 10^5$
iodine-132	$4 \cdot 10^6$	$2 \cdot 10^6$	$4 \cdot 10^5$	–	–	–	$4 \cdot 10^5$	$3 \cdot 10^5$	49,536
tellurium-133m	–	–	–	–	–	–	$4 \cdot 10^5$	$8 \cdot 10^5$	$1 \cdot 10^5$
tellurium-133	–	–	–	–	–	–	$2 \cdot 10^5$	$7 \cdot 10^5$	$1 \cdot 10^5$
iodine-133	$3 \cdot 10^6$	$3 \cdot 10^6$	$5 \cdot 10^5$	–	–	–	$3 \cdot 10^5$	$3 \cdot 10^5$	51,854
xenon-133m	–	–	–	$6 \cdot 10^6$	$5 \cdot 10^6$	$8 \cdot 10^5$	–	–	–
xenon-133	–	–	–	$1 \cdot 10^7$	$6 \cdot 10^6$	$1 \cdot 10^6$	–	–	–
tellurium-134	–	–	–	–	–	–	$7 \cdot 10^5$	$1 \cdot 10^6$	$2 \cdot 10^5$
iodine-134	$1 \cdot 10^6$	$3 \cdot 10^6$	$5 \cdot 10^5$	–	–	–	$2 \cdot 10^5$	$3 \cdot 10^5$	51,220
iodine-135	$2 \cdot 10^6$	$1 \cdot 10^6$	$2 \cdot 10^5$	–	–	–	$2 \cdot 10^5$	$2 \cdot 10^5$	27,041
xenon-135m	–	–	–	$4 \cdot 10^5$	$7 \cdot 10^5$	$1 \cdot 10^5$	–	–	–
xenon-135	–	–	–	$4 \cdot 10^6$	$4 \cdot 10^6$	$6 \cdot 10^5$	–	–	–
cesium-137	–	–	–	–	–	–	$2 \cdot 10^6$	$2 \cdot 10^6$	$2 \cdot 10^6$
xenon-138	–	–	–	$3 \cdot 10^5$	$1 \cdot 10^6$	$2 \cdot 10^5$	–	–	–
cesium-138	–	–	–	$5 \cdot 10^5$	$2 \cdot 10^6$	$2 \cdot 10^5$	$7 \cdot 10^5$	$3 \cdot 10^6$	$3 \cdot 10^5$
sum	$1 \cdot 10^7$	$1 \cdot 10^7$	$2 \cdot 10^6$	$2 \cdot 10^7$	$2 \cdot 10^7$	$4 \cdot 10^6$	$1 \cdot 10^7$	$1 \cdot 10^7$	$3 \cdot 10^6$

C. PRA Appendices

Appendix C.1. Fission Product Vent System Component Reliability Data

Fission Product Vent System and Vented Fuel System Component Unreliability Data

	Group	Component	Component Failure Mode	Description	Reactor Type	Publication Date	Data Source	Operational Failure Data, Lambda					Demand Failure Data, Q					Comments
								Dist'n	5th Percentile	Median	95th Percentile	Error Factor	Dist'n	5th Percentile	Median	95th Percentile	Error Factor	
Fission Product Vent System and Fuel System	Motor Operated Valve	MOV FTO/C	Change State	Motor Operating Valve - Fail to change state	HTGR	1987	MHTGR PRA	Log Normal	-	-	-	-	Lognormal	5.00E-03	6.00E-03	7.00E-03	1.2	1 order of magnitude less than MOV iso
		MOV BL	Bypass Leak	Motor Operating Valve - Bypass leak	HTGR	1987	MHTGR PRA	Log Normal	3.00E-07	3.00E-06	3.00E-05	10	Log Normal	-	-	-	-	1 order of magnitude less than MOV iso
		MOV SOP	Spurious Operation	Motor Operating Valve - Spurious Operation	HTGR	1987	MHTGR PRA	Log Normal	3.00E-07	3.00E-06	3.00E-05	10	Log Normal	-	-	-	-	1 order of magnitude less than MOV iso
	MOV Isolation	MOVI FTO/C	Change State	Motor Operating Valve Iso - Fail to change state	HTGR	1987	MHTGR PRA	Log Normal	-	-	-	-	Log Normal	3.00E-05	1.00E-04	3.00E-04	3.16	HTGR MOV Isolation Valve
		MOVI BL	Bypass Leak	Motor Operating Valve Iso - Bypass leak	HTGR	1987	MHTGR PRA	Log Normal	3.00E-07	3.00E-06	3.00E-05	10	Log Normal	-	-	-	-	HTGR MOV Isolation Valve
		MOVI SOP	Spurious Operation	Motor Operating Valve Iso - Spurious Operation	HTGR	1987	MHTGR PRA	Log Normal	3.00E-07	3.00E-06	3.00E-05	10	Log Normal	-	-	-	-	HTGR MOV Isolation Valve
	Motor Operated Control Valve (MOVC)	MOVC FTO/C	Change State	MOV Modulating/Control - Fail to change state	HTGR	1987	MHTGR PRA	Log Normal	-	-	-	-	Log Normal	3.00E-05	1.00E-04	3.00E-04	3.16	HTGR Isolation Valve
		MOVC EL	External Leak	MOV Modulating/Control - External Leak	HTGR	1987	MHTGR PRA	Log Normal	6.00E-08	1.00E-07	2.00E-07	1.83	Log Normal	-	-	-	-	HTGR MOV Modulating
		MOVC SOP	Spurious Operation	MOV Modulating/Control - Spurious Operation	HTGR	1987	MHTGR PRA	Log Normal	3.00E-07	3.00E-06	3.00E-05	10	Log Normal	-	-	-	-	HTGR MOV Isolation Valve
		MOVC FO	Control/Operate	MOV Modulating/Control - Fail to Operate/Control	HTGR	1987	MHTGR PRA	Log Normal	2.40E-06	2.60E-06	2.90E-06	1.10	Log Normal	-	-	-	-	HTGR MOV Modulating
	Check Valve (CKV)	CKV FTO/C	Change State	Check Valve- Fail to change state	HTGR	1987	MHTGR PRA	Log Normal	-	-	-	-	Log Normal	1.00E-04	3.00E-04	9.00E-04	3.00	HTGR CKV Passive Iso
		CKV SOP	Spurious Operation	Check Valve - Spurious Operation	HTGR	1987	MHTGR PRA	Log Normal	1.00E-07	1.00E-06	1.00E-05	10.00	Log Normal	-	-	-	-	HTGR CKV Passive Iso
		CKV BL	Bypass Leak	Check Valve - Bypass Leak	HTGR	1987	MHTGR PRA	Log Normal	1.00E-06	3.00E-06	3.00E-05	5.48	Log Normal	-	-	-	-	HTGR CKV Passive Iso
	Manual Valve (XVM)	XVM FTO/C	Change State	Manual Valve- Fail to change state	HTGR	1987	MHTGR PRA	Log Normal	-	-	-	-	Log Normal	2.00E-05	6.00E-05	1.00E-04	2.24	HTGR XVM
		XVM EL	External Leak	Manual Valve - External Leak	HTGR	1987	MHTGR PRA	Log Normal	6.00E-09	2.00E-08	6.00E-08	3.16	Log Normal	-	-	-	-	HTGR XVM
		XVM SOP	Spurious Operation	Manual Valve - Spurious Operation	HTGR	1987	MHTGR PRA	Log Normal	6.00E-09	2.00E-08	2.00E-07	5.77	Log Normal	-	-	-	-	
	HTA Module	HTA Adsorber	Bypass	Adsorber - Target Value	-	-	Target Value	Log Normal	1.00E-07	1.00E-06	1.00E-05	10	Log Normal	-	-	-	-	PNNL-22563 Carbon Loading 3.3E-3/h
		HTA Adsorber	Overload	Adsorber - Target Value	-	-	Target Value	Log Normal	1.00E-07	1.00E-06	1.00E-05	10	Log Normal	-	-	-	-	PNNL-22563 Carbon Loading 3.3E-3/h
		HTA Filter	Bypass	Filter	-	-	Target Value	Log Normal	1.00E-07	1.00E-06	1.00E-05	10	Log Normal	-	-	-	-	Target Value with high uncertainty
		HTA Filter	Plugged	Filter	Combined	-	EGG-SSRE, EFDA, NUREG	Log Normal	3.00E-07	3.00E-06	3.00E-05	10	Log Normal	-	-	-	-	4.8E-6 (EGG-SSRE), 3.1E-6 (EFDA), 3.1E-7 (NUREG), 3E-6 (INEEL Fusion)
	Compressor Module	Compressor	Fail to Run	Compressor	Combined	-	JAERI TPL, GCR DB, EGG-SSRE, INEEL TPL, NUREG	Log Normal	5.00E-06	5.00E-05	5.00E-04	10	Log Normal	-	-	-	-	1E-5 (GCR), 7.4E-4 (JAERI), 1E-4 (EGG-SRE), 3E-4 (INEEL TPL), 8.5E-5 (NUREG)
		Compressor	Fail to Start	Compressor	Combined	-	JAERI TPL, EGG-SSRE, INEEL TPL, NUREG	Log Normal	-	-	-	-	Log Normal	1.00E-05	1.00E-04	1.00E-03	10	5.2E-5 (JAERI), 5E-3 (EGG-SRE), 1E-4 (INEEL TPL), 1.7E-2 (NUREG)
		Heat Exchanger	All	Heat Exchangers - General	HTGR	1987	MHTGR PRA	Log Normal	1.00E-06	3.00E-05	3.00E-04	17.32	Log Normal	-	-	-	-	
	LTA Module	Liquid Nitrogen Cooling System	All	Cooler	HTGR	1987	MHTGR PRA	Log Normal	1.00E-06	3.00E-06	9.00E-06	3	Log Normal	-	-	-	-	
		LTA Adsorber	Bypass	Adsorber - Target Value	-	-	Target Value	Log Normal	1.00E-07	1.00E-06	1.00E-05	10	Log Normal	-	-	-	-	PNNL-22563 Carbon Loading 3.3E-3/h
		LTA Adsorber	Overload	Adsorber - Target Value	-	-	Target Value	Log Normal	1.00E-07	1.00E-06	1.00E-05	10	Log Normal	-	-	-	-	PNNL-22563 Carbon Loading 3.3E-3/h
		LTA Filter	Bypass	Filter	-	-	Target Value	Log Normal	1.00E-07	1.00E-06	1.00E-05	10	Log Normal	-	-	-	-	Target Value with high uncertainty
		LTA Filter	Plugged	Filter	Combined	-	EGG-SSRE, EFDA, NUREG, INEEL Fusion	Log Normal	3.00E-07	3.00E-06	3.00E-05	10	Log Normal	-	-	-	-	4.8E-6 (EGG-SSRE), 3.1E-6 (EFDA), 3.1E-7 (NUREG), 3E-6 (INEEL Fusion)
		Heat Exchanger	All	Heat Exchangers - General	HTGR	1987	MHTGR PRA	Log Normal	1.00E-06	3.00E-05	3.00E-04	17.32	Log Normal	-	-	-	-	
	General	Piping-Weld	Leak	Welds	HTGR	1987	MHTGR PRA	Log Normal	3.00E-08	3.00E-07	3.00E-06	10	Log Normal	-	-	-	-	Same as EGG Gas, same order of
		Piping-Leak	All (per foot)	Piping - General (Need to calculate with length included)	HTGR	1987	MHTGR PRA	Log Normal	2.00E-11	2.00E-10	2.00E-09	10	Log Normal	-	-	-	-	EGG Gas 3E-10, same order of magnitude for PWR NRC data. HTGR data used.
		Vessel	All	Vessel - All (Leak)	HTGR	1987	MHTGR PRA	Log Normal	1.00E-09	1.00E-08	3.00E-08	5.48	Log Normal					Same as EGG Gas, same order of magnitude for PWR. NRC data.
		Gasket	Leak	Gaskets	HTGR	1987	MHTGR PRA	Log Normal	3.00E-07	3.00E-06	9.00E-06	5.48	Log Normal	-	-	-	-	Same as EGG Gas, same order of magnitude for PWR. NRC data.
		Flange / Closure	Rupture	Flange and Closure	HTGR	1987	MHTGR PRA	Log Normal	3.00E-10	3.00E-09	3.00E-08	10	Log Normal					Same as EGG Gas, same order of magnitude for PWR. NRC data.
		Instrumentation	All	General	HTGR	1987	MHTGR PRA	Log Normal	1.00E-07	1.00E-06	1.00E-05	10	Log Normal	-	-	-	-	
	Group	Component	Component Failure Mode	Description	Reactor Type	Publication Date	Data Source	Dist'n	Mean	Alpha	Beta	Error Factor	Dist'n	Mean	Alpha	Beta	Error Factor	Comments
	EDG - SBO	EDG-SBO FTLR	Load/Run	EDG-Station Blackout Fail to Load/Run	PWR	2010	NUREG	-	-	-	-	-	Beta	1.01E-02	4.500	4.402E+02	2.0	First 1 hour
		EDG-SBO FTR	Run	EDG-Station Blackout Fail to Run	PWR	2010	NUREG	Gamma	1.30E-03	1.500	1.155E+03	3.3	-	-	-	-	-	Beyond 1 hour
		EDG-SBO FTS	Start	EDG-Station Blackout Fail to Start	PWR	2010	NUREG	-	-	-	-	-	Beta	4.32E-02	1.094	2.423E+01	4.0	

Note Lognormal distributions, EF = SQRT($\lambda_{95\%}/\lambda_{5\%}$)

Appendix C.2. SPAR-H Worksheets for Human Reliability Analysis

HRA Worksheets for LP/SD

SPAR Human Error Worksheet

Plant: EM[2] **Initiating Event:** N/A **Basic Event :** Generic **Event Coder:** N/A

Basic Event Context: Generic operator interaction with Fission Product Vent System

Basic Event Description: Generic operator interaction with Fission Product Vent System

Does this task contain a significant amount of diagnosis activity? YES [X] (start with Part I–Diagnosis) NO [ ] (skip Part I – Diagnosis; start with Part II – Action) Why?_____

PART I. EVALUATE EACH PSF FOR DIAGNOSIS

A. Evaluate PSFs for the Diagnosis Portion of the Task.

PSFs	PSF Levels	Multiplier for Diagnosis		Please note specific reasons for PSF level selection in this column.
Available Time	Inadequate time	P(failure) = 1.0	[ ]	
	Barely adequate time (≈ 2/3 x nominal)	10	[ ]	
	Nominal time	1	[ ]	
	Extra time (between 1and 2 x nominal and > 30 min)	0.1	[ ]	
	Expansive time > 2 x nominal & > 30 min	0.1 to 0.01	[ ]	
	Insufficient Information	1	[X]	
Stress/ Stressors	Extreme	5	[ ]	
	High	2	[ ]	
	Nominal	1	[ ]	
	Insufficient Information	1	[X]	
Complexity	Highly complex	5	[ ]	
	Moderately complex	2	[ ]	
	Nominal	1	[ ]	
	Obvious diagnosis	0.1	[ ]	
	Insufficient Information	1	[X]	
Experience/ Training	Low	10	[ ]	
	Nominal	1	[ ]	
	High	0.5	[ ]	
	Insufficient Information	1	[X]	
Procedures	Not available	50	[ ]	
	Incomplete	20	[ ]	
	Available, but poor	5	[ ]	
	Nominal	1	[ ]	
	Diagnostic/symptom oriented	0.5	[ ]	
	Insufficient Information	1	[X]	
Ergonomics/ HMI	Missing/Misleading	50	[ ]	
	Poor	10	[ ]	
	Nominal	1	[ ]	
	Good	0.5	[ ]	
	Insufficient Information	1	[X]	
Fitness for Duty	Unfit	P(failure) = 1.0	[ ]	
	Degraded Fitness	5	[ ]	
	Nominal	1	[ ]	
	Insufficient Information	1	[X]	
Work Processes	Poor	2	[ ]	
	Nominal	1	[ ]	
	Good	0.8	[ ]	
	Insufficient Information	1	[X]	

Rev 1 (1/20/04)

Reviewer: Lenhof

Plant: EM^2 **Initiating Event:** N/A **Basic Event :** Generic **Event Coder:** N/A

Basic Event Context: Generic operator interaction with Fission Product Vent System

Basic Event Description: Generic operator interaction with Fission Product Vent System

B. Calculate the Diagnosis Failure Probability.

(1) If all PSF ratings are nominal, then the Diagnosis Failure Probability = 1.0E-2
(2) Otherwise, the Diagnosis Failure Probability is: 1.0E-2 x Time x Stress or Stressors x Complexity x Experience or Training x Procedures x Ergonomics or HMI x Fitness for Duty x Processes

Diagnosis: 1.0E-2x ____ x ____ x ____ x ____ x ____ x ____ x ____ x ____ = | 1.0E-2 |

C. Calculate the Adjustment Factor IF Negative Multiple (≥3) PSFs are Present.

When 3 or more negative PSF influences are present, in lieu of the equation above, you must compute a composite PSF score used in conjunction with the adjustment factor. Negative PSFs are present anytime a multiplier greater than 1 is selected. The Nominal HEP (NHEP) is 1.0E-2 for Diagnosis. The composite PSF score is computed by multiplying all the assigned PSF values. Then the adjustment factor below is applied to compute the HEP:

$$HEP = \frac{NHEP \cdot PSF_{composite}}{NHEP \cdot \left(PSF_{composite} - 1\right) + 1}$$

Diagnosis HEP with Adjustment Factor = | 1.0E-2 |

D. Record Final Diagnosis HEP.

If no adjustment factor was applied, record the value from Part B as your final diagnosis HEP. If an adjustment factor was applied, record the value from Part C.

Final Diagnosis HEP = | 1.0E-2 |

Reviewer: Lenhof

Plant: EM^2 **Initiating Event:** N/A **Basic Event :** Generic **Event Coder:** N/A

Basic Event Context: Generic operator interaction with Fission Product Vent System

Basic Event Description: Generic operator interaction with Fission Product Vent System

Part II. EVALUATE EACH PSF FOR ACTION

A. Evaluate PSFs for the Action Portion of the Task, If Any.

PSFs	PSF Levels	Multiplier for Action		Please note specific reasons for PSF level selection in this column.
Available Time	Inadequate time	P(failure) = 1.0	☐	
	Time available is ≈ the time required	10	☐	
	Nominal time	1	☐	
	Time available ≥ 5x the time required	0.1	☐	
	Time available is ≥ 50x the time required	0.01	☐	
	Insufficient Information	1	☒	
Stress/ Stressors	Extreme	5	☐	
	High	2	☐	
	Nominal	1	☐	
	Insufficient Information	1	☒	
Complexity	Highly complex	5	☐	
	Moderately complex	2	☐	
	Nominal	1	☐	
	Insufficient Information	1	☒	
Experience/ Training	Low	3	☐	
	Nominal	1	☐	
	High	0.5	☐	
	Insufficient Information	1	☒	
Procedures	Not available	50	☐	
	Incomplete	20	☐	
	Available, but poor	5	☐	
	Nominal	1	☐	
	Insufficient Information	1	☒	
Ergonomics/ HMI	Missing/Misleading	50	☐	
	Poor	10	☐	
	Nominal	1	☐	
	Good	0.5	☐	
	Insufficient Information	1	☒	
Fitness for Duty	Unfit	P(failure) = 1.0	☐	
	Degraded Fitness	5	☐	
	Nominal	1	☐	
	Insufficient Information	1	☒	
Work Processes	Poor	5	☐	
	Nominal	1	☐	
	Good	0.5	☐	
	Insufficient Information	1	☒	

Reviewer: Lenhof

Plant: EM^2 **Initiating Event:** N/A **Basic Event :** Generic **Event Coder:** N/A

Basic Event Context: Generic operator interaction with Fission Product Vent System

Basic Event Description: Generic operator interaction with Fission Product Vent System

B. Calculate the Action Failure Probability.

(1) If all PSF ratings are nominal, then the Action Failure Probability = 1.0E-3
(2) Otherwise, the Action Failure Probability is: 1.0E-3 x Time x Stress or Stressors x Complexity x Experience or Training x Procedures x Ergonomics or HMI x Fitness for Duty x Processes

Action: 1.0E-3x ____ x ____ x ____ x ____ x ____ x ____ x ____ x ____ = **1.0E-3**

C. Calculate the Adjustment Factor <u>IF</u> Negative Multiple (≥3) PSFs are Present.

When 3 or more negative PSF influences are present, in lieu of the equation above, you must compute a composite PSF score used in conjunction with the adjustment factor. Negative PSFs are present anytime a multiplier greater than 1 is selected. The Nominal HEP (NHEP) is 1.0E-3 for Action. The composite PSF score is computed by multiplying all the assigned PSF values. Then the adjustment factor below is applied to compute the HEP:

$$HEP = \frac{NHEP \cdot PSF_{composite}}{NHEP \cdot \left(PSF_{composite} - 1\right) + 1}$$

Action HEP with Adjustment Factor = **1.0E-3**

D. Record Final Action HEP.

If no adjustment factor was applied, record the value from Part B as your final action HEP. If an adjustment factor was applied, record the value from Part C.

Final Action HEP = **1.0E-3**

Reviewer: Lenhof

Plant: EM^2 **Initiating Event:** N/A **Basic Event :** Generic **Event Coder:** N/A

Basic Event Context: Generic operator interaction with Fission Product Vent System

Basic Event Description: Generic operator interaction with Fission Product Vent System

PART III. CALCULATE TASK FAILURE PROBABILITY WITHOUT FORMAL DEPENDENCE ($P_{w/od}$)

Calculate the Task Failure Probability Without Formal Dependence ($P_{w/od}$) by adding the Diagnosis Failure Probability from Part I and the Action Failure Probability from Part II. In instances where an action is required without a diagnosis and there is no dependency, then this step is omitted.

$P_{w/od}$ = Diagnosis HEP 1.0E-2 + Action HEP 1.0E-3 = **1.10E-2**

Part IV. DEPENDENCY

For all tasks, except the first task in the sequence, use the table and formulae below to calculate the Task Failure Probability With Formal Dependence ($P_{w/d}$).

If there is a reason why failure on previous tasks should not be considered, such as it is impossible to take the current action unless the previous action has been properly performed, explain here: _____

Dependency Condition Table

Condition Number	Crew (same or different)	Time (close in time or not close in time)	Location (same or different)	Cues (additional or no additional)	Dependency	Number of Human Action Failures Rule ☐ - Not Applicable. Why?_____
1	s	c	s	na	complete	When considering recovery in a series e.g., 2nd, 3rd, or 4th checker If this error is the **3rd error in the sequence**, then the dependency is at least **moderate**. If this error is the **4th error in the sequence**, then the dependency is at least **high**.
2				a	complete	
3			d	na	high	
4				a	high	
5		nc	s	na	high	
6				a	moderate	
7			d	na	moderate	
8				a	low	
9	d	c	s	na	moderate	
10				a	moderate	
11			d	na	moderate	
12				a	moderate	
13		nc	s	na	low	
14				a	low	
15			d	na	low	
16				a	low	
17					zero ✓	

Using $P_{w/od}$ = Probability of Task Failure Without Formal Dependence (calculated in Part III):

For Complete Dependence the probability of failure is 1.
For High Dependence the probability of failure is $(1+ P_{w/od})/2$
For Moderate Dependence the probability of failure is $(1+6 \times P_{w/od})/7$
For Low Dependence the probability of failure is $(1+19 \times P_{w/od})/20$
For Zero Dependence the probability of failure is $P_{w/od}$ ✓

Calculate $P_{w/d}$ using the appropriate values:

$P_{w/d}$ = (1 + (_____ * _____))/ _____ = **N/A**

Reviewer: Lenhof

Appendix C.3. Normal Operation Fault Trees

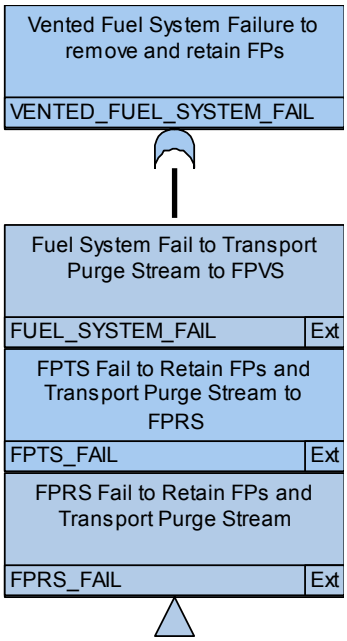

Figure C.3-1: Vented Fuel System Fault

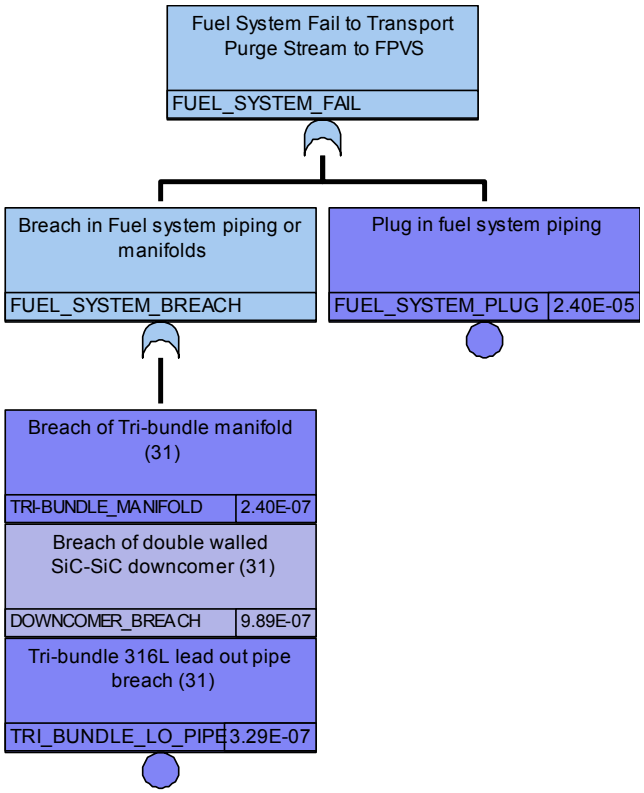

Figure C.3-2: Fuel System Fault Tree

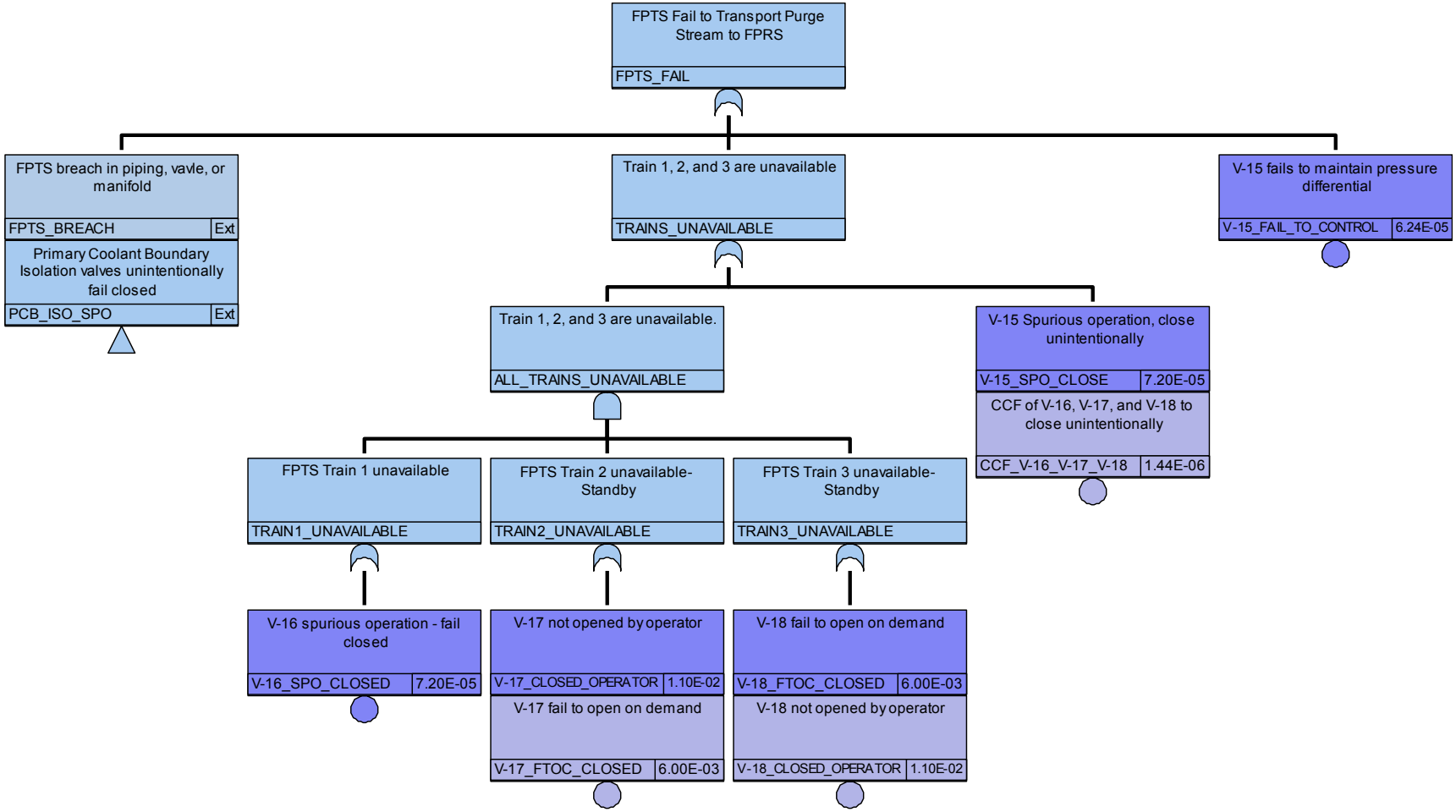

Figure C.3-3: Fission Product Transfer System Fault Tree

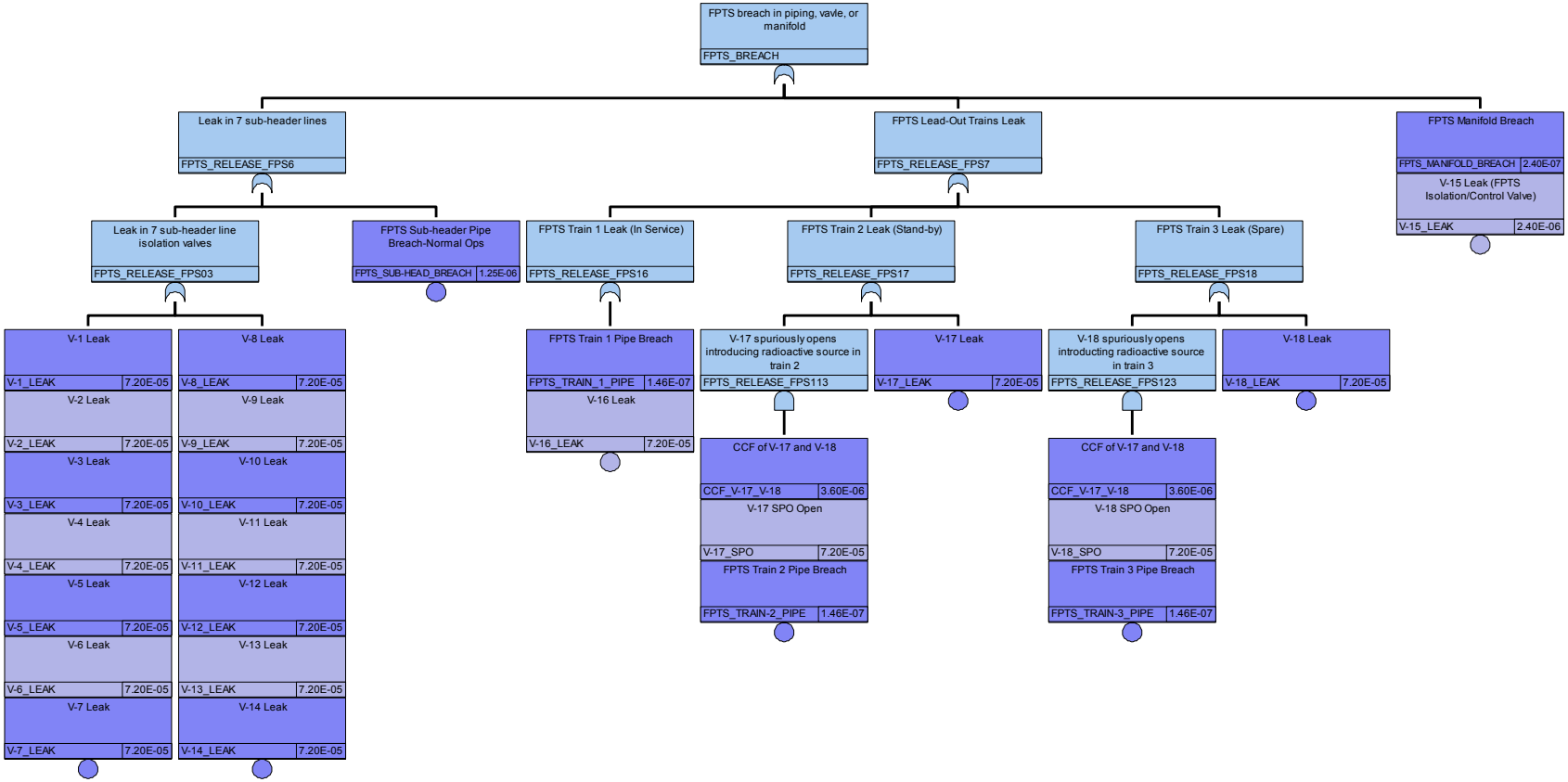

Figure C.3-4: FPTS Breach Fault Tree

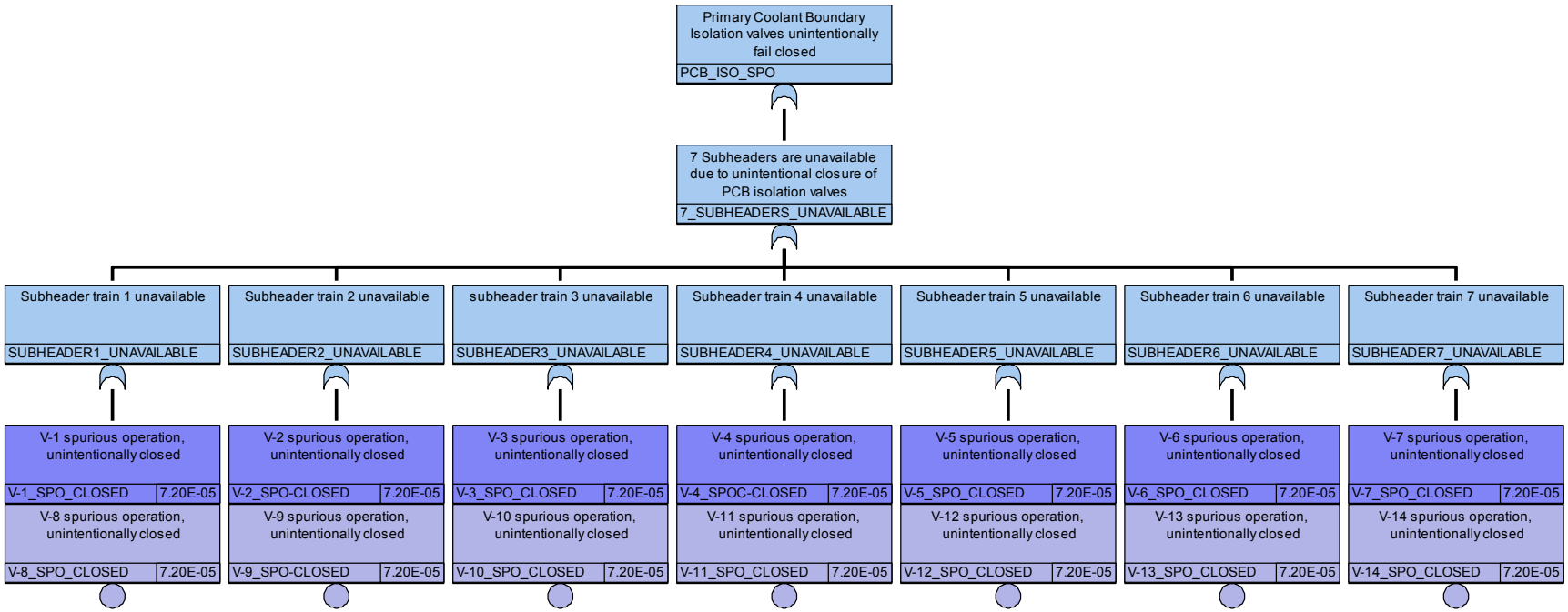

Figure C.3-5: PCB Isolation Valve Fault Tree

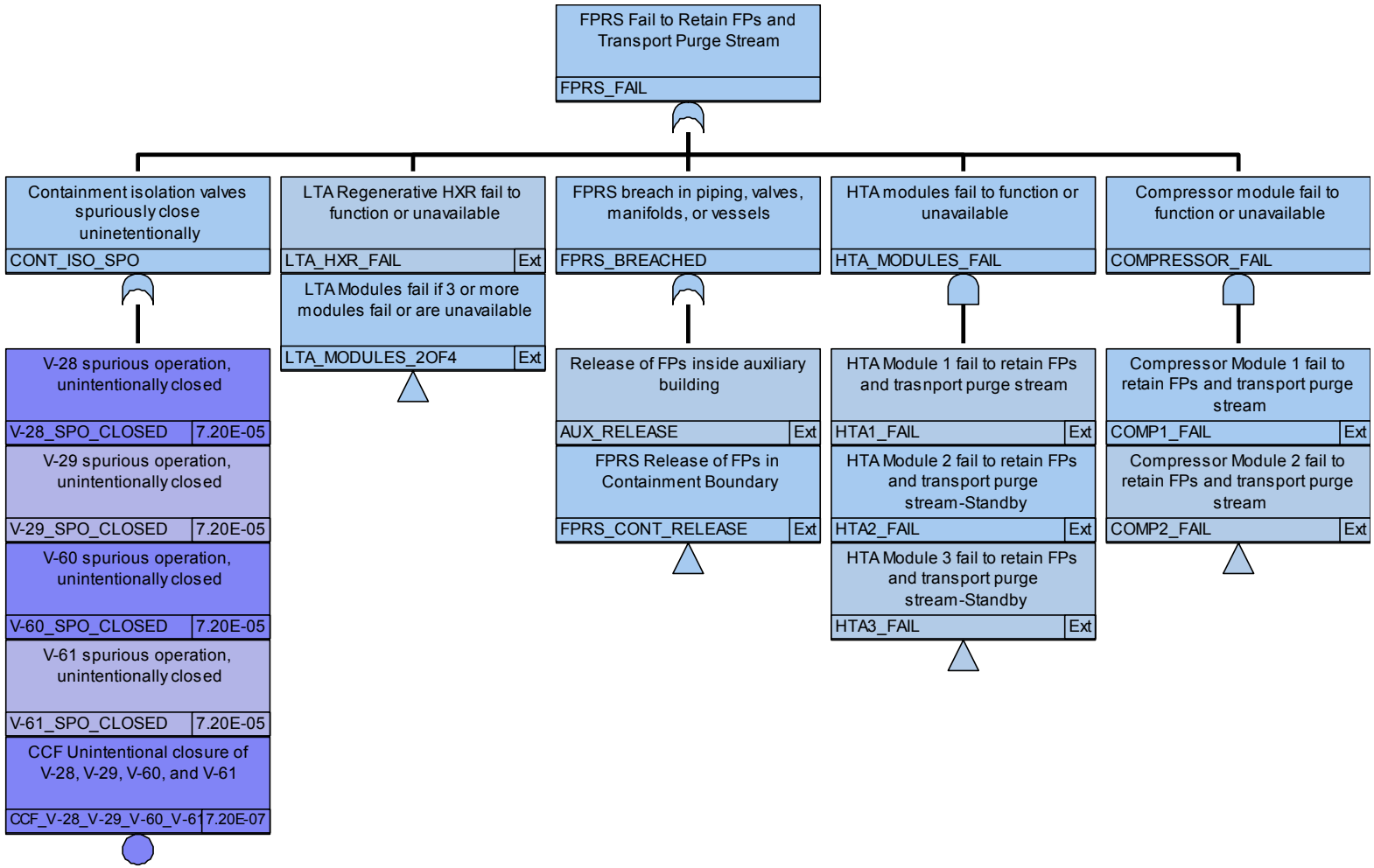

Figure C.3-6: Fission Product Retention System Fault Tree

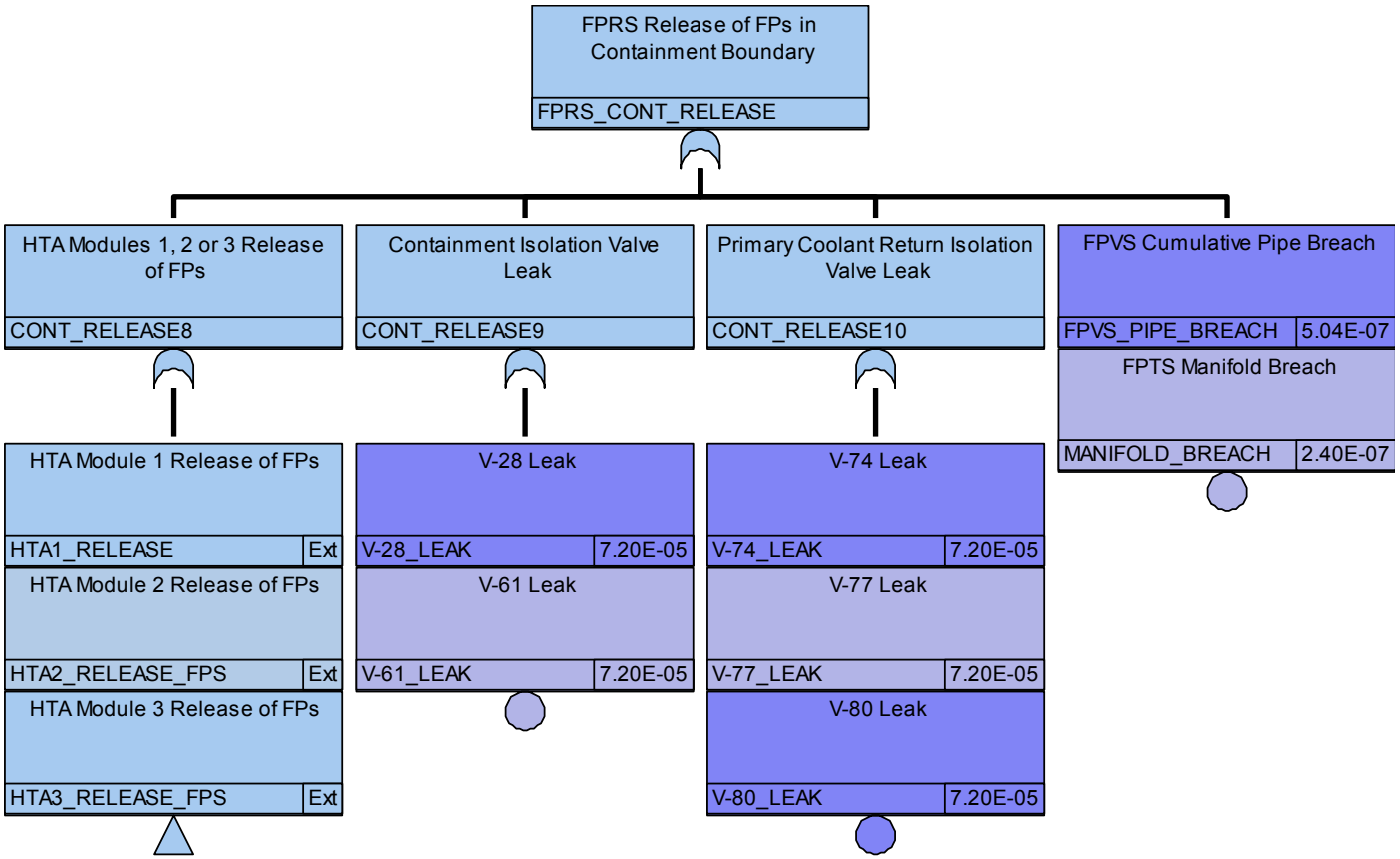

Figure C.3-7: FPRS Containment Release Fault Tree

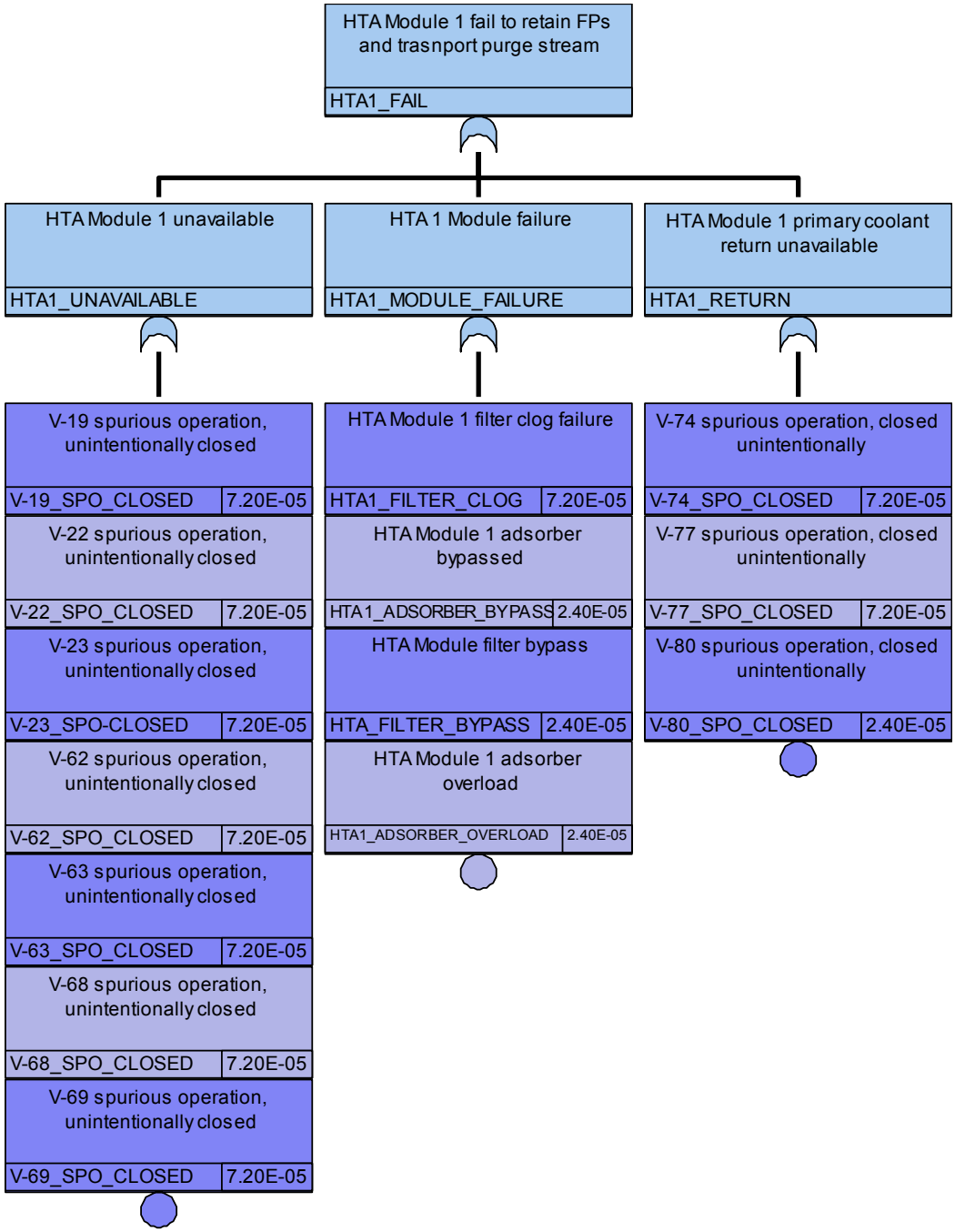

Figure C.3-8: High Temperature Adsorber Module 1 Fault Tree

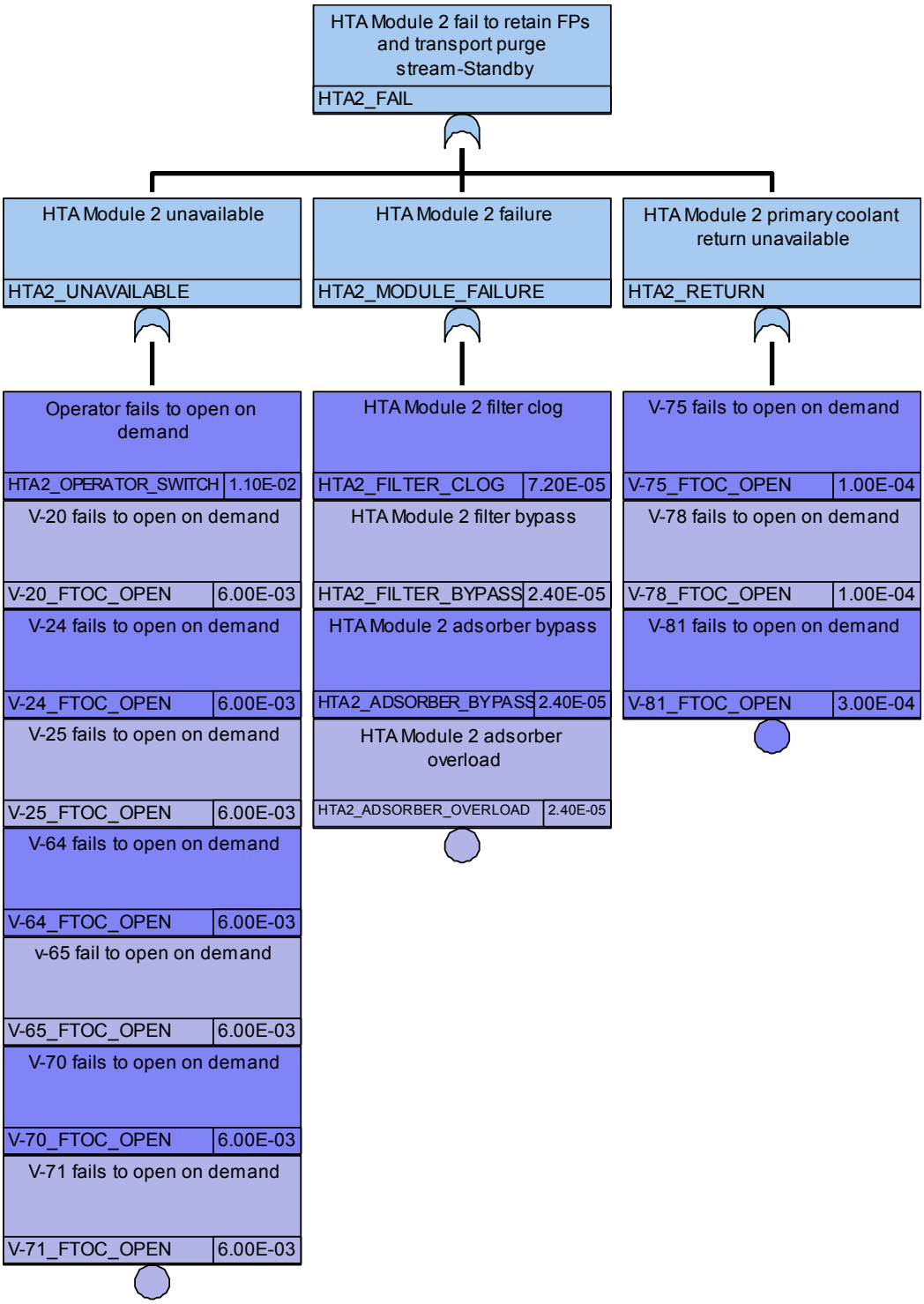

Figure C.3-9: High Temperature Adsorber Module 2 Fault Tree

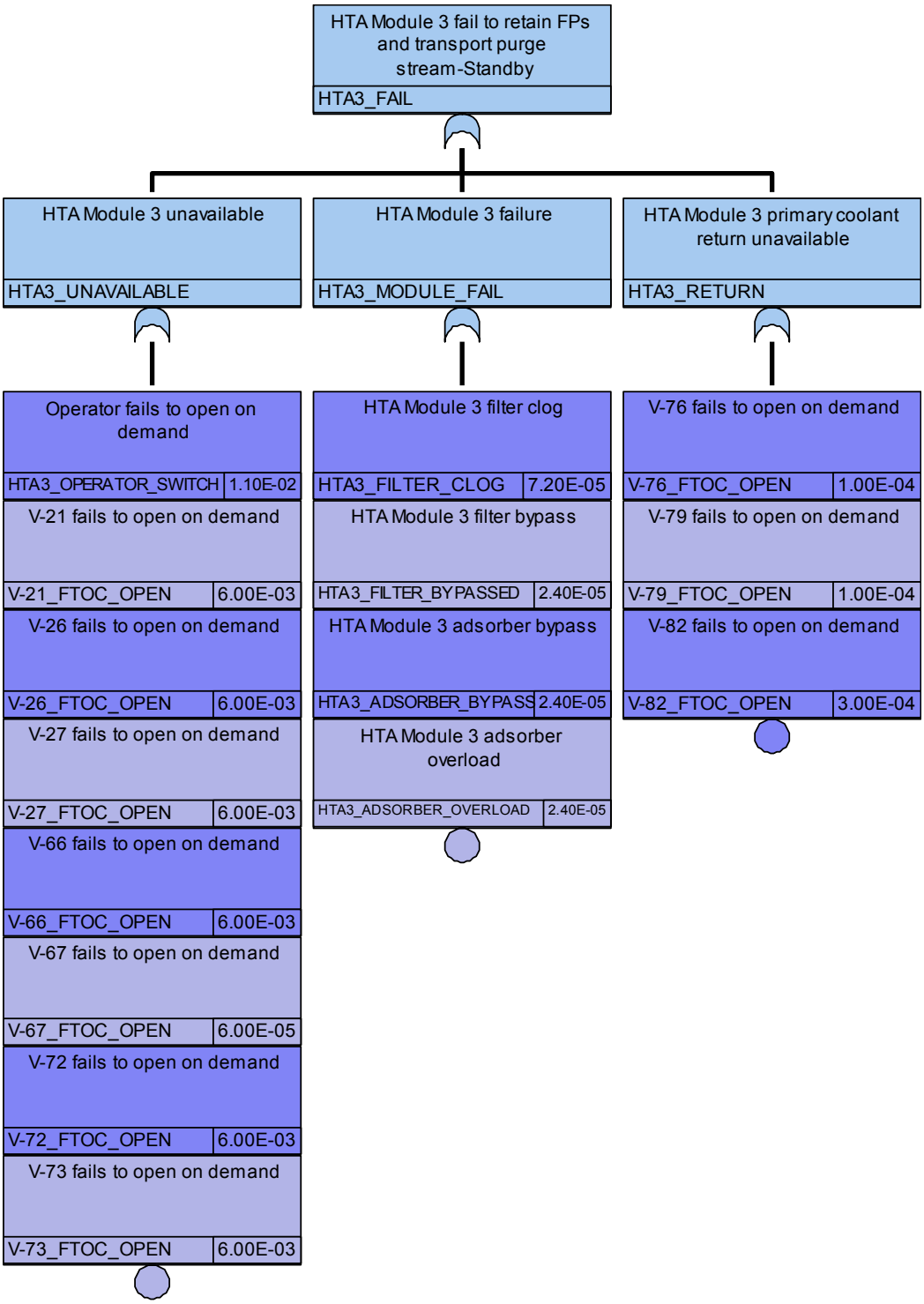

Figure C.3-10: High Temperature Adsorber Module 3 Fault Tree

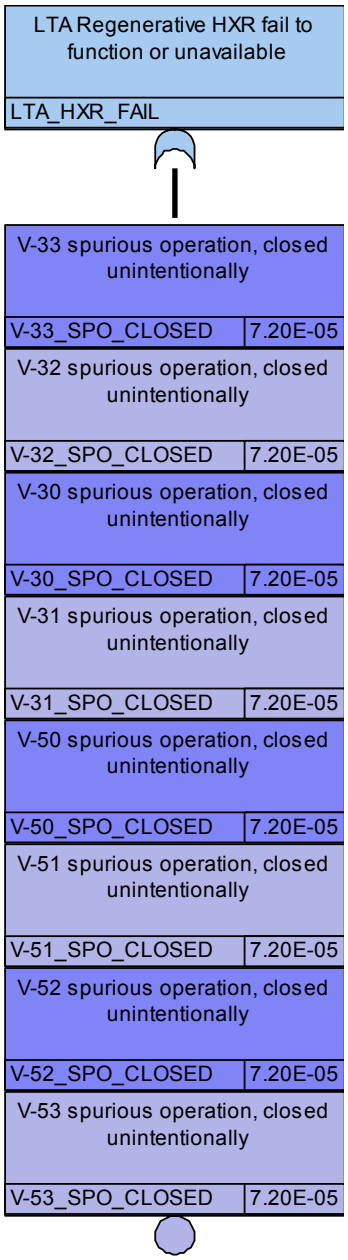

Figure C.3-11: LTA Regenerative Heat Exchanger Fault Tree

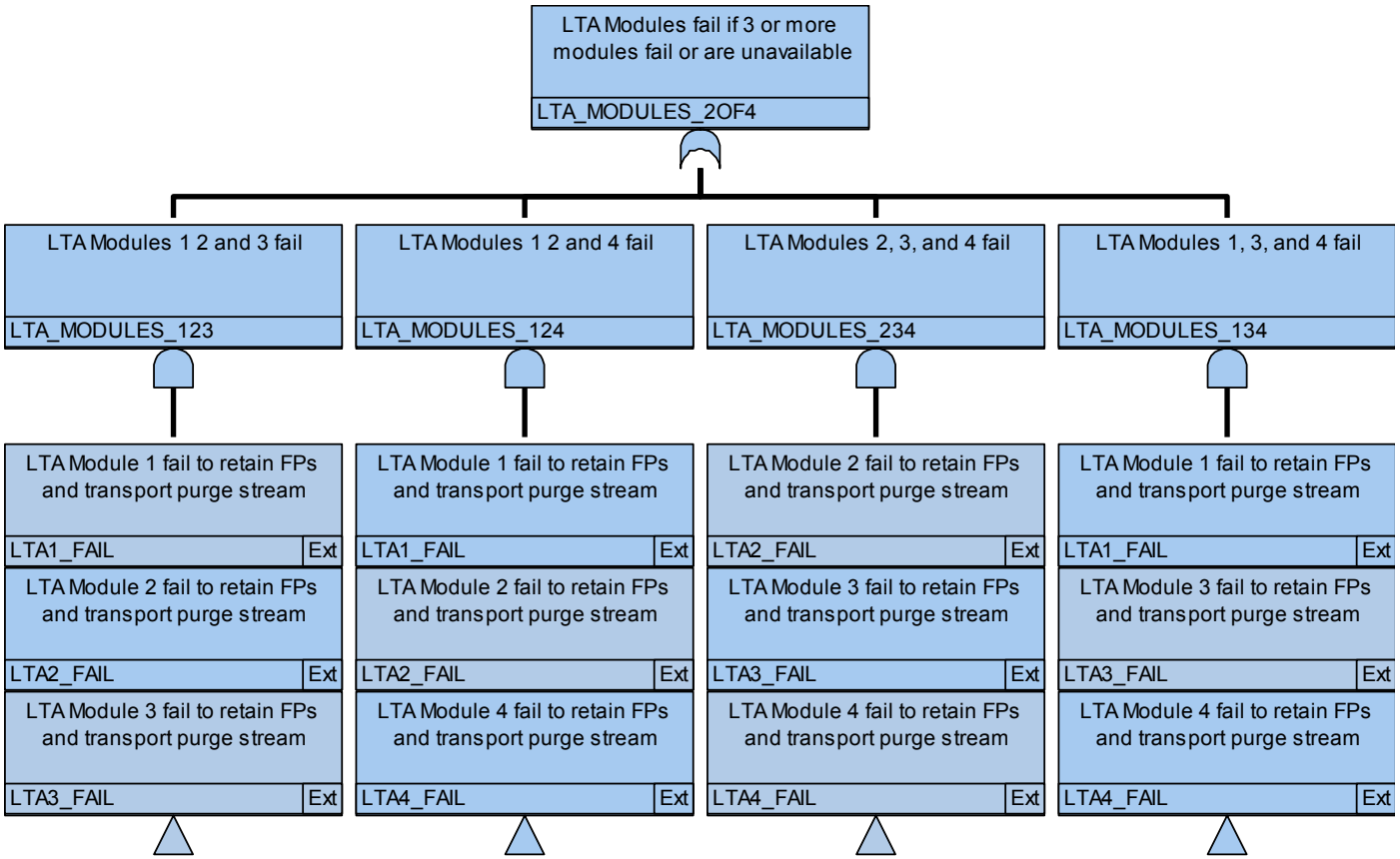

Figure C.3-12: Low Temperature Modules Fault Tree

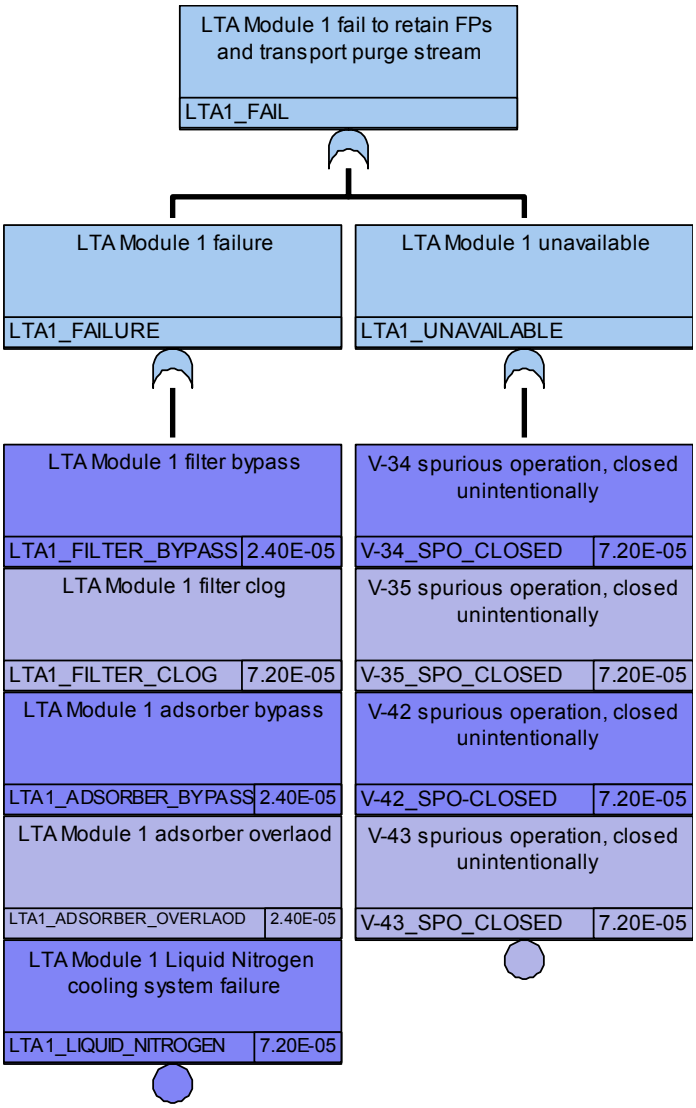

Figure C.3-13: Low Temperature Adsorber Module 1 Fault Tree

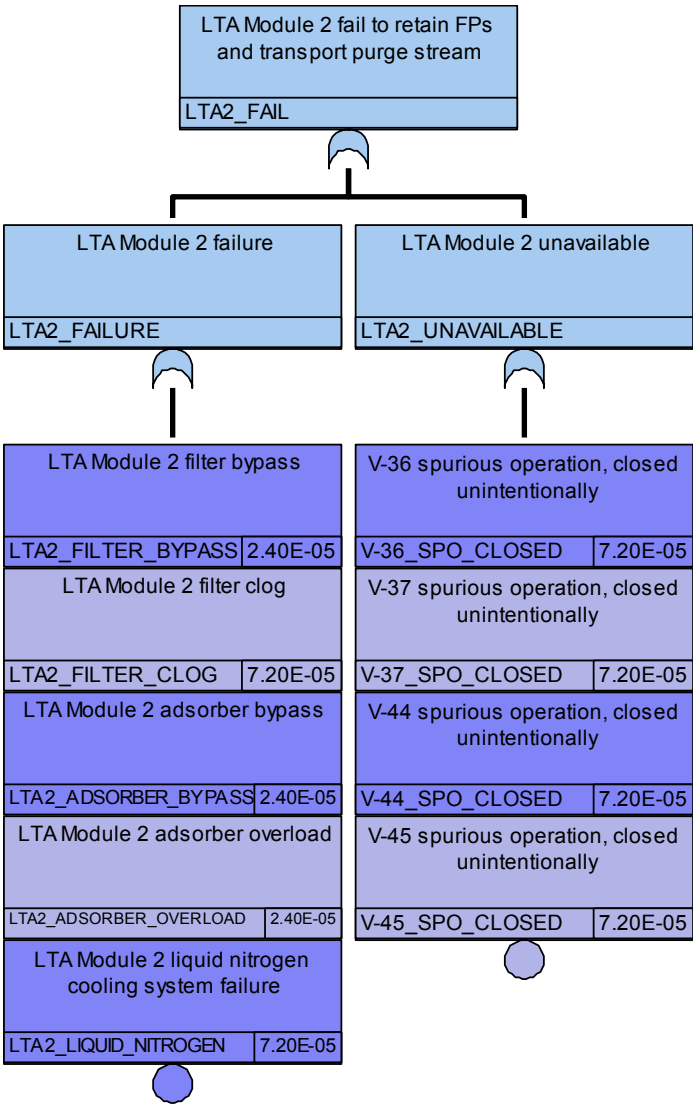

Figure C.3-14: Low Temperature Adsorber Module 2 Fault Tree

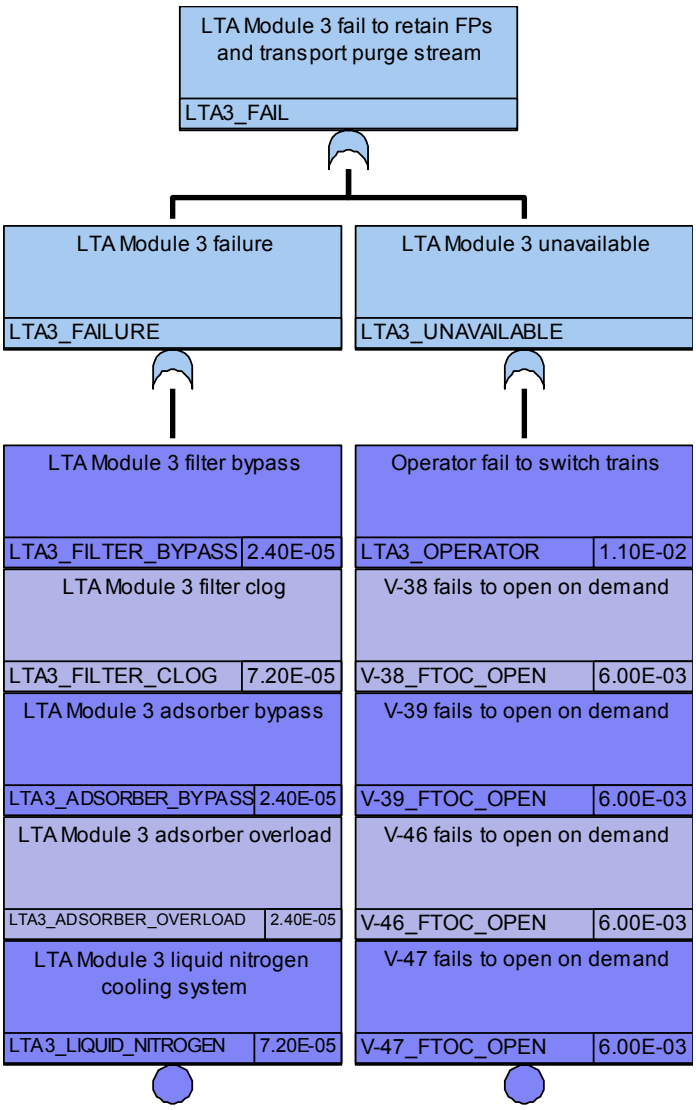

Figure C.3-15: Low Temperature Adsorber Module 3 Fault Tree

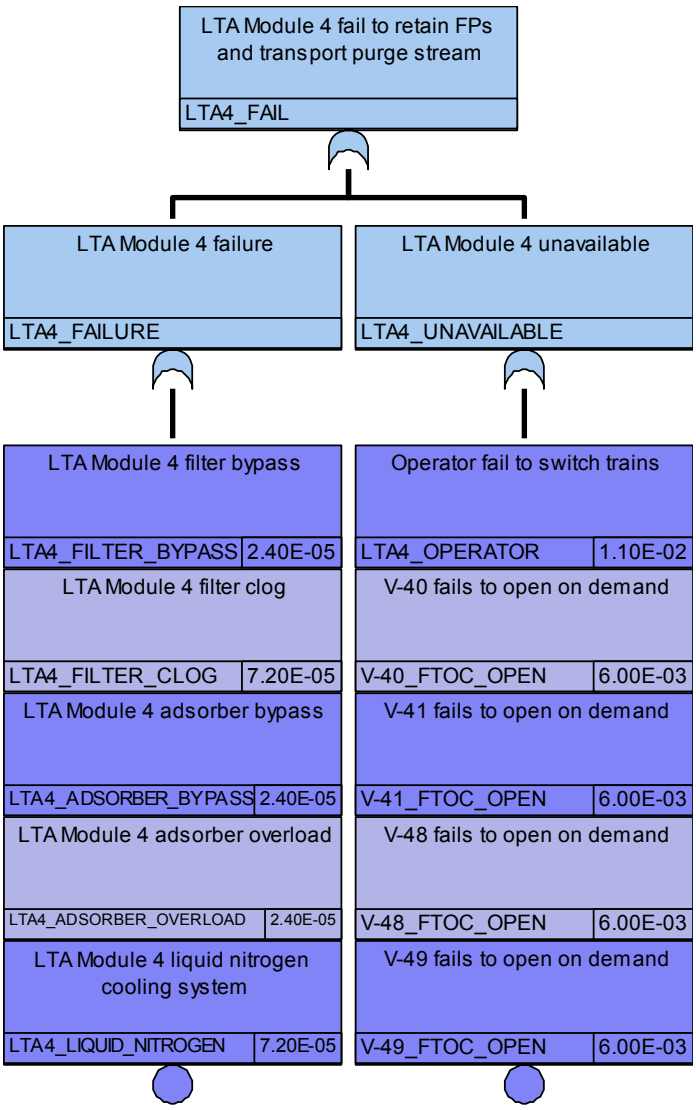

Figure C.3-16: Low Temperature Adsorber Module 4 Fault Tree

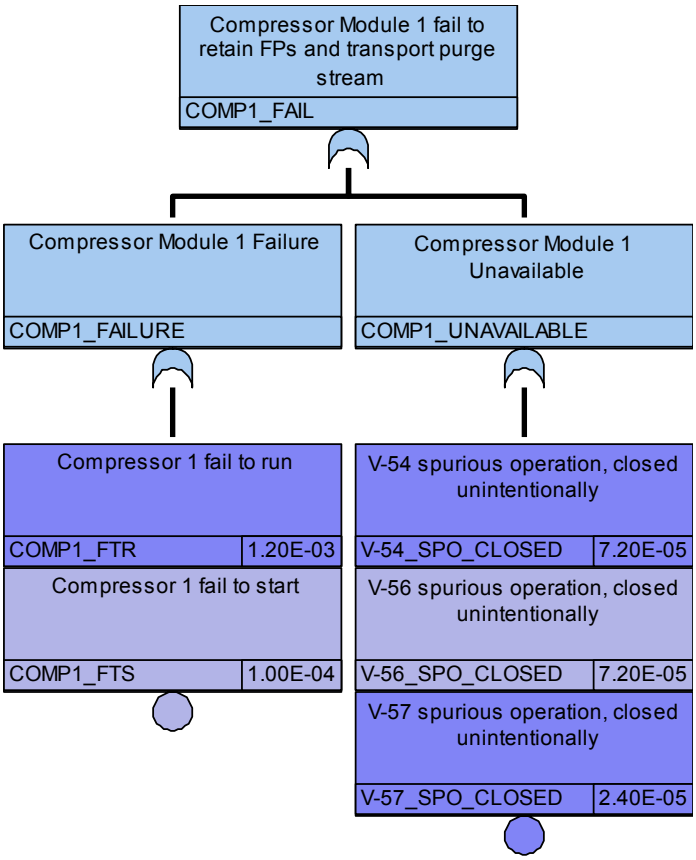

Figure C.3-17: Compressor Module 1 Fault Tree

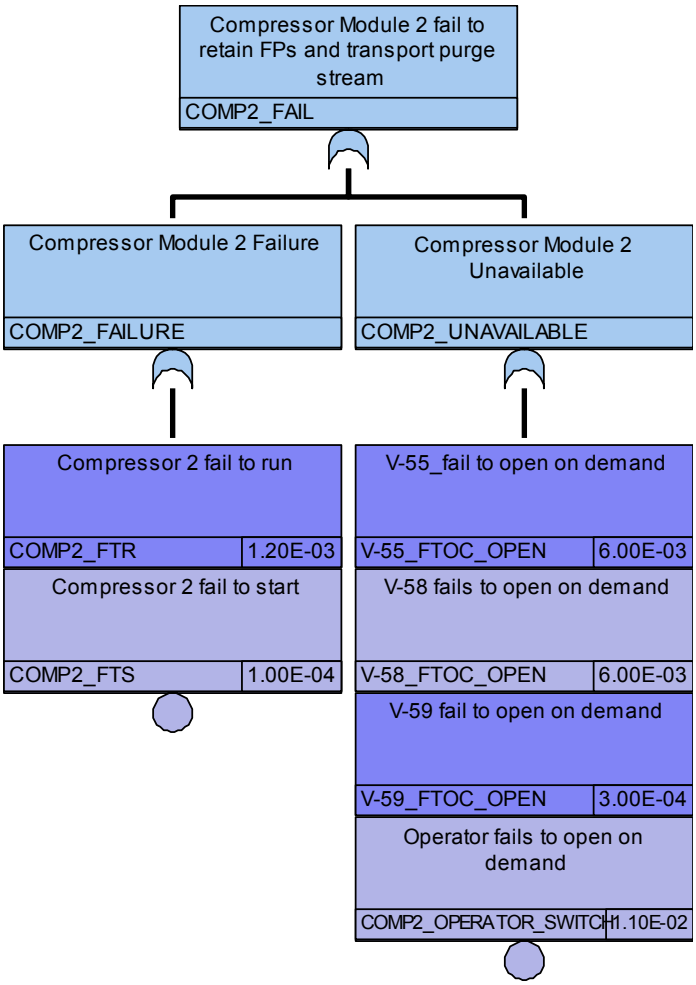

Figure C.3-18: Compressor Module 2 Fault Tree

Appendix C.4. Accident Condition Fault Trees

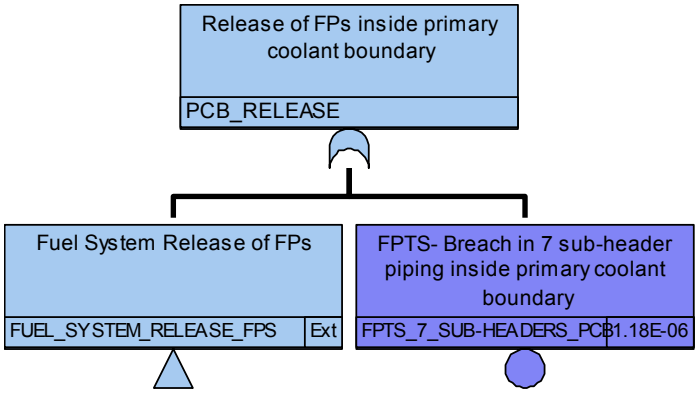

Figure C.4-1: Release in Primary Coolant Boundary Fault Tree

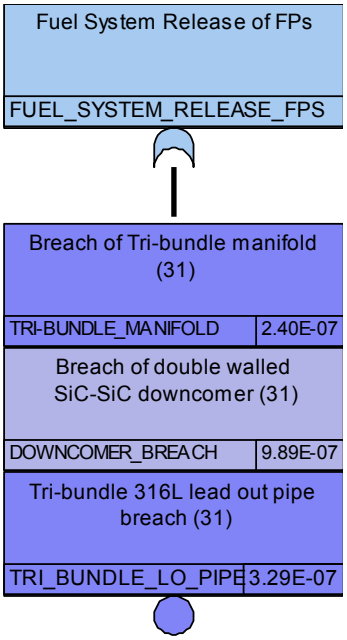

Figure C.4-2: Fuel System Fault Tree

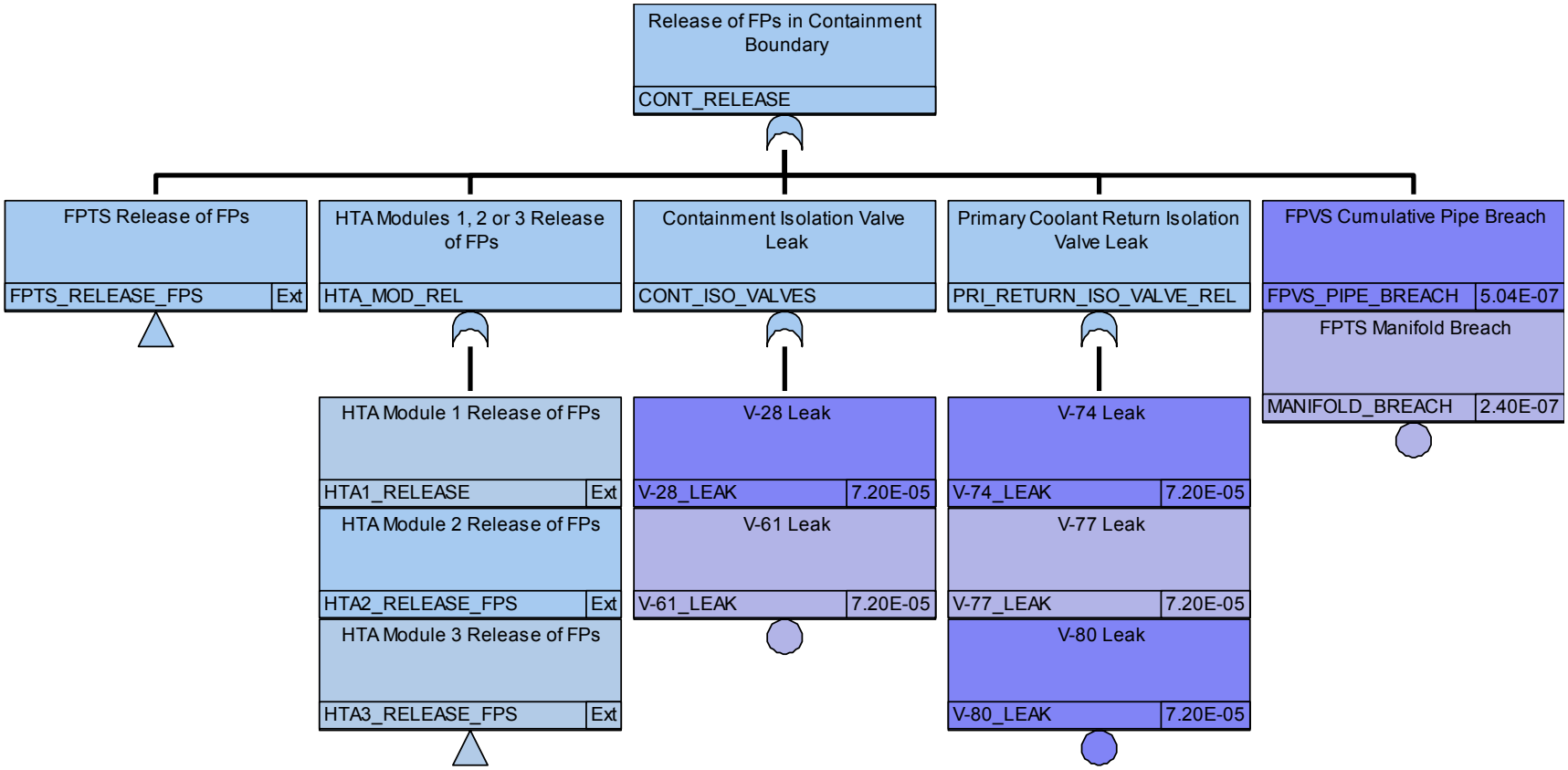

Figure C.4-3: Release in Containment Boundary Fault Tree

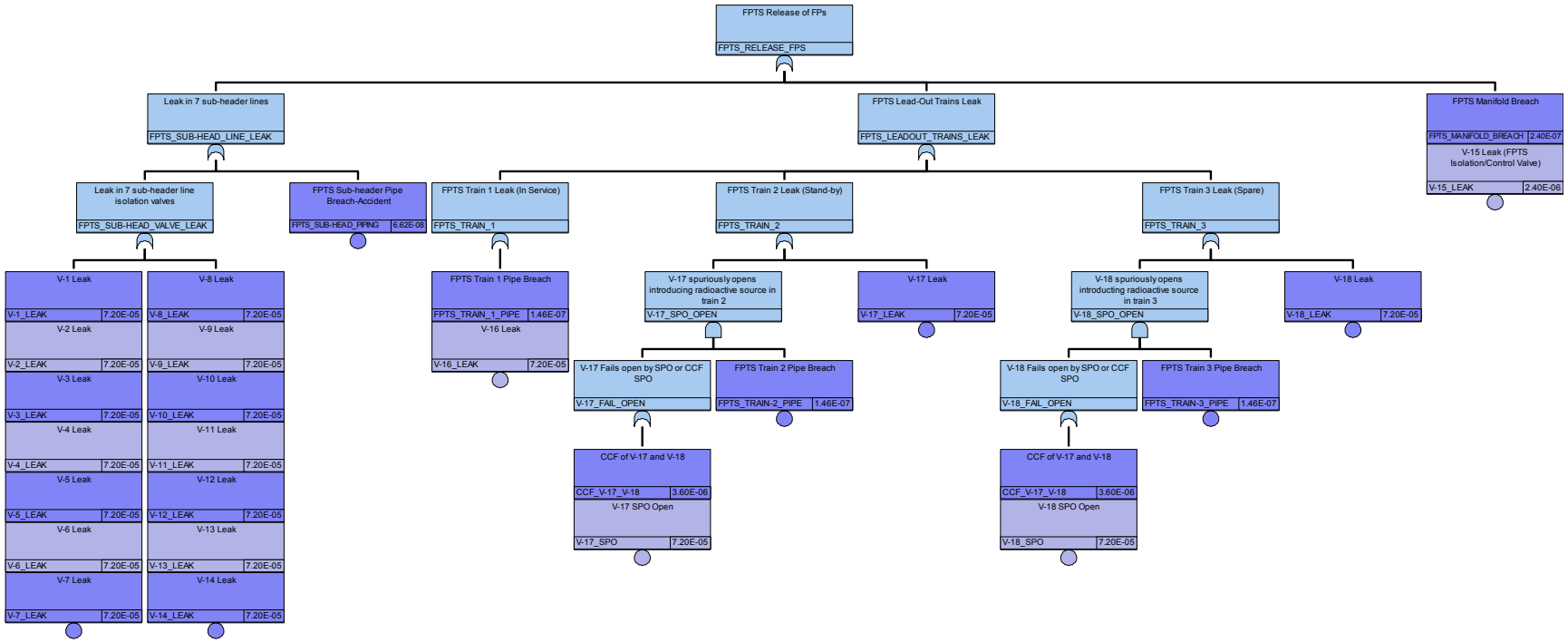

Figure C.4-4: Fission Product Transport System Fault Tree

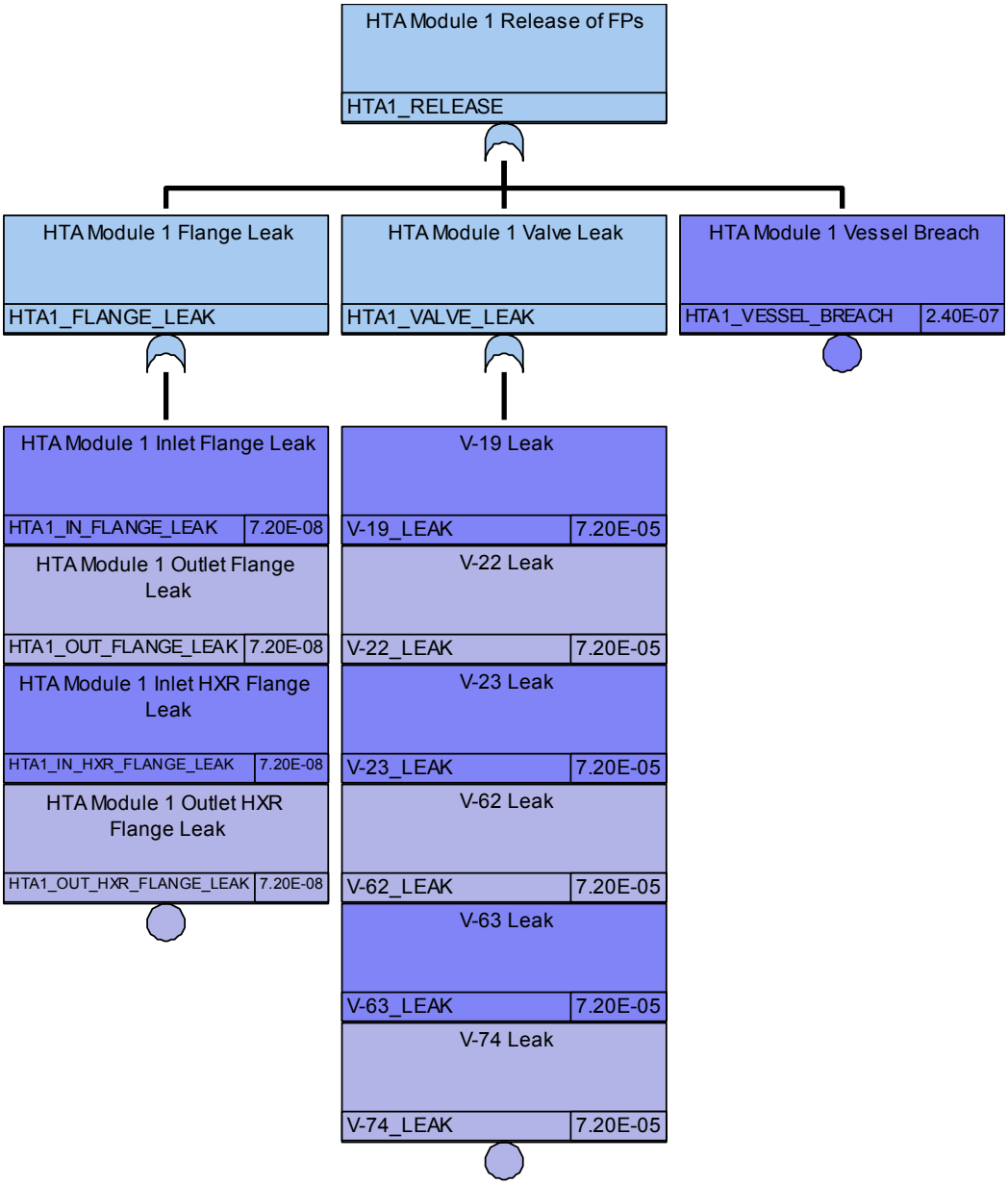

Figure C.4-5: High Temperature Adsorber Module 1 Fault Tree

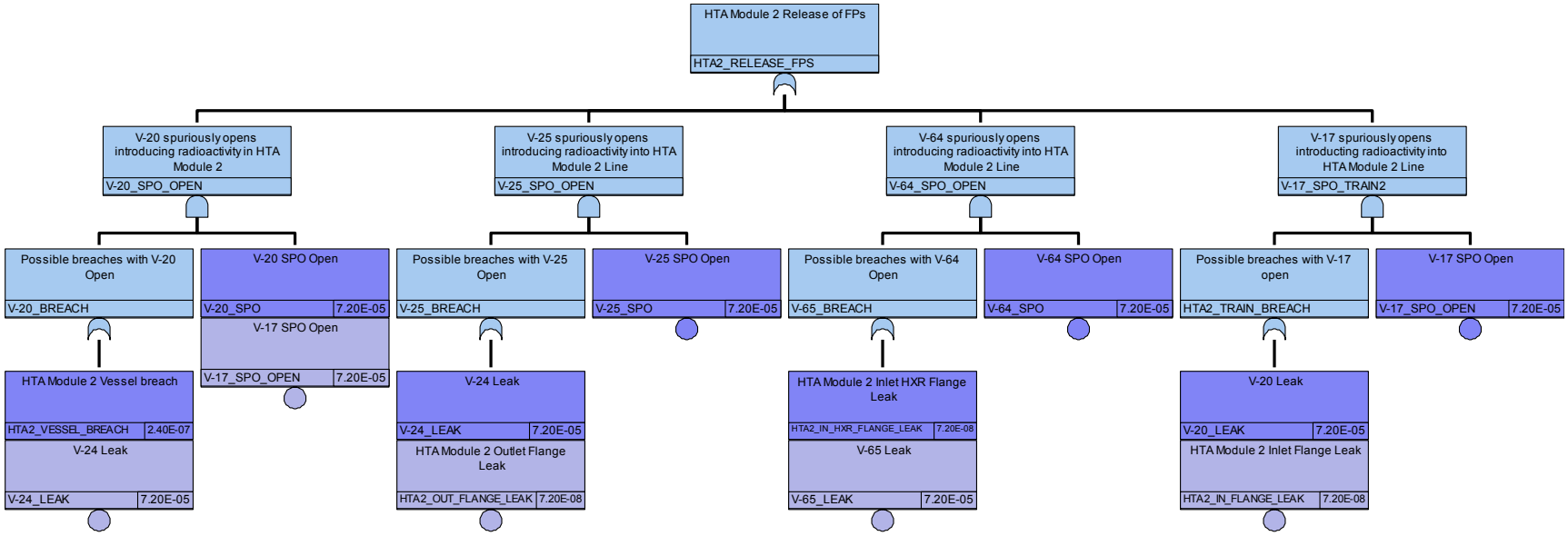

Figure C.4-6: High Temperature Adsorber Module 2 Fault Tree

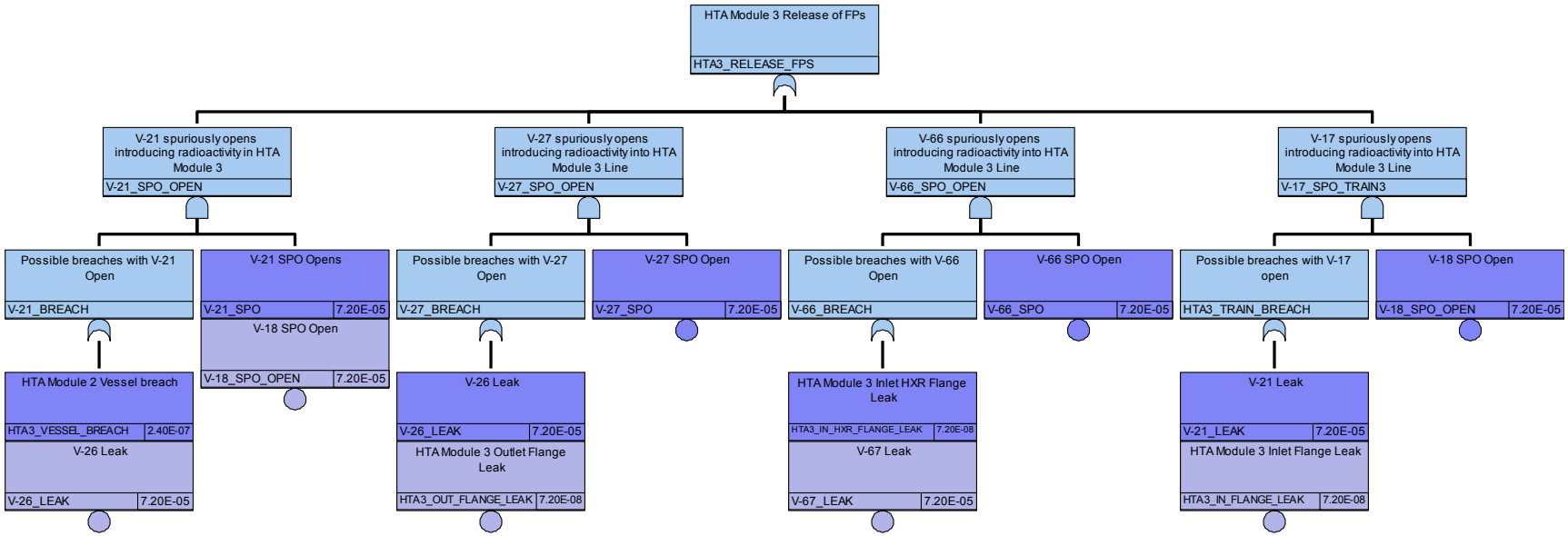

Figure C.4-7: High Temperature Adsorber Module 3 Fault Tree

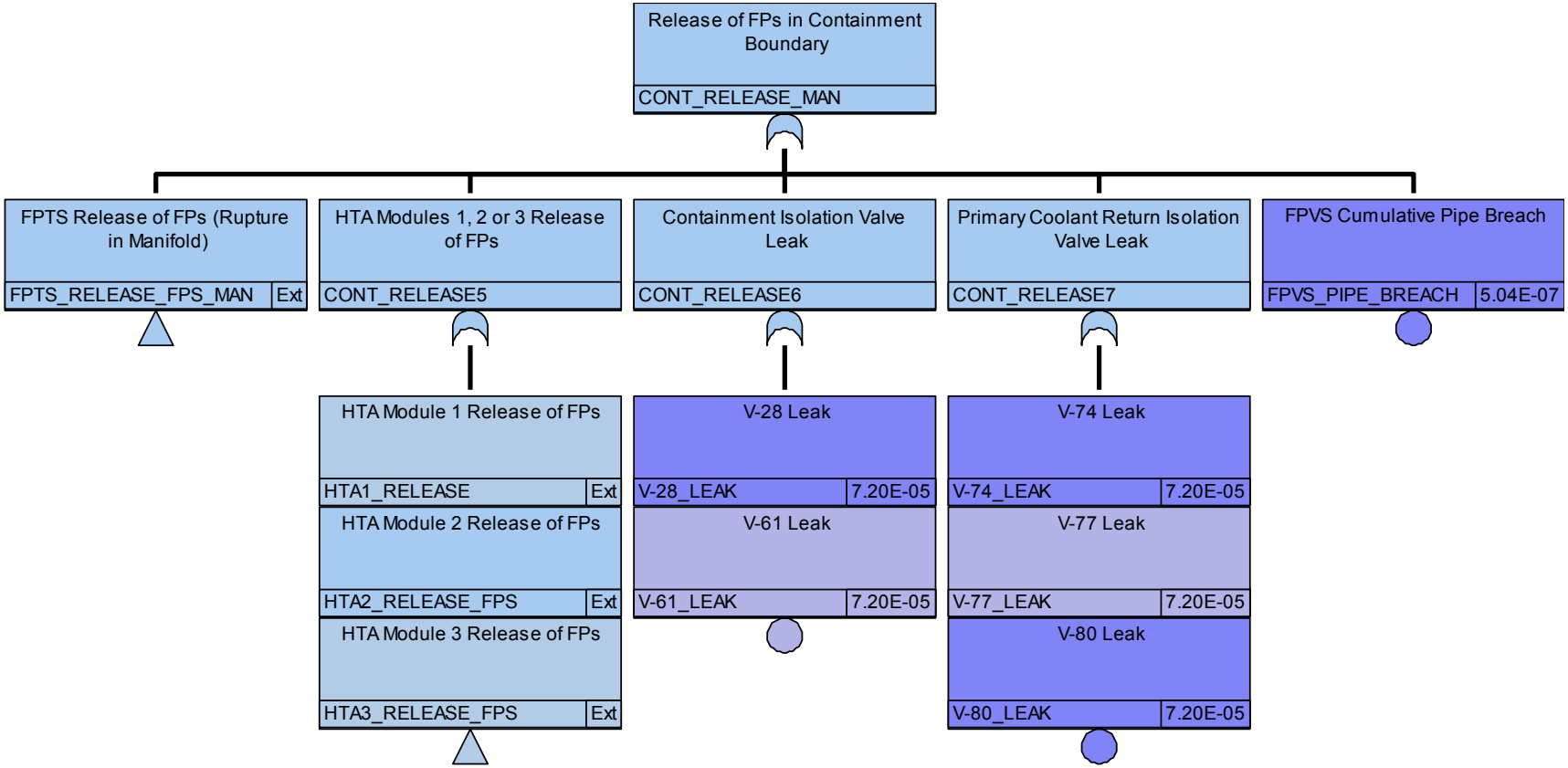

Figure C.4-8: Release in Containment Boundary Fault Tree (Rupture in Manifold)

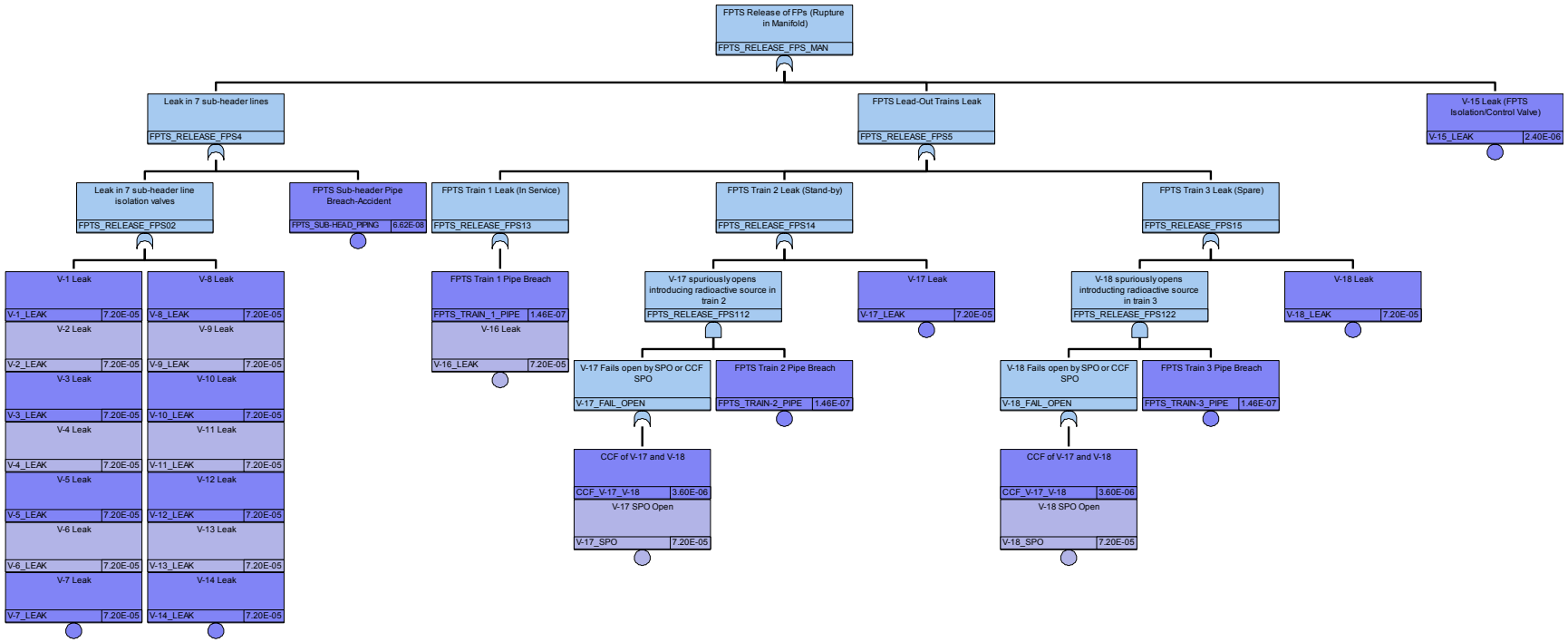

Figure C.4-9: Fission Product Transport System Fault Tree (Rupture in Manifold)

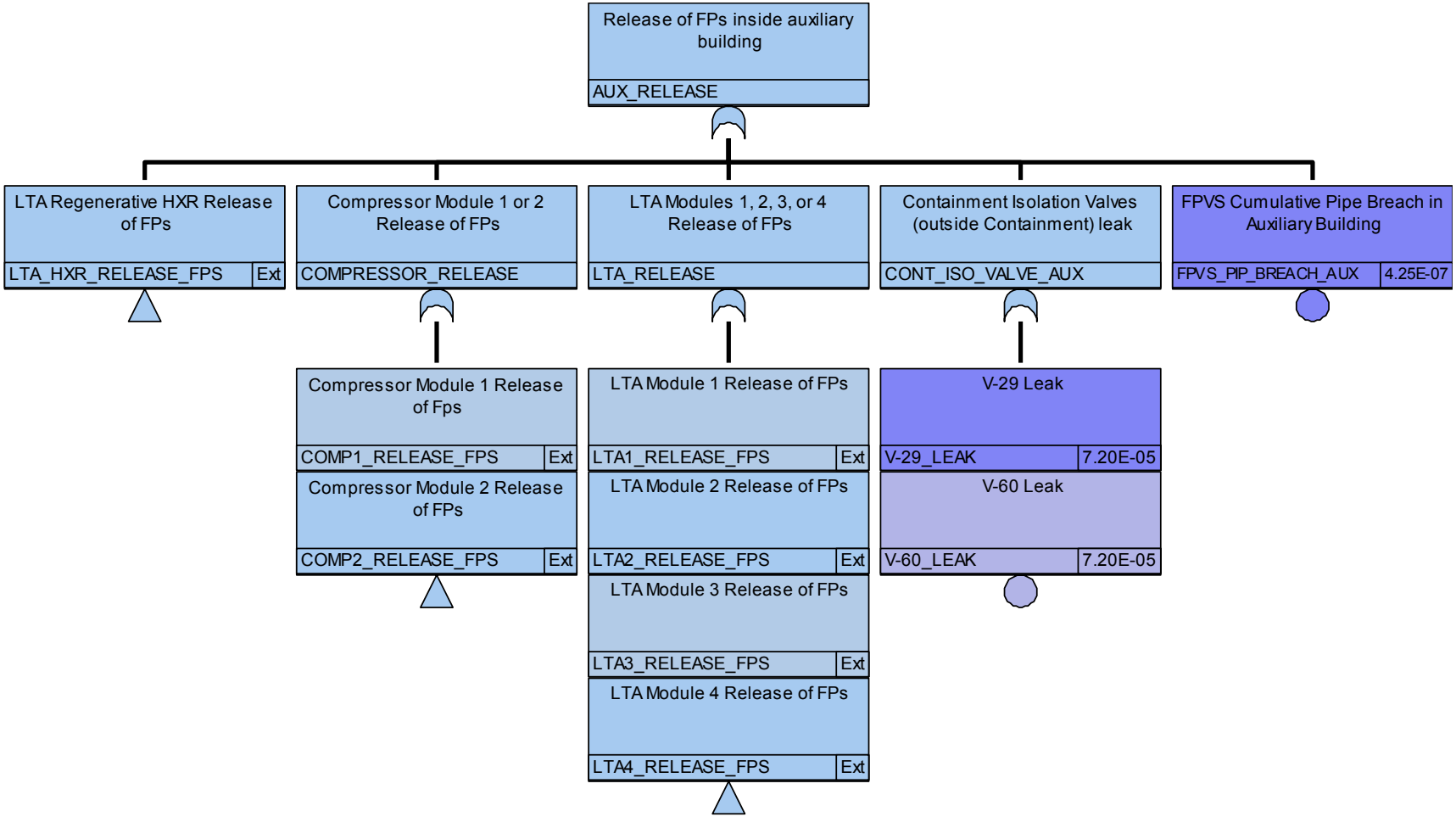

Figure C.4-10: Release in Auxiliary Building Boundary Fault Tree

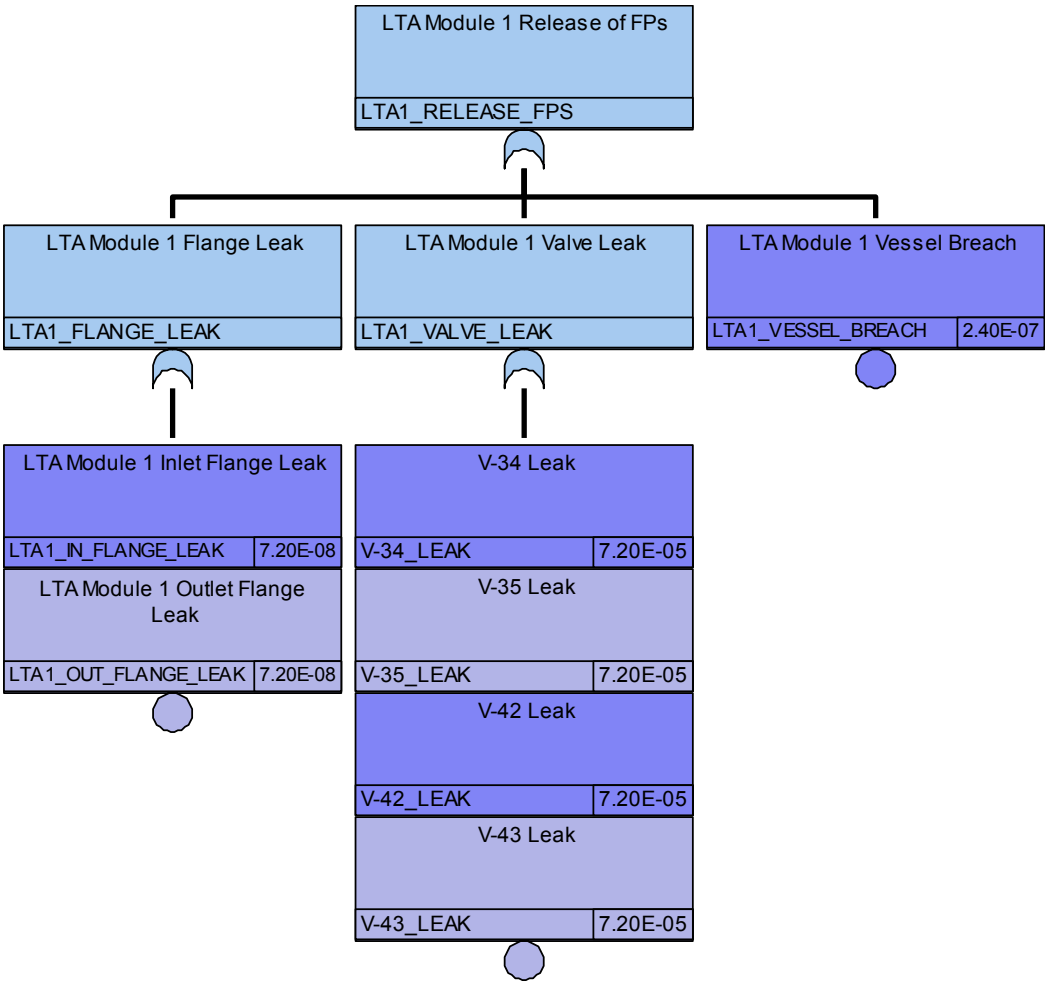

Figure C.4-11: Low Temperature Adsorber Module 1 Fault Tree

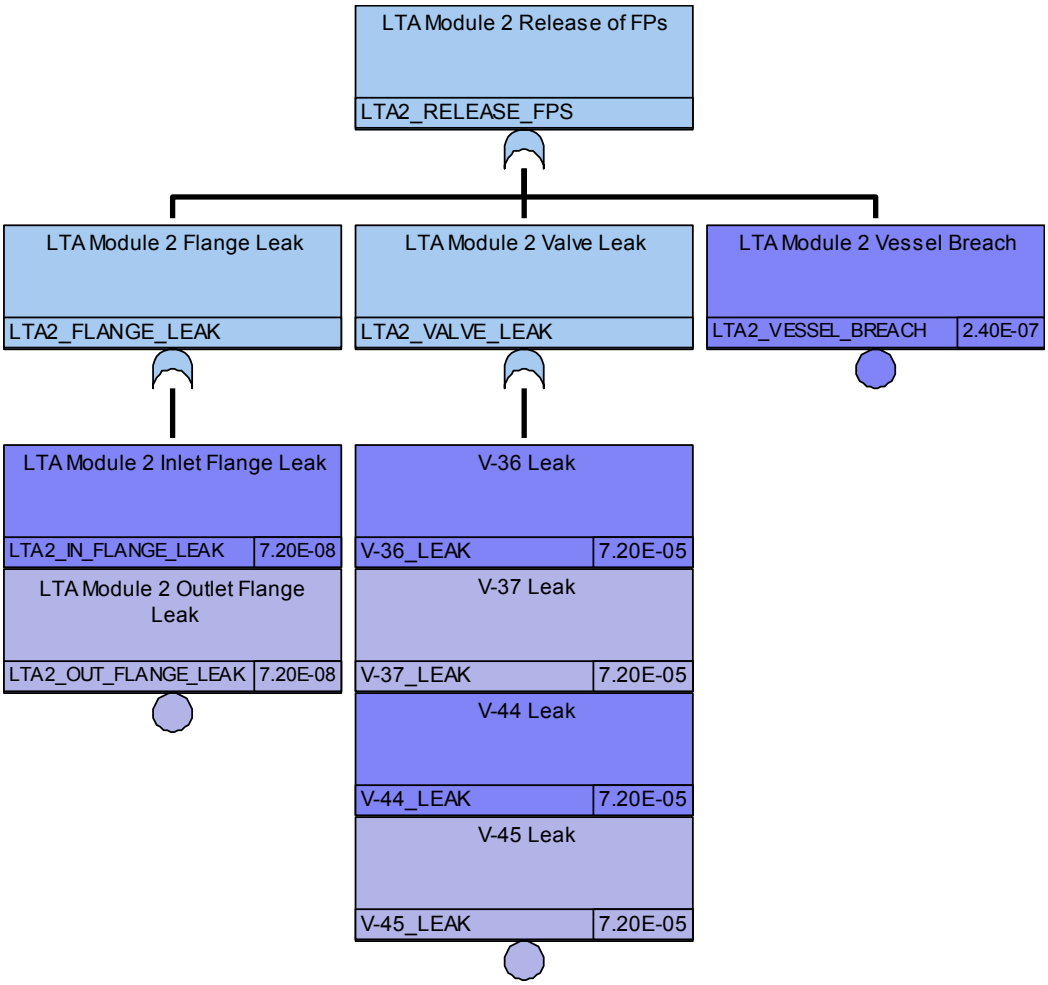

Figure C.4-12: Low Temperature Adsorber Module 2 Fault Tree

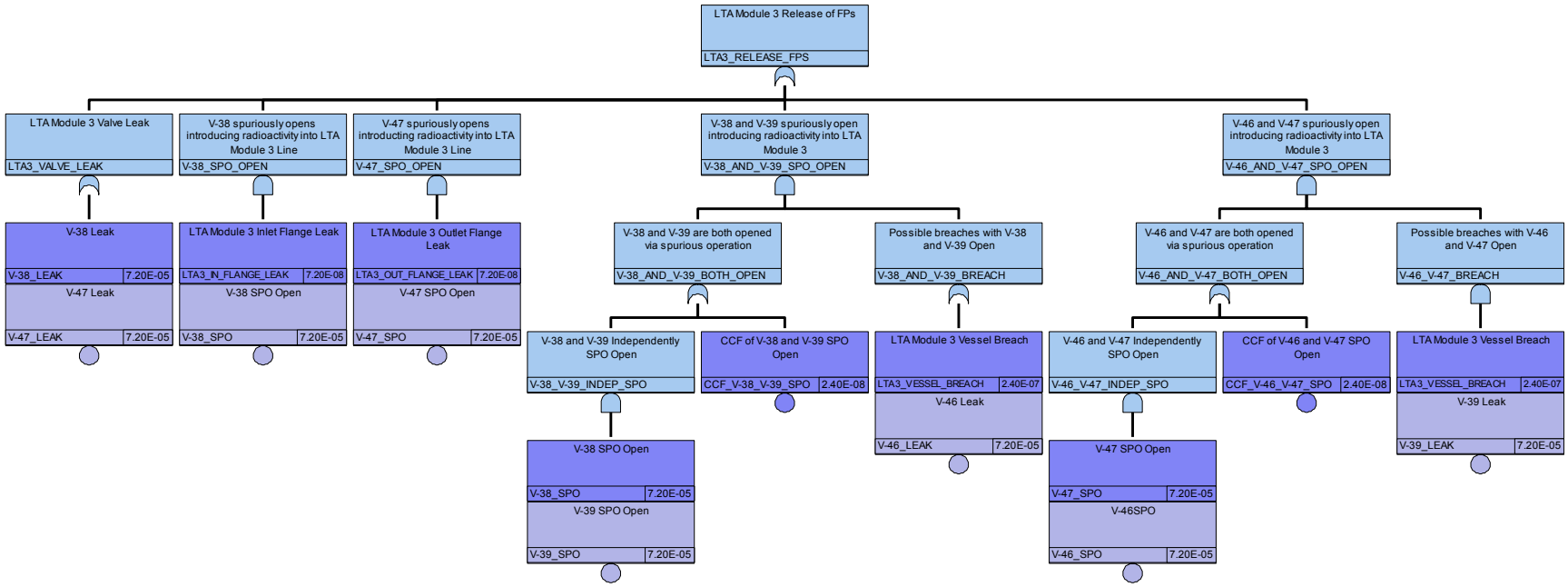

Figure C.4-13: Low Temperature Adsorber Module 3 Fault Tree

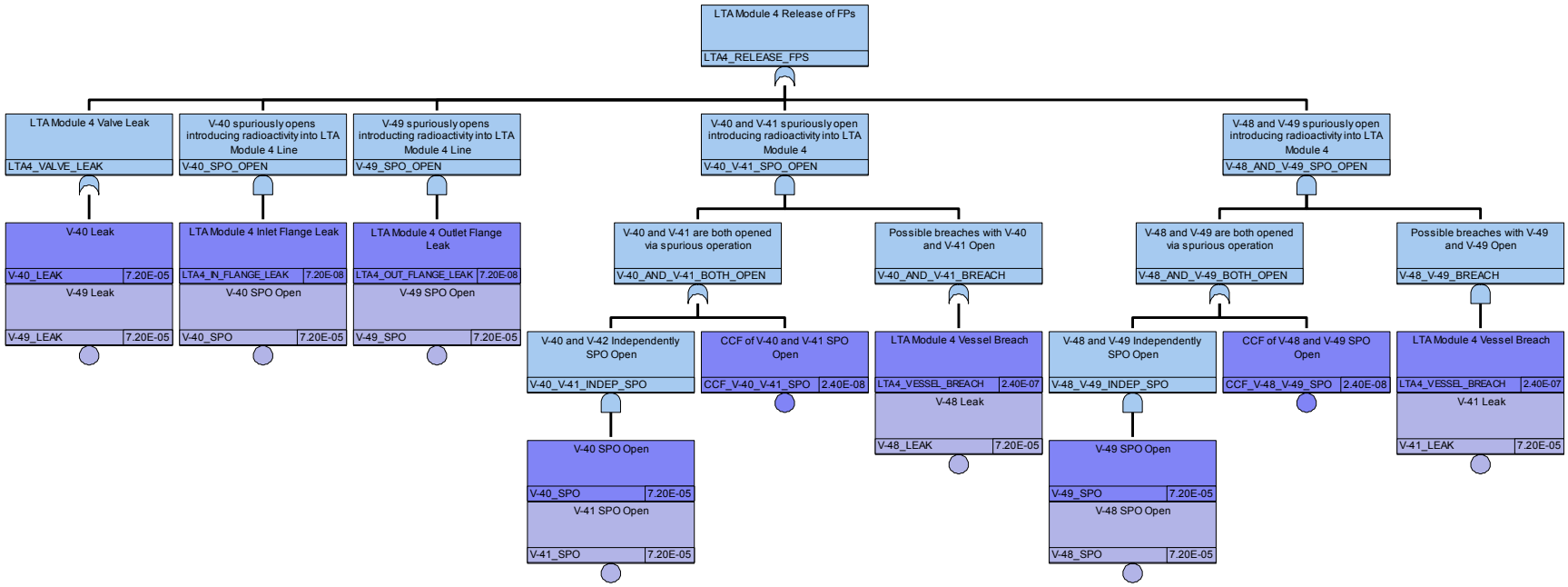

Figure C.4-14: Low Temperature Adsorber Module 4 Fault Tree

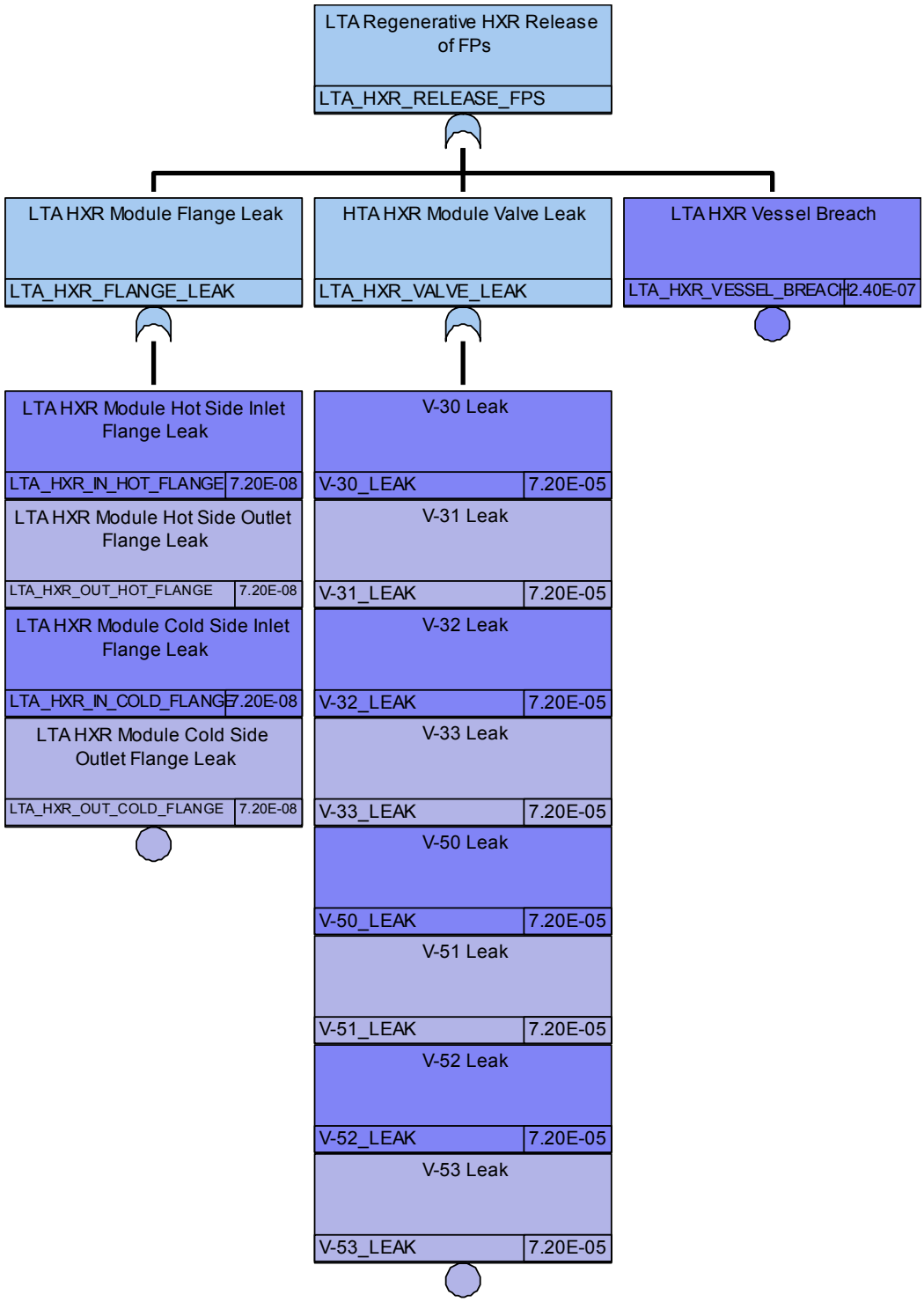

Figure C.4-15: LTA Regenerative Heat Exchanger Module Fault Tree

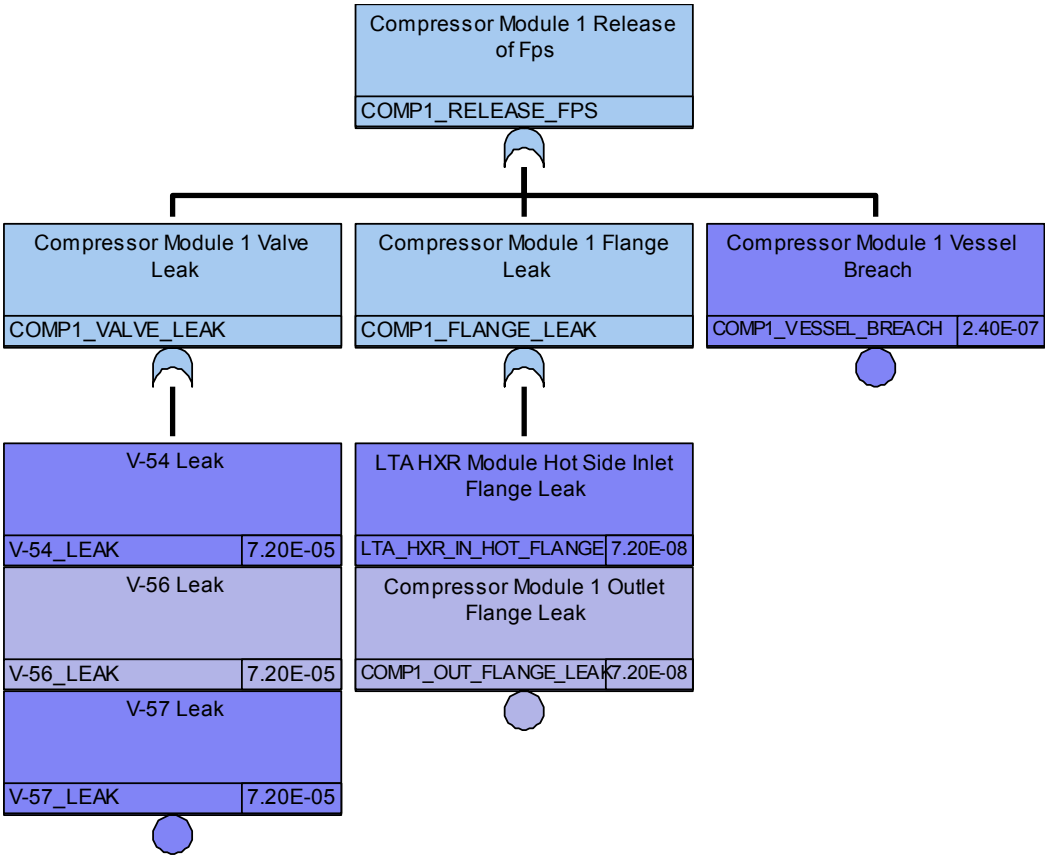

Figure C.4-16: Compressor Module 1 Fault Tree

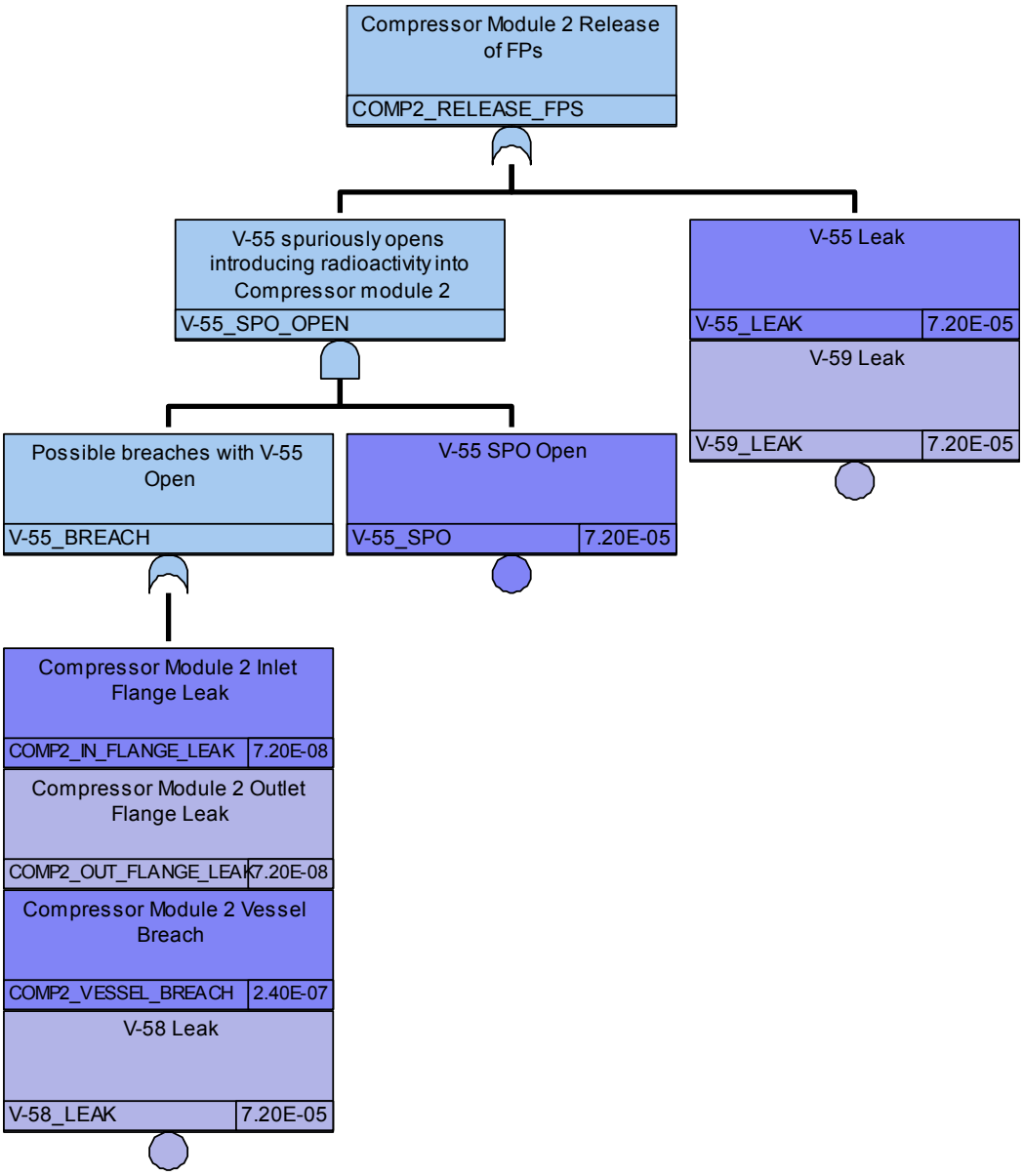

Figure C.4-17: Compressor Module 2 Fault Tree

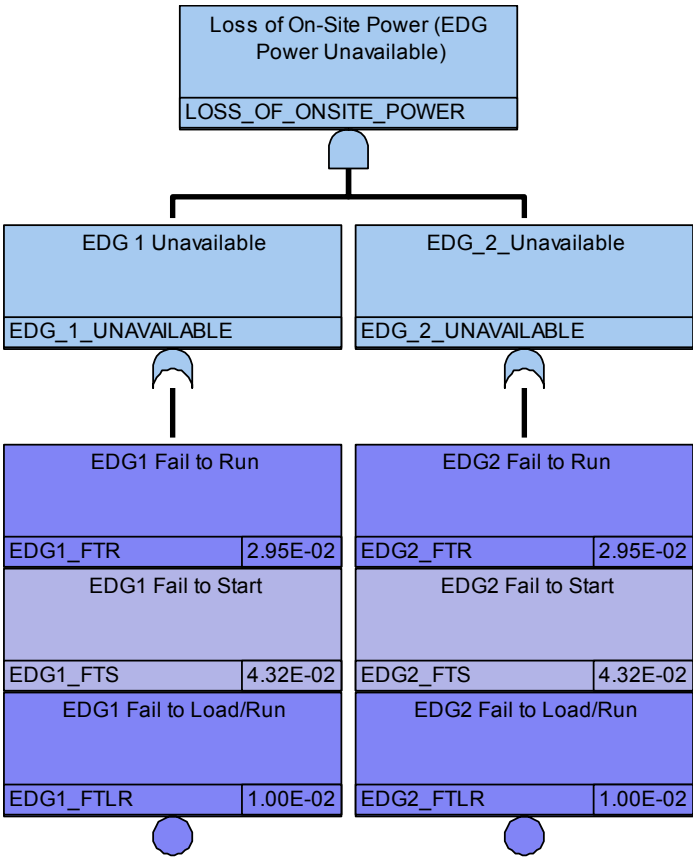

Figure C.4-18: Loss of On-site Power Fault Tree

Appendix C.5. Event Trees

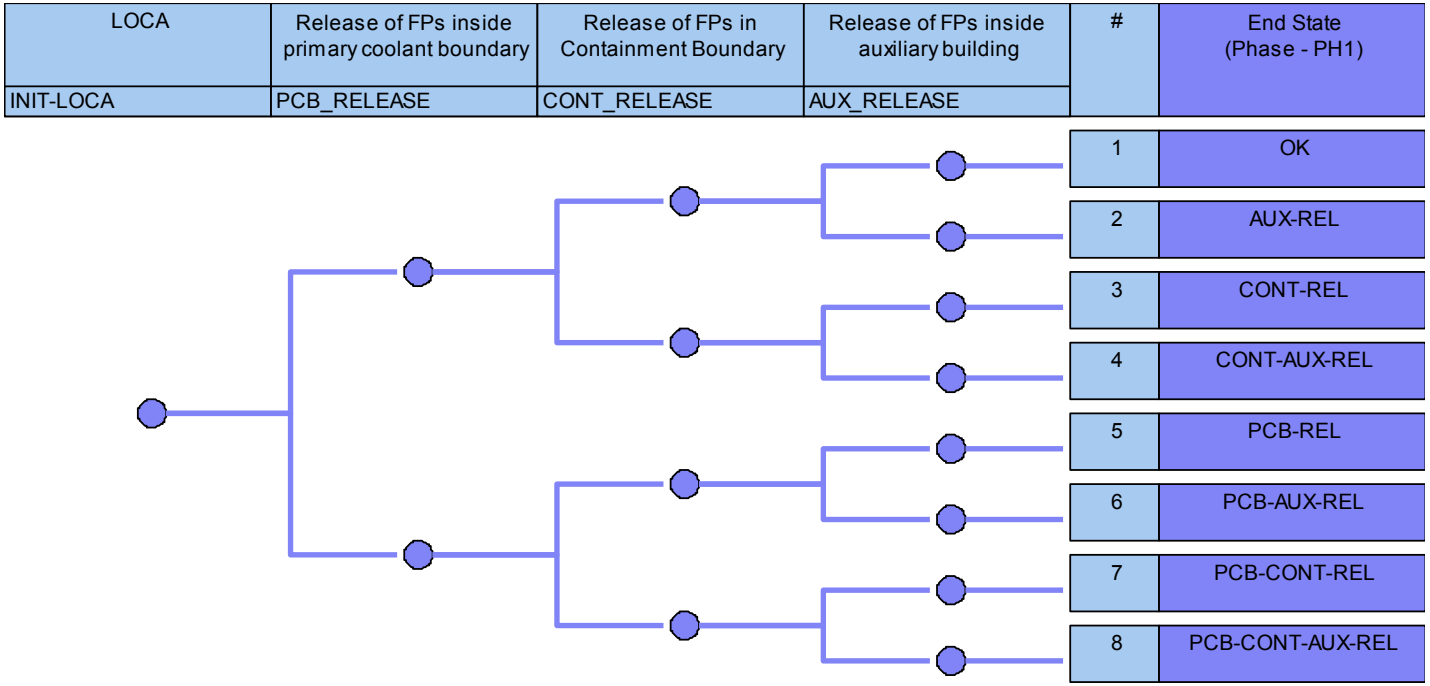

Figure C.5-1: LOCA Event Tree

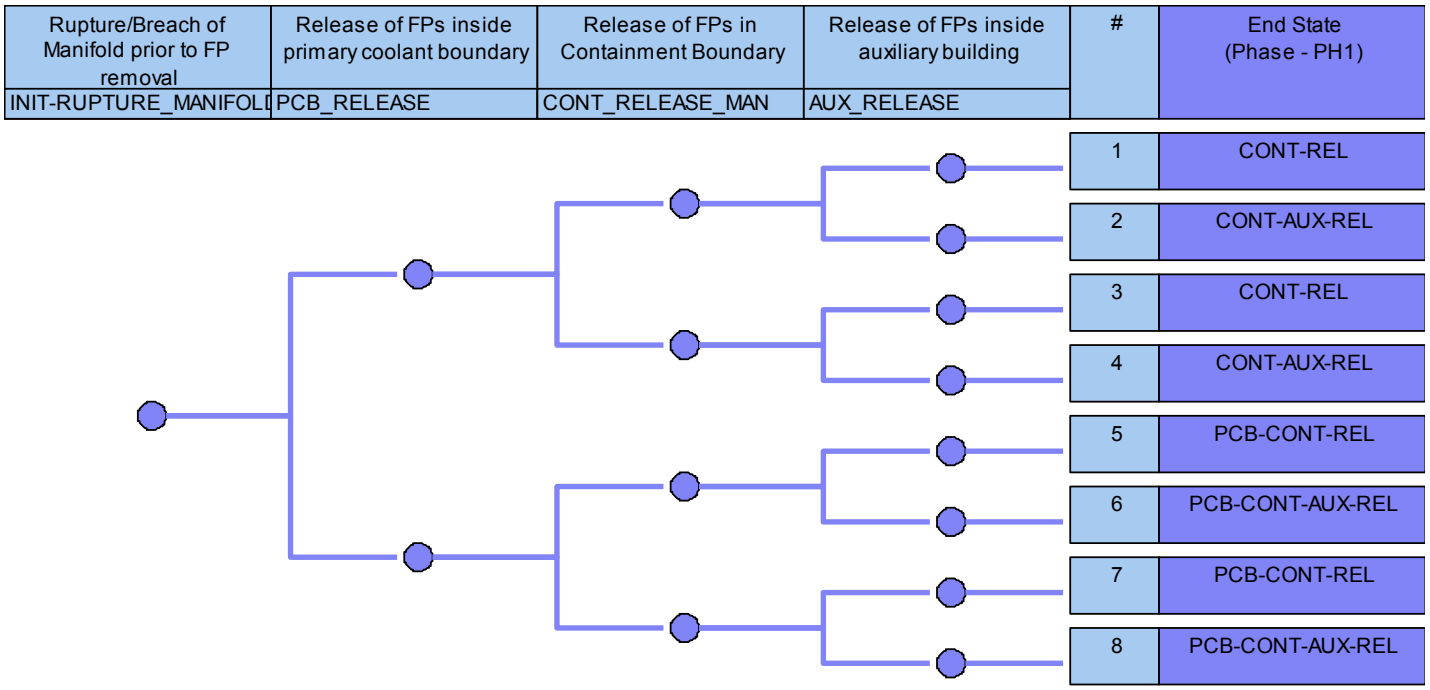

Figure C.5-2: Manifold Breach Event Tree

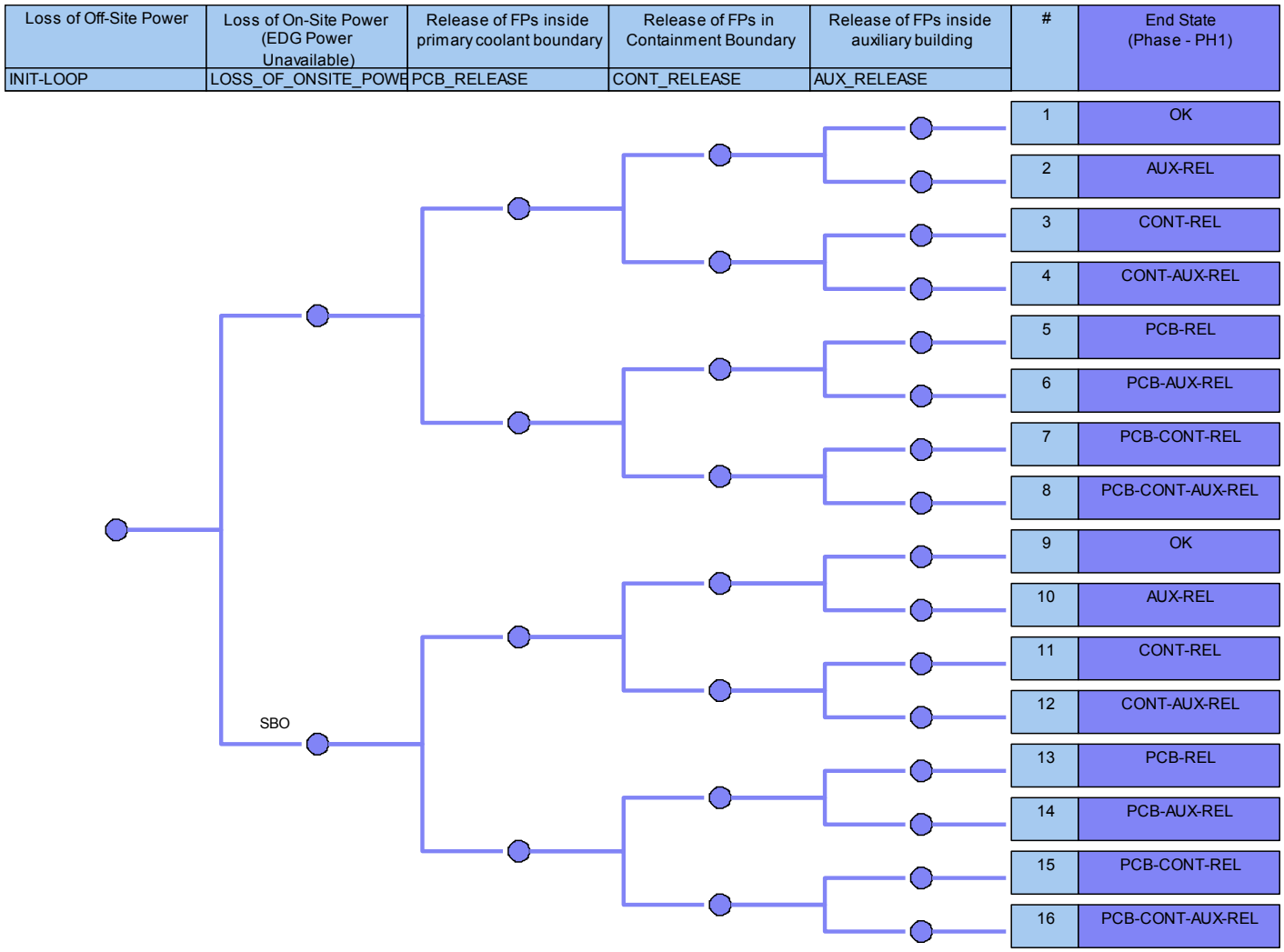

Figure C.5-3: SBO Event Tree

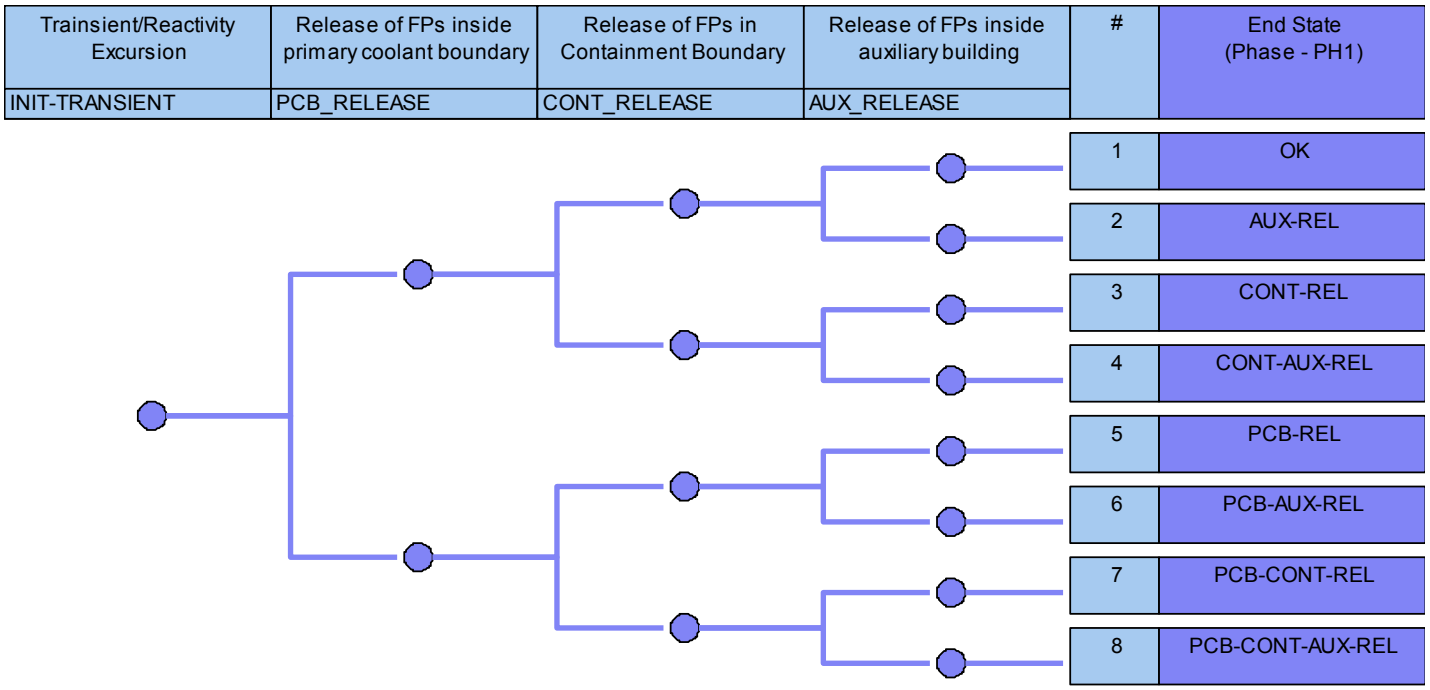

Figure C.5-4: Reactivity Transient Event Tree

Appendix C.6. SAPHIRE Results for Level 1 and Level 2

Table C.6-1: Normal Operations: Fault Tree Results

Name	Cut Set Count	Point Estimate	Mean	Median	5th	95th	Standard Dev.	Skew	Kurtosis
AUX_RELEASE	57	1.94E-03	1.94E-03	1.76E-03	1.00E-03	3.47E-03	8.88E-04	3.22E+00	2.83E+01
COMP1_FAIL	5	1.47E-03	1.56E-03	7.43E-04	1.70E-04	5.06E-03	3.90E-03	1.90E+01	5.84E+02
COMP1_RELEASE_FPS	6	2.16E-04	2.19E-04	1.44E-04	4.05E-05	6.15E-04	2.59E-04	5.57E+00	5.90E+01
COMP2_FAIL	6	2.44E-02	2.50E-02	1.78E-02	1.27E-02	5.57E-02	2.98E-02	1.06E+01	1.83E+02
COMP2_RELEASE_FPS	6	1.44E-04	1.44E-04	8.98E-05	2.11E-05	4.29E-04	2.05E-04	8.25E+00	1.32E+02
CONT_RELEASE	58	1.95E-03	1.95E-03	1.76E-03	1.00E-03	3.47E-03	8.99E-04	3.54E+00	3.43E+01
FPRS_CONT_RELEASE	33	7.21E-04	7.28E-04	5.93E-04	2.54E-04	1.63E-03	5.37E-04	4.25E+00	3.81E+01
FPRS_FAIL	6703	3.57E-03	3.58E-03	3.35E-03	2.16E-03	5.73E-03	1.22E-03	2.44E+00	1.78E+01
FPTS_BREACH	21	1.23E-03	1.23E-03	1.06E-03	5.24E-04	2.47E-03	7.06E-04	2.72E+00	1.58E+01
FPTS_FAIL	42	2.37E-03	2.37E-03	2.16E-03	1.29E-03	4.16E-03	9.75E-04	2.19E+00	1.20E+01
FPTS_RELEASE_FPS	25	1.23E-03	1.22E-03	1.06E-03	5.26E-04	2.48E-03	6.75E-04	2.51E+00	1.41E+01
FUEL_SYSTEM_FAIL	4	2.56E-05	2.41E-05	1.06E-05	1.82E-06	8.94E-05	5.05E-05	1.05E+01	1.90E+02
HTA1_FAIL	14	8.16E-04	8.28E-04	6.90E-04	3.05E-04	1.81E-03	5.70E-04	4.01E+00	3.65E+01
HTA1_RELEASE	11	4.32E-04	4.29E-04	3.15E-04	1.02E-04	1.12E-03	4.03E-04	4.53E+00	4.83E+01
HTA2_FAIL	15	5.24E-02	5.24E-02	4.61E-02	4.10E-02	8.32E-02	2.38E-02	8.76E+00	1.30E+02
HTA2_RELEASE_FPS	8	1.56E-08	1.53E-08	5.24E-09	6.31E-10	5.66E-08	4.50E-08	1.70E+01	4.63E+02
HTA3_FAIL	15	4.68E-02	4.60E-02	4.03E-02	3.54E-02	7.36E-02	2.23E-02	1.25E+01	3.16E+02
HTA3_RELEASE_FPS	8	1.56E-08	1.60E-08	5.29E-09	6.46E-10	5.35E-08	8.62E-08	4.69E+01	2.76E+03
LTA_HXR_FAIL	8	5.76E-04	5.69E-04	4.44E-04	1.70E-04	1.35E-03	5.15E-04	6.36E+00	8.15E+01
LTA_HXR_RELEASE_FPS	13	5.76E-04	5.68E-04	4.42E-04	1.73E-04	1.36E-03	4.49E-04	3.83E+00	3.51E+01
LTA_MODULES_2OF4	3420	1.27E-06	1.28E-06	8.66E-07	3.81E-07	3.17E-06	2.78E-06	4.17E+01	2.36E+03
LTA1_FAIL	9	5.04E-04	5.00E-04	3.97E-04	1.72E-04	1.14E-03	4.19E-04	6.14E+00	8.06E+01
LTA1_RELEASE_FPS	7	2.88E-04	2.85E-04	1.96E-04	5.43E-05	7.85E-04	3.17E-04	4.97E+00	4.65E+01
LTA2_FAIL	9	5.04E-04	5.10E-04	4.08E-04	1.78E-04	1.17E-03	5.17E-04	2.24E+01	9.79E+02
LTA2_RELEASE_FPS	7	2.88E-04	2.86E-04	1.93E-04	5.38E-05	7.91E-04	3.42E-04	7.33E+00	1.19E+02
LTA3_FAIL	10	3.47E-02	3.52E-02	2.84E-02	2.36E-02	6.52E-02	2.73E-02	1.04E+01	1.78E+02
LTA3_RELEASE_FPS	8	1.44E-04	1.40E-04	7.76E-05	1.44E-05	4.53E-04	2.08E-04	5.62E+00	5.62E+01
LTA4_FAIL	10	3.47E-02	3.49E-02	2.83E-02	2.35E-02	6.65E-02	2.49E-02	9.08E+00	1.39E+02
LTA4_RELEASE_FPS	8	1.44E-04	1.41E-04	7.48E-05	1.31E-05	4.75E-04	2.15E-04	5.32E+00	4.76E+01
PCB_ISO_SPO	14	1.01E-03	1.00E-03	8.52E-04	3.99E-04	2.11E-03	6.40E-04	3.32E+00	2.50E+01
PCB_RELEASE	4	2.74E-06	2.76E-06	1.74E-06	4.91E-07	8.20E-06	3.73E-06	7.14E+00	9.98E+01
AUX_RELEASE	57	1.94E-03	1.94E-03	1.76E-03	1.00E-03	3.47E-03	8.88E-04	3.22E+00	2.83E+01

Table C.6-2: Accident Conditions: Fault Tree Results

Name	Cut Set Count	Point Estimate	Mean	Median	5th	95th	Standard Dev.	Skew	Kurtosis
AUX_RELEASE	57	1.94E-03	1.94E-03	1.75E-03	9.92E-04	3.52E-03	8.64E-04	2.33E+00	1.24E+02
COMP1_RELEASE_FPS	6	2.16E-04	2.17E-04	1.44E-04	4.04E-05	5.95E-04	3.17E-04	1.24E+01	4.52E+01
COMP2_RELEASE_FPS	6	1.44E-04	1.40E-04	8.94E-05	2.18E-05	4.18E-04	1.79E-04	7.05E+00	8.83E+01
CONT_RELEASE	58	1.95E-03	1.94E-03	1.74E-03	9.90E-04	3.50E-03	9.56E-04	4.51E+00	2.94E+01
CONT_RELEASE_MAN	56	1.95E-03	1.95E-03	1.74E-03	9.92E-04	3.53E-03	9.26E-04	3.78E+00	2.58E+01
FPTS_RELEASE_FPS	25	1.23E-03	1.21E-03	1.06E-03	5.29E-04	2.38E-03	7.16E-04	5.75E+00	1.52E+01
FPTS_RELEASE_FPS_MAN	24	1.23E-03	1.22E-03	1.06E-03	5.29E-04	2.41E-03	6.79E-04	3.00E+00	3.57E+01
FUEL_SYSTEM_RELEASE_FPS	3	1.56E-06	1.57E-06	9.18E-07	2.35E-07	4.79E-06	2.50E-06	8.23E+00	3.00E+02
HTA1_RELEASE	11	4.32E-04	4.36E-04	3.27E-04	1.06E-04	1.11E-03	4.08E-04	4.39E+00	2.54E+02
HTA2_RELEASE_FPS	8	1.56E-08	1.62E-08	5.30E-09	6.44E-10	5.76E-08	5.38E-08	1.66E+01	1.39E+01
HTA3_RELEASE_FPS	8	1.56E-08	1.66E-08	5.20E-09	6.20E-10	5.05E-08	1.02E-07	3.91E+01	3.00E+01
LOSS_OF_ONSITE_POWER	9	6.82E-03	6.69E-03	5.03E-03	1.21E-03	1.79E-02	5.70E-03	2.25E+00	8.95E+00
LTA1_RELEASE_FPS	7	2.88E-04	2.89E-04	1.93E-04	5.30E-05	8.27E-04	3.44E-04	6.14E+00	9.57E+00
LTA2_RELEASE_FPS	7	2.88E-04	2.93E-04	1.96E-04	5.27E-05	8.14E-04	4.31E-04	1.80E+01	8.64E+00
LTA3_RELEASE_FPS	8	1.44E-04	1.46E-04	7.68E-05	1.34E-05	4.78E-04	2.49E-04	8.46E+00	1.00E+01
LTA4_RELEASE_FPS	8	1.44E-04	1.44E-04	7.57E-05	1.35E-05	5.08E-04	2.11E-04	4.37E+00	9.29E+00
LTA_HXR_RELEASE_FPS	13	5.76E-04	5.67E-04	4.53E-04	1.66E-04	1.30E-03	4.57E-04	5.12E+00	6.17E+00
PCB_RELEASE	4	2.74E-06	2.76E-06	1.73E-06	5.01E-07	7.81E-06	3.91E-06	8.61E+00	5.29E+01

Table C.6-3: Accident Conditions: Event Tree Results

IE	End State	Point Estimate (1/ Year)	Cut Set Count	Mean (1/ Year)	Median (1/ Year)	5th (1/ Year)	95th (1/ Year)	Standard Dev. (1/ Year)	Skew	Kurtosis
LOCA	Total	3.90E-07	1337	3.95E-07	1.39E-07	1.34E-08	1.47E-06	9.48E-07	9.86E+00	1.56E+02
	AUX-REL	1.94E-07	45	1.88E-07	6.79E-08	6.12E-09	7.07E-07	4.67E-07	9.98E+00	1.52E+02
	CONT-REL	1.95E-07	46	1.99E-07	6.82E-08	6.44E-09	7.77E-07	4.59E-07	8.01E+00	1.05E+02
	CONT-AUX-REL	3.79E-10	1026	3.99E-10	1.20E-10	1.00E-11	1.48E-09	1.45E-09	2.08E+01	6.69E+02
	PCB-REL	2.74E-10	4	2.45E-10	6.36E-11	4.56E-12	1.00E-09	7.63E-10	1.40E+01	3.27E+02
	PCB-AUX-REL	5.33E-13	108	5.79E-13	1.23E-13	7.46E-15	2.05E-12	2.76E-12	2.72E+01	1.05E+03
	PCB-CONT-REL	5.33E-13	108	5.53E-13	1.22E-13	7.89E-15	1.95E-12	2.40E-12	2.16E+01	7.00E+02
	PCB-CONT-AUX-REL	0.00E+00	0	0.00E+00	0.00E+00	0.00E+00	0.00E+00	0.00E+00	0.00E+00	0.00E+00
Manifold Rupture	Total	8.79E-05	1253	9.05E-05	3.21E-05	3.27E-06	3.08E-04	2.78E-04	1.77E+01	5.08E+02
	CONT-REL	8.76E-05	1	8.51E-05	3.36E-05	3.46E-06	3.17E-04	1.83E-04	8.08E+00	1.05E+02
	CONT-AUX-REL	1.70E-07	45	1.70E-07	5.91E-08	5.50E-09	6.37E-07	4.42E-07	1.18E+01	2.24E+02
	CONT-REL	1.71E-07	42	1.71E-07	5.84E-08	5.63E-09	6.59E-07	4.25E-07	1.10E+01	1.98E+02
	CONT-AUX-REL	3.32E-10	945	2.98E-10	1.05E-10	8.58E-12	1.12E-09	7.01E-10	8.45E+00	1.08E+02
	PCB-CONT-REL	2.40E-10	4	2.28E-10	5.88E-11	4.08E-12	8.35E-10	8.61E-10	1.63E+01	3.72E+02
	PCB-CONT-AUX-REL	4.67E-13	108	4.79E-13	1.11E-13	6.23E-15	1.83E-12	1.59E-12	1.19E+01	2.17E+02
	PCB-CONT-REL	4.67E-13	108	4.35E-13	1.07E-13	7.38E-15	1.65E-12	1.86E-12	2.45E+01	8.26E+02
	PCB-CONT-AUX-REL	0.00E+00	0	0.00E+00	0.00E+00	0.00E+00	0.00E+00	0.00E+00	0.00E+00	0.00E+00
LOOP	Total	2.41E-04	11862	2.41E-04	1.83E-04	5.62E-05	6.18E-04	2.00E-04	2.83E+00	1.76E+01
	AUX-REL	1.19E-04	55	1.17E-04	8.70E-05	2.49E-05	3.08E-04	1.08E-04	3.43E+00	2.30E+01
	CONT-REL	1.20E-04	56	1.19E-04	8.80E-05	2.55E-05	3.13E-04	1.06E-04	3.26E+00	2.34E+01
	CONT-AUX-REL	2.33E-07	1743	2.36E-07	1.57E-07	3.88E-08	6.92E-07	2.98E-07	1.27E+01	3.98E+02
	PCB-REL	1.68E-07	4	1.71E-07	8.68E-08	1.63E-08	5.67E-07	3.05E-07	8.76E+00	1.34E+02
	PCB-AUX-REL	3.27E-10	164	3.30E-10	1.59E-10	2.37E-11	1.14E-09	6.57E-10	1.05E+01	1.82E+02
	PCB-CONT-REL	3.28E-10	151	3.44E-10	1.56E-10	2.66E-11	1.13E-09	8.15E-10	1.21E+01	2.18E+02
	PCB-CONT-AUX-REL	0.00E+00	0	0.00E+00	0.00E+00	0.00E+00	0.00E+00	0.00E+00	0.00E+00	0.00E+00
	AUX-REL	8.17E-07	399	8.00E-07	4.57E-07	6.80E-08	2.65E-06	1.12E-06	4.61E+00	3.65E+01
	CONT-REL	8.18E-07	398	8.09E-07	4.42E-07	6.87E-08	2.72E-06	1.23E-06	7.57E+00	1.33E+02
	CONT-AUX-REL	1.59E-09	7614	1.56E-09	7.96E-10	1.12E-10	5.31E-09	2.56E-09	7.46E+00	1.10E+02
	PCB-REL	1.15E-09	36	1.10E-09	4.42E-10	4.56E-11	4.10E-09	2.17E-09	6.68E+00	7.59E+01
	PCB-AUX-REL	2.08E-12	621	2.13E-12	6.85E-13	6.50E-14	7.62E-12	8.31E-12	3.05E+01	1.31E+03

IE	End State	Point Estimate (1/ Year)	Cut Set Count	Mean (1/ Year)	Median (1/ Year)	5th (1/ Year)	95th (1/ Year)	Standard Dev. (1/ Year)	Skew	Kurtosis
	PCB-CONT-REL	2.08E-12	621	1.99E-12	6.80E-13	6.22E-14	7.88E-12	4.84E-12	9.20E+00	1.33E+02
	PCB-CONT-AUX-REL	0.00E+00	0	0.00E+00	0.00E+00	0.00E+00	0.00E+00	0.00E+00	0.00E+00	0.00E+00
Transient	Total	2.73E-03	4448	2.69E-03	9.67E-04	9.33E-05	1.04E-02	6.49E-03	1.15E+01	2.16E+02
	AUX-REL	1.36E-03	55	1.31E-03	4.61E-04	4.41E-05	5.01E-03	3.47E-03	1.67E+01	5.29E+02
	CONT-REL	1.36E-03	56	1.38E-03	4.86E-04	4.44E-05	5.29E-03	3.28E-03	9.79E+00	1.66E+02
	CONT-AUX-REL	2.65E-06	1809	2.83E-06	8.86E-07	6.88E-08	1.07E-05	9.46E-06	2.00E+01	6.01E+02
	PCB-REL	1.92E-06	4	1.97E-06	4.54E-07	3.26E-08	7.00E-06	8.77E-06	2.27E+01	7.26E+02
	PCB-AUX-REL	3.73E-09	167	3.47E-09	8.61E-10	5.62E-11	1.48E-08	9.92E-09	1.26E+01	3.04E+02
	PCB-CONT-REL	3.74E-09	170	4.22E-09	8.23E-10	5.25E-11	1.27E-08	4.56E-08	6.16E+01	4.12E+03
	PCB-CONT-AUX-REL	6.57E-12	2187	5.84E-12	1.20E-12	7.12E-14	2.44E-11	2.05E-11	1.18E+01	2.02E+02
	Total	3.06E-03	18900	3.07E-03	1.35E-03	3.10E-04	1.04E-02	6.72E-03	1.09E+01	2.04E+02

Appendix C.7. Accident Progression Event Trees

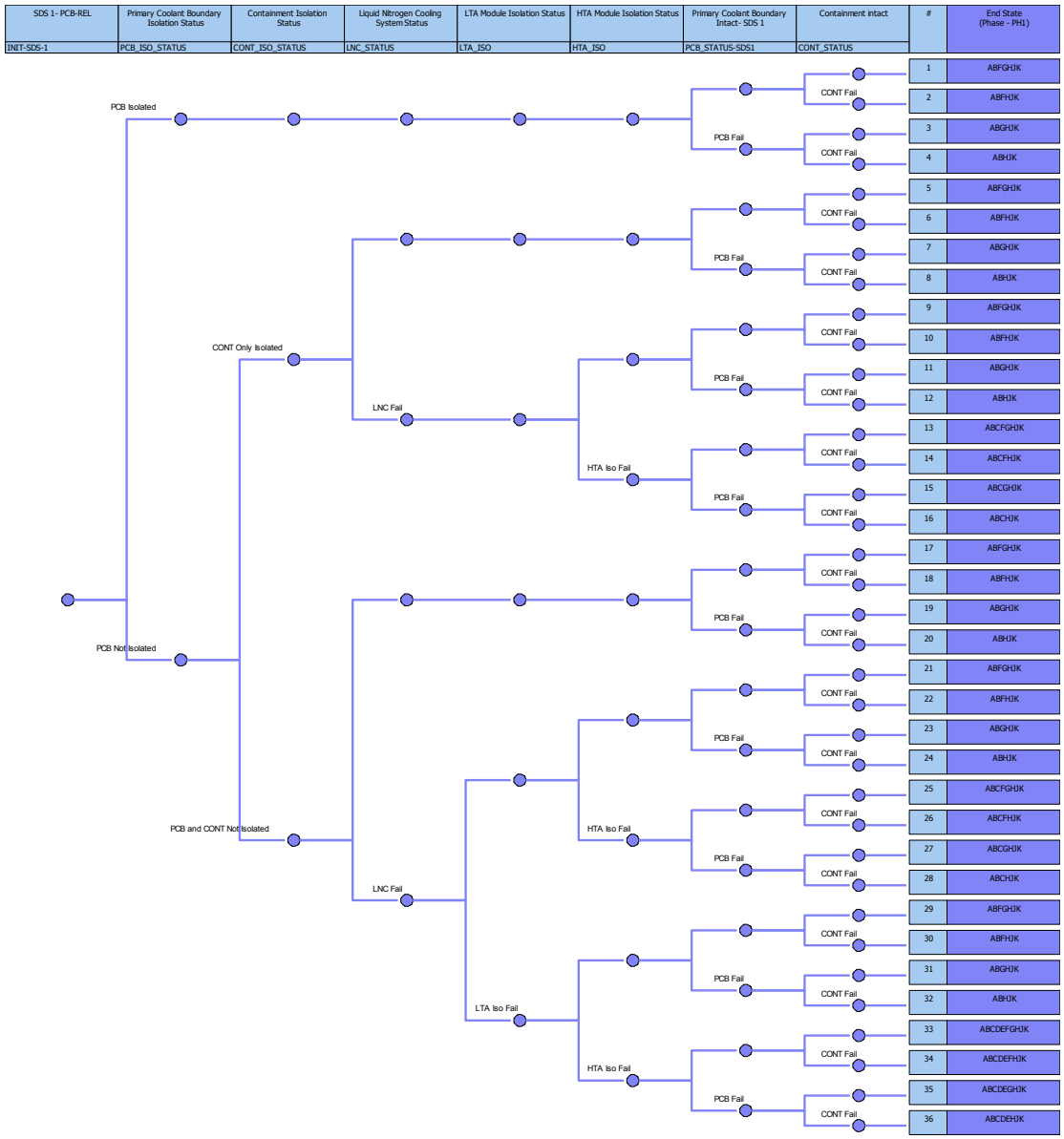

Figure C.7-1: Accident Progression Event Tree – SDS 1

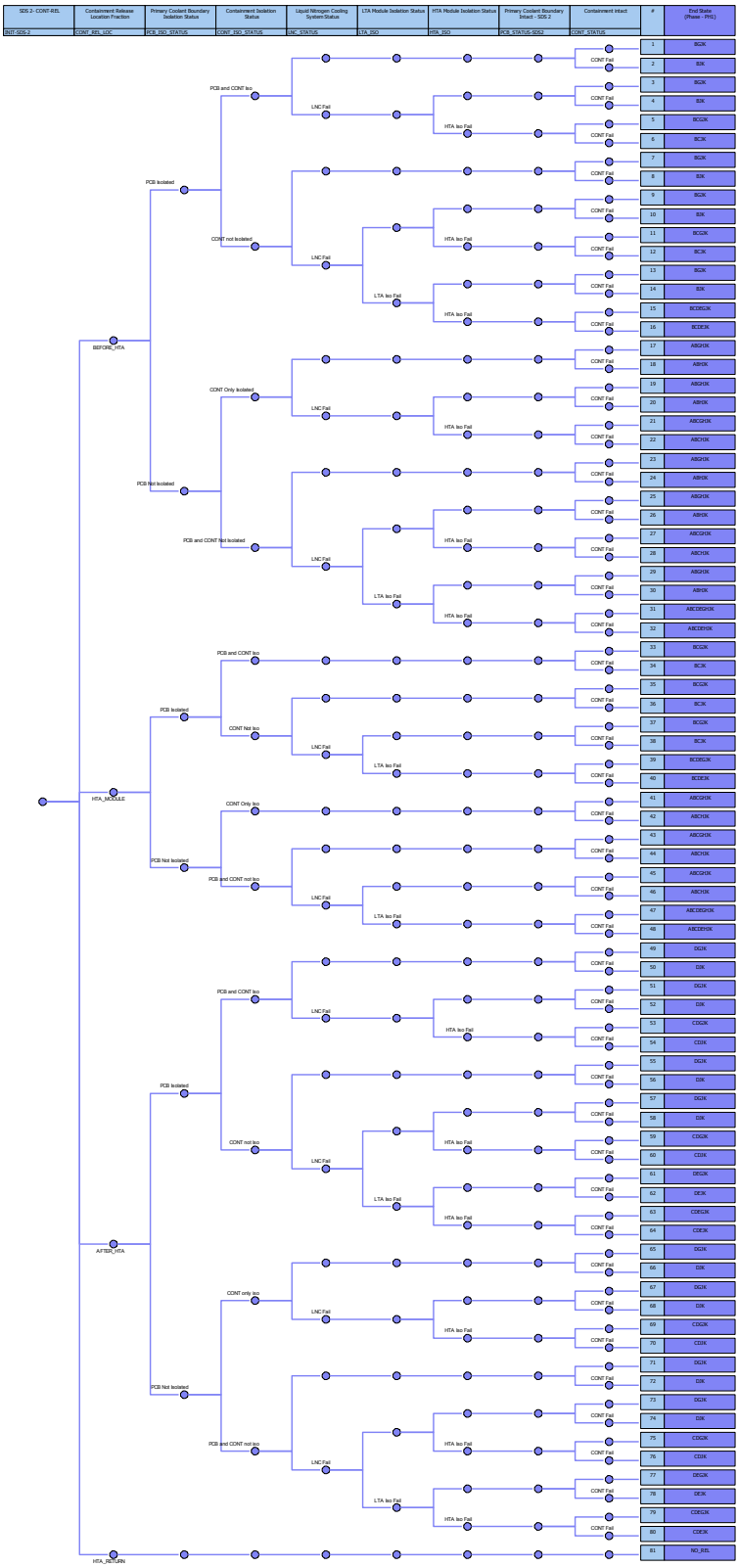

Figure C.7-2: Accident Progression Event Tree – SDS 2

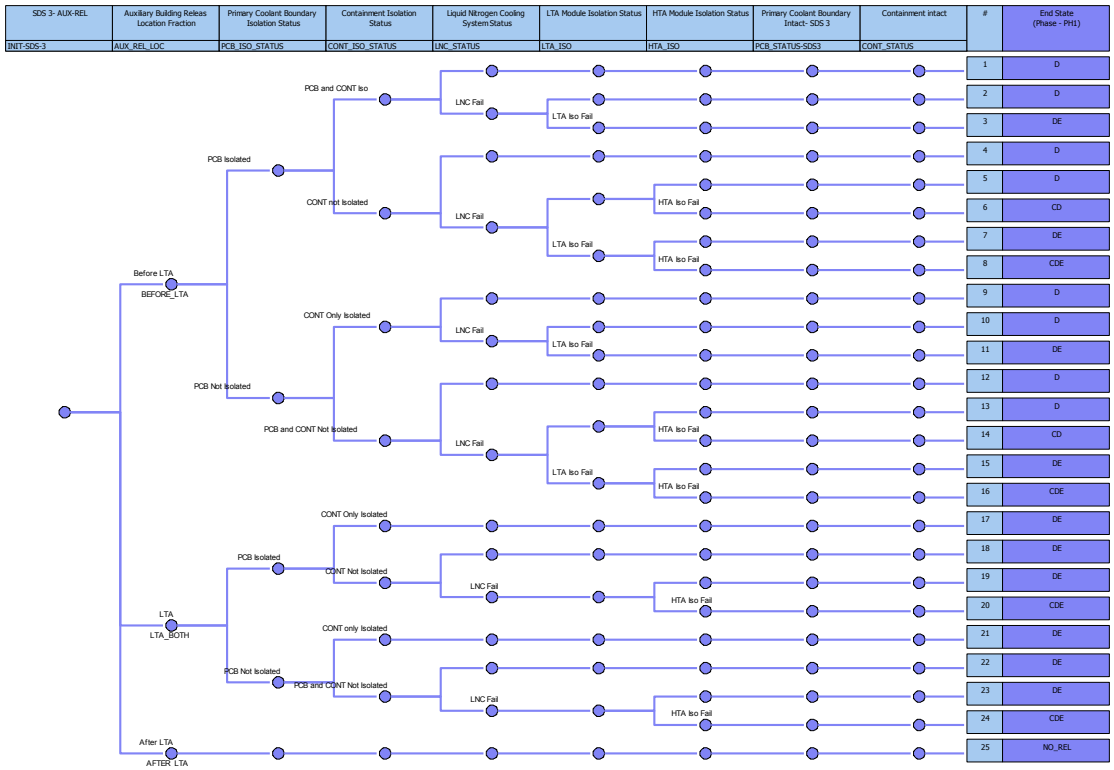

Figure C.7-3: Accident Progression Event Tree – SDS 3

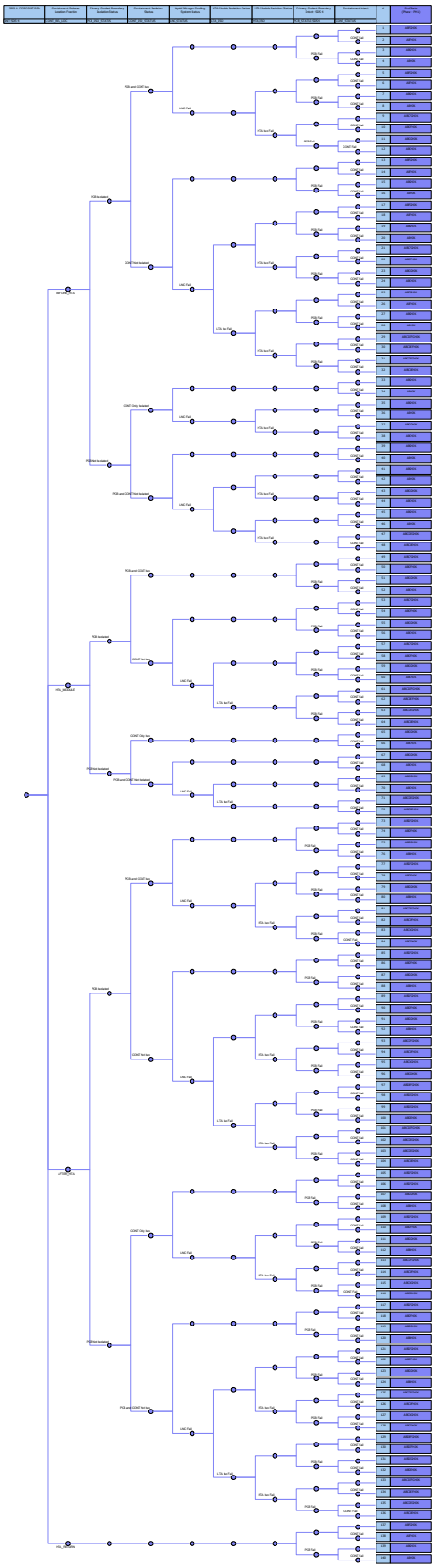

Figure C.7-4: Accident Progression Event Tree – SDS 4

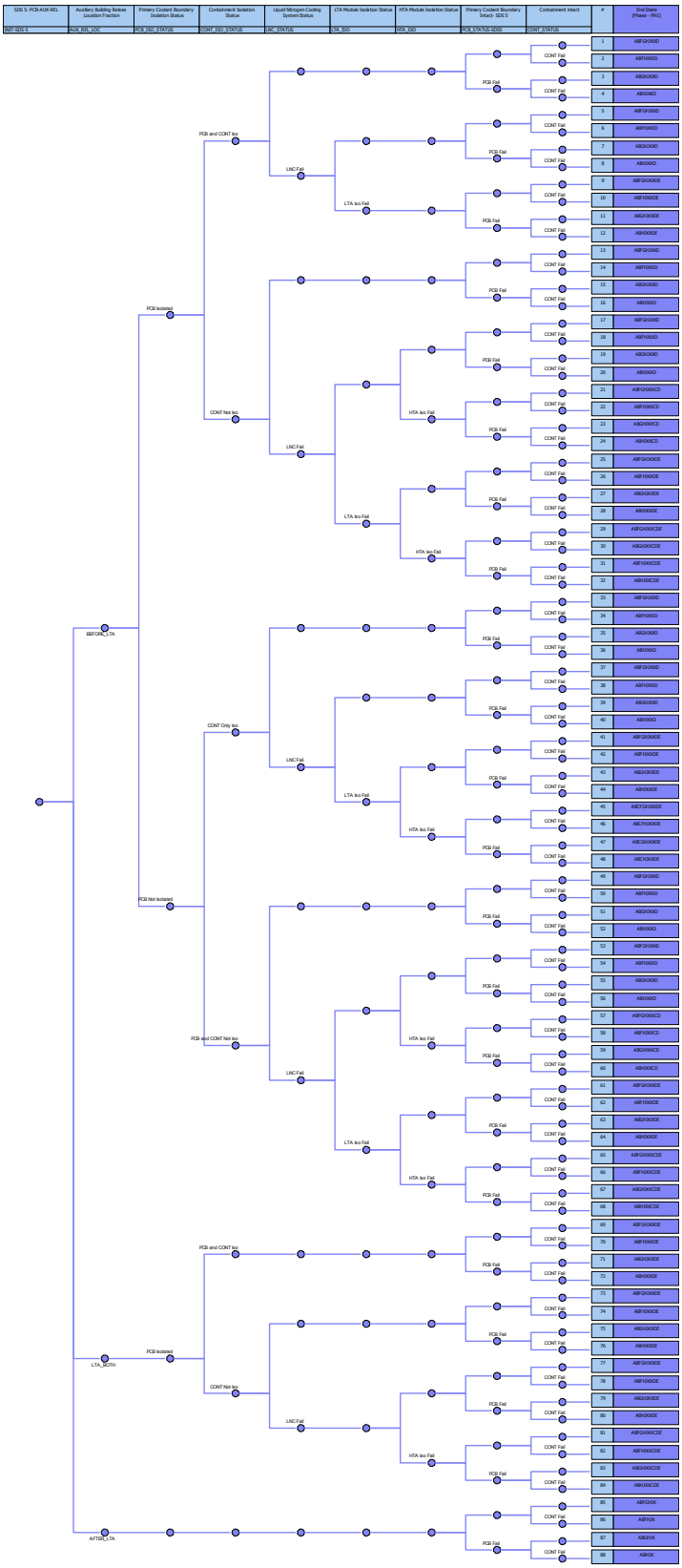

Figure C.7-5: Accident Progression Event Tree – SDS 5

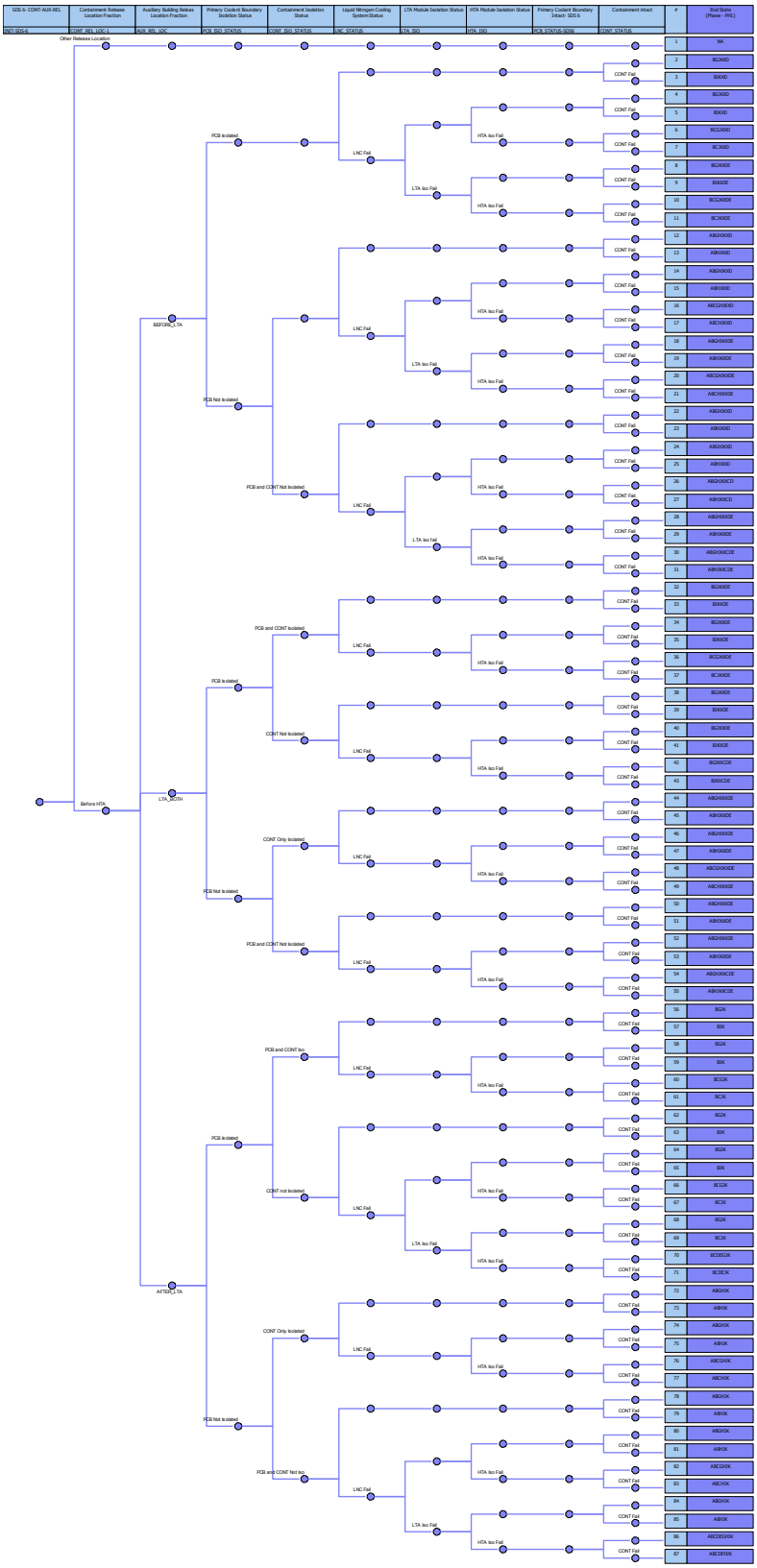

Figure C.7-6: Accident Progression Event Tree – SDS 6-1

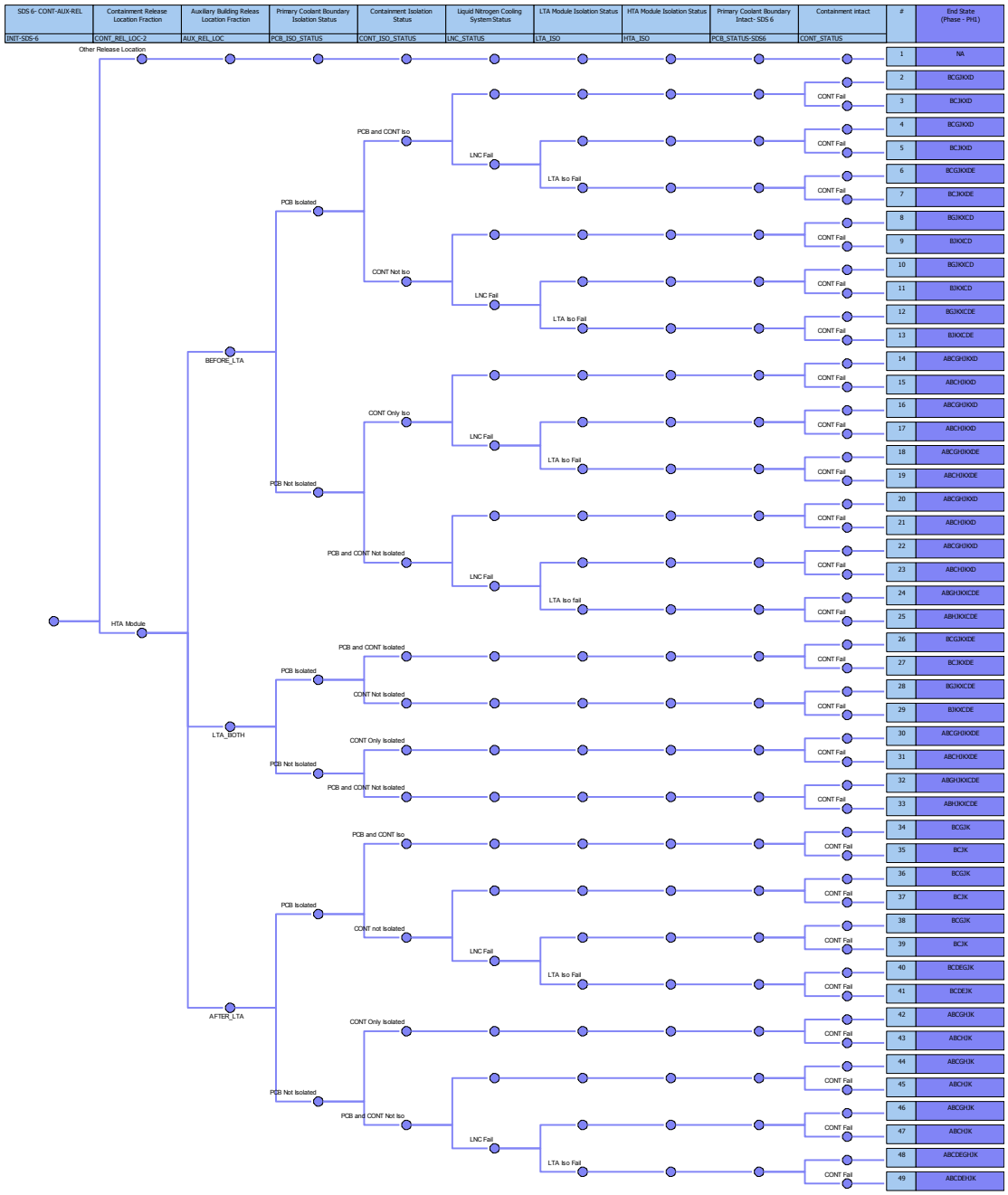

Figure C.7-7: Accident Progression Event Tree – SDS 6-2

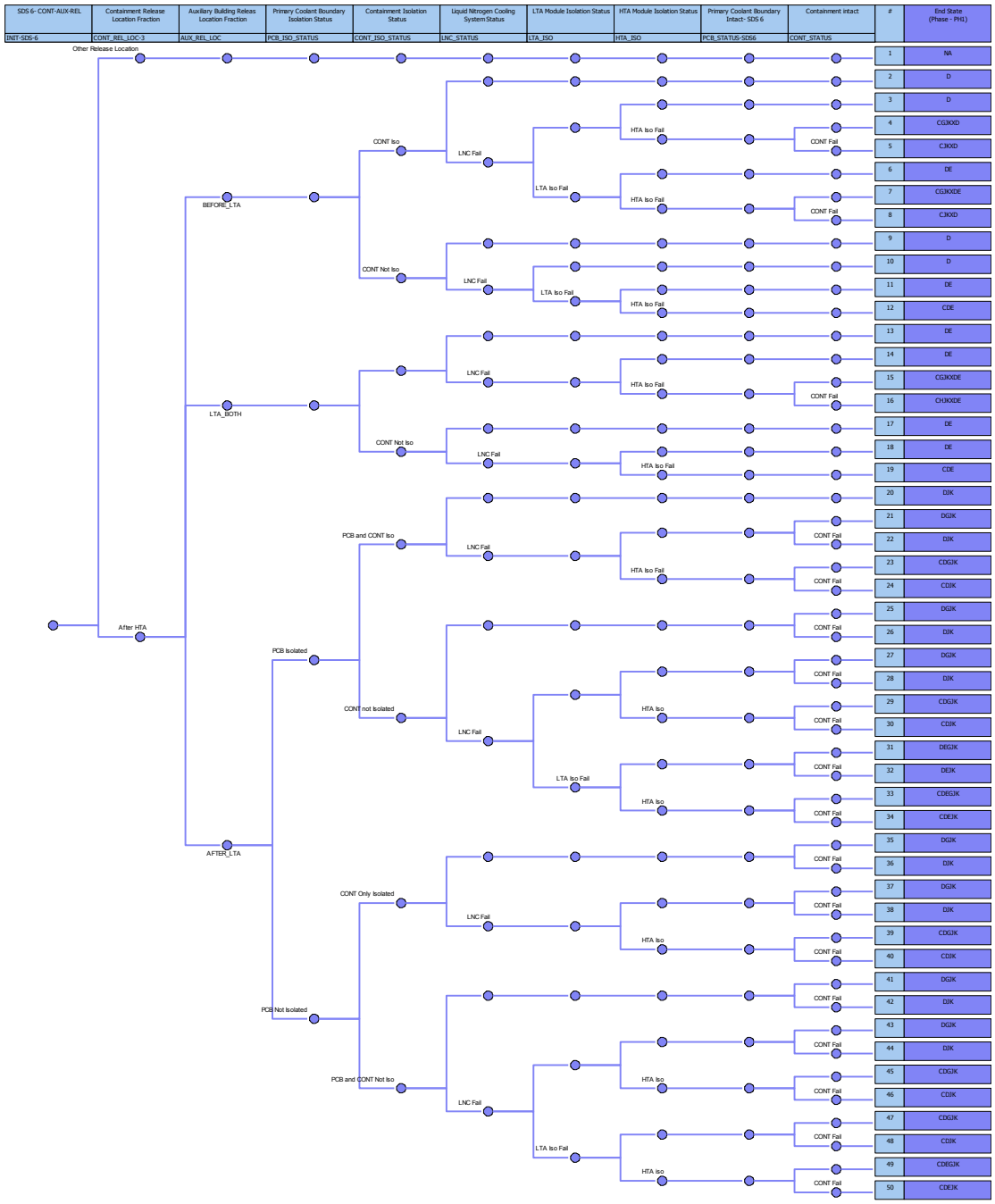

Figure C.7-8: Accident Progression Event Tree – SDS 6-3

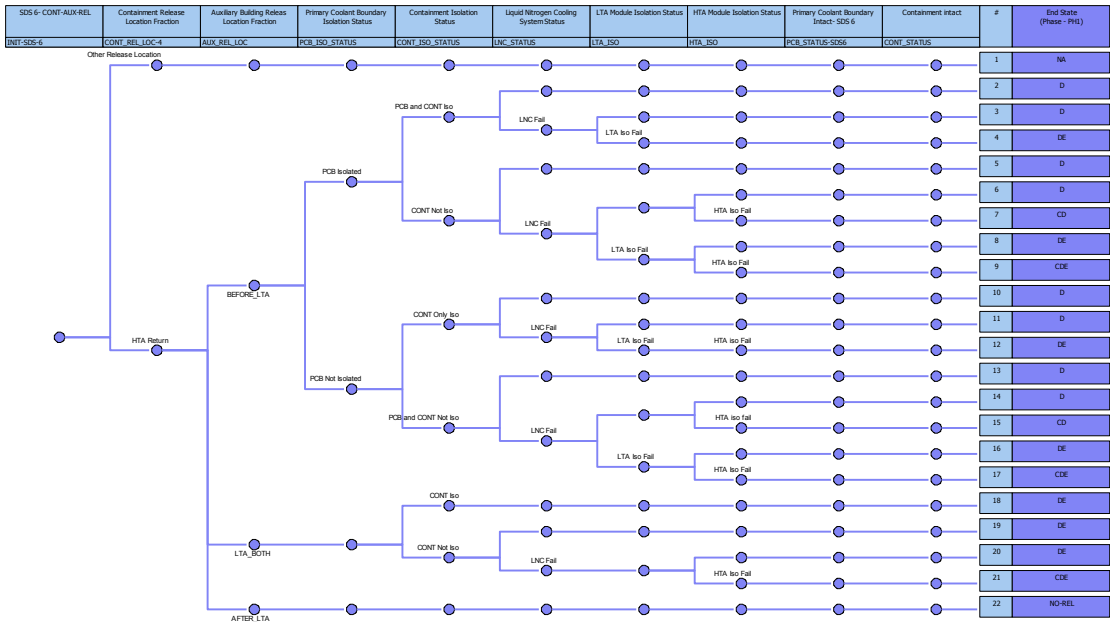

Figure C.7-9: Accident Progression Event Tree – SDS 6-4

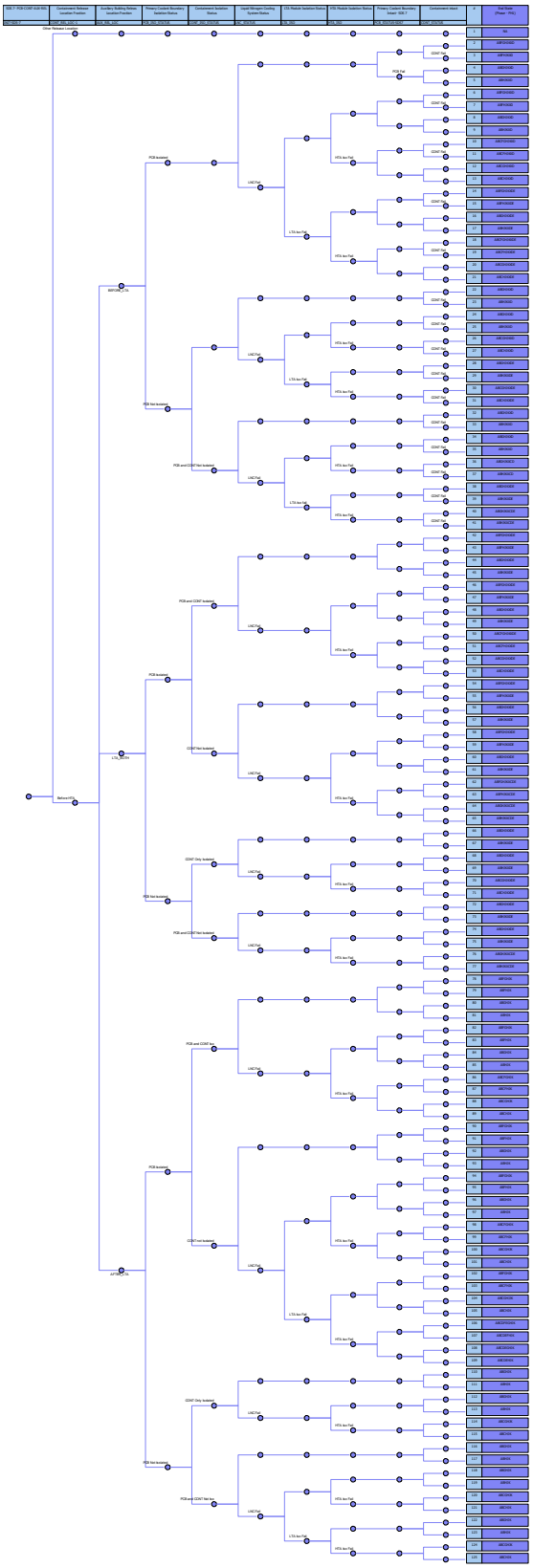

Figure C.7-10: Accident Progression Event Tree – SDS 7-1

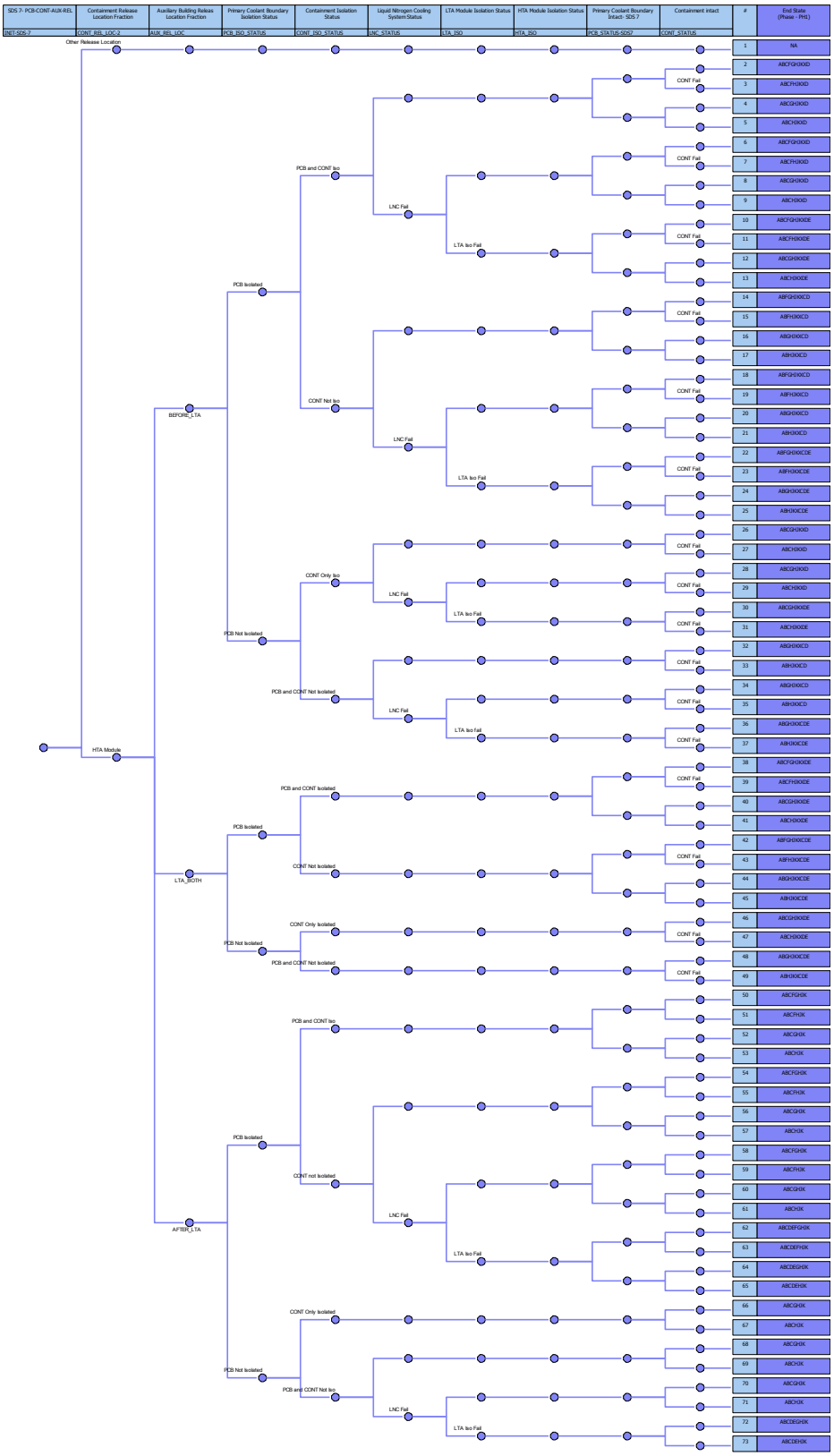

Figure C.7-11: Accident Progression Event Tree – SDS 7-2

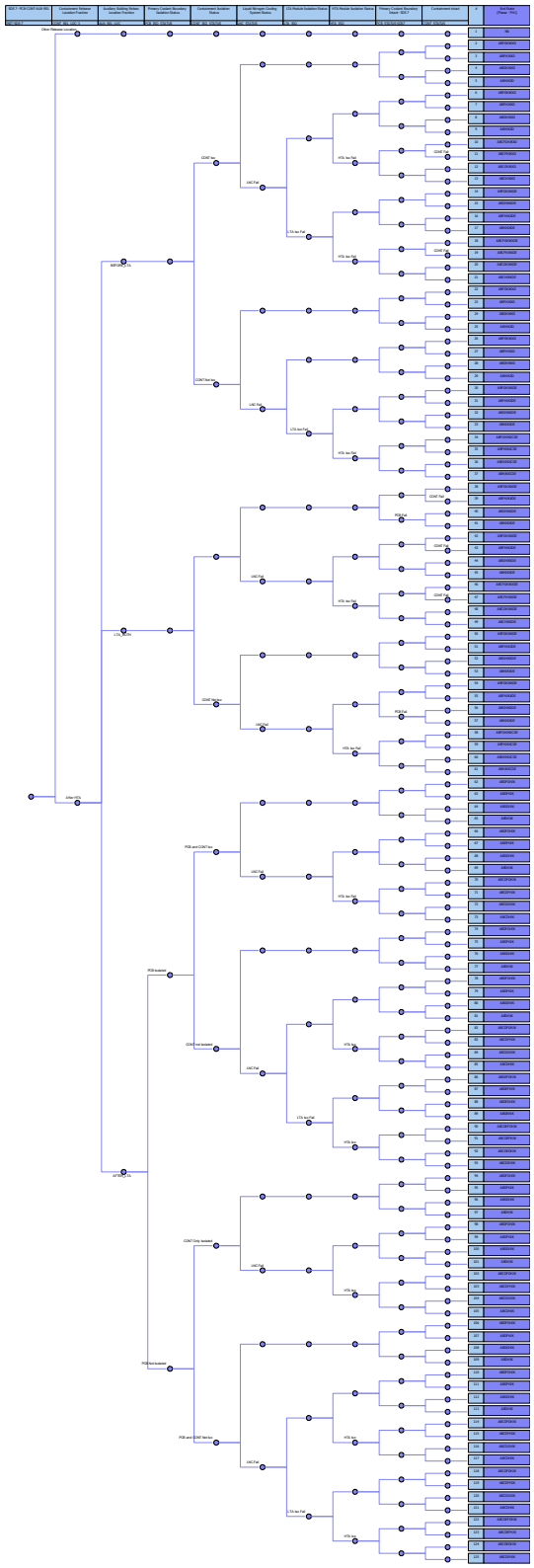

Figure C.7-12: Accident Progression Event Tree – SDS 7-3

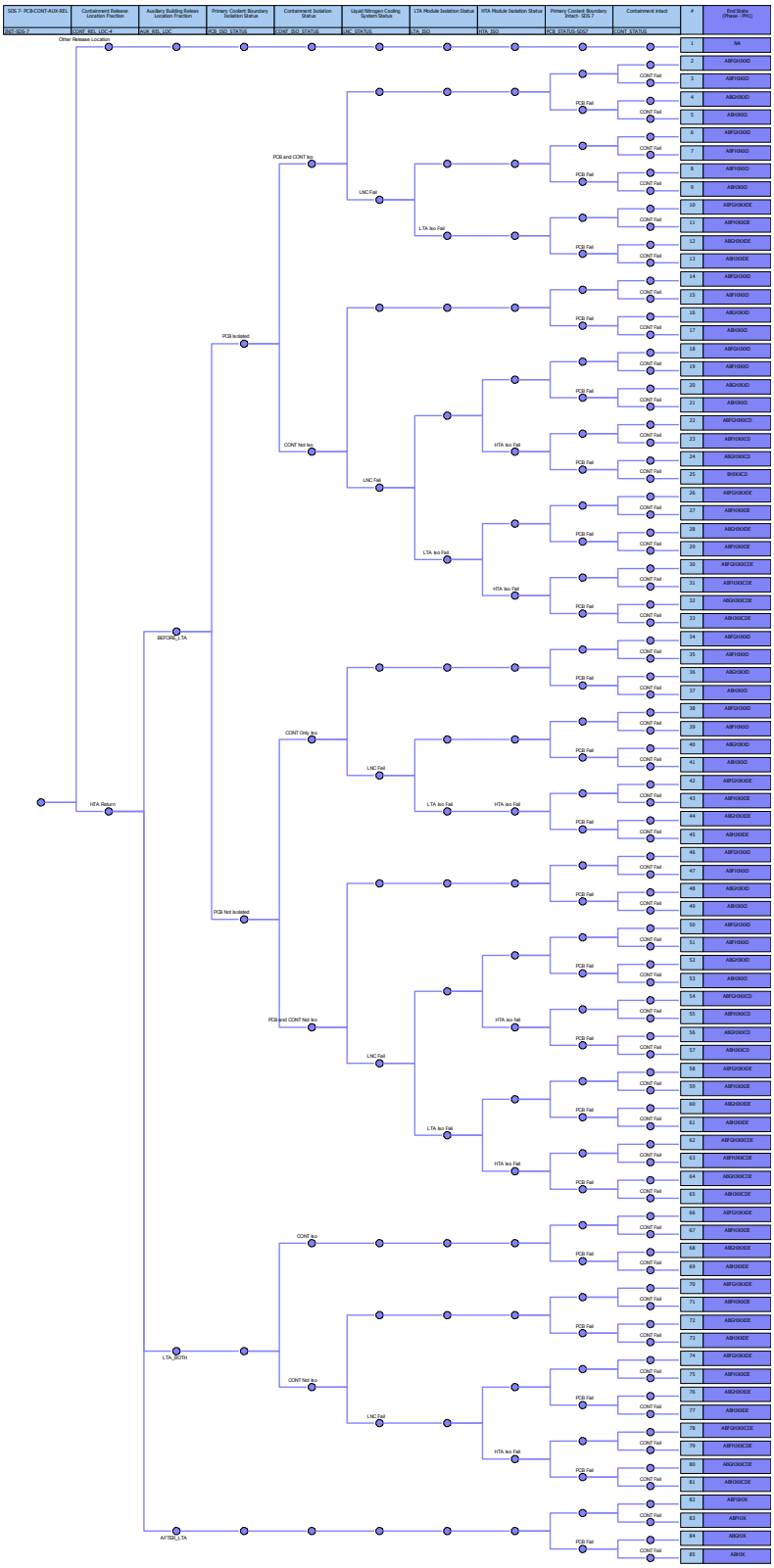

Figure C.7-13: Accident Progression Event Tree – SDS 7-4

Appendix C.8. STELLA Results

Table C.8-1: STELLA Activity Estimates

Activity (Ci) in the Fission Product Vent System										
Location	Plateout in PCB		Piping from core to HTA		HTA Contents		Piping from HTA to LTA		LTA Contents	
Nuclide	BOL	EOL	BOL	EOL	BOL	EOL	BOL	EOL	BOL	EOL
Krypton - 85m	-	-	3.34E+01	3.34E+01	-	-	2.97E+01	2.97E+01	2.45E+05	4.72E+04
Krypton - 85	-	-	2.73E-03	2.73E-03	-	-	2.73E-03	2.73E-03	8.82E+04	7.77E+04
Krypton - 87	-	-	2.09E+02	2.09E+02	-	-	1.86E+02	1.86E+02	4.37E+05	7.45E+04
Krypton - 88	-	-	7.29E+01	7.29E+01	-	-	6.47E+01	6.47E+01	3.39E+05	6.21E+04
Rubidium - 88	-	-	5.99E+02	5.99E+02	3.32E+05	6.37E+04	1.42E+00	1.42E+00	3.39E+05	6.21E+04
Rubidium - 89	-	-	1.70E+03	1.70E+03	7.31E+05	1.14E+05	-	-	-	-
Strontium - 89	-	-	9.20E-03	9.20E-03	7.32E+05	1.14E+05	-	-	-	-
Tellurium - 127m	-	-	5.54E-03	5.54E-03	2.30E+04	9.95E+03	-	-	-	-
Tellurium - 127	-	-	8.14E-01	8.14E-01	3.65E+04	1.22E+04	-	-	-	-
Tellurium - 129m	-	-	4.38E-02	4.38E-02	5.77E+04	1.93E+04	-	-	-	-
Tellurium - 129	-	-	1.24E+01	1.24E+01	6.30E+04	1.64E+04	-	-	-	-
Tellurium - 131m	-	-	3.15E+00	3.15E+00	1.68E+05	3.20E+04	-	-	-	-
Tellurium - 131	-	-	9.30E+01	9.30E+01	1.10E+05	1.82E+04	-	-	-	-
Iodine - 131	2.13E+04	5.60E+03	5.62E-01	5.62E-01	4.32E+05	9.34E+04	-	-	-	-
Tellurium - 132	-	-	1.01E+01	1.01E+01	1.26E+06	2.69E+05	-	-	-	-
Iodine - 132	1.13E+05	1.85E+04	2.49E+02	2.49E+02	2.28E+06	4.36E+05	-	-	-	-
Tellurium - 133m	-	-	5.04E+02	5.04E+02	7.66E+05	1.16E+05	-	-	-	-
Tellurium - 133	-	-	1.48E+03	1.48E+03	6.13E+05	9.18E+04	-	-	-	-
Iodine - 133	1.40E+05	2.66E+04	3.46E+01	3.46E+01	2.65E+06	4.49E+05	-	-	-	-
Xenon - 133m	-	-	1.59E+01	1.59E+01	-	-	1.59E+01	1.59E+01	4.15E+06	7.77E+05
Xenon - 133	-	-	5.76E+00	5.76E+00	-	-	5.76E+00	5.76E+00	5.50E+06	1.13E+06
Tellurium - 134	-	-	1.17E+03	1.17E+03	1.35E+06	2.04E+05	-	-	-	-
Iodine - 134	1.69E+05	2.65E+04	9.73E+02	9.73E+02	2.87E+06	4.43E+05	-	-	-	-
Iodine - 135	1.50E+05	2.48E+04	1.29E+02	1.29E+02	1.35E+06	2.23E+05	-	-	-	-
Xenon - 135m	-	-	7.69E+02	7.69E+02	-	-	7.69E+02	7.69E+02	6.33E+05	1.00E+05
Xenon - 135	-	-	9.73E+01	9.73E+01	-	-	9.73E+01	9.73E+01	3.49E+06	5.92E+05
Cesium - 137	1.52E+05	1.44E+05	5.14E-02	5.14E-02	1.37E+06	1.29E+06	-	-	-	-
Xenon - 138	-	-	3.23E+03	3.23E+03	-	-	2.86E+03	2.86E+03	1.07E+06	1.58E+05
Cesium - 138	2.55E+05	2.39E+04	2.40E+03	2.40E+03	2.29E+06	2.15E+05	3.51E+01	3.51E+01	1.50E+06	2.21E+05
sum	1.00E+06	2.70E+05	1.38E+04	1.38E+04	1.95E+07	4.23E+06	4.07E+03	4.07E+03	1.78E+07	3.30E+06

Table C.8-2: STELLA Power Estimates

Power (W) in the Fission Product Vent System										
Location	Plateout in PCB		Piping from core to HTA		HTA Contents		Piping from HTA to LTA		LTA Contents	
Nuclide	BOL	EOL	BOL	EOL	BOL	EOL	BOL	EOL	BOL	EOL
Krypton - 85m	-	-	8.33E-02	8.33E-02	-	-	7.38E-02	7.38E-02	6.09E+02	1.17E+02
Krypton - 85	-	-	4.20E-06	4.20E-06	-	-	4.20E-06	4.20E-06	1.36E+02	1.20E+02
Krypton - 87	-	-	2.67E+00	2.67E+00	-	-	2.37E+00	2.37E+00	5.57E+03	9.49E+02
Krypton - 88	-	-	1.02E+00	1.02E+00	-	-	9.08E-01	9.08E-01	4.76E+03	8.73E+02
Rubidium - 88	-	-	9.72E+00	9.72E+00	5.38E+03	1.03E+03	2.30E-02	2.30E-02	5.50E+03	1.01E+03
Rubidium - 89	-	-	3.07E+01	3.07E+01	1.32E+04	2.06E+03	-	-	-	-
Strontium - 89	-	-	3.22E-05	3.22E-05	2.56E+03	3.99E+02	-	-	-	-
Tellurium - 127m	-	-	2.96E-06	2.96E-06	1.23E+01	5.31E+00	-	-	-	-
Tellurium - 127	-	-	1.25E-03	1.25E-03	5.63E+01	1.88E+01	-	-	-	-
Tellurium - 129m	-	-	8.05E-05	8.05E-05	1.06E+02	3.54E+01	-	-	-	-
Tellurium - 129	-	-	4.41E-02	4.41E-02	2.24E+02	5.84E+01	-	-	-	-
Tellurium - 131m	-	-	3.21E-02	3.21E-02	1.72E+03	3.26E+02	-	-	-	-
Tellurium - 131	-	-	6.40E-01	6.40E-01	7.55E+02	1.25E+02	-	-	-	-
Iodine - 131	7.33E+01	1.93E+01	1.93E-03	1.93E-03	1.49E+03	3.21E+02	-	-	-	-
Tellurium - 132	-	-	2.03E-02	2.03E-02	2.54E+03	5.42E+02	-	-	-	-
Iodine - 132	1.83E+03	3.00E+02	4.03E+00	4.03E+00	3.69E+04	7.05E+03	-	-	-	-
Tellurium - 133m	-	-	6.12E+00	6.12E+00	9.31E+03	1.41E+03	-	-	-	-
Tellurium - 133	-	-	1.54E+01	1.54E+01	6.36E+03	9.52E+02	-	-	-	-
Iodine - 133	8.40E+02	1.59E+02	2.07E-01	2.07E-01	1.59E+04	2.69E+03	-	-	-	-
Xenon - 133m	-	-	2.17E-02	2.17E-02	-	-	2.17E-02	2.17E-02	5.66E+03	1.06E+03
Xenon - 133	-	-	6.49E-03	6.49E-03	-	-	6.49E-03	6.49E-03	6.19E+03	1.28E+03
Tellurium - 134	-	-	7.37E+00	7.37E+00	8.50E+03	1.28E+03	-	-	-	-
Iodine - 134	3.06E+03	4.81E+02	1.76E+01	1.76E+01	5.21E+04	8.03E+03	-	-	-	-
Iodine - 135	1.74E+03	2.88E+02	1.50E+00	1.50E+00	1.57E+04	2.59E+03	-	-	-	-
Xenon - 135m	-	-	2.42E+00	2.42E+00	-	-	2.42E+00	2.42E+00	1.99E+03	3.14E+02
Xenon - 135	-	-	3.23E-01	3.23E-01	-	-	3.23E-01	3.23E-01	1.16E+04	1.97E+03
Cesium - 137	1.71E+02	1.62E+02	5.79E-05	5.79E-05	1.54E+03	1.46E+03	-	-	-	-
Xenon - 138	-	-	4.30E+01	4.30E+01	-	-	3.82E+01	3.82E+01	1.42E+04	2.10E+03
Cesium - 138	5.16E+03	4.85E+02	4.87E+01	4.87E+01	4.64E+04	4.37E+03	7.12E-01	7.12E-01	3.04E+04	4.49E+03
sum	1.29E+04	1.89E+03	1.92E+02	1.92E+02	2.21E+05	3.48E+04	4.50E+01	4.50E+01	8.66E+04	1.43E+04

Table C.8-3: STELLA Mass Accumulation Estimates

Mass Accumulation (g) in the Fission Product Vent System										
Location	Plateout in PCB		Piping from core to HTA		HTA Contents		Piping from HTA to LTA		LTA Contents	
Nuclide	BOL	EOL	BOL	EOL	BOL	EOL	BOL	EOL	BOL	EOL
Selenium - 80	-	-	9.13E-06	9.13E-06	2.58E+02	2.58E+02	-	-	-	-
Bromine - 81	-	-	1.27E-05	1.27E-05	3.60E+02	3.60E+02	-	-	-	-
Selenium - 82	-	-	1.94E-05	1.94E-05	5.50E+02	5.50E+02	-	-	-	-
Krypton - 83	-	-	3.15E-05	3.15E-05	-	-	2.79E-05	2.79E-05	8.90E+02	8.90E+02
Krypton - 84	-	-	5.46E-05	5.46E-05	-	-	4.84E-05	4.84E-05	1.54E+03	1.54E+03
Krypton - 85m	-	-	4.06E-06	4.06E-06	-	-	3.60E-06	3.60E-06	2.97E-02	5.73E-03
Krypton - 85	-	-	6.96E-06	6.96E-06	-	-	6.96E-06	6.96E-06	2.25E+02	1.99E+02
Rubidium - 85	-	-	5.24E-05	5.24E-05	1.67E+03	1.78E+03	4.14E-09	4.14E-09	1.12E+02	3.62E+01
Krypton - 86	-	-	9.99E-05	9.99E-05	-	-	8.86E-05	8.86E-05	2.83E+03	2.83E+03
Krypton - 87	-	-	7.38E-06	7.38E-06	-	-	6.54E-06	6.54E-06	1.54E-02	2.62E-03
Rubidium - 87	-	-	1.11E-04	1.11E-04	3.54E+03	3.72E+03	3.37E-08	3.37E-08	2.10E+02	3.58E+01
Krypton - 88	-	-	5.81E-06	5.81E-06	-	-	5.15E-06	5.15E-06	2.70E-02	4.95E-03
Rubidium - 88	-	-	4.95E-06	4.95E-06	2.74E-03	5.27E-04	1.17E-08	1.17E-08	2.80E-03	5.14E-04
Strontium - 88	-	-	1.10E-07	1.10E-07	1.61E+02	3.09E+01	1.30E-10	1.30E-10	1.65E+02	3.02E+01
Rubidium - 89	-	-	1.24E-05	1.24E-05	5.32E-03	8.30E-04	-	-	-	-
Strontium - 89	-	-	3.17E-07	3.17E-07	2.52E+01	3.93E+00	-	-	-	-
Yttrium - 89	-	-	8.32E-13	8.32E-13	3.34E+02	5.21E+01	-	-	-	-
Cadmium - 111	-	-	1.89E-05	1.89E-05	5.34E+02	5.34E+02	-	-	-	-
Tellurium - 126	-	-	1.95E-05	1.95E-05	5.52E+02	5.52E+02	-	-	-	-
Tellurium - 127m	-	-	5.71E-07	5.71E-07	2.37E+00	1.02E+00	-	-	-	-
Tellurium - 127	-	-	3.10E-07	3.10E-07	1.39E-02	4.64E-03	-	-	-	-
Iodine - 127	1.71E+01	1.89E+01	4.99E-06	4.99E-06	1.78E+02	1.77E+02	-	-	-	-
Tellurium - 128	-	-	7.53E-05	7.53E-05	2.13E+03	2.13E+03	-	-	-	-
Tellurium - 129m	-	-	1.45E-06	1.45E-06	1.91E+00	6.39E-01	-	-	-	-
Tellurium - 129	-	-	5.91E-07	5.91E-07	3.01E-03	7.83E-04	-	-	-	-
Iodine - 129	5.29E+01	5.73E+01	1.54E-05	1.54E-05	5.35E+02	5.32E+02	-	-	-	-
Tellurium - 130	-	-	2.35E-04	2.35E-04	6.64E+03	6.64E+03	-	-	-	-
Tellurium - 131m	-	-	4.30E-06	4.30E-06	2.29E-01	4.36E-02	-	-	-	-
Tellurium - 131	-	-	1.62E-06	1.62E-06	1.91E-03	3.16E-04	-	-	-	-
Iodine - 131	1.71E-01	4.51E-02	4.52E-06	4.52E-06	3.48E+00	7.51E-01	-	-	-	-
Xenon - 131	-	-	8.27E-05	8.27E-05	-	-	8.27E-05	8.27E-05	2.66E+03	2.67E+03
Tellurium - 132	-	-	3.25E-05	3.25E-05	4.08E+00	8.69E-01	-	-	-	-

Mass Accumulation (g) in the Fission Product Vent System										
Location	Plateout in PCB		Piping from core to HTA		HTA Contents		Piping from HTA to LTA		LTA Contents	
Nuclide	BOL	EOL	BOL	EOL	BOL	EOL	BOL	EOL	BOL	EOL
Iodine - 132	1.09E-02	1.78E-03	2.39E-05	2.39E-05	2.19E-01	4.19E-02	-	-	-	-
Xenon - 132	-	-	4.43E-04	4.43E-04	-	0.00E+00	4.43E-04	4.43E-04	1.59E+04	1.59E+04
Tellurium - 133m	-	-	1.97E-05	1.97E-05	3.00E-02	4.55E-03	-	-	-	-
Tellurium - 133	-	-	1.30E-05	1.30E-05	5.38E-03	8.04E-04	-	-	-	-
Iodine - 133	1.24E-01	2.35E-02	3.05E-05	3.05E-05	2.34E+00	3.96E-01	-	-	-	-
Xenon - 133m	-	-	3.54E-05	3.54E-05	-	-	3.54E-05	3.54E-05	9.25E+00	1.73E+00
Xenon - 133	-	-	3.07E-05	3.07E-05	-	-	3.07E-05	3.07E-05	2.93E+01	6.04E+00
Cesium - 133	1.52E+03	1.84E+03	4.44E-04	4.44E-04	1.37E+04	1.66E+04	1.59E-09	1.59E-09	3.99E+03	8.23E+02
Tellurium - 134	-	-	3.51E-05	3.51E-05	4.05E-02	6.11E-03	-	-	-	-
Iodine - 134	6.32E-03	9.94E-04	3.64E-05	3.64E-05	1.08E-01	1.66E-02	-	-	-	-
Xenon - 134	-	-	6.81E-04	6.81E-04	-	-	6.81E-04	6.81E-04	2.40E+04	2.40E+04
Iodine - 135	4.25E-02	7.01E-03	3.66E-05	3.66E-05	3.82E-01	6.31E-02	-	-	-	-
Xenon - 135m	-	-	8.45E-06	8.45E-06	-	-	8.45E-06	8.45E-06	6.95E-03	1.10E-03
Xenon - 135	-	-	3.81E-05	3.81E-05	-	-	3.81E-05	3.81E-05	1.37E+00	2.32E-01
Cesium - 135	2.04E+03	2.26E+03	6.69E-04	6.69E-04	1.84E+04	2.03E+04	2.86E-08	2.86E-08	2.60E+03	4.42E+02
Xenon - 136	-	-	7.60E-04	7.60E-04	-	-	6.74E-04	6.74E-04	2.15E+04	2.15E+04
Cesium - 137	1.75E+03	1.66E+03	5.92E-04	5.92E-04	1.58E+04	1.49E+04	-	-	-	-
Barium - 137	-	-	1.57E-11	1.57E-11	5.81E+02	5.50E+02	-	-	-	-
Xenon - 138	-	-	3.34E-05	3.34E-05	-	-	2.96E-05	2.96E-05	1.10E-02	1.63E-03
Cesium - 138	6.01E-03	5.65E-04	5.68E-05	5.68E-05	5.41E-02	5.09E-03	8.29E-07	8.29E-07	3.54E-02	5.23E-03
Barium - 138	-	-	7.42E-07	7.42E-07	1.94E+03	1.82E+02	5.08E-09	5.08E-09	9.86E+02	1.46E+02
sum	5.39E+03	5.83E+03	4.92E-03	4.92E-03	6.79E+04	6.99E+04	2.21E-03	2.21E-03	7.76E+04	7.10E+04

Table C.8-4: Source Term Estimates

Source Term Estimates by Source Term Group (Ci)										
Source Term Group	ALL FPVS		BGJK		DE		D		BCGJK	
Nuclide	BOL	EOL	BOL	EOL	BOL	EOL	BOL	EOL	BOL	EOL
Krypton - 85m	2.45E+05	4.72E+04	3.35E+01	3.35E+01	2.45E+05	4.72E+04	2.97E+01	2.97E+01	3.35E+01	3.35E+01
Krypton - 85	8.82E+04	7.77E+04	2.72E-03	2.72E-03	8.82E+04	7.77E+04	2.72E-03	2.72E-03	2.72E-03	2.72E-03
Krypton - 87	4.37E+05	7.49E+04	2.11E+02	2.11E+02	4.37E+05	7.47E+04	1.87E+02	1.87E+02	2.11E+02	2.11E+02
Krypton - 88	3.39E+05	6.23E+04	7.31E+01	7.31E+01	3.39E+05	6.22E+04	6.48E+01	6.48E+01	7.31E+01	7.31E+01
Rubidium - 88	8.47E+04	1.55E+04	1.52E-02	1.52E-02	8.47E+04	1.55E+04	6.42E-02	6.42E-02	2.09E+00	4.13E-01
Rubidium - 89	4.61E+00	7.56E-01	4.35E-02	4.35E-02	0.00E+00	0.00E+00	0.00E+00	0.00E+00	4.61E+00	7.56E-01
Strontium - 89	4.57E+00	7.13E-01	9.28E-09	9.28E-09	0.00E+00	0.00E+00	0.00E+00	0.00E+00	4.57E+00	7.13E-01
Tellurium - 127m	1.44E-01	6.22E-02	1.38E-07	1.38E-07	0.00E+00	0.00E+00	0.00E+00	0.00E+00	1.44E-01	6.22E-02
Tellurium - 127	2.28E-01	7.63E-02	2.04E-05	2.04E-05	0.00E+00	0.00E+00	0.00E+00	0.00E+00	2.28E-01	7.63E-02
Tellurium - 129m	3.61E-01	1.20E-01	1.10E-06	1.10E-06	0.00E+00	0.00E+00	0.00E+00	0.00E+00	3.61E-01	1.20E-01
Tellurium - 129	3.94E-01	1.03E-01	3.11E-04	3.11E-04	0.00E+00	0.00E+00	0.00E+00	0.00E+00	3.94E-01	1.03E-01
Tellurium - 131m	1.05E+00	2.00E-01	7.88E-05	7.88E-05	0.00E+00	0.00E+00	0.00E+00	0.00E+00	1.05E+00	2.00E-01
Tellurium - 131	6.89E-01	1.16E-01	2.36E-03	2.36E-03	0.00E+00	0.00E+00	0.00E+00	0.00E+00	6.89E-01	1.16E-01
Iodine - 131	2.70E+00	5.84E-01	1.40E-05	1.40E-05	0.00E+00	0.00E+00	0.00E+00	0.00E+00	2.70E+00	5.84E-01
Tellurium - 132	7.89E+00	1.68E+00	2.52E-04	2.52E-04	0.00E+00	0.00E+00	0.00E+00	0.00E+00	7.89E+00	1.68E+00
Iodine - 132	1.42E+01	2.73E+00	6.24E-03	6.24E-03	0.00E+00	0.00E+00	0.00E+00	0.00E+00	1.42E+01	2.73E+00
Tellurium - 133m	4.80E+00	7.39E-01	1.27E-02	1.27E-02	0.00E+00	0.00E+00	0.00E+00	0.00E+00	4.80E+00	7.39E-01
Tellurium - 133	3.87E+00	6.12E-01	3.82E-02	3.82E-02	0.00E+00	0.00E+00	0.00E+00	0.00E+00	3.87E+00	6.12E-01
Iodine - 133	1.66E+01	2.81E+00	8.52E-04	8.52E-04	0.00E+00	0.00E+00	0.00E+00	0.00E+00	1.66E+01	2.81E+00
Xenon - 133m	4.15E+06	7.77E+05	1.59E+01	1.59E+01	4.15E+06	7.77E+05	1.59E+01	1.59E+01	1.59E+01	1.59E+01
Xenon - 133	5.50E+06	1.13E+06	5.76E+00	5.76E+00	5.50E+06	1.13E+06	5.76E+00	5.76E+00	5.76E+00	5.76E+00
Tellurium - 134	8.49E+00	1.31E+00	2.96E-02	2.96E-02	0.00E+00	0.00E+00	0.00E+00	0.00E+00	8.49E+00	1.31E+00
Iodine - 134	1.80E+01	2.79E+00	2.43E-02	2.43E-02	0.00E+00	0.00E+00	0.00E+00	0.00E+00	1.80E+01	2.79E+00
Iodine - 135	8.45E+00	1.40E+00	3.24E-03	3.24E-03	0.00E+00	0.00E+00	0.00E+00	0.00E+00	8.45E+00	1.40E+00
Xenon - 135m	6.35E+05	1.02E+05	7.88E+02	7.88E+02	6.34E+05	1.01E+05	7.88E+02	7.88E+02	7.88E+02	7.88E+02
Xenon - 135	3.49E+06	5.92E+05	9.67E+01	9.67E+01	3.49E+06	5.92E+05	9.67E+01	9.67E+01	9.67E+01	9.67E+01
Cesium - 137	8.55E+00	8.09E+00	1.28E-06	1.28E-06	0.00E+00	0.00E+00	0.00E+00	0.00E+00	8.55E+00	8.09E+00
Xenon - 138	1.07E+06	1.64E+05	3.31E+03	3.31E+03	1.07E+06	1.61E+05	2.94E+03	2.94E+03	3.31E+03	3.31E+03
Cesium - 138	3.75E+05	5.54E+04	5.99E-02	5.99E-02	3.75E+05	5.54E+04	1.60E+00	1.60E+00	1.44E+01	1.41E+00
sum	1.64E+07	3.10E+06	4.54E+03	4.54E+03	1.64E+07	3.10E+06	4.13E+03	4.13E+03	4.66E+03	4.56E+03

Source Term Estimates by Source Term Group										
Source Term Group	DGJK		BJK		BCJK		ABFGHJK		DJK	
Nuclide	BOL	EOL	BOL	EOL	BOL	EOL	BOL	EOL	BOL	EOL
Krypton - 85m	2.97E+01	2.97E+01	3.35E+01	3.35E+01	3.35E+01	3.35E+01	3.35E+01	3.35E+01	2.97E+01	2.97E+01
Krypton - 85	2.72E-03	2.72E-03	2.72E-03	2.72E-03	2.72E-03	2.72E-03	2.72E-03	2.72E-03	2.72E-03	2.72E-03
Krypton - 87	1.87E+02	1.87E+02	2.11E+02	2.11E+02	2.11E+02	2.11E+02	2.11E+02	2.11E+02	1.87E+02	1.87E+02
Krypton - 88	6.48E+01	6.48E+01	7.31E+01	7.31E+01	7.31E+01	7.31E+01	7.31E+01	7.31E+01	6.48E+01	6.48E+01
Rubidium - 88	1.60E-06	1.60E-06	1.52E+02	1.52E+02	2.09E+04	4.13E+03	1.52E-02	1.52E-02	1.60E-02	1.60E-02
Rubidium - 89	0.00E+00	0.00E+00	4.35E+02	4.35E+02	4.61E+04	7.56E+03	4.35E-02	4.35E-02	0.00E+00	0.00E+00
Strontium - 89	0.00E+00	0.00E+00	9.28E-05	9.28E-05	4.57E+04	7.13E+03	9.28E-09	9.28E-09	0.00E+00	0.00E+00
Tellurium - 127m	0.00E+00	0.00E+00	1.38E-03	1.38E-03	1.44E+03	6.22E+02	1.38E-07	1.38E-07	0.00E+00	0.00E+00
Tellurium - 127	0.00E+00	0.00E+00	2.04E-01	2.04E-01	2.28E+03	7.63E+02	2.04E-05	2.04E-05	0.00E+00	0.00E+00
Tellurium - 129m	0.00E+00	0.00E+00	1.10E-02	1.10E-02	3.61E+03	1.20E+03	1.10E-06	1.10E-06	0.00E+00	0.00E+00
Tellurium - 129	0.00E+00	0.00E+00	3.11E+00	3.11E+00	3.94E+03	1.03E+03	3.11E-04	3.11E-04	0.00E+00	0.00E+00
Tellurium - 131m	0.00E+00	0.00E+00	7.88E-01	7.88E-01	1.05E+04	2.00E+03	7.88E-05	7.88E-05	0.00E+00	0.00E+00
Tellurium - 131	0.00E+00	0.00E+00	2.36E+01	2.36E+01	6.89E+03	1.16E+03	2.36E-03	2.36E-03	0.00E+00	0.00E+00
Iodine - 131	0.00E+00	0.00E+00	1.40E-01	1.40E-01	2.70E+04	5.84E+03	1.40E-05	4.20E-05	0.00E+00	0.00E+00
Tellurium - 132	0.00E+00	0.00E+00	2.52E+00	2.52E+00	7.89E+04	1.68E+04	2.52E-04	2.52E-04	0.00E+00	0.00E+00
Iodine - 132	0.00E+00	0.00E+00	6.24E+01	6.24E+01	1.42E+05	2.73E+04	6.24E-03	6.33E-03	0.00E+00	0.00E+00
Tellurium - 133m	0.00E+00	0.00E+00	1.27E+02	1.27E+02	4.80E+04	7.39E+03	1.27E-02	1.27E-02	0.00E+00	0.00E+00
Tellurium - 133	0.00E+00	0.00E+00	3.82E+02	3.82E+02	3.87E+04	6.12E+03	3.82E-02	3.82E-02	0.00E+00	0.00E+00
Iodine - 133	0.00E+00	0.00E+00	8.52E+00	8.52E+00	1.66E+05	2.81E+04	8.52E-04	9.85E-04	0.00E+00	0.00E+00
Xenon - 133m	1.59E+01	1.59E+01	1.59E+01	1.59E+01	1.59E+01	1.59E+01	1.59E+01	1.59E+01	1.59E+01	1.59E+01
Xenon - 133	5.76E+00	5.76E+00	5.76E+00	5.76E+00	5.76E+00	5.76E+00	5.76E+00	5.76E+00	5.76E+00	5.76E+00
Tellurium - 134	0.00E+00	0.00E+00	2.96E+02	2.96E+02	8.49E+04	1.31E+04	2.96E-02	2.96E-02	0.00E+00	0.00E+00
Iodine - 134	0.00E+00	0.00E+00	2.43E+02	2.43E+02	1.80E+05	2.79E+04	2.43E-02	2.44E-02	0.00E+00	0.00E+00
Iodine - 135	0.00E+00	0.00E+00	3.24E+01	3.24E+01	8.45E+04	1.40E+04	3.24E-03	3.36E-03	0.00E+00	0.00E+00
Xenon - 135m	7.88E+02	7.88E+02	7.88E+02	7.88E+02	7.88E+02	7.88E+02	7.88E+02	7.88E+02	7.88E+02	7.88E+02
Xenon - 135	9.67E+01	9.67E+01	9.67E+01	9.67E+01	9.67E+01	9.67E+01	9.67E+01	9.67E+01	9.67E+01	9.67E+01
Cesium - 137	0.00E+00	0.00E+00	1.28E-02	1.28E-02	8.55E+04	8.09E+04	1.30E-06	7.20E-04	0.00E+00	0.00E+00
Xenon - 138	2.94E+03	2.94E+03	3.31E+03	3.31E+03	3.31E+03	3.31E+03	3.31E+03	3.31E+03	2.94E+03	2.94E+03
Cesium - 138	4.00E-05	4.00E-05	5.99E+02	5.99E+02	1.44E+05	1.41E+04	5.99E-02	6.00E-02	4.00E-01	4.00E-01
sum	4.13E+03	4.13E+03	6.90E+03	6.90E+03	1.23E+06	2.71E+05	4.54E+03	4.54E+03	4.13E+03	4.13E+03

Source Term Estimates by Source Term Group								
Source Term Group	BGJKXDE		BGJKXD		BCGJKXDE		BCGJKXD	
Nuclide	BOL	EOL	BOL	EOL	BOL	EOL	BOL	EOL
Krypton - 85m	2.45E+05	4.72E+04	6.32E+01	6.32E+01	2.45E+05	4.72E+04	6.32E+01	6.32E+01
Krypton - 85	8.82E+04	7.77E+04	5.45E-03	5.45E-03	8.82E+04	7.77E+04	5.45E-03	5.45E-03
Krypton - 87	4.37E+05	7.49E+04	3.97E+02	3.97E+02	4.37E+05	7.49E+04	3.97E+02	3.97E+02
Krypton - 88	3.39E+05	6.23E+04	1.38E+02	1.38E+02	3.39E+05	6.23E+04	1.38E+02	1.38E+02
Rubidium - 88	8.47E+04	1.55E+04	7.94E-02	7.94E-02	8.47E+04	1.55E+04	2.15E+00	4.77E-01
Rubidium - 89	4.35E-02	4.35E-02	4.35E-02	4.35E-02	4.61E+00	7.56E-01	4.61E+00	7.56E-01
Strontium - 89	9.28E-09	9.28E-09	9.28E-09	9.28E-09	4.57E+00	7.13E-01	4.57E+00	7.13E-01
Tellurium - 127m	1.38E-07	1.38E-07	1.38E-07	1.38E-07	1.44E-01	6.22E-02	1.44E-01	6.22E-02
Tellurium - 127	2.04E-05	2.04E-05	2.04E-05	2.04E-05	2.28E-01	7.63E-02	2.28E-01	7.63E-02
Tellurium - 129m	1.10E-06	1.10E-06	1.10E-06	1.10E-06	3.61E-01	1.20E-01	3.61E-01	1.20E-01
Tellurium - 129	3.11E-04	3.11E-04	3.11E-04	3.11E-04	3.94E-01	1.03E-01	3.94E-01	1.03E-01
Tellurium - 131m	7.88E-05	7.88E-05	7.88E-05	7.88E-05	1.05E+00	2.00E-01	1.05E+00	2.00E-01
Tellurium - 131	2.36E-03	2.36E-03	2.36E-03	2.36E-03	6.89E-01	1.16E-01	6.89E-01	1.16E-01
Iodine - 131	1.40E-05	1.40E-05	1.40E-05	1.40E-05	2.70E+00	5.84E-01	2.70E+00	5.84E-01
Tellurium - 132	2.52E-04	2.52E-04	2.52E-04	2.52E-04	7.89E+00	1.68E+00	7.89E+00	1.68E+00
Iodine - 132	6.24E-03	6.24E-03	6.24E-03	6.24E-03	1.42E+01	2.73E+00	1.42E+01	2.73E+00
Tellurium - 133m	1.27E-02	1.27E-02	1.27E-02	1.27E-02	4.80E+00	7.39E-01	4.80E+00	7.39E-01
Tellurium - 133	3.82E-02	3.82E-02	3.82E-02	3.82E-02	3.87E+00	6.12E-01	3.87E+00	6.12E-01
Iodine - 133	8.52E-04	8.52E-04	8.52E-04	8.52E-04	1.66E+01	2.81E+00	1.66E+01	2.81E+00
Xenon - 133m	4.15E+06	7.77E+05	3.18E+01	3.18E+01	4.15E+06	7.77E+05	3.18E+01	3.18E+01
Xenon - 133	5.50E+06	1.13E+06	1.15E+01	1.15E+01	5.50E+06	1.13E+06	1.15E+01	1.15E+01
Tellurium - 134	2.96E-02	2.96E-02	2.96E-02	2.96E-02	8.49E+00	1.31E+00	8.49E+00	1.31E+00
Iodine - 134	2.43E-02	2.43E-02	2.43E-02	2.43E-02	1.80E+01	2.79E+00	1.80E+01	2.79E+00
Iodine - 135	3.24E-03	3.24E-03	3.24E-03	3.24E-03	8.45E+00	1.40E+00	8.45E+00	1.40E+00
Xenon - 135m	6.35E+05	1.02E+05	1.58E+03	1.58E+03	6.35E+05	1.02E+05	1.58E+03	1.58E+03
Xenon - 135	3.49E+06	5.92E+05	1.93E+02	1.93E+02	3.49E+06	5.92E+05	1.93E+02	1.93E+02
Cesium - 137	1.28E-06	1.28E-06	1.28E-06	1.28E-06	8.55E+00	8.09E+00	8.55E+00	8.09E+00
Xenon - 138	1.07E+06	1.64E+05	6.25E+03	6.25E+03	1.07E+06	1.64E+05	6.25E+03	6.25E+03
Cesium - 138	3.75E+05	5.54E+04	1.66E+00	1.66E+00	3.75E+05	5.54E+04	1.60E+01	3.01E+00
sum	1.64E+07	3.10E+06	8.67E+03	8.67E+03	1.64E+07	3.10E+06	8.79E+03	8.69E+03

Appendix C.9. Consequence Results

Table C.9-1: TEDE at EAB for 2 Hours (BOL)

Source Term Group ID	Release Frequency	TEDE at EAB=400 m (rem)	TEDE at EAB=800 m (rem)	TEDE at EAB=1600 m (rem)	TEDE at EAB=3200 m (rem)	TEDE at EAB=8000 m (rem)
BGJK	9.60E-04	7.80E+00	2.50E+00	1.20E+00	6.50E-01	3.00E-01
DE	4.44E-04	4.70E+03	1.50E+03	7.30E+02	3.90E+02	1.80E+02
D	3.85E-04	5.00E+01	1.60E+01	7.70E+00	4.20E+00	1.90E+00
BCGJK	2.90E-04	8.80E+00	2.80E+00	1.40E+00	7.40E-01	3.40E-01
DGJK	6.09E-05	7.00E+00	2.20E+00	1.10E+00	5.80E-01	2.70E-01
BJK	2.97E-05	1.10E+01	3.60E+00	1.80E+00	9.50E-01	4.40E-01
BCJK	8.96E-06	9.80E+03	3.10E+03	1.50E+03	8.30E+02	3.80E+02
ABFGHJK	2.03E-06	7.80E+00	2.50E+00	1.20E+00	6.50E-01	3.00E-01
DJK	1.94E-06	7.00E+00	2.20E+00	1.10E+00	5.80E-01	2.70E-01
BGJKXDE	5.61E-07	4.70E+03	1.50E+03	7.30E+02	3.90E+02	1.80E+02
BGJKXD	4.86E-07	1.50E+01	4.60E+00	2.30E+00	1.20E+00	5.70E-01
BCGJKXDE	1.69E-07	4.70E+03	1.50E+03	7.30E+02	3.90E+02	1.80E+02
BCGJKXD	1.47E-07	1.60E+01	4.90E+00	2.40E+00	1.30E+00	6.10E-01
ALL FPVS	N/A	4.70E+03	1.50E+03	7.30E+02	3.90E+02	1.80E+02

Table C.9-2: Cancer Incidence at EAB for 2 Hours (BOL)

Source Term Group ID	Release Frequency	Cancer Incidence at EAB=400 m (risk)	Cancer Incidence at EAB=800 m (risk)	Cancer Incidence at EAB=1600 m (risk)	Cancer Incidence at EAB=3200 m (risk)	Cancer Incidence at EAB=8000 m (risk)
BGJK	9.60E-04	4.70E-03	1.50E-03	7.30E-04	3.90E-04	1.80E-04
DE	4.44E-04	2.80E+00	8.80E-01	4.40E-01	2.40E-01	1.10E-01
D	3.85E-04	3.00E-02	9.40E-03	4.70E-03	2.50E-03	1.20E-03
BCGJK	2.90E-04	5.30E-03	1.60E-03	8.20E-04	4.40E-04	2.00E-04
DGJK	6.09E-05	4.20E-03	1.30E-03	6.50E-04	3.50E-04	1.60E-04
BJK	2.97E-05	6.80E-03	2.10E-03	1.10E-03	5.70E-04	2.60E-04
BCJK	8.96E-06	5.90E+00	1.80E+00	9.20E-01	5.00E-01	2.30E-01
ABFGHJK	2.03E-06	4.70E-03	1.50E-03	7.30E-04	3.90E-04	1.80E-04
DJK	1.94E-06	4.20E-03	1.30E-03	6.50E-04	3.50E-04	1.60E-04
BGJKXDE	5.61E-07	2.80E+00	8.90E-01	4.40E-01	2.40E-01	1.10E-01
BGJKXD	4.86E-07	8.90E-03	2.80E-03	1.40E-03	7.40E-04	3.40E-04
BCGJKXDE	1.69E-07	2.80E+00	8.80E-01	4.40E-01	2.40E-01	1.10E-01
BCGJKXD	1.47E-07	9.50E-03	3.00E-03	1.50E-03	7.90E-04	3.70E-04
ALL FPVS	N/A	2.80E+00	8.80E-01	4.40E-01	2.40E-01	1.10E-01

Table C.9-3: Cancer Fatalities at EAB for 2 Hours (BOL)

Source Term Group ID	Release Frequency	Cancer Fatalities at EAB=400 m (risk)	Cancer Fatalities at EAB=800 m (risk)	Cancer Fatalities at EAB=1600 m (risk)	Cancer Fatalities at EAB=3200 m (risk)	Cancer Fatalities at EAB=8000 m (risk)
BGJK	9.60E-04	3.90E-03	1.20E-03	6.00E-04	3.30E-04	1.50E-04
DE	4.44E-04	2.30E+00	7.40E-01	3.60E-01	2.00E-01	9.10E-02
D	3.85E-04	2.50E-02	7.80E-03	3.90E-03	2.10E-03	9.70E-04
BCGJK	2.90E-04	4.40E-03	1.40E-03	6.80E-04	3.70E-04	1.70E-04
DGJK	6.09E-05	3.50E-03	1.10E-03	5.40E-04	2.90E-04	1.40E-04
BJK	2.97E-05	5.70E-03	1.80E-03	8.80E-04	4.80E-04	2.20E-04
BCJK	8.96E-06	4.90E+00	1.50E+00	7.60E-01	4.10E-01	1.90E-01
ABFGHJK	2.03E-06	3.90E-03	1.20E-03	6.00E-04	3.30E-04	1.50E-04
DJK	1.94E-06	3.50E-03	1.10E-03	5.40E-04	2.90E-04	1.40E-04
BGJKXDE	5.61E-07	2.40E+00	7.40E-01	3.70E-01	2.00E-01	9.10E-02
BGJKXD	4.86E-07	7.40E-03	2.30E-03	1.10E-03	6.20E-04	2.90E-04
BCGJKXDE	1.69E-07	2.30E+00	7.40E-01	3.60E-01	2.00E-01	9.10E-02
BCGJKXD	1.47E-07	7.90E-03	2.50E-03	1.20E-03	6.60E-04	3.10E-04
ALL FPVS	N/A	2.30E+00	7.40E-01	3.60E-01	2.00E-01	9.10E-02